AFRL-RX-WP-TR-2013-0086

NANOMATERIALS COMMERCIALIZATION CENTER

Leone Hermans-Blackburn and Richard A. Maresca

Wright Brothers Institute, Inc.

FEBRUARY 2013
Final Report

AIR FORCE RESEARCH LABORATORY
MATERIALS AND MANUFACTURING DIRECTORATE
WRIGHT-PATTERSON AIR FORCE BASE, OH 45433-7750
AIR FORCE MATERIEL COMMAND
UNITED STATES AIR FORCE

NOTICE AND SIGNATURE PAGE

Using Government drawings, specifications, or other data included in this document for any purpose other than Government procurement does not in any way obligate the U.S. Government. The fact that the Government formulated or supplied the drawings, specifications, or other data does not license the holder or any other person or corporation; or convey any rights or permission to manufacture, use, or sell any patented invention that may relate to them.

Qualified requestors may obtain copies of this report from the Defense Technical Information Center (DTIC) (http://www.dtic.mil)

AFRL-RX-WP-TR-2013-0086 HAS BEEN REVIEWED AND IS APPROVED FOR PUBLICATION IN ACCORDANCE WITH ASSIGNED DISTRIBUTION STATEMENT.

//SIGNED//
ASHLEY B. SUTHERLAND, Program Mgr
Soft Matter Materials Branch
Functional Materials Division

//SIGNED//
KATIE E. THORP, Chief
Soft Matter Materials Branch
Functional Materials Division

//SIGNED//
KAREN R. OLSON, Deputy Chief
Functional Materials Division
Materials & Manufacturing Directorate

This report is published in the interest of scientific and technical information exchange and its publication does not constitute the Government's approval or disapproval of its ideas or findings.

REPORT DOCUMENTATION PAGE

Form Approved
OMB No. 0704-0188

1. REPORT DATE *(DD-MM-YY)*	2. REPORT TYPE	3. DATES COVERED *(From - To)*
February 2013	Final	25 October 2006 – 30 January 2013

4. TITLE AND SUBTITLE
NANOMATERIALS COMMERCIALIZATION CENTER

5a. CONTRACT NUMBER
FA8650-06-3-9024

5b. GRANT NUMBER

5c. PROGRAM ELEMENT NUMBER
62102F

6. AUTHOR(S)
Leone Hermans-Blackburn, Ph.D. and Richard A. Maresca (Wright Brothers Institute, Inc)
Dr. Rick Simons (NanoRDC, LLC)
Ian Winfield, Iain Brooks, and Edward Yokley (Integran Technologies)
Shihai Zhang (Strategic Polymer Sciences, Inc.)

5d. PROJECT NUMBER
4347

5e. TASK NUMBER
10

5f. WORK UNIT NUMBER
X02T (11500102)

7. PERFORMING ORGANIZATION NAME(S) AND ADDRESS(ES)
The Wright Brothers Institute Inc.
5000 Springfield St #100
Dayton, OH 45431-1263

8. PERFORMING ORGANIZATION REPORT NUMBER
WBI-2013-1

9. SPONSORING/MONITORING AGENCY NAME(S) AND ADDRESS(ES)
Air Force Research Laboratory
Materials and Manufacturing Directorate
Wright-Patterson Air Force Base, OH 45433-7750
Air Force Materiel Command
United States Air Force

10. SPONSORING/MONITORING AGENCY ACRONYM(S)
AFRL/RXAS

11. SPONSORING/MONITORING AGENCY REPORT NUMBER(S)
AFRL-RX-WP-TR-2013-0086

12. DISTRIBUTION/AVAILABILITY STATEMENT
Approved for public release; distribution is unlimited.

13. SUPPLEMENTARY NOTES
Approved by 88ABW Public Affairs Office: Case number 88ABW-2013-2585 on 04 JUN 2013. Report contains color.

14. ABSTRACT

This report describes the activities of a collaborative project order (CPO) agreement between the Air Force Research Laboratory Materials and Manufacturing Directorate (AFRL/RX) and the Wright Brothers Institute (WBI), in which the Pennsylvania Nanomaterials Commercialization Center served as principal subcontractor, principal performer of all project work and principal interface with AFRL/RX. In this CPO, the PANanoCenter, working with AFRL and its core industry partners defined a Technology Roadmap. Based on that Roadmap, the PA NanoCenter funded a number of technology development projects that as a direct result of the funding could advance the technology for both the commercial and/or non-commercial stakeholders. In October 2009, with input from the AFRL an additional technology thrust was added to the Technology Roadmap which focused on nanomaterials for new energy applications. Energy is expanded to include (a) Generation; (b) Conversion; (c) Utilization and (d) Storage. The PA NanoCenter has been able to fund a total of 46 projects, 59 technologies and 19 commercial products have been developed. These are technologies that have been evaluated by the customer and assessed for the potential market.

15. SUBJECT TERMS
technology transfer, technology commercialization, government-industry collaboration, nanomaterials

16. SECURITY CLASSIFICATION OF:			17. LIMITATION OF ABSTRACT:	18. NUMBER OF PAGES	19a. NAME OF RESPONSIBLE PERSON (Monitor)
a. REPORT	b. ABSTRACT	c. THIS PAGE			Ashley B. Sutherland
Unclassified	Unclassified	Unclassified	SAR	468	19b. TELEPHONE NUMBER *(Include Area Code)* (937) 255-3180

REPORT DOCUMENTATION PAGE Cont'd

6. AUTHOR(S)

Dr. Alicyn Rhoades (Bayer MaterialScience)
Robert Barsotti (Arkema)
Metin Sitti (NanoGriptech)
Minkyu Song (NanoLambda, Inc.)
Dr. B. Erik Ydstie (Industrial Learning Systems)
Mark A. Snyder, James F. Gilchrist and Prof Raymond Pearson (Lehigh University)
Bahram Nabet, Ph.D. and Ed Sullivan (NanoGrass Solar)
Dr. Rong Kou and Dr. Christian E. Shaffer (EC Power)
Dr. Jason Gu (SenSevere)

7. PERFORMING ORGANIZATION NAME(S) AND ADDRESS(ES)

NanoRDC, LLC
526 S. Main Street
Akron, OH 44311

Integran Technologies
2541 Appletree Drive
Pittsburgh, PA 15241

Strategic Polymer Sciences, Inc.
200 Innovation Blvd State
College, PA 16803

Bayer MaterialScience
100 Bayer Road
Pittsburgh, PA 15205

Arkema
900 1st Avenue
King of Prussia, PA 19026

NanoGriptech
5520 Raleigh Street
Pittsburgh, PA 15217

NanoLambda, Inc.
510 William Pitt Way
Pittsburgh, PA 15238

Industrial Learning Systems
4244 Yarmouth Drive
Allison Park, PA 15101

Lehigh University
111 Research Drive
Bethlehem, PA 18015

NanoGrass Solar
860 Skyline Drive
Erdenheim, PA 19038

NanoGripTech
5520 Raleigh Street
Pittsburgh, PA 15217

EC Power
200 Innovation Blvd.
State College, PA 16083

SenSevere
7070 Forward Avenue
Pittsburgh, PA 15217

TABLE OF CONTENTS

LIST OF TABLES

I. Executive Summary

This report describes the activities of a Collaborative Project Order (CPO) agreement between the Air Force Research Laboratory Materials and Manufacturing Directorate (AFRL/RX) and the Wright Brothers Institute (WBI), in which the Pennsylvania NanoMaterials Commercialization Center has served as a major subcontractor, principal performer of all project work and principal interface with AFRL/RX. CPO 9024 was initiated in October 2006 and has been serially renewed or extended on an annual basis since its inception through April of 2013.

This final technical report summarizes the three major components and deliverables that have been successfully achieved during the course of this program. These derive from the statement of work described in the Attachment of the Subrecipient Agreement# WBSC 9024 PN between Wright Brothers Institute (WBI) and the Pennsylvania NanoMaterials Commercialization Center (PA NanoCenter), as modified under Mod 8 (August 10, 2011). The Prime Agreement is FA8650-06-3-9024.

A. TECHNOLOGY AREA PLANNING

The Pennsylvania NanoMaterials Commercialization Center, working with AFRL, and its core industry partners defined a Technology Roadmap. The Roadmap is a 5-page document that has been periodically upgraded and fashioned to most effectively engage and communicate the technology needs to the PA NanoCenter stakeholders. It defines the specific focus of nanomaterials and its application to (A) Active Functional Materials; (B) Passive Functional Materials and (C) New and Enhanced Structural Materials.

The PA NanoCenter funded a number of technology development projects that as a direct result of the funding could advance the technology for both the commercial and/or non-commercial stakeholders. This development is evident as project teams have reported on the success to leverage the funding and secure next stage engineering dollars and joint development agreements with the commercial or noncommercial stakeholder. For the contract period November 2006 through January 2013 the PA NanoCenter opened 10 rounds of proposals submissions. A total of 338 technology commercialization proposals were submitted and 46 were funded by the PA NanoCenter.

In October 2009, with input from the AFRL representative on the PA NanoCenter's Technology Advisory Committee, an additional technology thrust was added to the Technology Roadmap which focused on nanomaterials for new energy applications. Energy is expanded to include (a) Generation; (b) Conversion; (c) Utilization and (d) Storage.
Traditionally the PA NanoCenter has used print and web media to showcase the Technology Roadmap. This is being expanded to include a more far reaching approach using social and virtual media.

The PA NanoCenter has matured its model and able to extract best practices to advance the goals of accelerating emerging technology commercialization. An example of this activity includes hosting a webinar series to support the goal of using the Technology Roadmap to communicate the nanomaterials industry and market needs of the stakeholders. The webinars provided a virtual forum for the technology provider and researchers to hear a *firsthand account* of the commercial and non-commercial partners in support of their contribution to the roadmap. The goal was to

engage in Q&A to evaluate and bring to light emerging technologies that match the market need. The PA NanoCenter managed the engagement and outcomes of potential partnerships.

B. PROJECT MARKETING AND SELECTION

The PA NanoCenter developed a visibility strategy to (a) market the technology commercialization program to the primary stakeholders and (b) showcase the technology developments of the portfolio organizations. The result was that the technology development being proposed and subsequently selected for funding (a) was aligned with a clear market need; (b) had a project team that includes the potential customer and (c) outlined a feasible path to prototype development.

The PA NanoCenter used a selection of media tools to showcase the program and the successes of the portfolio companies and their technology development projects. The marketing formats included (i) an official web site; (ii) quarterly electronic newsletters; (ii) press releases and announcements; and (iv) regular presentations at conferences and meetings. In addition, the Center facilitated targeted university-industry workshops to match market (and AFRL needs) with university technology capabilities. AFRL representatives attended the workshops.

The PA NanoCenter continued to expand the visibility of the program by launching a series of marketing initiatives. These included the complete re-design of new brochures, publishing business success stories on the website, e-newsletters and submitting these to print media publications like TEQ- publication by the Pittsburgh Technology Council with national distribution and specific academic communications. The new brochure highlights case studies, economic impact data and is intended to showcase the impact of nanotechnology as it applies to the advanced materials industry.

The PA NanoCenter also expanded its resources and engaged qualified consultants to broaden the network and develop new opportunities for the commercialization of emerging nanotechnologies. These activities focused on (i) funding and partner opportunities for the portfolio companies and their technologies as well as the (ii) strategic development opportunities for the PA NanoCenter.

The PA NanoCenter assembled a 21 person Technical Advisory Committee (TAC) that reviewed and vetted all proposals submitted for funding. The TAC includes participation from the PA NanoCenter's four university partners (Carnegie Mellon University, University of Pittsburgh, Penn State University and Lehigh University), partner and portfolio companies, federal labs (AFRL, INL, NETL), serial entrepreneurs and early stage investors. The individuals on the TAC had expertise and extensive experience in a combination of technical, new business and product development. After a 2-stage review process the TAC recommended prospective projects to the PA NanoCenter Board of Directors for the approval of funding.

The TAC was charged with the following activities under the joint supervision of the TAC chair and the PA NanoCenter's Executive Director:

- Form sub-committees of the TAC as needed and as requested by the PA NanoCenter's board for the purposes of making changes to the TAC charter, addition of new members or other ways to improve the review process for the PA NanoCenter. One such sub-committee was formed to

develop the Energy component of the Technology Roadmap (as described in the Technology Area Planning section above)

- The PA NanoCenter developed the proposal criteria and review process that has been continually improved and used for each proposal round.

- An IP Policy (and subrecipient agreement) for both university and company participation was implemented. The PA NanoCenter had increasing and innovative proposals submitted while meeting the federal IP requirements.

C. PROJECT MANAGEMENT

The PA NanoCenter managed the project management of all funded technology developments under this agreement. This project management was designed to increase the probability of successful outcomes for the PA NanoCenter's projects. The project management support included:

- A requirement that prior to project start, each project plan follow the PA NanoCenter's standardized Statement of Work (SOW).

- Defining measurable milestones and deliverables that match the scope and timeline for the project.

- Outline congruent technical and commercialization development tasks for the SOW.

- A documented change order process.

- Regular (every two -three months) project reviews with formal progress reports.

- Other advice and support provided by the PA NanoCenter to its project partners on technical, manufacturing or business issues as needed.

The PA Nano Center facilitated regular, annual Technology Showcase Days at the AFRL facilities in Dayton, Ohio. The one-day meetings were designed to showcase the technology developments of the portfolio companies to the AFRL program managers and contractors. This typically took the form of a series of presentations and one-on-one engagements. The PA NanoCenter was actively involved with follow-up communications to leverage any opportunity for continued development of the technology towards commercialization.

The PA NanoCenter has been able to fund a total of 46 projects, 59 technologies and 19 commercial products have been developed. These are technologies that have been evaluated by the customer and assessed for the potential market. The economic impact of the investments show that 92 jobs have been created and 129 jobs have been retained. The funded technologies have been able to leverage the invested funding to the amount of 54.2M. The leveraged funds represent private, federal and engineering dollars that the portfolio organizations are able to secure for next stage and joint developments.

Appendix – Final PA NanoCenter Subcontractor Project Reports

Pa NanoCenter has final reports for the following projects. They are included in the Appendix.

Table 1. PA NanoCenter Subcontractors

Plextronics, Inc.	2180 William Pitt Way, Pittsburgh, PA 15238	07-001	03/22/2007- 03/25/2008
NanoRDC, LLC	526 S. Main Street, Akron OH 44311	07-002	03/16/ 2007- 08/31/ 2007
Integran Technologies	2541 Appletree Drive, Pittsburgh, PA 15241	07-005	09/26/2007- 09/15/2008
Plextronics, Inc.	2180 William Pitt Way, Pittsburgh, PA 15238	07-009	05/28/2008- 05/26/2009
Strategic Polymer Sciences, Inc.	200 Innovation Blvd. State College PA 16803	09-012	11/18/2008- 11/16/2009
Bayer MaterialScience	100 Bayer Road Pittsburgh, PA 15205	09-013	12/18/2008- 12/18/2009
Arkema	900 1st avenue King of Prussia, PA 19026	09-021	05/07/2009- 06/30/2010
NanoGriptech	5520 Raleigh Street Pittsburgh, PA 15217	09-020	05/06/2009- 06/05/2010
Kurt Lesker	1925 Route 51, Clairton PA 15205	10-023	11/06/2009- 11/23/2010
NanoLambda, Inc.	510 William Pitt Way, Pittsburgh PA 15238	10-022	10/29/2009- 10/28/2010
Industrial Learning Systems	4244 Yarmouth Drive Allison Park PA 15101	10-035	06/03/2010- 06/02/2011
Liquid- X	4400 Fifth Avenue Pittsburgh, PA 15213	10-039	10/14/2010- 09/30/2011
SolarPA	8740 Lyon Valley Road, New Tripoli PA 18066	10-040	09/30/2010- 09/30/2011
Lehigh University	111 Research Drive Bethlehem PA 18015	11-046	06/07/2011- 12/15/2011
NanoGrass Solar	860 Skyline Drive Erdenheim PA 19038	11-047	06/02/2011- 12/15/2011
NanoGripTech	5520 Raleigh Street Pittsburgh, PA 15217	2011-0050	05/26/2011- 06/30/2012
EC Power	200 Innovation Blvd. State College PA 16083	2011-0057	01/26/2012- 01/08/2013
SenSevere	7070 Forward Avenue Pittsburgh PA 15217	2011-0058	12/20/2011- 10/31/2012

APPENDIX - FINAL PA NANOCENTER SUBCONTRACTOR PROJECT REPORTS
Appendix A – 07-001 (Plextronics, Inc)

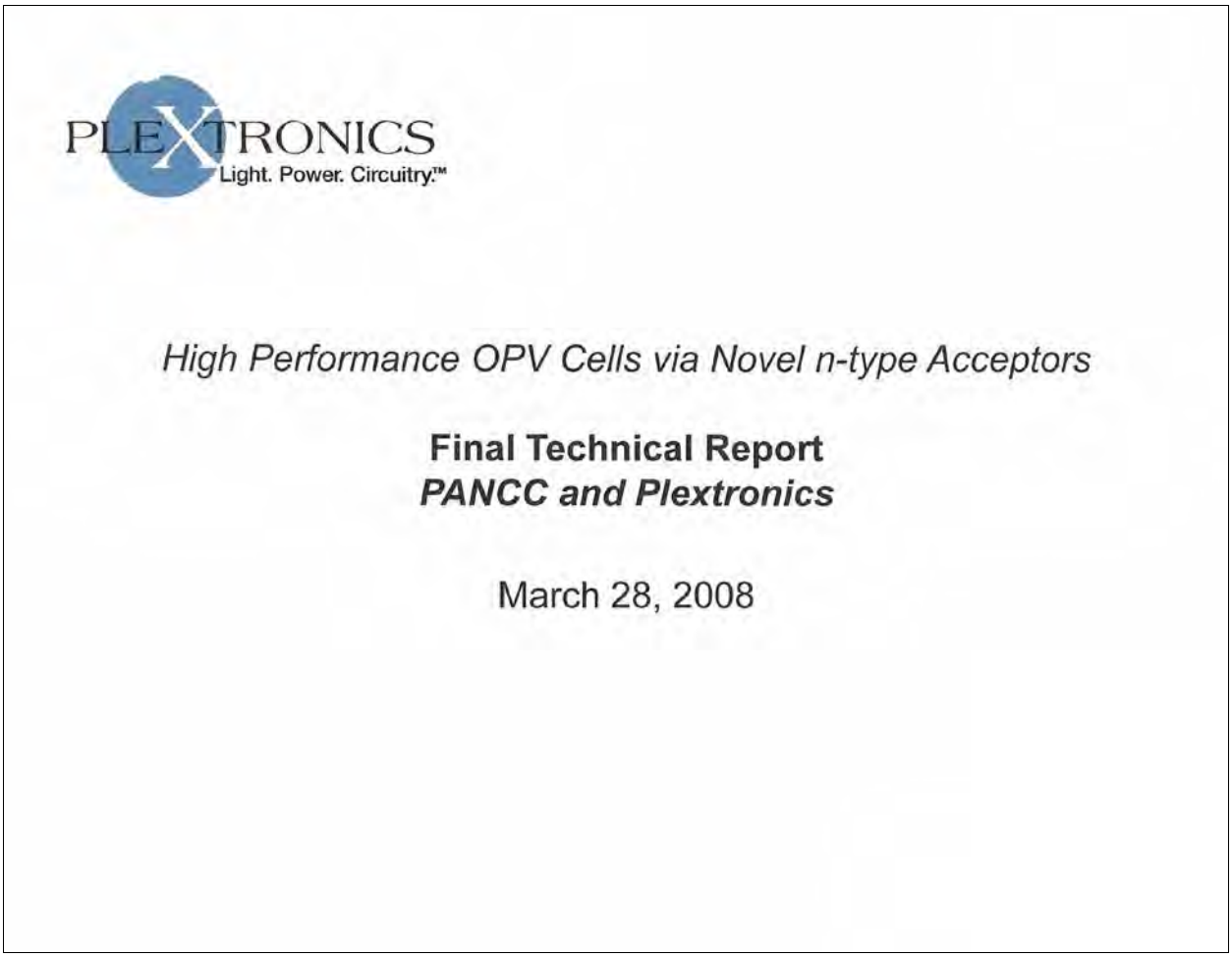

PLEXTRONICS
Light. Power. Circuitry.™

Novel n-type Project Stage Summary

Iteration	n-Type Purity	LUMO Level (eV)	Jsc	Voc	FF	Eff.	Notes
Baseline	< 98%	-4.11	9.4	0.82	0.65	~ 5%	4/30/2007 Completed
Cycle 1	99%	-4.11	9.5	0.85	0.68	5.3%	6/14/2007 Completed
Cycle 2	99.5%	-4.0	9.56	0.86	0.67	5.51	9/19/2007 Completed
Cycle 3	> 99.5%	< -4.0	10.5	> 0.90	> 0.7	5.8%	5.7% Achieved Completed
Fine Tune Promising Materials	>99.95	-4.0	10.3	0.85	0.7	6.14%	2/12/2008 Completed

PLEXTRONICS
Light. Power. Circuitry.™

Plextronics n-types for OPV
Final Stage Deliverables

- **Fine tune promising materials:**
  - C60-indene bisadduct – Jalapenos: S, T, W, U, U2, U3, U4, X, X2,X3
  - Jalapeno X – achieved best performance at 6.1% (World Record)
  - C60-indene trisadduct (Habanero) optimization
- **Screening new n-types:**
  - C60-PCBM-indene monoadduct (Chili-PCBM),
  - C60-PCBM-indene bisadduct (Chipotle),
  - C70-bis-PCBM (Barker)
  - C60-bis-PCBM (Tepin)
- Milestone: Fine tune promising n-types identified as likely candidates for OPV commercialization scale-up and module manufacture
- Deliverables: Final technical report and prototype OPV device utilizing new fullerene material (03/25/2008)

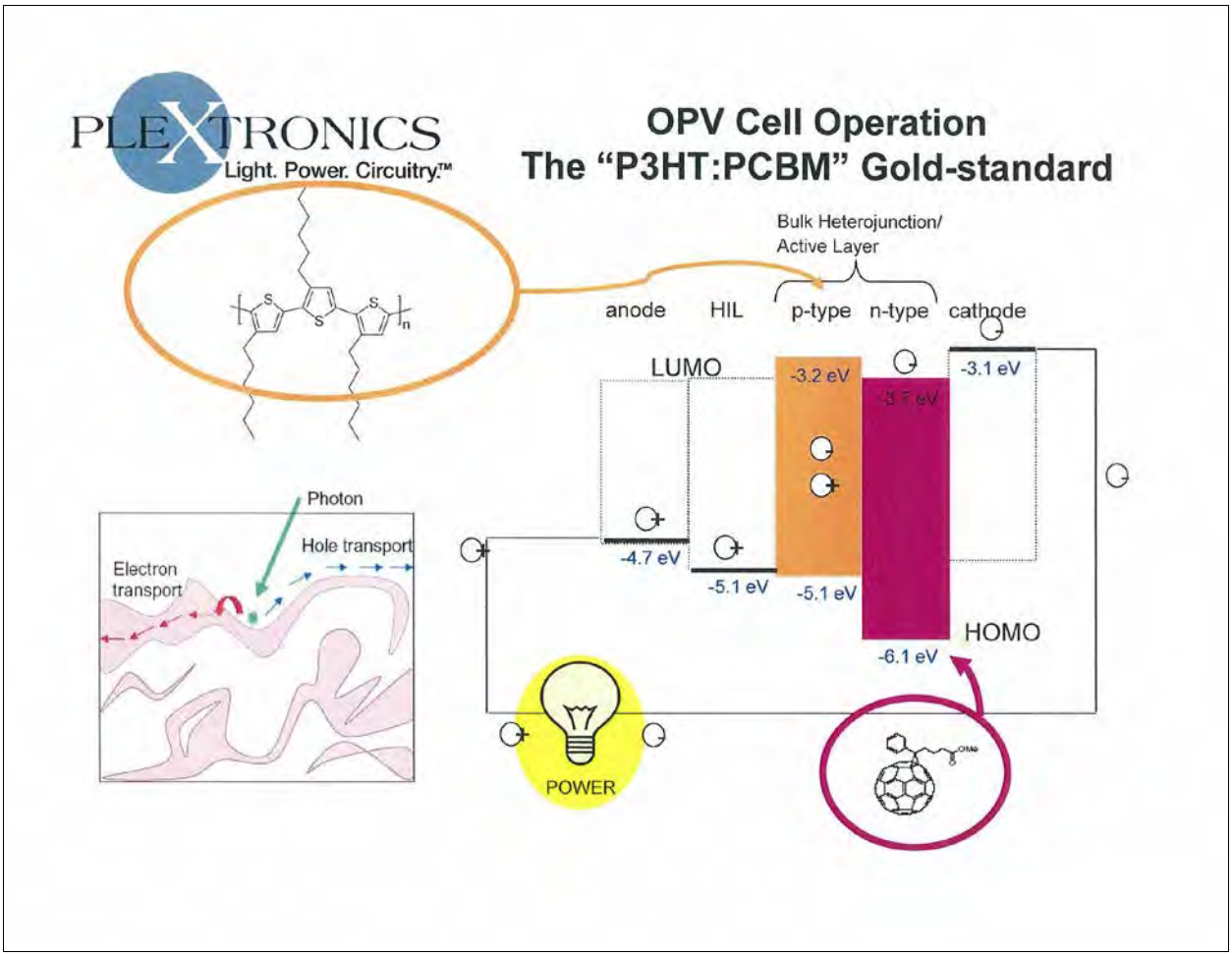

PLEXTRONICS
Light. Power. Circuitry.™

Material Properties and OPV Cell Operation

ASTM 1.5 Reference Solar Spectrum

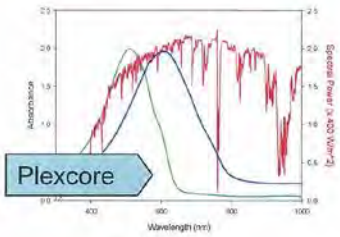

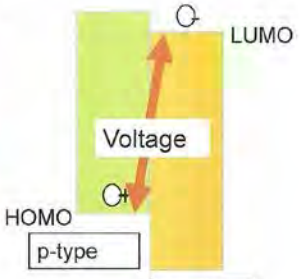

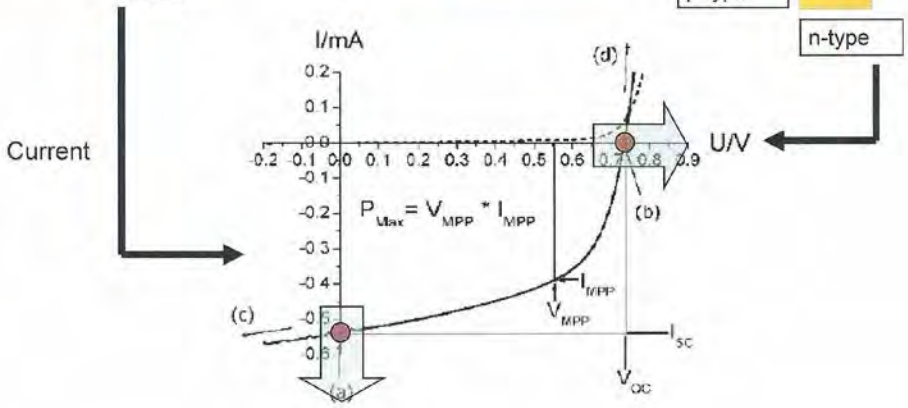

PLEXTRONICS
Light. Power. Circuitry.™

New internal record – 6.1 %
Jalapeno:P3HT Active Layer

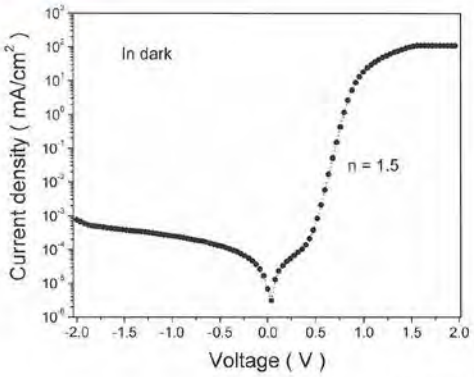

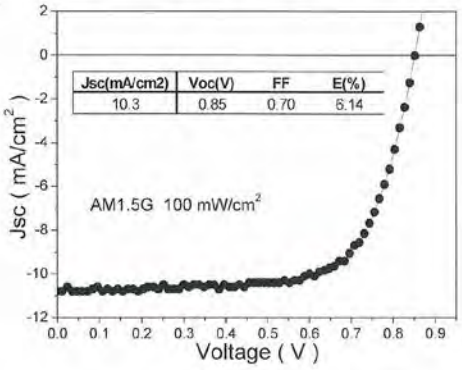

J-V curves in dark (a) and under 1 sun illumination (b)

- Further elimination of unwanted isomers and impurities significantly improve the performance of Jalapeno and results in new record 6.1%.
- Excellent fill factor (FF) = 70%.
- High photocurrent Jsc = 10.3 mA/cm^2 – First reproducible > 10 mA/cm^2 n-type
- This device currently in queue at NREL

PLEXTRONICS NREL Certification of Plexcore PV-F3

Light. Power. Circuitry.™

Jul 17, 2007 11:50 Device Area: 0.096 cm^2

Spectrum: AM1.5-G (IEC 60904) Irradiance: 1000.0 W/m^2

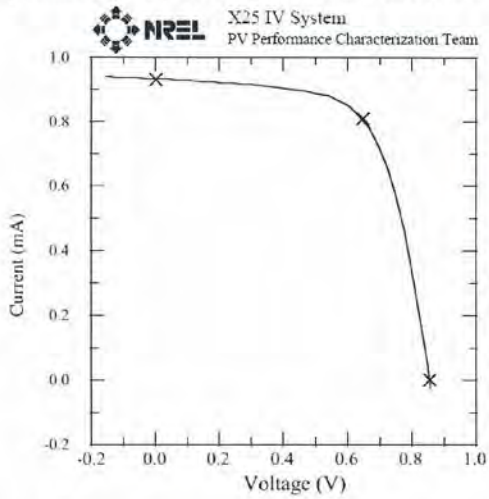

- World-record OPV efficiency
- NREL certified at 5.4%
- Single Photoactive Layer

I_{max} = 0.80664 mA	V_{oc} = 0.8563 V
V_{max} = 0.6452 V	I_{sc} = 0.93132 mA
P_{max} = 0.52048 mW	J_{sc} = 9.7013 mA/cm^2
Efficiency = 5.42 %	Fill Factor = 65.26 %

NREL X25 IV System
PV Performance Characterization Team

PLEXTRONICS
Light. Power. Circuitry.™

Computational Analysis of n-Type LUMO Levels

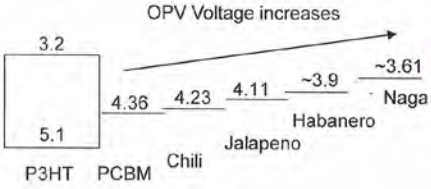

- Shallow LUMO improves Voltage
- Control of Voltage with no losses in current and FF can lead to very high efficiencies

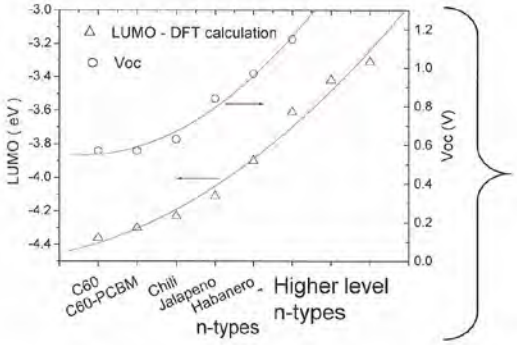

- n-type LUMO correlates with OPV device voltage
- Strategy is to ensure control of
  - morphology
  - energy levels
- Novel n-types can enable > 7% OPV devices

PLEXTRONICS Light. Power. Circuitry.™

Materials and Device Development Update

Materials Development

- During the course of this program Plextronics has evaluated > 40 n-type materials in active layer formulations.
- Plextronics module scale-up is currently focused on Jalapeno:P3HT
- Extensive iterative optimization around key parameters such as purity, formulation and device fabrication complete
- Plextronics has eliminatated unwanted isomers and impurities and significantly improved the performance of n-type materials leading to novel design rules:
  - Voltage of OPV cells scales with LUMO level of n-type (p-type fixed)
  - PCBM and Pepper substitutions give different voltage response allowing tuning of Voc and cell optimization
- 7% and beyond is expected from this approach

Lab-Cell OPV Device Development

- Plextronics fabricated lab-cell devices on 2" x 2" patterned ITO-coated glass substrates (~ 20 ohm/square).
- Plextronics have continued their development efforts and have since achieved internally tested lab-cell efficiencies of 6.1%.
- Plextronics continues to optimize the most promising material set. The devices have been sent to NREL testing facility for certification.

PLEXTRONICS
Light. Power. Circuitry.™

Novel n-type Summary

N-type	Jsc(mA/cm^2)	Voc (V)	FF	Efficiency
Barker	3.9	0.68	0.52	1.38
Tepin	7.6	0.71	0.67	3.61
Chili-PCBM	9.4	0.8	0.7	5.26
Chipotle	4.4	0.95	0.48	2.04
Habanero	5.6	1.0	0.47	2.61

Barker – bis-C70-PCBM
Tepin – bis-C60-PCBM
Chili-PCBM – mono-indene-C60-PCBM
Chipotle – bis-indene-C60-PCBM
Habanero – tris-indene-C60

- Tepin and Chili-PCBM are excellent n-types, far superior to C60-PCBM
- However, Jalapeno remains the champion n-type with P3HT

PLEXTRONICS
Light. Power. Circuitry.™

Tepin:P3HT

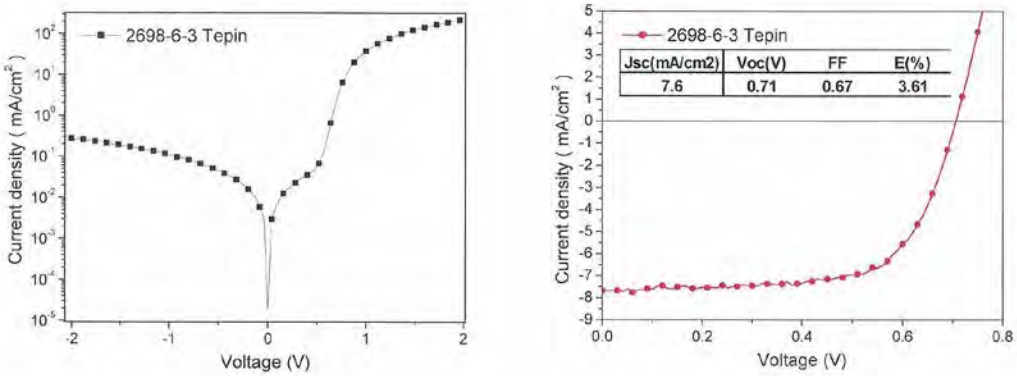

J-V curves in dark (a) and under 1 sun illumination (b)

- Good voltage of 0.71 V which is higher than in PCBM (0.6V)
- Good short circuit current and fill factor of 0.67 which can be improved after further optimization of morphology and thickness.

PLEXTRONICS
Light. Power. Circuitry.™

Barker:P3HT

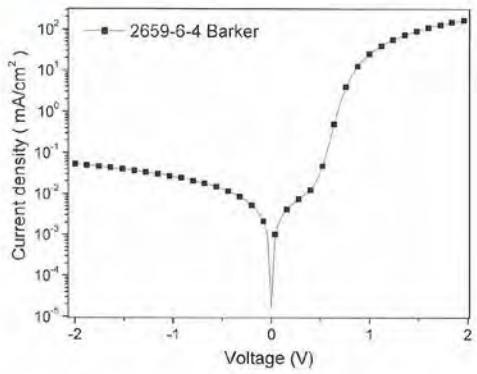

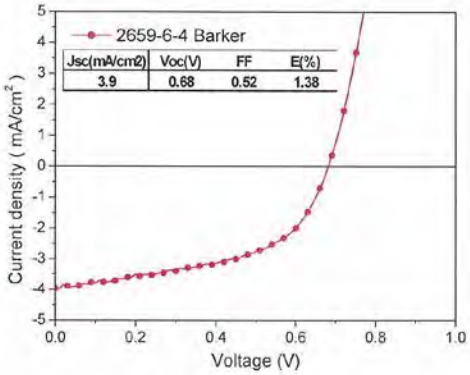

J-V curves in dark (a) and under 1 sun illumination (b)

- Open circuit voltage of 0.68 V is lower than in Tepin (0.71V) but higher than in PCBM (0.6V)
- Short circuit current and fill factor are low. Probably, could be improved after further optimization of morphology and thickness.

PLEXTRONICS
Light. Power. Circuitry.™

Chili-PCBM:P3HT
A *new efficient n-type*

Jsc(mA/cm2)	Voc(V)	FF	E(%)
9.4	0.80	0.70	5.30

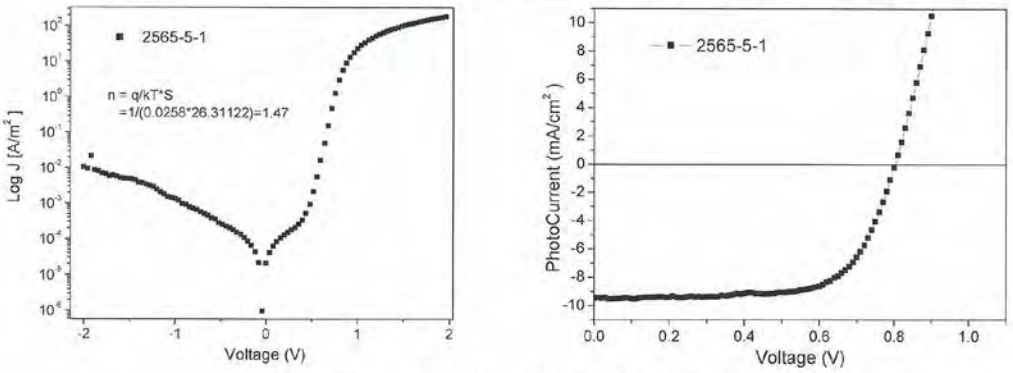

J-V curves in dark (a) and under 1 sun illumination (b)

- Application of our knowledge for developing of new n-types and advanced purification processing results in development of new efficient n-type – Chili-PCBM.
- High Voc = 0.8 V
- Excellent fill factor (FF) = 70%.
- High photocurrent Jsc = 10.3 mA/cm2.

PLEXTRONICS
Light. Power. Circuitry.™

Chipotle:P3HT

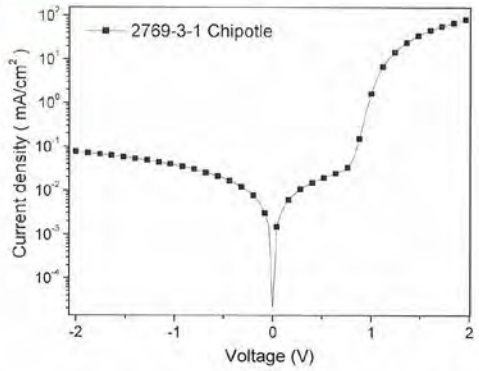

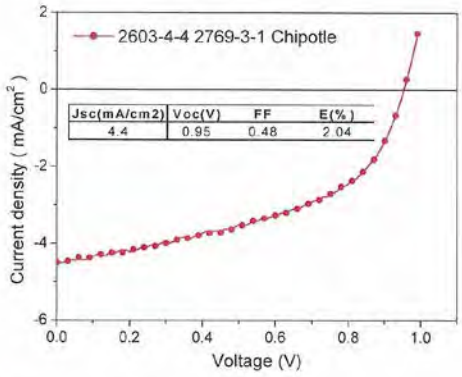

J-V curves in dark (a) and under 1 sun illumination (b)

- Very high dark current at backward bias -> leak currents due to non-optimal morphology and vertical phase separation
- Voltage of 0.95 V is high as expected.
- Fill factor is low -> bad morphology.
- Morphology needs to be improved.

PLEXTRONICS Light. Power. Circuitry.™

Data Summary of Novel n-Types

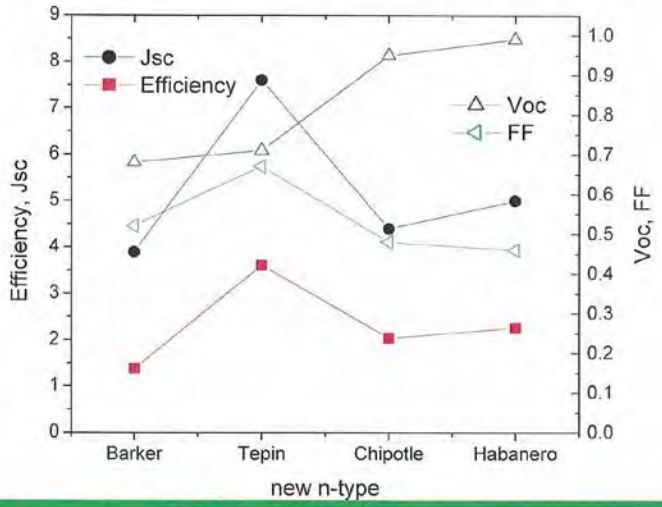

- New n-types show predicted Voc increase.
- However, short circuit current (Jsc) and fill factor (FF) are low.
- The most promising pepper are Habanero and Chipotle with high Voc.

PLEXTRONICS Light. Power. Circuitry.™

n-Type LUMO Scales with Voc

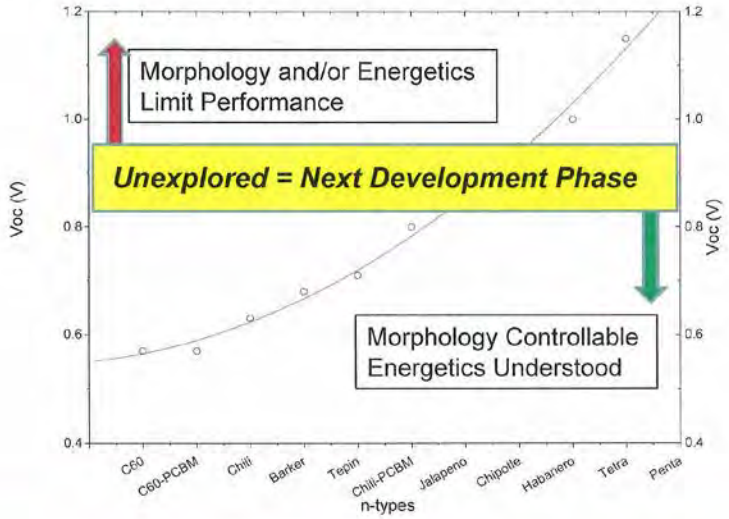

- The most promising pepper are Habanero and Chipotle with high Voc.
- Tetra and Penta have demonstrated poor performance in OPV devices due to abundant coverage of C60 cage with functional groups.

PLEXTRONICS
Light. Power. Circuitry.™

Fine Tune Promising Materials

Jalapeno
Habanero

PLEXTRONICS
Light. Power. Circuitry.™

Improving Jalapeno to > 6%

Device #	p-type	n-type*	Jsc	Voc(V)	FF	E(%)	Pave	Best
2603-1	P3HT(TO-01-100R)	PCBM 99%	9.78	0.61	0.66	3.87	0.35	3.92
2603-2	P3HT(TO-01-100R)	Jalapeno U3	8.68	0.85	0.65	4.70	0.43	4.79
2603-3	P3HT(TO-01-100R)	Jalapeno U4	7.48	0.82	0.54	3.29	0.30	3.40
2603-4	P3HT(TO-01-100R)	Jalapeno U2	9.65	0.83	0.70	5.58	0.51	5.63
2603-5	P3HT(TO-01-100R)	Jalapeno U3	9.07	0.85	0.68	5.15	0.47	5.18
2603-6	P3HT(TO-01-100R)	Jalapeno U4	7.55	0.82	0.58	3.56	0.32	3.67
2603-7	P3HT(TO-01-100R)	Jalapeno U2	9.54	0.84	0.70	5.48	0.50	5.59

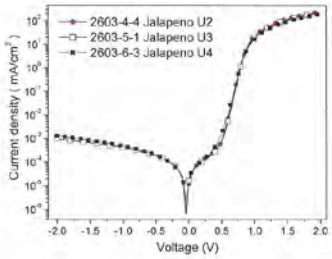

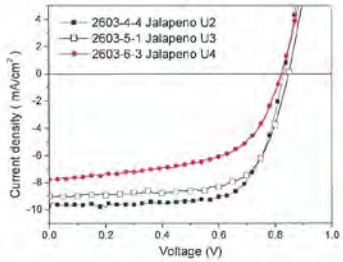

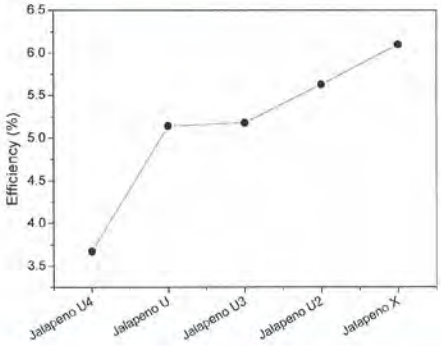

The data and plots demonstrate recent advancement in purification process of our best n-types – Jalapeno. Jalapeno X contains undetectable traces of impurities (>0.01%).

PLEXTRONICS
Light. Power. Circuitry.™

Optimization of Habanero

Device #	p-type	n-type*	Jsc	Voc(V)	FF	E(%)	Pave	Best
2476-2	P3HT(TO-01-100R)	Habanero 2+3	2.45	0.96	0.36	0.85	0.08	0.86
2476-5	P3HT(TO-01-100R)	Habanero 4+5	2.81	0.99	0.36	1.00	0.09	1.02
2476-7	P3HT(TO-01-100R)	Habanero Old	5.52	1.00	0.47	2.55	0.23	2.61

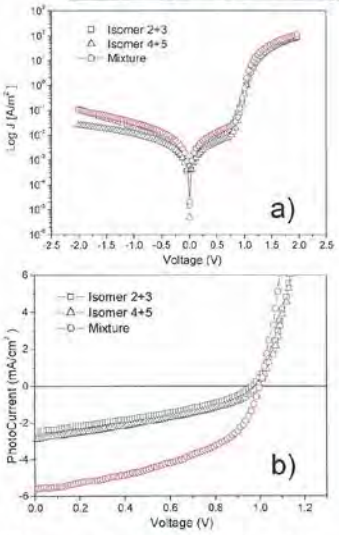

J-V curves in dark (a) and under 1 sun illumination

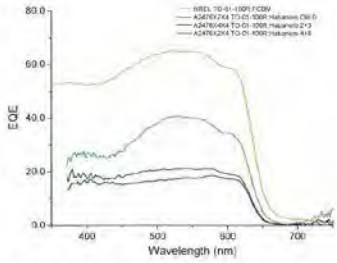

External quantum efficiency of OPV devices with 3 batches of Habanero

- OPV devices with various blends of P3HT and Habaneros show similar dark J-V curves.
- J-V curves under 1 Sun illumination differ significantly with mixtures of Habanero isomers demonstrating best performance.

PLEXTRONICS Light. Power. Circuitry.™

Habanero – Annealing Response

	Jsc(mA/cm2)	Voc(V)	FF	E(%)
No annealing	5.1	0.96	0.46	2.28
175C/30min	5.62	1.0	0.47	2.61

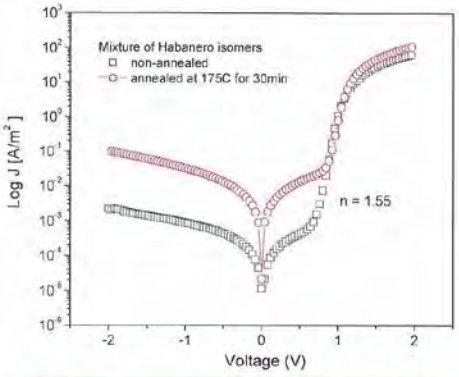

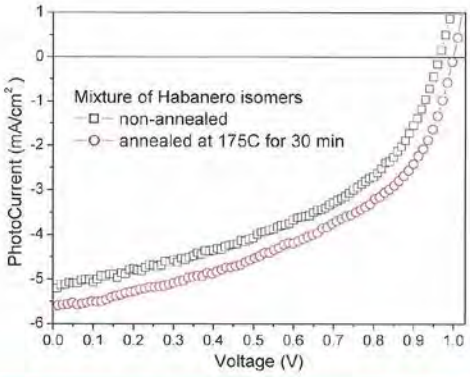

- OPV devices with mixtures of Habanero isomers shows similar performance without annealing and with annealing at 175C for 30 min.
- Annealing at 175C for 30 min is not optimal.
- Need DOE around p:n ratio and annealing conditions.

PLEXTRONICS
Light. Power. Circuitry.™

Raman mapping of P3HT:Habanero and P3HT:Jalapeno blends

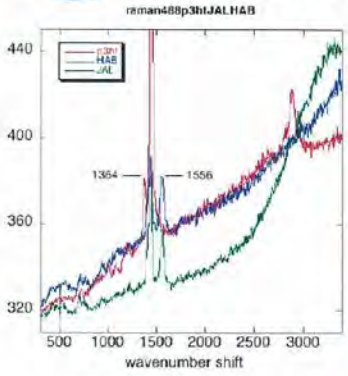

individual Raman spectra
1364 peak for P3HT (C_β-$C_{\beta'}$)
1556 peak for JAL and HAB

Composition Profile vs. lateral dimensions
Morphology vs. Area

blend 1364cm-1 map

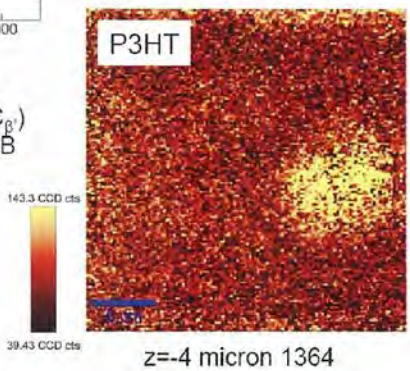

z=-4 micron 1364

blend 1556cm-1 map

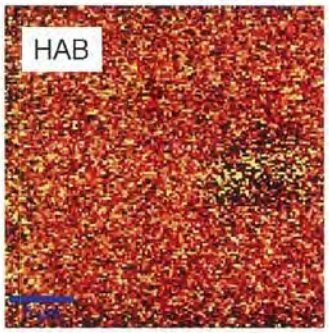

z=-4 micron 1556

PLEXTRONICS
Light. Power. Circuitry.™

Raman microscopy: Smaller aggregation in P3HT:Habanero vs. P3HT:Jalapeno

Combined Raman Mapping
P3HT:Habanero

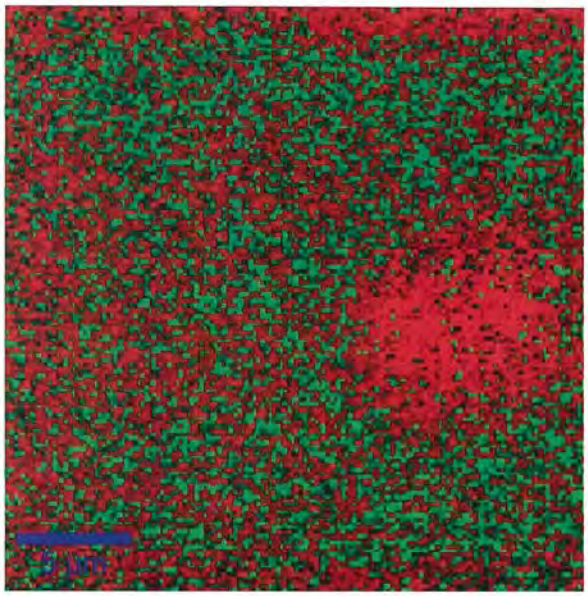

Combined Raman Mapping
P3HT:Jalapeno

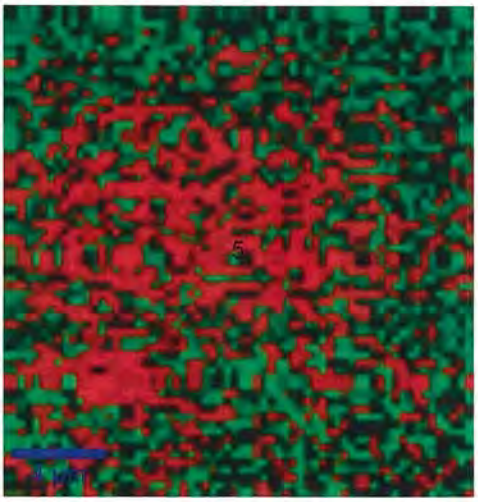

P3HT = Red
Peppers = Green

PLEXTRONICS
Light. Power. Circuitry.™

PL quantum efficiency and fast dynamics

A)

Dynamics Comparison
Pumped 3.2 eV; Probed 0.954 eV

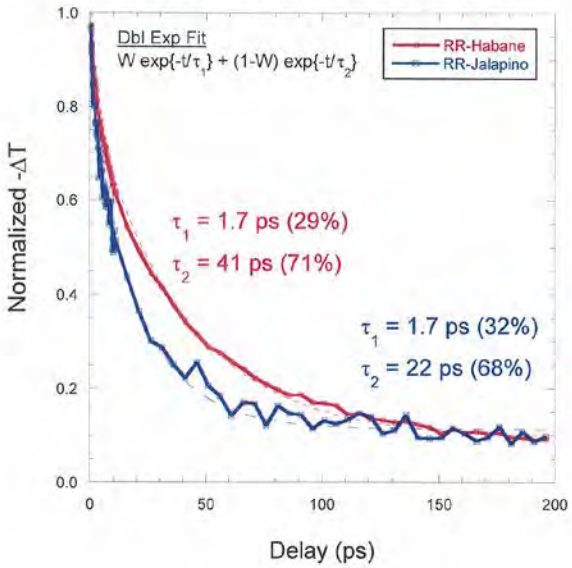

B)

RR P3HT:Habanero (1.2:1) QE = 1.70%
RR P3HT:Habanero (1.2:1) annealed QE = 1.22%

RR P3HT:Jalapeno (1.2:1) QE = 1.21%
RR P3HT:Jalapeno (1.2:1) annealed QE = 0.67%

A) Combining this data with J-V measurement, we can conclude that either morphology is not optimal in P3HT:Habanero blend or photoinduced charge transfer is not efficient.

B) Photoluminescence quantum efficiency of blends of P3HT and Habanero before and after annealing is higher than in blend of P3HT with Jalapeno indicating different scale of phase separation in two blends.

PLEXTRONICS
Light. Power. Circuitry.™

Comparison of FTIR PA absorption P3HT:Jalapeno vs. P3HT:Habanero

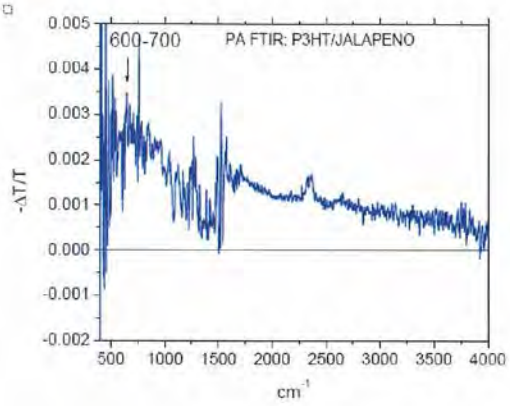

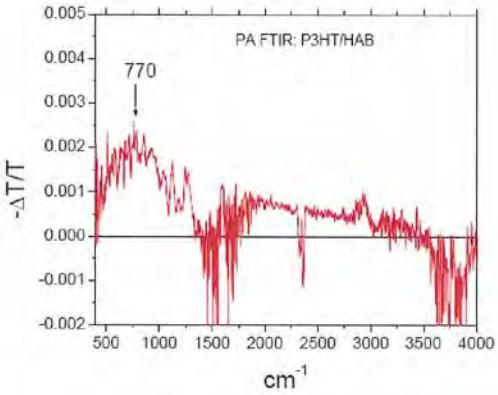

Peak shift to higher wavenumber is indication of less interchain interaction and probably more disorder in P3HT:Habanero blend. Polarons in P3HT:Jalapeno blend is less localized and have more freedom to move.

PLEXTRONICS Light. Power. Circuitry.™

Internally Tested Champion Module

LA OPV v.2/*P3HT:Jalapeno Active Layer*

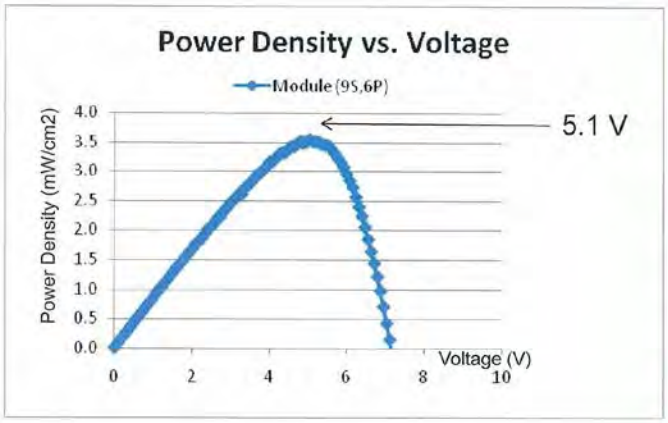

1.6% vs. Full Area
3.5% vs. Active Area

V_{pmax} = 5.1 V
I_{pmax} = 75 mA

P_{pmax} = 385 mW

Minimum Voltage for Li+ Ion charger is ~ 4.2V

THIS IS PRE-BURN IN and ACTUAL LIFETIME EVALUATION IN PROGRESS

PLEXTRONICS Light. Power. Circuitry.™

NREL Certified LA OPV v.2 Module

P3HT:PCBM as active layer

Device ID: 2752
Mar 18, 2008 10:49
Spectrum: AM1.5-G (IEC 60904)

Device Temperature: 25.0 ± 1.0 °C
Device Area: 232.800 cm^2
Irradiance: 1000.0 W/m^2

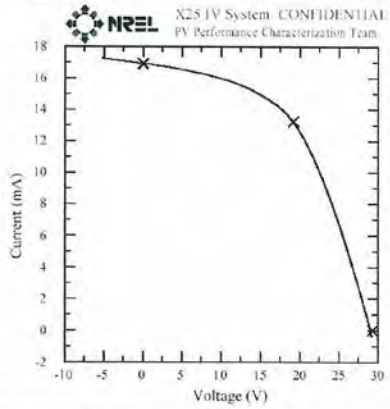

V_{oc} = 29.3466 V	I_{max} = 13.210 mA
I_{sc} = 16.906 mA	V_{max} = 19.1466 V
J_{sc} = 0.072618 mA/cm^2	P_{max} = 0.2529 W
Fill Factor = 50.98 %	Efficiency = 1.09 %

- Tested in 54s configuration (full series)
- Active Area Efficiency = 2.3%
- Measured at Plex to 1.2%
- Plex/NREL measurement differences:
  - 232.8 cm^2 vs. 225 cm^2
  - Slight change in FF
- Shelf-life stable after 192 h
- Next submission in April 08

27

PLEXTRONICS
Light. Power. Circuitry.™

PANCC Project Summary 2007-2008

- Set of new n-types with various LUMOs have been developed.
- n-type with high LUMOs are very sensitive to impurities and isomer distribution
- Purification is especially critical to observing intrinsic performance of n-type with high LUMOs
- **Further elimination of unwanted isomers and impurities significantly improve the performance of Jalapeno and results in new record 6.1%.**
- The most promising new n-types are identified – Habanero and Chipotle.
- Optimization of morphology of Habanero and Chipotle is in progress.
- Transient spectroscopy will be applied to high indenes for testing limit of LUMO of n-types.
- Jalapeno has been chosen as the best candidate for scale-up to commercial module production (in progress)

Appendix B – 07-002 (NanoRDC, LLC)

NanoRDC
Nanoparticles for Polymer Composites

METAL COMPLEXES FOR ENHANCED DISPERSION OF NANOMATERIALS

OCTOBER 19, 2007

FINAL PROJECT REPORT: NANOMATERIALS COMMERCIALIZATION CENTER, CONTRACT NUMBER NANO-07-002

BY DR. RICK SIMONS

NANORDC LLC
526 SOUTH MAIN STREET 811
AKRON OH 44311

NanoRDC
Nanoparticles for Polymer Composites

METAL COMPLEXES FOR ENHANCED DISPERSION OF NANOMATERIALS

By Rick Simons

NanoRDC LLC
526 South Main Street, #811
Akron OH 44311

INTRODUCTION

Applications for carbon nanotubes (CNT) are enormous due to their mechanical, thermal and electronic properties. The electrical properties of CNT make them ideal conductive fillers in nanocomposites. Incorporation and dispersion of CNT into polymers has proven difficult due to the inherent bundling of the CNT due to van der waal forces and incompatibility at the polymer/CNT interface.(1) Mechanical methods of dispersing nanotubes has demonstrated the dispersion of the CNT as small bundles dispersed throughout the polymer matrix.(2) Other attempts to aid the dispersion of CNT include functionalizing the nanotubes with a covalently bonded group thus separating the bundles into individual nanotubes.(3,4,5,6,7,8,9) This method is primarily useful for dispersing nanotubes in organic solvents. Mixing functionalized nanotubes in pristine polymer matrix requires extensive functionalization and the inherent properties of the nanotubes can be altered tremendously. Ideally, non-covalent modification of the nanotubes is preferable so that the nanotube properties are not disturbed. Non-covalently, the dispersion of nanotubes in aqueous media is achieved by using ionic surfactants such as sodium dodecylsulfate. (10) However, surfactants have limitations with organic solvents and this limits their usefulness in polymeric systems. Another non-covalent method of dispersing nanotubes in polymers is to pre-treat the nanotubes with oligomeric and polymeric highly conjugated and highly aromatic systems. These systems are employed to interact with the nanotubes through π-π interaction and to effectively wrap themselves around and separate the nanotubes. This method has found promise with polyimide/SWNT nanocomposite applications.(11,12,13). NanoRDC has been developing a proprietary treatment for carbon nanomaterials. Our approach is a non-covalent interaction between nanomaterials, preferably nanotubes, and metal alkyl sulfates. Our initial investigations have demonstrated that silver-4,4-bipyridine-dodecyl sulfate is a very effective reagent for increasing the dispersion of CNT into aqueous and organic solvents, plastics and composite matrices. The technology has many benefits and advantages. First, the reagent is non-selective and will operate effectively on any nano-graphitic type materials such as carbon fiber (CF), carbon nanotubes (CNT) and carbon black (CB). Second, the amount of metal complex adsorbed onto the surface is controlled by the steric requirements of the alkyl metal sulfates, and on average, the degree of treatment is approximately 10-35 wt% depending on the graphitic surface type (i.e. CF, CNT or CB) and the sterics of the alkyl sulfate anion. Third, although silver was the initial metal investigated, our results have demonstrated that copper can be used effectively as a cost efficient

replacement for silver. Fourth, maybe out of the scope of this project, but we have discovered that our treated nanotubes can be used to produce aqueous dispersions of CNT that are far superior to any technology on the market. We are currently pursuing the use of aqueous CNT dispersions to produce conductive latex gloves for the electronic industries.

OBJECTIVE:

The main objective of this project was to demonstrate the feasibility of producing treated carbon nanotubes (t-CNT) for use as electrical conducting fillers with improved dispersibility into themoplastics. The t-CNT will be useful to plastic compounders because they will enable compounders to use existing melt compounding equipment to produce conductive plastics. In these regards, the treated carbon nanotubes will have tremendous commercial value. NanoRDC plans to work closely with BMS to produce a treated Baytube with increased dispersibility. The treated Baytubes will be marketed to plastic compounders as electrically conductive filler.

NanoRDC worked together with BMS to optimize both the treatment technology and the compounding parameters. The present project was sub-divided into 5 specific tasks (See Task descriptions below). Specifically, Task 1 was to be completed by NanoRDC at the NanoRDC facility in Akron, OH. Task 2 was to be completed by BMS at the facility in Germany.

PROJECT PLAN

TASK 1 – SYNTHESIS AND CHARACTERIZATION OF TREATED CARBON NANOTUBES (T-CNT)

- Define operating parameters and throughput rates for effective debundling and dispersion quality

Milestone: Optimum parameters and rates established
Estimated time for completion: 2 months (March 1 – May 1, 2007)
Deliverable: Brief Report on preparation and dispersion of t-CNT

TASK 2 – MELT COMPOUNDING AND EVALUATION

- Prepare t-CNT composites with polymers of interest (e.g. polyurethane, polycarbonate, nylon)
- Optimize compounding process for each system
- Evaluate and optimize parameters that effect injection molding
- Optimize electrical conductivity for systems of interest

Milestone: Reproducible procedures for preparation of optimized t-CNT polymer composites are established
Estimated time for completion: 5 months (May 1 – October 1, 2007)
Deliverable: Report on melt compounding and evaluation of t-CNT

NanoRDC
Nanoparticles for Polymer Composites

TASK 3 – COORDINATE SCALE-UP WITH BAYER MATERIALSCIENCE (BMS)
- Develop engineering specifications
- Develop manufacturing processes
- Transfer materials and protocols to BMS
- Provide problem-solving support for the scale-up process

Milestone: Technology successfully scaled by BMS
Estimated time for completion: (May 1 – October 1, 2007)
Deliverable: Brief report on the scale-up to production
9/19/2007 Page 2 of 2

TASK 4 – DEVELOP AND VALIDATE WITH BAYER MATERIALSCIENCE A STRATEGIC MARKETING PLAN AND A STRATEGIC BUSINESS PLAN TO BRING TCNT POLYMER COMPOSITES TO THE MARKET
Target date: (July 1 – October 1, 2007)
Deliverable: Copies of marketing and business plans

TASK 5 – FIRST DRAFT OF JOINT IP AND LICENSING AGREEMENT WITH BAYER MATERIALSCIENCE
Target date: (August 1 – October 1, 2007)
Deliverable: Copy of joint IP and licensing agreements

TASK 1

Originally, Task 1 was planned to provide BMS with 1 KG of CNT treated with a silver complex. The 1 KG was supplied to BMS for evaluation, and subsequently, BMS determined that an additional 3 KG of treated CNT would be needed for complete evaluation. As part of Task 1, NanoRDC completed the following.

1. NanoRDC had originally developed the treatment of CNT using a bench-top procedure. We treated the original 1 KG of CNT at a scale of 10 g per batch according to the following procedure. Sodium dodecyl sulfate (1.5 g) was added to an aqueous solution (5 mL) of silver nitrate (0.85 g) and the resulting mixture stirred for 10 minutes in 20 mL chloroform. The resulting solution was added to a chloroform (500 mL) suspension of CNT (10 g) and sonicated for 5 minutes. A chloroform solution (200 mL) of 4,4-bipyridine (0.75 g) was added and the suspension was sonicated for an additional 5 minutes. The resulting suspension was collected in a 5- gallon bucket. Approximately 100 batches were treated and collected according to the aforementioned procedure. The treated CNT were eventually filtered under reduced pressure and the treated CNT were washed with chloroform. The treated CNT were dried at 80 °C for 3 hours to give approximately 1200 g

of treated CNT. The percentage of treatment was determined to be ca. 20 wt % by thermal gravimetric analysis (TGA).

2. Pilot Scale Dispersion Operation: A pilot scale dispersion operation was designed and assembled to accommodate larger scale treatment and/or dispersion of CNT. The operation is illustrated in the following schematic and consists of a 110 liter tank that contains the CNT, the dispersing liquid and the treatment chemicals. From this tank, the dispersed CNT are pumped through a flow cell that houses a sonicating horn. Within the flow cell, the bundles of CNT are de-agglomerated so that the treatment can be applied to the surface of individual CNT rather than bundles of CNT. The flow cell and sonicating horn operate at a preset 20 KHz and the sonicating power (watts) is controlled by a generator. The phenomenon responsible for de-agglomeration of the CNT bundles is cavitations at the CNT surface. There is a direct relationship between the amount of cavitations and the pressure of the sonicating medium within the flow cell and surrounding the sonicating horn. For instance, the degree of cavitations and amount of de-agglomeration is increased with increasing pressure. Other parameters such as flow rate through the flow cell and viscosity are also important and play a role in the efficiency of the dispersing operation. The maximum efficiency as a function of pressure can be approximated by monitoring the power consumed/converted from the system generator (watts). Our work showed that a pressure of 25-30 psi is sufficient to achieve excellent de-agglomeration. In addition, the pressure must be non-pulsating. Our initial choice of pumps was a peristaltic pump because it contained no valves that could be clogged with nanoparticles, however, the natural operation of the pump is pulsating and this proved unacceptable. We found that the correct parameters such as flow rate and pressure and the need to pump slurry could be met by a progressive cavity pump with an inverter duty motor and controller.
3. Efforts to reduce cost of treatment.
    a. It was realized early that the cost of chemicals needed for the treatment, including the dispersing medium were quite expensive. For instance, laboratory scale purchase of silver nitrate cost approximately 250 USD per 100 grams (100 g will treat 1 KG CNT). NanoRDC investigated the replacement of the silver nitrate with copper nitrate because copper nitrate could be purchased at the same scale for 25 USD per 100 g. Initial investigations into the replacement suggested that the copper was a viable alternative to the more expensive silver; however, BMS expressed their interest in not replacing the silver with copper in the treatment formulation.
    b. The dispersing medium (chloroform) was also a cost concern. The price for chloroform is ca. 250 USD per 25 L. In order to reduce the amount of chloroform consumption and reduce the price, we set up a large scale distillation operation. All used chloroform was distilled for re-use.

4. Treatment of 3 KG CNT: Due to engineering difficulties and time restraints, we completed the treatment of 3 KG CNT using our initial bench-top operation according to Task 1 #1.

NanoRDC
Nanoparticles for Polymer Composites

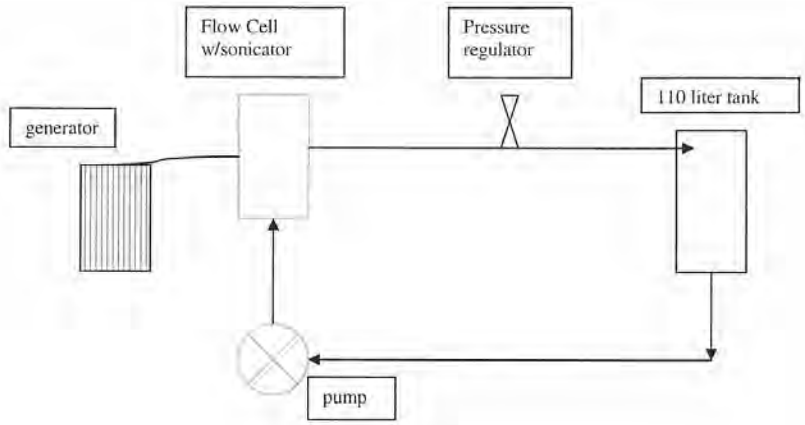

TASK 2

FORMATION OF CNT/POLYMER COMPOSITES.

According to Task 2, NanoRDC initially sent BMS 1 KG of treated CNT for evaluation. BMS responded back to NanoRDC that they had some engineering difficulties and the results were not scientifically relevant. BMS expressed to NanoRDC that they would need an additional 3 KG of material to complete Task 2. According to Task 1, NanoRDC sent BMS an additional 3 KG of silver treated CNT for evaluation.

BMS performed melt compounding trials. The choice of thermoplastic was polycarbonate and the trials were run with loadings of 2, 3, 5 and 7.5 wt % filler. Polycarbonate was chosen as the test thermoplastic because BMS had previously performed trials with polycarbonate and CNT filler and they have a potential market for polycarbonate/CNT composite materials. While NanoRDC ran its trials in nylon and polyurethane, the decision to run the trials in polycarbonate makes a lot of sense. For example, there was a need to test the treated verses untreated CNT dispersion into a thermoplastic that had been extensively examined. NanoRDC found in their previous studies that when using less shear and lower mixing times, there is a great enhancement in dispersion of treated CNT when compared to untreated CNT. However, as the mixing time and the degree of

shear are increased, the gap in performance between the treated and untreated CNT filled composites narrows. For instance, NanoRDC found that there is a large increase in performance resulting from treated CNT and a short mix time on a banbury type mixer when compared to a similar test using untreated CNT. The gap in performance is narrowed considerably when the mixing is done on a twin screw extruder because of the increase in shear provided by the twin screw configuration.

The filler was either treated CNT from NanoRDC or untreated CNT. The melt compounding was performed using a twin screw extruder and the press plaques were prepared using compression molding techniques. The results are summarized in the Table below. The following Table shows that the surface resistivity of the resulting composite materials is lower/better when using the untreated CNT. For example, at 2 wt % the surface resistivity of the composites with untreated CNT measured two orders of magnitude lower than the composites with the same level of treated CNT. Also, as the loading of treated CNT is increased from 2 wt % to 7.5 wt %, the surface resistivity measurements show an increase which is the opposite of what would be expected. In comparison, the untreated CNT gave the expected result. For example, with increasing CNT loading, the surface resistivity decreases gradually to a final value of 1.0E+01 ohms/sq.

Data Summary for Polycarbonate/CNT Composites Data Summary

Wt % CNT	Surface resistivity (ohms/sq)	Surface resistivity (ohms/sq)
	Baytubes C 150 P	Ag-functionalized Baytubes
2	1.24E+02	1.10E+04
3	4.30E+01	3.3E+04
5	2.70E+01	1.9E+04
7.5	1.00E+01	1.0E+05

TASK 3

Task 3 was designed to coordinate the scale-up of the treatment operation and transfer the protocols to BMS. During the course of the project, issues arose that changed the directions and goals of BMS. The most pressing issues are listed.

1. The treatment operation proved to be quite expensive and labor intensive. For example the use of chloroform as the dispersing and treatment medium led to cost issues and environmental as well as safety issues.

2. A business decision was made by BMS to concentrate on selling CNT as a commodity product. BMS would sell the CNT as an untreated material. This became a more favorable option for a couple of reasons.
    a. New technology developed by BMS made it possible to offer CNT at a very reasonable cost to its customers. This allowed the end user to add higher loadings to the composites materials without adding to much expense.
    b. The development of melt-compounding techniques advanced with regard to dispersing the CNT into thermoplastics. This enabled end-user to disperse the untreated CNT into their polymers more efficiently.
    c. In the case of polycarbonate, the treated CNT gave poor results when compared to the untreated CNT.

In conclusion, the advances in the production of CNT and advances in the dispersion techniques left little advantage in treating the CNT. Specifically, for melt-compounding applications, the treated CNT were more expensive and left little advantage. And in some cases the treatment of the CNT could be a hindrance. For example, the trials run at BMS, show better results when using the untreated CNT. Finally, the best scenario is to achieve the desired performance using the untreated CNT because the treatment adds a variable in the final product that could be adverse to the performance. For instance, when compounding advanced composite materials, the addition of additives (e.g. plasticizers, anti-oxidants) is common. These materials and their interaction with one another have been well studied. The addition of treatment, in the form of treated CNT, into the composite formulation adds a variable that is not well studied and could possibly be problematic.

TASK 4

The purpose of Task 4 was to begin and coordinate a strategic alliance and business plan between the BMS and NanoRDC. Originally, it was envisioned that BMS would license the technology from NanoRDC. Currently, the CNT are being produced at the Bayer (Germany) facility and it made good sense to perform the treatment at the same location as the CNT manufacturing process. As stated in Task 3, it became obvious to NanoRDC and BMS that this was not going to be an option due to reasons already stated. As a result of the issues stated in Task 3, NanoRDC has focused on producing aqueous CNT dispersions. Our new business model revolves around this decision and an executive summary is presented as Appendix A.

TASK 5

The purpose of Task 5 was to develop and draft a joint IP and licensing agreement. As stated in Task 3 and Task 4 above, the treatment of CNT became an unfavorable option due to cost and safety issues.

NanoRDC
Nanoparticles for Polymer Composites

CONCLUSIONS FROM TASK 1-5

During the course of the present project, several items arose involving the a) treatment technology b) cost of CNT and c) the melt compounding technology and these items changed the goal of NanoRDC and BMS. Final remarks on these issues are addressed below.

Treatment Technology: While there were many reports that stated that sonication was the most effective method of de-agglomeration of CNT bundles, the reports focused on bench top operations involving small scale batches. To our knowledge, there were no reports of large scale operations that would have industrial applications. This gave NanoRDC little information to guide the engineering of the envisioned continuous operating CNT treatment operation. Several issues arose that were problematic.

1. The use of chloroform as the dispersing medium added material limitations and/or specifications to the equipment used in the operation. For example, all piping, gaskets, seals, shafts and more specifically, any part of the operation that would come in contact with the chloroform must meet compatibility requirements. In most cases this was achieved by the use of Viton® (flouroelestomer) and/or stainless steel. The downside was the added expense and availability of the more specialized components such as the flow cell/sonicator and the progressive cavity pump.
2. The pressure/efficiency of cavitation relationship was not well documented and establishing the correct parameter (pressure, viscosity, and flow rate) for the pilot operation was experimental in the beginning.

Cost of Raw Materials: With the advancement of the technology involving the CNT manufacturing, the price of CNT reduced considerably. Actually, the price of the CNT became less than the price of the treatment when you considered the cost of treatment chemicals and the cost of operating the treatment facility.

Advancements in Melt-Compounding Techniques: The melt compounding of CNT into thermoplastics has evolved considerably and experienced compounders can achieve excellent dispersion of CNT into thermoplastics resulting in high performance composite materials using existing equipment.

NanoRDC
Nanoparticles for Polymer Composites

FUTURE DIRECTIONS

While it has become obvious that treatment of CNT for enhanced dispersibility is not feasible when considering melt-compounding, it might still have applications in other areas. Some examples are listed below:

1. Aqueous CNT dispersions have become a major focus for NanoRDC. The main reasons for this are due to technology and business decisions. Regarding the technology, it is more environmentally friendly and less labor intensive. When considering the business aspects, NanoRDC is a small startup company and our best outcomes will result from pursuing niche high end products.
2. Applications where the use of shear is limited might benefit from the treatment. For instance, in the case of carbon nanofibers, excessive shear has been shown to damage the carbon nanofibers.
3. In applications where the CNT can re-agglomerate. Aqueous and organic solutions of CNT, under prolonged storage, can re-agglomerate and be held tightly together by intermolecular forces. This would require the CNT to be de-agglomerated by the use of shear. This might not be a viable option depending on the applications and end-user capabilities.
4. Applications where the use of the treatment adds a property to the CNT. For example, the addition of silver complex to the surface of the CNT could add an anti-microbial action to the CNT.

NanoRDC
Nanoparticles for Polymer Composites

APPENDIX A. EXECUTIVE SUMMARY FOR NANORDC LLC

THE COMPANY

NanoResearch, Development and Consulting LLC (NanoRDC) operates an office and laboratory in Akron, Ohio. Our mission and the goal of founder, Rick Simons, is to commercialize *useable* compositions of carbon nanotubes (CNT).

THE PROBLEM

Applications for CNT are enormous due to their mechanical, thermal and electronic properties. However, dispersion of CNT into aqueous and/or organic media has proven difficult and expensive due to the inherent bundling/aggregation of the CNT.

THE SOLUTION

NanoRDC has developed a cost effective chemical additive and dispersion process that produces stable aqueous CNT dispersions. The CNT dispersions have several benefits that add value for the customers.

THE BENEFITS

1. The CNT are treated and dispersed into water as single CNT strands rather than aggregates. Depending on the application, this lowers the cost of the final product by as much as 50% because the desired electrical properties are achieved with lower CNT loadings.
2. Our dispersions can be custom formulated regarding % solids and viscosity. Additionally, it could be advantageous to pre-disperse additives.
3. Our CNT dispersions produce high end products with unique properties and specifications.
4. Our customers can now produce high-end nano products using their existing manufacturing operation(s).

THE APPLICATIONS

1. Electrical conductivity for latex materials e.g. gloves and finger cots
2. Conductive coatings and paints
3. Conductive textiles
4. Thermal conductivity for a range of polymers

TECHNOLOGY OVERVIEW

Our CNT dispersions are compatible with any waterborne applications and impart excellent electrical properties to applications and products. This remarkable technology is owned by NanoRDC LLC and protected with an International Patent Cooperation Treaty. This is the result of two years of research and development by NanoRDC and collaborations with CNT suppliers and experts in the field of commercializing nano products. In 2006, NanoRDC was awarded a grant from the Pennsylvania NanoMaterials Commercialization Center to advance the technology toward

commercialization. Currently, NanoRDC seeks strategic partnerships and/or customers that will result in mutual financial benefits for all parties.

COMPETITIVE ADVANTAGE

NanoRDC's competitive advantage is our position within the carbon nanotube supply chain. Our patented technology describing the treatment of CNT and their use to impart value to advanced composite materials enable end users to market advanced products with added value and unique properties. In addition, we hold a strong hold on high end markets that incorporate CNT. As a startup nanotechnology company, we will maintain our competitive advantage by co-developing and marketing high end nanoproducts with strategic partners that have existing customer base and a reputation for producing cutting edge products.

PROPOSED BUSINESS MODEL

NanoRDC current business model is to focus on niche markets that have annual sales of one to two billions USD. The niche markets will be pursued based on the following criteria.

1. Annual sales of 1-2 billion USD.
2. High potential for market growth.
3. Unique position on the market due to our patented technology and/or trade secrets. We will form strategic partnerships that will promote a monopoly on the chosen niche markets, however, we will never license our technology to carbon nanotube suppliers. This will protect our position within our own markets.

EMERGING NANOTUBE MARKETS

Conductive Gloves:

Even the slightest static existing in the work environment can be destructive to electronic components. As the speed and intricacy of electronic devices increases, they become more vulnerable to disturbance from static. Conductive gloves are electrically-conductive, thereby eliminating static discharge which would ruin delicate electronic parts. NanoRDC has the capability to produce treated carbon nanotubes which can be dispersed throughout the latex (untreated nanotubes will not disperse). Because of the properties of NanoRDC's treated nanotubes, very little would be needed as filler material in the latex. Because of this, the gloves can be made very thin, which is favorable when working with tiny, delicate parts; unlike the bulky ESD (electrostatic dissipative) gloves that are on the market right now. Workers can work faster and have greater dexterity while using these novel "nanogloves." NanoRDC's treated nanotubes are superior to competitors' because of technology developed that allows the nanotubes to keep their ideal properties and characteristics while dispersed throughout a material. The conductive glove market has annual sales of over one billion USD. NanoRDC has formed a strategic partnership with the largest international manufacturer of conductive gloves.

NanoRDC
Nanoparticles for Polymer Composites

Conductive coatings

Conductive coatings are marketed world wide as a material that can be applied to devices, buildings and in general to any article that needs ESD and/or RFI protection. State of the art is to incorporate silver powder and/or copper coated silver powder into an aqueous dispersion containing a binder (e.g. polyurethane). Our aqueous dispersions of carbon nanotubes will allow the manufacture of conductive coatings using CNT instead of precious metals. The combination of lower loadings of CNT needed and the reduced price of CNT when compared to precious metals will produce a conductive coating market with added value to the customers. For instance, in any composite material, the highest quality is obtained when the loading of fillers is low. The cost savings resulting from the low loadings and raw material cost can be passed on to customer to promote sales and market growth.

CONTACT INFORMATION

www.nanordc.com
Rick Simons email: rsimons@nanordc.com
330-983-7886 cell

Disclaimer: The data reported here were generated using generally accepted laboratory methods and is believed to be an accurate representation of the typical characteristic of the materials tested. NanoRDC LLC. makes no claims or warrantees herein as relates to the suitability of the materials tested for any intended use.

REFERENCES

[1] **Tasis, D., N. Tagmatarchis, A. Bianco, M. Prato**. 2006 Chemistry of Carbon Nanotubes. Chemical Reviews **106**: 1105-1136.
[2] **Park, C., Z. Ounaies, K. A. Watson, R. E. Crooks, J. G. Smith Jr. S. E. Lowther**. 2002 Dispersion of single wall carbon nanotubes by in-situ polymerization under sonication. Chem Phys Lett **364**: 303-306.
[3] **Chen, J., M. A. Hamon, H. Hu, Y. Chen, A. M. Rao, P. C. Eklund**. 1998 Science **282**: 95-??.
[4] **Niyogi, S., M. A. Hamon, H. Hu, B. Zhao, P. Bhowmik, R. Sen**, 2002 Chemistry of Single-Walled Carbon Nanotubes. Acc Chem Res **35**: 1105-1113.

[5] **Singh, C., M. S. P. Shaffer, K. K. K. Koziol, I. A. Kinloch, A. H. Windle**. 2003 Towards the production of large-scale aligned carbon nanotubes. Chemical Physics Letters **372**: 860-865.
[6] **Banerjee, S., S. S. Wong**. 2002 Structural Characterization, Optical Properties, and Improved Solubility of Carbon Nanotubes Functionalized with Wilkinson's Catalyst. J. Am. Chem Soc. **124**: 8940-8944.
[7] **Bahr, J. L.; J. M. Tour.** 2001 Highly functionalized carbon nanotubes using in situ generated diazonium compounds. Chem Mater **13**: 3823-3824.
[8] **Dyke, C. A.; Tour, J. M.** 2003 Solvent-Free Functionalization of Carbon Nanotubes. J. Am. Chem. Soc. 2003, **125**, 1156-1157.
[9] **Holzinger, M., J. Abraham, P. Whelan, R. Graupner, L. Ley, F. Henrich**, 2003 Functionalization of Single-Walled Carbon Nanotubes with (R-)Oxycarbonyl Nitrenes. J. Am. Chem. Soc. **125**: 8566-8580.
[10] **Islam, M. F., E. Rojas. D. M. Bergey, A. T. Johnson, A. G. Yodh**, 2003 High Weight Fraction Surfactant Solubilization of Single-Wall Carbon Nanotubes in Water Nano Lett **3**: 269-273.
[11] **Star A., Y. Liu, K. Gant, L. Ridvan, J. F. Stoddart, D. W. Steuerman**. 2003 Noncovalent Side-Wall Functionalization of Single-Walled Carbon Nanotubes. Macromolecules **36**: 553-560.
[12] **Chen R. J., Y. Zhang, D. Wang, H. Dai**. 2001 Noncovalent sidewall functionalization of single-walled carbon nanotubes for protein immobilization. J. Am. Chem. Soc. **123**: 3838-3839.
[13] **Star A., D. W. Steuerman, J. R. Heath J. F. Stoddart**. 2002 Starched carbon nanotubes. Angew Chem Int Ed **41**: 2508-2512.

NanoRDC
Nanoparticles for Polymer Composites

Pennsylvania NanoMaterials Commercialization Center
Attn: Alan G. Brown, Ph.D., Ms. Jeanne Straw
2000 Technology Drive
Pittsburgh, PA 15219-3110

10/17/2007

Final Federal Finacial Report
Contract # Nano-07-002

Cost Element	Period 3/17/07 to 5/31/07	Period 6/1/07 to 10/1/07	YTD Period 3/17/07 to 10/1/07	Budget
Direct Labor				
Labor	15,000	18,250	33,250	$29,250
Other Direct				
Sub-cost	1,000	1,000	2,000	$10,000
Supplies	4,000	4,000	8,000	$7,000
Other	4,000	4,000	8,000	$5,000
Total Other Direct Cost and expenses	9,000	9,000	18,000	$22,000
Total Project Cost and expenses	23,000	28,250	51,250	$51,250
Cost Share	20,600	8,895	29,495	$20,600

Please Make Check Payable for **$5,000** to NanoRDC LLC

I certify to the best of my knowledge and belief the data is correct and that all outlays were made in accordance with the agreement conditions.	Signature:
	Name:
	Date:

NanoRDC LLC 526 S. Main Street, #809B, Akron Ohio 44311 (330) 376-1893

NanoRDC
Nanoparticles for Polymer Composites

EXPLANATION FOR CHANGES TO ORIGINAL BUDGET

Labor:
Initially we had budgeted $ 29,250 for labor. This amount inceased to $ 36,000 for two reasons. First, the project was extended from 8/31/07 to 10/1/07. Second, the treatment of the CNT proved to be more labor intensive and NanoRDC hired a lab technician.

Sub-contractor Cost:
The initial budget of $ 10,000 was reduced to $ 2,000. Originally, we had planned to do test the efficiency of the pilot operation/flow by SEM analysis. However, the entire 4 KG was tested by bench top procedures. The sub-cost accrued are due to engineering of the pilot operation. The flow cell had to be mounted on the wall of the lab. However, a metal bracket had to be constructed at the machine shop and the lab wall had to be reinforced before the flow cell could be mounted.

The budget for laboratory rent also increased from the original budgeted amount of $5,000 to $8,000 for the project period due to our move into the incubator.

The In-Kind Contributions were purchased that were not part of the original In-Kind items

Additional In-Kind Contributions
Progressive cavity pump-----$3900
Flow cell----------$ 4995

Original In-Kind Contributions

IN-KIND CONTRIBUTIONS		
CONTRIBUTOR	**ITEM**	**COST**
NANORDC	PILOT PLANT HARDWARE	2000
NANORDC	SONICATOR	4200
NANORDC	CHEMICALS	2000
BMS	PURCHASE OF t-CNT	10,000
BMS	NANOTUBES	2400
TOTAL		**20600**

NanoRDC LLC 526 S. Main Street, #809B, Akron Ohio 44311 (330) 376-1893

Appendix C – 07-005 (Integran Technologies)

INTEGRAN
TECHNOLOGIES U.S.A. INC.

Co-Axially Nano-Structured Electrical Wire with Enhanced Strength-to-Weight and Optimized Conductivity

Final Technical Report – Task T5

2008-11-15

OUR FILE NO: **2007-PEN-603-0297**

Authors: Ian Winfield, Iain Brooks, & Edward Yokley

INTEGRAN TECHNOLOGIES U.S.A. INC., 2541 APPLETREE DR., PITTSBURGH, PA 15241, USA.

Page No. 1

Co-Axially Nano-Structured Electrical Wire with Enhanced Strength-to-Weight and Optimized Conductivity

Technology Development Report – Task T3

2008-07-17

OUR FILE NO: **2007-PEN-603-0297**

PREPARED BY:

IAN WINFIELD
RESEARCH ENGINEER

IAIN BROOKS
PROJECT LEADER

EDWARD YOKLEY
PRINCIPAL INVESTIGATOR

REVIEWED BY:

GINO PALUMBO
SENIOR SCIENTIST

APPROVED BY:

_____

ROBERT HEARD

PROJECT MANAGER AND COMPANY PRESIDENT

DISCLAIMER

INTEGRAN TECHNOLOGIES U.S.A. INC. TAKES REASONABLE STEPS TO ENSURE THAT ALL WORK PERFORMED SHALL MEET THE INDUSTRY STANDARDS AND THAT ALL REPORTS SHALL BE REASONABLY FREE OF ERRORS, INACCURACIES OR OMISSIONS. **INTEGRAN TECHNOLOGIES U.S.A. INC. DOES NOT MAKE ANY WARRANTY OR REPRESENTATION WHATSOEVER, EXPRESS OR IMPLIED, WITH RESPECT TO THE MERCHANTABILITY OR FITNESS FOR ANY PARTICULAR PURPOSE OF ANY INFORMATION CONTAINED IN THIS REPORT OR THE RESPECTIVE WORKS OR SERVICES SUPPLIED OR PERFORMED BY INTEGRAN TECHNOLOGIES U.S.A. INC.** INTEGRAN TECHNOLOGIES U.S.A. INC. DOES NOT ACCEPT ANY LIABILITY FOR ANY DAMAGES, EITHER DIRECTLY, CONSEQUENTIALLY OR OTHERWISE RESULTING FROM THE USE OF THIS REPORT.

EXECUTIVE SUMMARY

The reel-to-reel wire plating tool capable of continuous production of co-axially nanostructured electrical wire is in operation at the Pittsburgh-based facility. Continuous wire lengths are limited only by the total continuous length of the supply-substrate wire, which is currently ~5000 ft. Single strand testing has been executed to evaluate the properties of the wire for iterative development and to provide preliminary product data of the optimized wire.

Table I summarizes the preliminary product data in comparison with the materials performance indices (MPIs) identified in Technology Development Report – Task T1 and the properties of the competing high-strength conductor material, beryllium-copper alloy CS95. Additionally, characterization has been executed to examine the surface morphology, the coating-substrate adhesion, and the diameter of the wire.

Table I – Summary of Preliminary Product Data

Material/MPIs	MPI-1 Tensile Strength *MPa (ksi)*	MPI-2 Ductility *%EL*	MPI-3 Conductivity *%IACS*
Materials Performance Indices - Targets	1025 (155)	6	56
NanoMetal Enhanced Conductor - Actual	**950 (138)**	**7-8**	**58-59**
CS95 - Beryllium-Copper Alloy	655 (95)	6	63

The preliminary product data indicates that the 38 gauge co-axially nanostructured electrical wire has good potential to ultimately provide a conductor material that can be utilized to realize weight savings in the electrical wiring systems of aircraft.

TABLE OF CONTENTS

1.0 INTRODUCTION

Aircraft electrical wiring accounts for a significant fraction of an aircraft's total weight and can be upwards of 5000lbs depending on the aircraft type.[1] With a constant drive for weight reduction in the aerospace sector, this creates a commercial opportunity for the development of a technology that can ultimately reduce the weight of electrical aircraft wiring. The most effective method of reducing the wire weight is to modify/substitute the conductor material (the metal core of the wire), as it accounts for the majority of the overall wire weight. However, stringent conductivity and strength requirements, among many others mentioned in this report, limit the selection of suitable materials. Thus, a new conductor material that exhibits both high-conductivity and high-strength is required.

A co-axially nano-structured electrical conductor with enhanced strength-to-weight and optimized conductivity is the proposed solution for a new material. By utilizing a proprietary process developed by Integran, a high-strength nanocrystalline metal can be electrodeposited onto a substrate in order to significantly enhance the overall strength of the conductor while maintaining a relatively high conductivity. The final result is the ability to meet design requirements using significantly less conductor material, resulting in an overall weight reduction.

It is anticipated that this concept would be a relatively simple drop-in for existing wire production processes because the vast majority of copper wire that is in use today is already coated (often by electroplating) for corrosion resistance. In addition, the nanomaterials will be applied by a proprietary electrodeposition technique that is straightforward, mature, easy to scale up to mass production quantities, and relatively inexpensive. Hence, the possibility exists for widespread sizeable electrical wire weight savings at a low overall cost and extremely low technical risk.

Preliminary mechanical and electrical testing results indicate that a significant weight reduction of greater than 30% can be realized by adopting the nano-structured design as the conductor material.

2.0 AIRCRAFT WIRE REVIEW

2.1 Aircraft Wire Types

Aircraft wire is generally categorized into two main types: power wire and signal wire. Signal wire accounts for the majority of wire on an aircraft and is exposed to relatively low electrical loading. This allows for utilization of small wire sizes, typically in the range of 24 to 20 AWG (nominal diameter - 0.0201 to 0.0320 in.). Signal wire is used for a number of functions including: flight control systems, feedback and monitoring systems, discrete DC low voltage supply, and safety ground wiring. Table 1 shows the relative amount of 24 AWG signal wire compared to the overall wire used in specific Airbus aircraft models. Power wire, on the other hand, is exposed to very large electrical loads and is utilized to supply power to the electronic equipment. Consequently, power wire sizes are of a relatively large diameter, in the range of 12 AWG (nominal diameter - 0.0808 in.), and are therefore kept as short as possible in order to minimize weight.[2,3,4,]

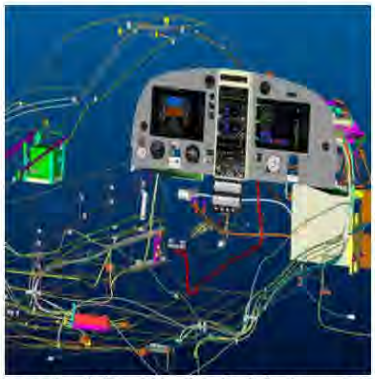

Figure 1 – Schematic of cockpit instrumentation and wiring (References for all figures can be found at the end of the report)

Table 1 - Approximate Lengths of Wiring on Commercial Aircraft

Aircraft Model	Total Length of Wires All Gauges, km	Total Length of 24 AWG Wire (signal wire) Only, km
Airbus A320	120	80
Airbus A340	300	200

Source: [5] Galenghien, J.L. and A. Synodinos

2.1 Wire Specifications and Standards

In order to ensure that aircraft wire can withstand the severe conditions experienced during flight—i.e. vibrations, bending loads, temperature changes, abrasion, etc.—the wire must meet certain standards. These standards are often military (*MIL*) or SAE

International (*AS*) approved, and specifications are consistent between the two. For example, documents *MIL-W-22759* and *AS22759* both cover the requirements for "Fluoropolymer-insulated single conductor electrical wires made with tin-coated, silver-coated, or nickel-coated conductors of copper or copper alloy". Specifications also exist for electrical connections, wire testing procedures, installation, etc. In some cases, *AS* or other new standards, such as Approved American National Standard (*ANSI*), supersede older existing *MIL* standards, but are for the most part equivalent.

Figure 2 – Example *of a 22759 wire showing* a) exposed conductor and b) insulation

Wire specifications, such as *AS22759*, define requirements for the wire as a whole, which consists of two primary constituents: a conductor (electrically conductive metal core material) and an insulator (electrically resistant polymer/composite exterior material). Since wire standards are specific to a certain insulator type, the requirements for the insulator are often included in the standard. Requirements for conductors, however, are commonly referenced to a secondary document, *MIL-W-29606,* which defines requirements for "Wire, Electrical, Stranded, Uninsulated Copper, Copper Alloy, or Aluminum, or Thermocouple Extension". This document has been superseded by a more current standard, *ANSI/NEMA WC 67*, consistent with *MIL-W29606* and including additional specifications for copper-clad steel. Thus, the *WC 67* standard is a fundamental guideline in the design of new conductor materials, outlining the requirements for strength, conductivity and other key performance characteristics

3.0 CONDUCTOR REVIEW

3.1 Conductor Construction

Conductors are most often constructed from a bundle of finer strands, rather than a large single end (solid) strand. This construction improves the flex fatigue life (the ability to withstand vibrations or repeated bending) of the conductor [6]. Stranding designs are generally either concentric lay (Fig. 3), assembled in a geometric arrangement of concentric layers helically wound about a central strand, or bunch-stranded (Fig. 4), strands twisted together with no specific geometric arrangement except for lay direction.

Conductors within a 30 to 10 AWG (minimum stranded diameter – 0.0105 to 0.106 in.) size range are constructed from a concentric lay of 7, 19, or 37 strands.[7,8,9] For example, a 26 AWG (min. stranded diameter - 0.0175 in.) conductor may consist of 19, size 38 AWG (nominal diameter – 0.004 in.) strands.[8] The construction is such that the cross sectional conductor area is near-equivalent to a solid, single end 26 AWG conductor. Conductor and wire sizes are often designated in AWG, or American wire gauge, and increase in diameter with decreasing gauge size.

Fig. 3 – Schematic of a concentric lay construction

Fig. 4 – Schematic of a bunch-stranded construction

Fig. 5 – Photograph of a 19 strand, concentric lay conductor

3.2 Conductor Specifications

ANSI/NEMA WC 67 is the current standard for uninsulated conductors used in electrical and electronic applications, replacing military standard *MIL-W-29606* as previously mentioned. *WC 67* defines requirements for the following conductor materials:

1. Bare (Uncoated) Copper (BC)
2. Tin Coated Copper (TCC)
3. Silver Coated Copper (SCC)
4. Nickel Coated Copper (NCC)
5. Heavy Nickel Coated Copper (NHC)
6. Silver Coated Copper Alloy (SCA)
7. Nickel Coated Copper Alloy (NHA)
8. Tin Coated Copper Alloy (TCA)
9. Heavy Nickel Coated Copper Alloy (NHA)
10. Silver Coated Ultra-High Strength Copper Alloy (SCU)
11. Nickel Coated Ultra-High Strength Copper Alloy (NCU)
12. Aluminum Strands (ALU)
13. Type K Thermocouple Extension Conductor (KPH, KPS, KNH, and KNS)
14. Nickel-Coated Copper-Clad Steel (NCCCS)
15. Silver-Coated Copper-Clad Steel (SCCCS)

Specifications are given for the construction of the conductors as well as the following conductor testing procedures and properties:

1. Diameter
2. Elongation to failure
3. Tensile or Break Strength
4. Conductor DC Resistance
5. Continuity of Coating
6. Coating Thickness
7. Weight
8. Solderability of Tin and Silver Conductors
9. Worksmanship

It is important to note that *WC 67* does not define requirements for flex fatigue life, crimpability (the ability for a conductor to be electrically connected via crimping to plastically deform the conductor), flexibility, or other important properties that may limit a material for use as a conductor. Yet, these are important properties to consider when designing a conductor material.

WC 67 outlines resistance requirements for all conductor types. However, strength requirements are only designated for copper alloys (often referred to as high-strength copper alloy) and ultra-high strength copper alloys. The requirements for strength and conductivity of nickel coated copper alloy (NHA) and nickel coated ultra-high strength copper alloy (NCU) conductors are displayed in Tables 2 and 3, respectively. It is beyond these requirements that a new conductor design must perform in order to successfully replace existing technologies.

Table 2 – Requirements for NCA Conductor

Size (AWG)	Configuration (count x AWG)	Max. Resistance (Ohm/1000ft)	Min. Tensile Break Strength (lbs)	Min. Elongation (%)
28	7 x 36	79.0	8.2	6
26	19 x 38	49.4	14.2	6
24	19 x 36	30.1	22.4	6
22	19 x 34	18.6	35.8	6
20	19 x 32	11.4	58.1	6

ANSI/NEMA WC 67 - Table 2E - Details of Alloy Conductors – (Nickel Coated High Strength Alloy)

Table 3 – Requirements for NCU Conductor

Size (AWG)	Configuration (count x AWG)	Max. Resistance (Ohm/1000ft)	Min. Tensile Break Strength (lbs)	Min. Elongation (%)
26	19 x 38	58.4	21.5	6
24	19 x 36	37.7	34.0	6

ANSI/NEMA WC 67 – Table 2E – Details of Alloy Conductors – (Nickel Coated Ultra High-Strength Alloy)

From Tables 2 and 3 it can be seen that NCU conductors require a higher minimum break strength than NCA conductors, approximately 1.5x stronger, while allowing for a greater maximum resistance. This effectively demonstrates that there is a generally accepted strength vs. conductivity trade off when designing conductor materials.

3.3 Strength vs. Conductivity Tradeoff

The strength vs. conductivity tradeoff must be accepted in designing a conductor material. This is because strengthening techniques, such as introducing alloying elements, heat-treating to produce second phase particles, increasing the grain boundary density (i.e. nano-structuring a material), or cold working to increase the dislocation density, all introduce scattering points for electrons traveling through the material. An increase in scattering points reduces the overall conductivity of the material (i.e. electrical attenuation). Figure 6, below, demonstrates this effect for the case of a copper-zirconium alloy. As zirconium is added to the alloy the tensile strength increases while the electrical conductivity (%IACS) is reduced. IACS stands for "International Annealed Copper Standard for conductivity" and represents the conductivity of a material relative to the conductivity of pure copper, which has a %IACS of 101%.

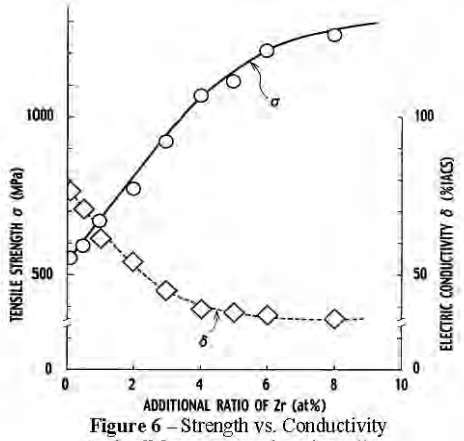

Figure 6 – Strength vs. Conductivity tradeoff for a copper-zirconium alloy

3.4 Current Conductor Materials

The majority of common conductor materials are copper-based alloys because of the high electrical conductivity of copper. Table 4 displays the relevant properties of some common alloys, as well as additional materials for comparison.

Table 4 - Properties of Common Conductors and Other Materials [3,9,10]

Material	Tensile Strength, MPa	%IACS	Density, kg/m^3	Min. %Elongation
Pure Copper	200	100%	8920	25%
C10200 (Cu - O_2 Free)	350	100%	8900	45%
PD135 (Cd-Cr-Cu Alloy)	480	91%	8940	n/a
C16200 (Cd-Cu Alloy)	485	89%	8890	6%
CS95 (Be-Cu Alloy)	655	63%	8830	6%
Pure Aluminum	125	57%	2670	6%
AISI 1095 Steel - Oil Quenched	1270	9%	7850	13%
304HN Stainless Steel	725	2%	8000	50%

Table 4 shows that one of the strongest copper alloys is CS95, which is a beryllium-copper alloy used to construct ultra-high strength copper alloy conductors.[11] The properties of stranded CS95 conductors, calculated on the basis of monolithic tensile

strength and conductivity, are shown in Table 5. These values are comparable to the specifications for ultra-high strength copper alloy conductor, Table 3, defined by *WC 67*. This is the "incumbent alloy to beat" in designing a new high-strength, high-conductivity conductor.

Table 5 - Theoretical Properties of CS95 Conductors, Stranded

Size (AWG)	Configuration (# x AWG)	Resistance (Ohm/1000ft)	Tensile Break Strength (lbs)	Elongation (%)
26	19 x 38	53.6	22.7	6
24	19 x 36	34.3	35.4	6

4.0 NANOMETAL ENHANCED CONDUCTOR DESIGN

4.1 Defining the Product

The first step in defining the product was to determine the specific wire type to target, be it signal wire or power wire. Due to the heavy electrical loading of power wires, conductivity requirements and minimum size constraints generally do not appear to allow for any reduction in weight/conductivity by reducing the amount of conductor material. Signal wires, on the other hand, offer significantly more flexibility in conductivity and size requirements, as they are used to carry lower electrical currents. Furthermore, signal wire accounts for the bulk of the overall wire weight on an aircraft. Thus, signal wire is the product of choice for this program.

Determining the conductor size and requirements was the second step in defining the product. Through interviews and conversations with industry professionals and wiring specialists, it was determined that 24 AWG CS95 conductor was the current standard.[12,13] Designers desired to use a 26 AWG wire in order to minimize weight contributions, but were often forced to increase the size to 24 AWG in order to meet strength requirements.

The target product was, thus, defined as a 26 AWG [19 x 38AWG (nominal diameter – 0.004 in.)] signal wire conductor, with a tensile break strength equal to or greater than that of a 24 AWG CS95 conductor, 35.4 lbs, and with a comparable resistance of less than 60 Ohm/1000ft (i.e. a conductivity of approximately 60 %IACS). To reiterate, the

goal is to provide the systems designer with a 26 AWG replacement option that is just as strong as the existing 24 AWG ultra-high-strength (CS95) copper material while still maintaining ~60 %IACS level of electrical conductivity. It is important to note that there may be many different NanoMetal + pairing material combinations that may meet the variety of conductor performance requirements for both aerospace and non-aerospace applications.

4.2 Design Requirements - Materials Performance Indices

Once the design requirements have been determined, identifying the proper Materials Performance Indicies (MPIs) provides a systematic method for material selection in the design process. In this case, designing a high-strength, high-conductivity conductor, the following MPIs have been identified as the most important design parameters:

MPI-1. Strength (Tensile Strength, MPa)
- Ensures that the conductor will meet strength requirements

MPI-2. Conductivity (%IACS)
- Ensures that the conductor will meet conductivity requirements

MPI-3. Ductility (%Elongation)
- Ensures that the conductor will have sufficient ductility to avoid catastrophic failure

MPI-4. Specific Strength (Tensile Strength/Density, MPa/(kg/m^3))
- Optimizes strength-to-weight ratio for maximum weight reduction and comparison with competitor designs based on lighter weight metals, i.e. aluminum

MPI-5. Strength-Conductivity Quotient (Strength*Conductivity, MPa*%IACS)
- Optimizes material to achieve maximum strength and conductivity

Other design parameters include flexibility, crimpability, and flex fatigue life, yet these are not intrinsic material properties and are dependant also on the geometry and configuration of the design. Ultimately, determining whether a design possesses these qualities requires prototyping and testing.

The strength and conductivity MPIs can be estimated by back calculation from the projected tensile break strength requirement of a 24 AWG CS95 conductor, 35.4lbs, and a resistance of less than 60 Ohm/1000ft. for a 26 AWG. The ductility MPI can be set by equating it to the % elongation of CS95, which is 6 %. These calculations yield the following results, with conservative rounding:

MPI-1 - Strength = 1025 MPa (Rounded up from 1022MPa)

MPI-2 - Conductivity = 57 %IACS (Rounded up from 56.4MPa)

MPI-3 - Ductility = 6 %EL

It is important to note that these MPIs may end up being beyond the final product design requirements and that, due to the myriad of product requirements and corresponding performance tradeoffs associated with aircraft electrical wire conductors, a material that does not meet all three MPIs should not necessarily be immediately discounted.

The identified MPIs facilitate material selection by limiting materials that do not pass the first three MPIs and then optimizing the final two MPIs to determine the best material. However, if the first two MPIs are applied to the currently available materials, see Figure 7, it is quickly established that no material is suitable for the required application, since no existing materials presently reside within the upper right hand quadrant. This generates a need for new materials or material combinations if enhanced performance is to be achieved. The incumbent high-strength Cu alloy, CS-95, has been highlighted in order to draw attention to the performance of the existing product with which the NanoMetal-enhanced design will likely compete.

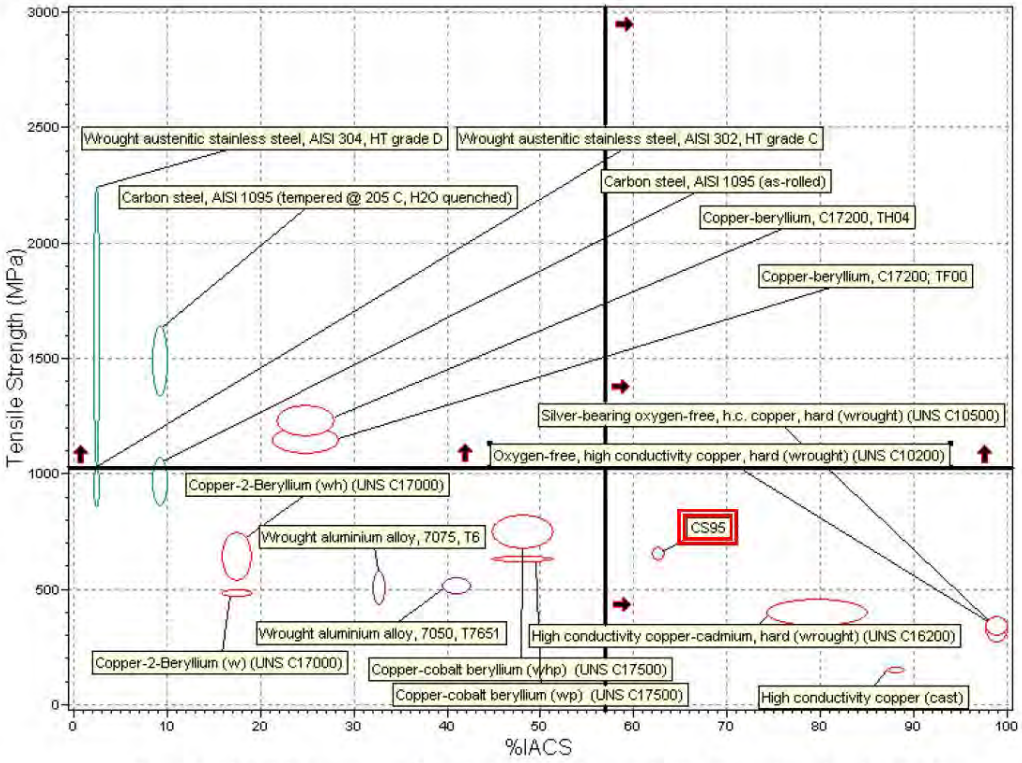

Figure 7 – Material property graph displaying strength and %IACS with horizontal and vertical lines representing the strength (MPI-1) and conductivity (MPI-2) MPIs, respectively.

4.3 Integran's Nanocrystalline Materials

Integran's process allows for the unique tailoring of material properties by controlling the grain size and chemical composition via precise control of the pulsed electroplating parameters and bath chemistry. The properties of some of Integran's nanomaterials are

shown in Table 6. As a result of grain refinement, tensile strength will increase and electrical conductivity will decrease. Thus, grain size control is one method by which the property trade-off can be optimized. Figure 8 illustrates the dependence of yield strength and conductivity of pure copper with respect to the grain size.

Table 6 - Properties of Integran's Nanomaterials

Material (Grain Size)	Tensile Strength, MPa	%IACS	Density, kg/m^3	Min. %Elongation
nNi (25nm)	1300	16%	8900	7%
nNi (100nm)	860	19%	8900	17%
nCu (~200nm)	665	80%	8920	21%
nCu + GBE-HT* (~1000nm)	300	93%	8920	28%
nCoP (10nm)	2000	6%	8900	6%
nNi-8%Fe (15nm)	1480	14%	8700	6%

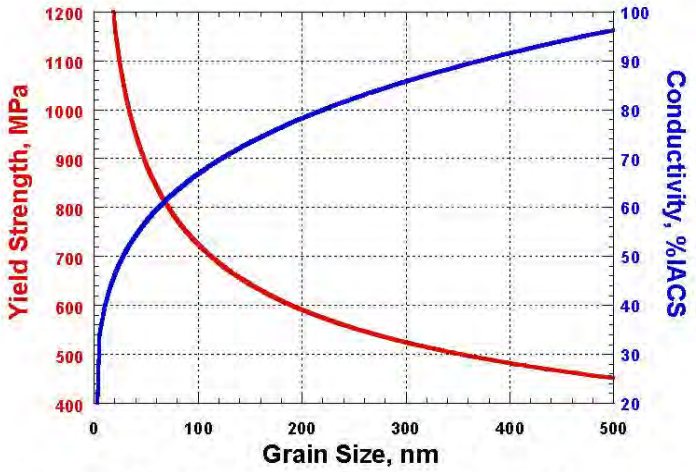

Figure 8 – Yield strength and conductivity of pure copper as a function of grain size

4.4 Conductor Design Concepts and Calculations

Design Concept-1, shown below in Figure 9, is the primary design and utilizes a commercially available copper core substrate in order to provide conductivity in conjunction with a load-bearing nanocrystalline metal outer layer to provide strength. Design Concept-2 is a secondary option that may, in some circumstances, be a better fit with customer performance needs.

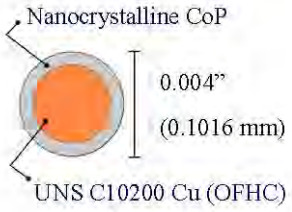

Figure 9 – Design Concept - 1

Figure 10 – Design Concept - 2

Theoretical calculations for the optimum conductor material combinations are shown in Table 7. Break stress and conductivity were calculated by using the rule of mixtures, while ductility was determined by choosing the lowest % elongation of the two materials (i.e. the NanoMetal coating). From the table it is seen that this Design Concept-1 can result in a conductor material that meets or surpasses MPIs 1, 2 and 3, if a 44% volume fraction of nCoP is applied to the copper substrate. All other coating materials meet the requirements for MPIs 2 and 3, but fail to meet the strength requirement defined by MPI-1. These coating materials, however, should not be immediately discounted as other factors may determine the final coating selection.

Table 7 - Theoretical Properties for Design Concept-1

Coating Material	Initial Strand AWG	Di In	Df in	Coating Thickness (in)	Coating Fraction (%)	Break Stress MPa	Conductivity %IACS	Ductility %EL	Density kg/m^3
nNi	40	0.0030	0.0040	0.00050	44	766	63	7	8900
nNi	39	0.0035	0.0040	0.00025	23	573	80	7	8900
nNi-8%Fe	40	0.0030	0.0040	0.00050	44	845	61	6	8813
nNi-8%Fe	39	0.0035	0.0040	0.00025	23	616	79	6	8853
nCoP	40	0.0030	0.0040	0.00050	44	1072	59	6	8900
nCoP	39	0.0035	0.0040	0.00025	23	737	78	6	8900
None	38	0.0040	0.0040	0.00000	0	351	100	45	8900

Table 8 shows that by replacing a 24 AWG CS95 wire with a 26 AWG nCoP coated copper wire, a weight reduction of approximately 35% is realized. A comparable weight reduction is seen for all NanoMetal + copper combinations, as they all have relatively the same density.

Table 8 – Wire Replacement Weight Savings for nCoP + Copper Conductor

Current Standard Wire Copper Beryllium - (CS95)					Replacement Wire nCoP Coated UNS C10200 Copper						
Wire Size AWG	Break Load lb-f	Resistance ohm/1000ft	Weight lb/1000ft	%IACS	Replace with: Size - Coating	Break Load lb-f	Resistance ohm/1000ft	Weight lb/1000ft	Strength Increase (%)	%IACS	Weight Reduction (%)
24	35	34.3	1.43	63	26 - 44% nCoP	37	57.3	0.921	4.8	59	35.5

Some potential limitations in terms of flexibility and ductility may be a concern for Design Concept-1, due to the nature of its construction (i.e. a very hard outer layer providing structural support to a soft internal substrate). Ductility is of considerable importance in application because conductor connection points are generally secured by crimping conductor ends. Thus, potential for failure at connection points may be accentuated for a design utilizing a relatively hard, load-bearing outer layer.

Design Concept-2 is proposed as a fallback option in the case that the applicability of Design Concept-1 becomes limited under certain circumstances. This secondary design utilizes a high strength-to-weight core material, such as high-strength steel or carbon

fiber, with the application of a thick fine-grained copper coating offering high-conductivity and high-strength with enhanced ductility. Applying the ductile, conductive thick coating as the outer layer should allow for sufficient "crimpability".

In order to identify optimal coating + substrate combinations from a calculations standpoint, comparisons of MPIs are shown in Table 9, with the two most promising designs from both design concepts highlighted. Projected weight reductions resulting from a 26 AWG wire replacement over 24 AWG CS95 wire are also provided.

Table 9 – MPI Comparisons

Design Concept #	Material Coating / Substrate	MPI-1 MPa	MPI-2 %IACS	MPI-3 %EL	MPI-4 MPa/(g/cm^3)	MPI-5 (MPa)*(%IACS)	Weight Reduction** (%)
-	Pure Copper	200	100	20	22.4	20000	-
-	CS95	655	63	6	74.2	41265	-
1	44% nNi / Cu	766	63	7	86.1	48270	35.5
1	44% nNi-8%Fe / Cu	845	61	6	95.9	51742	36.1
1	44% nCoP / Cu	1072	59	6	120.5	63296	35.5
2*	75 % nCu / Steel	1098	62	9	126.9	68411	37.3
2*	75% nCu+HT / Steel	827	72	9	95.5	59886	37.3

*Design Concept -2 calculations utilize a high-carbon steel substrate: tensile strength = 2400 MPa, hardness = 59 Rc.

**Weight reduction upon switching from a 24 AWG CS95 conductor to a 26 AWG NanoMetal + substrate conductor.

Optimal NanoMetal + substrate combinations show a specific strength (MPI-4) increase of 62-71% from the traditional CS95 material, resulting in a final potential weight reduction of ~36%. Figure 11 shows a material comparison on the basis of specific strength and %IACS (conductivity), with the applied MPI-2 cutoff of 57 %IACS. It can be seen that the NanoMetal + substrate designs result in the highest potential specific strength for materials meeting the conductivity cutoff of MPI-2.

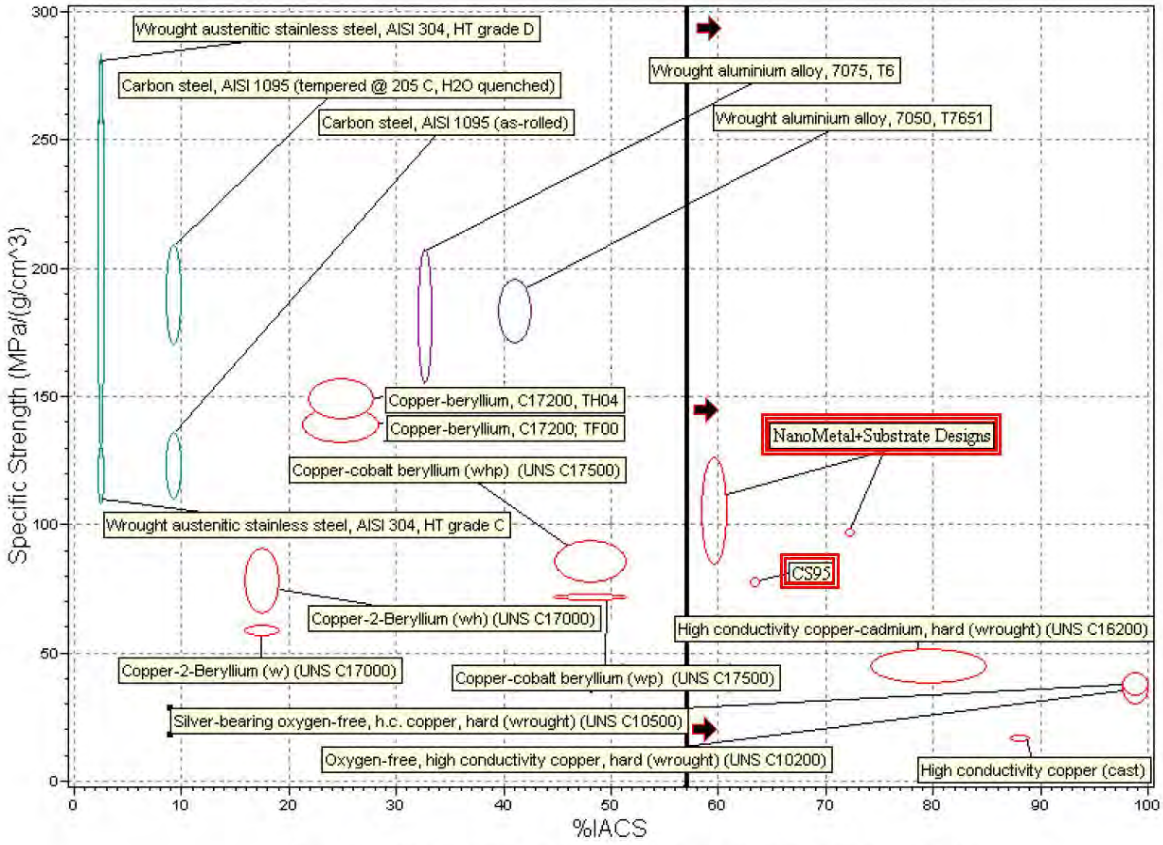

Figure 11 – Material property graph displaying specific strength and conductivity with MPI-2, conductivity, applied (vertical line)

Again, it is important to note that identified MPIs alone may not be sufficient in determining the final product, i.e. a specific NanoMetal + substrate combination. Additional properties and processing costs/considerations will undoubtedly impact the final design decision to some extent as well.

5.0 PROTOTYPE REEL-TO-REEL WIRE PLATING TOOL

5.1 Continuous Wire Plating

Continuous reel-to-reel wire electroplating is a well-established and widely practiced technology with processing patents dating back to the mid-to-late 1800's [1,2]. The plating of wire is normally carried out in order to provide corrosion protection, whereby metal coatings such as tin, nickel, cobalt, or silver are applied to the electrical and/or structural wires [3]. Operating in a continuous process allows for consistency in the quality of the finished wire and is also the most economical production method. In most cases the process involves feed (un-spooling) and take-up (re-spooling) mechanisms that effectively pull the wire through a series of cleaning/surface activation and plating tanks/cells and, sometimes, other processing steps to produce the final metal coated wire. Section 5 goes into specific detail on the reel-to-reel (continuous) wire plating tool designed and constructed to produce NanoMetal-enhanced conductor prototypes.

5.2 Initial Prodcut

While the reel-to-reel line as constructed is capable of producing various wire sizes and coating-substrate combinations of co-axial wire, a specific design concept was chosen as the initial product. Figure 12 shows a schematic for this design: a high-strength nanocrystalline Co-P coating, with a thickness of ~0.0005", in conjunction with a conventional copper core substrate, with a diameter of ~0.003". Calculations in the T1 report have shown that this design concept was the most promising in terms of strength and conductivity [4]. The final construction of the conductor will consist of 19 concentrically laid strands of the 0.004" diameter NanoMetal coated wire to result in a size 26 AWG conductor.

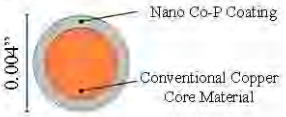

Figure 12 – Schematic of NanoMetal coated conductor (Coating thickness = 0.0005")

5.3 Initial Challenge and Design Constraint

The relatively small diameter, ~0.003", of the conventional copper substrate wire in combination with the inherently low strength of copper posed a major constraint for the design and fabrication of the reel-to-reel wire plating tool. A calculated yielding load of less than 1 lb set stringent requirements on both the drive system (feed and take-up devices) and the potential number of friction points (e.g. electrical connections, guide rollers, etc.) in the plating line in order to ensure that the wire would not break during the electroplating process.

5.4 Description of Reel-to-Reel Wire Plating Line

5.4.1 Overview of Reel-to-Reel Wire Plating Line

The reel-to-reel wire plating line is comparable to existing wire plating lines and involves similar chemical cleaning and activation steps as well as similar plating and activation cell designs. A color-coded schematic of the constructed wire line is shown in Figure 13, with an arrow indicating the direction of wire travel. The single stranded wire passes through a series of rectangular line cells (supported by the scaffolding). Each cell is constantly fed solution from its respective sump (reservoir) tank sitting below. Wire feed and take-up mechanisms (red) are stationed at the start and end, respectively. It is important to note that components such as the plumbing, heaters, controllers, and rectifiers are not shown for simplicity.

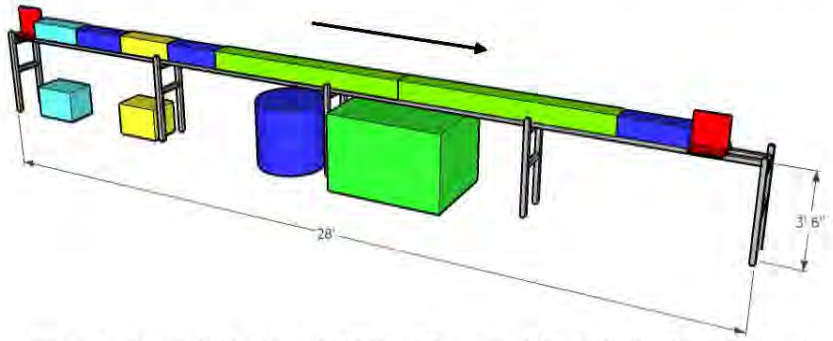

Figure 13 – Schematic of reel-to-reel wire plating line. Arrow indicates the direction of wire travel. (For simplicity the plumbing, heaters, controllers, and rectifiers are not shown in this diagram).

The path of the wire is as follows:

1. Substrate wire un-spools at feed mechanism (red, left)
2. Wire is cleaned by anodic polarization in an alkaline solution (light blue)
3. Wire is rinsed in de-ionized water (dark blue)
4. Wire is activated and further cleaned in an acidic solution (yellow)
5. Wire is rinsed in de-ionized water (dark blue)

6. Wire enters first electroplating cell and is cathodically polarized to deposit nanocrystalline metal (green).
7. Wire enters second electroplating cell and is further coated with nanocrystalline metal (green).
8. Wire undergoes a final rinse (dark blue).
9. Finally, the NanoMetal coated wire is re-spooled at the take up-mechanism (red, right).

A photograph of the wire plating line is shown below in Figure 14. The footprint dimensions are approximately 28' long x 5' wide.

Figure14 – Photograph of reel-to-reel wire plating line
(Wire travel direction is left-to-right)

The following sections provide more detailed descriptions of the components of the reel-to-reel wire plating line: drive mechanism, line cells, sump tanks, and structural scaffolding.

5.4.2 Drive Mechanism

The wire drive mechanism was designed and constructed with the ability to pull various wire sizes and types at a constant and monitored speed, with constant tension. The drive mechanism consists of two components; a wire feed device and a wire take-up device, which are shown schematically in Figures 15 and 16, respectively. A photograph of the drive mechanism is shown in Figure 17. The design is such that the take-up mechanism controls the line speed of the wire with a DC drive motor, while the feed mechanism controls the line tension with a torque motor. The torque motor has the ability to apply torque on the order of 1 Oz-in, allowing for the application of tension to the small diameter copper wire without yielding.

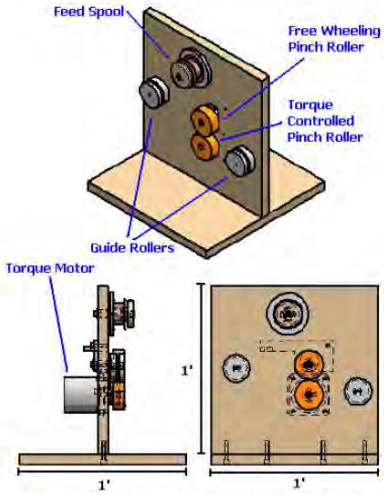

Figure 15 – Wire feed mechanism. Clockwise from top: 3-D view, front view, and side view.

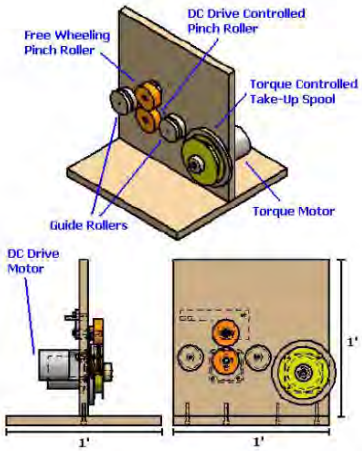

Figure 16 – Wire take-up mechanism. Clockwise from top: 3-D view, front view, and side view.

Figure 17 – Photograph of the drive mechanism showing wire feed (left) and wire take-up (right). Note: In operation, the actual spread between feed and take-up is approximately 25 ft.

Control of the entire drive mechanism is carried out on a single unit, shown in Figure 18. A digital controller is used to set the precise line speed and to monitor the length of plated wire. Analog controllers are utilized to control the torque motors on both the feed and take-up mechanisms. The torque motor on the feed mechanism controls line tension of the wire while the take-up torque motor ensures that the take-up spool is constantly in operation. Independent operation of the drive control and the take-up spool allows for a constant line speed regardless of the amount of wire on the take-up spool.

Figure 18 – Photograph of drive mechanism control unit.

5.4.3 Line Cells – Design and Design Strategy

Many wire plating techniques utilize idler rollers to direct the wire into various electrolyte baths and through other processing steps. However, as previously mentioned, the small size and low strength of the copper substrate wire places constraints on the number of "friction points" (e.g. rollers) along the plating line. A buildup in friction across the wire could cause it to break during production and, thus, friction must be kept to a minimum. In order to eliminate the need for rollers, the line cells were designed such that the wire enters and exits through narrow slits at opposite ends of each cell. This design, schematically shown in Figure 19, is similar to previous designs used to plate wire [5] and also minimizes the number of bends that the wire must make during processing, producing a straighter finished wire.

During processing, the wire passes into the cell through the slit at point A and then into solution through the slit at point B. The wire is plated (or activated/rinsed depending on the type of cell) between points B and C, until it exits solution at point C and finally exits the cell at point D. Naturally, solution will spill out of the slits at points B and C. This spill over is captured between baffles A and B (and C and D) and drained through exit ports to the sump tank via a piping system. Thus, each cell is designed to self-contain its spill over. To maintain the liquid level in the cell, each is constantly fed solution from its respective sump tank. A photograph of an activation cell showing the exit port drains between the outer baffles and the solution feed inlet positioned in the middle is shown in Figure 20.

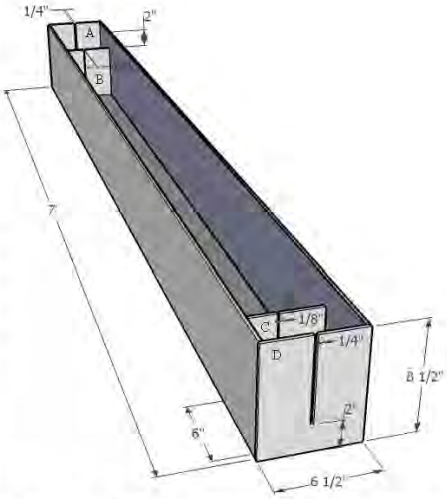

Figure 19 – Schematic of line cell, specifically, a plating cell. Activation and rinse cells are similar, but shorter in length.

Figure 20 – Top view photograph of an activation cell showing inner and outer baffles with exits ports on either end, and the inlet feed (grey) positioned in the middle.

5.4.4 Processing Steps

In order to execute the necessary processing steps for producing the NanoMetal coated wire, two size lengths of line cells were designed and constructed: activation/rinse cells with a length of 2 ft (Figure 9) and plating cells with a length of 7 ft (Figure 8). The details of the processing steps are as follows:

1. Activation Cell 1 (Volume ~ 8L) - The first processing step is a 10% *Soak 5000*™ alkaline cleaner. The solution is heated to approximately 140°F and the wire is subject to an anodic polarization utilizing mild steel cathodes on either side of the wire. Electrical contact is made through a sliding metal contact that is kept moist with a wet, lint-free sponge. This processing step cleans the wire of oil and debris to ensure complete continuity of the NanoMetal coating.
2. Rinse Cell 1 (Volume ~ 8L) - The wire is rinsed in a de-ionized water cell to remove excess alkaline solution.
3. Activation Cell 2 (Volume ~ 8L) - The wire is the subject to a room temperature activation in 7.5% Hydrochloric Acid. This step "activates" the wire by removing any oxides on the surface, ensuring a good bond between the wire and NanoMetal coating.
4. Rinse Cell 2 (Volume ~ 8L) - The wire is rinsed in a de-ionized water cell to remove excess acid solution.
5. Plating Cell 1 (Volume ~ 50L) - The wire is coated with NanoMetal in the first electroplating cell by cathodic polarization in the Co-P electrolyte utilizing titanium

anode baskets containing electrolytic-grade metal cobalt rounds on either side of the wire. The electrical contact is made in the same manner as Step 1. Operating conditions for the electroplating cell can be found in the Co-P Technical Data Sheet [6].

6. Plating Cell 2 (Volume ~ 50L) - The wire then enters the second electroplating cell whereby the same conditions as the previous cell are applied and the wire is further coated with NanoMetal.
7. Rinse Cell 3 (Volume ~ 8L) - A final de-ionized water rinse is applied to the wire.

Currently, the copper core supply wire is clean enough to by-pass the alkaline activation step without any negative impact on coating-to-substrate adhesion. However, the design retains the capability to clean the wire in an alkaline solution should the need arise.

In order to prevent the formation of a double layer coating (i.e. the formation of two independent, circumferential NanoMetal layers with an oxide barrier film in between) a "bridge" was constructed to maintain submersion of the wire between plating cells, which is shown in Figure 21. Prior to the use of the bridge, the double layer coating formed during processing (shown in Figures 22 and 23) was determined to be detrimental to the final mechanical properties of the conductor. Namely, the tensile elongation was limited to approximately 3.5 % EL at failure, with an average tensile elongation at failure of approximately 2.5 %EL. Electrical testing showed negligible differences in the electrical conductivity of wires with and without the dual-layer coating. However, the limited tensile elongation required elimination of the dual-layer coating.

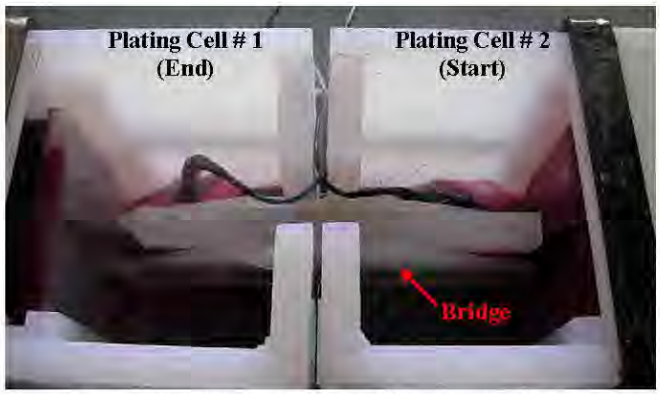

Figure 21 –Top view photograph of the "bridge" connection between plating cells.

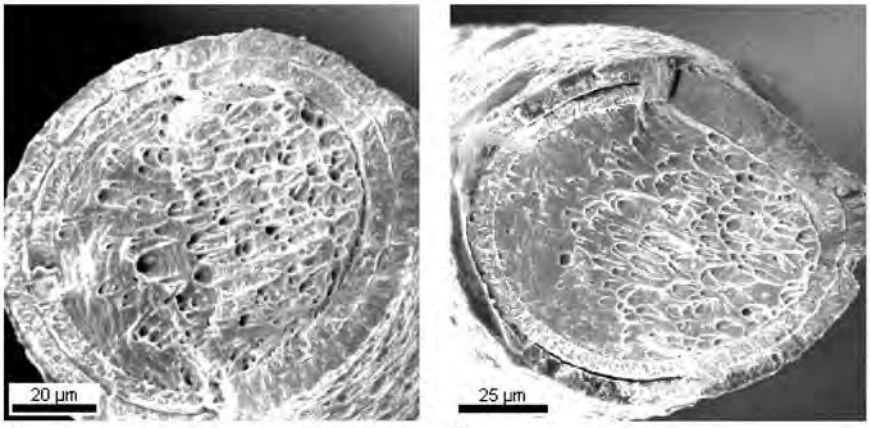

A B

Figure 22 – Scanning electron micrographs of the fracture surfaces of co-axially nanostructured wire exhibiting a double-layer NanoMetal coating encompassing the copper substrate wire. Note: Micrographs are from different fractured wires.

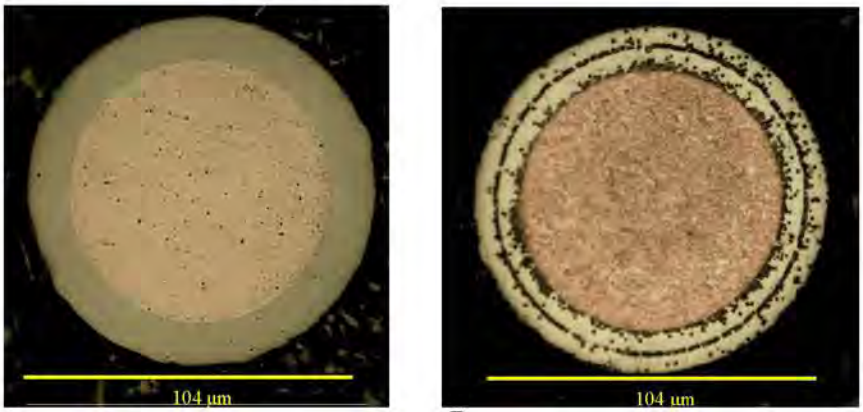

A B

Figure 23 – Optical micrographs showing the cross-sections before (A) and after (B) etching in Nitol of co-axially nanostructured wires exhibiting a dual coating layer of nCoP encompassing the copper core substrate. Note: Black spots in Fig. 7A are a result of polishing contamination and are not part of the microstructure.

5.4.4 Electrical Connections

The original locations of electrical contacts (to the wire) were placed at the beginning or end of each plating cell (e.g. beginning of Plating cell 1 and Plating Cell 2, OR beginning of Plating Cell 1 and end of Plating Cell 2). However, it was found that the current distribution across the wire was extremely non-uniform and that the majority of the coating was being applied within the first 1-2ft. (from the electrical contact) of the plating cell. This was determined by stopping both the applied current and the drive mechanism simultaneously, then removing the section of wire within the plating cell, and finally measuring the diameter along the submerged length (6 ft.) of the wire. Table 10 shows the measurements result from this analysis, which indicate that plating of the wire is only occurring within the first 24inches of submersion. This finding, however, did yield a very promising conclusion: the small diameter wire can be coated with NanoMetal at much higher plating rates than previously thought, thus allowing for a higher overall throughput.

Table 10 – Wire Diameter on Length
(When plating with a single electrical contact)

Location (Approx), inches	Diameter, µm
0 (Start)	82
6	97
12	105
18	107
24	109
30	109
36	
42	
48	
54	
60	
66	
72 (End)	109

The problem of plating only at a select area was solved by utilizing three electrical contacts across the plating cell. The current locations of the electrical contacts are: (1) at the entrance to Plating Cell # 1, (2) at the "bridge" between Plating Cell # 1 and Plating Cell #2, and (3) at the exit of Plating Cell #3. A photograph of the electrical contact at the entrance to Plating Cell #1 is shown in Figure 24. A wet, lint-free sponge is utilized on the top of the electrical contact to help maintain physical contact to the electrical connection to prevent arcing and to cool the wire.

Figure 24 – Photographs of the electrical (sliding) contact located at the entrance to Plating Cell # 1.

It is important to note that the electrical contacts located at the entrance of Plating Cell # 1 and the exit of Plating Cell # 2 are not submerged with plating solution, while the electrical contact at the "bridge" between the plating cells is submerged with plating solution. This effectively demonstrates the processing flexibility in terms of the ability to scale up to a higher-through put plating line.

5.4.6 Sump Tanks and Plumbing system.

Sump tanks and a plumbing system are required in order to maintain the solution level in each line cell. Additionally, the use of sump tanks provides a reservoir where control and monitoring of the solution temperature and chemistry can be executed without interfering with the electroplating process. A photograph of the electroplating sump tank, which feeds Plating Cells 1 and 2, is shown in Figure 25, with a description provided in the figure caption.

Figure 25 – Photograph of the electroplating sump tank showing the plumbing system. Solution is pumped from the side outlet near the bottom of the tank, through a fine particle filter column, and then fed up to the electroplating line cells above, which then drain back into the sump.

Figure 26 – Photograph of the temperature controller for the electroplating sump tank.

In total, four sumps are utilized in the wire plating line: an alkaline sump, an acid sump, an electroplating sump, and a rinse water sump (see Figure 2). Each sump tank and its respective line cell(s) utilize its own pump and plumbing system in order to maintain solution flow. To maintain and monitor the temperature of the alkaline and electroplating solutions, submerged heating elements, thermocouples, and temperature controllers are utilized. Figure 26 shows a photograph of the electroplating sump temperature controller.

5.4.7 Structural Scaffolding

A 28 ft long U-strut channel scaffold was constructed to support the line cells, drive mechanism, and control units of the reel-to-reel wire plating line. The scaffold provides a raised and level surface where the line tanks can rest, and allows for the easy mounting of the plumbing system and control units. Thus, the system is a "stand-alone" set-up requiring no additional supports such as desks or ceiling brackets and is easy to breakdown for shipping to a new location, if necessary. Additionally, the scaffold can be very easily modified to accommodate any future adjustments to the wire plating line.

5.4.8 Laser Micrometer

In order to ensure that the wire plating tool is properly operating during sample production, a method of continuous diameter measurement is required. The most effective and accurate option is to utilize a laser micrometer at the out-put end of the wire plating tool. This provides the necessary response variable for sample production, and will allow for accurate measurement of samples prior to mechanical and electrical testing.

The laser micrometer used is the Xploreline 13xy/200/B dual axis (two beam) measuring unit. Data is collected and recorded on a PC unit.

5.4.9 Spooling Unit

A proper spooling unit was necessary to produce customer samples on a properly packaged spool, allowing the customer to un-spool the sample for single strand testing or for braiding to produce a stranded conductor. Without the wire spooling unit, samples of appreciable length (>200 ft.) can not be properly packaged and will very likely incur damage or breakage during un-spooling attempts by the customer. Additionally, the wire spooling unit provides a simple and effective way to prepare customer samples of a specific length.

The spooling unit used is a the Modular Wire Takeup System (MTS), with a winding pitch modified to meet the needs of the small diameter wire (~100μm) produced in this reel-to-reel line, manufactured by Showmark Corporation

5.4.8 Production Considerations

The throughput rate of the reel-to-reel wire plating line is dependant on the line speed of the wire, which is in turn limited by the plating rate and the total submerged wire length within the electroplating cells. Currently, the wire plating line is designed to produce NanoMetal coated wire at a rate of 2-3 ft/min. However, the production rate may be increased by maximizing the plating rate and the current density applied to the wire. The implementation of these methods, however, will be limited by the current carrying capacity of the wire and the electroplating reaction kinetics.

Further improvements in the throughput rate of the wire are available by increasing the submerged line length within the plating electrolyte. This could realized by running multiple wires through the line cells with a number of independent drive systems, adding additional plating cells in series to increase the linear length of the plating area, or by simply adding additional wire plating lines that would operate in parallel. These methods

of increasing production are only limited by the amount of available footprint space and will be explored as the program progresses.

5.5 Initial Sample Production

Initial samples produced were of lengths up to 150 ft on 4 inch spools. A photograph of some preliminary samples is shown below in Figure 27. These samples were used for iterative sample development, procurement of preliminary wire data (mechanical, electrical, characterization), and to provide initial customer samples. To generate interest a customer sample kit containing various wire samples and corresponding data was produced. The sample kit communicates the value of the NanoMetal coated electrical conductor, comparing it to the current high-strength electrical conductor alloy, CS95 (Beryllium-Copper). The samples contained in the kit are 1' in length and are appropriate for interactions with customers insofar as the NanoMetal strengthening value proposition is clearly demonstrated.

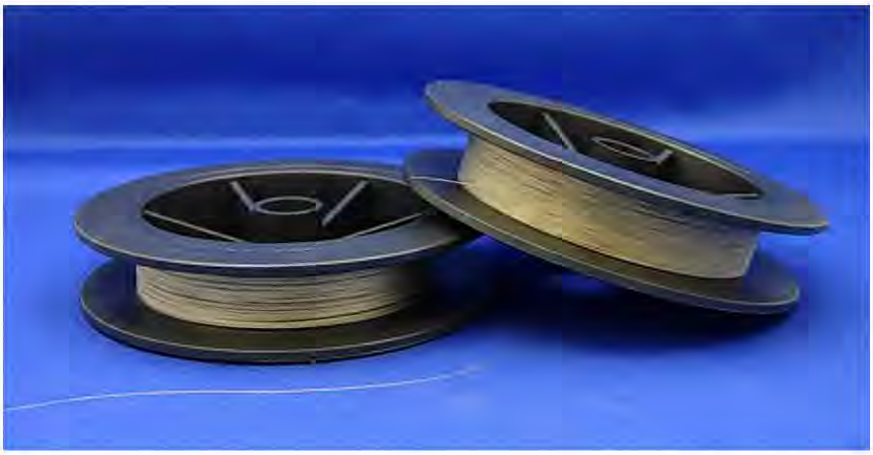

Figure 27– Photographs of some initial wire samples (44 Vol.% nCoP on OFHC Cu, d = ~107μm). Wires are packaged on 4"diameter spools (3.75" barrel).

6.0 WIRE SAMPLE CHARACTERIZATION & TESTING - METHODS

6.1 Surface Characterization and Diameter

Surface characterization of the co-axially nanostructured electrical wires was executed by scanning electron microscopy in order to observe the surface morphology of the wire samples. A JEOL – JSM 840A SEM was utilized to record images ranging from 500x – 1200x magnification.

The diameter of the wires was measured utilizing an optical microscope with bottom lighting to observe the shadow cast by the wire. Digital images were recorded and measured utilizing Image-Pro Express analysis software to determine the wire diameter. Additionally, wire diameters were measured using a hand-held digital micrometer.

6.2 Coating-Substrate Adhesion

The coating-substrate adhesion was qualified by analyzing the fracture surface of the tensile specimens. Scanning electron microscopy, utilizing the same set-up described in 2.1, was executed to examine for areas of delamination between the substrate and coating by recording images ranging from 800x – 2200x magnification.

6.3 Mechanical Testing – Tensile

Tensile testing was executed utilizing an Instron-3365 Tensile Tester fixed with Capstan-style wire grips in order to determine the tensile break strength and elongation at failure. A photograph of the wire grips mounted onto the tensile tester is shown in Figure 28. Tensile testing was carried out on individual wire strands utilizing methods described in *ANSI/NEMA WC 67: Standard for Uninsulated Conductors Used in Electrical and Electronic Applications* [1]. Further tensile testing will involve bundled 19-stranded conductor wires for final evaluation.

A B

Figure 28 – Photographs of the tensile testing set-up, utilizing capstan-style wire grips.

6.4 Electrical Testing – Resistivity/Conductivity

The electrical resistivity of the conductor was determined utilizing a 4-point probe set up with a Hewlett-Packard 6632A System DC Power Supply to provide the current and a Hewlett-Packard 34420 Nano Volt/Micro Ohm Meter to measure the voltage differential. Testing was executed on individual wire strands utilizing methods described in *FED Test Method STD. No. 228 – Method 6021* [2]. From the resistivity of the wire, the conductivity was calculated by comparing the resistivity to that of pure copper. Additionally, testing of pure copper wire was executed to verify the accuracy of the test apparatus. Further electrical testing will involve bundled 19-stranded conductor wires, tested in accordance with *ANSI/NEMA WC 67* for final evaluation.

6.5 Handling and Flexibility

The handling and flexibility of the NanoMetal-enhanced conductor was qualitatively assessed by ductility wrap testing through a modified ASTM E 290 test. In this test, the wire is wrapped around a mandrel of a known diameter and is then observed for any

surface damage (e.g. microcracking). If there is no surface damage, then the wire is given a pass for the given diameter.

7.0 WIRE SAMPLE CHARACTERIZATION & TESTING - RESULTS

7.1 Surface Characterization

Scanning electron micrographs of the co-axially nanostructured electrical wire revealed the cauliflower morphology, which is typical of electrodeposited NanoMetals. Scanning electron micrographs of the wire surface are shown in Figure 29. This surface morphology is not expected to have negative impacts on the performance of the wire as the individual "nodes" are typically less than 5 microns in diameter. However, a simple electro-polishing step could be added to the plating line to smoothen the surface if future performance evaluations indicate problems arising from the surface morphology. It should be noted that the nodular surface morphology could be advantageous for the application of organic/inorganic insulator coatings.

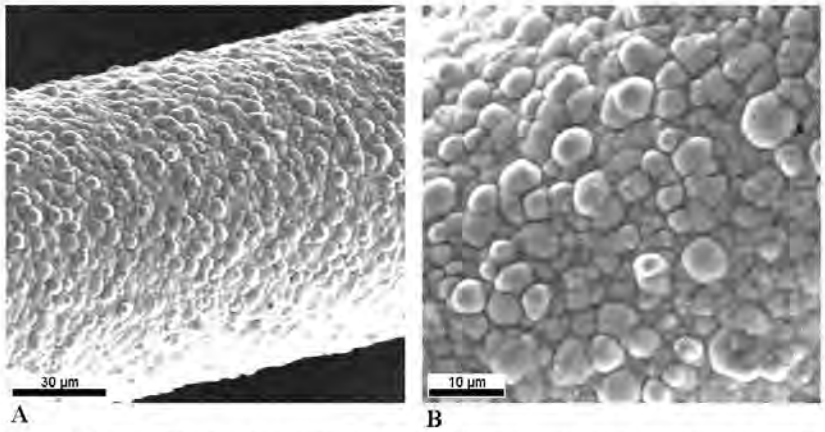

Figure 29 – Scanning electron micrographs of the co-axially nanostructured electrical wire surface at (A) 500x and (B) 1200x magnifications. The micrographs revealed the cauliflower morphology which is typical of electrodeposited NanoMetals.

Diameter measurements of the wires confirmed that the size was within the 38 gauge range of 0.0040" – 0.0043" (0.102 – 0.109 mm), with a diameter of approximately 0.0042 (0.107 mm). Processing conditions were set to target this diameter in order to achieve a NanoMetal volume fraction of 44%, the target volume fraction determined by the preliminary design calculations. The final diameter of the co-axially nanostructured wire was slightly larger than originally predicted due to the variability in diameter of the 40 gauge copper substrate wire, which can range from 0.0030" – 0.0032" (0.076-0.081 mm) and tends to be closer to the upper range with a measured diameter of 0.00315" (0.080 mm).

Diameter measurements along the length of the co-axially nanostructured wire verified the consistency of the diameter with negligible variance. Additionally, measurements by the optical microscope in conjunction with analysis software were in agreement with diameter measurements by the digital micrometer.

7.2 Coating-Substrate Adhesion

Scanning electron micrographs of the wire fracture surface, fracture by uniaxial tension, showed good adhesion between the NanoMetal coating and the copper substrate. Figure 30 shows scanning electron micrographs of fractured wire surfaces revealing good adhesion and no delamination.

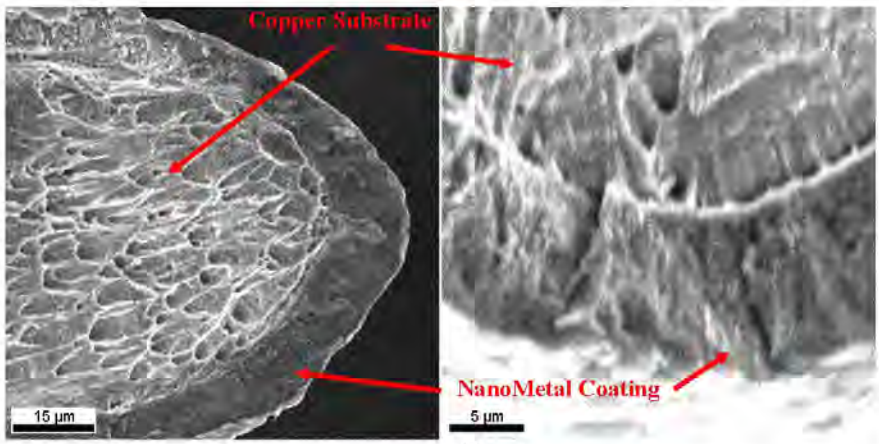

Figure 30 – Scanning electron micrographs of the fracture surfaces of co-axially nanostructured electrical wires at 800x (A) and 2200x (B) magnifications.

7.3 Mechanical Testing – Uniaxial Tensile to Failure

Tensile testing results were in relatively close agreement with the properties predicted in Technology Development Report – Task T1. Table 1 shows the predicted conductor properties in comparison with the actual properties, as well as those of the competing high-strength beryllium-copper alloy CS95.

From Table 1 it can be seen that the tensile strength of the co-axially nanostructured electrical wire exceeds that of the CS95 alloy by approximately 1.4-1.5x. However, the tensile strength failed to meet the criteria set forth by MPI-1 (tensile strength $\geq$ 1025 MPa) by approximately 7%. The tensile elongation exceeded the criteria set by MPI-3.

Table 11 – Tensile Properties

Material	Tensile Strength Mpa (ksi)	Elongation at Failure %EL
NanoMetal Enhanced Conductor - Predicted	1072 (155)	6.0
NanoMetal Enhanced Conductor - Actual	950 (138)	7-8
CS95 - Beryllium-Copper Alloy [3]	655 (95)	6.0
Bare OFHC Cu Wire	300 (44)	10-12

Stress-strain curves obtained from the uniaxial tensile testing of the NanoMetal-enhanced conductor and the bare OFHC copper core are shown below in Figure 31. It can be seen that applying the NanoMetal to the copper core yields an overall strength increase of approximately 320%.

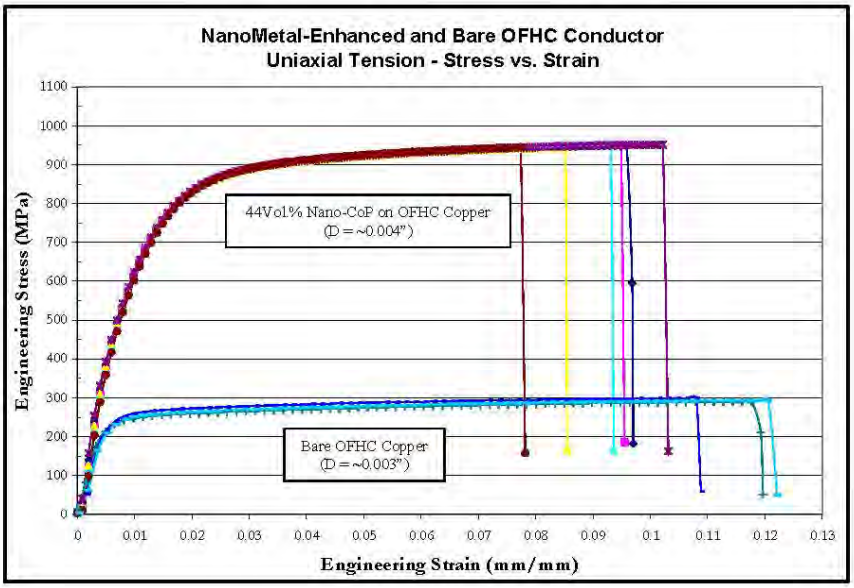

Figure 31– Stress-strain curves obtained from uniaxial tensile testing of the coaxially nanostructured electrical wire and the bare OFHC copper core substrate.

From the stress-strain curves the yield strength of the wire was determined to be approximately 525-550 MPa (76-80 ksi), by the 0.2% off-set method. The yield strength of the co-axially nanostructured wire is greater than 8x the yield strength of the copper conductor material (~65 MPa). The significantly enhanced yield strength indicates that the co-axially nanostructured electrical wire will exhibit notable improvements in fatigue resistance compared to both copper and CS95 conductor wire.

It is also important to note that the ductility of the nano-CoP coated wire is not significantly decreased from the original ductility of the core OFHC copper substrate, indicating that the NanoMetal has good ductility. Scanning electron micrographs of fracture surfaces of the NanoMetal-enhanced conductor are shown in Figure 32. A significant reduction in area can be observed indicating that the conductor material

exhibits good ductility. Furthermore, in some cases, the wire exhibited a ductility of greater than 10 %EL at failure, while still maintaining a tensile strength of 950 MPa. This further reinforces the fact that the wires can exhibit relatively high ductility.

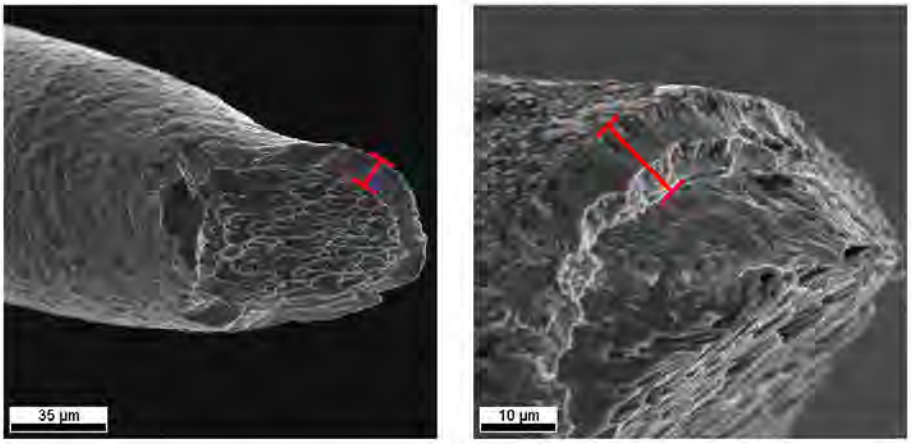

A B

Figure 32 – Scanning electron micrographs of showing fractures surfaces of the NanoMetal-enhanced conductor from uniaxial tensile testing at magnifications of (A) 400x and (B) 1100x. A significant reduction in area can be observed indicating that the NanoMetal-enhanced conductor exhibits good ductility. Red lines mark the NanoMetal coating.

The tensile properties along the length of the produced wire were relatively consistent, with a few exceptions. In some cases, wire samples exhibited a limited ductility of less than 6% EL. The exact mechanism of the limited ductility may vary depending on the sample (i.e. there could be more than one cause that leads to limited ductility). It is believed that the limited ductility could be a result of one or more of the following: damage (kinks) to the core conductor prior to plating, damage to the sample after processing but prior to testing, improper samples testing (i.e. not uniaxial tension), and/or poor substrate-to-coating adhesion.

7.4 Electrical Testing – Resistivity/Conductivity

Results of the electrical testing determined the conductivity of the co-axially nanostructured electrical wire to be in close agreement with the properties predicted in Technology Development Report – Task T1. Table 2 summarizes the predicted and actual electrical properties of the wire, as well as those of the competing CS95 alloy. The electrical conductivity of the co-axially nanostructured wire met the criteria set by MPI-3, an electrical conductivity of $\geq$ 57 %IACS.

Table 12 – Electrical Properties

Material	Resistivity μΩ-cm	Conductivity %IACS
NanoMetal Enhanced Conductor - Predicted	2.90	59
NanoMetal Enhanced Conductor - Actual	2.90-2.95	58-59
CS95 - Beryllium-Copper Alloy	2.71	63

7.5 Handling and Flexibility

The handling and flexibility assessment of the NanoMetal-enhanced conductor showed promising results. Scanning electron micrographs of the undamaged surface of the wire in the ductility wrap testing are shown in Figure 33. The diameter of this mandrel is 0.024" which corresponds to a wrap ductility of 14% [Wrap Ductility = (Wire Diameter) / (Wire Diameter + Mandrel Diameter) * 100]. This is a promising result in terms of the ability of the wire to be processed into a stranded conductor and to be flexed, bent, properly handled, and crimped in service.

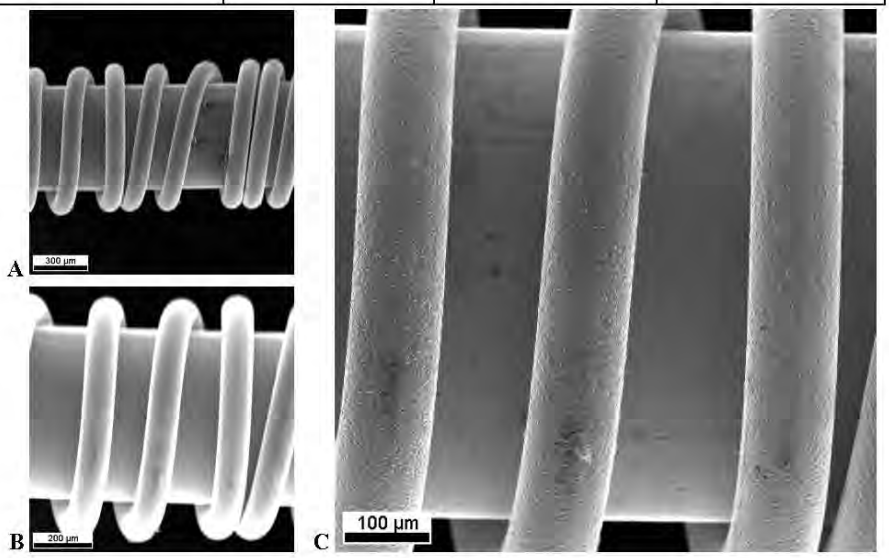

Figure 33 – Scanning electron micrographs of the NanoMetal-enhanced conductor wrapped about a mandrel of 0.024"in diameter at magnifications of (A) 43x, (B) 70x, and (C) 100x. The absence of surface damage can be observed, indicating a "Pass" for a mandrel of this diameter.

8.0 PITTSBURGH BASED TECHNOLOGY AND MARKETING CENTER

Design and development of the reel-to-reel wire plating line was conducted at Integran Technologies in Toronto, ON, Canada. The line has recently been relocated and reconstructed in the new Pittsburgh Based facility located at 2580 Smallman St., Pittsburgh, PA 15222. Installation of a ventilation system and safety equipment (e.g. eye wash, spill control kit) has been completed. The reel-to-reel plating line is operational. A photograph of the wire line at the Pittsburgh based location is shown in Figure 34.

Figure 34 – Photograph of the reel-to-reel wire plating line in the new Pittsburgh facility.

9.0 FINAL REMARKS

The reel-to-reel continuous wire plating tool is in operation and production of the 38 gauge co-axially nanostructured electrical wire is underway. Preliminary product data shows promising results with actual properties that exceed MPIs 2 and 3 and a tensile strength that nearly meets MPI 1. A summary of the preliminary product data in comparison with the MPIs and the properties of competing high-strength conductor CS95 are shown below in Table 4.

Table 4 – Summary of Preliminary Product Data

Material	Tensile Strength MPa (ksi)	Ductility %EL	Conductivity %IACS
Materials Performance Indices - Targets	1025 (149)	6.0	56
NanoMetal Enhanced Conductor - Actual	950 (138)	7-8	58-59
CS95 - Beryllium-Copper Alloy	655 (95)	6.0	63

The preliminary product data indicates that the co-axially nanostructured electrical wire has good potential to ultimately provide a conductor material that can be utilized to realize weight savings in the electrical wiring systems of aircraft. Additionally, the wire design may be modified to meet various product requirements by altering the substrate or coating materials and by varying the NanoMetal-to-substrate material volume ratio.

REFERENCES

[1] National Electrical Manufacturers Association, *ANSI/NEMA WC 67: Standard for Uninsulated Conductors Used in Electrical and Electronic Applications*, Rosslyn, Virginia (2005)

[2] Federal Test Method Standard No. 228 (1967)

[3] Fisk, E., *Developments in Alloy Conductors*, Wire and Cable Technology International, (2003)

Appendix D – 07-009 (Plextronics, Inc)

Fabrication of Flexible Organic Photovoltaic Devices *via* Semi-Continuous Processing

Contract Number: Nano-07-009

June 8th 2009

Table of Contents

Executive Summary

The Pennsylvania NanoMaterials Commercialization Center along with Plextronics Inc. has come together in a yearlong project to investigate and make semi-continuous processed organic photovoltaic devices. The project was broken up into 5 milestones each consisting of a commercial development portion, involving key business planning areas such as cost analysis of flexible vs. rigid, market opportunity, market entry points, and VOC, and technical deliverables related to materials, equipment, optimization, and device performance. This work has lead to an understanding of the current and potential future markets for organic photovoltaic devices constructed on flexible substrates and has demonstrated the feasibility of manufacturing such devices. This report will outline Plextronics' technical accomplishments, from the screening of potential substrates through the construction of devices, and review their commercial findings.

Technology Development

Summary

The technical development began with the proposal of a semi-continuous process to make flexible organic photovoltaic (OPV) devices. Substrate candidates were screened for compatibility with the proposed process along with Plexcore® PV ink systems. Initial concerns about the efficacy of flexible substrates were quelled by making small area devices on Polyethylene terephthalate (PET) by spin coating the organic layers. Parallel efforts focused on obtaining uniform films of the desired thickness on the Mini-Labo Microgravure™ coater. With the proper mesh gravure roller and optimizing the coating parameters both the hole transport layer (HTL) and photoactive layers could be made reproducibly in a roll to roll manner. The device architecture involved a couple different patterns of indium tin oxide (ITO), one to optimize the chance of getting a working diode (3mm tab) and the other to drive up efficiency (2mm stripe). Both designs made functioning organic solar cells. The substrates were purchased in rolls with our substrate design already formed with the ITO. Onsite we coated both the HTL and photoactive inks in a roll to roll manner before cutting the substrates out for the final stages of processing. Annealing, laser ablation (depending on substrate) and cathode deposition were carried out in a nitrogen glove box. With a more efficient design and tighter tolerances the 2mm stripe design required laser ablation of the organic layers from certain areas of the ITO. The champion device had an active area efficiency of 0.98% and area of 93.5 cm^2, well above the goal of 50 cm^2

Milestone 1

Tasks for Milestone 1

Sign development contract documentation on 05/27/2008, Plextronics invoices $50,000.

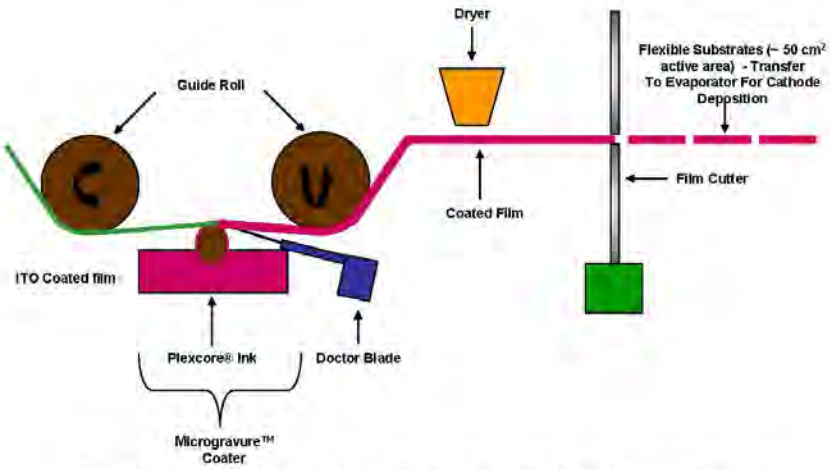

Figure 1. Plextronics' proposed semi-continuous processing using gravure coater

Milestone 2

Tasks for Milestone 2

1. Define initial materials specifications for flexible OPV devices.
2. Develop Laboratory scale flexible OPV devices.
3. Initiate development of Roll-to-roll (R2R) OPV process.

Deliverables for Milestone 2

1. Update report on materials screening and performance specifications for prototype flexible OPV device.
2. Report on development and testing of prototype of flexible laboratory scale OPV device.
3. Secure, install and make operational the Microgravure™ coater to be used in the R2R OPV fabrication process.

In order to enable rapid evaluation of OPV performance on flexible substrates, polyethylene terephthalate (PET) was chosen as the substrate. PET is readily available and, when supplied as heat-treated, it is able to withstand reasonable annealing temperatures. Additionally, there are commercial sources of PET with custom-patterned ITO so we were able to obtain suitable substrates to make OPV devices. Other flexible polymeric films such as polyethylene naphthalate (PEN), polyimide (PI) and polycarbonate (PC), were considered as substrate material.

For the active layer ink our initial tests were run with our Plexcore® PV 1000 and Plexcore® PV 2000 ink kits. These inks have a proven track record for performance, shelf life, and consistency. Other active layer material evaluated was the Plexcore® PV 1100 ink kit which utilizes less aggressive solvents which are more appropriate for a manufacturing process due to EH&S issues with o-dichlorobenzene.

For device fabrication ITO-patterned PET was cut to 2"x2" squares to match our current design on glass and was then cleaned by sonication for 20 minutes each in an optical soap, DI water, and finally isopropyl alcohol (IPA). The flexible substrates were attached to glass substrates with double sided tape or a reversible adhesive which provides a platform for fabrication in our current equipment. Before spinning the HTL the PET films were UV ozone treated for 10 minutes to clean / treat the surface. The HTL was spun in air and then annealed in the nitrogen atmosphere of a glove box for 15 minutes at 120°C (see Table 1). Next, the active layer was spin coated onto the substrates and also annealed in the glove box for 15 minutes at 120°C. The cathode was then deposited by thermal vapor deposition. Encapsulation was achieved via a UV cure epoxy and a glass microscope slide.

Table 1: Spin conditions

Film	Spread	Spin	Anneal
HTL	3 sec @ 350 RPM	1 min @ 500-1500 RPM (depending on formulations)	120 °C for 15 minutes
Active Layer	3 sec @ 350 RPM	1 min @ 400 RPM	120 °C for 15 minutes

Testing was done with both forward and reverse bias to show a functioning diode (see Figure 2). Table 2 contains the results of an OPV device made on the PET substrates. These results are representative of other devices made in the same manner and clearly show our technology is capable of a 2% efficient flexible OPV device.

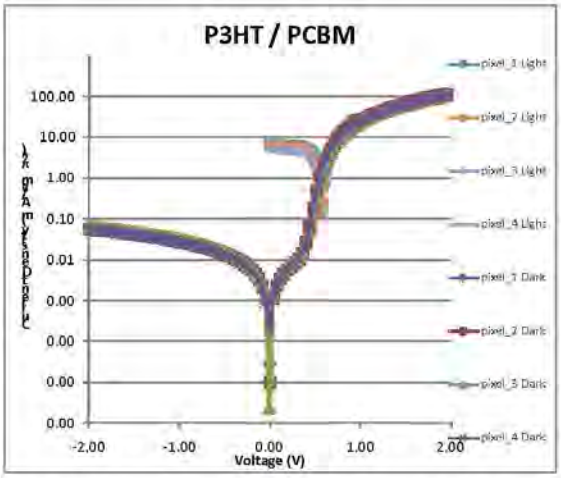

Figure 2 OPV cells on PET substrate using P3HT/PCBM active layer

Table 2: Flexible OPV Device – Performance Metrics

Pixel	Jsc	Voc	FF	E(%)
1	6.27	0.58	0.55	**2.00**
2	6.13	0.57	0.54	**1.88**
3	5.43	0.58	0.54	**1.70**
4	6.77	0.57	0.54	**2.07**

The lab space for the Microgravure unit was secured and the electrical and ventilation installed. The Microgravure unit was to be set up and operational by the end of this milestone however there was a "hiccup in vendor's ordering / follow-through process." The Microgravure was installed and operational by the end of September.

Milestone 3

Tasks for Milestone 3

1. Continued screening/development of materials for flexible OPV devices.
2. Continued development of laboratory scale flexible OPV devices.
3. Develop Microgravure™ coating process for organic materials.

Deliverables for Milestone 3

1. Update report on materials screening and performance specifications for prototype flexible OPV device.
2. Report on development and testing of improved prototype of flexible laboratory-scale OPV device.
3. Demonstrate R2R coating process for organic materials.

The Mini-labo instrument is on site and fitted with the proper engineering controls. Shown below in Figure 3 on a bench top, actual coating was done with the instrument placed in a fume hood.

Figure 3 Mini-Labo Microgravure unit

Using literature data and in-house screening methods it was decided that PET was the best substrate for this project Table 3. PET has been proven effective in roll to roll processing, is available with our ITO pattern at a reasonable price, has high transparency, and is chemically and thermally compatible with our processing.

Table 3 Substrate screening metrics

		literature data			Plextronics data						Hll wetting		contact angle	
					Thermal stability**				chemical compatibility*		MeOH wipe	MeOH wipe + 1 min UV ozone	MeOH wipe	MeOH wipe + 1 min UV ozone
Substrate material	Trade name	Elongation at break MD (%)	Tensile strength MD (psi)	Glass Transition (°C)	100 °C	140 °C	160 °C	180 °C	DIC	Toluene	treated / front	treated / front	treated / front	treated / front
PET	Melinex 504	180	26000		ok	slight deformation	bends easily	bends easily; cloudy	ok	ok	ok	ok	90?	9.1
PET	Melinex 454	150	28000		ok	slight deformation	slight deformation; cloudy	slight deformation; cloudy	ok	ok	ok	ok	36.6	12
PET	Melinex ST504				ok	ok	cloudy	bends; cloudy	ok	ok	ok	ok	38.6	na
Unfilled PEN	Teonex Q65	60	31900	120	ok	ok	ok	ok	ok	ok	ok	ok	<10	<10
PET	from Sheldahl				ok	ok	ok	ok	ok	ok	ok	ok	37.2	<10

Our PV 1000 and PV 2000 ink kits that produce ~3.5% and 5.0% efficiency on glass respectively were the main inks for this test. Although the PV 1000 and 2000 contain halogenated solvents that is not an issue for this small scale testing. Non halogenated inks may also be screened as they become available.

The film thickness of these thin organic films cannot be measured on PET substrates with our profilometer or elipsometer. The substrate is too soft to scratch only the organic for the step height analysis of the profilometer and PET poses reflectance problems for the elipsometer. To verify our film thickness we initially used the spectral absorbance of our inks on glass with films of known thickness, and then correlated the UV-vis absorption at a specific wavelength to the film thickness. This enabled us to get a rough idea of the film thickness on PET. Later in the project a Filmetrics spectral reflectance instrument was used to determine organic film thickness. Figure 4 depicts the absorbance profile and measured thickness of the films on glass. Figure 5 depicts the adjustability the Microgravure coater has based on these absorbance calculated thicknesses.

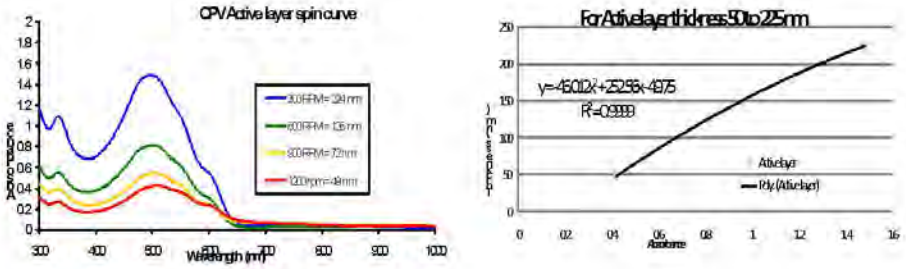

Figure 4 Photoactive layer absorbance on glass (left) and measured thickness (right).

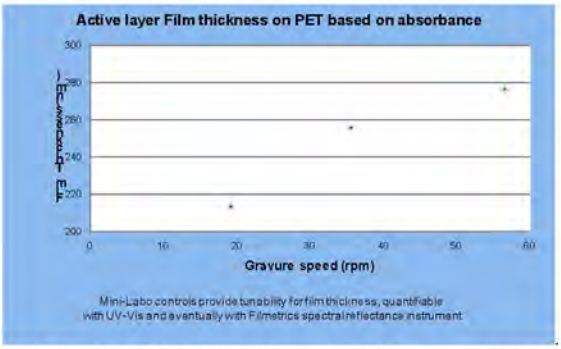

Figure 5 Film thickness can be controlled by gravure speed

Typically spun films have an R_q in the single digits as measured by AFM. The Microgravure coated film in Figure 6 is not much rougher than a typical spun film.

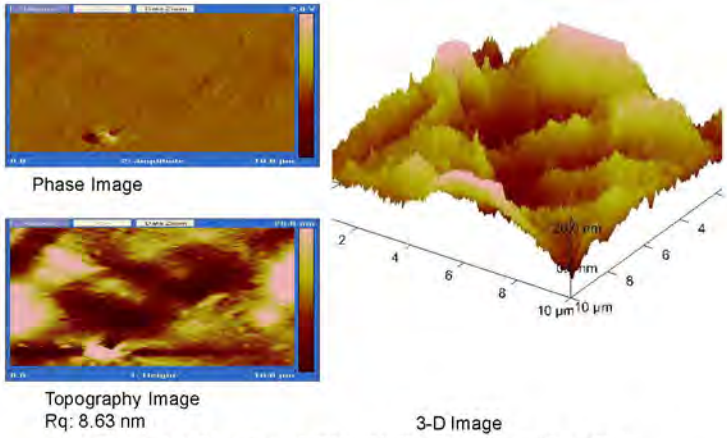

Figure 6 AFM images of P3HT/PCBM photoactive ink on PET

Using Gen 1.5 ITO pattern on PET device efficiencies for PV 1000 and PV 2000 were ~ 2 and ~3% respectively. The organic layers were spun on the PET and the devices were processed just as rigid substrates.

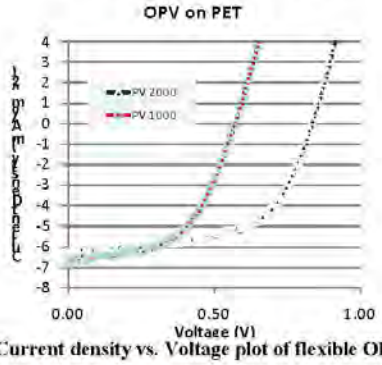

Figure 7 Current density vs. Voltage plot of flexible OPV device.

Table 4 Key solar cell metrics for lab cell device

Champion Device Performance		
	PV 1000	PV 2000
Jsc	6.77 mA/cm²	6.25 mA/cm²
Voc	0.57 V	0.84 V
FF	0.54	0.58
Efficiency	2.07%	3.07 %
Pmax	0.19	0.28

For making an OPV device with a stripe design, a laser is required to remove the organics from specific areas of the stripe design ITO pattern to optimize efficiency. While ITO is resistant to the 248 nm eximer laser the PET substrates are not impervious. Laser testing was conducted to define laser parameters required for removing organics without harming the ITO on the PET substrates. Many laser controls are available to adjust such as: voltage, hertz, aperture size, # of attenuators, # of passes, and speed.

Milestone 4

Tasks for Milestone 4

1. Define materials specifications for prototype flexible OPV device.
2. Continued development of laboratory scale flexible OPV devices.
3. Develop process optimization for large area flexible OPV processing.

Deliverables for Milestone 4

1. Final report on materials, process and performance specifications for prototype flexible OPV device.
2. Report on development and testing of improved prototype of flexible laboratory-scale OPV device.
3. Report on optimized process for large area flexible OPV processing.

Technical Milestones

- **Define materials specifications for prototype flexible OPV device.**

In order to enable rapid evaluation of OPV performance on flexible substrates, polyethylene terephthalate (PET) was chosen as the substrate. There are commercial sources of custom patterned ITO on PET so we were able to obtain suitable substrates to evaluate performance on flexible substrate via spin coating of the organic layers. PET film is compatible with the process we intend to employ, the thermal conditions required, and the inks that the substrate will be exposed. Internal testing also proved that the wetting properties of the inks on the film will be acceptable. The specific film chosen is Melinex ST504; a clear, high gloss, heat stabilized, roll of film that is 7 mil thick. It is provided with 60 Ohms/Sq patterned ITO and a protective film on both sides of the substrate. This was the lowest resistivity flexible substrate available off-the-shelf. Internal testing confirmed the resistivity of the ITO.

For the active layer ink our initial tests were run with poly 3-hexylthiophene/[6,6] phenyl C_{61} butyric acid methyl ester (P3HT/PCBM) in o-dichlorobenzene. This ink along with our aqueous based HTL ink comprises our PV1000 ink kit. These inks have a proven track record for performance, shelf life, and consistency. Other active layer materials to be evaluated will be the PV2000 ink kit which is a blend of proprietary p/n – type semiconductors enabling high efficiency. Our testing has also concluded that Microgravure coated films of uniform thickness can be made reproducibly and within our targeted thickness range.

- **Continued development of laboratory scale flexible OPV devices.**

For device fabrication, the ITO-patterned PET was processed as described in previous milestones. Improvements in performance have been gained by adjusting the annealing conditions and improvements in handling the substrates. Figure 8 highlights the improvements in performance since the previous milestone. Table 5 shows the solar device metrics typically used to characterize performance.

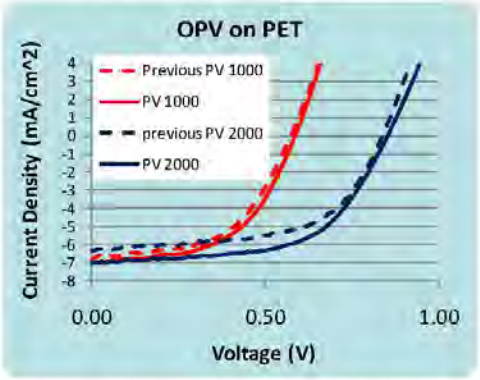

Figure 8 Current density vs. Voltage plot of flexible OPV device.

Table 5 Key solar cell metrics for lab scale flexible prototype.

Champion Device Performance		
	PV 1000	PV 2000
Jsc	8.09 mA/cm^2	6.98 mA/cm^2
Voc	0.60 V	0.85 V
FF	0.45	0.58
Efficiency	2. 17%	3.47 %
Pmax	0.20	0.31

- **Develop process optimization for large area flexible OPV processing.**

The Filmetrics thin film measurement system arrived has the ability to measure thin films on the flexible PET substrate. In-house techniques such as profilometry and elipsometer proved incapable of reliable results. The Filmetrics tool uses spectral reflectance to determine film thickness. It is non destructive, quick, and relatively easy once set up.

Using the Microgravure we were able to make films with uniformity similar to spin coating. This uniformity was achieved by adjusting the speed of the web, the speed of the gravure, tension on the film, and annealing conditions such as fan speed and temperature. Knowing the final concentrations of our inks let us choose a gravure mesh that would get make films of the desired thickness. The ratio of the gravure and web speed also gives minor adjustability in film thickness. Using the Filmetrics and the Microgravure film thickness could be measured and predictably controlled in our targeted range.

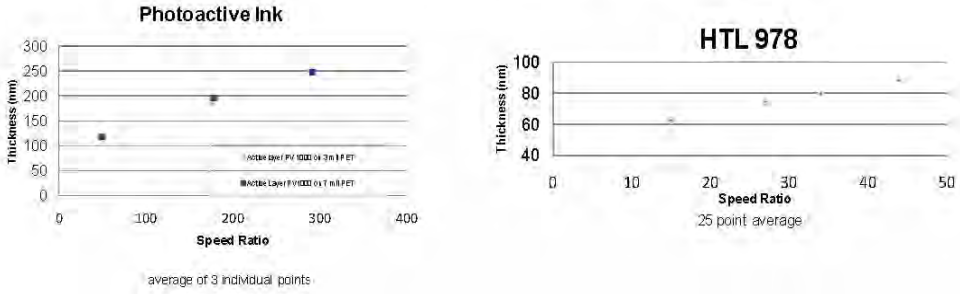

Figure 9 Thickness vs. speed ratio of the photoactive (left) and HTL (right) inks as measured with the Filmetrics system.

Annealing is a key parameter for device performance specifically with the photoactive inks. A designed experiment was set up look at the time and temperature of both the HIL and the active layer anneal steps. The HTL performed as expected at reduced times at 150°C and experienced only minor dips in JSC at 100°C. The Photoactive ink saw more of a hit specifically in fill factor at reduced temperatures, Figure 10.

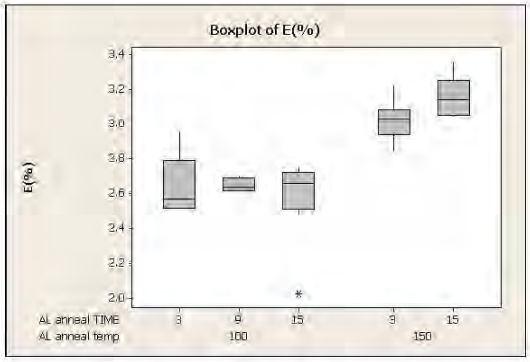

Figure 10 Lower annealing temperatures of the photoactive ink have an adverse effect on efficiency

For the large area substrates it was decided to use several patterns to optimize the chance of success in the project. Substrates with tabs were designed to not require laser ablation. It is difficult to ablate the organic layers without damaging the ITO underneath, specifically because the PET is more susceptible to laser damage than standard glass substrates. Laser ablation of the organic layers enables a more efficient device architecture. All of the substrates have an active area greater than 50 cm^2 which is required for Milestone 5.

Figure 11 Each of the 8 patterns is a substrate design (some are duplicates).

Milestone 5

Tasks for Milestone 5

1. Produce large area (~50 cm2) large area R2R prototype OPV device.
2. Evaluate large area (~50 cm2) large area R2R prototype OPV device.

Deliverables for Milestone 5

1. Demonstration and evaluation of large area prototype device *via* semi continuous R2R process.
2. Final Report.

Two major ITO patterns were made to optimize success for this project. The 3 mm tab design has loose tolerances to make alignment easy and does not require any laser ablation. Although this design is almost certain to produce a photovoltaic cell, the design is not geared towards a highly efficient OPV device. The best performance with this design was 0.13% (active area). The 2 mm stripe design has much tighter tolerances and requires laser ablation of the organic layers, but is more architecturally sound. The best efficiency with the 2 mm stripe design was 0.98% E (active area).

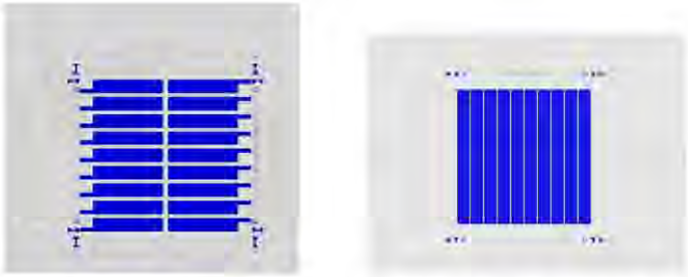

Figure 12 The 3 mm tab substrate with active area of 95.4 sq cm (left), and the 2mm stripe design with active area of 93.5 sq.cm (right).

These large area PET substrates were coated on the Mini-Labo Microgravure first with the HTL. The film was then rewound and coated with the Active layer. The substrates were then cut to size and annealed in the glovebox on a hotplate @ 120°C for 15 minutes (in some cases additional annealing was done just before deposition of the cathode). The 3mm tab design was then placed in the evaporator for cathode deposition, leads cleaned, and then tested. The 2 mm strip requires laser ablation of the organic layers from a section of the ITO prior to cathode deposition. It is imperative that the laser does not harm the ITO and is in the proper location

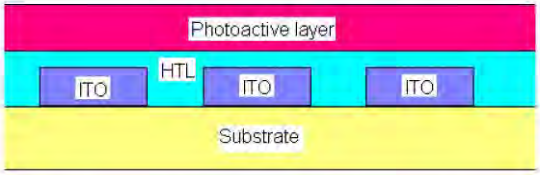

Figure 13 Cross section of device prior to laser ablation

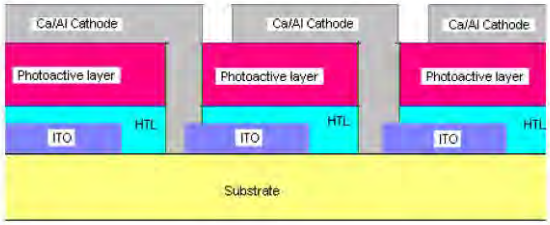

Figure 14 Proper cathode placement after laser ablation of organic layers

The major challenges of the stripe design are the alignment of the laser, alignment of the cathode, and laser power. If the laser is too strong it will damage the ITO and increase the resistance, or even short out the device. If the laser does not remove all of the organic layers the cathode will not contact the ITO. To accommodate variances in the film thickness and laser power, resistance testing was done on a test substrate prior to laser ablation of the actual device.

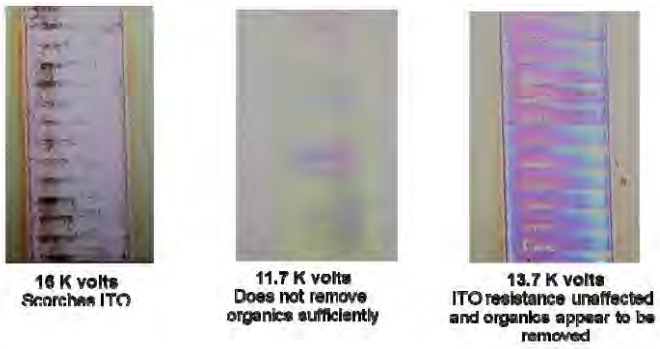

Figure 15 50x microscope view of laser ablation at 175 Hz, stage motion 20 mm/sec, 2 passes, and 2 attenuators.

With successful alignment and laser ablation the 2mm stripe design did boost the efficiency.

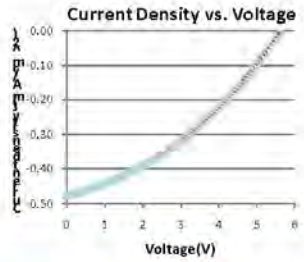

Champion Device Performance	
Jsc	0.48 mA/cm²
Voc	5.66 V
FF	0.36
Active area Efficiency	0.98%
Pmax	90.67

Substrate	0.007" PET with 60 Ohm/sq ITO 93.5 cm²
HTL	~ 50 nm of Plexcore PV 1000 HTL
Active layer	~ 200 nm of Plexcore PV 1000 photoactive ink
Cathode	10 nm Ca/200 nm Al

Figure 16 Champion device performance and conditions via semi R2R processing conditions

Summary

PV 1000 ink kit, both HTL and photoactive ink, coupled with ITO patterned PET was successfully coated on the Microgravure. These films were then cut and transferred to a glove box for annealing and laser ablation (depending on the design) a second anneal can be performed just before placement in the evaporator for cathode deposition. After Ca/Al cathode deposition the devices were tested immediately upon removal from the glove box because of lack of encapsulation. Active area efficiency of 0.98% was achieved on a 93.5 sq. cm ITO patterned device via semi-continuous roll-to-roll processing.

Commercialization

Summary

Flexible OPV presents a number of unique features that have the possibility of opening unique market opportunities that would not be possible to achieve utilizing a rigid substrate. The key to market success with OPV is to identify those applications for which OPV's value proposition aligns with the needs of the customer. This work has identified market opportunities, qualified which of those opportunities represented possible markets for entry for OPV technology, and gathered customer feedback to identify the key decision metrics and identify product opportunities.

Initial investigations ranked a number of possible markets on the basis of market size and growth potential. Individual markets were then systematically ranked based on the alignment of their needs with OPV's performance. From this, Consumer Power and Consumer Indoor markets were found to be the best fit for the near term performance levels. This analysis indicates that performance must be improved to serve the larger on grid markets, but that there are also a number of smaller markets that can be served in the interim period, providing a roadmap that shows a natural progression from off-grid to on-grid applications.

Next, a detailed investigation of the manufactured cost was performed to quantify the advantages of flexible OPV. This analysis showed that the cost of flexible modules is dominated by materials costs and that, currently, those materials are too high to be competitive for on-grid applications. This result agrees with the ranking performed previously, but also gives insight to what would be needed to create cost competitive flexible OPV. It was found that substrates and encapsulation materials that provide the necessary barrier properties are simply too expensive and would need to realize significant cost reductions to enable OPV to be a truly game changing technology.

Recognizing that the current cost structure excluded on-grid applications, the final step was to find alignment between potential markets and OPV's near term expected performance to identify potential entry markets for this technology. Through customer interactions, Plextronics identified the driving needs for consumer battery charging applications, powering electrophoretic/electrochromic display applications, powering various military applications, driving educational applications, and thin film battery charging applications. From these, the emerging technology around electrophoretic and electrochromic displays was quickly found to align with the strengths of OPV. Similarly the charging of thin film batteries was found to be a good fit. In both these cases, the weight savings afforded by the flexible form factor as well as the flexibility itself meshed well with the envisioned applications for these technologies.

Overall, Plextronics' analysis showed that for near term applications, those markets that value the unique properties of a flexible OPV device, i.e. the weight savings and flexibility, would be

accepting of OPV technology whereas those applications that are more cost driven would gravitate to rigid designs because of its lower cost.

Milestone 2

Tasks for Deliverable 2

- Perform market opportunity analysis to define key materials and efficiency requirements for flexible OPV processing.

Deliverables for Milestone 2

- Report on market opportunity analysis.

Plextronics has identified a number of markets for flexible OPV products and has performed an initial ranking as to which of those markets are most attractive. Initial analysis shows that flexible OPV does not yet have the performance to compete in on-grid applications as these tend to have rigorous performance demands. The intent of this exercise is to identify those applications that better align with OPVs near term performance levels. Table 6 gives descriptions of the major off-grid market segments that have been investigated.

Table 6 Off-grid market descriptions

Category	Application Segments	Market Description
Remote Industrial	• Communications & Telemetry • Cathodic Protection • Transportation Signals • SCADA (Supervisory Control and Data Acquisition) • Homeland defense	• Requires a high degree of reliability • Buyer is PV-knowledgeable • Requires less product support • Typically power modules >75 watts, though can use lower wattage module for some mobile applications
Remote Habitation	• Water Pumping • Village Power • Outdoor Lighting • Other miscellaneous applications	• Competitive with other renewables • Buyer is PV-knowledgeable in industrialized countries, but not in developing countries • Large market in developing countries • Requires high reliability/product support • Typically power modules 50 watts to 75 watts, growing market for 100-watt modules
Consumer Power	• Recreational • Automotive, etc.	• Buyer PV-knowledgeable • Industrialized countries • Niche market • Requires little product support • Independence is a key driver • Smaller modules, <70 watts
Grid-Connected	• Residential • Commercial • Utility (Distribution and Central)	• Considered too expensive • Long lifetime required • Growing in industrialized countries • Potential utility fit for concentrators • Power modules >124 watts
Consumer Indoor	• Consumer and Novelty Items	• Saturated market • Broad base • Reliability not required • Low margin • Products have short life

As a first screening of these markets, they were assessed for their potential market growth and the existing market size. The results are plotted in Figure 17.

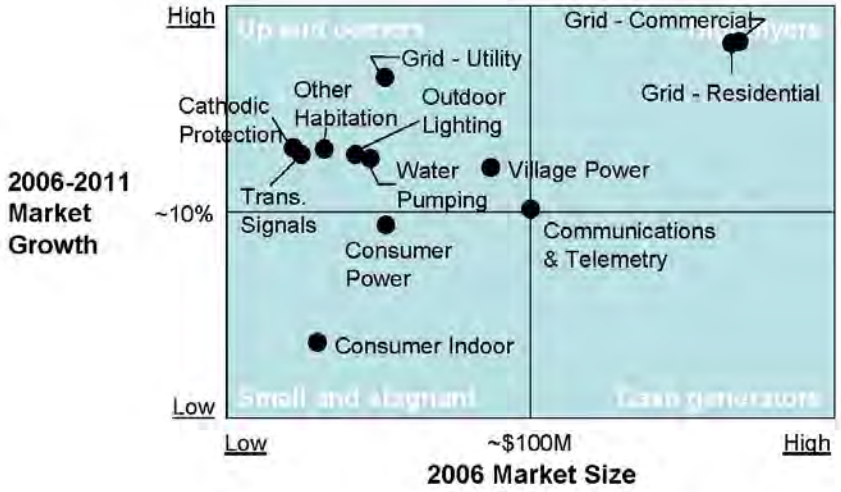

Figure 17 Market attractiveness of various off-grid market segments

From this we can see that the on-grid application represent large markets with large growth potentials and represent the longer term gal for OPV technology. For this analysis a method of ranking the many market segments that are currently small, but have large growth potential as those represent the potential for OPV to capture large market share. A number of criteria were chosen on which to rank the different markets, the definitions of which are given in Table 7.

Table 7 Definitions of market ranking criteria

Key Filters	Description
Market Attractiveness	A measure of the size and growth rate of the application segment
Efficiency	A measure of the required power density; important for space-constrained applications
Lifetime	The required MTBF for the application segment; typically quantified by T_{80}
Weight	The importance of a light-weight product for the application segment
Durability	The importance of product ruggedness for the application segment
Flexibility	The importance of product ruggedness for the application segment

The different criteria were each assigned a weight and each market segment was ranked, with a total score derived by multiplying the ranking by the weight for that category. The results of this ranking are shown in Table 8. From this Consumer power application and Consumer indoor applications are found to be the best fits with OPV. The on-grid markets rank highly, due mostly to large market size. Additionally remote transportation signaling was an unexpected application with which OPV was fairly well aligned.

Table 8 Market ranking results

Segment	Market	Efficiency	Lifetime	Power	Weight	Flexibility	Scaled Score	Comments
Communications and Telemetry							19-22	High reliability required; stationary application
Cathodic Protection							33	High reliability required; stationary applications
Transportation signals							30	High reliability required; some portable application improve value proposition
Water Pumping							33	Impact of product failure is high
Village Power							44-48	Remote Homes, Remote Facilities, and Desalination require large output modules
Outdoor Lighting							19-22	Billboard and Signage requires large output modules
Other Habitation							26	
Consumer Power							41-74	Portable applications improve value proposition
Grid Residential							44	Flexible attractive for BIPV; space constrained application; modules >100W
Grid Commercial							41	~50% of modules sold >200W
Grid Utility							22	~60% of modules sold >200W
Consumer Indoor							52-63	Portable applications improve value proposition

Milestone 3

Tasks for Deliverable 3

- Carry out analysis of manufacturing cost comparison for rigid versus flexible OPVs.

Deliverables for Milestone 3

- Preliminary report on cost-comparison of flexible *vs.* rigid processing for OPVs.

Summary

- At present, flexible OPV modules are more expensive to manufacture than on rigid glass substrates. Today's air and water sensitive active layer materials require stringent barrier properties to deliver >1yr lifetime. This drives flexible OPV costs substantially higher than on glass which is a low cost, high quality barrier.
- Above a certain minimum scale, module cost is dominated by material costs. As a result, high throughput of roll printing does not provide substantial cost benefits
- Compared with other vacuum deposited thin film PV technologies, OPV (rigid or flexible) is more capital efficient. Roll processing provides an even further advantage
- The key to delivering cost competitive flexible OPV is to reduce the material cost to parity with glass-based OPV. Once achieved, the capital efficiency of roll processing promises to deliver low cost per watt and high return on invested capital (ROIC). The primary lever to reduce cost is to improve the air stability of the active layer materials, thereby eliminating the need for expensive barrier solutions. Another option is to drive down the cost of flexible barriers and/or find alternatives to the solutions available today
- The potential of extremely high capital efficiency of roll processing offers the possibility of low cost per watt and high ROIC once a competitive flexible product can be delivered to serve the mass grid-connected markets
- In the near term, flexible OPV can successfully serve markets where its unique value propositions outweigh the added expense. As input costs decline, additional markets will open in the medium term. In the long term, flexible OPV may be a major source of on-grid generation capacity.

For this deliverable, four cases were modeled to compare the manufacturing of OPV on rigid an flexible substrates. The first two cases utilize Gen 5 and Gen 8.5 rigid glass substrates with areas of 1.43 m^2 and 5.72 m^2 respectively. The Gen 5 case is our base case for comparison and the Gen 8.5 represents a scaled up process that is also capable of higher throughput. In addition, to represent the advancement in OPV materials that would occur in the time it would take to scale to the larger substrate size, the efficiency, assumed to be 5.7% for the Gen 5 module, is increased to 7% for the Gen 8.5 module. For the flexible cases, a 0.5 m web width was used in both the base case and the higher throughput case. Again, we assume the base case to have a module

efficiency of 5.7% and the high throughput module to be at 7%. The difference in these cases is based on the an inversion of the device architecture and the switch from a polymer substrate to a metal substrate which, together, allows us to transition from a 3m/min web speed in our base case to a 30 m/min web speed in the high throughput case. These assumptions are summarized in Table 9.

Table 9 Modeling assumptions.

	Rigid – Base	Rigid – High Tput	Flexible – Base	Flexible – High Tput
Module efficiency	5.7%	7%	5.7%	7%
Substrate size	Gen 5 (1.4m^2)	Gen 8 (5.7m^2)	0.5m width	0.5m width
Electrode deposition	Vacuum	Vacuum	Screen-printing	Continuous printing (gravure, flexographic)
Electrode patterning	Etch paste, shadow mask	Etch paste, shadow mask	na	na
Capacity	150K starts/yr	350K starts/yr	3 m/min 1.58M linear m/yr	30 m/min 15.8M linear m/yr

Using Plextronics' sophisticated manufacturing cost model, the CapEx cost for the manufacturing facility, the total annual plant output, and the cost per watt were calculated. The results are shown in Table 10. As we can see, the throughput benefits of flexible processing are outweighed by the increased materials costs based on today's known technology and costs. To understand why this is, we must examine the breakdown of the cost.

Table 10 Modeling Results

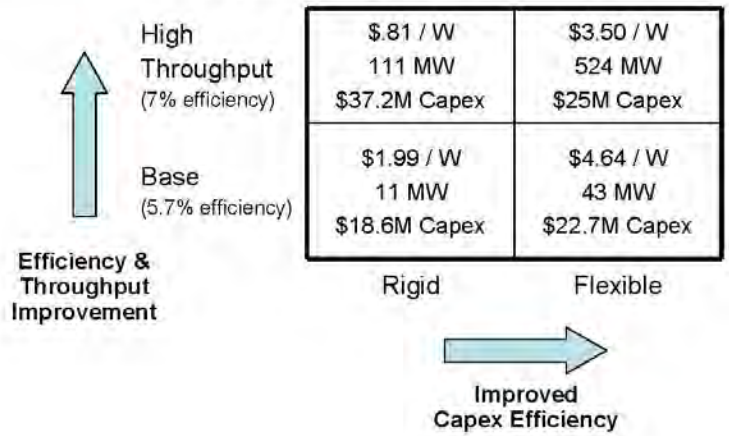

Figure 18 shows the cost pareto for the four modeled cases. In all cases, the materials costs are the dominant cost driver with the materials being more and more dominant as we move to higher and higher throughput processes. This is expected as the higher throughput allows the fixed costs to be spread over a larger number of devices.

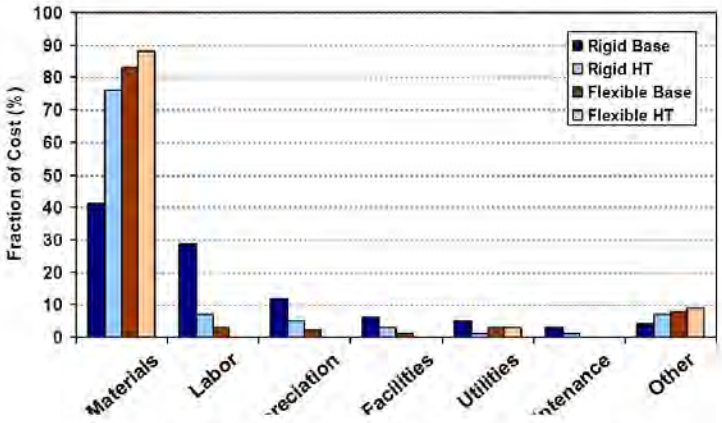

Figure 18 Distribution of costs from the modeled scenarios

Next we investigate the effects of scale and saw that, as plant capacity increased, the cost per watt leveled off as shown in Figure 19. This shows that, after some initial economies of scale are realized, there are no more cost reductions that can be achieved simply by increasing throughput.

This corresponds to the production level where the variable cost of the module dominates the cost structure.

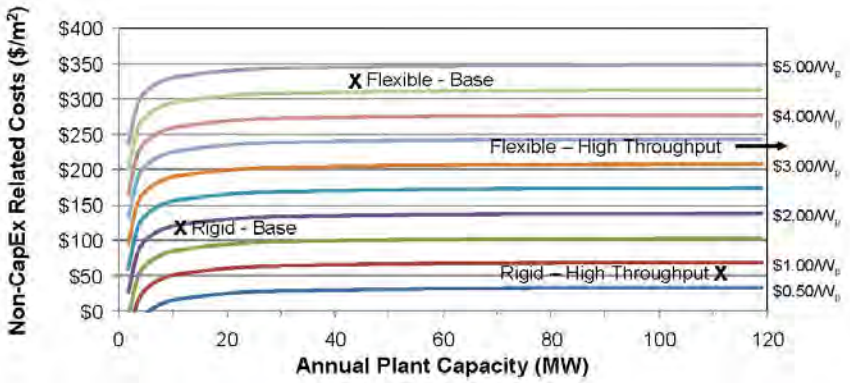

Figure 19 Cost isoquants showing the location of the modeled scenarios

Having found the materials cost to be an important driver, we next looked at a breakdown of the costs that go into a module. The breakdown of materials costs for flexible and rigid OPV modules as modeled are shown in Figure 20. For the flexible module, it is clear that the materials costs are being dominated by the substrate and encapsulation costs whereas the rigid module cost is driven by the cost of the active layer materials. It should be noted that these two cases use the same cost for the active layer inks so the comparison is a valid one.

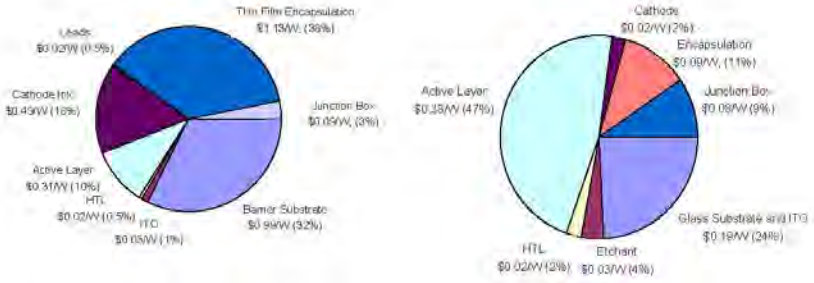

Figure 20 Cost Breakdown for flexible (left) and rigid (right) OPV modules (2012$s)

Conclusions

- Flexible OPV is more capital efficient than rigid OPV

The speed of continuous roll processing enables manufacturing high volumes with relatively low capital investments. This high throughput and low CapEx investment minimizes the contribution of depreciation to the module cost.

- Module cost dominated by variable costs

Materials are largest cost contributor for either flexible or rigid OPV. Rigid cost contributors are led by active layer materials. Or flexible, on the other hand, substrate and encapsulation materials account for almost 2/3rd of the total cost for flexible OPV.

- In the short term, rigid OPV delivers a lower cost overall

The lower materials cost for rigid translates to a lower overall unit cost. Modeling indicates that reducing the cost of flexible substrates and barrier films will go a long way to making Flexible OPV cost competitive. If it can be proven to be cost competitive, flexible OPV has the potential to deliver high ROIC due to its capital efficiency.

- Materials costs must be comparable in order for flexible to realize the full benefit of throughput and be less expensive than rigid.

Modeling indicates that, were barrier substrates to be cost competitive with glass, and thin film encapsulation costs were to be in line with their rigid counterparts, flexible OPV would be poised to deliver very competitive costs as low as $.65/W.

Milestone 4

Tasks for Deliverable 4

- Continued analysis of manufacturing cost comparison for rigid versus flexible OPVs.

Deliverables for Milestone 4

- Update report on cost-comparison of flexible *vs.* rigid processing for OPV

Initially Milestone 4 was proposed to represent continued refinement of the commercial analysis for flexible OPV. Additional analysis requires additional inputs and the technical side of this project reached a chosen design more quickly than was originally intended. This lack of new inputs on materials or process selection meant additional analysis was not meaningful. This update was a report confirming of our previous findings based on customer interactions that occurred since Milestone 3.

Milestone 5

Tasks for Deliverable 5

- Define strategic market entry points for flexible OPVs.

Deliverables for Milestone 5

- Report on VOC analysis for large-area flexible OPV devices.

Flexible OPV devices have the potential to be used in a number of widely different markets by a variety of end users. This report outlines Plextronics' efforts to investigate the more promising applications for OPV and convey the feedback gathered from customers in those markets. The markets investigated were:

- Consumer battery charging products
- Electrophoretic/electrochromic displays
- Military applications
- Education
- Thin film battery charging applications

Consumer battery charging products

Students at Carnegie Mellon University were chosen to represent technology-savvy consumers who would qualify as early adopters of new technology such as OPV. In a group discussion focused on the requirements for a solar charging product, they repeatedly stressed that integration was a key requirement for them and they expressed little interest in having a separate charging device. Though not stated explicitly, the requirements described exclude a rigid solution for a number of reasons. To achieve the conformability and integration into the end product, it was concluded that rigid OPV would be prohibitive and flexible OPV was required.

Electrophoretic/electrochromic displays

The second market/application that was investigated was powering electrophoretic and/or electrochomic displays such as the e-Ink display in the Amazon Kindle. The power requirements for these devices match up well with OPV's current performance. The current incarnation of these devices are rigid readers and could be integrated with a rigid OPV panel to provide power. Based on our contacts with leading companies in both electrophoretics and electrochromics, this industry looks to take advantage of the inherently thin, flexible nature of the display and readers that can be rolled are already being worked on. Clearly this drives the

requirement that the OPV be flexible as well, ideally co-deposited on the same flexible substrate, further reducing the cost to produce them.

Figure 21 – Electrophoretic displays on the Amazom Kindle (left) and an electrochromic display on a smart card (right).

Be it flexible readers or displays for smart cards, there are numerous potential applications for this technology and that translates into a tremendous potential for OPV, specifically flexible OPV, to power those devices. This market represents a great opportunity for flexible OPV.

Military applications

Military interest in OPV stems from an increase demand to power field equipment and also a desire to decrease the weight and bulk of the charging gear. Currently batteries comprise 15-20% of a soldiers gear and a typical SOF team member deploys with 27 lbs of batteries. Continually increasing amounts of communication and sensor gear necessitates more and more batteries and creates the need to recharge those batteries in the field. Flexible OPV has the potential to be a very good fit in this market as it will be able to meet the flexibility and durability requirements at a significantly lower cost than competing technologies.

Figure 22 - A typical soldier's gear (left) contains a significant amount of battery weight. Solar charging tents (right) are currently being tested as a method of charging these batteries.

The current performance of flexible OPV devices, however, must be improved before they will be ready to serve this need. Additional work on efficiency and encapsulation will enable these applications.

Education

One market that was not originally going to be considered was the education market. This comprises custom demonstration units for schools and museums to help teach about renewable energy and solar power. After being approached by the Carnegie Museum to participate in a upcoming exhibition, we identified a number of unique requirements for customers in this market. As these products tend to be displays that are not necessarily interactive, durability is not as much as a factor compared to some of the other applications already discussed. Instead, the aesthetic requirements, lead to a strong design for a conformable photovoltaic device that can be easily integrated into the displays, in this case robots. Flexible OPV fits this need nicely. Additionally, OPV's performance under artificial lighting and in lower lighting conditions compared with other PV technologies is and additional benefit as it lends some flexibility to the exhibit designer who can now use less light to operate the devices. The improved performance also means that there is less of an efficiency requirement for the flexible OPV devices in these kinds of applications.

In our discussions with the Carnegie Museum, we were also introduced to another application for OPV. As part of their Powdermill Nature Reserve, there is a program that is working on tracking the migratory patterns of golden eagles using GPS units attached to the birds. These devices are currently powered by high efficiency solar cells. These cells are very difficult to use as they are rigid and mounting them is inherently very difficult because of that. The people

leading this project had a clear desire for a flexible solution as it would be more durable and easier to work with while also, ideally weighing less. Flexible OPV however is not am ideal match to this application due to the efficiency requirements. Currently, the size of the required OPV device would be too large, though, with gains in efficiency, applications such as this could open up.

Thin film battery charging applications

Thin film batteries, new emerging class of battery technology, present unique charging opportunities, especially for technologies like OPV. These are low power, extremely thin batteries designed to power small semi-disposable circuits such as sensors, smart card, etc. Typically these batteries will have power capacities of mAh. Clearly this is not very much power, but it is ideally suited to the niches it is targeting.

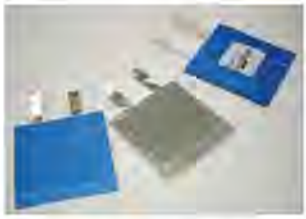

Figure 23 Typical Thin Film Batteries.

Like the electrophoretic displays discussed earlier, there is a desire to find a charging technology that can mirror the thinness of the product. Flexible OPV can achieve that level of thinness and, even with its current performance, can meet the charging requirements. Currently, major players in this market have expressed interest in using OPV to charge their batteries and a number of demonstrations have already been carried proving the suitability of the technology.

Conclusions

Taken together the feedback received from the customers in the various markets serves to highlight the point that, when it comes to OPV, there is no "one size fits all" solution. Different applications place different demands on the photovoltaics and, because of that, align differently with the current OPV capabilities and track differently with it projected performance. Some applications such as the thin film battery charging and the electrophoretic/electrochromic

displays align well with OPV's near term expected performance. Other applications such as consumer battery charging present more rigorous requirements and must be thought of as longer term fits to the technology.

In all cases, however, there were some common threads from which we can gain insight into the factors that will lead to OPV's final acceptance as a commercial technology. In all cases, flexible OPV was a valued solution because of its durability and conformability compared to rigid substrates. Flexible OPV is inherently more durable than its rigid counterpart and, by virtue of its flexibility, can endure uses that would damage a rigid OPV module. Additionally, many of the applications had a desire to have the OPV element become part of the design rather than an element that needed to be designed around. Flexible substrates enable this type of design integration. Overall we feel that there are a number of opportunities for flexible OPV in both the near and short term and the key to commercial success if finding those applications where OPV's unique value proposition is best aligned with the customer's needs.

Appendix E – 09-012 (Strategic Polymer Sciences, Inc)

Nanostructured High Energy Density Film Capacitors for Compact Implantable Defibrillators

Strategic Polymer Sciences, Inc.

Shihai Zhang
200 Innovation Blvd, #237
State College, PA 16803
Email: szhang@strategicpolymers.com
Phone: (814)238-7400 ext 224

Awarded: November 15, 2008

Table of Contents

1. Introduction

In this program, Strategic Polymer Sciences, Inc (SPS), teaming up with St. Jude Medical (SJM) and the Pennsylvania State University (PSU), has been working together to develop compact film capacitors by utilizing nanotechnology and SPS proprietary high dielectric constant polymer thin capacitor films. This advanced capacitor can be used in pulsed power applicatioins such as implantable cardioverter defibrillator (ICD), external automatic defibrillator, military directed energy weapons systems to reduce their size/weight/cost and improve their reliability.

Two families of polar fluoropolymers have been developed by Dr. Qiming Zhang at PSU. The first are terpolymers of vinylidene fluoride (VDF), trifluoroethylene (TrFE), and chlorofluoroethylene (CFE) or chlorotrifluoroethyelen (CTFE) with K of 50 and energy density of 10 J/cc. The other family consists of copolymers of VDF with CTFE (P(VDF-CTFE)) and VDF with hexafluoropropylene (HFP, P(VDF-HFP)) with K about 12-20 and DBS up to 700 V/μm. Energy density above 25 J/cc has been achieved at the film level. SPS was founded by Dr. Qiming Zhang and Mr. Ralph Russo in 2006 to commercialize these high-performance polymers for energy storage. SPS has obtained exclusive licenses from PSU for all these PVDF-based materials and related blends and nanocomposites.

Figure 1 benchmarks the performance of SPS capacitor film with commercial biaxially oriented PP (BOPP, K =2.2) and polycarbonate (PC, K= 3.2) capacitor film. SPS capacitor films have similar dielectric breakdown strength as the commercial BOPP and PC film, but with a dielectric constant that is 4-20 times higher than the latter.

Therefore, SPS PVDF copolymer capacitor films have significantly higher energy density than the commercial BOPP and PC based on the same test protocol. For example, at 600 V/μm, the directly measured discharged energy density of SPS01, SPS03-c, and SPS03-d is 24.2 J/cc, 17.0 J/cc, and 15.6 J/cc, respectively, while it is only 4.6 J/cc for PC and 3.7 J/cc for BOPP.

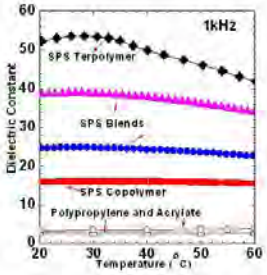

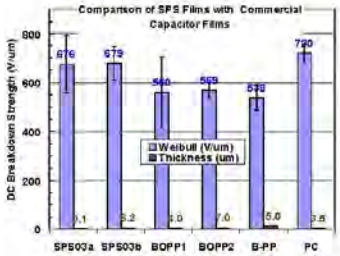

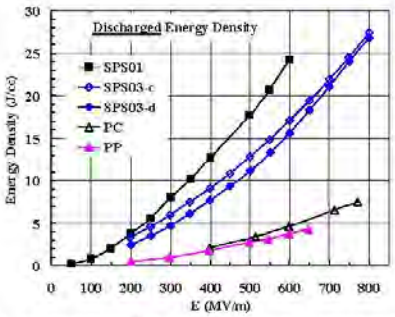

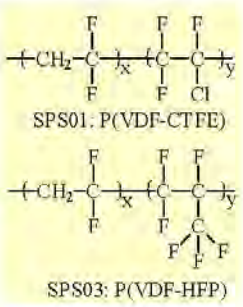

Fig 1. Capacitor film performance of selected SPS polar fluoropolymers benchmarking with commercial BOPP and PC capacitor films.

Recent development efforts at SPS have demonstrated that the high-performance capacitor film can be inexpensively manufactured with current capacitor film production facility, paved the way for future film commercialization. In a typical processing line, film with thickness of 50~100 μm is extruded from polymer melt through a film die, and is then stretched in two directions to get thinner film with improved electrical and mechanical performance. Figure 2 illustrates the capacitor film manufacturing process. The production machine is widely used by the packaging film and capacitor film industry.

Figure 2. Capacitor film manufacturing process.

Prior to the start of this project, SPS had developed its first generation capacitor films and prototype capacitor devices for military direct-energy weapon applications. Rolls of capacitor film with thickness of 10 μm was metallized and wound into capacitors (Fig 3, SPS private funding) in early 2008.

More recently in June 2008, it was demonstrated that the capacitor film with thickness 3-4 μm can be produced by using state-of-the-art capacitor film processing machine (Figure 4, Sponsored by US DoD and private funding). A roll of 3 μm film with length over 1,500 m was produced.

Figure 3. SPS 1st generation film capacitors.

However, it should be pointed out that the previous development had only demonstrated the feasibility of commercial scale manufacturing capability. The polymer resin, capacitor film, metallization, and capacitor winding still did not have the high quality required to achieve the high energy density, high reliability, and lifetime at the packaged capacitor level. The defects from the resin and the film significantly reduce the operating electric field and energy density in

the packaged large prototype capacitors. For example, in lab-scale capacitor film with area of 1 cm^2 (capacitance from 100 pF to 1 nF), the average dielectric breakdown strength is higher than 600-700 V/μm and the discharged energy density is up to 27 J/cc. However, in a 100 μF prototype capacitor using over 1 m^2 active capacitor film, the dielectric breakdown strength decreased to less than 200 V/μm and the discharged energy density was lower than 2 J/cc.

Figure 4. SPS capacitor film. Left: 3 μm film roll > 1,500 m long; Middle/right: 2.26 μm film. The 2.26 μm film broke after running for 3 min and the processing should be further improved to produce a large roll of capacitor film.

In addition to the relatively poor resin and capacitor film quality, the first generation wastes about 30-40% of the energy during the charge-discharge process due to the high leakage current, dielectric loss, and remnant polarization.

2. Project Achievements

Currently, polypropylene (PP) dominates the film capacitor market. Capacitor grade PP resin has been continuously improved in the last sixty years in terms of purity, chain isotactic regularity, crystallinity, and molecular weight distribution by Exxon Mobile and Borealis. On the other hand, PP capacitor film quality has also been improved since 1950's and 2.5 μm thick PP capacitor film is now commercially available for certain applications. The main manufacturers of PP capacitor film include Toray, Kopafilm, Bollore, Steinerfilm, etc. The dielectric breakdown strength of PP film capacitors has been improved from below 100 V/μm in 1950's to over 700 V/μm now for pulsed power applications. It takes over 60 years and costs likely hundreds of million dollars R&D for PP capacitor film to achieve the current excellent performance and market dominance.

SPS was founded in 2006 to develop the P(VDF-HFP) based resin and capacitor film. With the support of the Pennsylvania NanoMaterials Commercialization Center (PA Nano) and others, significant progresses have been made to enable the transfer of the high energy density film capacitor technology from an academic lab to prototype devices that can be tested by different potential customers. Within less than 4 years and $3M investment, large scale production of capacitor resin and film has been demonstrated, and the high energy density has been achieved in prototype capacitors.

The main achievements of the PA Nano project include:

1. Significant improvement in capacitor resin quality. Special resin compositions and manufacturing process have been developed by Solvay Solexis. The new resins are developed for high speed manufacturing of ultrathin capacitor film with high purity.
2. Capacitor film manufacturing has been improved. At the end of the project, it was demonstrated that 2.0 μm thick capacitor film can be produced at pilot scale and capacitor film rolls with length over 3,000 m has been produced. Prior to the project, the capacitor film thickness of stable manufacturing was limited to 3.0 μm.
3. The defect level in the capacitor film has been reduced from 30/100 cm^2 to less than 5/100 cm^2.
4. Nanodielectric blocking layer deposition has been developed to achieve high charge discharge efficiency.
5. Prototype capacitors with 2 μm thick film have been developed.
6. Discharged energy density over 6 J/cc has been achieved in large prototype capacitors.
7. Prototype capacitors have been delivered to various commercial and military customers for evaluation.
8. A provisional patent was converted into a formal US patent application.
9. Technical results have been presented in two major conferences.
10. The capacitor film products have been marketed at two major tradeshows.
11. Sell of capacitor film has been started to niche markets.
12. Three additional employees have been hired to work on the capacitor development programs.

3. Summary of Technical Milestones

In this very aggressive project, we performed capacitor resin development, ultrathin capacitor film production, silicon nitride deposition, and capacitor winding and test. This final report summarizes the main milestones in the order of technical logic.

3.1. Silicon Nitride Deposition

Milestone 3, March 2009

Optimization of PECVD of Si_3N_4 nano dielectric blocking layer: targeting Si_3N_4 dielectric breakdown strength > 800 V/μm, energy density > 10 J/cc, efficiency > 80% at 37 °C, deposition temperature below 150 °C.

The deposition of Si_3N_4 is controlled by several parameters: *plasma intensity, feeding gas ratio, feeding gas flow rate, deposition temperature, distance between film and plasma source*, etc. It was reported that the quality of Si_3N_4 is dramatically influenced by the deposition conditions. The breakdown strength, dielectric constant, dielectric loss, resistivity, and even

composition vary with the deposition conditions. Therefore, the deposition was systematically optimized to achieve high dielectric constant, low dielectric loss, high resistivity, and high dielectric strength without damaging the PVDF-copolymer capacitor film.

A design of experiment was performed to find the relationship of the deposition condition with the Si_3N_4 performance by depositing it on silicon wafer (Table 1). The Run Order represents the randomized order of experiment. The factors include plasma intensity, chamber temperature, and the distance between the film and the plasma.

Table 1. Design of Experiment Chart for the Optimization of Si_3N_4 PECVD

Run	T (°C)	SiH_4/NH_3	RF Power (W)	Deposition rate (nm/s)*
1#	*T1*	*G1*	*P1*	*3.8*
2#	T1	G2	P2	8.5
3#	T1	G3	P3	10.4
4#	*T2*	*G1*	*P2*	*3.7*
5#	*T2*	G2	P3	7.6
6#	*T2*	G3	P1	6.7
7#	*T3*	*G1*	*P3*	*4.0*
8#	T3	G2	P2	7.6
9#	T3	G3	P1	8.0

The Si_3N_4 on Si wafer was characterized by dielectric breakdown strength since their dielectric constant is similar. Figure 5 presents the dielectric breakdown strength of three of the best conditions.

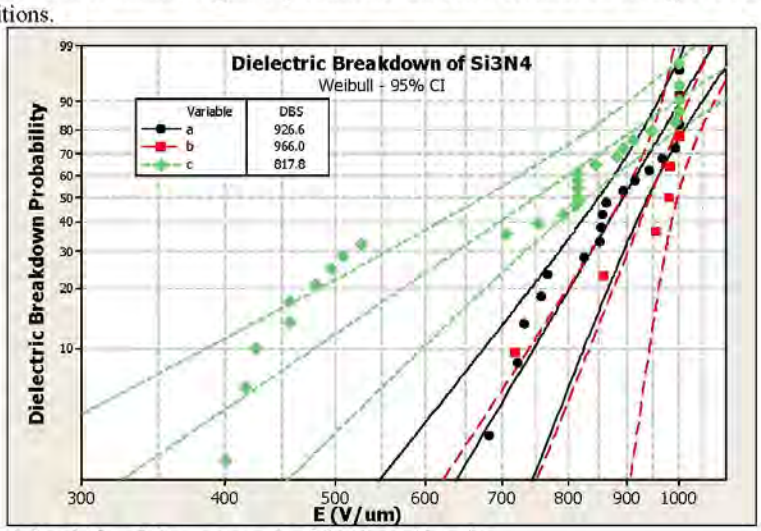

Figure 5. Dielectric breakdown strength of Si_3N_4 on Si wafer.

All three samples have Weibull dielectric breakdown strength above 800 V/μm.

The 800 V/μm dielectric breakdown strength for Si_3N_4 is an internal target at SPS. The goal for this target is to make sure the quality of silicon nitride is good enough for the final bilayer capacitor film. The silicon nitride will be coated at the surface of SPS capacitor film and the bilayer capacitor film will be operated at an electric field below 400 V/μm. The 800 V/μm breakdown strength of neat Si_3N_4 will ensure that it can work with high reliability in the bilayer capacitor film.

The discharged energy density and efficiency of the Si_3N_4 layer on Silicon wafer were measured by SPS and the results are summarized in Figure 6.

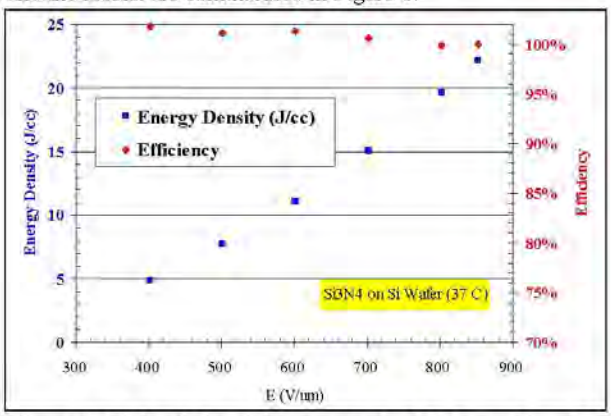

Figure 6. Dielectric breakdown strength of Si_3N_4 on Si wafer.

The pure Si_3N_4 (with a thickness of ~1 μm) can discharge energy of 19.6 J/cc with an efficiency of 99.8% at 800 V/μm.

The same Si_3N_4 sample with thickness of 1.2 μm was also delivered to the customer for their evaluation. They used a Keithley sourcemeter to measure the energy density of the Si_3N_4 film and Figure 7 summarizes their test results.

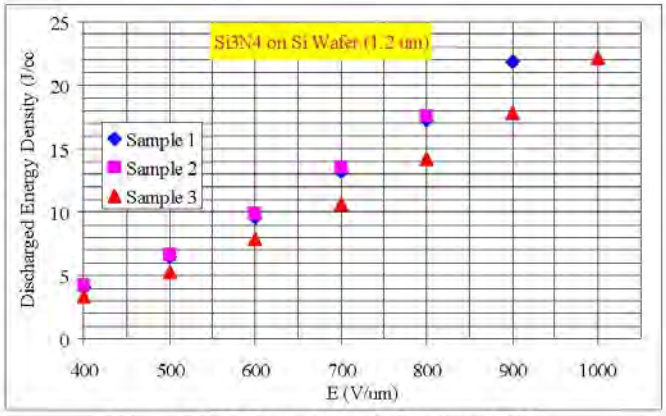

Figure 7. Discharged energy density of Si_3N_4.

At 800 V/μm, energy density of over 17 J/cc can be achieved.

Although the pure silicon nitride itself is a very good dielectric material for energy storage, it will be prohibitively expensive (even for medical devices) since more than 1,000,000 layers must deposited layer by layer to accumulate the thickness necessary for a large ICD capacitor. On the other hand, as an inorganic material, Si_3N_4 will be brittle for thickness above μm and cannot be wound into a round capacitor.

Milestone 5, October 2009:

Develop and test the process for deposition of the blocking layer on the polymer film. Will produce lab-scale capacitor film with nano blocking layer to achieve the following specs:

- energy density > 10 J/cc
- efficiency > 80% at 37 °C

Based on the deposition procedure optimized in Milestone 3, Si_3N_4 was deposited onto 2 μm capacitor film to improve the charge discharge efficiency. The deposition procedure is defined in Table 2:

Table 2. Plasma Enhanced Deposition of Si_3N_4 on 2 μm-thick Capacitor Film

Run	T (°C)	SiH_4/NH_3	RF Power (W)	Deposition rate (nm/s)
Optimized	*150*	*50/100*	*450*	*3.5*

The deposition was performed for 600 seconds to accumulate 2.1 μm thick Si_3N_4. The total thickness of the final capacitor film is 4.1 μm.

40 nm thick Aluminum was deposited on both sides of the capacitor film using thermal evaporation under high vacuum. To minimize the damage to the capacitor film during the thermal evaporation, the substrate was cooled with -10 °C recirculation fluid.

Figure 8 shows pictures of the metallized SPS capacitor film.

Figure 8. Si_3N_4-coated capacitor film with Al electrode on both sides.

The Si_3N_4-coated capacitor film was then tested with the capacitor charge-discharge system developed by SPS. The charged energy density and discharged energy density were calculated from recorded voltage/current/time data. The charge-discharge efficiency was calculated from the ratio of discharged/charged energy. The test was performed at 37 °C. SPS used a high-performance Trek 5/80 power amplifier, which is controlled by LabView program through a NI DAQ. The high-speed DAQ collects voltage and current data every 0.015 second.

Figure 9 summarizes the test results.

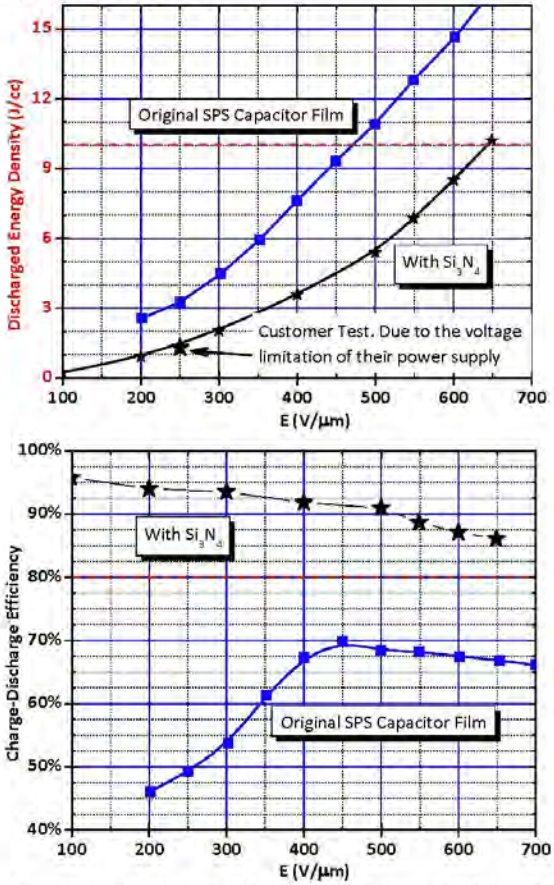

Figure 9. Energy density and efficiency of Si_3N_4-coated capacitor film. Red dashed lines in the figures refer to the proposed target energy density and efficiency. The customer requested energy density of 4 J/cc (capacitor) and efficiency above 75%.

The discharged energy density increases gradually with increasing electric field. 3.6 J/cc can be discharged at 400 V/μm, and it increases to 10.1 J/cc at 650 V/μm.

The charge-discharge efficiency is an important parameter required by the customer. Original uncoated SPS capacitor film has efficiency of ~60%.

The Si_3N_4 coated capacitor film has charge-discharge efficiency of 96% at 100 V/μm. It decreases to 92% at 400 V/μm, and 86% at 650 V/μm. The lower efficiency at higher electric field is a result of the increased charge injection at high voltage. The role of the Si_3N_4 is to reduce the charge injection.

The test results of uncoated SPS capacitor film are also included in Figure 2 for comparison. the original film has energy density of 16.5 J/cc at 650 V/μm, as compared with 10.1 J/cc for the Si_3N_4 coated film sample. However, the efficiency of original SPS capacitor film is only 67%, well below that of the Si_3N_4 coated capacitor film.

3.2. First Generation Ultrathin Capacitor Film Production

Milestone 2. February 2009

Make initial rolls of capacitor film at partner facility to the following specs:

- thickness of 2.5 μm
- thickness variation < ±5%
- width > 650 mm
- length > 1,000 m.

Three rolls of capacitor film have been produced in a continuous 40-hour film production trial:

Table 3. Roll Information of SPS High Energy Density Capacitor Film

No.	Thickness (μm)	Length (m)	Width (mm)	
PA Nano-01	2.5	393	690	All meet milestone of February 15, 2009.
PA Nano-02	2.5	3,043	690	
PA Nano-03	2.5	1,509	690	

The thickness distribution of Roll No 02 is summarized in Figure 10.

Start:	10.12.2008 12:21:17 PM	Thickness Act:	2.55	Scans:	265
End:	10.12.2008 1:38:03 PM	Thickness Set:	2.50 µm	LineSpeed:	40.0 m/min
Machine:	Bal	Length:	3043 m	2-Sigma:	0.086
Campaign:	sim_BOPVDF_V.5100-188_	Width:	650 mm	2-Sigma %:	3.392 %

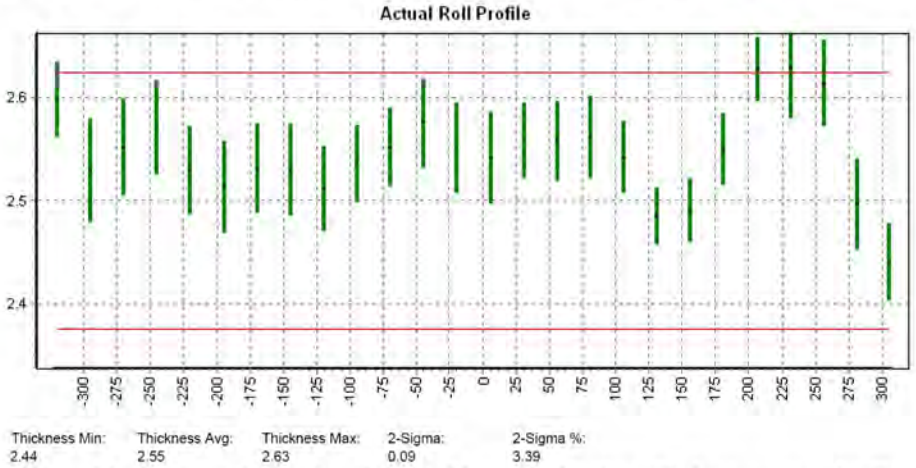

Thickness Min:	Thickness Avg:	Thickness Max:	2-Sigma:	2-Sigma %:
2.44	2.55	2.63	0.09	3.39

Figure 10a. Thickness distribution along the film width direction. Thickness measured with online IR thickness monitor. The thickness variation is less than 3.4% in the width direction.

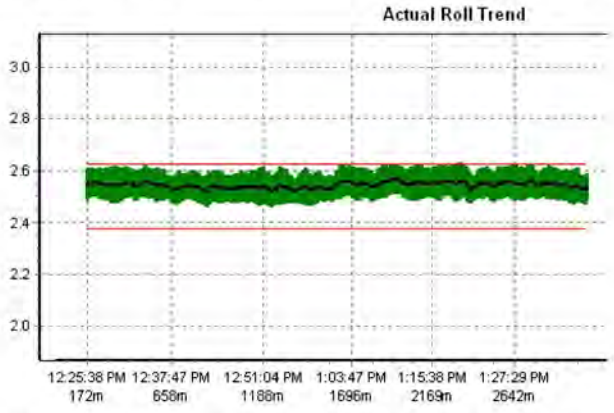

Thickness Min:	Thickness Avg:	Thickness Max:	2-Sigma:	2-Sigma %:
2.52	2.55	2.57	0.02	0.83

Figure 10b. Thickness distribution of roll No 02. The thickness uniforminity is better than 0.83%.

The pilot-scale capacitor film production was performed at Brückner, Germany after evaluating the capability of three potential machine manufacturers.

Since SPS has accumulated lots of experience in the capacitor film production from 2007 to 2008 and has done a thorough homework before the trial, film with thickness of 3 μm was achieved after 12 hours and wound film rolls with length over 2,500 m were successfully collected.

However, it took another 18 hours to successfully produce 2.5 μm film. Although the thickness was reduced by only 0.5 μm, or 17% from 3 μm, winding the 2.5 μm thick film represents a tremendous challenge for the winding control system. The tension that applied on the film must be controlled very carefully. If the tension is too tight, there will be wrinkles along the machine direction and the film will also break easily. If the tension is too low, the film may be wrapped onto anyone of the rollers and broken eventually. The film was running at a speed of ~40 m/min.

With fine adjustment of the winding system and film stretching process, the 2.5 μm film was finally wound onto a 6 in ID tube with length above 3,000 m. There was not film breakage and the winding was switched to another winding tube to continue the winding.

Figure 11 shows pictures of the large roll of 2.5 μm thick capacitor film produced by SPS in December 2008.

Figure 11. SPS high energy density capacitor film rolls with film thickness of 2.5 μm.

The 2.5 μm capacitor film produced at Brückner was evaluated in SPS lab and inside a class 1,000 cleanroom.

The thickness was verified with optical interference approach assuming a refractive index of 1.42 for the polymer. Nine locations were measured on a 4 in by 4 in sample and the results were summarized in Table 4.

Table 4. Thickness Measurement of SPS Capacitor Film Roll No. 02

Position	1	2	3	4	5	6	7	8	9	Mean	Std Dev
t (μm)	2.513	2.543	2.524	2.515	2.503	2.539	2.582	2.598	2.577	2.544	0.034

Figure 12 presents a summary of the energy density and efficiency.

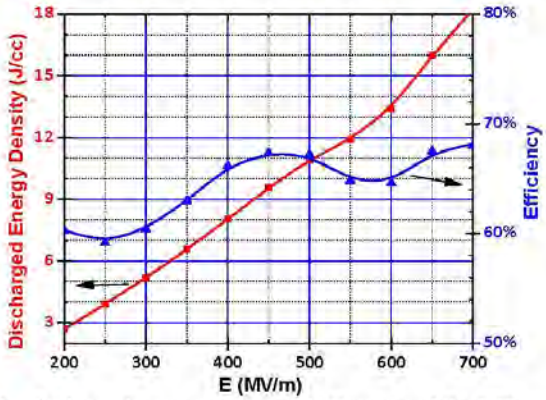

Figure 12. The discharged energy density and efficiency of the SPS capacitor film.

The energy density of the capacitor film is over 10 J/cc and meets the requirement of the ICD capacitors. However, the charge-discharge efficiency is only 60%~70% and below the 70% requirement of the ICD application.

3.3. First Generation ICD Capacitor Development

Milestone 4, July 2009:

Develop First Generation Prototype Capacitors for ICD Application Based on 2.5 μm Thick SPS Capacitor Film:

- Establish baseline technical performance of current SPS film capacitors based on 2.5 μm thick film technology
- Capacitance > 100 μF
- Deliver Energy > 35 J to 50 Ω resistor at 37 °C.

The metallization of the 2.5 μm capacitor film was performed using a roll-to-roll process. Under vacuum, the capacitor film was first treated with plasma to clean and activate the surface. This improves the adhesion between the P(VDF-HFP) capacitor film with the evaporated metal electrode.

The design of the metallization is critical to the electrical performance. There are several parameters that require attentions:

- The type of metal.
- The thickness of the electrode and the surface resistivity.
- The metallization pattern.
- Width of the capacitor film, width of the free margin.

Considering the above four factors and learning from the metallization design of film capacitors for automatic external defibrillators, a heavy edge metallization pattern with Al electrode was used to metallize the 2.5 μm thick ICD capacitors (Figures 13 and 14).

Film width of 30 mm was selected to optimize the winding efficiency. There is 2.5 mm wide margin at one edge of the film that was not metallized. 2.5 mm was used for the required 850 V operation voltage of the capacitor without flashover around the free margin. This can be determined by the known surface resistivity of the capacitor film.

The metallization pattern is a heavy edge design. The main body of the film has very thin Al electrode with surface resistivity of 100 Ω/□, and the edge has thicker Al electrode with surface resistivity of 10 Ω/□. The thin electrode in the active film area is used to facilitate the self-healing and increase the energy density of the ICD film capacitor. The heavy edge was used to enhance the end connection with external power supply and load.

During the metallization process, there were problems with handling the capacitor film due to the strong static charges and the smooth film surface. The metallization machine was designed to metalize 3 μm thick polypropylene (PP) capacitor film, which has 100% higher mechanical modulus than P(VDF-HFP). Several special tools and tricks were developed to enable the handling of the capacitor film.

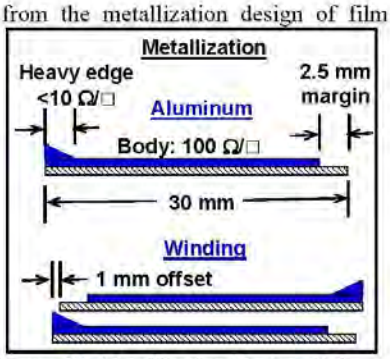

Figure 13. Metallization Design of the ICD Capacitor Film.

Figure 14. A roll of the metallized 2.5 μm thick P(VDF-HFP) capacitor film. There are still wrinkles in the film roll.

The metalized 2.5 μm film was wound into prototype capacitors. 64 capacitors with 80 μF capacitance and 50 capacitors with 120 μF capacitance were produced. Table 5 summarizes the capacitor design and dimensions.

Table 5. Design of Prototype Capacitors Based on 2.5 μm Thick P(VDF-HFP) Capacitor Film

Capacitance (uF)	Film Length (m)	Total Film Area (m^2)	Active Film Area (m^2)	Capacitor Width (mm)	Capacitor Diameter (mm)	Capacitor Vol (cc)	Capacitor Weight (g)	Packaging Eff (%)
80	94	2.82	2.26	30.34	21.96	11.5	20	49%
120	141	4.24	3.39	30.66	25.73	15.9	28	53%

It can be seen from Table 5 that the packaging efficiency of the 120 μF is only 53%, that is, only 53% of the volume is active capacitor film while other 47% consists of inactive film area such as free margin, offset area, winding mandrel and wrapping materials. The efficiency is even lower for the smaller 80 μF capacitors.

The packaging efficiency can be improved in the future by using smaller winding mandrel and narrower free margin. At this time, the goal of this project is to demonstrate the voltage performance of the prototype capacitors.

Figure 15 shows pictures of the prototype capacitors.

Figure 15. Pictures of the Prototype ICD Capacitors.

Table 6 and Table 7 summarize the electrical performance and the dimensions of the 80 μF and 120 μF capacitors, respectively.

Table 6. Capacitance and Dimensions of the 80 μF Prototype Capacitors

SPS08b17-	100 Hz		1000 Hz		10000 Hz		Diameter	Height	Gross Volume	Weight
170-80-10XX	Cp (μF)	D	Cp (μF)	D	Cp (μF)	D	cm	cm	cc	g
1001	77.065	0.05124	69.78	0.29727	7.036	4.3818	21.72	30.38	**11.25**	19.50
1002	77.026	0.06152	67.70	0.37936	2.270	9.8473	22.09	30.09	**11.53**	19.81
1003	77.081	0.06728	72.19	0.21670	5.373	6.2864	21.79	30.21	**11.26**	19.99
1004	77.357	0.03308	74.68	0.13311	12.950	4.1341	21.80	30.76	**11.48**	20.32
1005	78.996	0.04562	69.78	0.29881	2.691	8.2550	21.81	30.37	**11.34**	20.36
1006	77.962	0.03376	77.43	0.13327	24.930	2.7091	21.85	30.58	**11.46**	20.39
1007	77.599	0.03612	76.88	0.21779	10.120	4.2481	21.88	29.93	**11.25**	20.29
1008	78.052	0.03392	73.02	0.25462	5.824	5.6574	21.87	30.48	**11.44**	19.72
1009	78.318	0.03061	77.06	0.09341	36.250	2.1007	21.91	30.38	**11.45**	19.84
1010	77.749	0.02765	77.43	0.13327	30.010	2.4639	21.88	30.58	**11.49**	20.18
1011	78.289	0.04930	76.40	0.21439	5.087	6.7159	21.89	30.30	**11.40**	20.33
1012	78.437	0.02745	74.91	0.13176	17.800	3.5114	22.10	29.87	**11.45**	20.51
1013	77.697	0.04306	73.88	2.16780	6.036	5.6924	22.01	30.12	**11.45**	20.40
1014	77.643	0.06520	64.74	0.55495	1.247	10.8700	22.07	30.23	**11.56**	20.21
1015	78.004	0.06590	67.70	0.37927	1.805	10.5440	21.95	30.12	**11.39**	19.92
1016	77.719	0.03539	74.44	0.13246	20.150	3.2758	21.93	30.36	**11.46**	19.62
1017	77.390	0.04239	72.43	0.29880	3.281	8.2174	22.03	30.26	**11.53**	19.51
1018	76.143	0.03041	77.08	0.09803	29.190	2.5597	21.96	30.50	**11.55**	19.56
1019	76.206	0.04946	69.55	0.29814	3.866	7.0510	22.00	30.21	**11.48**	19.72
1020	76.375	0.03805	74.21	0.17697	2.450	3.6615	21.97	30.44	**11.53**	19.81
1021	75.281	0.03180	74.16	0.13559	20.120	3.5606	21.97	30.29	**11.48**	19.99
1022	76.359	0.04351	74.36	0.21513	6.435	5.7702	21.99	30.65	**11.63**	19.99
1023	77.390	0.03153	74.44	0.13792	17.790	3.3734	21.94	30.46	**11.51**	19.93
1024	77.124	0.03932	74.92	0.13630	13.720	4.1353	22.10	29.15	**11.18**	19.93
1025	76.103	0.07992	74.44	0.13792	10.930	4.1999	22.20	29.22	**11.30**	20.01
1026	76.387	0.02897	73.82	0.09540	29.220	2.5610	22.09	30.42	**11.65**	20.15
1027	76.663	0.03115	76.97	0.13640	23.030	3.1541	22.15	30.33	**11.68**	20.27
1028	76.190	0.04491	70.24	0.29571	4.030	7.4547	22.12	30.40	**11.68**	20.39
1029	75.475	0.03359	72.14	0.13630	15.740	3.2791	22.24	30.65	**11.90**	20.39
1030	53.608	0.37289	63.57	0.12039	8.314	4.9612	22.13	30.49	**11.72**	20.08
1031	75.504	0.03112	73.18	0.13559	12.940	4.1087	22.18	30.41	**11.72**	20.08
1032	76.561	0.04478	70.24	0.29555	3.405	6.9195	22.15	30.36	**11.69**	19.78
1033	76.915	0.03496	76.82	0.09203	23.620	3.7704	22.20	30.45	**11.78**	20.05
1034	76.827	0.02978	74.40	0.13792	23.070	3.1579	22.18	30.55	**11.78**	20.40
1035	78.030	0.06616	69.78	0.29727	2.705	7.7918	22.30	30.49	**11.90**	20.38
1036	76.928	0.03672	74.44	0.13711	14.690	3.3104	22.45	30.43	**12.04**	20.48
1037	77.479	0.03529	74.44	0.13792	13.090	3.5329	21.72	30.44	**11.27**	19.41
1038	73.585	0.01354	76.45	0.14392	29.130	2.5680	21.71	30.33	**11.22**	19.43
1039	77.681	0.03997	73.87	0.21439	5.092	6.4629	21.75	30.33	**11.26**	19.12
1040	78.081	0.03330	77.43	0.13792	23.980	5.5303	21.69	30.24	**11.17**	19.04
1041	78.228	0.04852	74.44	0.13697	11.840	3.8530	21.79	30.24	**11.27**	19.12
1042	77.660	0.03083	76.82	0.08271	29.220	2.5540	21.77	30.44	**11.32**	19.38
1043	78.081	0.03733	73.88	0.21678	6.347	5.7923	21.76	30.31	**11.27**	19.58
1044	58.240	0.08782	74.62	0.11717	12.530	4.2374	21.79	30.21	**11.26**	19.59
1045	77.315	0.02837	76.91	0.09203	27.040	3.0169	21.84	30.42	**11.39**	19.88
1046	77.842	0.02205	76.82	0.09503	29.230	2.7551	21.88	30.43	**11.44**	19.75
1047	77.298	0.03229	77.15	0.13096	20.050	3.2618	21.92	30.59	**11.54**	19.84
1048	78.087	0.02608	76.91	0.13176	22.060	3.2405	21.74	30.07	**11.16**	19.42
1049	78.186	0.07494	59.91	0.45503	1.325	13.2300	21.83	30.22	**11.31**	19.66
1050	79.375	0.04362	76.34	0.21361	5.783	7.2541	21.81	30.45	**11.37**	19.84
1051	78.643	0.03384	76.91	0.13176	21.060	3.1513	21.87	30.43	**11.43**	20.03
1052	78.226	0.03779	76.91	0.13176	24.920	2.6929	22.06	30.37	**11.60**	20.25
1053	76.192	0.02353	74.15	0.09123	27.060	2.7668	21.92	30.62	**11.55**	20.26
1054	75.227	0.02732	74.13	0.09820	35.760	2.2302	22.12	30.60	**11.75**	20.14
1055	77.111	0.04514	69.33	0.29565	2.758	8.3400	21.82	30.32	**11.33**	19.69
1056	76.663	0.03428	73.59	0.13744	21.480	3.9087	21.96	30.00	**11.36**	20.31
1057	76.188	0.03422	73.40	0.17593	8.636	4.9601	21.92	30.28	**11.42**	19.55
1058	76.370	0.03959	74.68	0.13191	17.780	3.3760	21.89	30.44	**11.45**	19.81
1059	76.016	0.03116	76.82	0.13172	29.190	2.5502	21.81	30.67	**11.45**	20.31
1060	75.190	0.04450	69.33	0.29565	3.123	8.5205	22.18	30.41	**11.72**	20.15
1061	76.620	0.03184	76.06	0.13592	23.970	3.4094	22.07	30.44	**11.64**	20.24
1062	75.375	0.07919	61.78	0.45801	1.279	13.7970	21.93	30.28	**11.43**	20.32
1063	76.938	0.07113	76.88	0.08901	29.150	2.5558	21.99	30.52	**11.59**	20.26
1064	76.342	0.02965	76.94	0.12811	26.030	2.8303	22.00	30.61	**11.63**	19.90

Table 7. Capacitance and Dimensions of the 120 μF Prototype Capacitors

	100 Hz		1000 Hz		10000 Hz		Diameter	Height	Gross Volume	Weight
	Cp (μF)	D	Cp (μF)	D	Cp (μF)	D	cm	cm	cc	g
1001	114.85	0.07342	112.0	0.67851	291.6	14.4320	25.68	30.79	15.94	28.19
1002	115.66	0.03667	112.9	0.17900	368.4	5.3852	25.59	29.89	15.37	27.92
1003	114.92	0.05242	112.5	0.32823	364.5	10.9830	25.65	30.44	15.72	27.66
1004	114.66	0.03476	112.1	0.15963	378.7	4.7671	25.70	30.46	15.79	27.62
1005	114.33	0.38610	111.7	0.19777	358.7	5.7328	25.75	30.32	15.78	27.82
1006	113.56	0.04006	111.1	0.21736	375.3	6.8421	25.79	31.49	16.44	27.60
1007	113.89	0.03284	111.4	0.14605	360.3	4.1503	25.80	30.66	16.02	27.69
1008	114.50	0.04025	11.8	0.20867	382.7	6.5792	25.76	30.31	15.79	27.77
1009	114.36	0.03274	111.9	0.14651	370.1	4.2974	26.02	30.57	16.25	28.60
1010	113.58	0.03460	111.1	0.16208	368.1	4.7997	25.82	30.48	15.95	28.51
1011	114.52	0.03516	112.1	0.17975	377.3	4.9560	25.96	30.78	16.28	29.18
1012	114.99	0.03397	112.6	0.15930	376.1	4.7952	25.93	30.92	16.32	28.96
1013	114.59	0.03583	111.9	0.17394	372.2	5.0015	25.89	30.71	16.16	28.48
1014	113.86	0.03849	111.2	0.19987	354.1	5.1350	26.01	30.61	16.26	27.89
1015	113.78	0.05500	111.3	0.25586	339.2	10.9110	26.00	30.56	16.22	28.21
1016	113.61	0.03705	111.2	0.18919	393.1	5.9826	25.94	30.49	16.11	28.12
1017	114.03	0.04368	111.3	0.25256	370.1	7.7150	26.07	30.63	16.34	28.31
1018	113.98	0.03466	111.5	0.16344	379.7	4.9483	26.05	30.61	16.31	28.31
1019	114.43	0.04579	112.0	0.28623	350.2	10.5440	25.64	31.07	16.03	27.70
1020	114.08	0.03444	111.6	0.16142	363.4	4.7278	25.56	30.69	15.74	27.94
1021	114.26	0.03390	111.8	0.15990	371.6	4.5875	25.55	31.14	15.96	28.15
1022	114.10	0.03699	111.6	0.18424	353.8	5.2253	25.54	30.72	15.73	27.89
1023	114.88	0.03288	112.4	0.14780	367.6	4.2943	25.62	30.97	15.96	27.56
1024	114.54	0.04219	112.1	0.23663	354.7	7.1509	25.64	30.63	15.81	27.53
1025	114.60	0.03449	112.2	0.16314	375.5	4.9249	25.63	30.94	15.95	27.44
1026	114.19	0.03424	111.7	0.15996	375.8	4.8123	25.77	30.84	16.08	27.57
1027	115.13	0.03642	112.6	0.17216	393.7	5.4384	25.69	30.62	15.86	27.67
1028	116.92	0.09154	115.6	0.49174	359.5	18.7480	25.64	30.73	15.86	27.67
1029	116.29	0.03903	112.8	0.18499	362.5	5.1342	25.65	30.44	15.72	27.97
1030	113.61	0.04726	110.8	0.28757	323.1	7.9880	25.28	30.65	15.38	27.52
1031	115.14	0.03743	112.3	0.18903	303.7	4.3967	25.38	30.95	15.65	27.56
1032	114.79	0.03599	112.3	0.17698	361.0	4.9986	25.36	30.67	15.48	27.43
1033	114.23	0.05934	111.9	0.35131	407.6	7.6748	25.60	31.66	16.29	27.28
1034	114.16	0.03495	111.6	0.16299	360.3	4.6302	25.58	30.44	15.64	27.30
1035	113.71	0.04011	111.1	0.20307	329.1	5.8573	25.60	30.62	15.75	27.45
1036	114.03	0.03442	111.4	0.16198	329.6	4.1860	25.55	30.48	15.62	27.39
1037	114.25	0.03472	111.4	0.16250	347.2	4.3517	25.67	30.45	15.75	27.58
1038	115.09	0.03472	112.1	0.20188	315.8	4.8668	25.62	30.51	15.72	27.81
1039	114.21	0.03517	111.8	0.16988	386.1	5.3177	25.74	30.73	15.98	28.09
1040	114.68	0.03938	112.2	0.20070	390.1	6.4753	25.74	30.60	15.92	28.38
1041	113.07	0.03613	110.7	0.17926	370.9	5.4337	25.80	30.62	16.00	28.43
1042	113.04	0.03431	110.6	0.15971	317.6	4.0881	25.80	30.74	16.06	28.34
1043	112.94	0.03783	110.5	0.19479	350.0	5.7070	25.87	30.66	16.11	28.21
1044	112.70	0.05705	110.0	0.34129	353.1	7.4921	25.93	30.46	16.08	28.11
1045	112.64	0.03347	110.2	0.15122	354.9	4.3037	25.95	30.52	16.13	28.06
1046	113.56	0.03967	111.0	0.20750	356.5	6.0640	25.98	30.46	16.14	28.16
1047	113.97	0.03786	111.5	0.19176	350.5	5.6659	25.92	30.62	16.15	28.24
1048	109.77	0.06956	101.9	0.16940	278.9	3.7636	25.93	30.32	16.00	28.52
1049	116.25	0.04187	113.8	0.23592	424.3	8.4429	25.59	30.79	15.83	28.15
1050	116.72	0.03626	114.1	0.16431	385.6	4.9937	25.50	30.58	15.61	28.07

The prototype capacitors were tested at SPS following the test protocol defined at the beginning of the project:

- Test done at 37 deg C
- Charge to 800 V at 10 mA constant current
- Discharge to 50 Ω load resistor
- Calculate discharged electric energy

At SPS internal test, the prototype capacitors can deliver an energy of 40-44 J.

After preliminary evaluation at SPS, five prototype capacitors were delivered to SJM for their evaluation.

Table 8. Prototype Capacitors Delivered to SJM

Capacitors made from 2.5 um thick film. 30 mm wide, 2.5 mm margin 1 mm offset	1000 Hz		Diameter	Height	Volume	Weight
	Cp (uF)	D	cm	cm	cc	g
SPS08B17-157-120-1002	110	0.042	2.606	3.163	16.86	
SPS08B17-157-120-1003	111	0.043	2.583	3.171	16.61	
SPS08B17-157-120-1004	106	0.044	2.608	3.166	16.90	
SPS08B17-157-120-1007	110	0.045	2.620	3.192	17.20	
SPS08B17-157-120-1009	108	0.044	2.606	3.243	17.29	

In general, SJM found most of the capacitors can pass their 850 V high-voltage test. They found the energy density is ~2.1 J/cc. In general, the capacitors can deliver the required 35 J energy for defibrillation, however, the energy density needs to be improved.

3.4. Second Generation Ultrathin Capacitor Film Production and High Energy Density Capacitors

Milestone 6, April 30, 2010:

Develop second generation film capacitors based on improved capacitor film to achieve energy density > 4 J/cc in the packaged capacitor

Thanks to the support of PA Nano, we produced P(VDF-HFP) capacitor film with thickness of 2.1 μm – 3 μm in December 2008.

In June of 2009, we worked with Steinerfilm on the metallization of the 2.1 μm capacitor film. A roll of 2.1 μm thick film with length of 1,300 m was used. However, the film was damaged in the roll-to-roll metallization process.

As part of the risk management plan, we decided to produce another batch of capacitor film using our private funding.

In October 2009, we performed a third-round of pilot production of high-dielectric constant capacitor film. As discussed in our last report, SPS and Solvay Solexis jointly developed a new P(VDF-HFP) resin which has optimized composition and high purity. Solvay produced 2,600 kg of such resin in September 2009 and SPS paid over €100,000 for the pilot film production. We produced 24 rolls of capacitor film with thickness from 2.0 μm to 7.0 μm. Table 9 lists the roll information of the 2.0 μm capacitor film.

Table 9. SPS 2.0 μm Capacitor Film Produced in October 2009

Roll	Thickness (μm)	Length (m)
SPS09-11	2.0	2,009
SPS09-12	2.0	1,509
SPS09-13	2.0	1,510
SPS09-14	2.0	1,680
SPS09-15	2.0	1,344
SPS09-16	2.0	2,510
SPS09-17	2.0	2,009

Figure 16 shows a picture of the 2.0 μm thick capacitor film roll.

Figure 16. A roll of SPS High-K capacitor film with thickness of 2.0 μm.

The special resin developed by SPS and Solvay exhibits significant improvement in the capability for producing ultrathin capacitor film. The commercial resin contains more gels and the ultrathin capacitor film breaks frequently during the film production due to poor resin quality and contamination. By contrast, production of 2.0 μm film with the new resin was very smooth.

Lab-scale evaluation of the capacitor film confirmed the improvement in film quality. Figure 17 summarizes the results.

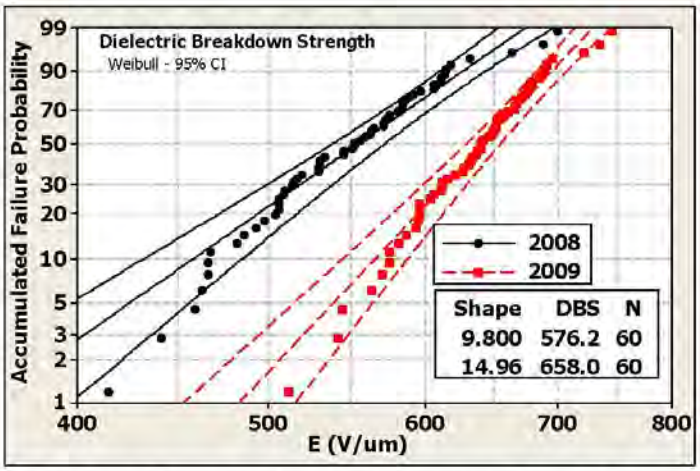

Figure 17. Dielectric breakdown strength SPS High-K capacitor film with thickness of 5.0 μm.

The capacitor film produced in 2008 has dielectric breakdown strength of 576 V/μm, and it increases to 658 V/μm in the 2009 capacitor film. More importantly, for the 60 tested specimens, there were 11 with DBS below 500 V/μm in the 2008 film, while all 60 specimens in 2009 film have DBS above 500 V/μm. This confirms the improvement in film quality, which is critical for implantable medical devices.

Since the 5 μm thick capacitor film has improved dielectric breakdown strength, a roll of 5.0 μm film with length of 2,510 m was used to fabricate the capacitors.

Figure 18 shows the design of the metallization. Figure 19 shows the pictures of the prototype capacitors.

For a 50 μF capacitor using 5 μm thick film, the active area is 3.14 m^2, which is about 8,000 times larger than the film test at lab scale (4 cm^2). Due to the existence of the free margin, the total film area is 4.48 m^2. To wind the 50 μF capacitor, 149 m long film was used for each capacitor.

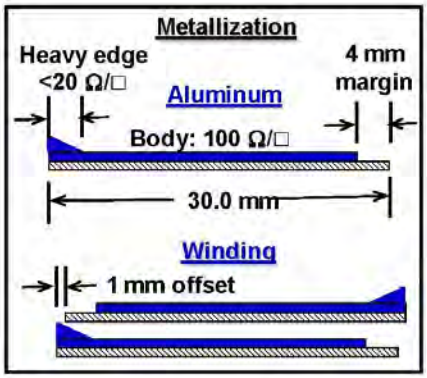

Figure 18. Metallization Design of the Prototype Capacitors Using 5 μm Thick Capacitor Film

Figure 19. Prototype Capacitors

The discharged energy density of the prototype capacitors was measured by using a special test setup developed by SPS following the same test protocol used by our primary customers such as medical defibrillator and navy railgun.

During the test, the capacitor is charged to preset voltage at constant current (~10 mA) using a modified Trek 5/80 amplifier. The capacitor is hold at the preset voltage for 10 seconds, and then discharges to a load resistor through a high power IGBT switch. The current flowing through the load resistor is recorded with an oscilloscope. A Labview program was developed to control the test process and record the charging and discharging data.

Figure 20 summarizes the discharged energy density.

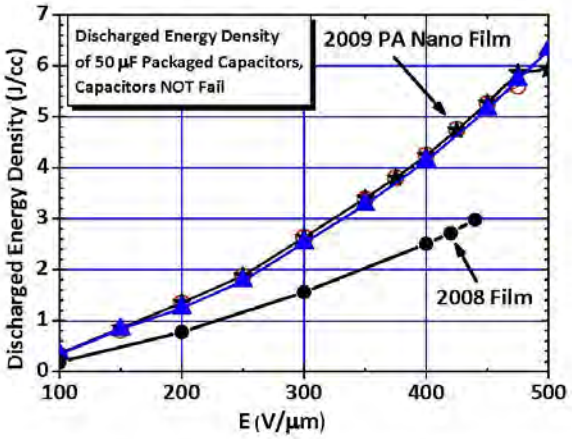

Figure 20. Energy density of prototype capacitors made with the new

capacitor film produced in 2009 as compare with the film produced in 2008 (prior to project start). Improvement in film quality leads to higher dielectric breakdown strength and higher energy density.

With the support from PA Nano, we produced capacitor film with higher film quality and higher dielectric breakdown strength, and the packaged prototype capacitors exhibit energy density over 6 J/cc, double the energy density of prototype capacitors made with film produced before the project started.

The metalized capacitors exhibit significant size reduction as compared with previous prototype capacitors. Figure 21 shows pictures of SPS capacitors made from 3.1 μm, 2.5 μm, and 2.0 μm capacitor film, as well as commercial PP capacitors with 3 μm thick capacitor film. Table 10 summarizes the size and capacitance density of these prototype capacitors.

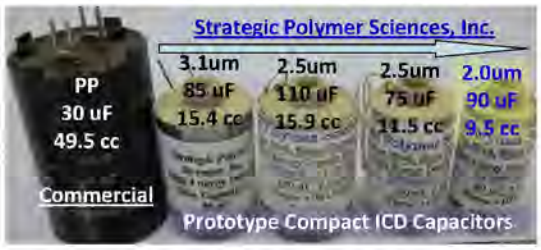

Figure 21. SPS prototype capacitors.

Table 10. Comparison of SPS Prototype Capacitors

Thickness	Capacitance (μF)	Diameter (mm)	Width (mm)	Volume cm^3	Weight (g)	μF/cm^3	μF/g
3 μm PP	30	Commercial for benchmark		49.5	67.3	0.61	0.45
3.1 μm	85	32.2	24.6	15.4	28	5.52	3.04
2.5 μm	110	30.7	25.7	15.9	28	6.92	3.92
2.5 μm	75	30.4	22.0	11.5	20	6.52	3.75
2.0 μm	89	32.5	19.3	9.5	15.7	9.37	5.67

It is clear that significant progress has been achieved in this project. Before the project, we produced 3.1 μm film and an 85 μF capacitor is about 15.4 cc in size and 28 g in weight. At the beginning of this project (April 2009), 2.5 μm was developed and a 110 μF capacitor has size of 15.9 cc and weight of 28 g. The capacitance density is improved from 5.52 μF/cc for 3.1 μm film to 6.92 μF/cc. At the end of the project, we reduced the film thickness by another 34% and produced the ultrathin 2.0 μm thick capacitor film. The capacitance density was further improved to 9.37 μF/cc.

It should be pointed out that these are only preliminary prototype capacitors and no optimization of capacitor design has been performed. For example, all current capacitors are wound around a core with diameter of 9.5 mm. The size of this core is about 2.1 cc, and it

contributes to 22% of the capacitor volume. By using much smaller winding core or no core, the size of the capacitor can be further reduced.

4. Summary of Commercial Milestones

The commercial milestones include customer test of SPS capacitor film and capacitors, cost analysis, IP development, and capacitor film marketing.

Milestone 2. February 15, 2009 (Completed)

Commercial capacitor film manufacturing evaluation, including

C1. Evaluation of the feasibility of commercial capacitor film production process.

C2. Cost analysis of capacitor films and manufacturing facilities

The production of the ICD capacitor base film with thickness down to 2.0 μm in a commercial scale has been demonstrated with the successful film run performed by SPS in October 2009.

However, the film line costs over $10 million US dollars and is well beyond SPS budget. Furthermore, the annual consumption of the ICD capacitor film is approximately 6,000 kg and it can be produced even with the pilot line in two weeks.

The machine manufacturer and the pilot line owner have offered SPS for toll manufacturing. Once the prototype capacitor performance developed in this program has been confirmed by the ICD manufacturer, SPS can lease the pilot film line for 2-3 weeks and continuously produce the polymer film for ICD capacitor application.

For the film run performed by SPS, the cost of the film is about $500/kg. However, this price can be reduced to below $150/kg if the film line is running continuously 24 hours a week and 7 days a week for 3 week.

One ICD capacitor will use less than 10 g SPS capacitor film. Assuming the film sale price is $1,000/kg, the film cost of one ICD capacitor is only $10, which is well below the current ICD capacitor price of $150.

SPS is also developing high energy density film capacitors for other military and commercial applications. If the market of the film is over 100,000 kg/year, SPS may consider buy a special film line to manufacture the high energy density capacitor film. With this model, the cost of the capacitor film will be less than $50/kg.

Milestone 3. March 27, 2009 (Completed)

C3. 2.5 μm film samples to customer for evaluation and customer send feedback

C4. Update on JDA agreement and potential licensing agreement.

The 2.5 um capacitor film produced by SPS in December 2008 was sent to the customer for evaluation. The customer measured the mechanical properties and concluded that the 2.5 um capacitor film is strong and sufficiently for winding capacitors.

CONFIDENTIAL: SPS has signed an official agreement with one ICD customer. The customer has paid SPS to obtain 18 months exclusivity period for capacitor evaluation. SPS will not entertain, accept or discuss with any other customers for the same application during the 18 months.

Milestone 4. July 15, 2009:

C5. Work with SJM to define the detailed specifications on the ICD capacitors and incorporate their feedback into technical development steps of Milestone 5.

SJM has provided a detailed requirement on the capacitor performance for the ICD application (see attached document). Table 11 summarizes their requirement.

	Voltage	Capacitance	Delivered Energy	Energy Density	Energy Efficiency	DSR	Leakage Current
Requirement	850 V	N/A	35 J	4 J/cc	75%	90%	0.3 mA
Current Status	850 V	80-120 μF	>35 J	2.1 J/cc	54%	84%	0.5 mA

While the current SPS film capacitors meet the voltage endurance and the delivered energy requirements, there are still several issues that need to be addressed for technology insertion. The most critical ones are the energy density and the energy efficiency.

High energy density is required to the implantable device. The energy efficiency is important to save the battery energy and extend the battery life.

To meet the customer requirements, SPS is planning to try several technical approaches:

1. Producing capacitor film with thinner thickness. The thinner the film thickness, the higher the capacitance density is. The capacitance density (and the energy density) is proportional to the square of the thickness.
2. Improve the capacitor winding design. Current capacitors have winding volumetric efficiency around 50%, and it should be improved to 75% to significantly improve the energy density. This can be achieved by using smaller winding mandrel and narrower free margin for metallization.
3. Improve resin and film quality. By reducing the defects in the resin and the film, energy loss can be minimized and voltage endurance can be improved. This will be done by cooperation with Solvay Solexis.
4. Utilizing the PECVD of Si_3N_4 to improve the energy efficiency and film quality. Higher film quality is critical to higher voltage endurance and energy density.

It should be noted that the development of the film capacitor is a very expensive process which is well beyond the resources of this project. Fortunately, SPS has obtained continuous support from the Department of Defense, Depart of Energy, and NIH on the development of the

advanced film capacitor technologies, and SPS is still working on these four approaches, as well as new polymer dielectric compositions.

Milestone 5. October 15, 2009:

C6. File formal US patents on ICD capacitor films.

SPS and Penn State filed a US patent on the nanostructured multilayer capacitor film technology.

Title "Methods to Improve the Efficiency and Reduce the Energy Losses in High Energy Density Capacitor Films and Articles Comprising the Same"

US Patent Application No.: 61/023,602, 2008

With our internal funding, SPS has also filed a new provisional patent on novel polymer dielectric compositions and another provisional patent on capacitor design:

"Low Cost Hybrid Film Capacitor Systems with High Energy Density and High Charging-Discharging Efficiency", 2010, 61/315,117

"Capacitor having high-temperature stability, High dielectric constant, low dielectric loss, and low leakage current", 2010, 61/314,355

Milestone 6. April 30, 2010: Film Capacitor and Capacitor Film Marketing and Future Plan

C7. Product Marketing: ICD capacitors, External Defibrillators, and Navy Railgun

C8. New Product Development

C9. Future Plan

With the support of the PA Nano commercialization fund, we have further improved the resin quality, film capability, and capacitor performance. We have recently produced prototype capacitors with energy density above 6 J/cc, doubled the energy density that was achieved before the PA Nano project.

- The improved capacitor film quality and capacitor performance encouraged us to launch our marketing and sales efforts. We attended the CARTS (Capacitors and Resistors Technology Symposium) USA 2010 at New Orleans, LA on March 15-18, 2010. We set up a booth to show SPS capacitor film products and advanced capacitors. Inquiries from several customers have been received and film sales have been started.
- We attended PCIM Europe (Power Conversion Intelligent Motion) on May 4-6, 2010 at Nuremberg, Germany to continue the marketing process.
- We delivered prototype capacitors to our ICD customers.
- We delivered prototype capacitors to the US Navy Railgun project for evaluation. We have had several phone conference with them to define the test protocol. However, the Navy is evaluating different technologies and they cannot make any decision now.

C8: New Product Development

- With the support of this PA Nano project, SPS has been able to integrate the capacitor resin development and production, pilot scale capacitor film manufacturing, film metallization, capacitor winding, and capacitor test and SPS has become the only US company with this broad expertise and capability.
- The success to deliver prototype capacitors in such a short term has impressed our DoD sponsors and SPS has won three additional SBIR Phase II projects and four SBIR Phase I projects to develop and commercialize our next generation film capacitors target at renewable energy applications. The sponsors include US Navy, Air Force (Wright Patterson), DOE, and NIH.
- With the government support, SPS is developing several novel film capacitor technologies at the same time:
  - High temperature film capacitors based on modified PTFE for power inverters in electric vehicles, wind mill, solar cell, and smart grid.
  - Wide temperature film capacitors that can operate from -55 °C to 300 °C.
  - Nanodielectric for railgun and high power microwave system.
  - Compact film capacitors for Radio Frequency accelerators.
- We were one of five companies in the nation that were invited by the DOE/DOD Interagency Advanced Power Group (IAPG) Capacitor Panel to discuss our capabilities in the development of advanced capacitors on Feb 4, 2010 in Washington, DC.
- We were invited for a second conference with Air Force, Navy, Army, and DOE to present our capacitor technology on April 26, 2010.

C9: Future Plan

- The development and commercialization of the ICD capacitor are still our priority with our new Air Force SBIR Phase II project and our NIH SBIR Phase II project.
- To reduce our risk, we have recently developed a new dielectric material which can meet the ICD customer's requirement on energy density and charge-discharge efficiency. A provisional patent is being filed before discussing with the customer.
- Marketing and sale of SPS high K capacitor film and high energy density film capacitor will continue. SPS is in the process of hiring a senior marketing manager to be in charge of the efforts.

5. Conclusions and Future Plan

This has been a very ambitious and aggressive project for Strategic Polymer Sciences, Inc. who has been trying to push the high energy density film capacitor technology to the commercial medical market. The PA Nano support has been critical to the progress made in the last two years. The pilot scale inexpensive capacitor film production has been significantly improved in three trials and large rolls of ultrathin capacitor film have been produced. The capability to produce high quality capacitor film using melt extrusion process distinguishes SPS from other

small capacitor companies which are using expensive solvent process and exotic polymer compositions at kilogram scale.

The progress made in this project has facilitated SPS secure more R&D funding to further improve the resin composition, capacitor film quality, and capacitor design. The three new patents have enabled SPS to expand the market from pulsed power system to power electronics DC bus capacitors which include hybrid electric vehicles, wind energy, solar energy, and smart grids. The novel film capacitors will facilitate the more efficient utilization of electricity, reduce the dependence of US on foreign resources, and help the war on climate change. The unique manufacturing capability and strong IP position will enhance the competitiveness of SPS in the renewable energy market.

Due to the unexpected technical challenges in handling ultrathin capacitor film, the PECVD of Si_3N_4 process has not been tested in the roll-to-roll process in this project. However, recent progress at SPS has revived our confidence in this technology. With the support of US Navy and Air Force, SPS is planning a roll-to-roll PECVD trial on 6 μm thick capacitor film, which will be performed at General Plasma at the end of June.

ICD capacitor still remains one of the highest priority and short term high profit margin market for SPS. SPS is continuing the development and two new customers have been asking for samples to evaluate.

Appendix F – 09-013 (Bayer MaterialScience)

Contract # Nano-09-013
Bayer MaterialScience LLC (BMS)
Final Report

Dear Drs. Brown and Hermans-Blackburn:

Please find attached the Final Report for the Force Sensing Pad project. Your support has enabled the development of a strong platform technology, completely enabled by nanoscience, at Bayer MaterialScience. We have also developed a good understanding and business case for the commercialization of a potentially industry-changing pressure sensitive pad for wheelchair patients. Final steps towards commercialization are still under internal discussion, but the work has clearly developed a nearly-commercial ready technology, business model and partners, and first class working prototype.

Thanks again for your support. We look forward to future endeavors with the PNCC.

Sincerely,

Dr. Alicyn Rhoades
Principal Investigator
Bayer MaterialScience LLC

Deliverables

Final Project Report
Payment: $29,850

Report Summary
Through the PNCC funded Force-Sensing Pad project, Bayer MaterialScience (BMS) worked together with partners from both the University of Pittsburgh and Carnegie Mellon University to develop a pressure-sensitive pad for the prevention of pressure ulcers in wheelchair patients. An in-depth market analysis revealed that existing market solutions which help caregivers and patients to minimize the occurrence of these preventable injuries are both too expensive and do not possess optimized physical properties for widespread adoption. BMS has developed a state of the art, nanotechnology-enabled solution for this major potential medical market in the PNCC flexible force sensing pad.

As stand-alone technologies, two patents have been filed detailing the composition of conductive components and flexible pad design. It is expected that both the wheel chair market application will be pursued, as well as other applications which stem from market-pull opportunities outside of the healthcare segment.

Project Team Review

BMS is one of the leading producers of polymers and high-performance plastics in North America and is part of the global Bayer MaterialScience business with nearly 14,900 employees at 30 sites around the world and 2006 sales of 10.2 billion euros from continuing operations. Our innovative developments in coatings, adhesive and sealant raw materials, polycarbonates, polyurethanes, thermoplastic urethane elastomers and functional films - including carbon nanotubes - enhance the design and functionality of products in a wide variety of markets, including the automotive, construction, electrical and electronics, household and medical industries, and the sports and leisure fields.

QoLT is a National Science Foundation Engineering Research Center (ERC) located in Pittsburgh whose mission is to transform the lives of people with reduced functional capabilities due to aging or disability. QoLT is a unique partnership between Carnegie Mellon and the University of Pittsburgh which brings together a cross-disciplinary team of technologists, clinicians, industry partners, end users, and other stakeholders to create revolutionary technologies that improve and sustain the quality of life for all people. By integrating information technologies and biomedical innovations, the resulting systems allow people to independently perform valued and necessary activities of daily living so that they can more fully participate in society.

Development Highlights

Significant progress was made though this project in when considering both the platform technology and the SmartSeat Application. The following are considered to be highlights:

Platform Development Highlights:

- System Materials Optimization
  - New formulation for CNT UV curable coating
  - Optimized dielectric layer
  - Robust
- System Design Optimization
  - Understand design impacts device efficiency
  - Three sensing capabilities co-exist on one film
  - Requires a balance of EE and materials expertise
- Manufacturing Optimization
  - Materials developed for high speed screen printing
  - Suitable for roll-to-roll applications

Smartseat Application Highlights:

- Significant Learning from Clinical Evaluation Trial
  - Feedback enabled optimization of material and design properties for hospital and patient application
- Butler Screenprinting Partnership
  - Materials optimized for the manufacture of this application at the appropriate scale
  - Identified knowledgeable, collaborative partner for future endeavors
- Software Interface for Clinicians
  - Medical staff expectations are now understood, and designs can be optimized to enable quick adoption
- Three Sensing Technologies
  - Pressure, temperature and moisture are critical to the medical application and have been integrated accordingly

The Evolution of the PNCC Force Sensing Pad

Early Prototype Pad:

The PNCC Force Sensing Pad started with an existing proof of concept pad that was a flexible polymer film sandwich with an 8 X 8 array of conductive carbon nanotube force sensing cells. The pad was manufactured by screen printing conductive silver ink traces on polyether polyurethane film, followed by a spray paint coating of a waterborne conductive CNT matrix over the silver traces. The rows and columns of the sensor array were connected to the external interface electronics over a 16 conductor ribbon cable.

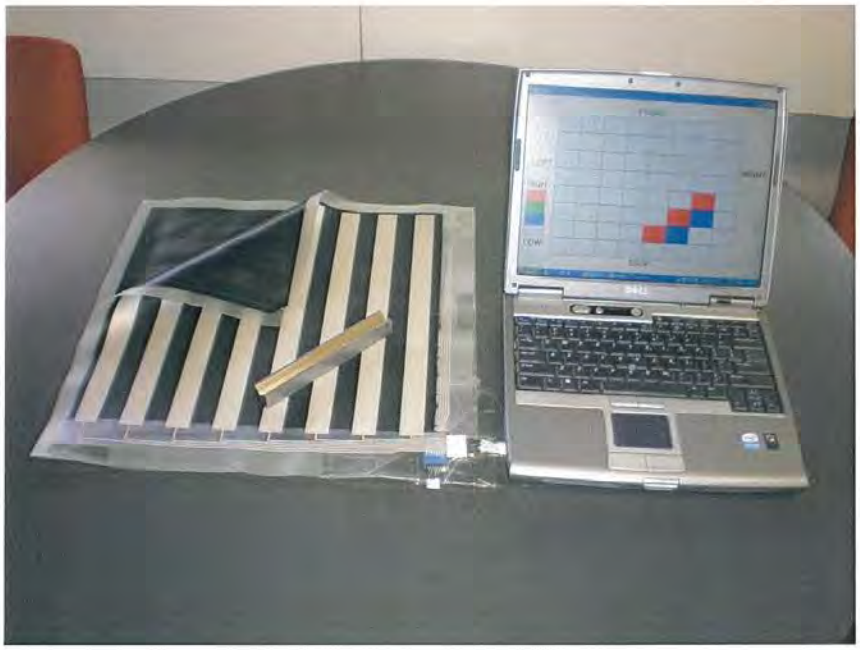

Figure 1 Early Prototype Pad

The main feature demonstrated by the pad was the highly flexible conductive carbon nanotube coating that could not be reproduced using existing carbon black coatings. A carbon black

coating would require a higher loading to achieve the same conductivity, resulting in a reduction in the flex properties of the coating. The early generation pad had limitations in hardware and software that restricted the response of the pad in pixel resolution, response time, and reliability of the ribbon cable interconnects. However, the pad clearly showed proof of concept, and the PNCC project goals were determined using this model as the starting point.

The first goal of the PNCC grant was to optimize design features of the early prototype device to meet specific application criteria that would be set forth by the joint effort of Bayer MaterialScience and Quality of Life Technology Center. As a competitive benchmark, the commercially available "X-Sensor®" pad was chosen and discussed in detail.

First Generation PNCC Force Pad

The critical application criteria for the force pad were established and included:

- A highly flexible polymer film substrate that would not interfere with the any cushion material on the wheelchair.
- A 16 X 16 force sensor array.
- The incorporation of temperature sensors on the pad would be very useful.
- The incorporation of a moisture sensor on the top of the pad would be very useful.
- The pad should be able to "breathe" and not interfere with the circulation of air between the patient and the cushion.
- The electronic interface should be located on the pad to reduce cabling.
- The pad software should match the basic human interface features of the X-Sensor® pad.
- The pad should match the performance specifications of the X-Sensor® pad.

With these goals in mind the first generation PNCC pad prototype was designed to test out the electronic circuitry with a 4 X 4 force sensor array and temperature and moisture sensors. The prototype pad was screen printed in-house to develop and evaluate the CNT conductive ink and dielectric ink, and to test the screen printing and pad assembly procedures.

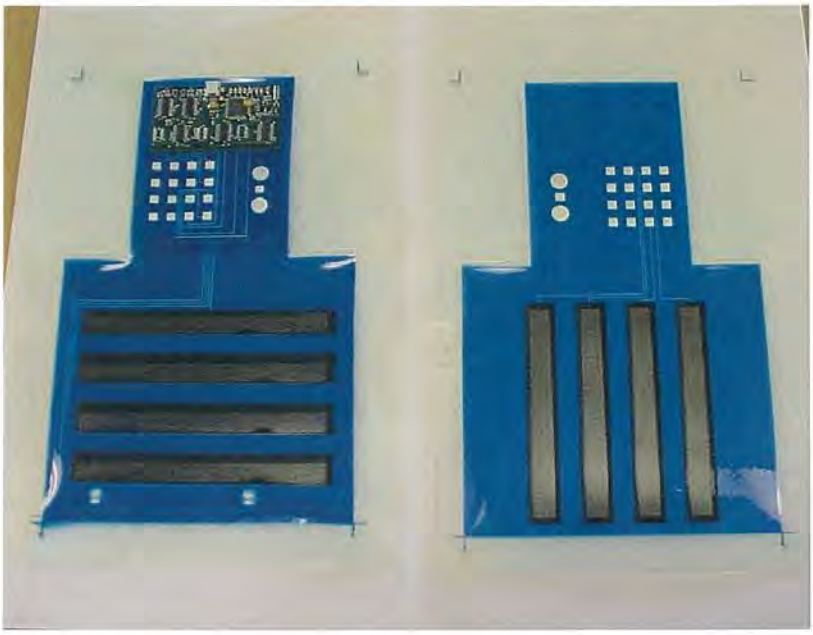

Figure 2 First Generation PNCC Pad prior to bonding the 2 films together.

Important lessons learned and observations with the first generation pad:

- The water based polyurethane CNT dispersion for the conductive coating would not work for screen printing because the coating would dry almost instantly on the screen fabric and clog the screen. This led to the development of a UV cured CNT conductive coating that would not dry on the screen and was very easy to use.
- The conductive CNT coating with a surface resistance from 10^4 to 10^6 is appropriate for this application.
- A method was developed to electrically and mechanically connect the printed circuit board to the force pad.
- The software and hardware for the electronic interface circuit was tested and scan rates for a 16 X 16 force sensor array can be as fast as 10 complete scans per second. The slow response of the early prototype pad was overcome with this model.

Second Generation PNCC Force Pad

Based on the results of the first generation prototype, the artwork for the larger 16 X 16 sensor array pad was generated.

Second Generation PNCC Force Pad

- Force sensing pad built on flexible TPU film
- Silk screened 17 layers
- Interface electronics mounted on pad
- New Material: UV cured conductive CNT coating

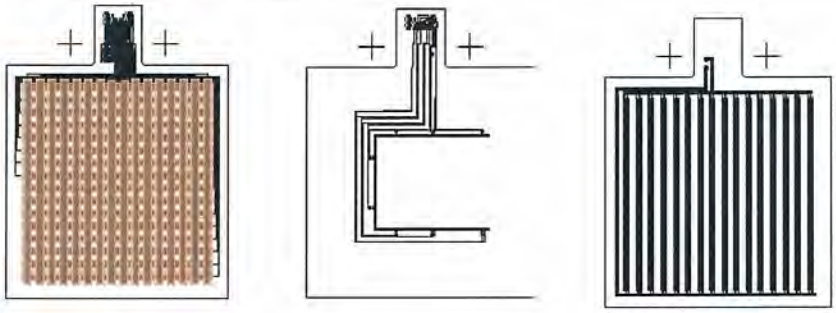

Figure 1. Second Generation PNCC Force Pad design for pressure, thermal, and moisture mapping.

Pads were screen printed at Butler Technologies. A number of problems were encountered with the screen printing process and are summarized in the following:

- The polyurethane films would curl and distort when sent through the oven for curing the silver ink and under the UV lamps for curing the UV inks.
- Due to the distortions in the film from the cure cycles, the registration between layers was off as much as +- 0.25".
- Two film thickness of 10 and 20 mils were used but the curling of the 10 mil films was so severe that it was eliminated from the trial.
- The UV cured dielectric ink generated numerous shorts between conductive layers through microscopic pinholes in the dielectric ink. The layers were increased from the normal two, to three prints per layer. This increased the thickness and reduced

the flexibility considerably. Even with three prints per dielectric layer there was still a rejection rate of 40 % due to electrical shorts.

- Adhesion of the Dielectric layer to the polyether polyurethane film was poor and would separate on some pads.
- A water based polyurethane contact adhesive was initially used for bonding the films. However, this system would clog the screen mesh and was not suitable for screen printing.
- Problems were encountered with mounting the thermistors to the pads and getting a secure mechanical and electrical bond.
- There were problems with interference or cross talk between force cells in the same row and the mathematical method being used to de-convolute the interference was not working. At the time it was thought that high resistance shorts between conductive layers was causing random leakage currents that could not be modeled and that the next run of pads using reformulated dielectric ink would eliminate the problem.

There were a number of things that did work well and included:

- The silver ink is very flexible and can survive repeated 1/8" bend radius stress.
- A method was developed to laminate the films to glass or metal as a carrier substrate. This eliminated the curling and distortions of the film and eliminated registration problems.
- A polyester polyurethane film was tested for adhesion to the inks and found to have excellent adhesion and was used in the next generation.
- A commercial UV cured contact adhesive for bonding the films together was tested and worked very well.
- A method was developed to bond and secure the thermistors to the force pads using a polyurethane thermoset adhesive prior to making the electrical connection with a silver epoxy and over coating with a UV cured polyurethane resin.

Eight fully functional pads were generated for testing. Two were delivered to HERL and one to the Human Interface Software (HIS) programmer for evaluation. After initial evaluation, HERL reported that the pads were too thick and stiff to be used as a wheelchair pad. HERL also reported that the recovery of the force cells after a weight was removed was slow and this was found to be due to tackiness of the CNT coating. Extensive testing of the pads by HERL was postponed until the third generation FS pad was produced to address these obvious issues. Delivery of a fully functional force pad was essential for the HIS programmer and rapid progress was made on the Human Interface Software while the third generation prototype pad was in development.

Third Generation PNCC Force Pad

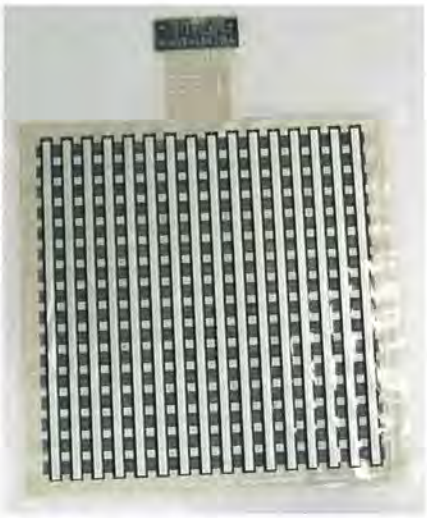

Figure 2. Third Generation PNCC Force Pad, assembled.

The screen printing process was moved to BMS for printing the next set of pads. The formulation of CNT conductive ink was adjusted to reduce the tackiness and improve the recovery rate of the force sensor cells. The formulation of the dielectric ink was adjusted to optimize viscosity, flow and surface tension to eliminate or reduce the number of pinhole shorts between conductive layers. Screen printing at BMS allowed the team to evaluate several formulations and complete significant in-house testing. However, the screen printing was done manually and therefore resulted in variable coating thicknesses; a problem that would not occur using professional screen printing machines. The pads were printed on 5 mil polyester polyurethane film laminated to glass sheets. The following observations were made on the third generation pads:

- Laminating the films to glass sheets allowed the registration between layers to be held to a very tight tolerance.
- Using the glass sheets allowed the film thickness to be reduced to 5 mils. The third generation force pads are very thin and flexible and received a favorable evaluation on comfort from HERL.
- The new formulation for the UV cured conductive CNT coating had very low tackiness and the recovery of the force cells after a force was removed was instantaneous.
- The polyester polyurethane films had excellent adhesion to all the inks used in printing the pads.

- Adhesive transfer tape was used to bond the two films together and worked very well.
- The thermistor sensors were bonded to the polyurethane film with a polyurethane adhesive prior to applying the silver epoxy electrical bond and the polyurethane protective coat. None of the thermistor bonds have failed (as of the date of this report?).
- The new UV-cured dielectric formulation is a significant improvement over the last generation dielectric coating. Even so, some films had to be rejected due to pinhole shorts. After extensive research, it was found that pinhole shorts in dielectric coatings are an industry wide problem and extreme measures are taken to reduce the failure rate. Rather than reformulating the dielectric coating, a design solution will solve the problem for FSP. The current pads are produced with two films with up to four silver and four dielectric layers on one film surface. Fourth generation pads isolate each of the three conductive silver patterns on individual films. In addition to the silver trace, each layer will be coated with one dielectric layer, existing only for abrasion and oxidation protection.
- The mathematical method for eliminating interference or crosstalk of force cells on the same row could not be implemented. The method failed when applied to the force pad where leakage currents, finite resistance of the signal traces and other variables caused singularities in the processing that were equivalent to a zero divisor. A literature search revealed an expired 1989 patent, U.S. Pat. No. 4,856,993 issued to Tekscan, which describes the use of a negative feed back virtual ground op-amp circuit that sums the currents from all sensor cells on a given row. All cells not being read are connected through a multiplexer to ground and contribute no current to the op-amp input. The cell of interest is connected to the positive drive voltage and is the only cell contributing a current to the op-amp circuit. This design was implemented and the crosstalk between cells on the same row was virtually eliminated. Under certain test conditions where large forces were being applied to a number of cells, cross talk could still be observed. Under normal pressure loads of a person sitting on a pad, the response was comparable to the Xsensor®[1]. Further improvements that will eliminate the crosstalk will be covered in the fourth generation FS pad.

HERL Testing of the PNCC and competitive XSensor® Pads

Two iterations of testing were completed, according to methods described in the Milestone 3 report. Both the flat-plate test and the Gel-buttock imprint test were used to compare the PNCC FSP to the competitive XSensor® FSP. Initial testing results were reviewed in April of 2010, and several problems with the testing setup were identified. After troubleshooting the technique, the two pads were re-tested in April of 2010. In summary, it was determined that the PNCC FSP performs at a competitive accuracy level to the XSensor® pad. Sample

[1] Xsensor® is a registered trademark of Xsensor® Technology Corporation.

Gel-buttock testing is shown below, which depicts the force sensing reading from each of the two pads.

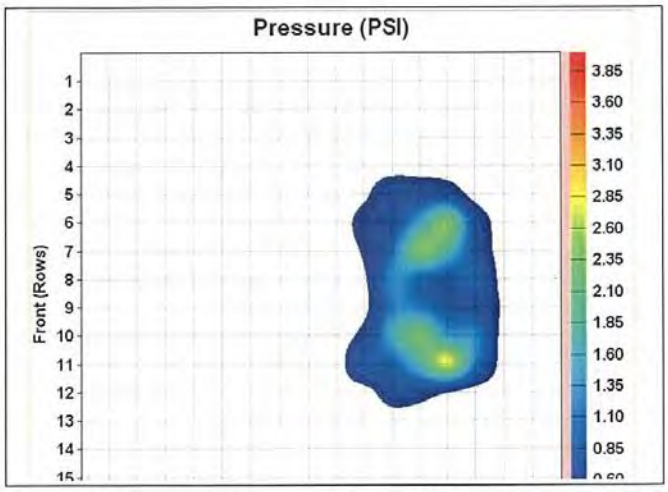

Figure 3. Gel-Buttock test fixture readout with 125 N force on PNCC pad. Sample data from repeatability study.

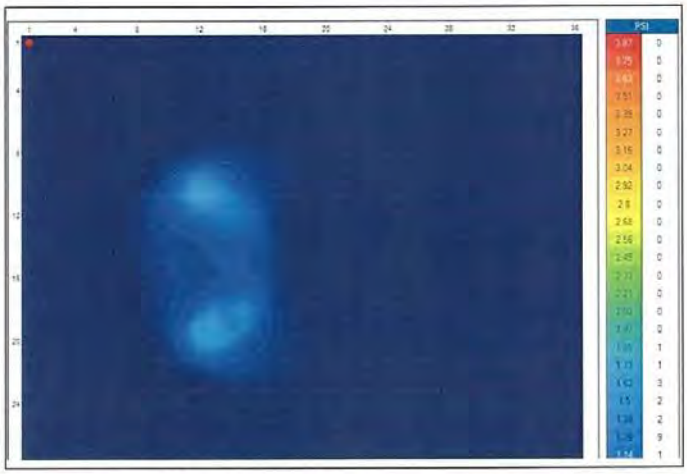

Figure 4. Gel-Buttock test fixture with 125 N force on the XSensor® pad. Sample data from repeatability study.

From the flat-plate testing, accuracy measurements were developed for both the Xsensor® and the PNCC pad at different force levels. From the following two charts, it is clear that both the PNCC and the XSensor® pads are measuring at a known interval from the true measurement. This error is repeatable up to a reasonable force for application (>200 N) and therefore, accurate calibration is possible as shown in the second plot.

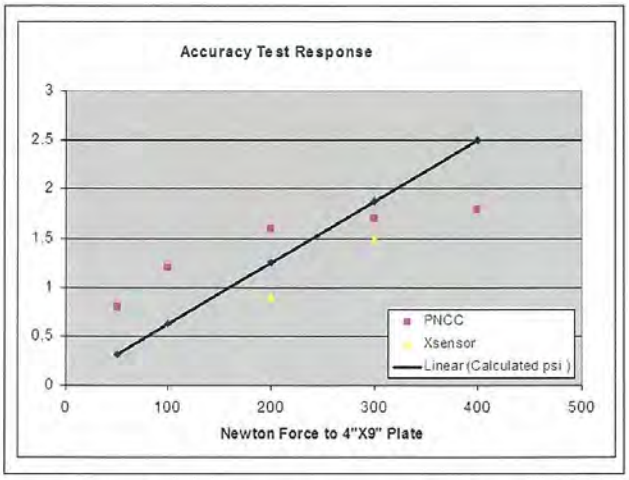

Figure 5. Accuracy test response from the flat-plate testing on both the PNCC and XSensor® pads. Both are linear and accurate within a certain force range, but both need calibration for accuracy.

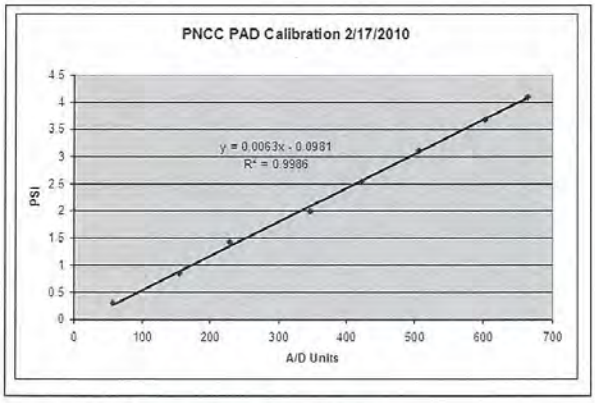

Figure 6. PNCC force readings after calibration.

Clinical Evaluation and Feedback of Force Sensing Pad

Three clinicians tried the pad in cooperation with three wheelchair patients. All clinicians have Physical Therapy background and have experience in prescribing wheelchairs. For the wheelchair users, two subjects are spinal cord injury patients and the other is a cerebrovascular accident patient. Two of them use the manual wheelchair and one person uses a power wheelchair. After using the device for three hours, both the clinician and the wheelchair patients provided feedback regarding the device. Their feedback is summarized in the following:

Table 1. Feedback from Wheelchair and Clinician user groups

	Pro	Con
W/C User	1. It is easy to use and good to see this information. 2. Knowing this information can help user correct their posture and manage pain efficiently. 3. Like one type of educational tool to teach and help user relieve pressure. 4. It is comfortable to sit on the map, and user is able to tell it was underneath him. 5. The device is small and could be operated easily.	1. Not sure is it worth to combine the Towel texture on the top of the device.
Clinician	1. It was convenient that this device can be plugged in computer with USB port. 2. It is good to know this information through testing.	Mapping 1. It was inconvenient to set up the orientation of the mapping without obvious indications and makers. 2. Pressure mapping crinkled easily. It would help to improve its flexibility. Software 3. The Software was not easy to use and interface should be friendly. 4. Interface is not clearly labeled. Temperature and moister value are not intuitive. 5. It is better to offer user to adjust color coding based on clinician preference. 6. It is inconvenient for clinician to compare different record during the evaluation. For example, comparing the data from different position and

		cushions. 7. This software cannot record user demographics and cushion information. 8. The usefulness of temperature and moister are still unknown. 9. Moisture value was kind of high; the data from the moisture sensor were questionable. Besides, we could not really tell the moisture value was from environment, clinician hands or user's hip. 10. Moister output had no time specific. 11. Software was not stable at all. Sometimes the system will freeze while closing the window.

In addition to the HERL study, BMS was able to follow up with one clinician for more detailed feedback. This feedback is summarized in the following:

Primary Materials Consideration

- Pad crinkles when sat upon or when it is over a soft mat. This is also common with the competitive pad and is a function of the pads being able to flex but not stretch.

Design Optimization:

- Cabling should come from the corner and not from the center of a side. This would simplify positioning the pad on more wheelchairs.
- Reports of the software crashing during the clinical evaluations most likely were from an intermittently shorted USB cable supplied by HERL.
- Clinician liked that the interface electronics were on the pad and had a simple USB cable instead of a wide ribbon cable to the computer with no additional boxes or power supplies.
- Clinician liked the display options including the 3D and color mapping with easy display rotation. Stated that patients want to see a color map response (red is bad, green is good) rather then a numerical response.
- Clinician stated that the Front/Back and Top/Bottom of the pads needed to be clearly marked.
- Clinician uses the mmHg scaling on pressure display and liked the option to choose range scaling (psi, newtons, mmHg).

Moisture and Temperature Sensing Feedback:

- Temperature output may be better as just one number reflecting the peak temperature on the pad instead of the 8 individual readings.
- Temperature and moisture readings are excellent ideas, but these aspects of the prototype need significant optimization.

- Moisture sensor to sensitive. High end of range should be water saturation.
- Clinician thinks a pad dedicated to moisture sensing would also useful.

General Feedback:

- Clinician thinks a pad with inflatable bladders and control feed back for pressure relief would be very useful.
- Clinician likes the pad and thinks it is relevant and has other applications. Likes the moisture sensor.

The Importance of User Feedback to Technology Development

In the true spirit of an integrated development project, the feedback obtained from clinicians, professional screen printers, internal material suppliers, and QoLT/HERL professionals culminated in the rationale behind the design iterations for the second, third, and upcoming fourth generation FS pads.

Source	General Topic	Feedback to R.H.	Impact to Project
HERL	Additional sensing capabilities	Moisture and thermal sensors would be very helpful to caregivers	Thermal and moisture sensing aspects were developed for the 2nd Generation pad
HERL	Pad design	2nd Generation pads were too thick and not flexible enough to be used as wheelchair pads	Efforts were made to thin the design for the 3rd generation, including reducing the TPU film thickness by 40%
HERL	Force sensing	HERL also reported that the recovery of the force cells after a weight was removed was slow	A less-tacky CNT coating was developed (UV cureable) which allowed for faster recovery and more accurate readings in real time
HERL	Sensing accuracy	High pressure loads were not being	RH determined the problem to be cross-

		properly detected	talk between neighboring loaded cells, and reconfigured the actual design of the pad to accommodate higher force loadings with less resistance in the wiring traces
Direct Clinician Feedback	Electronic interface	Clinicians revealed that the software has several positive attributes (3D mapping, etc) which will be maintained in future designs	RH/Bayer MaterialScience is able to aide future investors with this advice
Direct Clinician Feedback	Electronics Interface	Interface needs to be optimized for ease of use, and needs to store and retrieve data appropriately	RH recommends benchmarking final software developments to competitive XSensor products
Direct Clinician Feedback	Moisture and temperature sensing	Moisture and temperature sensing devices are not reported in useful units	RH worked with clinicians to establish "useful" units. This data will be incorporated into future software revisions
Manufacturing partnership feedback	Ease and practicality of manufacture	Waterborne coatings were not optimized for screenprinting, and clogged the screens.	RH/TW developed an alternative UV cureable coating which allowed for accurate and clean screenprinting

Refinement and Validation of Business Model

The development of a sound business case for the FSP has required a clear understanding of the market drivers, size, and segmentation in order to build an appropriate value proposition for BMS. After this initial value proposition, a value chain assessment was developed to examine the cost/benefit to BMS for participation in each stage of the value chain. Based on these calculations, a proposal for business development is being prepared and will be presented to BMS leadership in the coming weeks.

Market Drivers

Several market drivers suggest that the FSP is a needed and appropriate device within the modern US healthcare system. These drivers include Medicare/Medicaid reimbursement, legislative requirements, legal liabilities, patient safety, rising health care costs, and a growing elderly population. In summary:

Reimbursement

- Centers for Medicare and Medicaid Services will no longer reimburse hospitals for Stages III and IV pressure ulcers that are not documented upon admission.

Legislative Requirements

- New Jersey passed the 'Bedsore Bill' requiring nursing homes to replace existing spring mattresses with pressure-relieving mattresses to prevent the development of bedsores.
- Similar legislation is expected to pass in other states.

Legal Liabilities

- 17,000 lawsuits are related to pressure ulcer cases per year.
- Average settlement ranges from $50,000 - $4,000,000.

Patient Safety

- 60,000 people die every year from pressure ulcer infections (Christopher Reeve, a victim).
- Approximately 1.8 million pressure ulcer cases per year.

Rising Healthcare Costs

- Healthcare spending at $2.5 trillion or 17.3% of GDP in 2009.
- $1.3 billion spent on surgical treatment of pressure ulcers in US.

Growing Elderly Population

- The 65+ population numbered 38.9 million in 2008, an increase of 4.5 million or 13.0% since 1998.

Market Size and Information

Pressure ulcers, or bedsores, are defined as any lesion caused by unrelieved pressure resulting in damage to the underlying tissue. They are primarily caused by immobility and are particularly common among nursing home residents. Pressure ulcers are often associated with insufficient turning and poor body alignment while the resident is confined to bed. Long periods of sitting in one position, such as in a wheelchair, can also cause the skin to breakdown.[2] Repeated skin wetting and abrasions from sheets can heighten the occurrence of pressure ulcers. A resident at risk can develop a pressure ulcer within two to six hours of the onset of pressure, making timely intervention critical. A pressure ulcer can form literally overnight, or in a matter of hours if there is unrelenting pressure in a vulnerable area.[3]

In 2006, 1.8 million American cases of pressure ulcers were recorded at a treatment cost of $1.3 billion.[4] Each year, 60,000 people die from pressure ulcer infections. In 2007, CMS reported 257,412 cases of *preventable* pressure ulcers as secondary diagnoses. For these cases the average cost was $43,180 *per hospital stay.* Pressure ulcer treatment cost is directly correlated with the severity of the incident. Stage II pressure sore can cost upwards of $15,000 to treat, a stage III can cost up to $30,000 and a stage IV up to $90,000. Most commonly, pressure ulcers are diagnosed in the Stage II phase. A significant number of these pressure ulcers result from wheelchair patient usage.

BMS will initially target the wheelchair market in both the hospital and nursing homes. Assuming a 3:1 ratio of wheelchairs to beds, a seven-year lifetime for beds and wheelchairs and projected prices per devices, an addressable market share at each stage in the value chain can be calculated.

Metric	Number	Annualized Number (7 year life)	Assumption/Reference
Number of hospital beds	951,045	135,864	2008 AHA survey
Number of nursing home beds	1,700,000	242,857	2004 National Nursing Home Survey
Number of hospital w heelchairs	317,015	45,288	Assumption: 3:1 ratio
Number of nursing home w heelchairs	566,667	80,952	Assumption: 3:1 ratio

Figure 7. Market size calculations

[2] http://www.medicalnewstoday.com/articles/39327.php

[3] Mary Jane Maloney, a nurse practitioner and certified wound specialist, and a consultant to many long-term care facilities in northeastern Ohio.

[4] National Pressure Ulcer Advisory Panel

Sensitivity Analysis	Low (10% market share)	Medium (25% market share)	High (50% market share)	Addressable Market Size
Distributor	$ 12,624,024	$ 31,560,060	$ 63,120,119	$ 126,240,238
Device	$ 11,992,823	$ 29,982,057	$ 59,964,113	$ 119,928,226
Sub-Assembly	$ 6,312,012	$ 15,780,030	$ 31,560,060	$ 63,120,119
Raw Material	$ 467,089	$ 1,167,722	$ 2,335,444	$ 4,670,889

Figure 8. Market share calculations.

Value Proposition

The following "soft" and "hard" value proposition elements can drive the demand for pressure ulcer monitors. The "hard" or quantifiable elements can be summarized as the pressure ulcer cost per bed or wheelchair, which can be utilized in value pricing the FSP. For hospitals, opportunities to reduce surgeries, hospital stays and legal fees could result in cost savings of $75,796 per bed or wheelchair. For nursing homes, the potential to reduce legal fees could result in cost savings of $26,250 per bed or wheelchair.

Patient Safety. The FSP will reduce the risk of pressure ulcers and related infection, help to avert mortality and surgery, and also reduce the dependence of the patient on the caregiver or nurse.

Productivity: The FSP will allow nurses and caregivers to spend less time shifting patients in wheelchairs, and also reduce the time that these professionals must spend updating the Braden Scale, which is used to gauge pressure ulcer development.

Cost Savings: The FSP will enable cost savings from the prevention of surgery. The FSP will also reduce the length of hospital stays and reduce legal costs associated with pressure ulcer litigation. Hospitals are under increasing pressure to provide proof that every logical method for pressure ulcer prevention was in place during a patient's hospital stay.

Element	Calculations	Hospital Cost	References
Number of preventable hospital pressure ulcers per year	257,412		CMS 2007
% of pressure ulcers that are non-heel related	70%		Dekeyser, Dejarger, Meyst, Evers - 1994
Number of addressable pressure ulcers per year	180,188		
Hospital Costs			
Surgical and hospital costs per pressure ulcer		$ 43,180	CMS 2007
Legal Costs			
Number of pressure ulcer law suits per year	17,000		Mayo Foundation for Education and Research
% of law suits from hospital neglect	50%		Variable: Assume 50% from hospital, 50% from nursing home
Average settlement per pressure ulcer law suit	$ 1,000,000		Rowe 1999
Law suit cost per pressure ulcer case (amortized)		$ 33,021	
Total Cost per Pressure Ulcer		$ 76,201	
Cost per Bed or Wheelchair			
Annualized number of hospital beds	135,864		AHA Survey, 2008
Annualized number of hospital wheelchairs	45,288		Assumption: 3:1 ratio
Total pressure ulcer cost per bed or wheelchair		$ 75,796	Assume equal cost for both bed or wheelchair

Figure 9. Value proposition for hospitals

Element	Calculations	Nursing Home Cost	References
Number of nursing home pressure ulcers per year	159,000		National Nursing Home Survey, 2004
Legal Costs			
Number of pressure ulcer law suits per year	17,000		Mayo Foundation for Education and Research
% of law suits from nursing home neglect	50%		Variable: Assume 50% from hospital, 50% from nursing home
Average cost per pressure ulcer law suit	$ 1,000,000		Rowe 1999
Law suit cost per pressure ulcer case (amortized)		$ 53,459	
Total Cost per Pressure Ulcer		$ 53,459	
Cost per Bed or Wheelchair			
Annualized number of nursing home beds	242,857		AHA Survey, 2008
Annualized number of nursing home wheelchairs	80,952		Assumption: 3:1 ratio
Total pressure ulcer cost per bed or wheelchair		$ 26,250	Assume equal cost for both bed or wheelchair

Figure 10. Value proposition for Nursing Homes

Competitive Solutions

The importance of medical reimbursement for care of pressure ulcers is not trivial, and in fact may be the primary driver for product adoption. CMS regulations state: "Effective October 1, 2008, the Centers for Medicare and Medicaid Services will no longer reimburse the higher diagnosis-related group rate for Stages III and IV PrUs that are not documented on admission. In addition, formation of pressure ulcers in the hospital also puts the institution at financial risk of lawsuits."

As a result, hospitals are now using this statute [CMS Regulation] as an opportunity to review their entire inventory of products used for preventive skin care to include pressure redistribution mattresses and chair cushions, positioning devices, skin cleansers, moisturizers and incontinence products. The use of pressure-redistributing support surfaces, consisting of beds, mattresses and chair cushions, is expensive and constitutes the biggest single part of a hospital's expenditure on pressure ulcer prevention. The lack of research on the efficacy and cost benefits of various pressure redistributing surfaces adds confusion to hospital decision making ability with regard to the competitive options that exist. These competitive options are outlined below.

Pressure Ulcer Prevention Techniques	Technologies/Products	Notes
Patient turning (every ~2hrs)	Hospital and long-term care procedure	• Labor intensive • Lawsuits a result of neglect
Skin inspection (every ~8hrs)	Hospital and long-term care procedure	• Labor intensive
Skin creams/moisturizers	Topical antimicrobial, which includes povidone-iodine and cadexomer-iodine products.	• Labor intensive, temporary • Other risk factors still present
Nutritional supplements	Arginine, glutamine, vitamins, ProStat®	• Pressure and shear stress risk factors still present
Comfort pads and cushions	Air, gel, foam, water	• Not effective over time • Prices range from $60 - $500
Pressure redistribution pads 	Aquila Airpulse, Ease Seating System G-100+ Ergo Air EDS 2000 Pegasus Airwave Altern8 Talley Trinity Medical Dynamic Cushion System, Huntleigh Healthcare, Talley Group, British Astec, Pegasus Airwave, Blue Chip Medical Products SenTech Medical Systems Graham-Field Health Products The Roho Group Invacare Corp Sunrise Medical Supracor	• Over $2,000 price (~ $2,980, Aquila Airpulse) • Efficacy unknown • Timed
Pressure mapping pads	Xsensor®, ROHO Group, Vista Medical, Tekscan, Huntleigh, KCI, iShoe, Tactex Controls, KINOTEX® sensor, NITTA Corp., Osaka, Japan)	• Over $2,000 price • Does not measure shear, temperature and other risk factors • Only a static assessment

Table 2. Competitive analysis

Value Chain Analysis

The value chain for the production and sale of the FSP includes four major participants, as shown below.

Figure 11. Major value chain participants for the commercialization of the FSP.

We have analyzed four different scenarios, each capturing the situation should BMS decide to pursue subsequent positions in the value chain. In the simplest case, BMS simply sells raw materials, and in the most aggressive, BMS would distribute the FSP. BMS has its core competencies in the raw material and sub-assembly stages and we see a strong opportunity for a start-up company to leverage these strengths to manufacture the device and distribute to nursing home and hospital institutions. It is important to establish the value for each player in the value chain, in order to minimize risk of any position that BMS decides to pursue.

In summary, the gross margin has been calculated for BMS participation in each scenario. The following variable costs are associated with each position in the value chain:

Raw Material Supplier	Sub-Assembly	Device Mfg	Distributor
Silver ink	Thermistors	Software	
Baytubes	Thermistor mounting	Circuit board	
Dielectric coating	Screen printing	Netbook	
UV Coating	Lamination		
TPU film	Curing		

Table 3. Costs associated with each stage of the value chain.

A preliminary margin analysis is given for each stage in the value chain where BMS could position itself. The estimated price, variable cost and gross margin per unit is given for each stage. At the sub-assembly stage, the screen printing process accounted for the majority of the total cost. The screen printing cost was estimated based on a roll-to-roll production process, assuming conservative 5,000 unit volumes. With higher unit volumes, economies of scale will reduce the variable cost at the sub-assembly stage.

The estimated price per unit at each stage was determined based on anticipated margins and value-added. The conservative distributor price was determined based on the potential cost

savings for hospitals and nursing homes (value-proposition) and competitive pressure redistribution and mapping pad prices.

The gross margin percentage is anticipated to be highest in the raw material and sub-assembly stages where the greatest value-add exists with the core materials and manufacturing processing. Given its core competencies in materials processing and manufacturing, BMS will likely position itself as a raw material supplier and/or a sub-assembler.

	Raw Material Supplier	Sub-Assembly	Device Mfg	Distributor
Price/unit	$37	$500	$950	$1000
Variable cost/unit	$17	$222	$461	$514
Gross margin/unit	$20	$278	$489	$486
% Gross margin	55%	56%	51%	49%

Table 4. Gross margin estimation for profit at each stage of the value chain.

Other Market Opportunities for the Platform Technologies

Market opportunities have been identified in footwear applications, security applications, mass transit, and automotive applications. Currently, Business Groups at BMS are actively exploring the market potential in these other segments. These non-medical market segments represent areas where BMS materials are currently used, and therefore existing channels to market may be tapped for rapid commercialization opportunities.

Conclusions and Recommendations

According to our internal calculations with regard to the Smart Seat application, there is a two-year timeline to commercialization which remains. The cost of this timeline is roughly $800,00 and includes consideration of further product development, regulatory approvals, and the development of effective business partnerships for final commercialization. It has also been calculated that the demand for this type of solution will grow at levels greater than the GDP. Given these and other favorable calculations, it is expected that BMS will support the further commercialization of the SmartSeat either via direct commercialization or through a licensing model with partner companies.

Project Financials

Category	Amount	Date/Status
Total Project Costs	$44,603.44	As of 6/30/2010
Outstanding Obligations	$24,000	As of 7/08/10
-- to CMU	$4000	
-- to Butler Technologies	$10,000	
-- Close-out labor	$10,000	
Funding Received	$219,000	As of 7/08/10
Outstanding Obligations	$79,850	
-- Milestone 4 payment	$50,000	Invoice submitted
-- Final Report payment	$29,850	Report submitted

Appendix G – 09-020 (NanoGriptech)

FINAL REPORT

Project Title: Biologically Inspired Polymer Micro/Nano-Fibers as New Sportswear Closure Materials

Project Leader: Metin Sitti

Name of Project Leader's Organization: nanoGriptech, LLC

Date: June 1st, 2010

Submitted to: Pennsylvania NanoMaterials Commercialization Center

TABLE OF CONTENTS

EXECUTIVE SUMMARY

Project Goal Statement

The goal of the project is to develop gecko foot-hair inspired polymer fiber adhesives as new sportswear closure materials. The desired sportswear closure specifications given in Table 1 were determined after discussions with Under Armour Inc. Our work plan includes material selection, fabrication, and testing of polymer fiber adhesives produced with various materials and geometries to achieve the mandated performance metrics listed in Table 1.

Table 1: Mandated specifications of the polymer fiber adhesives for sportswear closure applications.

Specification Number	Specification Name	Desired Specification
S1	Shear force	10 N/cm^2 in dry conditions and 5 N/cm^2 in wet conditions
S2	Peel force	0.5 N/cm in dry and 0.3 N/cm in wet conditions
S3	Durability	Number of cycles over the product life: • 1k cycles – 90% of original strength • 2k cycles – 70% of original strength • 5k cycles – 65% of original strength
S4	Usability	Open and close forces of <0.5 kgf per inch
S5	Closure patch size	25 mm x 25 mm
S6	Water-resistance	20 kPa (3 psi) for 2 minutes
S7	Washability	Water cleaning (with a temperature up to <93° C)
S8	Flexibility	Flexible fiber arrays conforming to body curvatures
S9	Sound	Silent closures for specific clothing closures

Technical Development

In order to measure the performance of fiber adhesives, a custom-built testing setup capable of performing peel, shear, and adhesion strength measurements was developed. This system is also capable of performing repeated peel and adhesion tests to assess the durability of the developed materials. First generation fiber adhesives were manufactured using a micromolding/dip transfer method with two-part polyurethanes. The resulting fibers had a specialized geometry where the fiber is cylindrical with a wider flat tip which we denoted as "mushroom tipped fibers". Various fiber geometries were tested in dry conditions resulting in a fiber design that achieved dry shear strengths of 5.64 ± 0.81 N/cm^2 (56% of S1) and peel strengths of 0.71 ± 0.30 N/cm (142% of S2). This design was also found to maintain up to 85% adhesion over 5000 cycles surpassing the high cycle requirements of S3 (Table 1). Fibers sticking to each other during fabrication and after repeated use were found to be detrimental to adhesive performance.

A one-step micromolding fabrication technique was designed to decrease collapse during fabrication and improve the speed and the reliability of manufacturing. To further improve manufacturing reliability and prevent fiber collapse, a stiffer two-part polyurethane was used as the fiber material. While the stiffer material solved the fiber collapse problem, adhesive performance was poor.

Our work with two-part polyurethanes provided us with valuable information in terms of fabrication and material properties. However, two-part polyurethanes are not suitable for high volume/high speed fabrication due to curing times in the order of hours. Therefore, we switched our efforts toward manufacturing fiber adhesives from UV curable polyurethanes provided by Bayer MaterialScience. The curing time for these materials ranges from milliseconds to minutes depending on the curing system. Along with manufacturing fiber adhesives from UV curable polymers, we also started focusing on adhesion in wet conditions. While performance in dry conditions proved to be satisfactory (8.04 ± 0.54 N/cm^2 in shear and 0.64 ± 0.02 N/cm in peel), wet performance magnitudes were so weak as to not be measurable. To improve wet performance, fiber tips were coated with a specialized material containing a substance called DMA using a dip transfer method. Fibers with the DMA coating demonstrated 11.46 ± 0.42 N/cm^2 in shear and 0.50 ± 0.06 N/cm in peel in dry conditions, and 5.26 ± 0.70 N/cm^2 in shear and 0.09 ± 0.04 N/cm in peel in wet conditions, which satisfied the specifications for Milestone 4. While coatings such as DMA remain as a solution for improving wet adhesion, the high cost for both material procurement and their manufacturing led us to use fibers without coatings and focus on the properties of the mating surface to improve the performance.

In light of the previous findings, the fourth and final generation fibers were designed to reduce collapse using a hardening additive. The harder fiber material was found to have less fiber failure (see Appendix A) and more repeatable performance. After testing several different materials provided by Bayer MaterialScience, the opposing flat contacting surface was also changed to a waterborne polyurethane dispersion, Bayhydrol UH XP 2592.

Comparing our best measured performances with the specifications from Table 1, we observe:

- **Shear Strength**: Shear strength of 11.38 ± 0.41 N/cm^2 (114% of S1) in dry and 4.77 ± 0.13 N/cm^2 (95% of S1) was achieved (see I.4.2.1).
- **Peel Strength:** Peel strength of 0.41 ± 0.07 N/cm (82% of S2) in dry and 0.23 ± 0.02 N/cm (77% of S2) in wet conditions was achieved (see I.4.2.1).
- **Durability:** The peel strength after 1000 cycles is approximately 60-65% of the initial value. While this value is below the desired performance mandated by specification number S3 (which requested maintaining 90% of the peel strength after 1000 cycles), we are encouraged by the fact that very little performance degradation is observed after the first 100 test cycles (see I.4.2.3).
- **Usability:** The opening force is ~1 N/inch which is about one fifth of 0.5 kgf/inch. This value is calculated based on the peel strength.
- **Closure Patch Size:** The smallest patch sizes used in this project are ~25 mm X 25 mm. However, during the course of the project, we developed a fabrication technique to manufacture larger patch sizes using many small patches (see I.4.1.2)
- **Water Resistance:** After subjecting our developed material to 20 kPa (3 psi) for 2 minutes, approximately 60% of the fibrillar array stayed in contact with the opposing surface (see Appendix B).
- **Washability:** After five wash cycles at 40 °C (recommended washing temperature is "cold" for the fabrics provided by Under Armour), performance showed no degradation (see I.4.2.4).
- **Flexibility:** The final generation fibers are made from flexible materials.
- **Sound:** Fiber adhesives are found to be more silent than hook-and-loop adhesives.

Commercial Development

In August of 2009 joint development agreements were made with Under Armour and Bayer MaterialScience. In the first term, IP rights were obtained from Carnegie Mellon University and a license agreement was signed with UC Berkeley. Adhesives were designed with the intention of being used as closures for outerwear.

In the second term, options for scaling up were evaluated and cost estimates were made. We found that a complete production line (including a customized roller, and UV cure system) would cost on the order of $250,000 with an estimated material cost of $0.21/in^2 for 1.2M unit volumes.

The first scaled up fiber arrays were made in the third term and attached by Under Armour to opposing fabric samples to form closures (see II.3.2). These fiber arrays were later modified to use a flat material as the mating surface.

With a modified closure design, three apparel prototypes were produced. A glove was fitted with a fibrillar adhesive wrist strap to replace a hook and loop closure. Hook and loop closures were replaced on a jacket on the front and wrists. Running shoes were prototyped with three fibrillar adhesive straps replacing the laces. In the fourth term commercial development focused on identifying possible patents.

I. TECHNICAL DEVELOPMENT

I.1. MILESTONE 2

Develop the first generation fiber adhesives, using commercial polyurethane elastomers, for dry conditions at room temperature. The adhesives would have properties roughly 50% of the desired S1, S2 and S3 product specifications as listed in Table 1.

I.1.1. T1: First-Generation Polymer Fibers

Produce the first-generation polymer fiber array samples using commercially available polyurethane elastomers. All consequent fiber array samples are prepared as one-inch square, vertically aligned mushroom shaped micro-fiber arrays.

The first generation polymer fibers were fabricated using a sequence of photolithography, micro-molding and mechanical peeling. First, the exact replica of the final fiber structure (master template) was fabricated via photolithography from SU-8 photoresist. Then this lithographically formed master template of SU-8 fibers was used to form a compliant negative mold, which is silicone rubber. After having fabricated cylindrical fiber arrays, mushroom-like tip shapes were obtained by a dip transfer process. Consulting with Under Armour, polymer fiber adhesives were fabricated on ~150 μm thick adhesive thermoplastic urethane (TPU) sheets to facilitate bonding to fabric. First generation fibers were fabricated using ST-1060 polyurethane (BJB Enterprises, Inc) whose Young's modulus is ~2 MPa. Figure 1 includes a scanning electron microscopy image of the fibers and a large scale picture of the flexible fiber array.

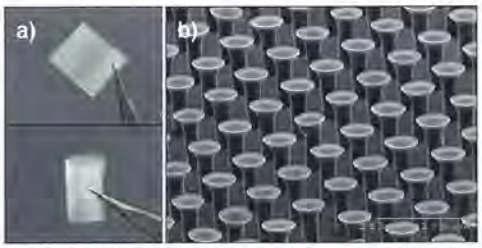

Figure 1: a) Photo of the flexible fiber sample. b) A scanning electron microscopy (SEM) image of sample **b** (see Table 2).

Table 2 details the dimensions of the resulting fibers. The tip diameter range between 1.5 to 2 times the stem diameter of the fiber for each sample.

Table 2: Dimensions of the first generation polymer fiber samples.

Sample Name	*Fiber Diameter (μm)*	*Fiber Length (μm)*	*Center-to-center spacing (μm)*
a	20	50	62
b	17	50	48
c	40	125	98
d	40	125	125
e	40	125	160
f	35	110	94

I.1.2. T2: Test Methods

Develop the test methods to measure the performance properties and compare to the desired specifications for dry conditions as listed in Table 1.

A custom testing setup was built to measure shear and peel resistance of the fibrillar adhesives (Figure 2).

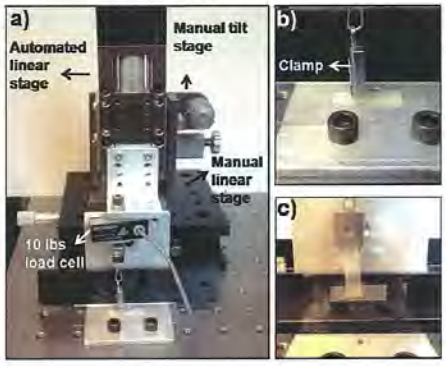

Figure 2: a) Picture of the test system used for shear and peel testing. Close up views for b) peel and c) shear testing.

All the peel experiments were conducted at 1 mm/s. However, we also conducted experiments on one sample at different speeds to demonstrate the effect of speed on peel resistance. The shear testing was performed at 0.1 mm/s for all samples.

Repeatability tests were performed with the same set up. Instead of the first fiber sample attached to the load cell, a 6 mm glass hemisphere is used to indent a fiber sample (Figure 3).

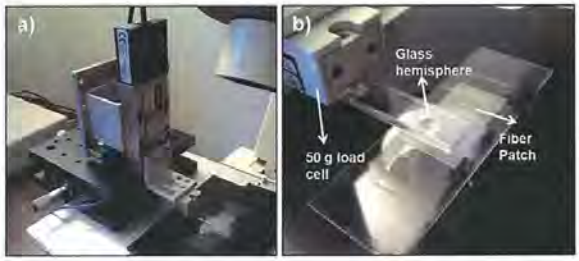

Figure 3: a) Repeatability testing setup in isometric view. b) Close up view of the hemispherical indenter and the fiber patch.

I.1.2. T3: Characterization

Characterize the performance of the first-generation fiber arrays in dry conditions.

Shear and Peel Testing

First generation fiber array samples listed in Table 2 made from ST-1060 polyurethane (BJB Enterprises, Inc.) were tested to quantify their peel and shear performance and compare with the desired specifications as listed in Table 1.

Table 3: Testing results for the first generation polymer fiber arrays. Listed values are the means of three measurements and the corresponding standard deviation. Bold (red) values indicate that the desired specifications are met.

Sample Name	*Shear Strength (N/cm^2)*	*Peel Strength (N/cm)*
a	3.89 ± 1.22	**0.49 ± 0.15**
b	**5.64 ± 0.81**	**0.71 ±0.30**
c	3.66 ± 0.47	**0.47 ± 0.10**
d	3.09 ± 0.30	**0.49 ± 0.01**
e	2.41 ± 0.19	0.24 ± 0.07
f	**5.31 ± 0.72**	**0.95 ± 0.08**

Figure 4 shows the effect of speed for peel and shear testing. Results from both peel and shear tests are evidence for viscoelastic behavior as expected from polyurethane elastomers.

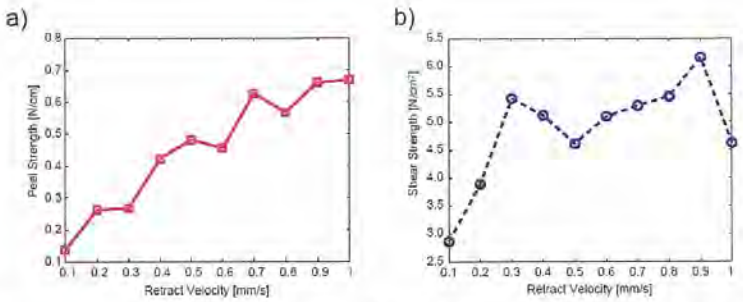

Figure 4: Rate dependence of a) peel, and b) shear strength for the first generation polymer fibers. All of the tests were performed with sample **b**.

Repeatability

Sample **f** was tested for 5000 adhesion cycles to quantify the performance decay for repeated use. Results in Figure 5 shows that the performance drops by 15% after 5000 cycles. The results are ~5% below the required performance at the 1000th cycle. However, the performance is well over the specifications for cycle numbers larger than 1000.

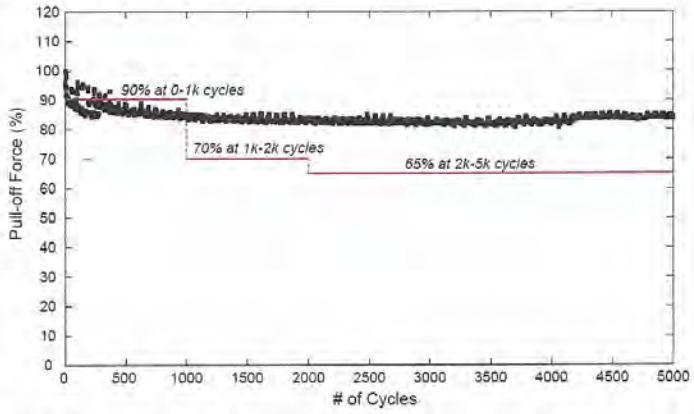

Figure 5: Adhesive performance of the fiber sample **f** for 5000 cycles and durability specification S3 (Table 1).

I.1.3. T4: Second-Generation Fiber Material Selection

Select the second-generation fiber materials from polyurethane products provided by Bayer MaterialScience.

Although the first generation polymer fibers performed well and satisfied the desired specifications, a major problem was fiber collapse during fabrication. Preliminary tests showed that permanent collapse could be prevented by using a stiffer material (such as ST-1085) for fiber fabrication. In addition,

polyurethanes used for Milestone 2 were two part polyurethanes. The curing times for two part polyurethanes are in the order of hours which make them less desirable for high volume manufacturing.

We consulted with Bayer MaterialScience for using fast curing UV curable polyurethanes as the fiber material. The fast curing capability of UV systems allows for very high volume and fast manufacturing. It was also possible to obtain a wide range of hardness values with these materials without drastically changing the material composition. This would allow us to isolate the effect of hardness and perform systematic experiments.

I.2. MILESTONE 3

Develop the second-generation, polymer fiber array adhesives for wet conditions at room temperature. The adhesives would have properties roughly 20% of the desired S1, S2 and S3 specifications given in Table 1 for wet conditions.

I.2.1. T5: Second-Generation Fiber

Produce the second-generation polymer fiber array samples using the polyurethane products provided by Bayer MaterialScience and test their performance in dry conditions.

As proposed in the Milestone 2 report, the collapse problem was reduced using a harder polyurethane (ST-1085) which also gave encouraging results as the potential second generation material. However, the feedback from Under Armour, based on the samples made from ST-1085, suggested that this material lost adhesion quickly over several uses and therefore was eliminated as the second generation fiber material. Therefore, we focused on improving the performance of the first generation fibers through improving the fabrication technique to eliminate collapse.

In addition, fiber fabrication from UV curable polyurethanes, supplied by Bayer MaterialScience, proved challenging to fabricate and set us back in our plan for the development of second generation fibers.

Manufacturing a One-step Mold

A process for manufacturing one-step molds has been developed as illustrated in Figure 6.

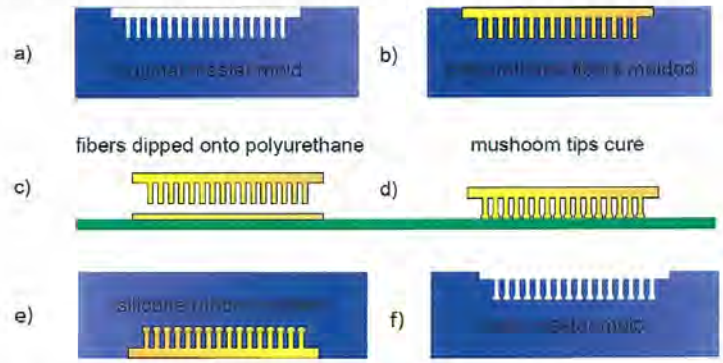

Figure 6: A one-step molding process creates a mold from existing fibers so that mushroom tips can be molded with the whole fiber array. a) A master mold made of silicone is prepared. b) Fibers are made on the master

silicone rubber mold with hard polyurethane. c) The array is dipped in a thin film of polyurethane. d) Mushroom tips are cured on a flat surface. e) A new silicone master mold is created by molding the silicone on the fibers. f) Fibers are mechanically peeled-off to obtain the mushroom tipped fiber mold.

Fiber collapse reduced significantly using this fabrication technique. In addition, this method allowed us to fabricate fibers from a wide variety of materials including UV curable polymers reliably. It also reduced the fabrication time by eliminating the spinning, dipping, and the extra curing stage in the original dipping based mushroom tip formation.

ST-1060 polyurethane was used as the fiber material. Fibers had a base diameter of 15 µm, a length of 50 µm, and a tip diameter of approximately 30 µm. The fibers were in a square packing arrangement with a uniform center-to-center spacing of 45 µm.

I.2.2. T6: Test Methods

Develop the test methods to measure the performance properties and compare to the desired specifications for wet conditions as listed in Table 1.

The experimental setup was similar to the setup used for previous tests as reported in I.1.2.

Shear Experiments and Results

For wet shear testing we placed a 0.1 ml water droplet on the center of the TPU film. The dry fiber array was then centered over the droplet and pressed onto the wet base. Figure 7 shows how shear forces were applied to the sample. Other than the light initial compressive load (preload) to bring the samples in contact, no normal compressive force was applied during shear testing. The speed of the stage was kept constant at 0.1 mm/s. The testing results can be seen in Table 4 and Figure 8.

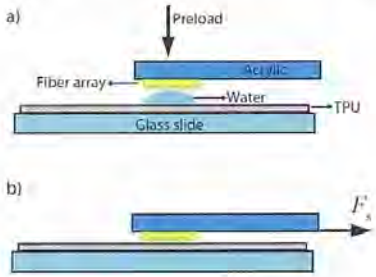

Figure 7: An illustration of the shear measurement. a) A preload is applied to the sample to allow the fibers to contact with TPU and push out excess water. b) A force is applied coplanar to the base of the fiber array.

Table 4: Measured and target shear strengths for fiber adhesives on TPU

	Shear Strength, dry (N/cm^2)	Shear Strength, wet (N/cm^2)
Measured	5.54 ± 0.77	1.77 ± 0.46
Target	5.00 (50%)	1.00 (20%)

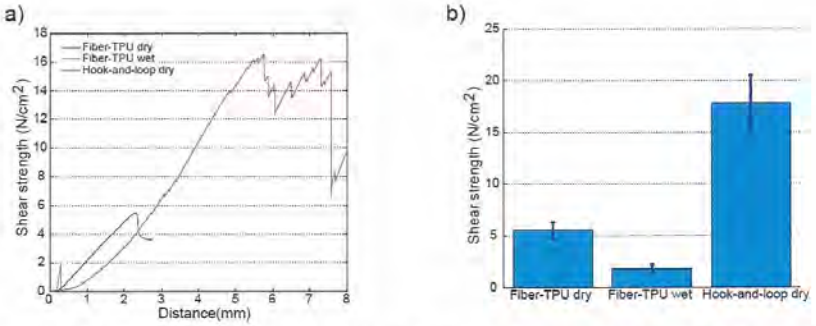

Figure 8: Shear measurement results. a) Sample force-distance data for wet and dry conditions. b) Average and standard deviation for 5 tests at 10 µm/s speed.

Peel Experiments and Results

Wet peel testing was set up similar to the shear testing. 0.1 ml water droplet was placed on the TPU surface and a light preload was applied manually to force the fibers into contact with the TPU film. After the preload was applied, the fiber film was pulled away vertically from the TPU film as illustrated in Figure 9. The test was repeated 5 times and the pulling speed was kept at 1 mm/s. Peel results are included in Table 5 and Figure 10.

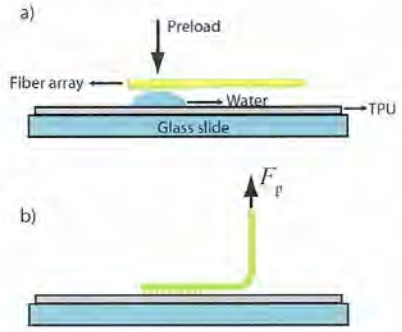

Figure 9: An illustration of the peel measurement. a) A preload is applied to the sample to allow the fibers into contact with TPU and push out excess water. b) Force is applied at 90o to the fiber array.

Table 5: Measured and target peel strengths for fiber adhesives on TPU

	Peel Strength, dry (N/cm)	Peel Strength, wet (N/cm)
Measured	0.151 ± 0.029	0.01 ± 0.01
Target	0.25 (50%)	0.06 (20%)

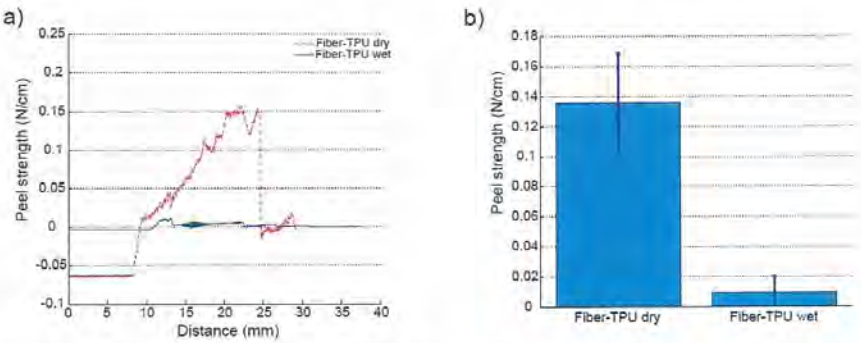

Figure 10: An illustration of the peel measurement. a) A preload is applied to the sample to allow the fibers to contact the TPU and push out excess water. b) Force is applied at 90° to the fiber array.

I.2.3. T7: Third-Generation Fiber Material Development

Develop the third-generation fiber materials with Bayer MaterialScience using performance and manufacturing as the primary criteria.

Initial tests performed to check the compatibility of several UV curable formulations (provided by Bayer MaterialScience) with silicone rubber showed that the UV polymers only partially cure on the silicone rubber with UVA exposure (UVA 400, HS Autshot). Also, initial findings suggested that a fusion curing system with Gallium bulb partially solved this problem leaving very thin tacky layer on the tips of the fiber adhesives.

Molding was also very challenging due to the high viscosity of the polymer and the fact that UV polymer does not wet the silicone rubber, both leading to the polymer not filling the holes in the silicone rubber properly and the formation of fibers with either no mushroom tips or smaller mushroom tips. To solve this problem, we added several silicone surfactants, tried formulations with lower viscosities, and performed molding under vacuum. Preliminary shear and peel test results are shown for UV curable fiber arrays in Table 6 and Figure 11.

Table 6: Measured and target peel strengths for fiber adhesives on TPU

	Shear Strength, dry (N/cm^2)	Peel Strength, dry (N/cm)
Measured	3.95 ± 1.29	0.52 ± 0.23
Target	5.00 (50%)	0.25 (50%)

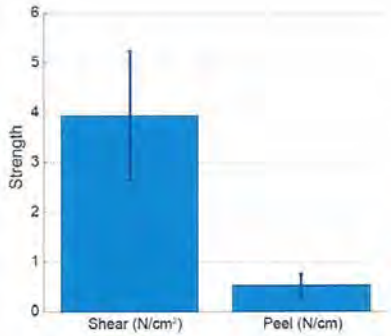

Figure 11: Shear and peel measurement results for fiber array made from UV curable polymer on TPU. Testing parameters are the same as described in section T6.

I.3. MILESTONE 4

Produce the third-generation fiber adhesives, using the modified polyurethane products, for dry and wet conditions in room temperature. The adhesives would achieve roughly 60% of the desired S1, S2 and S3 specifications given in Table 1 in dry conditions and roughly 30% of the desired specifications in wet conditions.

I.3.1. T8: Third-Generation Fiber

Prepare the third-generation polymer fiber array samples using modified polyurethane samples provided by Bayer MaterialScience.

I.3.1.1. Materials

Two types of UV curable polyurethanes were used as the third generation fiber material. The first material (Material 1) was a mixture of Desmolux 2491 (Bayer MaterialScience) and Genomer 1122 (Rahn USA Corp.) at 75% and 25 % by weight, respectively. The second material (Material 2) we used was Desmolux 2491 without any additives. Young moduli for Material 1 and Material 2 were calculated to be 2.6 MPa and 5.3 MPa, respectively. The Young modulus of the first and second generation fibers were about 2 MPa.

Figure 12: Top-view optical microscope images of a) 15, b) 40, and c) 50 µm base diameter fibers.

We used three different fiber geometries for testing. Dimensions of these fibers are listed in Table 7. In addition, optical microscope images are shown in Figure 12.

Table 7: Geometrical dimensions of the fiber arrays.

Sample Name	Base diameter (μm)	Tip diameter (μm)	Center-to-center Spacing (μm)	Area Coverage (%)
15 μm	15	31	45	37
40 μm	40	71	90	49
50 μm	50	98	120	52

I.3.1.2. Fabrication Method

UV curable polyurethanes were used as the third generation fiber materials. The manufacturing process was similar to the one-step molding described in I.2.1.

Since the affinity of UV curable polymers to silicone rubber is less than that of two-part polyurethanes, molding was performed under vacuum to force the UV material into the holes. With the help of Bayer MaterialScience, we have investigated possible additives that would reduce the viscosity and help improve the affinity of UV material to silicone rubber. Proper additives are likely to eliminate vacuum molding requirements.

Recall that, when cured against silicone rubber, UV curable polymers left an uncured tacky surface which affected the durability of the fibers. We determined that it was the trapped oxygen in the silicone rubber that caused oxygen inhibition on the surface of the polymer, a known condition with UV curable polymers. In light of these problems, the fabrication method was modified to ensure proper curing of the material. In this fabrication method, the molded UV curable polyurethane was exposed to UV light (400 W UVA lamp, H&S AutoShot) for a short period of time (approximately 1 min) to ensure that fibers hold their shape and peel from the rubber mold without damage. Then, to prevent oxygen inhibition, peeled fibers were cured in vacuum for 4 min. This fabrication method eliminated the curing problem and improved the performance and the durability of the fiber adhesives drastically.

I.3.2. T9: Characterization

Characterize the performance properties of the third-generation fibers in dry and wet conditions at room temperature as listed in Table 1.

I.3.2.1. Characterization Methods

Shear experiments were performed using the setup illustrated in Figure 13. This setup is almost identical to the experimental setup used previously but includes minor modifications to improve contact and obtain more repeatable results. Experiments were performed at speeds of 0.01 mm/s, 0.1 mm/s, and 1mm/s. The contact area was approximately 1 cm^2 for all tests. Reported results are the mean and the standard deviation of 3 tests per testing speed.

Testing was performed in "dry"," wet", and "wicking" conditions. Dry conditions refer to conditions at room temperature. For experiments in "wet" conditions, the sample was soaked in water until it gets completely wet. Testing was performed while the sample was still wet. Experiments which will be referred to as "wicking" were performed after the wet sample was dried with a wicking fabric for 1 min.

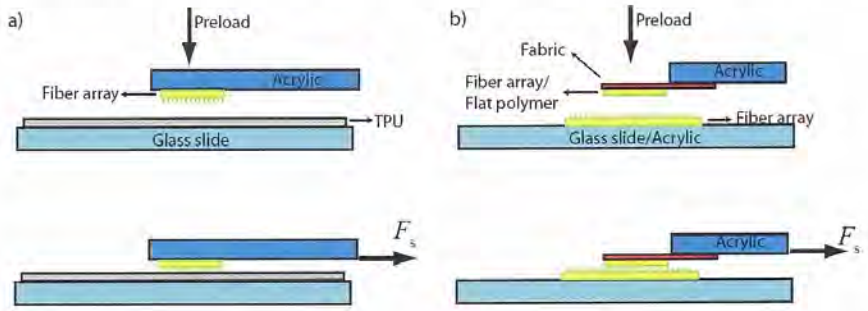

Figure 13: Illustration of a) shear testing method used previously, and b) current testing system.

Peel Testing:

Experimental setup illustrated in Figure 14 was used to carry out peel experiments. As in shear experiments, peel experiments were also performed in similar fashion to the work conducted previously. Experiments were performed at a speed of 1mm/s. The width of contact area was approximately 1 cm for all tests. Reported results are the mean and the standard deviation of three tests per testing speed. Dry, wet and wicking experiments were performed for peel following the same conditions explained in shear experiments.

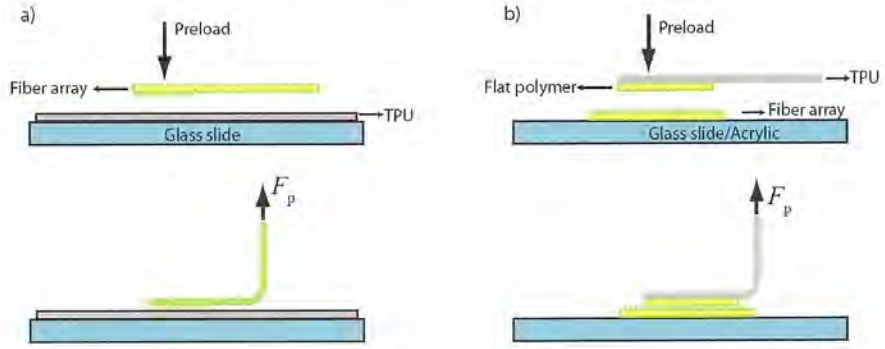

Figure 14: Illustration of a) peel testing method used previously, and b) current testing system.

Testing Results

The results from shear and peel testing under dry, wet, and wicking conditions for Material 1 can be seen in Table 8. The dash sign "-" in tables stands for values that could not be measured accurately due to the resolution limit of the load cell. All the results reported in the tables below are measurement results at 1 mm/s for both peel and shear measurements.

All the geometries were tested with fiber made of Material 1. These results were used to guide us to select the best performing geometry as the 50 μm fibers. **While the dry condition performance was over the desired values for fiber-flat measurements with 50 μm samples, in wet conditions, both peel and shear were practically nonexistent**. These results led us to select Material 2 as the fiber material.

Table 8: Shear and peel results for Material 1.

Condition	Specification	Test surface	Material 1			Desired Values
			15 μm	40 μm	50 μm	
Dry	Shear Force (N/cm^2)	Flat	3.18 ± 0.28	7.15 ± 0.30	8.04 ± 0.54	6.0
		Fiber	3.26 ± 0.08	2.40 ± 0.33	3.31 ± 0.20	
	Peel Force (N/cm)	Flat	0.36 ± 0.02	0.56 ± 0.01	0.64 ± 0.02	0.3
		Fiber	0.11 ± 0.03	0.24 ± 0.02	0.55 ± 0.13	
Wet	Shear Force (N/cm^2)	Flat	-	0.07 ± 0.0	-	1.5
		Fiber	-	-	-	
	Peel Force (N/cm)	Flat	-	-	-	0.09
		Fiber	-	-	-	
Wicking	Shear Force (N/cm^2)	Flat	0.69 ± 0.22	0.19 ± 0.25	0.11 ± 0.07	1.5
		Fiber	0.98 ± 0.49	0.82 ± 0.16	1.38 ± 0.33	
	Peel Force (N/cm)	Flat	-	-	0.19 ± 0.09	0.09
		Fiber	-	-	0.06 ± 0.03	

Testing results for Material 2 are listed in Table 9. While dry results were lower than that obtained from Material 1, they matched the desired values for fiber-flat measurements. Surprisingly for wet measurement, we saw a drastic improvement with Material 2 where both shear and peel results in wet conditions matched the desired values. Wet results included testing with both tap water and di-ionized water.

Table 9: Shear and peel results for Material 2.

Condition	Specification	Test surface	Material 2	Desired
			50 µm	Values
Dry	Shear Force (N/cm^2)	Flat	6.08 ± 0.40	6
		Fiber	4.64 ± 0.16	
	Peel Force (N/cm)	Flat	0.56 ± 0.04	0.3
		Fiber	0.18 ± 0.02	
Wet	Shear Force (N/cm^2)	Flat	2.74 ± 0.82*	1.5
		Fiber	1.99 ± 0.20†	
	Peel Force (N/cm)	Flat	0.11 ± 0.04*	0.09
		Fiber	0.08 ± 0.07†	

* di-ionized water, † tap water

I.3.3. T10: Test Methods for Temperature Performance

Develop the test methods to measure the shear and peel forces and characterize the durability of the polymer fiber arrays at temperatures that range roughly from -10 °C to +40 °C.

Characterization Methods

Temperature experiments were performed with the test setup shown in Figure 15. This setup uses a Peltier device to control temperature. A styrofoam box was used to insulate the test area. A slit in one face allows a string to pull on the sample inside the box from outside. Automated linear stages were used in the same configuration as other shear and peel tests to control vertical and horizontal motion. A temperature probe was inserted into the test area through a small hole.

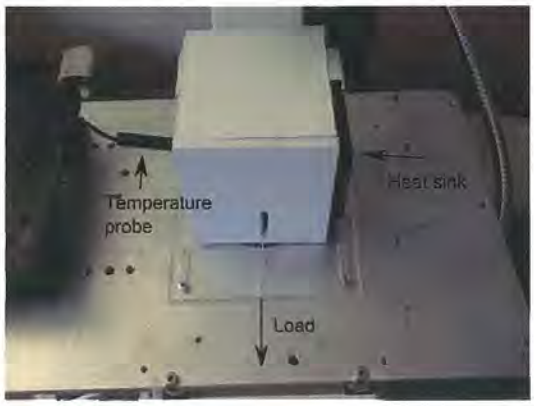

Figure 15: Temperature test setup

Results Summary

The results from temperature experiments can be seen in the figure below (Figure 16).

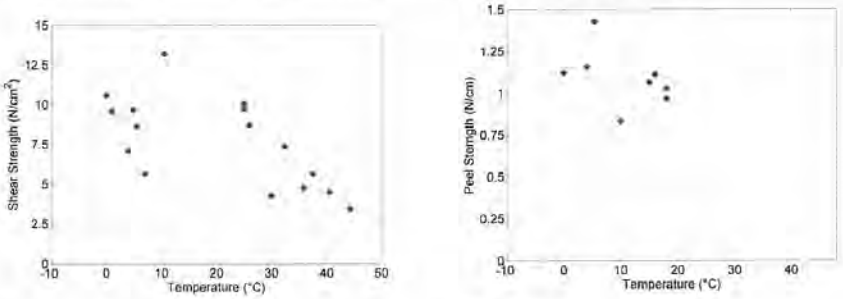

Figure 16: Results for shear (left) and peel (right) at various temperatures.

Results from temperature testing demonstrated that shear and peel strength generally decrease as temperature increases. For peel testing the Peltier device failed during testing and higher temperatures could not be reached.

I.3.4. T11: Forth-Generation Fiber Material Development

Develop the fourth-generation fiber materials with Bayer MaterialScience by modifying the array material to perform according to desired product specifications in dry and wet conditions at a variety of temperatures.

I.3.4.1. DMA Coating

Although we observed an improvement with Material 2 where both shear and peel results in wet conditions matching the desired values, it was of interest to additionally enhance the performance in wet conditions. For this purpose, we coated 50 µm mushroom fibers of Material 2 with 3,4-dihydroxyphenylalanine (DOPA) which is a modified amino acid that contains a unique catechol moiety and found in adhesive proteins in marine organisms, such as mussels and polychaete, showing strong adhesion in aquatic conditions.

A lightly crosslinked DOPA-containing polymer, hereafter will be abbreviated as DMA, was prepared by adding divinyl crosslinking agent, ethylene glycol dimethacrylate, and a photo-initiator, Irgacure 819, to monomer mixtures of dopamine methacrylamide and 2-methoxyethyl acrylate (Figure 17). DMA coated fiber arrays were prepared by a dipping process into a thin layer of DMA–dimethyl formamide solution. Then, the crosslinked coating was obtained by exposure to ultraviolet light (400 W UVA lamp, H&S AutoShot) for 1 minute.

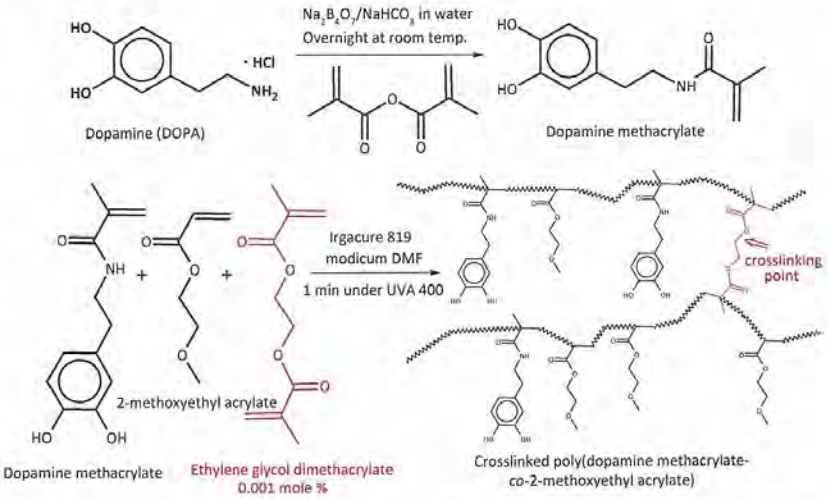

Figure 17: Illustration of the synthesis of dopamine methacrylate and crosslinked poly(dopamine methacrylate-*co*-2-methoxyethyl acrylate).

Testing results for the DMA coated Material 2 are listed in Table 10.

Table 10: Shear and peel results for fourth generation fiber material.

Condition	Specification	Test surface	DMA coated Desmolux 2491 50 µm	Desired Values
Dry	Shear Force (N/cm^2)	Flat	11.46 ± 0.42	6
		Fiber	7.82 ± 0.80	
	Peel Force (N/cm)	Flat	0.50 ± 0.06	0.3
		Fiber	0.56 ± 0.11	
Wet	Shear Force (N/cm^2)	Flat	5.26 ±0.70*	1.5
		Fiber	3.62 ± 0.77*	
			2.91 ± 0.14†	
	Peel Force (N/cm)	Flat	0.09 ± 0.04*	0.09
		Fiber	0.11 ± 0.04*	

* di-ionized water, † tap water

I.3.4.2. Repeatability:

Repeatability tests were performed for uncoated Desmolux 2491 fibers and DMA coated Desmolux 2491 fibers. All fibers for these tests were 50 µm in diameter and ~100 µm in length. Figure 18 shows the percentage strength to cycle number obtained with a 6mm glass sphere test.

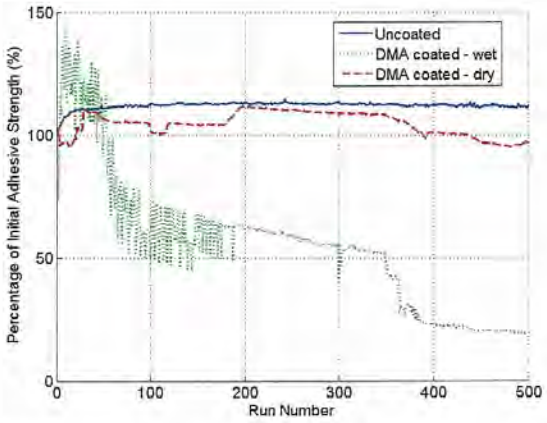

Figure 18: Repeatability for uncoated fibers and DMA coated fibers

I.4. MILESTONE 5

Produce the optimized fiber adhesive using the tailored polyurethane materials to perform at a variety of temperatures in dry and wet conditions. In room temperature conditions, the performance would have properties greater than 60% of the desired S1, S2 and S3 specifications given in Table 1 in dry conditions and greater than 30% of the desired specifications in wet conditions.

For this milestone, along with efforts to optimize the fiber material, we focused our attention on the material selection for the adhering surface. It is possible to achieve desired properties by controlling both the fiber and the adhering surface materials. In that regard, Bayer MaterialScience provided us with several candidate materials to choose from. Testing was performed for all to determine the best adhering material. Results are reported for the adhering surface which performed the best in dry and wet conditions.

I.4.1. T12: Fabricate Fourth-Generation Polymer Fiber

Fabricate the fourth-generation polymer fiber array samples using the tailored polyurethane material.

I.4.1.1. Materials

Desmolux XP 2491 (Bayer MaterialScience): Desmolux XP 2491 is used for the fabrication of fibrillar adhesives either as it is or as a major component in other formulations. It is an unsaturated aliphatic

urethane acrylate resin which contains isobornyl methacrylate as UV reactive group. Once exposed to UV light or electron-beam, it forms a very highly flexible elastomer.

Desmolux XP 2491 was primarily developed as coatings for application by roller coating, spraying, curtain coating and printing on wood, cork, furniture, paper, parquet, plastics, glass and films. It can also be used to formulate temporary (strip) coatings.

The viscosity of the material can be adjusted by using standard thinners (mono-, di-, tri- or tetraacrylic acid esters) or solvents such as butyl acetate. The UV curing of formulations based on Desmolux XP 2491 requires the use of standard commercial photoinitiators. The addition is up to 5% or in concentrations that satisfy the reactive requirements of the application. In case of electron beam curing, good passivation is essential to avoid the risk of surface inhibition.

SR 351 (Sartomer Company, Inc.): SR 351 (trimethylolpropane triacrylate) is used as a hardener in Desmolux XP 2491 as it increases the crosslinking density of the final cured product. It is a trifunctional, low viscosity, low volatility liquid monomer which offers fast curing response during free-radical polymerization. It provides weatherability, hardness and water, chemical, abrasion and heat resistant performance properties.

Bayhydrol UH XP 2592 (Bayer MaterialScience): Bayhydrol UH XP 2592 is used as a coating on the opposing surface of fibrillar adhesives. It is a solvent-free polyurethane dispersion which contains oxidatively drying groups in the backbone. The product is based essentially on a polyester backbone which also contains unsaturated natural oils (soy and peanut) which are what oxidatively cure. A polyester structure such as this which contains these natural oils is commonly referred to as an alkyd resin. The polyurethane is formed by reaction of the OH functional alkyd with an aliphatic diisocyanate (isophorone diisocyanate). During the production of the product, this polyurethane is formed first, and then dispersed into water to form the dispersion. Once the product is applied to a substrate, the water evaporates and the oxidative curing takes place which adds some more crosslinking to the resin.

Bayhydrol UH XP 2592 was primarily developed for direct adhesion to metal surfaces, but it has also been found to work well on other substrates such as wood and plastic.

I.4.1.2. Scaled-up Manufacturing Method

Using UV curable polymers and silicone rubber, a large scale mold can be manufactured cheaply and accurately. Uniform fiber arrays are made using a mushroom mold with a one-step molding process. The mold has raised edges with the thickness of the original master fiber array (see I.2.1). These edges are used to maintain a uniform thickness. The fibers are made with a UV polymer (Desmolux XP 2491). Up to eight adjacent fiber arrays are molded using the following process (Figure 19).

A small amount of UV material (enough to cover the surface) is spread onto the mushroom mold. The mold is placed in a vacuum chamber long enough for bubbles to disappear from the mold surface. The mold is removed from the vacuum chamber and the bubbles are manually removed by scraping. More UV material is added and a polypropylene sheet is placed on top to squeeze out excess material and flatten the back surface. The material is cured under UV light for 1 min (the lamp must be warmed up before starting the curing process). After partially curing, the fiber array is demolded. The array is placed in a portable vacuum chamber and cured for 6 minutes while under vacuum. Once fully cured, razor

blades are used to cut two parallel sides on the fiber array so that fibers adjacent fibers from a continuous line.

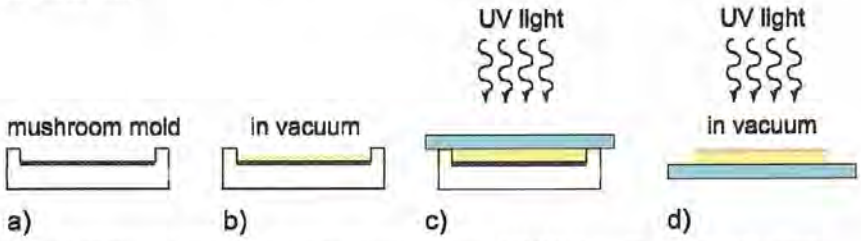

Figure 19: UV fiber curing: a) a silicone mushroom mold is prepared, b) UV polymer fills mushroom fiber mold under vacuum, c) UV light partially cures fibers, d) UV light fully cures demolded fibers under vacuum.

The fiber arrays are arranged with the fiber side down on a flexible sheet of thermoplastic polyurethane (TPU) which sits on a flat rigid surface to align the fiber tips to the same plane. The arrays are put in a row so that the razor-cut edges are as close to each other as possible. Figure 20 illustrates how the fiber arrays are arranged.

Figure 20: Arranging fiber arrays so that fiber surfaces are coplanar and edges are close.

Mounting the arrays to a rigid surface is necessary so that the fiber surface can be exposed for molding. Figure 21 illustrates the mounting process. Small cracks between arrays need to be sealed so that the material used for mounting the fibers does not seep onto the fiber surface during mounting (Figure 21 (a)). A seal fabricated from the UV curable polymer is applied carefully into the cracks between fiber arrays (Figure 21 (b)) and cured quickly (Figure 21 (c), around 1 min). If the UV material is not cured soon after being applied, it too will seep onto the fiber surface. It may be necessary to seal the cracks in several stages to avoid seepage.

With the cracks sealed, a large batch of UV material is applied to the back of the fiber arrays and a rigid, clear surface like acrylic is placed carefully so that no bubbles remain in the material. Large bubbles may affect the surface of the fibers. The UV material is fully cured (Figure 21 (d)) leaving the fibers permanently attached to a rigid surface.

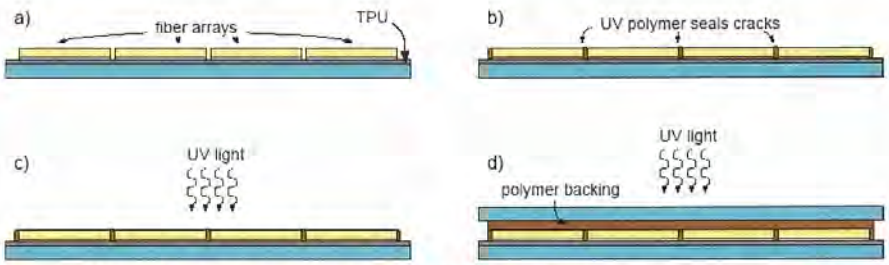

Figure 21: Mounting the fibers on a rigid surface, a) arranged fibers, b) UV polymer fills cracks, c) polymer is cured with UV light, d) more polymer is added and is cured onto acrylic backing.

After the fiber arrays are mounted to a rigid surface, the bottom surface can be removed and the TPU is carefully peeled off of the fiber surface. With the fiber surface up, a 1/8 inch thick window is placed outside the edges of the fibers, as illustrated in Figure 22 (a) which describes the mold-making process. Around 5g/in^2 of Silicone rubber (Dow Corning HSII) is poured to fill the window (Figure 22 (b)). A rigid backing material is placed on top of the silicone and weight is applied to the top surface to squeeze out excess silicone rubber and make the mold bottom flat (Figure 22 (c)). After 24-48 hours of curing the mold is ready to be demolded. If demolded carefully it should be possible to make another mold using the same fiber arrays. The final mold is illustrated in Figure 22 (d).

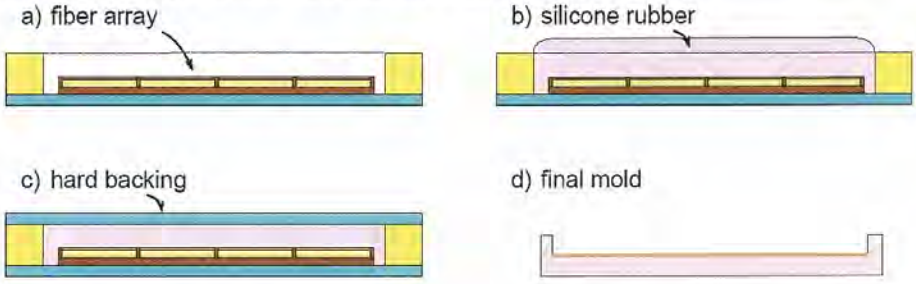

Figure 22: Mold-making, a) a window is placed around fibers, b) silicone rubber is poured, c) a rigid backing material flattens silicone rubber, d) mold is demolded and ready to be used.

I.4.1.3. Flat Surface Manufacturing Method

Methods for manufacturing a flat surface to mate with the fiber surface were explored this term. Various Bayer MaterialScience polyurethane dispersions (PUDs) were tested (see I.4.3). PUDs are waterborne polymers that cure once water evaporates. Flat coatings of PUDs can be made with simple knife coating techniques. Samples used for our experiments were made at Bayer MaterialScience by curing the material directly onto a paper backing. In order to better control surface quality transfer coating may be used. Figure 23 demonstrates how knife coating is used for PUDs.

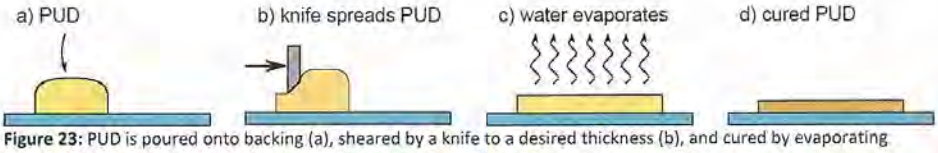

Figure 23: PUD is poured onto backing (a), sheared by a knife to a desired thickness (b), and cured by evaporating water (c). The final coating will be thinner than the layer sheared by the knife because of lost mass (d).

I.4.2. T13: Performance Characterization

Characterize the product performance of the fourth-generation fiber array samples in dry and wet conditions and in the temperature range of -10° C and 40°.

I.4.2.1. Dry and Wet Performance

Shear and peel performances were measured both in dry and wet conditions using previously-reported measurement setups. Results for the highest performing fiber sample/substrate combination are presented in Table 11. This optimized performance was measured for fibers fabricated from a UV-curable polyurethane (Desmolux XP 2491, Bayer MaterialScience) with a hardening additive (1% by weight, SR 351, Sartomer Company, Inc.) on a polyurethane dispersion-coated substrate (Bayhydrol UH XP 2592, Bayer MaterialScience). For all of these results, the measured values are compared with the desired benchmark values for this phase of the project, which are listed in the last column of the table. Results for other evaluated samples and substrates are presented and discussed in more detail in Section I.4.3.

Table 11: Dry and wet shear and peel results for fourth-generation fiber arrays

Condition	Specification	Testing speed (mm/s)	Desmolux XP 2491 + 1% 351 hardener on UH XP 2592 substrate	Desired Values
Dry	Shear Force (N/cm^2)	0.1	6.41 ± 0.37	6.0 N/cm^2
		1.0	11.38 ± 0.41	
	Peel Force (N/cm)	1.0	0.41 ± 0.07	0.3 N/cm
Wet	Shear Force (N/cm^2)	0.1	1.50 ± 1.08	1.5 N/cm^2
		1.0	4.77 ± 0.13	
	Peel Force (N/cm)	1.0	0.23 ± 0.02	0.09 N/cm

For all testing configurations, the benchmark desired values for this fourth generation material were surpassed. In shear testing, increasing the test speed tenfold from 0.1 mm/s to 1.0 mm/s increases the measured shear force significantly in line with the data reported for previous milestones.

I.4.2.2. Temperature Performance

Experimental Setup

For shear and peel testing, a temperature control system was designed to maintain temperatures between -10 °C and 40 °C. Figure 24 shows the system configured for shear testing. A water-cooled Peltier device is used to either heat or cool an aluminum testing surface. The fiber sample is placed in contact with the aluminum and cooled/heated via conduction from the surface.

Figure 24: Testing configuration and cooling system. The temperature control system uses a water cooling system (a) to keep the Peltier device (b) from overheating. The Peltier device is controlled by a voltage regulator (c) and its temperature is monitored by a probe near the sample (d).

For each test, the fiber array and opposing flat surface were put in contact at room temperatures and kept in contact for 10 min while the temperatures was adjusted. This prevented frost and condensation from forming on the interface. Because the surroundings were at room temperature (between 22 °C and 27 °C) condensation and frost formed at rates that we don't expect to experience in real world applications where the surface is likely to be close to the surrounding temperature. Contact time has the tendency to increase shear and peel strength somewhat but our room temperature tests were relatively close to previous tests with short contact times. Before each test the entire system is brought back to room temperature and the sample is dried in a vacuum desiccator for 10 minutes.

Results

Our tests showed, as expected, that shear and peel strength were highest at cold temperatures and decreased consistently as temperature increased. The results can be seen below (Figure 25).

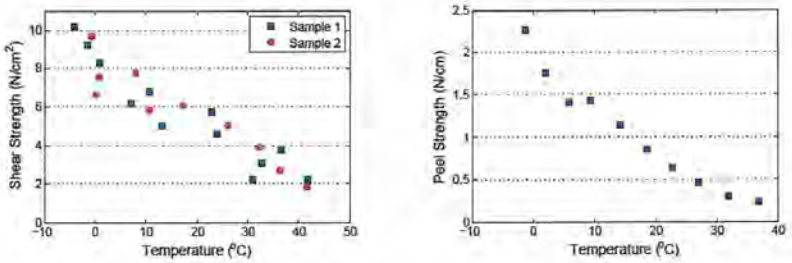

Figure 25: Temperature-dependent results for shear testing at 0.1 mm/s (left) and peel testing at 1 mm/s (right).

I.4.2.3 Durability Performance

Cyclical Peel Testing: Experimental Setup

Recall that the repeatability tests we performed previously were in adhesive contact using a hemispherical glass as the adhering surface. Although the results from that type of testing are very informative, fibers do not experience the type of loading they undergo in a typical peel or shear experiment. In order to better assess the durability of the fibers under use as closures, an automated preloading mechanism was fabricated and incorporated into our peel force characterization apparatus, as illustrated in Figure 26. This mechanism automatically presses the fiber sample back into contact with the test substrate after each test cycle, allowing for data collection for multiple cycles without a human operator.

To collect data, the fiber array (**A**) is first manually pressed into the substrate (**B**). Then, using a computerized controller and data collection software, a linear stage (**C**) is actuated to move a spring-loaded preloading roller mechanism (**D**) toward the substrate. As the mechanism comes into contact with the substrate, the rubber roller rolls down along the length of the substrate, evenly pressing the fiber tips into contact until a predefined preload force, measured by a 10 lb load cell (**E**), is reached. At this point, the stage is retracted away from the fiber/material interface, peeling the sample as it is withdrawn. Now, the apparatus works as before, using the same load cell to measure the peeling force required to separate the fibers from the substrate. When the test ends, the top section of the fiber array is still in contact with the substrate, allowing the process to be repeated for any desired number of test cycles by iteratively preloading the rest of the fiber array back into the substrate and peeling it off.

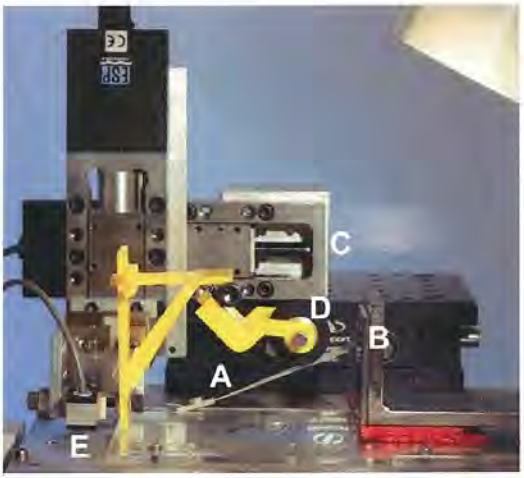

Figure 26: Peel testing apparatus with automated preloading mechanism which allows for multiple cycle durability evaluation. A fiber array sample (A) is first manually brought into contact with a test substrate (B). A linear stage (C) controls the motion of a spring-loaded preloading roller mechanism (D) which evenly presses the fibers into the substrate as the mechanism moves toward it. As the mechanism is retracted, the peel force required to separate fiber/substrate interface is measured by a load cell (E).

Cyclical Peel Testing: Results

This apparatus was used to collect data for 1000 peel cycle iterations for hardened fibers (fabricated from Desmolux XP 2491 with the addition of 1% by weight SR-351) on a Bayhydrol UH XP 2592 substrate. The results of this testing are illustrated in Figure 27. The sawtooth nature of the data in this figure is reflective of the automated air-conditioned laboratory environment and the temperature dependence on the peel strength, which was observed and discussed in Section I.4.2.2. As the air-conditioning is activated, the environment cools slightly and the peel strength increases modestly. Once the room temperature set-point is reached, the air-conditioning turns off, and as the room warms up, performance declines slightly. This cycle is repeated as the thermostat alternately triggers and cuts off the cooling in the room. From this data, we can see that the peel strength after 1000 cycles is approximately 60-65% of the initial value. **While this value is below the desired performance mandated by specification number S3 (which requested maintaining 90% of the peel strength after 1000 cycles), we are encouraged by the fact that very little performance degradation is observed after the first 100 test cycles.** Because we do not have a dedicated setup for this type of testing and data collection for 1000 cycles requires approximately 15 hours, we were unable to test for higher cycle numbers at this point in time, as it would prevent us from being able to run other tests or evaluate fabricated samples in our lab.

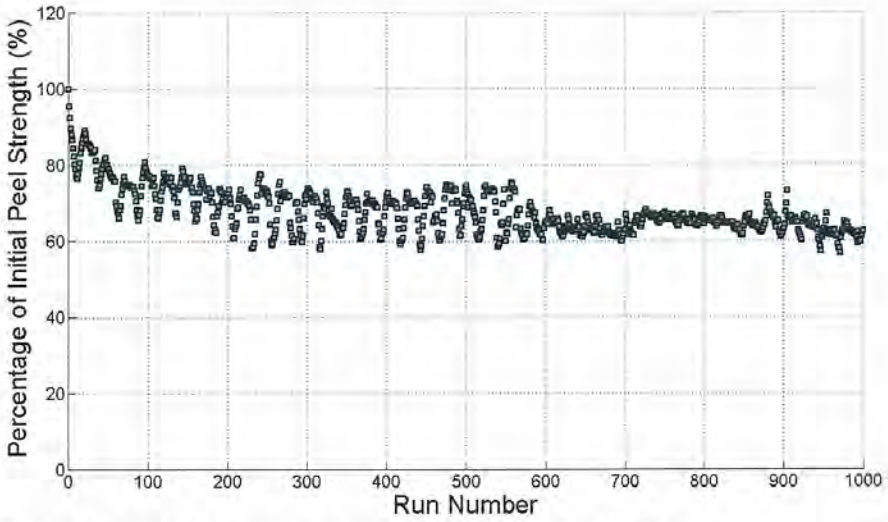

Figure 27: Durability evaluation of fourth generation fibers for 1000 cycles of peeling.

Fiber Loss Quantification: Experimental Setup

Another way of characterizing the durability of the fibrillar materials is to quantify the damage to the fibers after repeated testing. To do this, we subjected a Desmolux XP 2491 fiber array with a hardening additive (1% by weight, SR 351) to 100 cycles of manual loading and peeling from a Bayhydrol UH XP 2592 substrate, stopping periodically to take a series of optical microscope images of the fibers. Image processing software was written to evaluate each of these fiber images to count broken and collapsed fibers after each periodic number of peel cycles. This software was run both in a fully automated way and with human supervision on each picture to evaluate its accuracy. Details of this software are discussed in Appendix A.

Fiber loss Quantification: Results

An optical microscope image of a typical fiber region after 100 cycles of testing is shown in Figure 28. **A** denotes a broken fiber, **B** denotes fibers that are merged, and **C** identifies an area of healthy fibers.

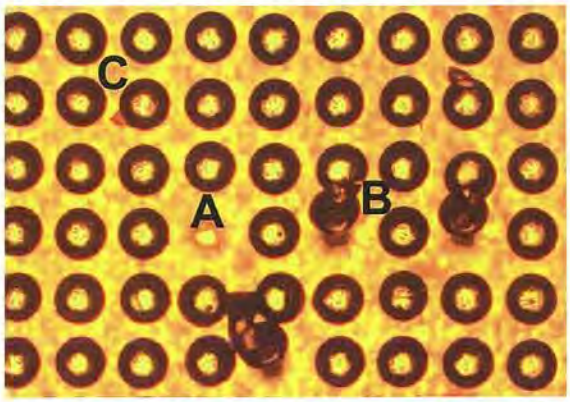

Figure 28: Optical microscope image of an array of fibers after 100 cycles of manual peel testing. **A** denotes a broken fiber, **B** denotes two merged fibers, and **C** identifies an area of healthy, undamaged fibers.

Using our software to count 90 similar images, a figure illustrating healthy and damaged (broken or merged) fibers is shown below. After 100 cycles of peel testing, 3.6% of fibers had been broken, 4.9% of fibers were merged, and 91.5% of fibers were healthy. Since merged fibers could unmerge with repeated testing or prolonged relaxation, 96.4% of the fibers in the array remained viable after this loading.

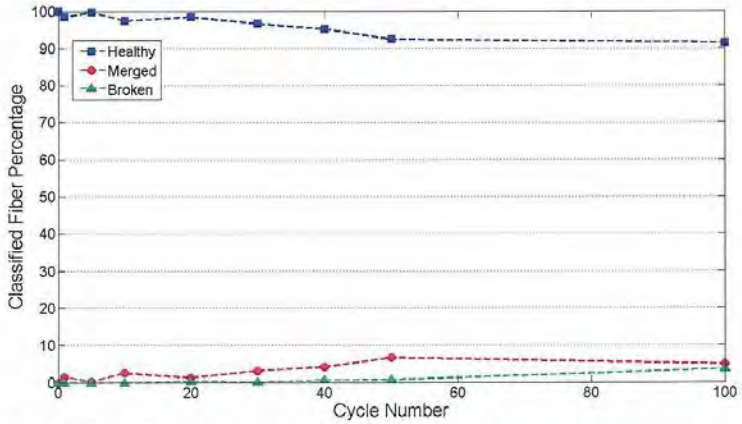

Figure 29: Results quantifying the percentage of Desmolux 2491 fibers with hardening additive which have merged or broken after repeated peel testing from a Bayhydrol 2592 substrate.

I.4.2.4 Washability Performance

Characterize the performance of the fourth-generation fiber material after being subjected to water cleaning between tests.

To evaluate the promise of the fourth-generation materials for commercial sportswear closure applications, testing was performed to see how subjecting the materials to repeated cleaning in an agitated mixture of 40° C water and laundry detergent for thirty minutes affected its performance. Once the samples have been washed, they were allowed to fully dry before being subjected to the same peel testing protocol described above. Figure 30 illustrates the effect of repeated washing on the performance of Desmolux XP 2491 fiber samples on a Bayhydrol UH XP 2592 substrate. **From this data, no performance deterioration is observed with repeated washing. However, it is important to understand the drying characteristics of the fiber adhesives.**

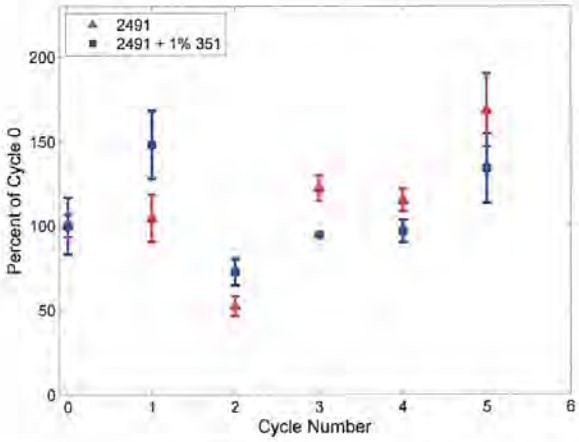

Figure 30: Peel performance of fiber samples after being subjected to repeated washing cycles.

I.4.3. T14: Fourth-Generation Optimization

Optimize the fourth-generation fiber material composition and/or chemistry using the test results by working together with Bayer MaterialScience.

After discussions with Bayer MaterialScience, it was determined that the UV-curable polyurethane used to fabricate the fibers which generated these results (Desmolux XP 2491) was the only reasonable material for the envisioned fabrication process. As such, options for optimization were limited to modifying the substrate to which the fibers would contact or incorporating a hardening additive (1% by weight, SR 351) into the uncured polymer. First, shear and peel testing was performed on Desmolux XP 2491 fiber samples on a variety of substrates provided by Bayer MaterialScience in both dry and wet conditions to identify which substrates resulted in higher shear and peel strengths. The results from these tests are presented in Table 12.

Table 12. Shear and peel results for fourth generation fiber arrays in contact with a range of substrates

Substrate	Dry		Wet	
	Shear Force (N/cm^2)	Peel Force (N/cm)	Shear Force (N/cm^2)	Peel Force (N/cm)
AH XP 2741	6.06 ± 1.29	1.11 ± 0.15	0*	0*
UH XP 2592	5.62 ± 0.11	0.72 ± 0.12	1.20 ± 1.62	0.25 ± 0.13
C84	4.86 ± 0.60	0.40 ± 0.22	**	**
XP 2637	4.50 ± 0.63	0.47 ± 0.03	**	**
124	4.44 ± 0.43		0*	0*
U 53	4.34 ± 0.32	0.55 ± 0.16	**	**
U XP 2643	3.53 ± 0.11	0.86 ± 0.03	0.16 ± 0.15	0.07 ± 0.06
ID DLU	3.45 ± 0.17			
PU 402 A	2.97 ± 0.32			
UH 340/1	2.65 ± 0.32			
U 42	2.60 ± 0.60			
U XP 2699	2.48 ± 0.16			
VP LS 2239/BL 5335	2.32 ± 0.15			

*Due to the hydrophilic nature of these materials, good contact could not be made between the fibers and substrate, and no wet shear or peel forces could be measured; ** Due to the similar hydrophilic nature of these materials, no wet shear or peel characterization was attempted.

After performing preliminary dry shear evaluation of our fibers on all of these substrates, only those materials which demonstrated dry shear forces in excess of 3.50 N/cm^2 were subjected to additional testing. Wet characterization of most of these substrates proved difficult. Due to the hydrophilic nature of many of these materials, a considerable build-up of water at the fiber/substrate interface prevented the tips from contacting the surface and making the wet shear and peel forces negligible. **After this wet characterization, it was determined that only the Bayhydrol UH XP 2592 substrate demonstrated promising performance in both wet and dry conditions, and as such, it was chosen as the contacting surface of choice for closure applications.**

Another level of performance enhancement was evaluated by adding a hardening agent to our fiber materials, now in contact with only the UH XP 2592 substrate. The results of shear and peel strength for fiber arrays with and without the addition of the hardening agent are presented in Table 13, as are comparisons of the number of merged fibers and peel strength performance after 1000 cycles, which were both determined using the techniques described in Section I.4.2.3.

Table 13. Shear and peel results for fibers in both with and without the addition of a hardening agent

Condition	Specification	Testing speed (mm/s)	Desmolux XP 2491	Desmolux XP 2491 + 1% SR 351 hardener	Desired Values
Dry	Shear Force (N/cm^2)	0.1	5.62 ± 0.11	6.41 ± 0.37	6.0 N/cm^2
		1.0	8.89 ± 0.39	11.38 ± 0.41	
	Peel Force (N/cm)	1.0	0.72 ± 0.12	0.41 ± 0.07	0.3 N/cm
Wet	Shear Force (N/cm^2)	0.1	1.20 ± 1.62	1.50 ± 1.08	1.5 N/cm^2
		1.0	3.55 ±0.74	4.77 ± 0.13	
	Peel Force (N/cm)	1.0	0.25 ± 0.13	0.23 ± 0.02	0.09 N/cm
Dry	Merged Fibers After 100 Cycles	N/A	30.8 %	4.9 %	Not specified
	Peel strength after 1000 cycles	1.0	40-50%	60-65%	90 % of initial strength

From these results, we can see that the addition of the hardening agent has resulted in significant increases in the shear strength of the specimens with a corresponding decrease in the dry peel strength due to the increased stiffness of the fibers. In doing our fiber loss quantification after 100 peel cycles, we also saw that the addition of the hardening agent resulted in a decrease in the number of merged fibers from 30.8% of the total array to only 4.9% of the array. This tremendous decrease in fiber collapse also helps explain how the hardened fibers maintain a greater percentage of their peel strength performance after 1000 cycles, while the observed peel strength of fibers without hardening agent was only 40-50% of their initial strength. Complete results for fiber loss quantification of both hardened and unhardened fibers are presented in Appendix A, as are data for the 1000 cycles of peeling for unhardened specimens. Considering all of these factors, **Desmolux XP 2491 fibers with the addition of a 1% by weight SR 351 hardening agent are proposed as the most desirable fiber material for sportswear closures.**

II. COMMERCIAL DEVELOPMENT

II.1. MILESTONE 2

Complete the Licensing and Joint Development agreements with the partners, Carnegie Mellon University and University of California -Berkeley.

II.1.1. C1: IP Rights Agreement with Carnegie Mellon University

An IP Rights agreement with Carnegie Mellon was successfully signed on June 30, 2009.

II.1.2. C2: Evaluation License Agreement with University of California-Berkeley

An evaluation License Agreement with UC Berkeley was successfully signed on May 4, 2009 for one year duration with the possibility of an extension.

II.1.3 C3: Joint Development Agreement with Under Armour

A Joint Development Agreement with Under Armour was successfully signed on August 4, 2009 for one year.

II.1.4. C4: Joint Development Agreement with Bayer MaterialScience

A Joint Development Agreement with Bayer MaterialScience is finalized successfully after negotiations. However, the agreement was signed in the week of August 10, 2009.

II.1.5. C5: First-Generation Fiber Array Samples for Under Armour

Four fiber array sample patches were mailed to Under Armour on Aug. 10th, 2009.

II.2. MILESTONE 3

Develop the first version of manufacturing scaling up options and cost analysis.

II.2.1. C6: Manufacturing Scale-up Options and Initial Manufacturing Cost Calculations

Current development efforts are focused on the selection/development of optimal polymer formulations for the near-term product applications identified above. One production system under preliminary consideration will be to use a roller-based system to directly fabricate the nano/micro fibers.

Roller-based systems offer the potential for very low production costs with high volumes. Such roller based systems have become standard in the polymer coating industry, and incorporate the type of UV cure systems that we are working on from a research level to a continuous production process. A complete production line (including a customized roller, and UV cure system) would cost on the order of $250,000. As a first pass in calculating unit costs, we estimated the initial cost of the fibrillar adhesive material at $0.21 in^2 for 1.2 M unit volumes. This cost will decrease over time due to economies of scale and the decreasing cost of the polyurethane material.

II.2.2. C7: Second-Generation Fiber Array Samples for Under Armour

We sent eight fiber samples to Under Armour for field testing. Their feedback from the first generation fibers was that during the process they attach the fibers to fabric, excessive heat and pressure damaged the fibers. Therefore, they could not provide us with any quantitative data. The second-generation samples were sent for field testing were still in the silicone rubber mold.

II.3. MILESTONE 4

Integrate the fiber adhesives into to the sporting fabrics.

II.3.1. C8: Attachment Method Design

Determine the method of attachment of the fiber array samples to the substrate for field testing at Under Armour. Under Armour will provide the textiles, adhesives, films and other materials to be used as substrates.

II.3.1.1. Scale-up Molds

In order to make samples large enough to be used on garments, a new mold-making process was used. Using an acrylic jig and acrylic tiles, we created a continuous surface of fibers that was about 9 inches long and 2 inches wide. With this mold we were able to attach a large array of fibers onto TPU leaving excess backing material to be ironed onto fabric. The scale-up mold and fibers obtained from this process can be seen below in Figure 31.

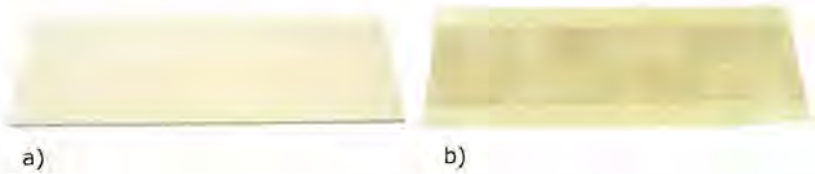

Figure 31: Scale-up mold (a) and fiber array (b).

The fiber array was attached to two fabric pieces with an iron so that the fiber arrays could adhere to each other to form an enclosure. The figure below shows the two closures obtained.

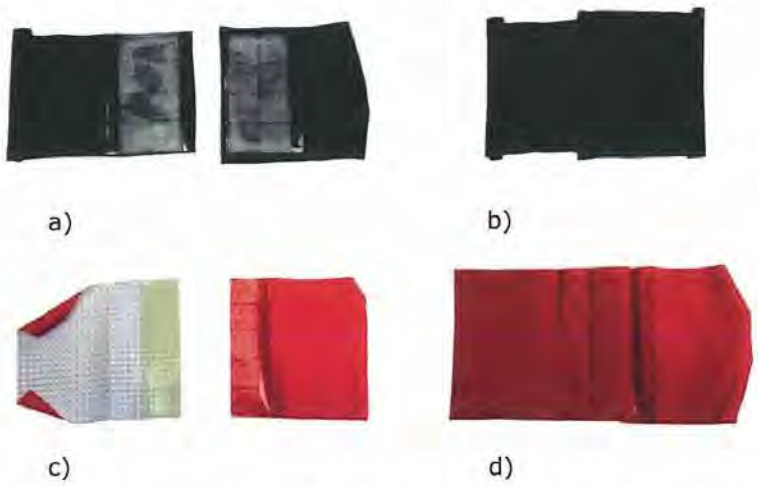

Figure 32: Enclosures, fabric 1 unnatached (a), fabric 1 attached (b), fabric 2 unattached (c), fabric 3 attached.

II.3.2. C9: Third-Generation Fiber Array Samples for Under Armour

Provide Under Armour with the third-generation fiber adhesive samples to for field-testing of 1the product specifications S4, S6, S7, and S8 as listed in Table 1.

II.3.2.1. Field Testing Results

The field testing results provided to us by Under Armour were brief. They were able to test the shear and peel qualitatively and reported that while shear was good, peel strength was poor and needed improvement. This was expected as the scaling-up introduces some irregularities on the surface. In addition, the samples we sent to Under Armour were very thick which decreases the peel performance significantly.

Figure 33: Fiber sample being sheared.

Figure 34: Fiber sample being peeled.

II.4. MILESTONE 5

Generate new IP where applicable.

II.4.1. C10: Patent Opportunities

Assess the patent filing opportunities with the partners on the fiber material design and manufacturing, fiber material composition, or fiber material integration to sporting fabrics

We have identified several contributions to fibrillar adhesive technologies that have been made throughout this project which we feel are significant and worth protecting through patents or trade secrets. The following sections serve as a preliminary assessment of patent opportunities. Future

discussions with Under Armour, Bayer MaterialScience, as well as consultation with patent lawyers will be necessary to determine the best course of action for each contribution.

II.4.1.1. Scaled-up Manufacturing Technique

Our manufacturing techniques for scaled-up fibrillar adhesive molding (I.4.1.2.) are novel and possibly patentable. We have developed a method to align the fiber surface of many small-scale fiber arrays (less than $1in^2$) and mount the fibers onto a rigid backing. This method requires UV curing and other non-obvious techniques and produces an almost continuous fiber surface.

II.4.1.2. Fiber Integration to Fabric

Throughout this project several methods for fiber integration to fabric have been developed. In one method fibers are molded directly onto a sheet of TPU. When heated, the TPU melts and can bond to fabrics. Waterborne polyurethane dispersions (PUDs) can also be used in place of TPU to attach fibers to fabric. Both TPU and PUDs are currently used in the textile industry however patents currently exist for attachment methods that apply specifically to hook and loop fasteners [1]. This precedence makes us more confident that a similar patent may be applicable to fibrillar adhesives.

Prototypes

Three prototypes have been made using fibrillar adhesives to demonstrate their uses in the apparel industry. The clothing we used for these prototypes was provided by Under Armour. We began with a wrist strap on a glove which can be seen below (Figure 35). The strap was made by molding fibers and attached to the non-stretch fabric using PUD. The fabric was then stitched to the glove. A flat opposing surface was molded directly onto the elastic wristband. The wrist strap stays attached throughout the full range of motion of the wrist.

Figure 35: A glove wrist strap being adjusted (left) and extended to a high loading position (right).

Figure 36 shows a pair of shoe prototypes which use fibrillar adhesive straps to replace laces. The straps and opposing flat surfaces were attached to fabric using PUD and were then stitched to the shoes.

Figure 36: Shoes with fibrillar adhesive straps (left) and a user adjusting a fibrillar adhesive strap (right).

Hook and loop closures were replaced by fibrillar adhesive closures on a light jacket (Figure 37). The fiber surface is attached to a fabric using PUD and the flat surface is molded directly onto a wicking fabric. Although these pieces of fabric were stitched to the jacket for the prototypes they would likely be attached directly to the jacket material in a full scale production.

Figure 37: A jacket closure prototype open (left) and being closed by a user (right).

II.4.1.3. Wicking Surface

During wet testing we found that by adding a wicking material either on or adjacent to the adhesive interface wet performance increases. This is useful for outerwear such as jackets and gloves. We demonstrated that wicking improved performance in Term 3 (see II.3.2.) and also demonstrated a method for integrating a wicking surface to a jacket closure. This wicking design and several unexplored options may be valuable as patents because of the large performance increase.

REFERENCES

[1] Hatch, Richard N. "Method for Adapting Separable Fasteners for Attachment to Other Objects." Patent 4,933,224. Jun. 12, 1990.

APPENDIX A

Fiber loss quantification software

Custom software was written to perform image analysis on optical microscope images of a fiber array to classify whether each fiber in the image is either broken, merged, or healthy. Screenshots of fiber images processed by this software are shown in Figure A1 below. This software begins by loading in a .jpg image captured by a camera during optical microscopy, as shown in Figure A1 (**A**). The image is then converted to black and white such that the fiber tips are separated from the background (**B**). Finally noise or dust is eliminated from the foreground and any incomplete fiber areas which are bordering on the edge of the image are also erased (**C**). At this point, by calculating and comparing the areas of the fibers left in the image, the program is capable of accurately classifying each area as either broken (areas which are significantly smaller than the average area), merged (areas which are significantly larger than the average area) or healthy (areas which are approximately average in size). It can also accurately count the number or merged fibers in each merged area by dividing the area of the merged area by the area of a healthy fiber.

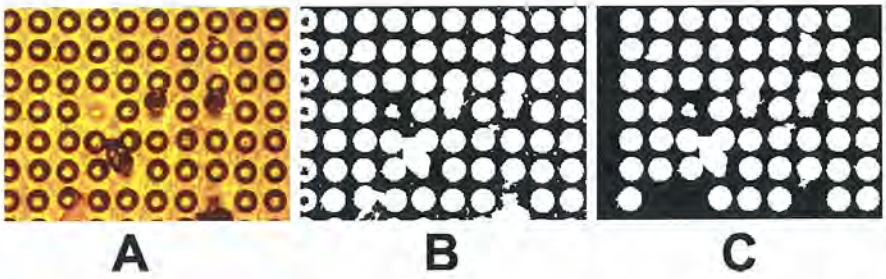

Figure A1. Screenshots from the fiber loss quantification software. **(A)**: Raw .jpg image captured during optical microscopy; **(B)**: The image is transformed into black and white, where the fiber areas are separated from the background; **(C)**: Specks of dust and noise are erased, as well as any incomplete fiber areas which are touching the image border.

While this program can be run with an operator who reviews the final image (such as the one shown in Figure A1 (**C**) who can review the counts for each image to ensure accuracy, it was also modified to automatically scan through a directory of fiber images and count and classify each one. By comparing the manual count with the automated count, we were able to determine that this software extremely accurate. Results comparing the manual and automatic count for both hardened and unhardened Desmolux XP 2491 are included in Table A1 and A2, respectively. While the close matching of these results demonstrates the robustness of the software, small inaccuracies in automated counting may need to be rectified in future generations of this software.

Table A1. Comparison of manual and automatic counts of broken, merged, and healthy fibers from a series of optical microscopy images of Desmolux XP 2491 fibers with a 1% hardening agent additive.

	Broken Fiber Percentage		Merged Fiber Percentage		Healthy Fiber Percentage	
Cycle Number	Manual Count	Automatic Count	Manual Count	Automatic Count	Manual Count	Automatic Count
1	0.0 %	0.0 %	0.0 %	0.6 %	100%	99.4 %
2	0.0 %	0.0 %	1.5%	1.6 %	98.4%	98.4 %
5	0.0 %	0.0 %	0.3%	0.6 %	99.7%	99.4 %
10	0.0 %	0.0 %	2.6%	2.8 %	97.4%	97.2 %
20	0.3 %	0.3 %	1.3%	1.9 %	98.4%	97.8 %
30	0.2 %	0.2 %	3.3%	3.6 %	96.6%	96.3 %
40	0.6%	0.6 %	4.2%	5.0 %	95.2%	94.4 %
50	0.8%	1.0 %	6.8%	7.2 %	92.4%	91.7 %
100	3.6%	1.2 %	4.9%	5.5 %	91.5%	93.3 %

Table A2. Comparison of manual and automatic counts of broken, merged, and healthy fibers from a series of optical microscopy images of Desmolux XP 2491 fibers with no hardening agent additive.

	Broken Fiber Percentage		Merged Fiber Percentage		Healthy Fiber Percentage	
Cycle Number	Manual Count	Automatic Count	Manual Count	Automatic Count	Manual Count	Automatic Count
1	0.3 %	0.3 %	1.3 %	1.3 %	98.4 %	98.4 %
2	1.1 %	0.9 %	0.0 %	0.9 %	98.9 %	98.1 %
5	1.0 %	0.6 %	2.9 %	3.4 %	96.1 %	96.0 %
10	0.0 %	0.0 %	3.5 %	5.7 %	96.5 %	94.3 %
20	0.6 %	1.0 %	8.7 %	9.5 %	90.6 %	89.4 %
30	1.1 %	0.9 %	11.8 %	11.7 %	87.0 %	87.5 %
40	0.5 %	0.4 %	18.0 %	16.8 %	81.5 %	82.8 %
50	0.2 %	0.1 %	21.8 %	21.0 %	78.0 %	78.9 %
100	1.4 %	0.9 %	30.8 %	23.9 %	67.8 %	75.2 %

Durability Performance for hardened and unhardened Desmolux XP 2491

Peel strength data for both hardened (1% by weight SR 351, Sartomer) and unhardened Desmolux XP 2491 fibers subjected to 1000 loading and unloading cycles is presented in Figure A2. Here, we can see that the sample without hardener gradually deteriorates in performance until the final peel strength is only 40-50% of the initial strength when testing began. Again, the sawtooth behavior of the curve is due to changes in environment temperature due to the laboratory's automated air conditioning system.

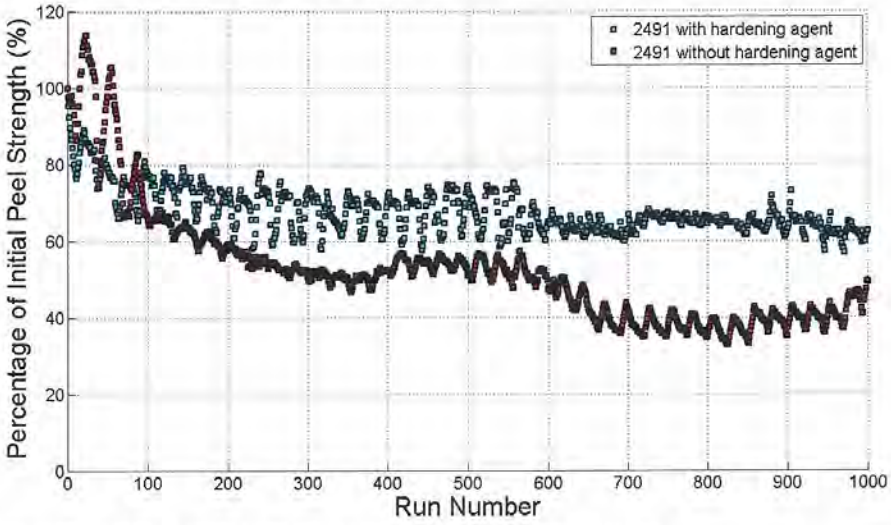

Figure A2: Durability evaluation of fourth generation fibers for 1000 cycles of peeling.

APPENDIX B

The water resistance measurements were performed in a pressure chamber. The fiber adhesive was brought in contact with the mating surface in dry conditions and the fiber adhesive/opposing surface was placed under water in a Petri dish. The dish was then placed in the pressure chamber and the chamber was pressurized to 20 kPa (3 psi). After subjecting our developed material to 20 kPa for 2 min, approximately 60% of the fibrillar array stayed in contact with the opposing surface as seen in Figure B1. While this system provides partial water resistance, a more effective sealing system could be manufactured using flat sealing flaps on the periphery of the fiber array.

Figure B1. Image of the fiber array after water resistance test at 20 kPa for 2 min. The clear area on the fringes of the left image indicates that water seeped in between the fibers. The opaque area at the center of the fiber arrays indicated that this region is completely dry and water could not penetrate in between the fibers. The image on the right is a close up view of the interface between the dry and wet regions of the sample.

Appendix H – 09-021 (Arkema)

A New Class of Nanostructured Toughening Agents for Wind Energy and Electronic Material Epoxy Applications

Final Report

July 5, 2010

Robert Barsotti, Ph.D.
Arkema Inc.
Corporate Research
900 First Avenue
King of Prussia, PA 19406

Professor Raymond Pearson
Lehigh University
Center for Polymer Science & Engineering
5 East Packer Avenue
Bethlehem, PA 18015

Background

The goal of this project was to commercialize nanoscale self-assembling block copolymer additives that will become the next generation of toughening agents for epoxies focusing on wind energy and electronic material applications. Prior to the start of the work on the PNMCC grant, Arkema had developed technology to make block copolymers using either controlled radical polymerization or anionic polymerization. Research had been performed on the use of block copolymers for toughening of epoxy resins. Several block copolymers grades had been commercialized under the Nanostrength® trade name. These grades allow for excellent toughening with good maintenance of Tg and modulus and had achieved low volume commercial success in epoxy prepreg applications such as sporting goods. A downside of these grades was the 10-20X increases in viscosity of the resin when using block copolymer toughening agents in epoxy resins at 5-10% loading. Many of the high volume opportunities for toughening of epoxies could not tolerate this viscosity increase. There was high motivation to develop block copolymer toughening agents which could achieve similar thermal and mechanical properties to commercial grades, but due so with much less effect on viscosity. In particular, wind energy and electronic materials applications were targeted as high growth markets where the unique properties of block copolymer toughening agents could bring value.

Commercial and technical efforts were carried out over the course of the grant to achieve the goal.

Interactions with Key Customers

The initial commercial efforts consisted in having detailed meeting with charter customers to understand the need for new technology. For wind energy applications, meetings were held with Hexion (largest manufacturer of epoxy resin for wind applications), Cook, Ashland, Interplastics (UPR/VER manufacturer for wind applications) TPI, MFG (two wind blade manufacturers) and GE (wind turbine manufacturer).

In the wind energy area, customers clearly stated that the major short-term technical need for toughening is in the area of structural adhesives. Increased fatigue life without sacrificing modulus is the critical property that could bring value to new adhesives.

Toughening of the wind blade composite potentially provides a large volume but long-term opportunity. Focus is needed on epoxy, vinyl ester resin (VER) and unsaturated polyester resin (UPR) systems, as it is not clear which technology will be dominant for wind blades. Fatigue improvements with minimal increase in viscosity are the key driving factors.

For electronic materials, meetings were held with Hexion (world leader in supply of epoxy resin for printed circuit boards, PCB), Endicott (PCB manufacturer) and Henkel (electronic adhesive fabricator) In electronic materials, a high volume opportunity exists

for toughening of printed circuit boards. Regulatory measures have forced the introduction of new materials into the industry. An opportunity exists for improved performance via introduction of a new toughener.

Electronic adhesives represent a lower volume, but high margin opportunity. These higher performance materials are constantly looking for improved properties (toughness, viscosity, CTE, Tg).

Establishing Applicative Manufacturing and Testing Techniques

Initial technical efforts were closely tied to the commercial development efforts. Working with charter customers, samples were provided to Arkema for evaluation of block copolymers in customer-specified resins. Customers also provided a blueprint for the manufacturer and testing of representative samples:

- For electronic and wind energy adhesives, material was purchased and plans were outlined for making adhesive samples. For adhesive testing, lap shear, T peal and double cantilever beam testing would be carried out.

- For PCBs, laminates would be made by first using solvent cast epoxy prepregs. The prepregs would then be formed into a laminate in a heated press. Testing of these materials would employ techniques such as falling weight dart drop and interlaminar fracture toughness.

- For wind energy composites, infusion processing would be performed to make test specimens. An infusion table was designed and purchased. Testing would include inter-laminar fracture toughness and flexural strength.

To better understand the relationship between block copolymer composition and mechanical and rheological properties, screening was also done in customer resins and clear cast cured resin samples (without any fiber reinforcement). This testing included viscosity measurements, single edged notched beam fracture toughness, tensile testing and dynamic mechanical analysis (for T_g measurement). Efforts were focused on maximizing mechanical properties while minimizing both viscosity and raw material cost. Initial results showed promise using block copolymer with an epoxy miscible block which contained reactive methacrylic acid units.

Market Analysis

The major commercial development effort for milestone 3 was complete market analysis of wind energy and electronic material applications. Market analysis was performed using customer interactions and information from SRI and Frost and Sullivan market reports, DOE 20% by 2030 report, American Wind Energy Association, talks in Wind Session at 2010 Materials Challenges for Alternative Energy Conference, Cocoa Beach, FL, and reports in Composites World (2008) and E Composites Inc. The charts below

(tables 1-4) illustrate the approximate market size and anticipated market growth for each of the following markets:

Table 1: Thermoset Resin Use For Wind Energy Composites

Thermoset Resin Consumption (MT)	2008	2012 (12% growth)	2025 (DOE report-US)
WW	86.4	136.0	
US	27.2	42.8	49.1

Table 2: Thermoset Resin Use For Wind Energy Adhesives

Thermoset Adhesive Consumption (kMT)	2008	2012 (12% growth)	2025 (DOE report-US)
WW	27	42.5	
US	8.5	13.4	31.4

Table 3: Thermoset Resin Use For Printed Circuit Boards

	2006		2011	
Epoxy Resin for PCB	Revenue ($ Mil)	Volume (kMT)	Revenue ($ Mil)	Volume (kMT)
US	38	13	42	14
Europe	30	10	33	11
Japan	368	32	433	144
Korea	258	86	347	116
Tawain	304	101	397	132
China	450	150	1074	301
Total	1448	392	2326	718

Table 4: Thermoset Resin Use For Electronic Adhesives

	Substrates (Epoxy Only)		Encapsulants (All)		Die Attach (All)	
Consumption of Electronic Chemicals (2006)	Revenue ($ Mil)	Volume (kMT)	Revenue ($ Mil)	Volume (kMT)	Revenue ($ Mil)	Volume (kMT)
US	245	5	140	3	34	1.0
Europe	180	4	100	2	25	0.8
Japan	509	10	271	5	41	1.3
Korea	562	11	219	4	54	1.7
Tawain	268	5	196	4	42	1.3
China			50	1	11	0.3
Total	1764	35	1310	26	260	8

The following conclusions were drawn from the market analysis and customer interactions:

- The wind energy composites market for turbine blades is an extremely high growth, high potential opportunity. Potential value of nano-structured

toughening agent is largely unknown as no toughening agents are currently used. Value chain is complex and most likely point of entry for block copolymers is with resin manufacturers. Motivation is very high amongst UPR and VER manufacturers. UPR and VER have value drivers over epoxy: lower cost resin and quicker processing time but need to match mechanical properties, including fatigue in order to compete. 4 UPR/VER resin manufacturers are involved with Arkema on the use of block copolymer toughening agents for potential fatigue improvements. Epoxy resin suppliers also have a motivation for improved toughening to a.) To continue to outperform UPR/VER and b.) To create longer, more durable blades for offshore applications.

- The printed circuit board (PCB) market is another large opportunity for block copolymers. Regulations have forced the use of new more brittle resins, requiring toughening agents that do not affect Tg. Most likely path is with resin manufacturers. 1 partner has been established in this area, but development has been slow due to competing priorities and limited resources.
- The wind energy adhesive market is a substantial opportunity. Toughening agents are used. Unknown is if nano-structured toughening agents will further enhance key property driver: fatigue. Path forward could be with resin suppliers or adhesive formulators. Major negative for the project is not finding the right partner in North America motivated to work on block copolymer toughening agents for epoxy adhesives. This is potentially due to the higher prevalence of tough acrylic based adhesives used in wind in the US. In Europe, however, two projects are underway using commercial Nanostrength® grades for epoxy wind blade adhesives.
- Electronic adhesives, encapsulants and substrates for semiconductors are highly fragmented lower volume opportunity markets. Path to market would be with the many formulators. Most likely not a good target unless existing grades (or those developed for wind infusion or PCB) fit into these markets.

Based on the above, wind blade composites and PWB have jumped to the front as the key markets with the best chance of success for block copolymers. Both markets are in need of improved toughening/ fatigue with limited effect on other properties. PWB needs a toughener that does not affect the T_g of resins, while wind blades are in need of a nanoscale toughener with limited effect on viscosity.

Block Copolymer Candidates for Customers

After initial screening, technical efforts focused on developing the appropriate block copolymers that could achieve excellent results in the customer provided resins. Key to the selected applications was achieving an understanding of the relationship between block copolymer morphology and viscosity. It was found that the use of a diblock as compared to a triblock could significantly reduce viscosity. It was further discovered that viscosity was directly related to the length of the epoxy miscible block. By choosing the appropriate block copolymers, performance of a commercial triblock (M52N, epoxy miscible block= 15K) could be matched with a diblock (NM27, epoxy miscible block=

15K) with ½ the viscosity. Further reduction in viscosity was possible using a diblock (XLV50, epoxy miscible block= 10K) with a shorter miscible block (Table 5). An optimal length miscible block length of ~10Kkg/mol was found to minimize viscosity but maintain nanostructuration of the rubbery domains.

Table 5: Rheological, Mechanical and Thermal Properties of Block Copolymer modified epoxies

Dicyandiamide cured	M52N (10%)	NM27 (10%)	XLV50 (10%)
K_{1C} (MPa.m$^{1/2}$)	1.82	1.86	1.89
G_{1C} (J.m^{-2})	1867	1552	1778
Tg by DMA (℃)	135.4	128.4	127.7
Viscosity (Pa.s) at 40℃	28.6	14	7.45

Three families of block copolymers were explored for toughening of epoxy, UPR and VER resins for wind energy composite or PCB applications, as shown in figure 1.

2nd Generation Candidates- Diblock Families

PBA-b-PMMA/DMA (80/20)
NM27 – 12k-b-15K

PMA/MA-b-PBA
XLV50- 10k-b-40k (10% Acid)
XLV31- 10k-b-21k (5% Acid)

PMA/DMA(60/40)-b-PBA
NM50- 10k-b-40k
NM30- 10k-b-20k

Figure 1: 2nd Generation diblock polymer candidates *(PBA=Polybutyl acrylate; PMMA=Polymethyl methacrylate; MA=Methacrylic Acid; DMA=Dimethyl Acrylamide; PMA=Polymethyl acrylate)*

A second significant technical finding was the ability to control morphology to optimize toughening. It had been previously understood that the use of block copolymers that formed a worm-like micelle as compared with the more traditional nanospherical micelle had a positive impact on toughening performance. The use of highly asymmetric block copolymers, such as NM50, (4:1 ratio of miscible to immiscible (rubbery) block) at very low loadings results in a vesicle morphology, with a core of resin surrounded by a spherical shell of block copolymer. This unique morphology was shown to be extremely effective in toughening resin systems at very low block copolymer loading levels (1.25-2.5%). Results of the use of NM50 in a VER system and NM30 in an epoxy system are shown below in figure 2 and 3.

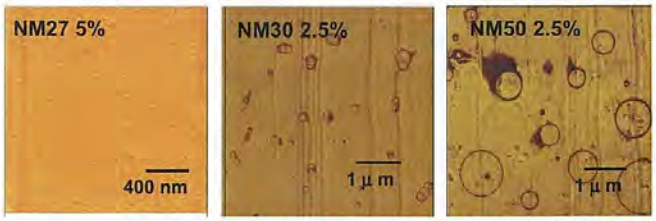

	NEAT	NM27 (5%)	NM27 (2.5%)	NM30 (2.5%)	NM50 (2.5%)
K_{1C} (MPa.m$^{1/2}$)	0.98	2.50	2.07	2.66	2.33
G_{1C} (J.m^{-2})	481	3533	1999	4375	3258
Viscosity (Pa.s) at 25°C	0.99	3.05	1.72	1.34	1.37
Tg by DMA (°C)	93.4	93.1	TBD	90.8	90.4

Figure 2: Atomic force microscopy (AFM) tapping mode phase images showing rubber morphology of NM27, NM30 and NM50 in an epoxy infusion system. Fracture toughness property measurements (K_{1C}, G_{1C}) show significant improvement with vesicle morphology (NM30 and NM50) at very low loading levels and subsequently very low viscosities.

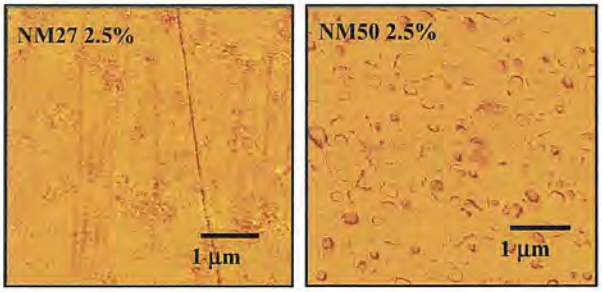

MEKP Cured	NEAT	NM27 (1.25%)	NM50 (1.25%)	NM50 (0.625%)
K_{1C} (MPa.m$^{1/2}$)	0.51	0.9	1.15	1.05
G_{1C} (J.m^{-2})	214	573	801	667
Viscosity (Pa.s) at 25°C	0.15	0.28	0.28	0.22

Figure 3: AFM tapping mode phase images showing rubber morphology of NM27 and NM50 in a VER infusion system. Fracture toughness property measurements (K_{1C}, G_{1C}) show significant improvement with vesicle morphology (NM50) at very low loading levels and subsequently very low viscosities.

Customer Feedback and Customer Status

Based on technical results and customer needs, products such as XLV50, NM27, NM50 and NM30 were sampled to resin manufacturers for wind energy composites and printed circuit boards. The most advanced development was with a VER resin manufacturer for wind energy. The customer was sampled with a PBA-b-PMMA/DMA polymer (NM27).

Static mechanical testing in both clear cast and infused composite samples done by the customer demonstrated significant improvements in toughening with NM27 while maintaining strength and modulus properties and an acceptable viscosity for infusion. As the true value driver for wind applications was fatigue, a plan was established for samples to be infused by the customer and tested at Lehigh University for 4 point bending fatigue. Figure 4 demonstrates the results of the testing, showing that significant improvements can be achieved by using as little as 3% NM27. Further improvements may be possible by incorporating NM27 along with using a controlled radical polymerization agent initiation system (IS300) from Arkema.

Stress Level	Thousands of Cycles to Failure			
	A- Control VER	B - VER with 3% NM27	C- Control Epoxy	D- VER with IS300 and 3% NM27
430 MPa	72 ± 26	119 ± 39	33 ± 21	129 ± 50
350 MPa	199 ± 121	335 ± 88	129 ± 40	847± 180
300 MPa	675 ± 113	938 ± 125*	> 1000*	>1000*

* ¾ samples tested from B did not fail at 1 Million Cycles. No failure was observed for samples C and D at 1 Million Cycles. Actual values for B, C and D at 300 MPa may be much higher.

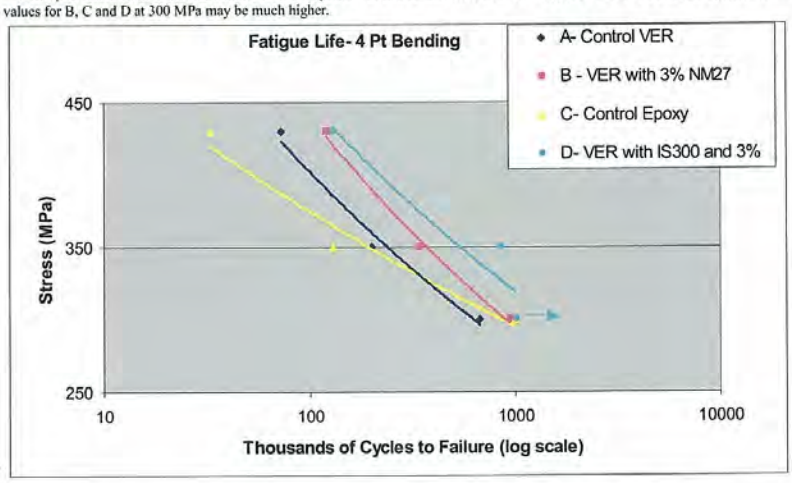

Figure 4: Fatigue testing of VER and epoxy control and NM27 modified VER systems.

Based on this data, the customer expressed interest in a joint development agreement (JDA) with Arkema. Negotiations on the JDA are nearly complete. The customer will get exclusivity for NM27 in all UPR/VER closed molding application in exchange for hitting certain volume thresholds. 1st significant commercial sales expected in 2012 with > 100 T potential in 2014.

3 additional UPR and VER resin manufacturers are active in evaluations of 2nd generation candidates. An epoxy resin manufacturer will be sampled with an optimized grades based on screening at Arkema in summer 2010.

In printed circuit boards, feedback was given on a commercial SBM (poly(styrene-b-butadiene-b-methylmethacrylate)) grade, E21, and acid modified diblock grades (XLV50). As shown in figure 5, nanostructuration was achieved with both block copolymers. These block copolymers greatly improved the toughness of the resin, as measured by the area under a tensile-stress strain curve. E21 and XLV50, however, slightly under-performed compared to a competitive modifier. Interest remains in the technology, potentially due to lower price point of block copolymer technology as compared to competitive materials. Based on application screening and block copolymer optimization, customer will be sampled with best performing block copolymers for PCB application. Improvement at low loading will be critical to offer an attractive price-performance value.

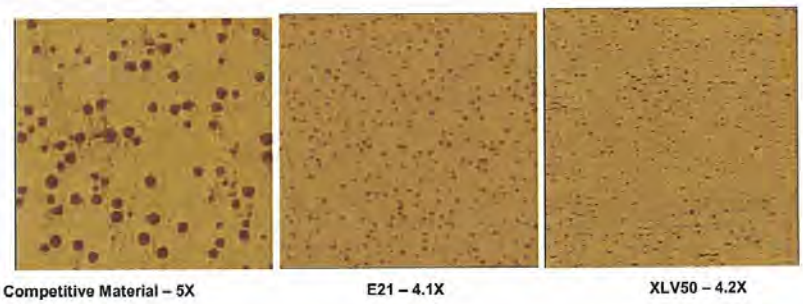

Figure 5: AFM tapping mode phase imaging of customer samples. The number adjacent to sample labels indicated relative performance in toughening as compared to unmodified control.

Application Testing and Grade Optimization

Infusion manufacturing of control and block copolymer modified samples has begun at Arkema, as shown in figure 6. Optimization of the process to achieve 60-70% fiber volume fraction is underway. Variables include tube diameter and fiberglass placement. After process is optimized, flexural strength and interlaminar fracture toughness testing will be performed to validate performance of block copolymers in infused composites.

Figure 6: Photograph of infusion table and infusion set-up during processing showing white resin inlet tube and black vacuum tube.

The process for making intermediate prepregs and printed circuit boards laminates was determined by testing the effect of several variables. Optimizing variables such as prepregging time and temperature, accelerator level, and pressure and temperature during lamination allowed for prepregs with the proper Tg and low/no voids to be manufactured. To screen candidate polymers for interlaminar fracture toughness, AFM imaging and gardner dart drop testing was performed. Two candidates were selected for initial testing:

- E21, a commercial SBM grade, which formed nanospherical rubber domains and showed decreased lateral damage during dart drop
- NM44, a DMA-PBA grade, which formed small vesicle aggregates and showed decreased through thickness damage during dart drop

Table 6 clearly demonstrates that E21 outperforms NM44, giving 4X improvement over the control during interlaminar fracture toughness measurement. NM50, NM30 and XLV50 will also be screened for ILF.

Table 6: Interlaminar Fracture Toughness Measurement on PCB composites

	Crack length calculated from compliance	Crack length measured
	Average G1C (J/m^2)	Average G1C (J/m^2)
Control	244 ± 21	144 ± 17
5% E21	723 ± 196	865 ± 338
5% NM44	188 ± 8	101 ± 8

Block copolymers are currently being optimized for scale-up at our micro-pilot facility in France. To minimize capitol costs, a study is underway to determine if the PMA/DMA-b-PBA family of polymers can be made using PBA-b-PMMA/DMA, eliminating the need to purchase a storage tank for methylacrylate monomer. Initial with a modified NM50 grade are very promising, showing equivalent or better rheological, mechanical

and thermal properties in an epoxy, VER and UPR system. A modified NM30 grade will be tested in the near future.

After scale-up, charter customer will be provided with additional material to continue their evaluations. Sampling will also be expanded to new customers in the wind energy composite and printed circuit boards markets.

Summary and Path Forward

Over the course of the year under the PNMCC grant significant progress was made in commercializing nanoscale self-assembling block copolymer additives for wind energy and electronic material applications. Key technical achievements were made in being able to a.) develop block copolymer with low effect on thermoset resin viscosity and b.) understand the composition necessary to make block copolymer form vesicle morphologies in thermosets to toughen at very low loading levels. Customer interaction resulted in obtaining both resin samples and knowledge on manufacturing and testing of samples. Block copolymer grades were optimized for wind energy and electronic material resins based on this interaction. Market analysis allowed the project to be focused on areas where the chance of success for block copolymers is the greatest. Charter customer have given feedback on the materials and one customer is very close to signing a joint development agreement with Arkema based on work done under the grant.

The path forward focuses on the following items:

- Scale-up of optimized grades
- Generation of a set of technical data on scaled-up grades in infused composites for promotion of the new materials (Interlaminar Fracture Toughness, Flexural Strength) in wind energy and other markets
- Additional fatigue studies on clear cast samples and infused composites to better understand structure property measurements for fatigue
- Additional interlaminar fracture toughness measurements on PWB samples to select optimum grade
- Technical support of charter customers to push commercialization of new grades
- Promotion of wind energy and electronic materials grades to broader audience

The PNMCC grant enabled critical technical and commercial developments to be undertaken, allowing for Arkema to be on the doorstep of commercialization of block copolymer grades for wind energy and electronic material applications.

Appendix I – 10-022 (NanoLambda, Inc)

Pennsylvania NanoMaterials Commercialization Center

Final Report (PA10-022)

- **Project Title: Ultra compact highly accurate LED Color monitoring sensor product development**
- **Project Leader: Min Kyu Song**
- **Name of Project Leader's Organization: NanoLambda**
- **Report submitted by: Min Kyu Song**
- **Date: April 30, 2011**

1

Introduction/ Summary

The objective of this proposed project is to develop an ultra compact, highly accurate LED color (wavelength) monitoring sensor to monitor the drift of LED color with 2nm accuracy, using the innovative nano-optic filter array technology.

Under this proposed project, an ultra compact, highly accurate LED color(wavelength) monitoring sensor will be developed using an innovative nano-optic filter array technology, and using high throughput monolithic nanoimprint process for a pilot production at low cost. We will implement this filter array process technology directly onto the CMOS image sensor wafers (ex., full 8" diameter wafer) as shown in Figure 10. It is feasible because the fabrication of nano-optic filter array is fully compatible with the existing CMOS image sensor process.

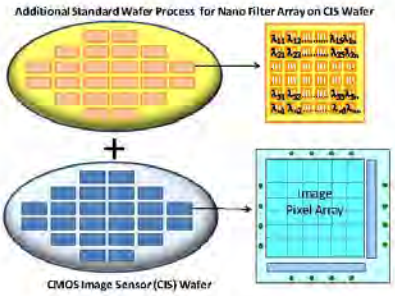

❑ Sectional view

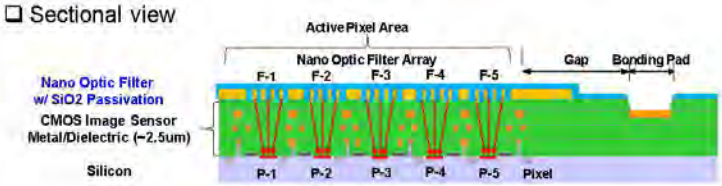

Wafer scale monolithic nano-optic filer array integration Concept

To fulfill the monolithic filter integration on the image sensor wafer, the CMOS image sensor wafers are supplied from the image sensor company. A new nanoimprint stamp including filter/chip aligning mark will be designed and fabricated. The monolithic integration process will be developed in collaboration with KIMM (Korea Institure of Materials and Machinery) with utilization of the NNFC (National Nano-Fabrication Center) in Korea.

During the last 16 months, we successfully followed the project schedule step by step.

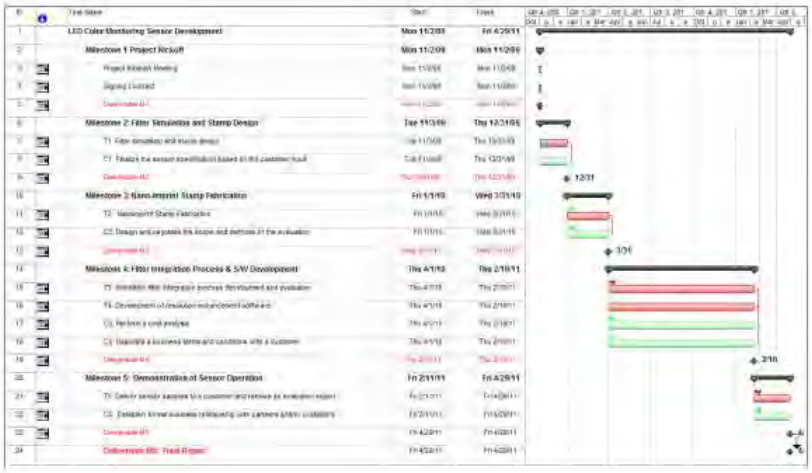

The detail milestone and deliverables were summarized as follows;

Milestone	Tasks	Period	Deliverables
Milestone 1	Project initiation meeting	11/2/09	*Signed contracts*
Milestone 2: Technical	T1: Filter design & simulation - *Goal: Design and simulate the AI nano-optic filter performance to have at least 15% peak wavelength transmission over the range (400nm~700nm), at 10nm incremental (5nm incremental around R, G, B LED wavelengths. Determine the nano-optic filter design for the stamp fabrication.*	11/3/09-12/31/09	*Report on the filter simulation result, and the stamp design layout*
Milestone 2: Commercial	C1: Finalize the sensor specification based on the customer input - *Goal: Finalize the sensor specification for the LED color monitoring with 2nm accuracy agreed with a customer*	11/3/09-12/31/09	*The agreed sensor specification*
Milestone 3: Technical	T2: Nano-imprint stamp fabrication - *Goal: Fabricate a Quartz stamp for UV nano-imprint with less than 10% variation of pattern width with minimum 100nm pattern depth*	1/1/10-3/31/10	*Report on the nano-imprint Stamp fabrication result (SEM images)*
Milestone 3: Commercial	C2: Design and negotiate the scope and methods of the evaluation - *Goal: Have a mutually agreed test and evaluation methods*	1/1/10-3/31/10	*A test scope & method document*

3

Milestone	Tasks	Period	Deliverables
Milestone 4: Technical	T3: Monolithic filter integration process development and evaluation - *Goal: Develop monolithic filter integration process using nano-imprint/ AI etch processes* T4: Development of resolution enhancement software - *Goal: Develop highly accurate LED color sensing software able to detect 2nm wavelength shift*	4/1/10-2/10/11	•*Report on the summary of filter integration process development* •*A monolithically filter integrated LED Color sensor sample* •*Demonstrate the 2nm wavelength shift detection using sample LEDs*
Milestone 4: Commercial	C3: Perform a cost analysis - *Goal: Have a volume based cost analysis for a mass production* C4: Negotiate a business terms and conditions with a customer - *Goal: Have a mutually agreed commercial terms and conditions draft*	4/1/10-2/10/11	*An estimated cost analysis* *A draft MOU*
Milestone 5: Technical	T5: Deliver sensor samples to a customer and receive an evaluation report - *Goal: Deliver samples to a customer, and Receive a customer's evaluation report*	2/11/11-4/30/11	*Evaluation report from a customer. Final Report*
Milestone 5: Commercial	C5: Establish formal relationship with partners and/or customers - *Goal:* Establish a commercial business relationship with a customer	2/11/11-4/30/11	*A formal business agreement document*

Part 1: TECHNOLOGY DEVELOPMENT

Milestone 1 (Date for completion: 11/2/09)

(*Deliverable: signed contracts, project initiation meeting*)

The project initiation meeting was held at nanoLambda office, and the contracts were signed on 11/2/09.

Milestone 2 (Date for completion: 12/31/09)

T1: Filter Design and Simulation *(Deliverable: Report on the filter simulation result, and the stamp design layout)*

- *Goal: Design and simulate the Al nano-optic filter performance to have at least 15% peak wavelength transmission over the range (400nm~700nm), at 10nm incremental (5nm incremental around R, G, B LED wavelengths. Determine the nano-optic filter design for the stamp fabrication*

- **Nano-optic filter simulation**

  - As a filter simulation tool, the FDTD (finite difference time domain) S/W from Lumerical Inc. was used, and the simulation steps were described.

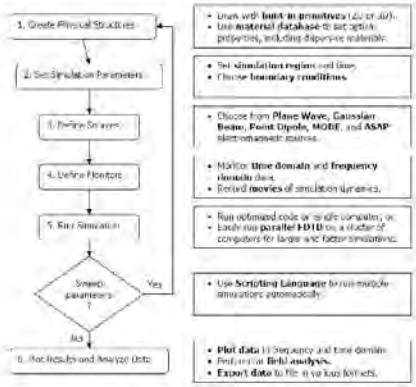

Figure1. FDTD simulation procedure

  - Various 2-D slit array structures were simulated when the aluminum is 80nm thick; i.e., rectangular array and hexagonal array structures with changing the pitch (200-400nm) and the x-slit size (130-280nm) have been simulated. In addition, different dielectric environment (i.e., air, and SiO2 passivation) was also investigated (page 15). Total 50 of different nano-optic filter structure have been simulated.

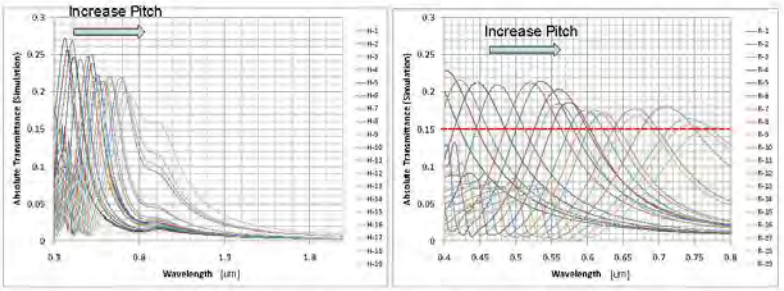

Figure2. Simulation result of rectagular array sturcture

- As a simulation result of the rectangular array structure, when the pitch increased, the peak wavelength was shifted longer side, and the intensity was decreased (Figure2).
- From the hexagonal array structure, the simulation results show the same trend of the rectangular array structure except shorter peak wavelength and higher intensity peak at the same pitch condition.
- After nano-optic filter was passivated with SiO2, the peak wavelength was shifted longer side and the peak intensity was increased from both rectangular and hexagonal array structures, and the amount of red-shift was increased as the pitch increased (Figure3).

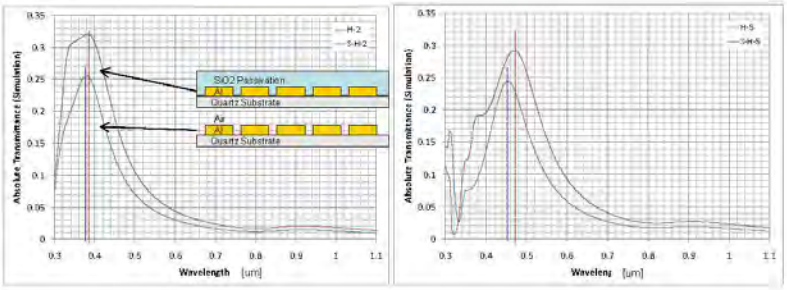

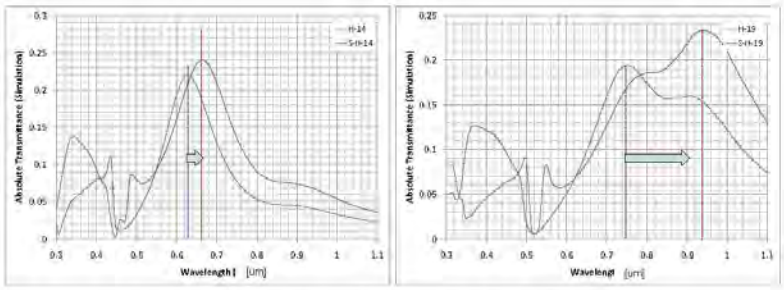

Figure3. Simulation result of peak wavelength shift

- Simulation results of the peak wavelength and the peak intensity by changing pitch when the dielectrics were air and SiO2. From the linear interpolation of each simulation results, the exact peak wavelength and peak intensity could be estimated even at any minor pitch variation. *Therefore, the simulation goal of nano-optic filter performance was achieved to have at least 15% peak wavelength transmission over the range (400nm~700nm)* (Figure4).

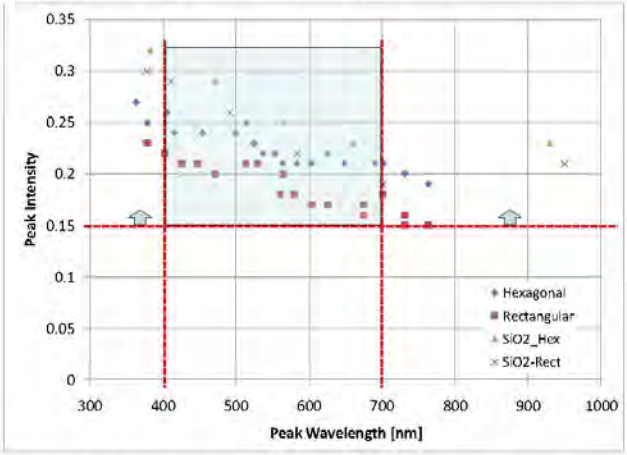

Figure4. Simulation results of various peak wavelength vs. peak intensity

- **Nano-imprint Lithography Stamp Design**
  - Figure5 shows the general SFIL (Step and Flash Imprint Lithography) stamp information.

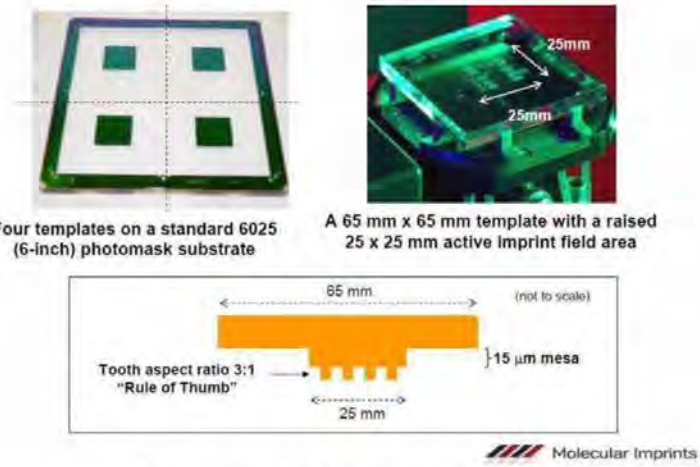

Figure5. General SFIL stamp information

- Figure6 shows the layout of CIS (CMOS Image Sensor) dies on the 8" diameter wafer. The nano-optic filter should be aligned on the active pixel area of each die.

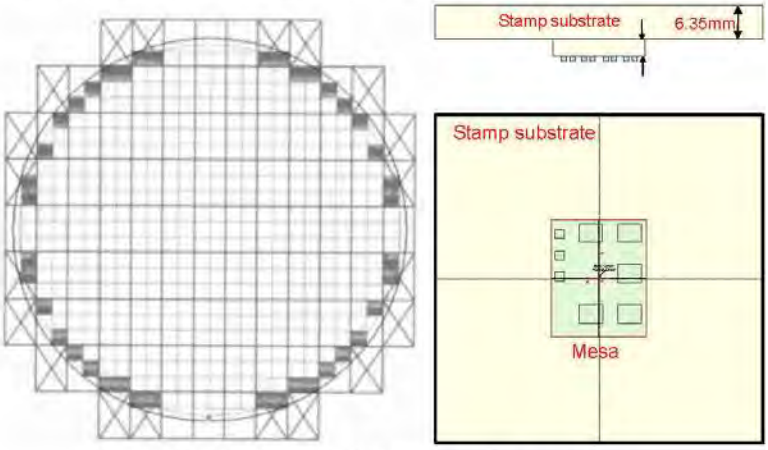

Figure6. Layout of CIS wafer and imprint stamp

- In order to nano-imprint on the CIS wafer, the imprint stamp was designed to cover several dies at each imprint. To be aligned the nano-optic filter on the CIS wafer, the filter layout was designed with mirror image effect (i.e., changing left & right) (Figure6)

- Figure7 shows the alignment marks for susbtrate (i.e, CIS wafer) and nano-optic filer layer which are very critical for aligning the filter layer and CIS wafer.

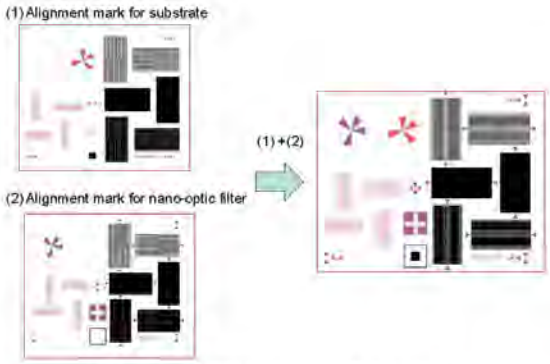

Figure7. Alignment mark information

- More detail filter dimension was described in the GDS II file, and it was delivered to the stamp manufacturer for stamp fabrication. *Therefore, new stamp design has been successfully made.*

Milestone 3 (Date for completion: 3/31/10)

T2: Nano-imprint stamp fabrication *(Deliverable: Report on the nano-imprint Stamp fabrication result (SEM images))*

- *Goal: Fabricate a Quartz stamp for UV nano-imprint with less than 10% variation of pattern width with minimum 100nm pattern depth*

- Once the stamp design was finalized at the previous milestone, it has been fabricated outside for 3 months. As a stamp material, quartz was used to penetrate UV. Stamp size is 65x65mm with 6.35mm thick. The stamp mesa area is 23.3x18.98mm^2 with 15um height. (Figure8)
- 3 step monitor patterns were located on the stamp to measure the pattern depth after stamp fabrication, and top view of SEM images were taken at the 6 different locations to see whether each pattern has been made correct. (Page 8)

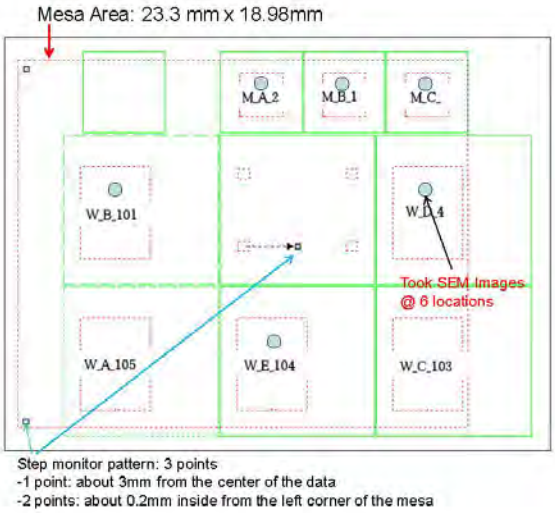

Figure8. Detail stamp mesa area map

- Various patterns (hole, cross, and dot) on the stamp were measured from top view SEM images on page. As a SEM result, the fabrication accuracy of each pattern was within the 10% hole-variation compared to the design value.
- From the x50 magnified optical microscope images, there is no defect on the stamp surface. (Figure9)

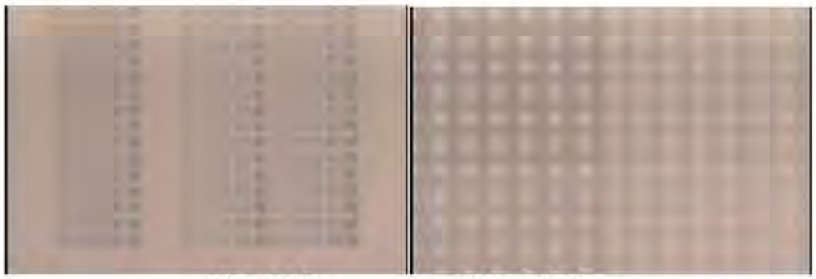

W_B_14 Area W_E_1048 Area

Figure9. Optical microscope images of imprint stam (x50)

- Finally, the fabricated stamp inspection results were summarized and each inspection test has passed. *Therefore, new stamp fabrication has been successfully made.*

10

Inspection Item	Specifications	Inspection result	Pass/ Not	Remarks
Hole width accuracy	Hole: ± 10 nm (X direction) Dot: as is Cross filter: ±10% (X direction and Y direction, target value, width of longitudinal direction) * Those points which are not included in the inspection points are provided as is.	Hole: +4.0nm～ +7.1nm Cross filter +3.1%～+6.7%	Pass	CD-SEM measurement and SEM image will be provided. Inspected patterns are as follows; Hole pattern width is evaluated in X direction. Cross filter width will be measured both X and Y longitudinal direction. M_A_21:94nm width hole M_B_14:200nm long cross M_C_7:184nm long cross W_B_1014:80nm width cross and 80nm width hole W_D_48:66nm width hole W_E_1048:80nm width dot 86nm width hole (Fig. 2 and Table 1)
Pattern depth accuracy	100 ～ 120 nm	111nm Step monitor Average	Pass	Pattern depth is measured by using the monitor pattern depth with stylus step measuring tool. The measured data will be attached.
Pattern inspection	Inspection using optical microscope	OK	Pass	Pattern area (W_B_1014 and W_E_1048) is observed by optical microscope (X50).

Table1. Imprint stamp inspection results

Milestone 4 (Date for completion: 2/10/11)

T3: Monolithic filter integration process development and evaluation *(Deliverable: Report on the summary of filter integration process development, and a monolithically filter integrated LED Color sensor sample)*

- *Goal: Develop monolithic filter integration process using nano-imprint/ Al etch processes*
  - The monolithic nano-optic filter integration process on a CIS wafer consists of approximately 13 steps, and the process flow chart is shown in Figure10.
  - Each consecutive process step is explained by showing the cross section view. (Figure11)

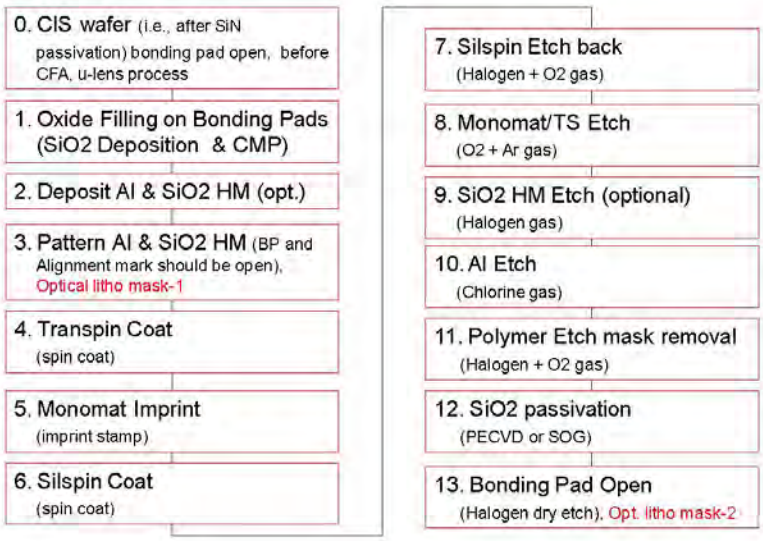

Figure10. Monolithic Filter Integration Steps

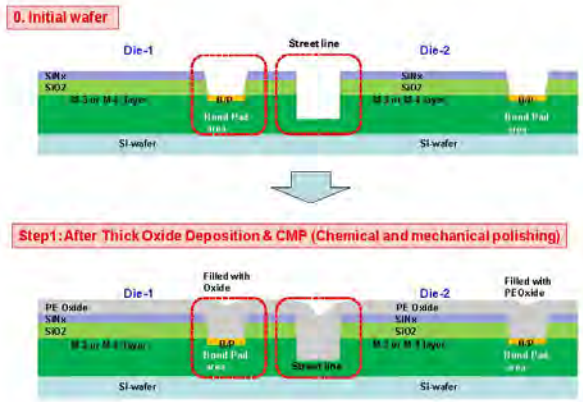

12

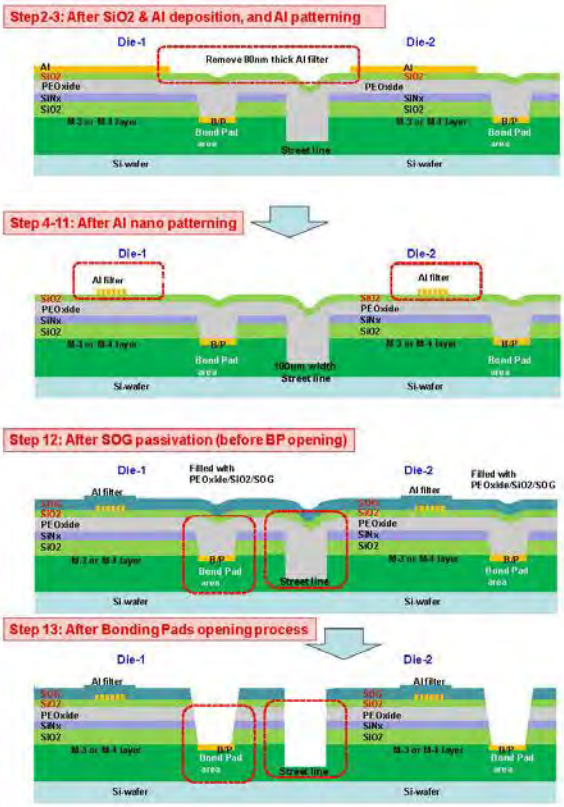

Figure11. Monolithic Filter Integration Steps

- Compared to the hybrid filter fabrication, new process development of monolithic filter integrateion has been addressed in red colors. (Table2)

13

Process Step	Issue
Flat CIS wafer surface: Oxide filling on grooves (B/P, scribe lines)	• Proper SiO2 deposition thickness and CMP (chemical mechanical polishing) process condition
Selective Al area patterning	• Open optical litho alignment keys, bonding pads, scribe lines
Imprint	• Precise alignment between imprint stamp and CIS wafer • Imprint Pattern Optimization o monomat seeping o uniformity o air-gap
Silspin coat	• Silspin uniformity
Polymer etch	• Etch non-uniformity
Al etch	• Etch non-uniformity due to pin-holes attack after consecutive PR process steps
Bonding pad opening	• Opening without damage bonding pads

Table2. Consideration of integration filters on a CIS wafer

- Since the CIS wafer surface morphology is not flat due to the bonding pad and scribe line are etched, surface planarization with SiO2 deposition & CMP process are required. The precise control of flat surface was achieved by monitoring various film characterization tools such as (1) (1) profilometer, (2) FIB cross section, (3) Spectroscopic ellipsometer. (Figures12-14)

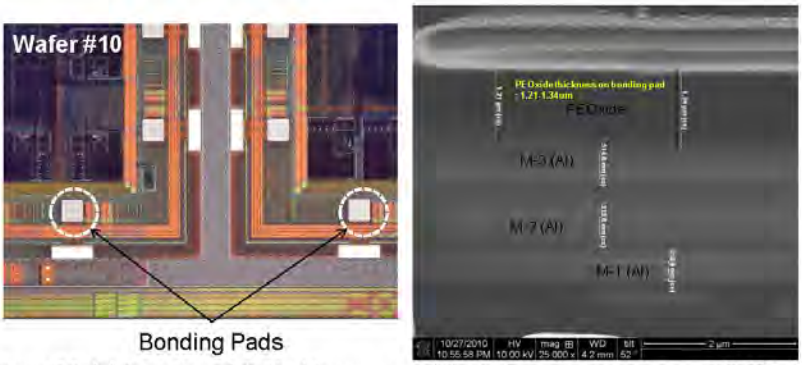

Figure12. (a) Top view of Optical Image , and (b) FIB Cross-section image of CMP treated CIS wafer

14

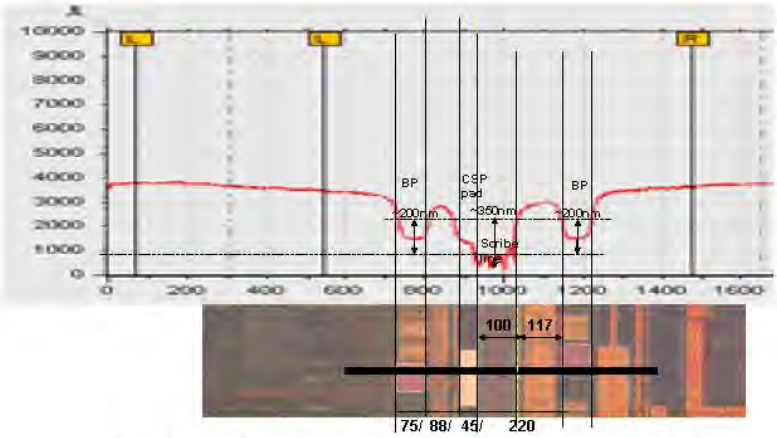

Figure13. Profilometer measurement of CMP treated CIS wafer

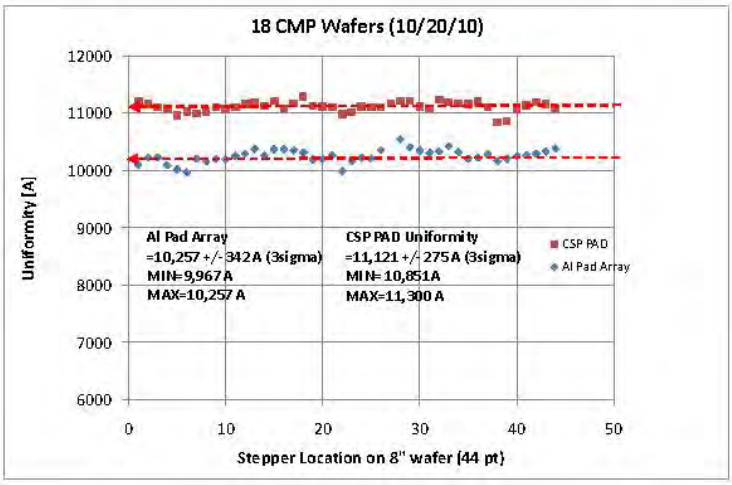

Figure14. Spectroscopic Ellipsometer results measured 44 different locations on 8" wafer

- The selective aluminum area patterning result to open optical lithography alignment keys, bonding pads, scribe lines is shown in Figure15.

15

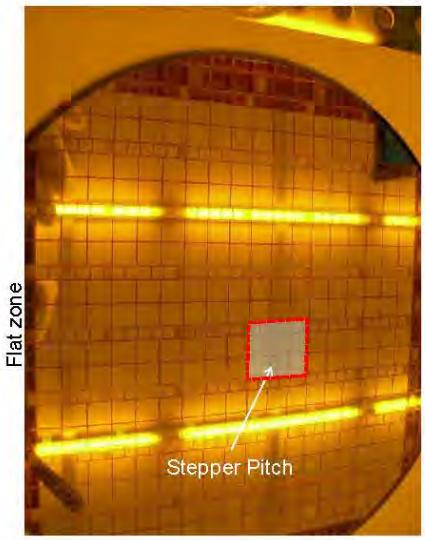

Figure15. Wafer Image of SAAD (Sective Aluminum Area Deposition)

- During the imprint process, the issues of alignment, monomat seeping, uniformity, air-gap have to be precisely controlled. These problems are solved by using various imprint alignment keys and optimized imprint recipe including monomat drop pattern layout. (Figures 16-20)

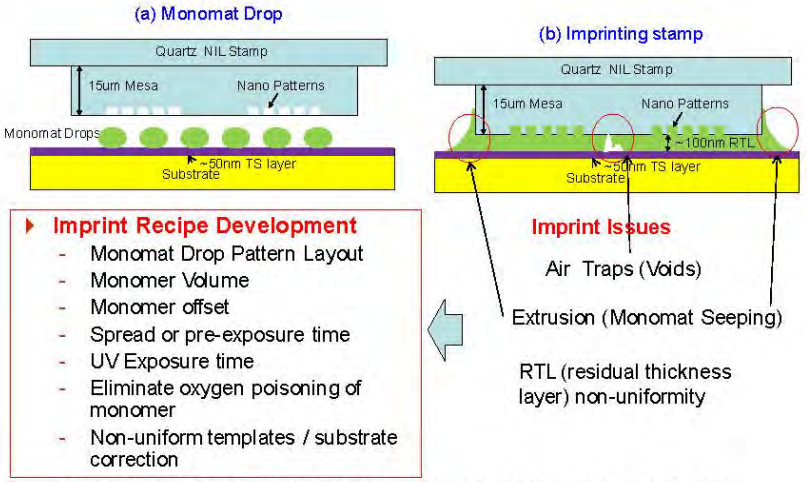

Figure16. Monomat Imprint Issues and Imprint Recipe Development

16

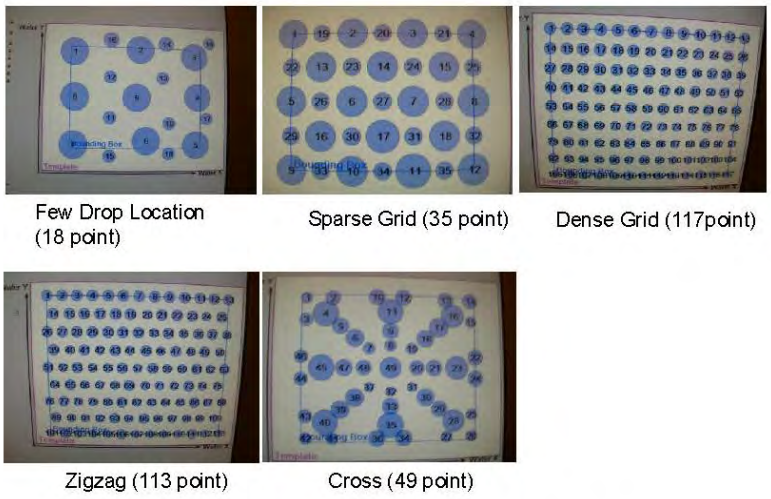

Figure17. Various Monomat Drop Pattern Layout

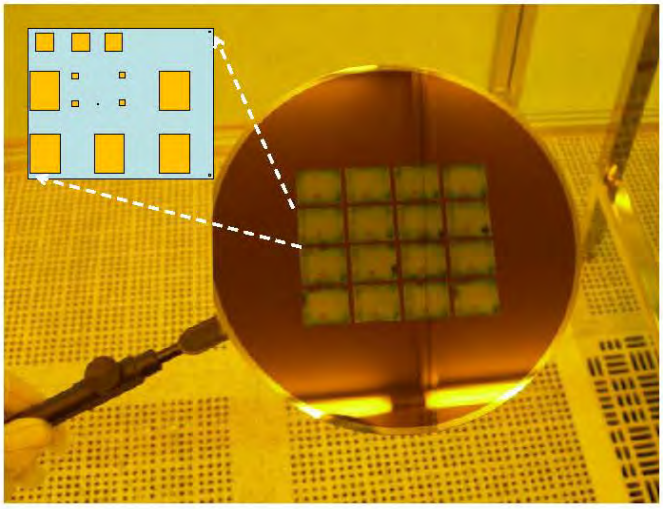

Figure18. Various Optimized Monomat Imprints on 8" Wafer (4 x 4 Imprints)

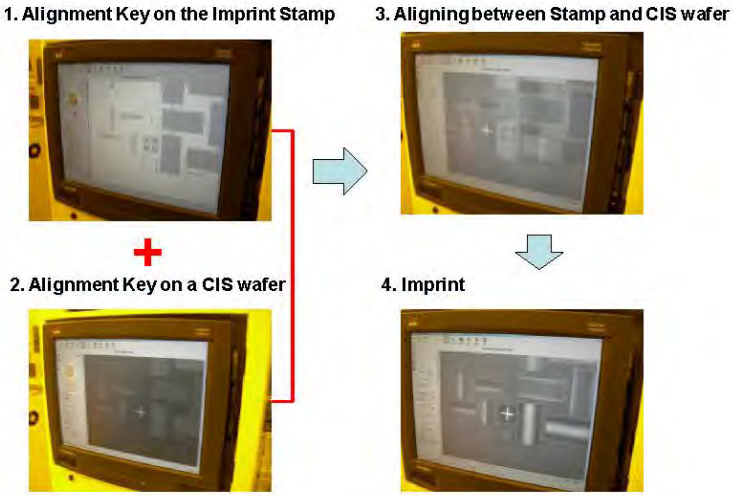

Figure19. Imprint Aligning Procedure

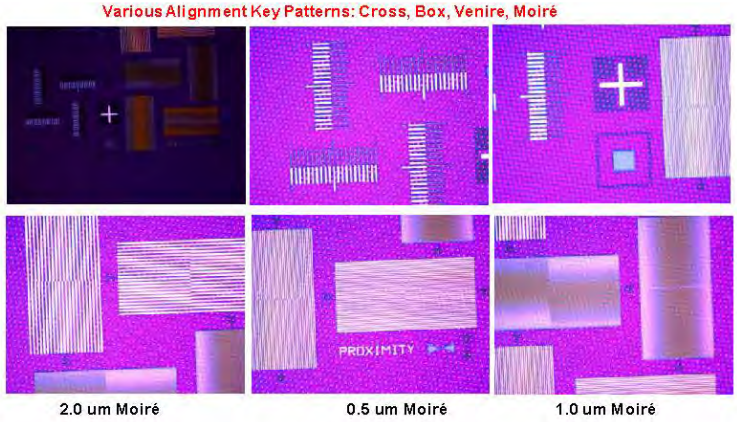

Figure20. Optical Images of overlapped alignment keys after monomat imprinting on a CIS wafer

- Uniform thickness of silspin on the wafer is very critical for following uniform etching step. Figure21 shows the silspin uniformity on a CIS wafer has been achieved by 2 step spin coating process. Figure 22 shows the silspin uniformity on the 8" dia wafer by measuring 8 different area. Figure 23 shows the uniform silspin coated on the monomat pattern surface.

18

❑ History of Sample Preparation
- Transpin coating (3000rpm, 40s)
- Case 1: Silspin coating (800 rpm, 35s) (baking 150 degree 1min)
- Case 2: Silspin coating (3000 rpm, 35s) (baking 150 degree 3min) X 2 times

❑ Cross section view of SEM image (ex., 1-position)

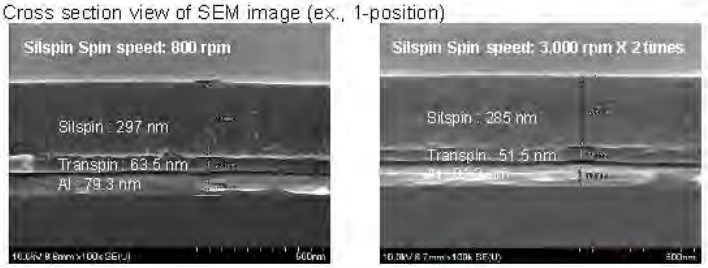

❑ Measured Silspin coating thickness

rpm speed	1 position (edge)	2 position (middle)	3 position (center)	Deviation (Ctr-Edge)
800rpm	297 nm	287 nm	278 nm	~20nm
3000rpm x2	285 nm	278 nm	274 nm	~10nm

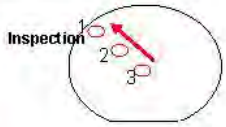

Figure21. Silspin coating uniformity improvemwnt by 2 step coating process

- Wafer no.: 3000rpm x 2 times, (New Silspin solution)
- Since Transpin thickness= ~720A (measured by Ellipsometer)
- Therefore, Avg. Silspin thickness = 3,690-720= ~2,970A

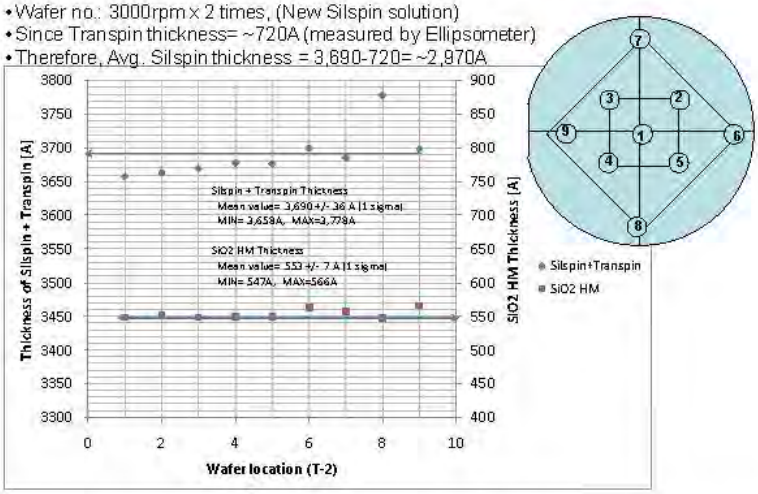

Figure22. Silspin thickness measurement on 8 wafer by spectroscopic ellipsometer

19

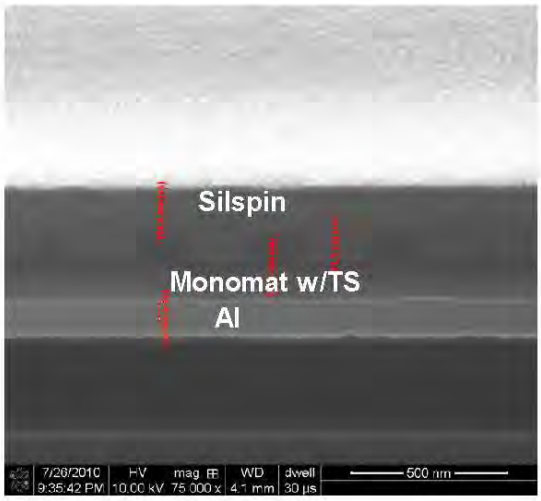

Figure23. Silspin uniformity on the monomat pattern

- The two step polymer etch processes (silspin etch-back and monomat etch) shoud be optimized by proper etch gases and etch time. Figure 25 shows how the incomplete polymer etch profiles are transferred to the next etch process such as SiO2 hardmask and Al etch.

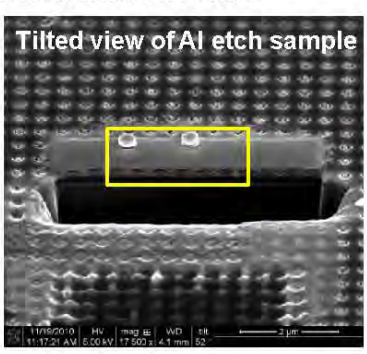

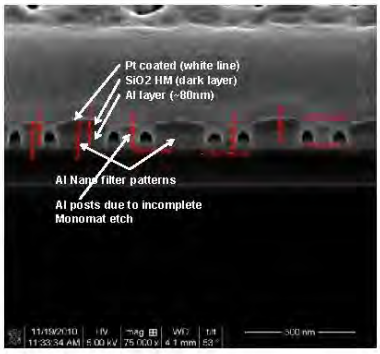

Figure25. Incompelete monomat etch process

- The proper aluminum pattern etch has been achieved with using SiO2 hardmask. Figure26 shows the optical image of nano filter integrated on the pixel arrays. The different color diplayed on each different filter integrated on the pixel arrays.
- Figure27 shows the cross sectional FIB image of Al nano filter patterns.

20

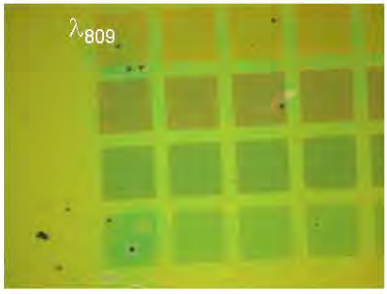

❑ Front Illumination &Reflection

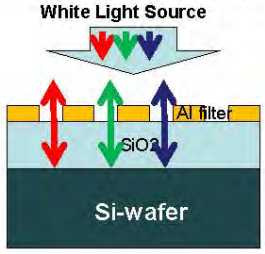

Figure26. Front illumination & reflection with white light source

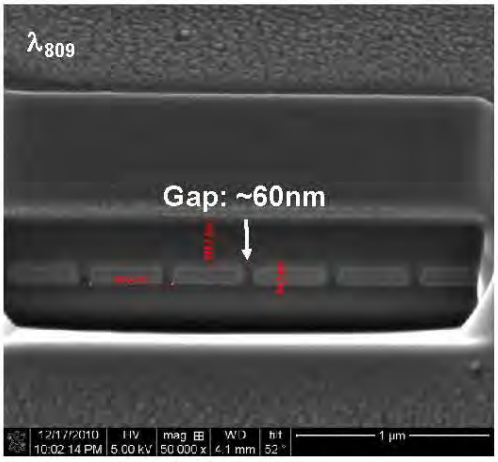

Figure27. FIB cross section of Al nano pattern

- Finally, the bonding pad opening process has been optimized by using proper etch target. (Figures 28-29)

21

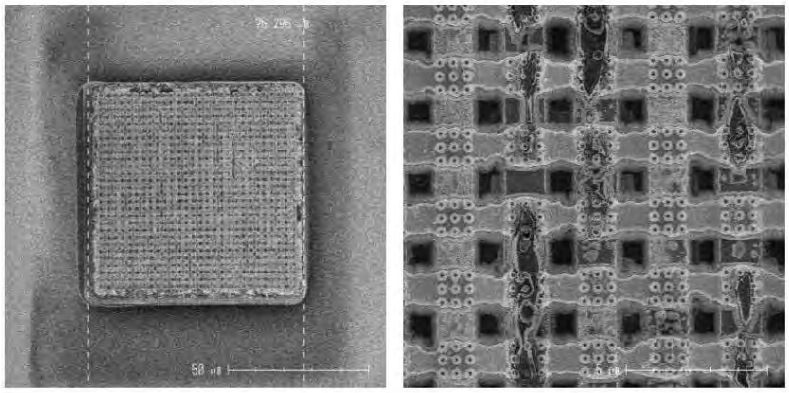

Figure28. CD-SE image of over etched bonding pad (a) Entire Pad, (b) magnified area

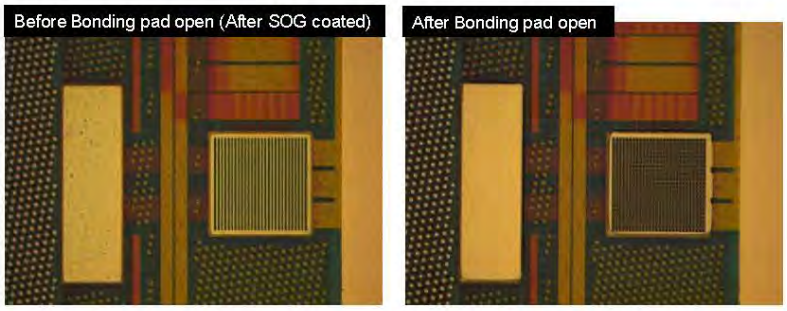

Figure29. Optical image of optimized bonding pad etched condition (a) before etch, (b) after etch

- *Therefore, the monolithically filter integrated on a CIS die was successfully made.* (Figures 30-31)
- All the monolihic filter integration process issues are solved and listed in Table3.

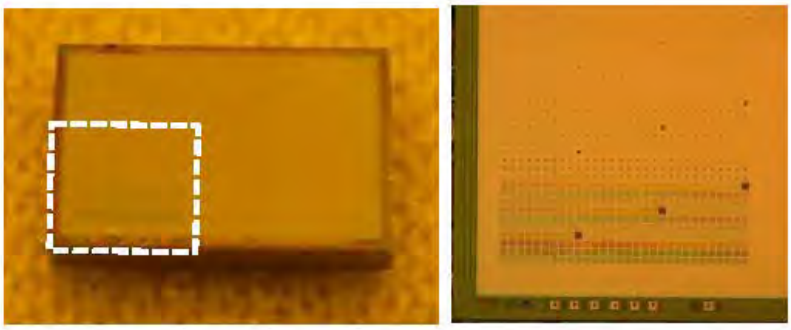

Figure30. (a) Monolithically nano optic filter integrated on a die, (b) magnified pixel array

Figure31. (a) Packaged optical part, (b) spectrum sensor module

23

Process Step	Issues	Solution
Flat CIS wafer surface: Oxide filling on grooves (B/P, scribe lines)	• Proper SiO2 deposition thickness and CMP (chemical mechanical polishing) process condition	→ Flat surface of CIS wafer was analyzed by (1) Profilometer, (2) FIB cross section, (3) Spectro-scopic ellipsometer
Selective Al area patterning	• Open optical litho alignment keys, bonding pads, scribe lines	→ Use optical litho masks (contact aligner, KrF scanner)
Imprint	• Precise alignment between imprint stamp and CIS wafer • Imprint Pattern Optimization ○ monomat seeping ○ uniformity ○ air-gap	→ Align with various alignment keys → Optimized imprint recipe including drop pattern layout
Silspin coat	• Silspin uniformity	→ Apply two step spin-coating
Polymer etch	• Etch non-uniformity	→ Optimized silspin-etch back & monomat etch condition
Al etch	• Etch non-uniformity due to pin-holes attack after consecutive PR process steps	→ Protect SiO2 hardmask
Bonding pad opening	• Opening without damage bonding pads	→ Proper tune the etch time

Table3. Monolithic filter integration process issue & solution

T4: Development of resolution enhancement software *(Deliverable: Demonstrate the 2nm wavelength shift detection using sample LEDs)*

- *Goal: Develop highly accurate LED color sensing software able to detect 2nm wavelength shift*
  - Different algorithms have been developed to reconstruct and enhance the resolution. Spectrum reconstruction method has been developed (Figures32-33)

24

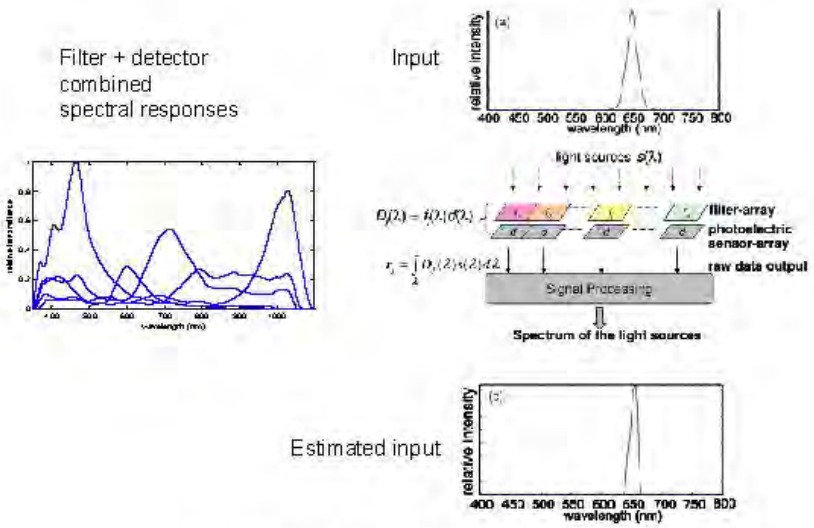

Figure32. Specterum reconstruction overview

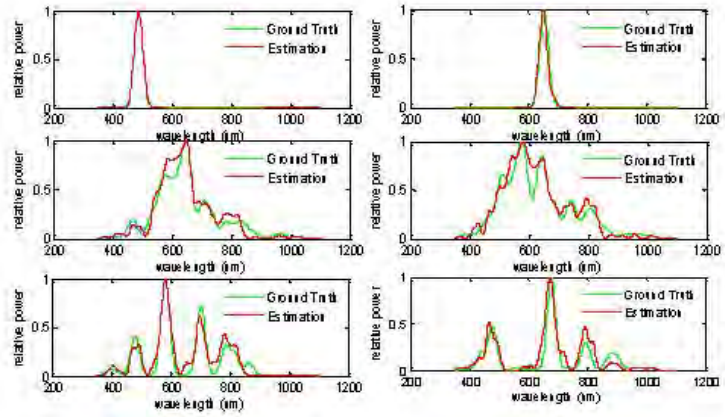

measured by a commercial spectrometer
measured by Spectrum Sensor

Figure33. Result of spectrum reconstruction method

25

- Training method also has been developed ,and by utilizing training data, measurement can exceed 2nm accuracy. See below graph showing filter output response to monochromatic light from 550nm – 554 nm. (Figure34)

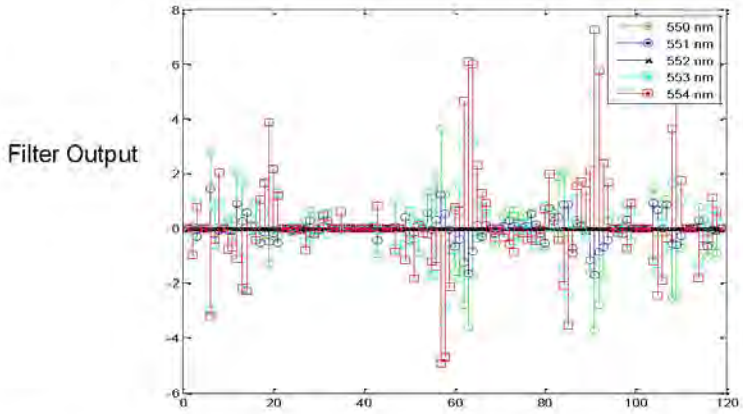

Figure34. Filter output response to monochromatic light from 550nm – 554 nm

Milestone 5 (Date for completion: 4/30/11)

T5: Deliver sensor samples to a customer and receive an evaluation report
(Deliverable: Evaluation report from a customer)

- *Goal: Deliver samples to a customer, and Receive a customer's evaluation report*

- A sample has been delivered to a potential customer and/or partner, WithLight Co., Ltd. in Jeonju city , South Korea. WithLight is an expert company highly specialized in LED measurement tools, equipment, and methods working with many companies and research institutes in the LED industry. WithLight and nanoLambda tested the sensor measuring the LED samples (Blue, Green, and Red) and compared the measurement results with the measurement results using existing test setup. (Figure 35)
- WithLight provided feedbacks and suggestions from the technical and business perspectives. WithLight and nanoLambda agreed on a Joint Development for commercial LED test equipment embedding nanoLambda's sensor.

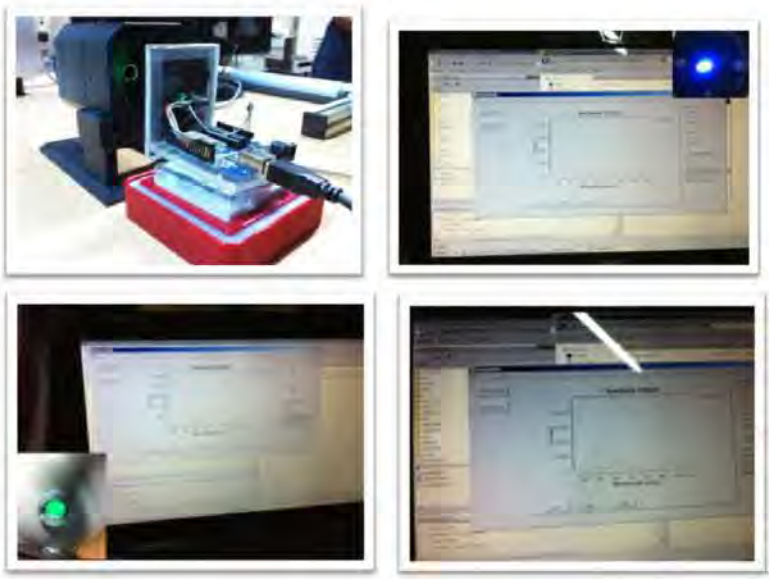

Figure35. Evaluation setup, and measurement blue, green, red LEDs

- The sensor and evaluation kit was delivered and tested measuring the sample LEDs
- The measurement has been done jointly with WithLight engineers and nanoLambda engineers, using both nanoLambda's sensor and existing test equipment
- WithLight provided an evaluation report with feedbacks and suggestions on
  - Stray light, Linearity, Transmittance, Dynamic range
  - Temperature dependency, Angle dependency
  - Suggested to build an automatic calibration setup with integrating sphere with monochromator with variable angle and distance capability.
  - Suggested an acceptable target technical number on CIE x,y value.
  - Suggested to write a draft specification of sensor chip

Part 2: COMMERCIAL DEVELOPMENT

Milestone 1 (Date for completion: 11/2/09)

(*Deliverable: signed contracts, project initiation meeting*)

The project initiation meeting was held at nanoLambda office, and the contracts were signed on 11/2/09.

Milestone 2 (Date for completion: 12/31/09)

C1: Finalize the sensor specification based on the customer input *(Deliverable: The agreed sensor specification)*

- *Goal: Finalize the sensor specification for the LED color monitoring with 2nm accuracy agreed with a customer*
- The customer inputs of LED color requirements were described, and other references such as Philips Lumileds and Cree were described.
- *Therefore, the finalization of the LED color sensor specification has been succesfully made.*

Milestone 3 (Date for completion: 3/31/10)

C2: Design and negotiate the scope and methods of the evaluation *(Deliverable: A test scope & method document)*

- *Goal: Have a mutually agreed test and evaluation methods*
  - Test and evaluation methods have been discussed with LED vendor, channel partner, and test equipment vendor, and a test method for single LED has been agreed upon. (Figure 35)
  - Test method for the single LED is considered the priority as a first step
  - CIE x, y value, peak wavelength, and binning data will be the main test items.
  - Test set-up and procedures for a single LED have been agreed upon.

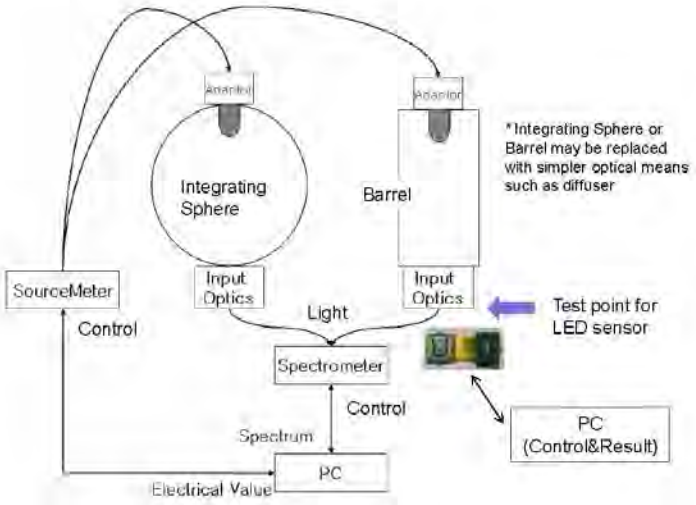

Figure35. Typical measurement setup

- The test results will be compared with the test results using commercial test equipment to evaluate the NanoLambda's LED sensor's performance.
- *Therefore, the scope and methods of the evaluation was successfully negotiated.*

Milestone 4 (Date for completion: 2/10/11)

C3: Perform a cost analysis *(Deliverable: An estimated cost analysis)*

- *Goal: Have a volume based cost analysis for a mass production*

- Cost analysis has been done based on the assumption
  # of wafer : at least 100 (volume> 100,000 ea chip case),
  and unit cost per wafer is $4500;
  CIS Wafer Price : $1500, nano filter integration : $1500, Test & Packaging : $1500
- Analysis summary

  If nano filter integration yield is 48%, the sensor chip cost becomes
  $ 2.12 (for 2.5 mm x 2.5 mm chip size)
  $ 3.05 (for 3.0 mm x 3.0 mm chip size)
  If nano filter integration yield improves to 70% from 48%, and unit cost per wafer reduced to $3000 from $4500, the sensor chip cost becomes
  $ 1.09 (for 2.5 mm x 2.5 mm chip size)
  $ 1.57 (for 3.0 mm x 3.0 mm chip size)

29

- *Therefore, the volume based cost analysis for a mass production was successfully performed .*

C4: Negotiate a business terms and conditions with a customer *(Deliverable: A draft MOU)*

- *Goal: Have Have a mutually agreed commercial terms and conditions draft*

- An MOU has been agreed and signed by and with WithLight, a LED measurement equipment vendor.
- The MOU includes commercial terms and conditions such as deliverables and the price ceiling for a minimum volume.
- *Therefore, the business terms and conditions with customers are successfully negotiated .*

Milestone 5 (Date for completion: 4/30/11)

C5: Establish formal relationship with partners and/or customers *(Deliverable: A formal business agreement document)*

- *Goal: Establish a commercial business relationship with a customer*

- A sample has been delivered to a potential customer and/or partner, WithLight Co., Ltd. in Jeonju city , South Korea. WithLight is an expert company highly specialized in LED measurement tools, equipment, and methods working with many companies and research institutes in the LED industry. Also nanoLambda signed a Purchase Agreement with "L" Electronics in Korea for evaluation kit, and nanoLambda received an order from company "S" cal in US for an evaluation kit. nanoLambda signed an MOU with Stanford University for a joint project as well. All these customers and partners are willing to collaborate to develop solutions for variety of different potential applications including LED or LED light measurement.
- *Therefore, the formal relationship with partners & customers were successfully established .*

WithLight

- WithLight wants to continue the relationship to develop the commercial LED measurement equipment product
- WithLight suggested a joint development project of a LED measurement equipment using nanoLambda's sensor.
- For the joint development, WithLight commented that they could also apply for Korea government funding.

- WithLight also suggested that they can support nanoLambda on certain development areas where nanoLambda needs help, such as on the embedded hardware and firmware design and development.
- WithLight and nanoLambda agreed on a joint development project.

Company, "L" Electronics

- "L" Electronics and nanoLambda signed a purchase agreement for an evaluation kit. Delivery Due: May 25, 2011, Amount: $3,200
- "L" Electronics wants to test and evaluate the sensor for many different applications including LED measurement.

Company, "S" Cal

- "S" cal placed an order and paid in advance ($3,200) for an evaluation kit.
- Their target application is the accurate color measurement and calibration of TV/Display (LED TV, 3D TV, LED projector etc.)

University of Stanford

- University of Stanford and nanoLambda signed an MOU for a collaboration
- As part of the ROSE(Remotely Operated Science Education) program, University of Stanford would like to use nanoLambda's Spectrum Sensor.

Part 3: VALUE PROPOSITION

- **How has the funding by PA Nano helped your company to grow?**

The funding by PA Nano for LED Color monitoring sensor has greatly help our business move forward for the commercialization. The successfully developed monolithic fabrication process proved that the mass production at a very low cost using nanoimprint process is feasible. We demonstrated our new sensor prototype at the international CES 2011 show. More than 500 potential partners, customers and investors visited and showed strong interests. We also tested our sample together with potential partners/customers and got feedbacks. More importantly, we got PO and sold our evaluation kits to a few selected alpha test customers for test and evaluation for their applications. Since we now verified that it's mass producible at low cost and now we better understand the market needs, the commercialization is finally foreseeable on the horizon. We plan to release our commercial product within a year.

- **What is the potential for job creation?**
  For the commercial product launch, we will need to hire five to ten more engineers within a year in various fields, such as optics, wafer process, software, test and applications, and sales.

- **Have you established any new partnerships with customers or commercialization partners resulting from the support of PA Nano?**
  We have established new partnerships with WithLight and Stanford University by signing an MOU. We have also established relationships for joint commercial product development, with potential customers such as LG in Korea and SpectraCal in US. Also collaborations with CMOS image sensors are under discussion with partner companies such as Avago, ClairPixel, Hamamatsu, and Siliconfile.

- **How has support from PA Nano accelerated your commercialization pathway?**
  Not only the funding but also the review and support from PA Nano have accelerated our commercialization pathway. The cost analysis along with the monolithic fabrication process developed and the test with WithLight under this PA Nano project have been the key milestones for the commercialization pathway. Since we verified that it's mass producible at low cost and we now understood more clearly what to improve, our commercialization efforts have become more predictable and can appeal better to potential customers, partners and investors. We can accelerate our commercialization efforts and tasks all in parallel.

Part4: Submission of the Final Report and Closeout Paperwork

Schedule summary for milestone and payments

Milestone	Date	Description	Payment
Milestone 1	11/2/09	Project kick off	10% of total - $19,745
Milestone 2	12/31/09	T1, C1	30% of total - $59,235
Milestone 3	3/31/10	T2, C2	20% of total - $39,490
Milestone 4	2/10/11	T3, T4, C3, C4	20% of total - $39,490
Milestone 5	4/30/11	T5, C5	10% of total - $19,745
Final Paperwork	4/30/11	Closeout docs	10% of total - $19,745

Appendix J – 10-023 (Kurt Lesker)

PANCC Copper Sputtering Trials
Kurt J. Lesker Company, Materials Division
February 7, 2011

Summary

Two copper targets of identical dimensions were sputtered under similar conditions. The resulting films were analyzed to identify differences in film quality or target performance. The targets used to produce the films were manufactured by different techniques. Integran USA, Inc produced a 99.998% pure copper target that was used to manufacture EJTNANOCUSAMPLE that was then used to deposit 100nm Cu films on silicon wafers ("I" samples). Nikko Metals USA, Inc produced a 99.9999%+ pure copper target that was used to manufacture EJTCU60SAMPLE that was then used to deposit 100nm Cu films on silicon wafers ("N" samples).

- Sputtering of the materials proved to be very similar, only noting a slight difference in sputtering voltage.
- A difference in appearance was noted after the targets were sputtered and removed from the chamber; the EJTNANOCUSAMPLE appeared to have porosity throughout.
- Film uniformity on wafer I1 was +/-12%; film uniformity on wafer N1 was 11.2%.
- AES analysis was performed to examine the depth profile of the films. The surface survey spectra showed copper, oxygen, and low levels of carbon present at similar concentrations on the two as-received samples; namely the surface and the interface between the copper film and the silicon substrate.
- TEM cross section data show that the copper layer thickness is 125nm on I3 and ~120nm on N3.
- In the I3 sample voids were detected at the substrate-film interface. No voids were detected in the N3 TEM sample
- In the STEM images, there also appears to be an interfacial layer between the copper and silicon substrate on both samples. This layer was also detected during the AES analysis.
- The average resistivity of wafer I4 was measured at 1.87×10^{-6} Ω·cm with a standard deviation of 6.76×10^{-8}; the average resistivity of wafer N2 was measured at 2.44×10^{-6} Ω·cm with a standard deviation of 7.48×10^{-8}.

"I" Samples: I1, I2, I3, I4

Target: Part # EJTNANOCUSAMPLE, nCu (copper) 99.998% pure, 6.00" diameter x 0.250" thick, Lot #: S008 / PRD053287
Substrate: 6" Si Wafer
Film thickness: 1280 Å
Power: ~1kW (574 Volts, 1.74 Amps)
Film uniformity (wafer I1): +/-12%

Target Impurities – EJTNANOCUSAMPLE, Lot # S008 / PRD053287

The target material was sent for full scan GDMS and IGA. The resulting purity including only metallic impurities was 99.9982%. Carbon and oxygen were detected at 23ppm and 36ppm, respectively.

Element	Concentration [ppm wt.]	Element	Concentration [ppm wt.]
Li	< 0.001	Ag	0.03
Be	< 0.001	Cd	0.02
B	< 0.001	In	< 0.005
F	< 0.01	Sn	1.2
Na	0.13	Sb	0.01
Mg	< 0.005	Te	< 0.05
Al	0.007	I	< 0.005
Si	0.008	Cs	< 0.005
P	2.1	Ba	< 0.001
S	0.11	La	< 0.001
Cl	0.03	Ce	< 0.001
K	0.4	Pr	< 0.001
Ca	< 0.01	Nd	< 0.001
Sc	< 0.001	Sm	< 0.001
Ti	0.005	Eu	< 0.001
V	< 0.001	Gd	< 0.001
Cr	< 0.005	Tb	< 0.001
Mn	< 0.005	Dy	< 0.001
Fe	< 0.001	Ho	< 0.001
Co	0.02	Er	< 0.001
Ni	0.04	Tm	< 0.001
Cu	Matrix	Yb	< 0.001
Zn	< 0.05	Lu	< 0.001
Ga	< 0.01	Hf	< 0.001
Ge	< 0.005	Ta	< 1
As	0.09	W	0.02
Se	< 0.05	Re	< 0.001
Br	< 0.05	Os	< 0.001
Rb	< 0.001	Ir	< 0.001
Sr	< 0.001	Pt	11
Y	< 0.001	Au	< 0.01
Zr	< 0.001	Hg	< 0.01
Nb	< 0.005	Tl	0.02
Mo	0.44	Pb	0.23
Ru	< 0.005	Bi	0.02
Rh	< 5	Th	< 0.001
Pd	0.02	U	< 0.001

Element	Concentration [ppm wt.]
C	23
N	< 10
O	36
S	
I	< 3

Figure 1. GDMS results (above) IGA results (below) for EJTNANOCUSAMPLE, nCu target, Lot # S008 / PRD053287

Sputtering Results – EJTNANOCUSAMPLE, nCu Target / Wafers I1, I2, I3, I4

The target sputtered very well and no problems were encountered while it was running. However, when the target was removed from the magnetron, the appearance was not as expected. The eroded nCu target displayed shallow porosity after sputtering as shown below. In

general the erosion of the target was not even. An alpha step was used to measure the film uniformity across the wafer I1 and the result was +/-12%.

Photo of eroded nCu Target after sputtering

"N" Samples: N1, N2, N3, N4

Target: Part # EJTCU60SAMPLE, Nikko Copper Target 99.9999% pure, 6.00" diameter x 0.250" thick, Lot# 07-0918-363 / VPU052919
Substrate: 6" Si Wafer
Film thickness: 1250 Å
Power: ~1kW (562 Volts, 1.78 Amps)
Film uniformity (wafer N1): +/-11.2%

Target Impurities – Customer (Altis Semiconductor) sample of Nikko Cu

The target material provided by a customer using the same material was sent for full scan GDMS and IGA. The resulting purity including only metallic impurities was 99.99996%. Oxygen was detected at 16ppm. GDMS and IGA results are listed below.

Element	Concentration [ppm wt]	Element	Concentration [ppm wt]
Li	< 0.001	Ag	0.22
Be	< 0.001	Cd	< 0.01
B	< 0.001	In	< 0.005
F	< 0.01	Sn	0.009
Na	< 0.005	Sb	0.002
Mg	< 0.005	Te	< 0.05
Al	0.001	I	< 0.005
Si	0.01	Cs	< 0.005
P	0.01	Ba	< 0.001
S	0.07	La	< 0.001
Cl	< 0.05	Ce	< 0.001
K	< 0.01	Pr	< 0.001
Ca	< 0.01	Nd	< 0.001
Sc	< 0.001	Sm	< 0.001
Ti	< 0.001	Eu	< 0.001
V	< 0.001	Gd	< 0.001
Cr	< 0.005	Tb	< 0.001
Mn	< 0.005	Dy	< 0.001
Fe	0.004	Ho	< 0.001
Co	< 0.001	Er	< 0.001
Ni	0.003	Tm	< 0.001
Cu	Matrix	Yb	< 0.001
Zn	< 0.05	Lu	< 0.001
Ga	< 0.01	Hf	< 0.001
Ge	< 0.005	Ta	< 1
As	< 0.005	W	< 0.001
Se	< 0.05	Re	< 0.001
Br	< 0.05	Os	< 0.001
Rb	< 0.001	Ir	< 0.001
Sr	< 0.001	Pt	< 0.01
Y	< 0.001	Au	< 0.01
Zr	< 0.001	Hg	< 0.01
Nb	< 0.005	Tl	< 0.005
Mo	< 0.005	Pb	< 0.005
Ru	< 0.005	Bi	< 0.005
Rh	< 5	Th	< 0.001
Pd	< 0.005	U	< 0.001

Element	Concentration [ppm wt]
C	< 10
N	< 10
O	15
S	
H	< 3

Figure 3. GDMS results (above) IGA results (below) for Nikko Cu target, customer supplied sample

Sputtering Results – EJTCU60SAMPLE, Nikko Cu Target / Wafers N1, N2, N3, N4

The target sputtered very well and no problems were encountered while it was running. When the target was removed from the magnetron, the appearance was typical and the erosion of the target was mostly even.

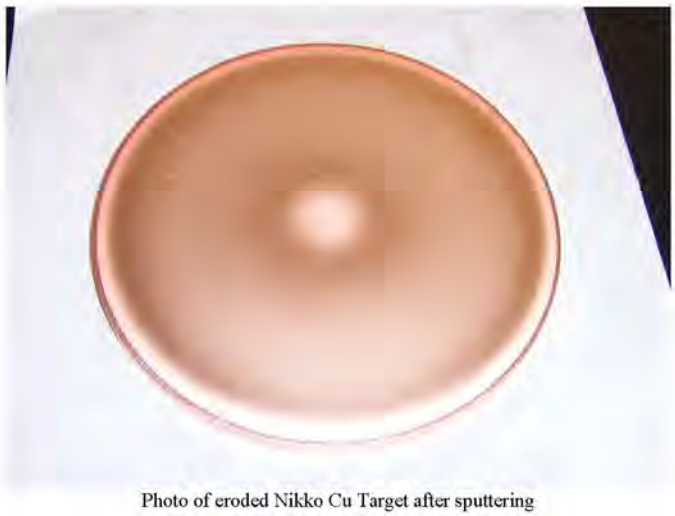

Photo of eroded Nikko Cu Target after sputtering

Copper Film Analysis – nCu (I2, I3) and Nikko (N2, N3)

Auger Electron Spectrometry (AES)

AES is a surface surveying technique that analyzes energy from Auger electrons generated by a sub-micron electron beam. The technique generates images using both secondary or backscattered electrons and also depth profiling through sputtering with an auxiliary ion beam.

AES was performed on both samples to determine depth profiles. The surface survey spectra showed copper, oxygen, and low levels of carbon present at similar concentrations on the two as-received samples. Spectra were also acquired mid-way through the sputter depth profiles and after the completion of the profiles. The data are summarized in Table I and Table II. The sputter depth profiles are copied below and show the presence of a very thin (~10-20Å) oxide layer on the copper layer. The copper layer was ~105nm on all samples. The thickness is an estimate and assumes that the copper sputters at the same rate as SiO_2.

The full AES survey data for both samples is outlined in ReportY0ABV589Cu.pdf. The depth profiles for each sample have been copied below.

AES Sputter Depth Profile: Wafer I3

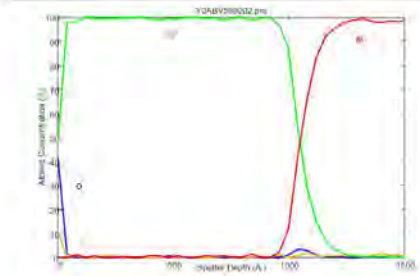

AES Sputter Depth Profile: Wafer N3

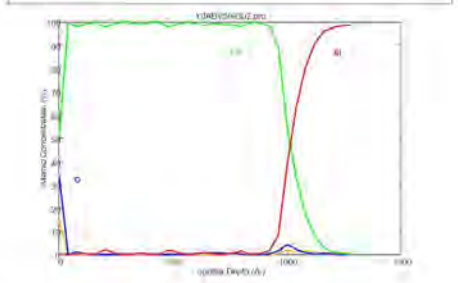

Table I. Concentration of Elements Detected on the As-Received Surface (in Atom%)

Filename	Sample ID	C	O	Si	Cu
	Wafer I2				
Y0ABV589101.spe	Surface	14	38	-	48
Y0ABV589104.spe	Mid pt in profile	-	-	-	100
Y0ABV589103.spe	Post Profile	-	-	100	-
	Wafer I3				
Y0ABV589201.spe	Surface	7	42	-	50
Y0ABV589204.spe	Mid pt in profile	-	-	-	100
Y0ABV589205.spe	Post Profile	-	-	100	-
	Wafer N3				
Y0ABV589301.spe	Surface	6	57	-	37
Y0ABV589304.spe	Mid pt in profile	-	-	-	100
Y0ABV589305.spe	Post Profile	-	-	100	-

Table II. Film Composition and Thickness based upon AES Profiles

Filename	Sample ID	C	O	Cu
Y0ABV589102	Wafer I2	<2nm	<2nm	~105nm
Y0ABV589202	Wafer I3	<2nm	<2nm	~108nm
Y0ABV589302	Wafer N3	<2nm	<2nm	~103nm

Scanning Transmission Electron Microscopy (STEM)

In STEM, a focused probe of electrons is rastered across a sample, transmitted through the sample and collected with detectors below the sample with the exception of secondary electron detection which takes place above the sample. There are 3 image modes which are denoted at the bottom of the image:

1. Transmitted Electron Mode (TE)- The detector is directly under the sample and yields a traditional TEM bright field image from diffraction contrast.
2. Z-Contrast Mode (ZC)- the transmitted electrons are collected underneath the sample on a high-angle annular dark field (HAADF) detector which yields atomic number contrast. High atomic number elements appear light in gray scale, low atomic numbers are dark.

3. Secondary Electron Mode (SE)- Just like traditional scanning electron microscope images (SEM). Secondary electrons are collected from the surface of the sample providing topographical and atomic number contrast information.

Scanning transmission electron microscope (STEM) surface analysis of wafers I3 and N3 showed variations in grain growth but uncovered no obvious defects. The secondary electron images, acquired at a magnification of 250X, show that both samples are free of particles, scratches, hazes, hillocks, pits, etc.

Secondary Electron Images: Wafer I3

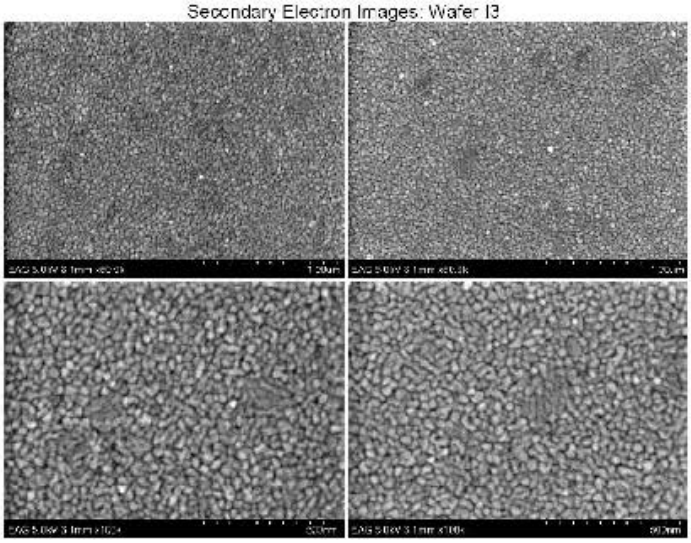

Secondary Electron Images: Wafer N3

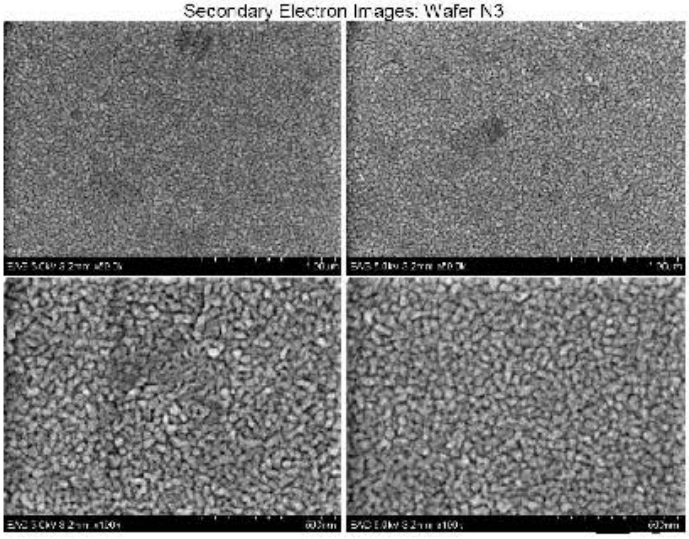

During FIB sample preparation, a carbon coating is applied to the samples. This is followed by sputtered platinum and FIB-applied platinum which are not visible in the images. Some of the images are rotated 90 degrees clockwise for layer thickness measurements. However the TEM cross section data show that the copper layer thickness is 125nm on I3 and ~120nm on N3. The data are summarized in Table III.

Table III. Film Composition and Thickness based upon TEM

Filename	Sample ID	C/O	Cu
Y0ABv589202	Wafer I3	~1nm	~125nm
Y0ABv589802	Wafer N3	~1nm	~120nm

Copper film thicknesses were measured to be 128 nm and 125 nm for I3 and N3 respectively.

Cross Section Image: Wafer I3

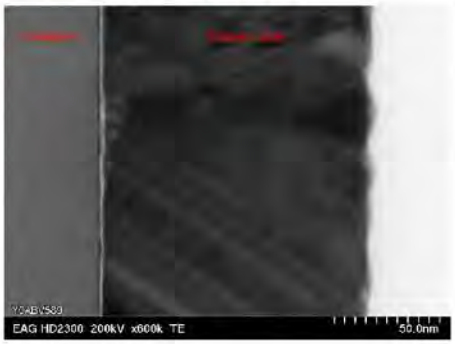

Cross Section Image: Wafer N3

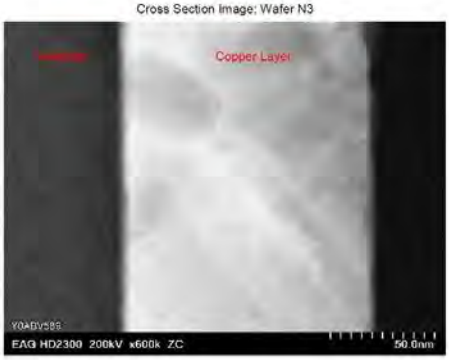

In the I3 sample voids were detected as can be seen in the image below on the left. No voids were detected in the N3 TEM sample as seen in the image below on the right.

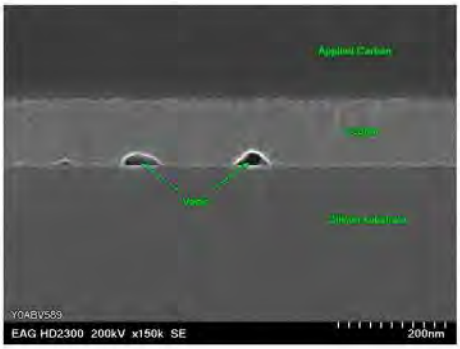

There also appears to be an interfacial layer between the copper and silicon substrate. Sample I3 is shown below on the left and sample N3 is shown below on the right.

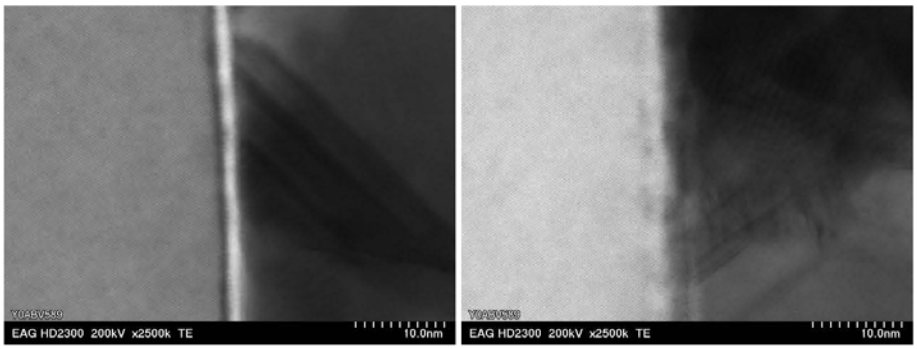

49 Point Resistivity Mapping

Electrical resistivity is a measure of a material's opposition to the flow of electric current. Electrical resistivity mapping was performed on the two samples. 2D and 3D maps were produced using the data obtained from the resistivity measurements.

The data for sample I4 is copied below. The set of data includes 3 sigma data. This is the data within 3 standard deviations of the average. 2D and 3D maps are shown below. The average resistivity was measured at 1.87×10^{-6} Ω·cm with a standard deviation of 6.76×10^{-8}.

Contour Map

1. Lot ID : TEST 49PT
2. Data File : t4(2).dat
3. Sample Size (mm) - Sample : 150 Flat : 57 Exclusion : 6
4. Thickness (um) : 0.1
5. Sample Material : Cu
6. Mat. Resistivity (ohm.cm) : 0.00E+00
7. Correction F : 4.53236
8. Probe Space (mm) : 1
9. TCoefficient : 0
10. TMeasure (°C) : 23
11 TReference (°C) : 23
12. MMode : Pattern 49 Site
13. Date : 1/18/2011 Time : 11:43:26 AM
14. Op ID : bjg
15. Analysis [ohm.cm] : 3 Sigma=Max : 2.02909E-06 Min : 1.73241E-06
1) Max : 2.00988E-06 2) Min : 1.75180E-06 3) Ave : 1.87216E-06
4) StDev : 8.76210E-08 5) Uni (%) : 6.89257E+00 6) Max-Min(Range) : 2.58080E-07
7 Ave (%) : 3.61192E+00
16. Description : t4(2) 2D 3Sigma

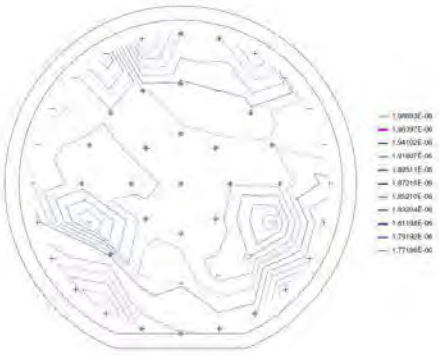

3D Map Analysis [ohm.cm]

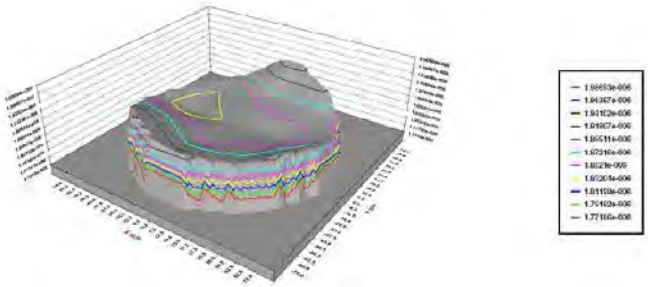

The data for sample N2 is copied below. The set of data includes 3 sigma data. This is the data within 3 standard deviations of the average. 2D and 3D maps are shown below. The average resistivity was measured at 2.44 x 10^{-6} Ω·cm with a standard deviation of 7.48 x 10^{-8}.

Contour Map

1. Lot ID : TEST 49PT
2. Data File : N2(2).dat
3. Sample Size (mm) : Sample= 150 Flat : 57 Exclusion : 6
4. Thickness (um) : 0.1
5. Sample Material : Cu
6. Mat. Resistivity (ohm.cm) : 0.00E+00
7. Correction F : 4.53236
8. Probe Space (mm) : 1
9. TCoefficient : 0
10. TMeasure (°C) : 23
11. TReference (°C) : 23
12. MMode : Pattern 49 Site
13. Date : 1/18/2011 Time : 11:58:03 AM
14. Op ID : hg
15. Analysis [ohm.cm] : 3 Sigma=Max : 2.60358E-06 Min : 2.28324E-06
1) Max : 2.57579E-06
2) Min : 2.30611E-06
3) Ave : 2.44193E-06
4) StDev : 7.47500E-08
5) Uni (%) : 5.52186E+00
6) Max-Min(Range) : 2.69680E-07
Ave (%) : 0.00000E+00
16. Description : N2(2) 2D 3Sigma

Project Title:

High Performance Nano-Structured Sputter Targets

Date of Submission:

March 30, 2011

Name and Organization of Principal Investigator:

Mr. Kevin Williams

Kurt J. Lesker Company

Telephone: *412-266-1166*

E-Mail: *kevinw@lesker.com*

Address of Principal Proposer:

P.O. Box 10, 1925 Route 51, Clairton PA 15025-3681

Names and Organizations of other Team Members:

Integran Technologies USA Inc. (Pittsburgh, PA)

Ian Winfield, Dr. Herb Miller and Dr. Robert Heard,

Kurt J. Lesker Company (Clairton, PA)

Rich Johnson and Heidi Siwik

Milestone 5 Deliverable

Summary/Status

This Milestone includes both a commercial and technical deliverable. A brief description of each deliverable with a status summary of each follows.

Commercial Deliverables:

Two (2) purchase orders for *n*Cu target qualification from semiconductor and/or GMR customers/OEMs.
Status: Partially Complete

Summary: Four customers have agreed to test targets which meet the specification: Intel, Applied Materials, TSMC and Altis Semi.

Technical Deliverable:

A 4" (OD) x 0.125" (thick) alternate material to be identified and produced based on customer feedback and technical feasibility. Purity and grain size analysis of sample.
Status: Not completed

Summary: A change in the Milestone deliverables was requested in order to delete this deliverable. The additional costs associated with replacing the deposition bath to increase purity and the increase the thickness of the prototype targets was determined more important in the development of the product than subsequent material development.

Shipment of prototype targets.
Status: Not completed

*n*Cu target which yields film characteristics and sputtering performance measured to meet customer specifications. The data will include the following:

- Film resistivity <2 ohm sq and thickness uniformity per 49 point resistivity mapping
  Status: Completed (see 2/7/11 report)
- Post sputtering target surface Ra < 1micron
  Status: Not completed
- Target with surface finish of 63RMS or better
  Status: Completed (see 2/7/11 report)
- TEM and SAM analysis to detect film defects
  Status: Completed (see 2/7/11 report)
- Cleaned and packaged product per customer specification
  Status: Completed (see 2/7/11 report)

Prototype delivered to respective customers for qualification.
Status: Not completed

Data showing how the performance of this manufactured product compares to the product produced using targets acquired from the top suppliers of Cu targets to the semiconductor industry.
Status: Completed (see 2/7/11 report)

Milestone Summary: After thorough review of technical results, it was determined that the electro-deposition process may not yield targets which meet the customer specifications/requirements. Further development would require substantial financial resources with an uncertain outcome. It was agreed by all

parties to end the project at this point.

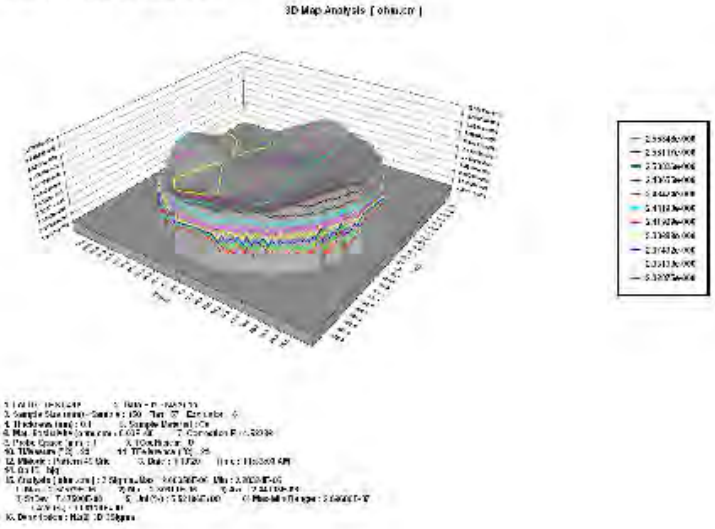

Appendix K – 10-035 (Industrial Learning Systems)

Final Report submitted to PA-Nano Materials Commercialization Center

Project Number:	**10-035**
Title:	**Continuous Production of Nano-Structured Solar Cells**
Submitted By:	**Dr. B. Erik Ydstie, CEO ILS**
Company:	**Industrial Learning Systems, Inc.**
Date Submitted:	**Aug 14, 2012**

Executive Summary: The objective of the development and commercialization project supported by the PA-Nano Materials Commercialization Center was to verify a new process for making silicon wafers to produce solar cells. Prototypes using machined graphite coated with silicon nitride and similar inert materials were used to demonstrate a new (patent pending) process for making thin, nano-structured films of silicon suitable for making solar cells. The new process promises to reduce capital and operating costs by a factor of 3 or more relative to current wafer production technology. This reduction paves the way for solar electricity to reach coal parity at about $0.40 per kWp in the foreseeable future (about 4 years). The proposed process is based on a concept that is easy to implement on an industrial scale in Western Pennsylvania. The PA manufacturing base has expertise in high temperature processing and ideally suited for this commercialization project and industrial development partners are easy to find. Industrial Learning Systems (iLS) has been negotiating potential development and commercial partnerships with the Alcoa Technical Center in New Kensington, Epiphany Tech in Vandergriff and Elkem ASA with offices in Moon Township. Basic research and development completed during the execution of the project show the feasibility of the process principles. We have shown that the process is capable of producing mono-crystalline wafers. We developed a water model at scale that shows feasibility of continuous production. We developed a new texturization process that reduce the reflectance level down to less than 8% for wafers produced in our lab. The impurity level is currently too high and difficult to control in the current experimental set-up. We will gain access to a more advanced pilot plant system in the fall of 2012 that will allow us to continue process development and control the process so that the required purity conditions are met. The new system is designed to produce 5 inch wide wafers at a rate of about 20" per minute. A number of companies and investors, including Mr. Andre Heinz and Applied Materials have expressed interest in investing once the process concept has been demonstrated at industrial scale.

Background: The Horizontal Ribbon Growth (HRG) process for continuous production of silicon wafers is motivated by how *ice freezes on water*. A molten bath of silicon is cooled from the top, below its freezing point. Solid silicon is less dense than liquid silicon (by about 4%) so that the sheet floats like ice on water as shown in **Figure 1**. The solid sheet is continuously removed, while liquid silicon is continuously replenished at the same rate. The continuous process promises to reduce the cost of mono-crystalline silicon wafers by a factor of 3 or more relative to the current technology. The main savings come from reducing waste by eliminating sawing (kerf losses) and by continuous operation at high production rate.

The production rate of the HRG process is not limited by the rate of solidification since

solidification is perpendicular to the process flow. This property distinguishes the process from many current technologies including the Czochralski and Edge Film Defined Growth (EFG) processes. Furthermore, directional solidification on a liquid substrate produces a mono-crystalline sheet of high quality by moving impurities to the melt.

Mathematical models and a full-scale water-model show that sheets with a thickness of 0.180 mm can be produced at a rate of 150 mm per min (See **Figure 1** on the right). Small scale, batch experiments have been used to produce single crystalline silicon wafers by solidification from the top of molten silicon as well as molten slags.

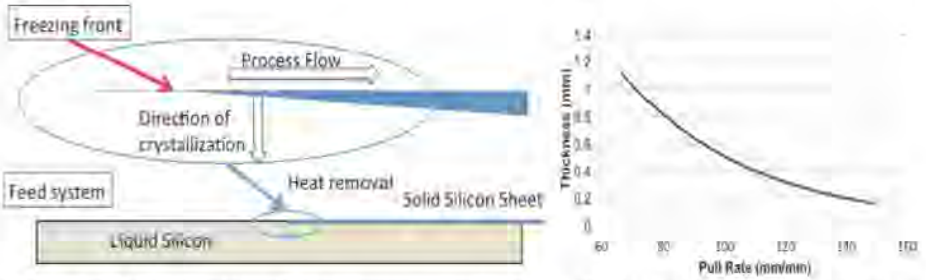

Figure 1: The HRG process for continuous manufacturing of silicon solar wafers is shown on the left. The figure on the right compares mathematical model results with a water model for pull rates from 1 to 2.5 cm per minute.

Major Conclusions

The program supported by the PA-Nano Materials Commercialization Center enabled us to demonstrate

1. The continuous process can produce small mono-crystalline wafers of silicon. Silicon losses were estimated to be less than 12 %.
2. The new texturization process new green chemicals reduces reflectance of Czochralski wafers to 10% of incident light while the reflectance of iLS wafers was about 8%. The silicon losses were estimated to be 4%.
3. We approached a number of potential partners and looked into how to finance the further development of the process. The most successful results:
    a. PA Nano funding and the results we obtained allowed us to write a strong NSF Phase I proposal. This was funded and led to the submission of the Phase II proposal in July 2012.
    b. Results from the research were presented at the IEEE Photovoltaics Specialist Conference in Austin TX. Here we made contact a major solar cell production company that is going to donate a major piece of equipment that will be used to develop and test the wafer production system at commercial scale.
4. The commercialization plan was completed. It was shown that price of silicon wafers can be reduced by a factor of three. We predict that cost of a solar cell produced in HRG process will be about $0.40 per Wp. Three commercialization options were evaluated, license, partner, build our own. In the current economic climate and in discussions with

potential investors we found that build our own is the best option to move forward.

The Road Ahead for iLS

The feasibility of the proposed approach was verified in high temperature batch and semi-continuous experiments to demonstrate thin sheet formation, extraction and texturization. We also verified that the proposed approach holds the potential to offer the following ***economic benefits*** over conventional wafering processes. The major ***challenges*** prevailing in this project are:

1. Controlled and continuous sheet formation with uniform thickness in the range of 150 to 250μm.
2. Optimization of the heat transfer processes to maintain smooth temperature gradient.
3. Automated extraction of mono-crystalline sheets with desired crystal orientation.
4. Control the impurity inclusion and segregation.
5. Capital investment towards better design, construction and implementation of the proposed methodology.
6. Identify investors willing to invest in industrialization once the process has been demonstrated at 1:1 scale.

In order to meet these challenges iLS has decided go ahead with the implementation of a pilot plant system capable of producing 5 inch wide wafers in a continuous process. This system will be installed in the fall of 2012 at U-PARC or at CMU. We are in process of investigating the different options to find the one that suits our needs best. The system, shown in the diagram below (Figure 2) consists of a crucible for melting silicon and a float chamber for wafer production. The system has several measurement and control devices and is connected to a computer control system that allows for precise control of the system. The system is housed in a cylindrical container as shown in Figure 3. The system can be evacuated to remove air and moisture and then be back-filled with inert argon gas and potentially low levels of nitrogen to stabilize the crystallization process. The system that will be installed is designed to be capable of producing 5inch wide wafers at 20 inches per minute. These specifications correspond to the ones used in the industrial case study. With significant NSF funding in Phase II, we will be able to operate and fine-tune the pilot plant system. A Gannt chart showing the project plan for 2013-2014 is shown below.

Tasks	Months							
	3	6	9	12	15	18	21	24
Objective 1 – Operate and Refine the Pilot Scale Float Process								
Task 1 – Design and modify float zone chamber								
Task 2 – Develop empirical models for control								
Task 3 – Automatic control of temperature profile in float zone								
Task 4 – Improved control of extractor system								
Task 5 – Heater installment and control at the exit and along the belt								
Objective 2 – Design of an Industrial Scale Demonstration System								
Task 6 – Develop scale-up models								
Task 7 – Optimization of process at different conditions								

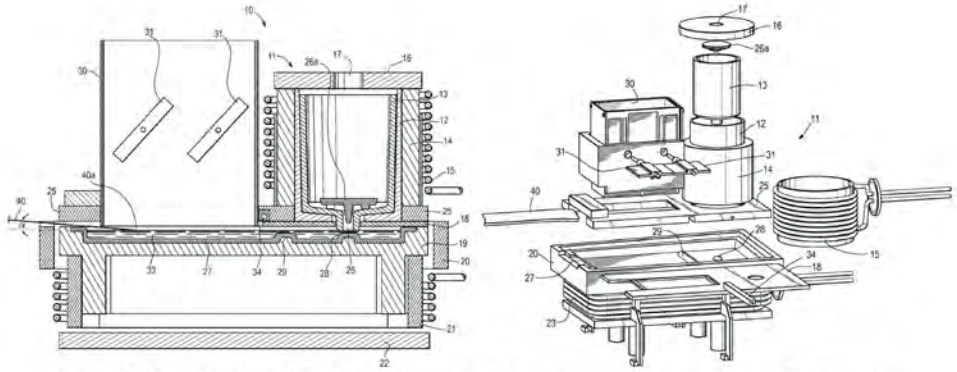

Figure 2: Detailed sketches of pilot plant design equipment for continuous float process.

Figure 3: Photos showing the pilot plant (left) and power supply and computer control system (right).

Overview of Progress Reports, Milestones and Results

During the execution of the project we produced 5 reports and accompanying presentations. These reports explain in detail progress made and a review of 6 Major Technical Milestones with 17 sub-categories and 5 Major Commercial Milestones with 6 sub-categories. The major

The contents of the reports and Technical Milestones are reviewed here

1. **Report 1: Submitted September 29, 2010**
    1. ***T1:*** *Produce prototype crystalline silicon sheets in small scale batch experiments.*

       Conclusion: We have been able to make wafer of 2cm × 2cm. We have also been able to produce ~5cm × 3cm. We have not been able to accomplish 400 μm thickness of wafer. Thickness of our wafer at present is 500 μm. On the technical development of our float process, the raw material (polysilicon) from Hemlock

has been used and is being used. Silicon from ALCOA is no longer in use for our wafering process due to technical difficulties in working with it.

2. ***T2:*** *Estimate the silicon loss – the silicon loss should be less than 10%.*

   Conclusion: No substantial weight loss was observed in making Silicon blocks of given dimension from polysilicon. Nearly 8% of Silicon loss was observed in a batch experiment, and calculation has been made by weighing a block and all the silicon wafers from the same block using precision microbalance.

3. ***T3:*** *Measure the impurities in the prototype sheets. These should not exceed 1ppm using less clean raw materials. Establish the solar conversion efficiency - should be around 12% or higher.*

   Conclusion: We have not been able to establish the solar conversion efficiency as well as impurity at ppm level. It became clear as the project progressed that it is not possible to achieve the required purity in the current experimental set-up. A further discussion and the road ahead is provided in Report 5.

4. ***T4:*** *Compare the impurity levels in different prototypes made from different test materials through the wafering process.*

   Conclusion: Currently we are using Hemlock polysilicon. We have not measured impurity level in ppm.

5. ***T5:*** *Evaluate various etching solutions to etch the surfaces of prototype wafers to a depth of 10-15 microns.*

   Conclusion: We have achieved nearly 12% reflectance level in our wafer. The optimum working solution in this direction is given in Table 1, **EXPT. 3**.

6. **T6:** *Evaluate the role of oxidizing agent (e.g. $Cr_2O_7^{2-}$) with acid etchant (HF) and other fluorine compounds. This may help in accomplishing better or controlled pyramidal structures and may require less "time" for texturization.*

   Conclusion: In this task, reflectance level has been brought down to 8%. The optimum working solution in this direction is given in Table 2, **Expt. 9**. We have been able to carry out this work at room temperature in short span of time of 5-20 min.

7. **T7:** *Establish the role of oxy-fluoride as a substrate in pre-texturization step. The idea is to study the role of fluoride ion impact on the surface of silicon wafer in the "form of nano-patterning". This is to test whether fluoride ion from oxyfluoride based glasses can enhance the process.*

   Conclusion: Though oxyfluoride glass powder helps in etching process (reflectance level is 12% in Cz Wafer), but it does not play any role in patterning of Silicon surface at nano-scale with F^- ion. There is no indication of Si-F formation.

8. ***T8:*** *Structural integrity and loss of minimal silicon materials are the two major determinants of the proposed cost-effective texturization zone. Wafer characterization, mainly the depth of Si thin-sheet before and after texturization, will be used to compute the loss of silicon.*

Conclusion: There is no change in structure integrity before and after etching the surface. As given in the Table 1, 2 and 3, our working solutions, e.g. EXPT. 3 and EXPT. 9 show a minimal loss of 2 and 4.7% respectively, much less than the target value of 8%.

9. ***T9**: Complete the experimental design to show a model for the equipment required for the wafering process that will be used for the design of the pilot plant system. Alcoa will provide input on the key design parameters that include the system dimensions, conductive, convective and radiative heat transfer, flow velocity of the inert gases and coolants, heating rate, pulling speed for the specific equipment. We will visit lab facilities at Alcoa to understand the design and operation of high temperature furnaces and on handling molten metals.*

   Conclusion: Our talks with Alcoa led to the conclusion that they are NOT the best partners for us in this project. We are exploring options with AMAT and Elkem. We also have input and project reviews from Alcoa engineers through Epiphany Tech.

10. **C1:** *Provide a Letter of Agreement from Alcoa that outlines the respective roles and requirements for the (a) Pilot process and the (b) experimental design for the wafering process.*

    Conclusion: A letter from Epiphany tech is attached. The letter expresses their interest and confidence in the project. At present Epiphany is working (work for hire) under an NDA. We have not developed a formal partnership yet.

2. Report 2: Submitted January 15, 2011

1. ***T10**: Control of the single nano-size of metal, metal oxides and/or both particles using wet-chemical etching approach.*
   Conclusions: We successfully employed **one-step wet-chemical approach at low dilution** in order to control the dispersion of gold nano-particle followed by coating of these nanoparticulates onto Si<100> and Si<111> wafers. Removal of gold nanoparticles led to the formation of a fine, random hillock sub-structure on the surface of silicon in nano-scale dimension. We have achieved nearly 4% reflectance level in our wafer. The optimum working solution in this direction is given in Table 1, EXPT. **37.**
2. **T11:** *Characterize the morphology (SEM and TEM), single nano-size of metal/metal oxide nanoparticles and spectral reflectivity of wafer.*
   Conclusions: In this task, we have successfully characterized the dispersion and coating of nano-particles on the surface of Silicon wafer using Scanning Electron Microscope (SEM) and X-ray Diffraction (XRD) measurements.
3. **C2:** *Establish cost of chemicals and develop computer tools for sensitivity analysis.We will estimate total market size, key competitors and industry value chain and cost analysis of product of scale-up. This analysis will help us understand the total market opportunity and the strategic approach for commercialization given the competitive landscape and our differentiating factors*
   Conclusions: We conducted a full analysis of the total market size, competitive

landscape and key players in each part of the value chain. Based on the study we conducted, we evaluated three potential commercialization strategies – build, partner, and license. Our full business plan that is attached to this report includes our study results. Total available market estimation and value chain description can be found in section 2 of business plan. Section 6 describes the competitive landscape and our cost advantage over the next 5-8 years. Section 7 describes the different commercialization options and the tradeoffs between them.

4. **C3:** *Wafer cost analysis*
   Conclusions: We successfully estimated the cost per wafer and cost per MW capacity. Our estimation concluded that we have a significant cost advantage over our competitors. The costs estimates can be found in the appendix of the business plan.

3. **Report 3: Submitted March 31, 2011**
   1. **T12:** *Wet-chemical self-assembly route will be employed and self-assembling block copolymer templates will be utilized to pattern an aqueous metal reduction reaction on silicon surfaces that allows nanoscale patterning.*
      Conclusions: We have successfully employed self-assembled polymer mask having a thickness level of 400 nm. However, the polymers used in this task did not yield any significant results, and did not form sufficient pattern at nano-scale. The minimum reflectance level of nearly 16-22% was measured in the sample etched by wet-chemical method – dilute HF-H_2O_2 solution. The best level of minimum reflectance obtained so far is 4% and is reported in the Milestone 3.
   2. **T13:** *Accomplish the impurity level of 1ppm or less in the prototype sheets. Establish the solar conversion efficiency - should be around 12-16% or higher."*
      Conclusions: Attempts made to accomplish the level of impurity in as-produced silicon sheet at 1 ppm or less remained unsuccessful. The level of impurity of 1.89 ppm obtained so far is the best result and is reported in the Milestone 2. The sheet produced in this method has been sent for purity (carbon) analysis. We have not been able to fabricate a cell with our as-produced sheet to measure solar conversion efficiency. Nevertheless, we have made progress in pulling experiment.
   3. **C4:** *We will identify potential partners among wafer manufacturers, equipment and process experts in the industry and we will initiate discussions with potential partners.* **Conclusions:** Identified Applied Materials as one of the potential partners. Other companies interested in the rooftop solar market (for example SunPower) would be a good partner, since our aim is to reduce the costs of high yield, mono crystalline panels.
   4. **C5:** *We will identify potential partners among wafer manufacturers, equipment and process experts in the industry and we will initiate discussions with potential partners.*
      Conclusions: Analysis of the feedback received from partner is being evaluated. Further discussion is provided in Report 5.

4. **Report 4: Submitted May 18, 2011**
   1. **T14:** *The wafering process has to lead to the texturization process producing*

solar grade silicon wafers. The pilot plant design will be focused to integrate both processes.

Conclusions: Although we have not been able to fabricate a cell with our as-produced sheet to measure solar conversion efficiency. We have successfully employed nano-texturization process to those wafers produced in our laboratory, Si<111> and other highly textured Silicon sheets along with Czochralski wafers, Si<111> using batch process. However, we could not manufacture any significant wafers using continuous method, and hence, the integration of pilot plant design remained halted.

2. **T15:** *Once the representation model is validated with the available experimental data, other important design parameters like equipment size will be tweaked to determine the sensitivity of those parameters.*

   Conclusions: Attempts were made to validate an all-inclusive model with the experimental data including equipment size. Due to on-going experiments and deviations in their results, availability of partial supportive data could not yield significant results in this task.

3. **T16:** *Operating parameters like temperature, extent of reaction, reaction time, process time etc. and their expected range of variation, acceptable minimum and maximum values will also be determined based on the model developed.*

   Conclusions: Since we are still continuing our experiment, therefore optimization of operating parameters like temperature, extent of reaction, reaction time, process time, creation of efficient cooling zone with respect to thickness etc. and their expected range of variation, acceptable minimum and maximum values and their determination based on the model still remain under observation and fruition.

4. **C6:** We will conduct a detailed cost analysis in order to understand required funds for commercialization of technology. We already have an initial estimate but based on technology development and the detailed theoretical pilot plant design, we will add more details to the budget and cost analysis. At this stage, we estimate the cost of fabrication will be cut by a factor of 4.

   Conclusions: A comprehensive business plan is tabulated.

5. **Report 5: Submitted August 6, 2012**

   1. **T17:** *Establish the solar conversion efficiency - it should be around 12% or higher to meet the goals of the project. As-produced wafers will be made of single crystalline silicon for higher solar conversion efficiency.*

      Conclusions: It was found that the as-produced wafers had the desired single crystal form. Thus, one important aspect of the process concept has been verified. The horizontal furnace system with the alumina tube and the graphite crucibles introduce a significant aluminum, carbon and oxygen impurities. We changed the experimental procedures and tried different argon flow rates and a range of different crucible materials. Even the best wafers where so heavily doped that it was not possible to obtain electrical property measurements needed to apply standard solar testing equipment. We have thereby established that the solar efficiency in our current set-up cannot reach the 12% mark. Further testing and experimentation is not merited until the purity issues have been addressed. We are

installing a new pilot plant system at ILS facilities in Pittsburgh in the fall of 2012 that will make it possible to control the impurity levels.

2. **T18:** The solidification and CFD models will be validated with the available experimental data.
   Conclusions: We developed CFD, solidification and heat transfer models that were validated against the water model experiments as well as high temperature experiments in a vertical furnace at CMU. We have used the model for sensitivity studies that show how wafer thickness depend on process and design parameters. A solidification model has been developed that show how impurities segregate. This model has been compared with experimental results for aluminum. We also developed stability models that show that the process should be stable provide the starter silicon material is sufficiently pure. The models furthermore show that it is feasible to produce a sheet at 10-20 cm per minute and that impurities are moved from the solid to the melt due to directional crystallization.
3. **C6:** Formulating a cost and business analysis for the proposed process. Propose a commercialization path in the business plan. We will conduct a detailed cost analysis in order to understand required funds for commercialization of technology. We already have an initial estimate but based on technology development and the detailed theoretical pilot plant design, we will add more details to the budget and cost analysis. At this stage, we estimate the cost of fabrication will be cut by a factor of 4.
   Conclusions: We have updated and refined the business plan in accordance with the requirements. The cost picture looks very promising even in view of the fact that prices have fallen sharply in the PV market during the past 2 years, mainly due to large-scale production and very aggressive pricing by Chinese manufacturers of solar cells and panels.

Appendix L – 10-039 (Liquid-X)

Liquid X Printed Metals
Final Technical Report submitted to the Pennsylvania NanoMaterials Commercialization Center, May, 9th 2012.

Throughout the duration of this project Liquid X Printed Metals (LXPM) has supplied regular reports (both oral and written) to the Pennsylvania NanoMaterials Commercialization Center (PANCC). To now fulfill the final report requirements we are submitting abbreviated highlights from the technical and commercial milestones outlined in the finalized statement of work.

Commercialization Highlights

Milestone 1; C1
The first commercial milestone was to engage Idea Foundry in relation to the commercialization strategy. Our meeting with the Idea Foundry provided an understanding of the resources they provide. However it was decided to use our in house resources to pursue a commercialization strategy. From this milestone, we developed specific Company Milestones and deadlines that ensured the advancement of the technology towards the needs of the Printed Electronics market.

Milestone 2: C2 – C5
During Milestone 2, Liquid X produced a comprehensive cost model for our silver and gold inks from benchtop to pilot and production scale. This milestone aided in driving our research into both internal and external scale-up efforts. This exercise also helped us to identify the most cost effective method to produce our silver and gold inks. Also included in this Milestone, we conducted a comprehensive market analysis in which we identified our top competitors, discovered over 50 different potential end use applications for our technology, identified potential customers within these applications, and determined our target markets for market entry points. We conducted a comprehensive competitive analysis to identify our key differentiating factors of Liquid X's ink.

Milestone 3, C6 – C7
In Milestone 3, we worked with a subgroup of our target customers to identify their target parameters of functional metallic inks and provide them with samples. From this exercise, we discovered that our value proposition will change depending on the end use application. For example, in RFID, they are looking for a low-cost, high performing (high conductivity) functional metallic ink. On the other hand, in Printed Circuit Board manufacturing, they currently use a subtractive method of removing copper foiled lined substrates to leave the etched out pattern producing a lot of waste. However, they need a highly conductive ink that can produce thin traces with narrow spacing in between. We also learned that the deposition vendor also plays an important role in the relationship with our customers. We have even pulled in the deposition vendors into some of our customer relationships to ensure our customers full support as they implement our additive solution.

Milestone 4, C8

During Milestone 4, we provided sample inks to Plextronics for use in a working device. We learned this was an iterative process. We also identified a need for a feasibility testing prior to the actual device testing. During the feasibility testing, we acquire our customer's target parameters and along with sample substrates to ensure the Liquid X's ink formulation will perform to expectation. By imploring this method, we are able to reduce our costs and shorten the development time with our customers.

Milestone 5; C9

In our final Milestone we executed development agreements with our customers. We have numerous ongoing projects with customers from various end use applications in which we are working to incorporate our ink into their products. We are also exploring possible licensing agreements with a few of our customers.

Technology Highlights

Milestone 2; T1 – T4

During this milestone we purchased, assembled, and successfully implemented use of a programmable Specialty Coating System GSP-8 to optimize the deposition of various silver inksets using numerous neat and mixed solvent delivery systems. We primarily focused on conductivity (σ) as our figure of merit (FOM) and regularly achieved σ ranges > 1×10^6 S/m. Parallel to these efforts we synthesized a new sulfur-containing family of silver inksets with low metallization temperatures on the order of 110°C (± 10°C) and scaled-up and validated our metathesis reaction between silver acetate and various short-chain carboxylic acids whose carbon content does not exceed 5 atoms. Batch-to-batch purity was assessed by elemental analysis.

Milestone 3; T5 – T7

On the synthetic front we took our new silver molecules (developed and synthesized in Milestone 2) and fabricated a variety of solutions at varying concentrations and solvent delivery systems. The evaluated delivery solvents spanned a range of polarities, viscosities, and boiling points. It was uncovered through collaboration with our partner – Plextronics - that the most desirable, optimized ink concentrations were 100 mg/mL (± 2 mg/mL), regardless of solvent.

Evolution of Metalonix Silver Deposition Conditions to Optimize Inksets for OPV Applications

Drop Casting	→	Spin Coating	→	Inkjet printing
Substrates: Inorganic - glass and silicon Organic – Kapton Polyurethane PET		Glass, Silicon, HTL (hole transport Layer) coated glass provided by Plextronics		Glass, Silicon, HTL coated glass, Full OPV architecture on glass, Kapton

After many experimental iterations, H-bonging solvents were deemed undesirable and toluene was selected as the ink solvent. Initial runs with the toluene delivery solvent met with limited success. Although the films were dense with low resistivities, negligible device performance was observed. The next iterative step for the ink progression was to test 3 inks, 1:1 toluene:diethyl ether, toluene, and 1:1 toluene: diethylene glycol dimethyl ether (at 100 mg/mL) in the jetting process. After the toluene or 1:1 tolene: diethylene glycol dimethyl ether based inks were identified a number of variable were chosen for optimization; these were a) annealing temperature, b) annealing time, and c) and solvent choice. The confusing top left graph (below) address c), and shows that after annealing for 30 min at up to 200°C the higher boiling solvent mixture provides essentially infinite resistance. At top right (address a)) the effect of temperature is measured and the lowest observed resistance values occur after rapid annealing at 200°C. Ultimately the influence of annealing time (addresses b) was investigated in the remaining lower left graph. It exhibits that after 300 minutes the resistance reaches a minimum. This impractical value was compromised to be 3 h at 200°C to yield 9 Ω/□ at 1550 nm (± 227 nm) thicknesses.

Figure 3.

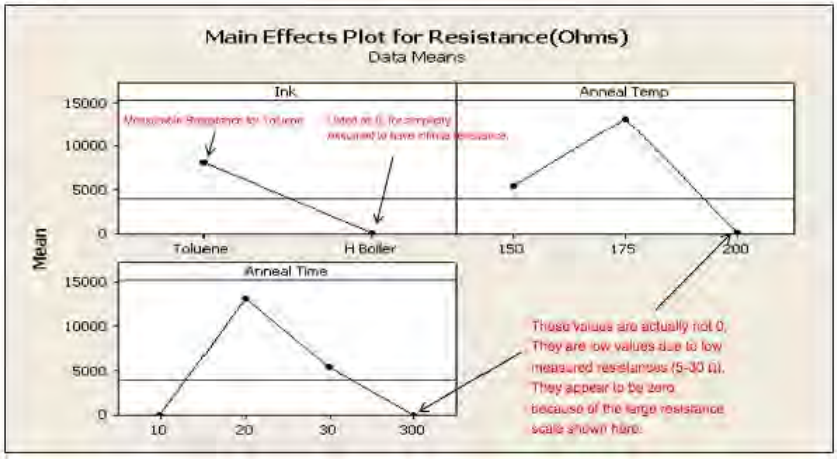

Ultimately, the device performance of inverted solar cell architectures was tested and measurable numbers realized. For a the ZnO/active layer/hole injection layer/Ag) the results are outlined in the table below. Admittedly the efficiencies modest, we did achieve active working devices all the while optimizing our ink processing conditions in the inverted solar cell architectures.

Table 1.

Ink Source	Anneal Time (h)	Jsc	Voc	FF	Eff (%)
Metalonix	3	0.15	0.56	0.2	0.017
Metalonix	3	0.14	0.53	0.21	0.015

Addressing adhesion was also critical - we have tested three types of devices. First, vapor deposited silver in inverted OPV device, Metalonix silver ink in inverted OPV devices, and Metalonix silver ink on Kapton plastic substrates. In both the OPV devices and Kapton tests (no surface treatment), Metalonix metalized silver inks adhered completely after performing the Scotch tape test. This is not true for the silver cathodes deposited by evaporation. As on can see in the below images, the silver cathode deposited by evaporation completely lifts off into the Scotch tape, whereas the Metalonix silver remains adhered after Scotch-tape lift off.

Figure 4. Plextronics Vapor Deposited Electrode Control Scotch Tape Test

Figure 5. Metalonix Ag Electrode Scotch Tape Test

Figure 6. Metalonix Ag Ink - Scotch Tape atop Drop Cast Sample on Kapton (left), Scotch Tape Removed from Kapton (right).

Milestone 4, T8 – T9

Given the relatively incompatible work function (ϕ = 4.7 eV) of silver metal with organic-based field effect transistor (OFET) materials, most notably poly(3-hexylthiophene) – P3HT, we decided to explore base gold as an electrode pad material ((ϕ = 5.1 eV). Our initial steps were to fabricate a gold-containing ink for inkjet printing. This molecule contains ~ 55% gold by weight, is completely soluble in organic aromatic hydrocarbons that are compatible with the desired printing process, and has the desired reaction to yield high-quality gold metal. After optimization we narrowed down suitable ink concentrations that contained 250 mg/mL of gold complex for jetting.

Initial experiments were produced via drop casting and spin-coating to assure that the conductivities of the desired films were suitable (1.6×10^7 S/m) for OFET fabrication. We then designed a pattern to jet onto p-doped Si coupons that had been etched and cleaned. Our pattern was 250 x 175 µm electrode pad pairs separated by 40 µm (channel length) into which we would subsequently drop-cast the active organic polymer - P3HT.

Figure 1 above shows the pattern and its dimensions. After jetting on both glass and Si, we discovered there to be multiple issues, related to both experiments and instruments. Concerning the latter, the 10 picoliter droplet inkjet head apertures were too large to accommodate our desired specifications. Upon printing, we had neither vertical nor horizontal planarized resolution leading to solid gold lines. As a remedy we purchased higher resolution cartridges with 1 picoliter (previously 10 picoliter) droplet delivery apertures. This yielded successful lateral resolution in that the Au electrode pads were now separated however the 40 µm spacing was not achieved due

Figure 1.

Figure 2.

to ink wetting the surface as seen in Figure 2.

Essentially, even in a low-boiling solvent delivery system and with a maximum platen temperature of 60°C the surface wetting issues cause the ink to bleed into the channel before metallization. To assess the extent of this challenge and successfully print these channel features, we designed an experiment consisting of a series of patterns in which the channel and electrode sizes were varied. This provided valuable design information concerning the wetting process. As can be seen in Figure 3, the wetting phenomenon was successfully exploited to fabricate the desired 40 μm electrode separation.

Silver lines were inkjet printed onto silicon and glass substrates using from 1-3 overprints and various concentrations of 100, 250, and 500 mg/mL. The simplest numbers to understand were the conductivities which reproducibly ranged from 2.5×10^5 S/m to 1.1×10^6 S/m throughout all samples. Furthermore, each line passed the scotch tape test and it was determined that they adhered well to glass and silicon. As expected, the thicknesses varied depending upon concentration and number of overprints, with the thinnest features being 230 nm and the thickest features being 1.2 μm. All linewidths ranged from 190 μm to 220 μm. Figure 4 shows various printed silver lines on a Si coupon that were used for these tests. Figure 5 shows an optical micrograph of a single line that exhibits a microstructure comprised crystalline silver grains.

Figure 3.

Figure 4.

Figure 5.

Milestone 5; T10 - 11

To expand available printing methods for our inks, we explored three more relevant deposition methods to test the applicability of our low viscosity inks. These were slot die coating, microgravure, and screen printing. This work was jointly undertaken with our partner and subcontractor, Plextronics.

The first printing method we explored was slot die coating using a 100 mg/mL concentration of silver ink to determine coating viability. The essential parameters to be evaluated were coating thickness (single pass vs. multiple passes), annealing temperature, and substrate type (glass and flexible). Before deposition could take place metrics had to be determined. Given the low viscosity of our toluene delivery vehicle, we scanned a dispense rate range of 15 – 150 μL/sec at a coating velocity of between 5 – 15 mm/sec. For this bracket set of metrics, we found the best deposition conditions (after 23 attempts) were 150 μL/sec at a velocity of 12 mm/sec using 3 overpasses of this silver ink to achieve > 200 nm thicknesses. Once the optimal metrics were determined, 13 glass plates and 2 flexible substrates polyethylene terephthalate (PET) were coated and the 4-point probe measurements were taken across the samples after annealing at 120°C (glass), 200°C (glass), 120°C (flexible), and 140°C (flexible). The below images show the gross silver coatings on these substrates which provided uniform silver films.

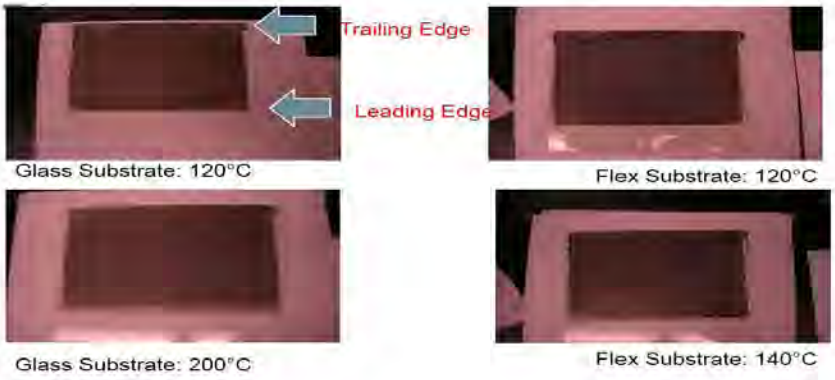

In addition to the above images, we took optical micrographs at 25x magnification and representative images are shown below. On all of the plates we observed formation of silver grains and crystallites. The largest grain size was found on the flexible substrates (after three

Glass Substrate: 120°C

Coat 3 passes of Ag Ink

Flex Substrate: 120°C

Glass substrate 200°C

Flex Substrate 140°C

coating passes) heated at 120°C while denser morphologies and smaller features were observed on glass at 120°C and on both glass and the flexible substrates at the higher temperatures. The origin of these morphological differences most likely involves ink-substrate surface interactions, and the four point probe measurements indicate higher conductivities on the glass substrate when compared to the organic substrates. These 4-point probe measurements and film properties are summarized in the below chart.

Substrate	# of coats	Thickness (nm)	Anneal Temp.	4 pt probe (ohm/square)
Glass	1	128	200	1
Glass	1	112	120	24
Glass	3	427	200	1
Glass	3	501	120	1
PET	3	Not measured	120	117
PET	3	Not measured	140	74

Microgravure was the next evaluated coating method. The essential parameters were ink concentration, dry time, dry method (forced air and hotplate), and microgravure cylinder speed (higher the speed, the thicker the coating deposited at a constant web speed). Once the optimal metrics were determined, 4 substrates were coated for each concentration of ink. The results are summarized in the below tables for 2 different ink concentrations of 100 mg/mL and 200 mg/mL.

- 100 mg/ml Solution

Conditions				
MG speed (m/min)	6	11.7	57.7	57.7
Web Speed (m/min)	0.5	0.5	0.5	0.5
Dry Method	Forced Air	Forced Air	Forced Air	Hot Plate
Dry Time (min)	2	2	2	5
Dry Temp (°C)	145	145	145	150
Ink Concentration	100 mg/ml	100 mg/ml	100 mg/ml	100 mg/ml
Coatable (Y/N)	No	Yes	Yes	Yes

- 200 mg/ml Solution

Conditions					
MG speed (m/min)	57.7	57.7	57.7	57.7	57.7
Web Speed (m/min)	0.5	0.5	0.5	0.5	0.5
Dry Method	Forced Air	Forced Air	Forced Air	Hot Plate	Hot Plate
Dry Time (min)	2	4	15	10	10
Dry Temp (°C)	145	145	145	120	90
Ink Concentration	200 mg/ml	200 mg/ml	200 mg/ml	200 mg/ml	200 mg/ml
Coatable (Y/N)	Yes	Yes	Yes	Yes	Yes

Ultimately, screen printing was undertaken using both a 100 and a 200 mg/mL ink concentrations of our silver to pattern a standard OPV anode. Not surprisingly, the low viscosity of the ink resulted in bleeding of the ink and a resulted in a halo pattern with poorly defined edges. Thus, we hypothesize the neat, low viscosity inks will require thickeners or additives before future screen printing will be attempted.

To date, we have developed four new gold inksets, all of which are toluene soluble. The gold inksets are typically based on small thioether neutral ligands which bind the Au^{1+} ion through their sulfur atoms and anionic carboxylates which are bound through a terminal oxygen. The deposition methods we have used for these inksets include spin coating and drop casting with

ultimate conductivities of 1.5 x 10^7 S/m. The shelf-life of the inksets has also improved; whereas previously gold complexes were indefinitely stored at -35°C we now have examples with shelf-lives exceeding months at 0°C.

In addition to the gold work we have continued the evolution of our silver inksets, and currently have greater than 12 examples of silver ink based on well-characterized coordination compounds. Given the synthetic tailorability of the inks, we have specifically developed and tested a wide range of compounds with the metric of solubility at the forefront or our design criteria. We now have unique silver compounds with solubilities that range from hydrocarbon soluble to polar protic solvent soluble. Examples of the latter include aqueous inks as well as alcohol and polyethylene glycol (PEG) soluble examples. The PEGs offer many possibilities for inks with tunable viscosities as well as opening up the realm of mixed solvent ink systems having orthogonal chemistries with organic substrates or organic/polymer coated materials.

Given the tailorability of the gold and silver complexes, we developed gold and silver inks that are soluble and miscible in each other. After annealing, the resulting metal films are a solid solution whose metal content is identical to the dissolved solution concentrations. This alloying process opens up a completely new area of discovering both new metallic phases as well as replicating known materials using low-temperature solution processing, all of which depends on the precursor chemistry. Without the synthetic ability to tailor and develop new metal complex inks, this process would have been impossible.

Below are images of the alloy lines containing different amounts of gold and silver. These were all deposited via inkjet printing. Even upon optical inspection, the silver to gold color change is readily apparent as the gold in silver content increases.

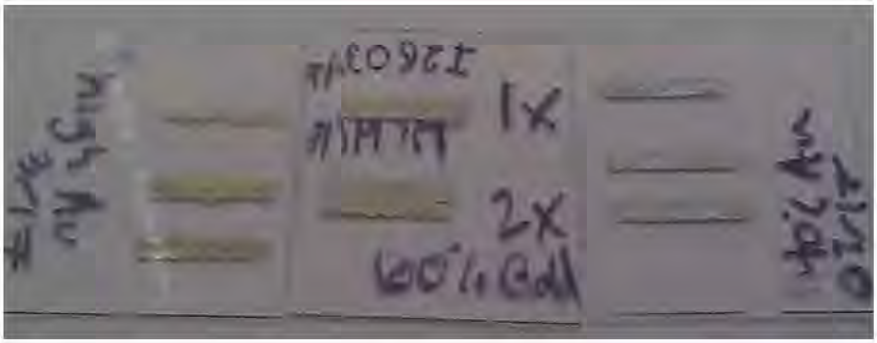

Increasing Au

Appendix M – 10-040 (SolarPA)

Final Project Report
SolarPA

A report to PANCC
June, 2011

1

Table of Contents

2

About SolarPA

- SolarPA is a Texas C corporation that was founded in 2006 and incorporated in 2010. The goal of the company is to create an industry changing technology which will both bring enable solar cell manufacturers to produce cells at higher efficiencies and lower costs, while producing a significant return for shareholders.
- SolarPA owns patent – pending coating technology called NanoCoat, exploitation of which will have important positive implications for photovoltaic (PV) systems economics and the utility of solar power. Application of NanoCoat on existing Si technologies appears to increase energy output by up to 8%. Upon broad dissemination, the value created by NanoCoat technology is measurable in billions of dollars based upon billions of watts of solar cells manufactured each year.

3

SolarPA's NanoCoat OverCoat

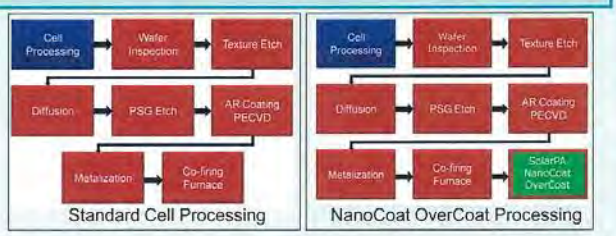

- NanoCoat OverCoat, a proprietary nanomaterial/polymer matrix deposited in liquid form over the top of a completed solar cell increases the efficiency of the solar cell by up to 8%

4

SolarPA's NanoCoat OverCoat

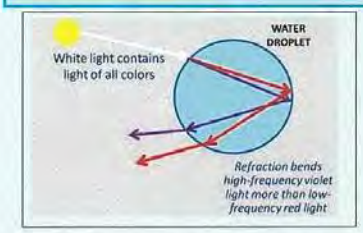

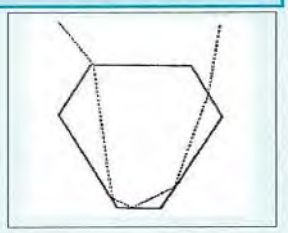

SolarPA technology utilizes proprietary nanocrystals to refract the light

5

SolarPA's NanoCoat OverCoat

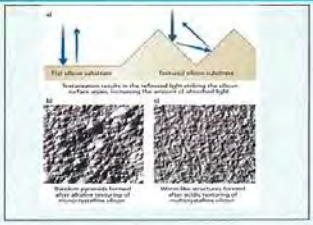

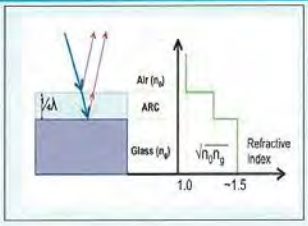

- NanoCoat eliminates the need for an etch that textures the silicon substrate to scatter light and increase efficiency.
- NanoCoat reduces sunlight reflection, which causes more photons to reach the solar cell, resulting in higher electricity output. The anti-reflective coating (ARC) increases solar cell performance by reducing the amount of reflected photons.

6

Milestone 2 Technology Deliverables

- SolarPA will evaluate and report on the performance of dip coating our nanomaterials without the use of a polymer on 25 solar cells and measure the relevant physical and electrical characteristics including wattage, efficiency, amperage and, adhesion dispersion and nanoparticle density and distribution. The results will be compared to control samples from SPI.
- Finalize a formulation for the most effective application and performance of the Nanocoat product. Nanocoat efficiency improvement anticipated >3%. Target specification is a uniform monolayer of the nanocrystals based on scanning electron micrograph (SEM) evaluation.

- SolarPA has demonstrated that it is capable of formulating and coating its proprietary nanomaterial based dispersion to achieve 3% improvement in efficiency by top-coating SPI solar cells utilizing its NanoCoat B formulation coated at 40 microns (wet) thickness. The adhesion of the nanomaterial is excellent; and, can form a monolayer at the optimized concentration and coating thickness. Further improvement is anticipated.

7

Milestone 2 - T1

- SolarPA will evaluate a dip coating method, utilizing optical measuring equipment, on the cells and compare to control samples of spin coating method which we suspect will give a more uniform coating over a 6-inch cell, while at the same time reduce processing complexity. Spin coating was used in our original technology development. Optical microscopic characterization methods will be used to measure the uniformity and density of the nanomaterial coatings.

- SolarPA has determined that both spin-coating and dip coating methodology produce an inferior coating on patterned solar cells. Superior control and uniformity are achieved by "blade-coating". This method has proven to be much more easily controlled when coating patterned (not flat) solar cells. Uniformity of the coating was ascertained by optical microscopy. Further optimization of the coating (wet coating thickness and nanomaterial concentrations) is expected; and, will be reported in Milestone 3.

8

Blade Coating Method

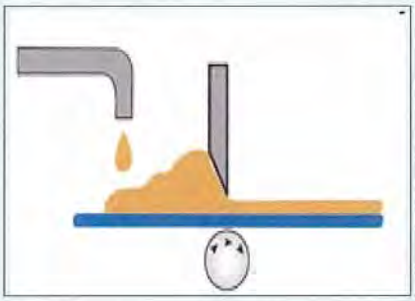

9

Milestone 2 - T2

- SolarPA will measure the efficiencies of 25 standard solar wafers provided by SPI and will top coat (i.e. a coating over the entire completed cells including the electrodes) the 25 cells with SolarPA's Nanocoat. The Nanocoat will be applied to the cells using SolarPA's proprietary nanomaterials suspended in a solvent.

- Upon receipt of solar cells from SPI, it was determined that 20 wafers supplied by SPI would be separated in to two groups. Each group would be measured (baseline) by SPI and re-measured by SolarPA at Lehigh University to insure correlation. Subsequently, each group would be sub-divided into two groups for coating testing.
- Using 1 cm x1 cm solar cells, four (4) formulations were tested in duplicate to insure reliable results. Upon selection of the two (2) best-in-class formulations, 5 full size SPI solar cells of each of the two best performing formulations were prepared at different coating thicknesses. The results of this testing are included in the technical data portion of this report.

10

Milestone 2 - T3

- SolarPA will evaluate the results without the use of a polymer vehicle that suspends the nanomaterials for uniform coating over the cell (using only the solvent as a vehicle for the nanomaterials). A polymer was used in our original technology development but has limited temperature applicability of 150C.

- SPI cells supplied are between 13.62 and 15.76% efficient. An improvement of nearly 4% has been demonstrated at this time

11

Milestone 2 – T4

- SolarPA will compare suspensions of different Nanocoat compositions, which will be comprised of different concentrations of these nanomaterials using different solvents to coat the 25 cells. The cells coated with Nanocoat material will then be measured again by SolarPA to determine the improvement in efficiency over the existing standard cells. SolarPA will repeat the coating process used to prepare the best performing solar cell (as determined by SPI) using 10 additional solar cells; and, conduct a check-test. All measurements will be made at room temperature.

- SPI cells supplied are between 13.62 and 15.76% efficient. An improvement of nearly 4% has been demonstrated at this time
- This improvement is based on a top coat of NanoCoat, meaning that the solar cells were already completed with electrodes. Efficiency enhancements of texture etch and ARC were already incorporated into the processing of the cells at SPI.
- We have named this product NanoCoat InnerCoat (no polymer matrix component).

12

NanoCoat A Efficiency (NanoCoat InnerCoat)

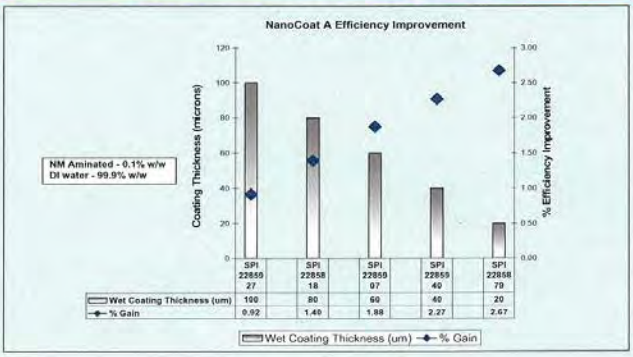

13

NanoCoat B Efficiency (NanoCoat InnerCoat)

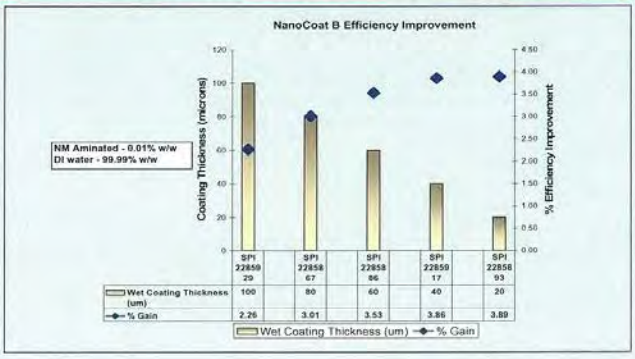

14

Efficiency Improvements Built into SPI's Completed Cells

- This improvement is based on a top coat of NanoCoat, meaning that the solar cells were already completed with electrodes. Efficiency enhancements of texture etch and ARC were already incorporated into the processing of the cells at SPI.
  - Not including any effect from hydrogen passivation, if you assume SPI's current cell is 16% efficiency, taking into account the change in reflectivity with AR coating you are looking at a drop to 12.4-13.6% efficiency without the AR coating. In other words the AR coating provides at least an 18-24% relative efficiency increase.
  - Regarding the texturing, the general rule of thumb is that it provides ~1%abs efficiency increase, or ~6.7% relative increase in efficiency.

15

Therefore…

- SolarPA's improvement of 4% is on top of up to a 30% improvement already built into SPI's completed cells because they are already fabricated with the texture etch and ARC.
- SolarPA intends to ultimately replace the texture etch and ARC with its NanoCoat as part of Milestone 4 (see next Slide).
- Efficiency enhancements of NanoCoat without the texture etch and ARC are expected to not only increase the efficiency above the up to 30% standard improvement, but the replacement of these steps by NanoCoat are expected to reduce the overall production cost of the solar cells.

16

SolarPA's NanoCoat InnerCoat OverCoat

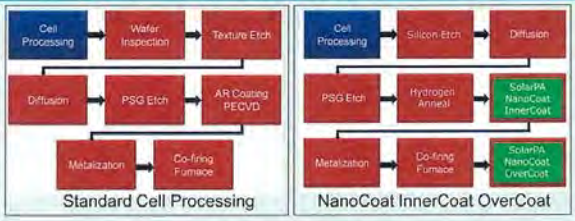

- Possibility of replacing Texture Etch and AR Coating PECVD with Hydrogen Anneal and SolarPA NanoCoat InnerCoat
  - AR Coating PECVD combines Hydrogen Anneal and PECVD
  - SolarPA will replace the PECVD portion only with NanoCoat InnerCoat

17

Milestone 2 - C1

- **Evaluate the cost savings in replacing texture etch with modified etch to remove wire saw damage. Evaluate the cost using NanoCoat and saw damage etch compared to texture etch.**

- SPI is expected to provide the cost of replacing texture etch within the next few weeks as they are in the midst of a process change at their factory that effects this cost. Nonetheless, SPI is anticipating the integration of NanoCoat B as a top-coat after metallization at this time.
- SPI anticipates evaluating Nano-Coat B in several other steps including: prior to ARC coating, and in the backside aluminum and top side silver metallization steps. This work will be performed in Milestone 4. In any event, the cost of using NanoCoat B per Solar Cell (as a top-coat) is quite compelling at less than $0.05 per cell (100 wafers per liter of NanoCoat B) or $0.013 per watt.

18

Milestone 3 - Commercial Deliverables

- Determine cost savings with substituting texture etch with non-texture wire saw damage etch.

- Cost savings will be significant; and, easily justify the integration of NanoCoat B into the process after wire saw etch rather than using an additional texture etch step. SPI solar cells from the wire saw (prior to texture etch) will be provided for testing in Milestone 3

19

Milestone 3 Technology Deliverables

- SolarPA will measure the electrical characteristics of 25 cells as a function of angle of incidence before and after coating with NanoCoat.
- Efficiency improvement anticipated is >3% at an angle of incident light perpendicular to the cell, but > 4% at grazing angles of incidence.

- SolarPA has completed the measurement of the electrical characteristics of solar cells as a function of angle of incidence before and after coating with Nanocoat as presented in the data portion of the SolarPA Milestone 3 report. Efficiency improvement using NanoCoat OverCoat at varying angles of incident light has been experimentally confirmed at an angle of incident light perpendicular to the cell,; and, at grazing angles of incidence less than 90°.

20

Milestone 3 – T5

- SPI will substitute the texturing chemical etch with the less corrosive etch on one lot of 25 wafers and then complete the manufacture of these cells using its standard processing.

- Cells were processed by replacing the texture etch with a nitric acid/hydrofluoric acid etch (10:1 ratio for 1 minute) to remove approximately 5 microns of the wafer surface damaged during wire sawing in a slurry
- No statistical improvement was observed in cells normally processed versus those cells where the texture etch was replaced by NanoCoat InnerCoat, as show in the graph on the next slide. All results fell within a standard deviation of 0.4%
- We plan on repeating the experiment by using Akrion's standard silicon etch process for better consistency and uniformity of etch.

21

Efficiency of Standard Solar Cells Vs. NanoCoat InnerCoat Cells

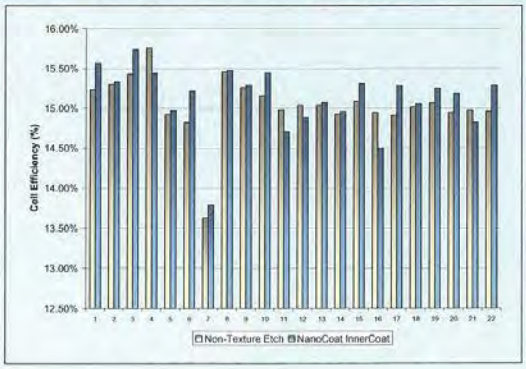

22

SolarPA's NanoCoat OverCoat

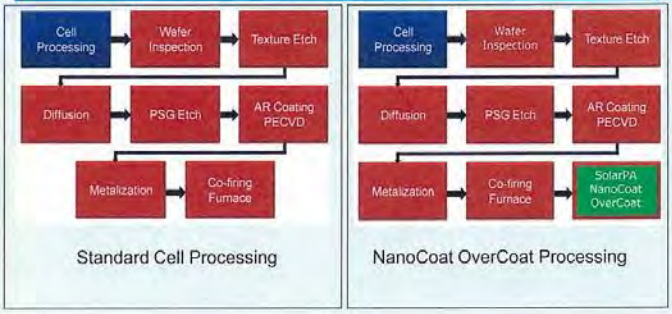

23

Milestone 3 – T6

- **SolarPA will measure the efficiency of the 25 solar cells and compare to control samples using the texturing chemical etch.**
- **SolarPA will measure efficiency as a function of the angle of incidence of the UV source to evaluate the effect of diffraction of incident light from the nanocrystals.**

- **SolarPA has identified NanoCoat OverCoat as the superior formulation for improving the efficiency of a solar cell with a top-coat. This formulation incorporates an Arkema UV transparent polymer to "suspend" the nanocrystals to maximize their positive impact on solar cell ef-ficiency.**
- **Completed solar cells coated with NanoCoat OverCoat, which contains nano-crystals in an Arkema Kynar matrix, show an flattened distribution of efficiency with angle of incidence of sunlight.**
- **At 90 degrees (normal incidence), cells with NanoCoat OverCoat exhibit an average efficiency increase of 10.1%,**
- **At 60 degrees, cells with NanoCoat OverCoat exhibit an average efficiency increase of 12.7%,**
- **At 30 degrees, cells with NanoCoat OverCoat exhibit an average efficiency increase of 21.9%,**

24

Efficiency of Completed Solar Cells Vs. Angle of Sunlight Incidence

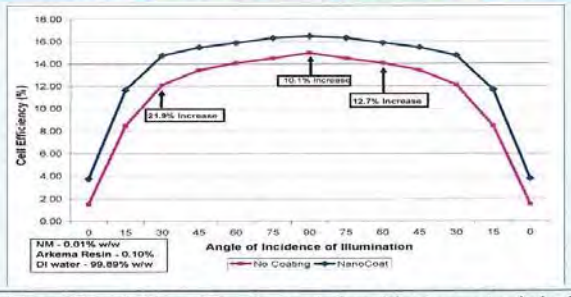

- NanoCoat **OverCoat** contains Nanomaterials in Arkema Kynar Matrix

25

Comparison With Actual Installed Panel With Tracking

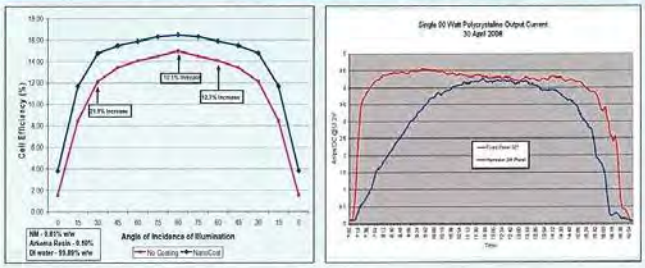

- Left – SolarPA chart from previous slide
- Right – Actual data for installed tracking versus fixed panel on a residence
  - SolarPA NanoCoat can eliminate the need for a tracking system while at the same time increase the efficiency of a standard solar cell by 10%

26

SolarPA's NanoCoat OverCoat Can Eliminate Expensive Tracking

- SolarPA technology can eliminate the need for expensive tracking systems, particularly on residential and commercial buildings

27

Milestone 3 – T7

- SolarPA will apply a NanoCoat OverCoat to the modified wafers provided by SPI using the "best performing" NanoCoat formulation and coating method developed in Milestone 2.

- Data show that as the thickness of the coating (containing nanocrystals in Arkema's Kynar matrix) decreases, efficiency of a completed solar cell increases to nearly an 8% relative improvement at a thickness of 40 microns (the height of the silver bussbars)

28

NanoCoat OverCoat Efficiency Increase on Completed Solar Cell

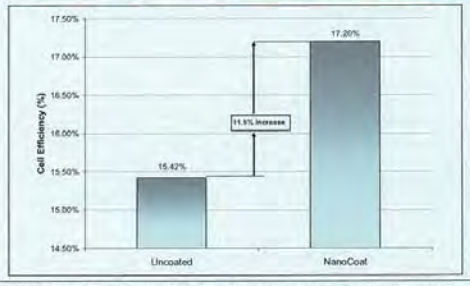

- NanoCoat C contains Nanocrystals in Arkema Kynar Matrix – our NanoCoat OverCoat product

29

Milestone 3 – T8

- SolarPA will measure the efficiency as a function of angle of incidence of the UV light source and document the improvement in efficiency and compare to control samples.
- NOTE: All 25 samples will be treated in exactly the same way; but, with varying pull-coating orientation with respect to light angle.

- Solar cells were measured with respect to the position of the bussbars as shown in the next slide
- There was no measurable difference in efficiency of the solar cells as a function of the pulling direction of the NanoCoat across the 6-inch wafer (vertical or horizontal to the bussbar)

30

Setup of Solar Cells for Measuring Efficiency Vs Angle

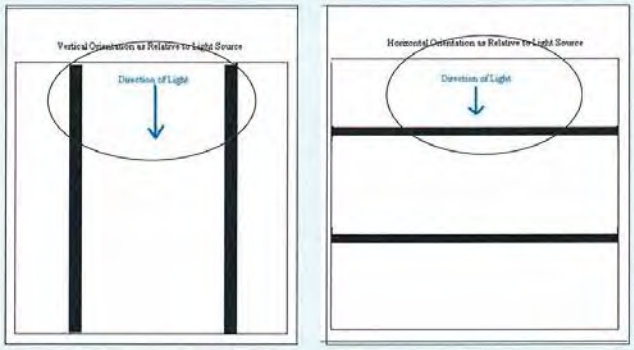

31

Efficiency Vs Angle Vs Cell Position

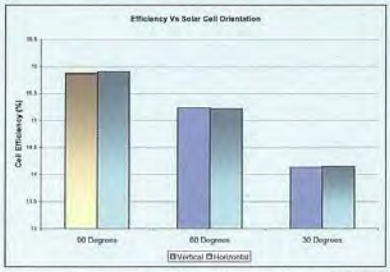

- As angle measurement departs from normal incidence (90 degrees) efficiency decreases
- Efficiency is the same for each cell when cells are measured and rotated in the horizontal position (see previous slide)

32

Milestone 3 – T9

- SolarPA will use scanning electron micrograph (SEM) measurements of the surface of the cells to evaluate orientation of the nanocrystals on the surface and its correlation with solar cell efficiency improvements at grazing incidence of the UV light.

- The orientation of the nano-crystals have been determined to be uniform by microscopic techniques including HRTEM., No effect upon efficiency relating to coating orientation vs. light angle was observed.

33

Milestone 3 – T9

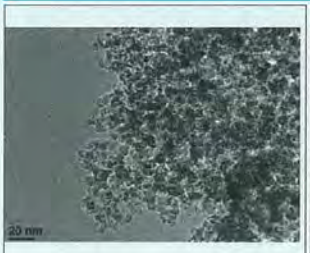

HRTEM Image of Polydispersed SolarPA "NanoCoat" Coating on Silicon (images courtesy NTC)

SEM Image of Monodispersed SolarPA "NanoCoat OverCoat" Coating on a Silicon Solar Cell

34

Milestone 3 - C1

- **Evaluate cost benefit and impact on selling price of NanoCoated solar cells with increased efficiency with grazing incidence of sunlight on the cell.**

- The experimental data generated confirms that a 40u coating thickness of NanoCoat OverCoat yields superior solar cell efficiency as compared to 60u, 80u, and 100u. This significantly improves the value proposition for using NanoCoat OverCoat to improve solar cell efficiency.
- It has been demonstrated that the negative effect of grazing angle effect on SPI solar cells is mitigated by the addition of NanoCoat OverCoat to the solar cell. While this does not impact the selling price of the product, it certainly adds to the cost benefit of using NanoCoat OverCoat.

  (as observed in Milestone 3 T-6)

35

Milestone 4 Technology Deliverables

- **SolarPA will measure the efficiency of 45 cells as a function of elevated temperature.**
- **A determination will be made regarding where Nanocoat can be employed in SPI's manufacturing line.**

- **The anticipated efficiency is >3% at an angle of incident light perpendicular to the cell, but > 6% at elevated temperature.**
- **SolarPA ultimately intends to License or enter into a Development Agreement with SPI.**

36

Milestone 4 – T10

- SPI will supply 15 silicon wafers to SolarPA that have been chemically etched in a non-texturing chemical bath (see Milestone 3). SolarPA will coat the wafers with NanoCoat and return them to SPI.

- Silicon wafers were etched at Akrion, Inc., Allentown PA, in a chemical bath to remove 5 microns of wire saw damage on each side of the wafer.
- The silicon wafers were subjected to a diffusion process and oxide etch at SPI prior to coating the wafers with NanoCoat.

37

Milestone 4 – T11

- SPI will process the silicon wafers in its standard manufacturing line and make a completed solar cell.

- Cells were processed by replacing the texture etch with a nitric acid/hydrofluoric acid etch (10:1 ratio for 1 minute) to remove approximately 5 microns of the wafer surface damaged during wire sawing in a slurry
- No statistical improvement was observed in cells normally processed versus those cells where the texture etch was replaced by NanoCoat InnerCoat, as show in the graph on the next slide. All results fell within a standard deviation of 0.19%
- As the nanocrystals in NanoCoat InnerCoat are held to the surface of the solar cell by weak van der Waals attraction after the solvent evaporates and the solar cell is subjected to temperature of 600 degrees C during subsequent processing, it is probable that the nanocrystals came off the surface of the cell. We intend to do a chemical analysis to try to detect whether any nanocrystals remained on the surface.

38

Efficiency of Standard Solar Cells Vs. NanoCoat InnerCoat Cells

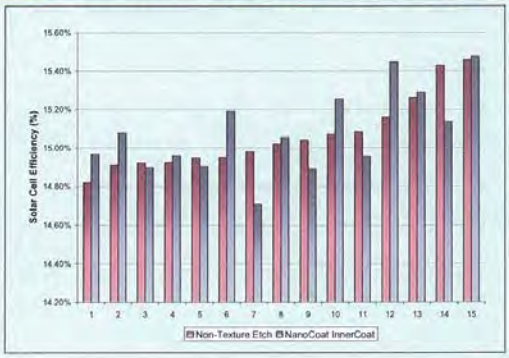

39

Milestone 4 – T12

- SolarPA will measure the efficiency of the two lots of 15 solar cells as a function of temperature up to 75C to compare efficiency of a NanoCoated cell versus a standard cell. (The temperatures inside a glass enclosed solar paned have been known to reach temperatures above 50C.)

- On this lot of cells the average increase in efficiency at 25 degrees C was 8.4%. At 50 degrees C the average efficiency was 10.4%.
- Both lots degraded with increasing temperature because of band-gap widening of the silicon
- The higher efficiency at higher temperatures means solar cells with NanoCoat OverCoat will operate at a higher efficiency in high-temperature regions such as a solar farm in a desert.

40

Efficiency of Completed Solar Cells Vs. Temperature

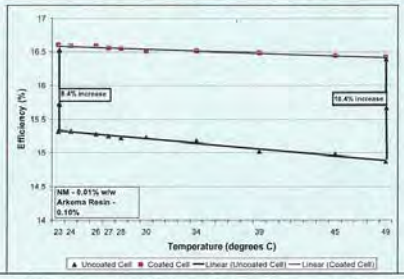

Efficiency Increase at 23 degrees C – 8.4%
Efficiency Increase at 49 degrees C – 10.4%

41

Milestone 4 – T13

- SPI will supply an additional 15 silicon wafers to SolarPA that have been chemically etched in a non-texturing chemical bath (see T11 of Milestone 4) and that have been further processed to include SPI's standard hydrogen anneal and antireflective coat steps, but do not contain the electrodes. SolarPA will coat the wafers with Nanocoat and return them to SPI.

- We were proceeding with evaluating a process of replacing the ARC deposition with NanoCoat InnerCoat. Wafers were coated and submitted to SPI for processing and evaluation.

42

Milestone 4 – T14

- SPI will process the silicon wafers in its standard manufacturing line and make a completed solar cell.

- SPI ceased production of solar cells before they could be processed. We will attempt to complete the evaluation once SPI is back in business.

43

Milestone 4 – T15

- SolarPA will measure the efficiency of the 15 solar cells as a function of temperature up to 75C to compare efficiency of a NanoCoated cell versus a standard cell.

- On this lot of cells the average increase in efficiency at 25 degrees C was 8.3%. At 50 degrees C the average efficiency was 10.5%.
- Both lots degraded with increasing temperature because of band-gap widening of the silicon
- The higher efficiency at higher temperatures means solar cells with NanoCoat OverCoat will operate at a higher efficiency in high-temperature regions such as a solar farm in a desert.

44

Efficiency of Completed Solar Cells Vs. Temperature

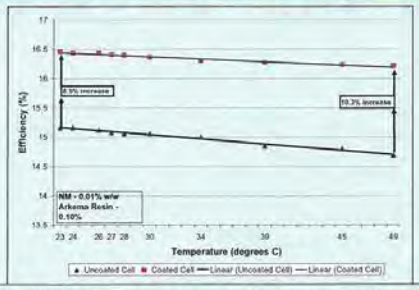

Efficiency Increase at 23 degrees C – 8.3%
Efficiency Increase at 49 degrees C – 10.5%

45

Milestone 4 - Commercial Deliverables

- Determine cost savings and potential selling price increases with substituting texture etch with non-texture wire saw damage and etch and the ability to offer a product with higher efficiency at elevated temperatures compared to standard cells.
- Enter into an Agreement with either SPI and/or another solar cell manufacturer as a potential customer for the technology.

- As there was no statistical difference between cells with no texture etch and cells with no texture etch plus NanoCoat InnerCoat, there was no potential savings to SPI by eliminating the texture etch and replacing it with NanoCoat.
- Solar Power Industries (SPI) wishes to continue investigative development with Solar PA regarding the industrial implementation of the NanoCoat material in both inner coat and outer coat implementations.
- In regards to the outer coat implementation, SPI intends to provide a source for finished cells for coating by Solar PA and provide test verification of efficiency improvements. This work may also extend to verification of cell improvements in a module configuration.

46

Milestone 4 – C3

- **Evaluate cost impact of the Nanocoat step at varying points in SPI's solar cell manufacturing line.**

- As the output of a solar plant is increased by 10% with the addition of the coating, a 50 MW plant now becomes a 55 MW plant.
- More importantly, this technology can move binned marginal efficiency cells above a company's minimum level to become useable. As much as 20% of annual production results in marginally efficient cells. If a 50 MW plant makes 10 MW (20%) of marginal cells at a production cost of $1 per watt (cells have gone through the entire production process), that's $10 million that would be lost but now reclaimed.

47

Milestone 4 – C4

- **Evaluate cost benefit and impact on selling price of NanoCoated solar cells with increased efficiency at elevated temperatures**

- **Increasing the efficiency of a cell by 8.4% fat room temperature will result in an 8.4% increase in the output of a solar cell. At elevated temperatures, the 10.4% increase in efficiency means a 10.4% increase in output (watts) of the cells. Thus, 10.4% less cells need to be installed in a solar farm in a hot climate to achieve the same output.**

48

Milestone 4 – C5

- Establish an overall selling price of Nanocoat based on process cost reduction by changing from standard process in C4.
- Conduct a cost benefit analysis of Nanocoat per Watt of power derived from the solar cell with SPI personnel. Upon successful completion of this program, and upon meeting our goal of a solar wafer (cell) with > 6% increased efficiency, we will offer the technology to Solar Power Industries via a License Agreement.

- Selling Price – Please see Slide 47
- Agreement – Please see Slide 48

49

Milestone 4 – C6

- The selling price of Nanocoat will be based on the above evaluations which will include raw material costs and royalties from benefits for process improvements and manufacturing savings.

- We can process 200 cells per liter of NanoCoat OverCoat
  - 2.86 panels per liter
  - COG is 0.05 cents per watt
  - COG is $3.50 per panel
  - COG is $10 per liter
- Selling price is twice the COG which includes royalties

50

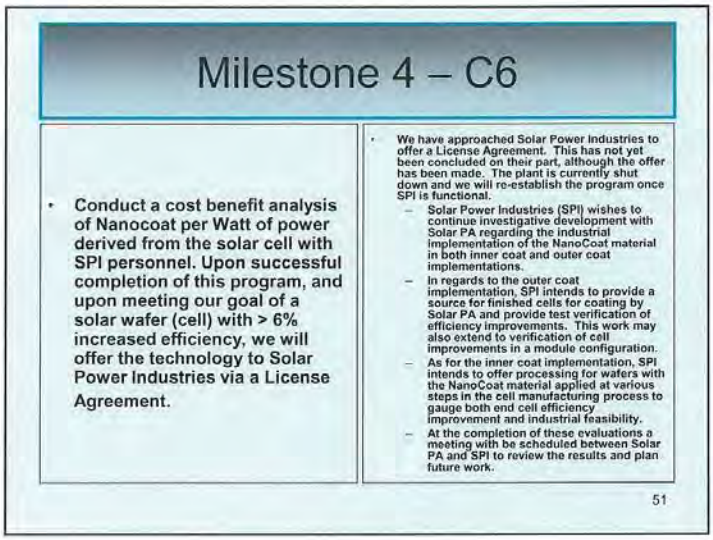

Appendix N – 11-046 (Lehigh University)

Utilization of Self-assembled Nanoparticles to Generate Electricity from Ambient Lighting

Mark A. Snyder (PI) and James F. Gilchrist
Lehigh University, Dept. of Chemical Engineering, Bethlehem, PA 18015

Final Report
May 14, 2012

The overarching focus of this pre-commercialization project was to develop the fundamental understanding of a novel materials platform towards commercialization of enhanced-efficiency dye sensitized solar cells (DSSCs). The proposed platform harnesses anode-embedded microlens technologies and anode structuring as a means for enhancing overall device efficiency towards commercial viability.

Technological efforts focused in three primary areas: **1)** extension of the anode-embedded convex and concave microlens technology to flexible substrates, **2)** optimization of microlens parameters (e.g., microlens feature size and degree of embedment) relative to device efficiency, and **3)** scale-up of the microlens technology from 1 cm^2 conventional test devices to broader-area DSSCs.

Microlens extension to flexible substrates The transition of microlens and structured anode technology from DSSCs packaged on bulky conductive glass (e.g., ITO, FTO) to ones packaged within flexible substrates, was studied (**Fig. 1**). Challenges presented by the inherent hydrophobicity of flexible substrates were overcome by the deposition of an intermediate TiO_2 sol gel layer, enabling assembly of high-quality microlens arrays on the conductive side of flexible substrates and their subsequent embedment within TiO_2 anodes. Microlens structure, including ordering and TiO_2 embedment, was quantitatively comparable to structures realized on conventional FTO- and ITO-based hard anode substrates. Deposited structures also displayed robustness to cyclic bending studies. As such, challenges with flexible devices originate not from the microlens technology, but rather the inherent limitations associated with sheet resistance of conductive flexible substrates and limited temperature stability thereof in comparison to solid FTO and ITO glass substrates. The latter precluded full-scale temperature treatments required for crystallization of TiO_2 anode structures and thereby led to parasitic device resistances.

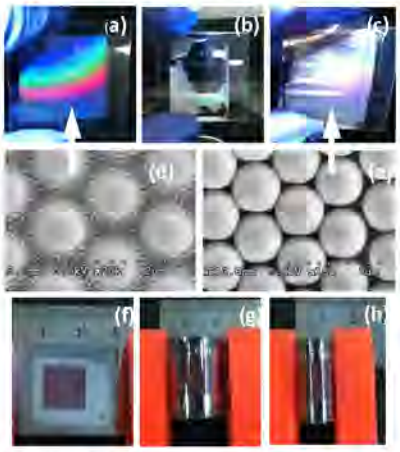

Fig. 1 Optical diffraction measurements and complementary SEM images of microlens structure on flexible ITO-PEN substrates by (a,d) binary deposition and (b) silica particle deposition. (c,e) show silica particle deposition on titania sol-gel modified ITO-PEN substrate. Images (f-h) show assessment of ITO-PEN anode (titania paste) supported, PEN/Ti/Pt counterelectrode mechanical stability by bending.

Optimization of microlens parameters relative to device efficiency Motivated by findings of anode-embedded microlens enhancement, a systematic study aimed at developing structure-properties relations governing the enhancement in DSSC efficiency observed through

incorporation of microlens technology within the anode structure was carried out. *Convex microlenses* are realized by convective assembly of ordered arrays of silica particles on titania-coated ITO glass, followed by back-filling of the interstices with titania sol gel and subsequent calcination to realize highly anatase titania structures. *Concave microlenses* are synthesized by a similar process with the use of polystyrene particles instead of silica. The polystyrene is ultimately burnt off during titania calcination, resulting in the templating of concave (periodic replica) microlenses. This processing affords two handles for tuning final microlens morphology—the *degree of back-filling of the titania sol* into either the convex silica microlenses or for replication of the sacrificial polystyrene microlenses and *control of microlens size*. Through systematic microlens fabrication, characterization, device packaging, and current-voltage (IV) testing (**Figs. 2 and 3**), we have determined that optimal device efficiencies are realized for microlens morphologies that minimize electron resistance and yield an optimum in current density. This corresponds, in the case of convex microlenses, to conditions for which combined thin coating of the silica particles with the titania sol gel layer and complete filling of the microlens interstices (58.3 μm/s) is realized. Similarly, in the case of concave microlenses maxima in open circuit voltage and current density are realized for complete filling of the interstices of sacrificial template particles. Systematic analyisis of microlens particle (convex) or feature (concave) size (**Fig. 4**) shows a clear optimum in device efficiency for 1 μm convex microlenses and ca. 0.5 μm concave lenses. In the former case, the optimal efficiency corresponds to an apparent optimum in the current density and in the latter case is due to a concerted effect of a maximum voltage and high current density.

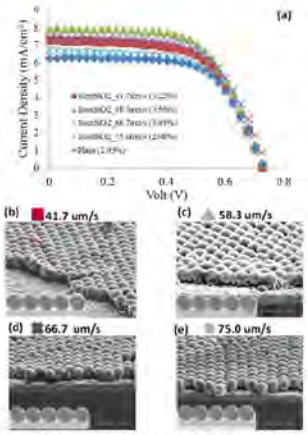

Fig. 2 Study of degree of titania infiltration of convex microlenses with (a) IV performance for various specified titania deposition rates (efficiency included parenthetically) and (b-e) corresponding SEM images showing titania morphology (schematized in insets).

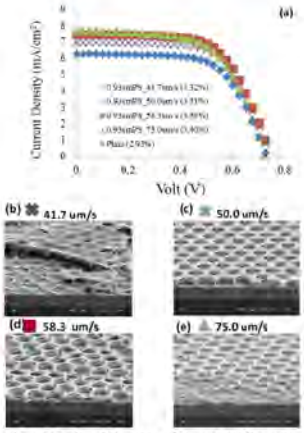

Fig. 3 Study of degree of titania infiltration for forming concave microlenses with (a) IV performance for various specified titania deposition rates (efficiency included parenthetically) and (b-e) corresponding SEM images showing titania morphology (schematized in insets).

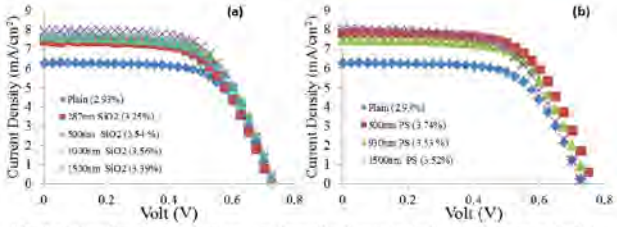

Fig. 4 Study of microlens feature size (specified) versus device performance for (a) convex and (b) concave microlenses, the latter formed by replication of polystyrene (PS) microlenses. Computed efficiencies are shown parenthetically.

Device scale-up by scale-down of active DSSC area Transitioning anode-embedded microlens technology from individual, lab-scale devices (i.e., 1 cm^2 active area) to larger scale platforms (ca. 10 cm^2 or larger) was studied. Uni-dimensional scale-up of microlens-incorporated DSSCs proved to be facile, with the need for only increased materials (i.e., microlense solution for deposition) and no deposition artifacts. While multidimensional scaling of devices (**Fig. 5**) led to lower efficiencies as a result of increased sheet resistances of the underlying FTO-glass anode/cathode supports, array-based devices in which small 1 cm^2 DSSCs were connected in parallel and in series (**Fig. 5cf**) proved promising. Specifically, *series connectivity* of arrays of smaller (1 cm^2) devices into an effective array area of 9 cm^2 resulted in array efficiencies (4.58%) greater than the average efficiency (4.19%) of any individual device composing the array. Incorporation of microlenses into each device within the array led to an increased array efficiency of 5.51%, underscoring the scalability of the microlens technology.

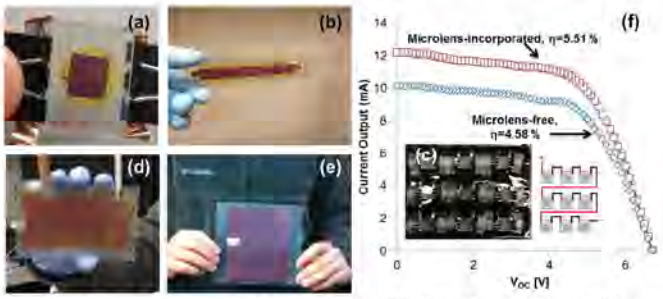

Fig. 5 Scale-up of conventional (a) 1 cm^2 device into (b) 9 cm^2 single and (c) array devices, (d) 66 cm^2, and (e) 168 cm^2 devices. Comparison of current-voltage (IV) performance of arrays of of 9 - 1 cm^2 microlens-free and microlens-incorporated DSSCs configured in series broader-area DSSCs.

Motivated by the sensitivity of device efficiency to sheet resistance, systematic studies of the areal confinement of the active DSSC region was studied by fabricating individual microlens-free DSSCs of varied size (**Fig. 6**). A clear inverse relation between cell efficiency and the size of the active region (microlens-free) has been identified for the first time, with the effect of microlens enhancement persisting.

Future technological outlook Coupled together, these findings suggest that series-connected arrays of small, active DSSC domains could provide significant advances in scalable DSSC technology. The ability to "print" such series-interconnected arrays in a roll-to-roll processing will be explored and could open exciting avenues for technological advancements and attracting commercial interest.

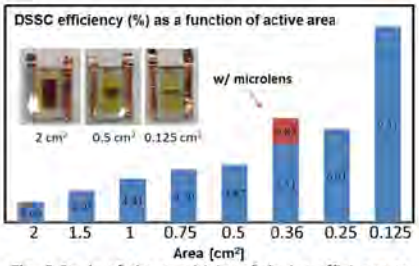

Fig. 6 Study of the sensitivity of device efficiency to dimensionality of the active area of DSSCs. Efficiency under solar simulated conditions for microlens-free (blue) and microlens-incorporated (red) DSSCs suggests an inverse proportionality of DSSC efficiency and dimensionality of the active area (example, inset).

Commercialization efforts focused on **1)** market assessment in collaboration with PAower Optics LLC and an external firm, Foresight, **2)** sharing technology advancements with potential commercial partners through oral presentations at various technical and industry-attended conferences, and **3)** establishing/developing relations with potential customer/collaborator companies (e.g., Boeing, Swatch Watch™).

Market assessment Commercialization efforts focused initially on preliminary market assessment in collaboration with PAower Optics LLC and an external firm, Foresight. Analysis led to conclusions about entry points into the consumer electronics market and identification of competing products, patents, and market barriers. In addition, a list of target companies was identified based upon the developed technology.

Technology presentations Outside of the AFRL showcase, numerous technological presentations were made during the course of this project, including:

- 2011 American Institute of Chemical Engineering Meeting in Minneapolis, MN
  P. Kumnorkaew, J.F. Gilchrist, and M.A. Snyder, "Anode Assembly and Templating Strategies for Improving Efficiency and Versatility of Dye-sensitized Solar Cells," 2011 AIChE Meeting, Minneapolis, MN. I
- Invited talk at the Composites at Lake Louise meeting in Lake Louise, Canada
  J.F. Gilchrist, X. Cheng, M.A. Snyder, N. Tansu, P. Kumnorkaew, A.L. Weldon, T. Muangnapoh, "Convective Assembly of Nanostructured Optical and Biofunctional Coatings", Composites at Lake Louise, 2011, Lake Louise, Canada
- Society of Rheology (DSSC-microlens technology introduced as motivation)
- American Physical Society's Division of Fluid Dynamics Meeting (DSSC-microlens technology introduced as motivation)

Fostering industrial interactions toward commercialization Efforts aimed to foster relations with potential customer/collaborator companies including with Boeing, with efforts focused on the translation of microlens technologies and DSSC devices for light-weight on-board powering of electronic devices, and Swatch Watch™, for flexible solar power for wrist watches and other portable electronics.

Appendix O – 11-047 (NanoGrass Solar)

From: Bahram Nabet, Ph.D.
NanoGrass Solar LLC
860 Skyline Drive
Erdenheim, PA 19038

To: Leoné Hermans-Blackburn Ph.D.
Program Manager
Pennsylvania NanoMaterials Commercialization Center

Subject: Final Project Report

Date: May 10, 2012

Dear Leoné:

Attached please find:

1. Property Closeout Certificate and
2. Report of Inventions and Subcontracts (DD Form 882 attached).
3. Final Financial Report

Since there was no template for the final report, I am attaching the detailed report based on the third milestone report that shows the cumulative technical and commercial work that was done during the course of this project.

Please let me know what else needs to be done to close this contract.

Thank you very much for your support.

Sincerely,

Bahram Nabet

Bahram Nabet, PhD.
NanoGrass Solar LLC

CC: Ed Sullivan, NGS

Final Project Report:

Below is based on Milestone 3 report to PA Nanocenter which details our cumulative technical and commercial accomplishments during the course of this project.

TECHNOLOGY DEVELOPMENT ACHEIVEMENTS

Task – Prepare the high efficiency light absorbing NW substrate consisting of GaAs /AlGaAs core-shell on the following non-crystalline substrates (c) poly-silicon and (d) transparent conductive oxide (TCO).

NGS: We had delayed the growth of GaAs nanowire on Si from Milestone 2 tasks. We have been able to reach this important milestone. We have started the preliminary work that is needed for growing nanowires on poly-silicon or transparent conductive oxides, however, we do not have the resources that we need to commit to that work. Instead we would like to build on the good results we have achieved on GaAs NW growth on GaAs and on Si substrates as detailed below.

Growth of GaAs/AlGaAs core-shell NW on Si.

This is has proven to be impossible for thin-film technology despite heavy investments in research labs and industry, and patent portfolios reaching up to 200. However, as stated in our proposal, the nanowire version can be grown since all that is required is the "adequate" transfer of the substrate crystallography to beneath the Au colloidal particles used in VLS growth. We are preparing a patent on the detail of the growth. Broadly, however, we orient the surface of Si so that it matches better with GaAs (111) planes. We produce a thin film of the latter plane first, then grow the GaAs NWs. The results are shown in figure below, where GaAs NWs, grown on GaAs substrate are also shown for comparison in the inset.

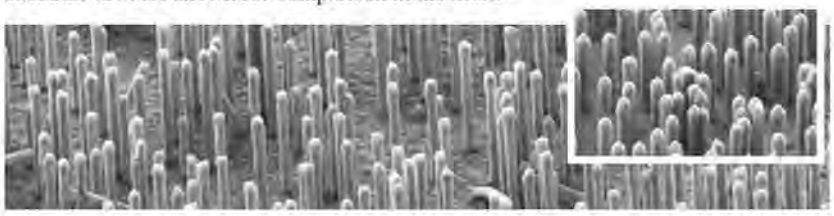

Figure 1. FE-SEM micrograph (45°tilt view) of GaAs/AlGaAs coreshell NWs grown on a GaAs/(111)Si substrate. Inset shows same NWs grown on GaAs susbtrate.

Several observations should be made:

1. The wires are oriented in the same direction and have relatively uniform height. There is a vertical yield ≥95%, i.e., 95% of the wires oriented in the same direction. This is comparable to what expected for growth on (111)GaAs.
2. The density of wires is similar to those grown on GaAs.
3. Wires have good stoichiometry
4. The uniformity of growth is comparable to GaAs, but the growth was done in small areas. Extension of this to large surfaces seems reasonable, but requires further refinement of the process.
5. The substrate in which NWs were grown should be compared in the figure and its inset. The inset has the smooth crystalline surface of GaAs, while the rough surface of Si prepared for NW growth is obvious in the heteroepitaxial case (GaAs on Si).

We have performed photoluminescence (PL) measurements in order to study the material quality and optical properties. Results are shown in figure 2.

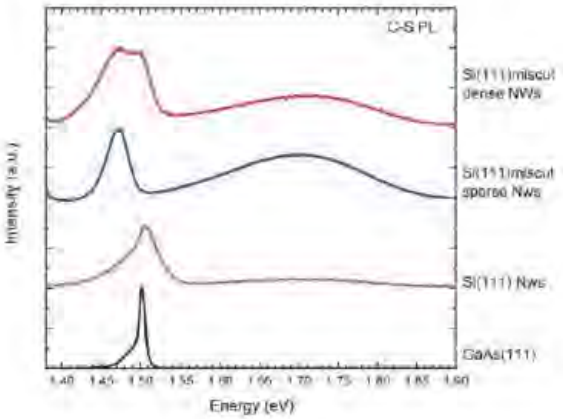

Figure 2. Comparison between 7K PL spectra of GaAs/AlGaAs coreshell NWs grown on various substrates: (i) standard (111)GaAs wafers, and GaAs buffers grown on (ii) exactly oriented, and (iii) 4° offcut (111)Si wafers.

Low temperature PL spectra recorded from dense arrays of core-shell NWs grown onto GaAs/Si hetero-substrates show emissions similar to what previously observed for growth on (111)GaAs wafers, although the NW core emissions appear generally much broader with respect to the latter case; also, a difference appears between PL emissions from NW arrays grown on exactly-oriented and 4° off-cut Si wafers (Figure 8): in the latter case the PL spectra appear also somewhat red-shifted and depending

on the density of NWs. the origin of such effects is not clear to date, and requires further investigation.

In summary, this is an important milestone for NanoGrass Solar. We have shown that we can grow high efficiency expensive GaAs nanowires on low cost substrate. Furthermore, we use only a fraction of GaAs material to achieve much higher absorption of light than.

Task - Characterize the *light* absorption properties of the as-grown substrates

NGS: Reflectivity measurements were performed on a) planar GaAs substrate, b) planar GaAs/AlGaAs substrate, and c) AlGaAs/GaAs core-shell NWs. Data is plotted in Figure 3 for the wavelength range that covers the solar spectrum.

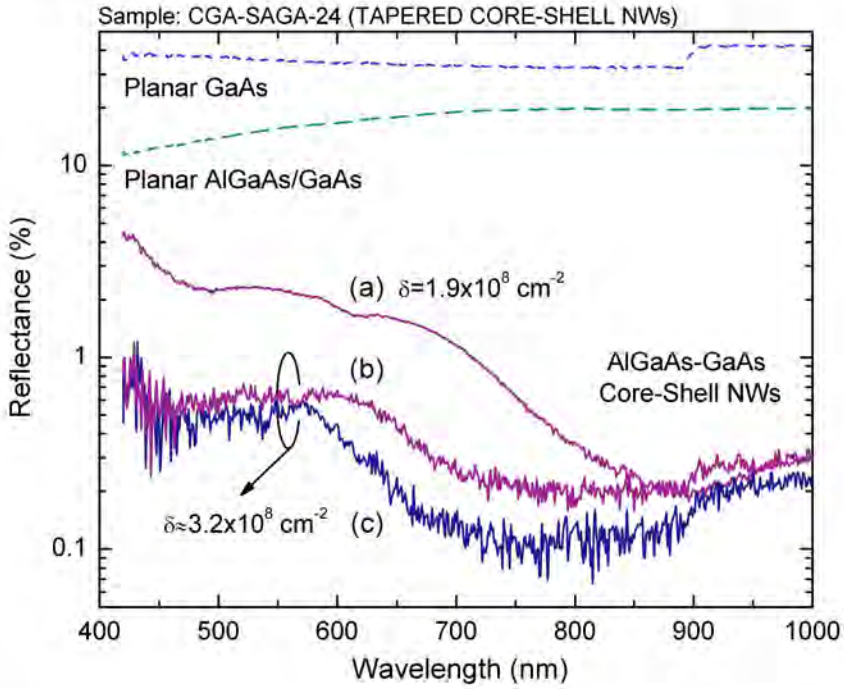

Figure 3. Measured reflectivity of planar GaAs, planar AlGaAs/GaAs, and AlGaAs/GaAs core-shells at 3 different wire densities.

It is seen that, as well known, GaAs reflects nearly 40% of incident radiation, absorbing 60% of the light. AlGaAs has a higher index of refraction, so it reflects about 20% of the light, for the whole range. Data for NWs of core-shell GaAs/AlGaAs is taken at 3 spots on the wafer with different NW density that were calculated from the SEM of these area. Curve (a) has ~$1.9 \times 10^8/cm^2$ NWs, while (b) and (c) had ~$3.2 \times 10^8/cm^2$. We observe that for these higher densities, corresponding to approximately 15% of the volume, reflectivity is less than 1% for the whole spectrum! For the lower NW density as well, less than 5% of the light is reflected even though less than 10% of the volume is occupied by wires. While we need to make correction to the experimental results by which do not account for the diffused light, and the light that is trapped between the NWs but is not absorbed, the results are remarkable as expected.

Task - Develop the optical PV devices on a single wire and calculate the efficiency.

This requires that we make both Ohmic and Schottky contacts to the wire. We have previously attempted this during milestone 2 period and were not successful in making Ohmic contacts. Partially the problem is the difficulty in electric transport measurements. The wires need to be harvested on a substrate that is pre-patterned. Then the should be located in a focused ion beam machine and next contacted by either ion beam induced deposition, or electron beam induced deposition. We have performed these delicate and expensive processes. The results have shown that we can make Schottky or blocking contacts. As a result we have data on single NW's response to light. In fact we have data for how fast these wires respond to light. However for a photovoltaic device, that is, for operation in the 4th I-V quadrant we must have an Ohmic contact so that a Metal-Semiconductor diode can be formed.

The same problem exists for planar thin-film devices. All Ohmic contacts, such as the source and the drain of a transistor are formed on a highly doped GaAs material. Hence we have launched the design of multi shell wires which, have an outer shell of doped GaAs. This is also uncharted territory in NW fabrication. Figure below shows the multi-shells that we have grown.

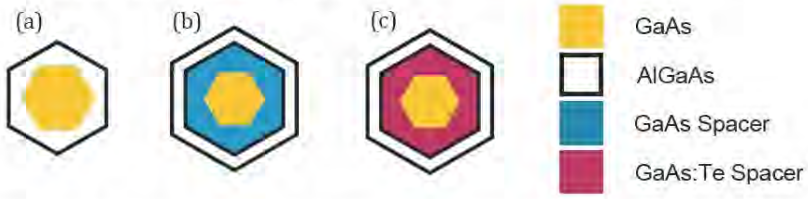

Figure 4. Schematics of asgrown GaAsAlGaAs coremultishell NWs. (a) represents a standard GaAsAlGaAs single core/single shell NW structure; (b) coreshell NW structure with an additional undoped GaAs shell overgrown around the GaAs core; and (c) same structure as in (b) but with the additional GaAs shell intentionally doped with Te.

These wires which have a doped outer shell have been grown. We are in the process of determining the conductivity of the outer shell so that we may produce our PV device.

Task - Develop the photodetector device on the nanowire array (NWA) substrate.

NGS: We have grown several dies for this purpose. We have performed first metallization on an array, but have observed unacceptable damage to the wires. We have changed the design so that the lower contact is doped GaAs. Te (n-type) doping of substrate is performed. We will use the multi shell structure shown in Figure 4 for this purpose.

Deliverables: - Show evidence of and report on the production of the NWA substrate that absorbs an order of magnitude more light than a thin film of the same material while occupying about 1/10th of the volume.

NGS: The result in figure 3 is the evidence of high absorption of light by NW. Furthermore we have been able to do this on Silicon substrate as Figure 1 of this report shows.

Commercial Achievements:

Tasks:

- Identify the PV cell manufacturers in generation II and III photovoltaics.
- Engage the R&D units of GE and Dupont in order to interest them in NGS technology
- Outline and compare the provisional cost structure with respect to the manufacture and selling price for (a) wafer, (b) equipment; and (c) PV cell manufacturers. Compare the competitive technologies and address what the market is willing to tolerate in terms of cost.

Deliverables:

- Provide a market analysis that includes the market size and potential customers in PV devices based on the NanoGrass technology.

NGS: Despite a plethora of bad news surrounding the PhotoVoltaic ecosystem over the past 18 months, grid-installed PV's have grown substantially through that same period and are expected to do so through 2012. According to a recent report by the Solar Energy Industries Association, installed PV increased 69% in Q2 2011 over the same period in 2010 and was up 17% overall through 2011. (see attached graph). This bodes well for NGS over the coming quarters and years. While the Federal Cash Grant expiration may have driven some of the 2011 growth, we believe strong programs pushing adoption over the next 5-10 years at the state level should accelerate this even more. (e.g. California's renewable portfolio standard, 33% renewable by 2020).

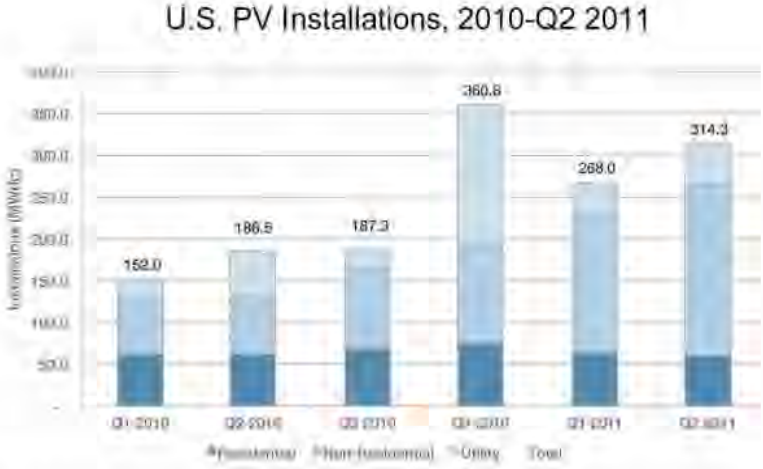

Figure 5. Most recent report on US PhotoVoltaic installations show a healthy expansion.

- Report on engaging potential partners/customers for R&D as well as device manufacture.

NGS: Through 2011, NGS has engaged prospective partners with the aim of establishing business development partnerships with varying degrees of R&D or commercialization. To be clear, our preferred path is not to directly manufacture PV's but to license our technology to functionally adjacent partners. To date, our efforts have been focused on core technology partners (nano-grass structure), material manufacturing partners and manufacturing process partners.

Most notably, NGS has finalized it's IP partnership with Drexel University to secure our rights with respect to the IP for the core Nano-Grass structures and is in the final stages of negotiation with University of Salento, Lecce, Italy to secure the worldwide rights to their proprietary nanowire manufacturing process. Also, we have been in negotiations with Bayer regarding a Joint Development Agreement and potential investment pending the preliminary results utilizing their polymers. Bayer has agreed to provide the samples to NGS at their cost for the purposes of advancing these discussions.

- Report on the commercialization strategy – outline (a) the most feasible market moving forward and (b) potential partnership/s. Provide a Letter of support from the partner and/or potential customer for the identified market.

NGS: NGS has begun soliciting private investors via a Private Placement Memorandum which will enable NGS to raise between $100K and $500k over the next two quarters. To date, NGS has raised $60K via this offering and intends to raise an additional $100K by the end of Q1 2012.

Appendix P – 11-050 (NanoGripTech)

FINAL REPORT

Project Title: Roll-to-Roll Manufacturing of Bio-Inspired Micro/Nano-Fiber Adhesives for Sports Apparel Applications

Project Leader: Metin Sitti

Name of Project Leader's Organization: nanoGriptech, LLC

Date: July 6, 2012

Submitted to: Pennsylvania NanoMaterials Commercialization Center

Project Goal Statement: The goal of the project was to develop gecko foot-hair inspired polymer fibrillar adhesives as new sports closure and glove gripping material applications. The desired sports apparel specifications given in Table 1 were determined after discussions with Under Armour Inc. Our work plan included material selection, roll to roll manufacturing, and testing of polymer fiber adhesives with various materials and geometry to achieve the desired performance metrics in Table 1. In any milestone below, the desired specifications was achieved by a fiber array and a flat closure surface or on a ball surface for a given sports application.

Specification Number	Specification Name	Desired Specification (mass-produced fibers)	Previous Measured Fiber Performance (small-batch fibers)
S1	Shear force (football glove)	3 N/cm^2 at 0.8 N/cm^2 load in contact with dry football and 1.5 N/cm^2 at 0.8 N/cm^2 load in contact with wet football	2.2 N/cm^2 at 0.8 N/cm^2 load (dry football) and 1.2 N/cm^2 at 0.8 N/cm^2 load (wet football)
S2	Shear force (closure)	10 N/cm^2 in dry conditions and 6 N/cm^2 in wet conditions	11.4 N/cm^2 (dry) 6.4 N/cm^2 (wet)
S3	Peel force (closure)	0.5 N/cm amount in dry conditions and 0.3 N/cm in wet conditions	0.7 N/cm (dry) 0.2 N/cm (wet)
S4	Durability	Number of cycles over the product life: • 1,000 cycles – 90% of original strength • 2,000 cycles – 70% of original strength • 5,000 cycles – 65% of original strength	1,000 cycles – 60-65% of original strength
S5	Usability	Open and close forces of <0.5 kgf per inch	Not yet measured
S6	Closure patch size	1 inch x 25 feet	1 inch x 1 inch
S7	Water-resistance	20 kPa (3 psi) for 2 minutes	40% water penetration at 3 psi for 2 minutes
S8	Washability	Water cleaning (with a temperature up to <93° C)	No performance loss at temperatures of 40° C
S9	Flexibility	Flexible fiber arrays conforming to body curvatures	Conform to ~12 mm diameter curvatures
S10	Incorporate fabric	Incorporate fabric backing into mass-production process	Incorporated fabric into small batch process
S11	Cost	Close to $0.1/inch when manufactured in high volumes (Lower than the cost of hook and loops, which is $0.36/inch. The cost of coil zippers is ~$0.01/inch.)	Around $0.5/inch excluding the labor and equipment costs

*Table 1: Specifications for **mass-produced fibers** using the roll-to-roll process for the target applications, compared with the previous performance of our **small-batch** fiber adhesives. These specifications were determined in collaboration with Under Armour.*

TABLE OF CONTENTS

A. EXECUTIVE SUMMARY

Technical Development

- **T1**: Computer simulation of the contact between the fiber and football surfaces determined that using a thicking and softer backing will increase the contact surface area of the fibers which will ultimately increase shear performance
- **T2**: Tests using BMS's Fusion curing systems using gallium and mercury bulbs demonstrated proper cureing of Desmolux 2491 in the silicone mold without nitrogen atmosphere or vacuum. Also, we demonstrated that nGt's two stage vacuum curing is compable to the Fusion system
- **T2**: Formulation studies have shown that Desmolux 2491 stiffness and adhesive properties decrease with time, however, testing of new formulation, F-75, show that this aging can be mitigated using other comonomers
- **T3**: Our second generation mass production system was designed and build with improved features that allow better process control
- **T4**: Initial samples produced from this system met or surpassed all Milestone 2 performance requirements
- **T5, T9**: A design criterion for adhesion to wet surfaces was developed in the computer model
- **T6**: An optimization study for photoinitator wt-% resulted in a 50% shear force enhancement for F-75 formulations; Peel strength was found to increase with decreasing photoinitiator, which was correlated to the formation of softer-tipped fibers (relative to bulk modulus) due to inhibition at the mold surface
- **T7**: The mass production system was modified to change roller location, quantify the effect of belt speed and temperature on the quality of the manufactured tape, and modified to use clear molds
- **T8**: 2nd generation fibers made using the mass-production system produced samples that exceeded final target shear strengths on closure surfaces, and exceeded peel values milestones in both wet and dry conditions
- **T10**: Studies were conducted to characterize the effect of mold transparency, lamp distance, lamp distance, curing temperature, and hardener concentration on fiber performance
- **T11**: Modifications to the roll-to-roll system eliminated the need for a post-mold vacuum curing step while improving material performance. Additionally, the system could now produce samples cured directly on non-transparent substrates like UA textiles
- **T12**: All project performance specifications were met at this time with the exception of dry shear strength on a football

- **T13**: Studies conducted at BMS resulted in high-performance samples produced using the Fusion microwave lamp system at speeds of up to 100 ft/minute, demonstrating the ability to scale up production rates

- **T14**: A simplified single roller system was built and successfully operated, and properly cured samples were produced from LED UV systems on loan from Phoseon. A 25' sample was produced using our mass-production system

- **T15**: All project performance specifications were met with the exception of dry shear on football substrates

Commercial development

- **C1**: A renewed Joint Development Agreement between nanoGriptech and Under Armour was signed in September 2011

- **C2**: Preliminary mass-produced fiber arrays were provided to UA for evaluation; Additionally, nGt prepared football glove sized fiber array that was laser cut and fitted onto a glove while on-site at UA in a joint prototyping effort

- **C3**: New fiber templates were fabricated in the CMU cleanroom, and studies identified the optimum backing thickness for football friction enhancement; This information was used to produce new samples for delivery to UA for evaluation

- **C4**: A preliminary system quote of $174,900 was received from PolyWorks Inc (North Smithfield, RI), for a customized roll-to-roll UV-curing production system. Additional quotes from alternative vendors (4 total) were procured in later Milestones

- **C5, C6**: Frequent communication and regular collaboration between nGt and UA has resulted several improved generations of micropatterned football glove and closure prototypes produced and evaluated in user studies and field trials

- **C7**: Possible IP generated during this project include the ultimate formulations used in this study, and the ability to directly cure micropatterned materials on opaque substrates using transparent molds

Directions for future development

- Under Armour and nanoGriptech are in the process of preparing and negotiating a term sheet for a joint development project which would involve UA partially funding a pilot production line in exchange for continued development of closure and football glove prototypes with milestones to meet for development, and delivery sales price and volume

- Additional technical hurdles include producing samples that satisfy the real-world environmental handling of UA's product line. This will be accomplished through repeated protyping and field trials in collaboration with the UA team

- Procurement, installation, and optimization of the pilot-scale production system

B. TECHNICAL DEVELOPMENT

B.1. MILESTONE 2 TECHNICAL DEVELOPMENT

B.1.1. T1 Fiber Adhesive Models

Develop fiber adhesive models for fibrillar parameter selection for both football and flat closure substrates in dry conditions

Basic Simulation Case

As was described in the Commericalization Grant proposal submitted to PA for this project effort, computational mathematical and physics modeling is a powerful tool used as a part of the fiber design process. The models provide a solid theoretical foundation for honing in on optimal design geometries and materials, based on the desired final performance outcome of the project. For the first quarter of this project the team developed a basic computational simulation model using COMSOL software on a single micro-fiber. The focus of the basic simulations were to predict the predict and estimate both the adhesion of the fiber to a smooth polymer surface and also a football receiver application.

In adhesion applications, the goal is to create and interaction between 2 surfaces with the maximum amount of surface area contact. In the case of fibers contacting the a smooth closure surface, much modeling work has been done by both nanoGriptech and other research groups in the world. However, the situation of a fibrillar adhesive contacting the surface of a football is a more difficult design and manufacturing challenge due to the rough dimpled surface of the football as shown in Figure 1.

Figure 1: Close up image of football surface.

The football surface is comprised of a repeating pattern of tiny spherical caps that are 420 µm in height and approximately 1.15 mm in radius (Figure 2). Fiber arrays fabricated at nanoGriptech range between 100 µm and 125 µm in length which are significantly short compared with the height of the repeating roughness pattern on football. This implies that the fiber array will not form full contact with the football surface. During our NSF STTR Phase I project, a compliant backing was added to the fiber array which showed significant shear performance improvement over fiber arrays without a compliant backing. This result was expected because the additional compliance of the backing aids in the conformation of the fiber array to the football roughness leading to an increased number of contacting fibers and thus improving performance. The study performed for the NSF project was preliminary and did not involve any numerical/theoretical modeling.

Figure 2: Cross-sectional view of a football surface (taken from NSF STTR Phase I final technical report)

To better understand the effective parameters and fiber adhesive design to given specifications, a Finite Elements (FE) study was designed to predict the shear performance of fibers on the football surface. Figure 3 shows the model and the elements of the simulation. The repeating pattern on the football surface is modeled as a hemisphere with 1.78 mm radius. Fiber array is modeled as a continuous 100 µm thick film and the effective fiber modulus was calculated directly from experimental data. Underneath the fibers, a 50 µm layer exists which is made of the same material as the fibers. The entire system is supported by a compliant backing whose modulus and thickness will be determined for best possible performance within the constraints given to us by UA.

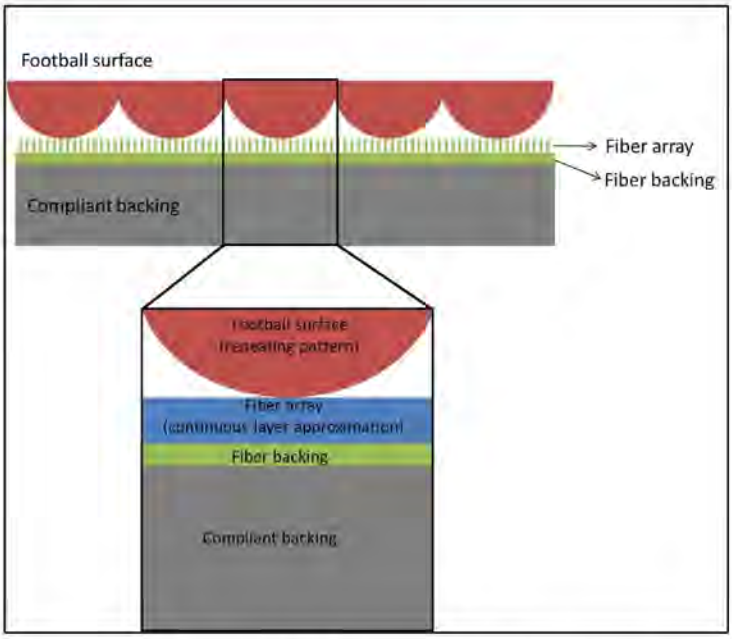

Figure 3: Depiction of the elements involved in the computational model for fibrillar contact with dimpled football surface.

Figure 4 shows the output of the computational model where the deflection of the fibers is viewed as a function of the football displacement. This analysis was performed in 42, 10 µm increments starting from initial contact of the fiber surface to the 420 µm indentation. This series of analyses were performed for fibers with two different backing thickness and moduli and with no backing. Figure 5 displays the effect of the backing thickness and moduli on the coverage area of the fibers. where E = Young's modulus of the compliant backing material and h = thickness of the compliant backing material. Note that contact pressure was calculated using the football displacement and moduli of the materials. It can be observed that for the same contact pressure

(displacement) between the fibrillar adhesive and the football surface that contact percentage improves when the compliant backing is thicker and softer. Therefore, a thicker, more compliant backing would allow the entire adhesive system to conform to the rough shape of the football and increase shear performance. As the model is further refined, more design and manufacturing data will be collected. This data will become part of a continuous loop to continually improve the fidelity of the model. The selection of the backing will be made together with UA to ensure that performance, fit, and comfort criteria are met for the receiver glove.

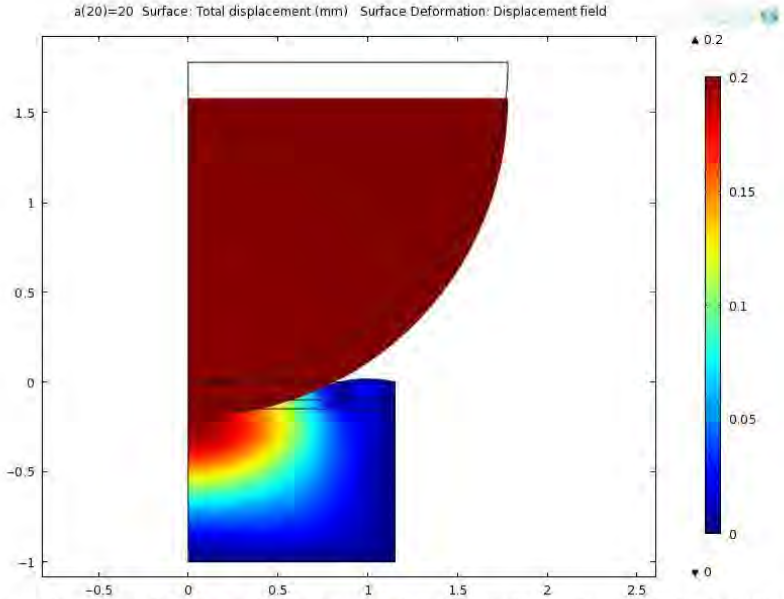

Figure 4: Comsol model displaying the displacement of the fiber surface as the football dimple is displaced 200 μm.

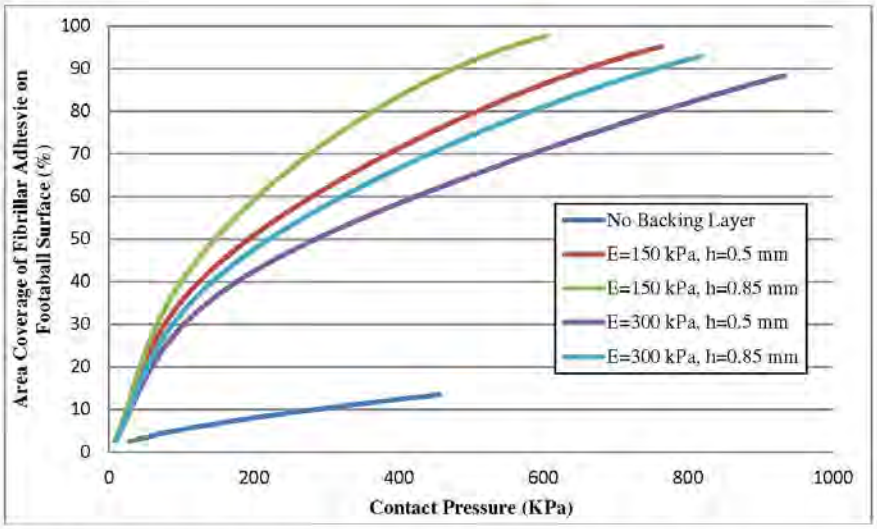

Figure 5: Area of fibular adhesive coverage on a football dimple surface versus the contact pressure using various backing layers (E=Young's modulus and h=thickness of the backing layer).

B.1.2. T2: Material Compositions for Mass-Production

Select and develop the polymer fiber material compositions for mass-production system and ideal material properties (i.e. tensile strength, elastic modulus, surface energy, hydrophobicity, and processing) and performance in dry conditions (S1, S2, S3, S4, S5) in collaboration with BMS. Materials should achieve 40% of specifications S1-S5 in Table 1.

Materials for fibrillar adhesives must have desired bulk mechanical properties, sufficient amount of surface energy, and the ability to be manufactured into fiber arrays quickly. Initial focus was placed on ST-1060 polyurethane (BJB Enterprises) because the material properties rendered it strong enough to be fully released from the silicone mold while being sufficiently soft to allow mushroom tips to bend into full contact with a surface. While this results in good adhesion performance, the full curing of the material exceeds 24 hours including a heat cycle, limiting production volume and increasing part cost. UV cured materials offer an advantage over two-part curing systems because curing occurs in minutes rather than days. Our partner Bayer MaterialScience (BMS) is an industry leader in UV-cured polyurethane polymers and has assisted us with formulation of their commercial materials. BMS's commercial UV cured polyurethanes consist of acrylate terminated polyurethane mixed with 20 wt-% of an additional acrylate (or methacrylate) monomer (Figure 6). When combined with a photoinitiator and exposed to UV light, the materials polymerize and create a crosslinked film. In this quarter, new formulations were prepared where the acrylate functional polyurethane was copolymerized with four different monomers in order to tune material properties.

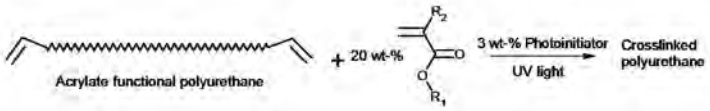

Sample	Where R_1 =	Where R_2 =
2491		CH_3
F74		H
F75	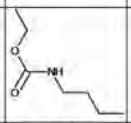	H
F76		H

Figure 6: Schematic of polyurethane UV curing system and chemical structure of comonomers used for tested formulations.

As detailed in our first PA Nano funded project, we have encountered several setbacks using our current formulation (BMS Desmolux XP 2491) and curing methods in order to obtain a fast curing polyurethane that will perform as well as the BJB ST-1060 2-part polyurethane system. First, it was found that any presence of oxygen would inhibit full curing of the resin with our H&S Autoshot UV light system. This results in a significant decrease of adhesive strength of the fibers along with a substantial amount of residue left on the adhering surface. This was overcome by using a two-stage curing process where the fibers were cured in the mold for one minute followed by peeling from the mold and curing for seven additional minutes in a vacuum chamber. While this method is sufficient for laboratory studies, it is not suitable for high volume production of fibular adhesives. Additionally, the Desmolux 2491 material is subject to aging. This was realized by the loss of adhesion and increase of residue left by older manufactured samples. In the following sections we describe our methods to characterize and overcome these problems with the UV curable polyurethane resin. We studied four different polymer formulations cured by different light sources and characterized their aging properties by testing adhesion performance over time.

B.1.2.1 Minimizing oxygen inhibition through lamp selection

Oxygen in the atmosphere and absorbed in the silicone mold inhibits full curing of the polyurethane using our light source at nGt. However by using different lamp types and light intensities, this inhibition can be mitigated. By curing with two light sources available at BMS's laboratory, we studied this effect on four monomer systems presented in Figure 6. The H&S Autoshot system has a mercury bulb similar to the one at nGt, while the Fusion system uses a gallium and mercury bulb which includes larger light spectrum and a higher intensity. All Autoshot samples were subject to UV light for eight minutes and Fusion samples were passed

twice through the belt system amounting to approximately one minute of exposure. Inhibition was characterized by visual inspection under a microscope. If residual material was observed during the first attachment and peel then material was deemed not fully cured.

All samples cured with the Autoshot displayed inhibition, while all samples cured with the Fusion system showed no residual material on the adhering surface. Figure 7 displays the shear strength of Desmolux 2491 cured using three processes involving both high and low intensity lamps and air and vacuum systems. Using the BMS's Autoshot system in atmospheric conditions yields uncured materials that have the lowest shear strength. However, when the vacuum is applied with a similar light source (nGt method), the fibers are fully cured and have shear strengths comparable with the high intensity Fusion system. For large volume production a Fusion system should be used because it provides fibular arrays with superior performance without a nitrogen atmosphere or vacuum conditions. For our formulation testing, the data shows that the two-step nGt method will give similar results to a production scale setup.

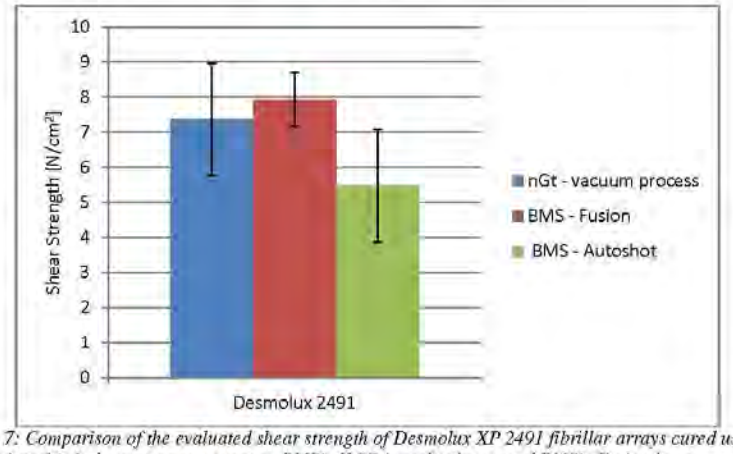

Figure 7: Comparison of the evaluated shear strength of Desmolux XP 2491 fibrillar arrays cured using nanoGriptech's in-house vacuum process, BMS's H&S Autoshot lamp, and BMS's Fusion lamp.

Figure 8 displays the shear strength of fibers produced from the four material formulations with the Autoshot and Fusion curing systems. There is no correlation to how a material will perform when not fully cured. As shown with 2491, shear strength will decrease when not fully cured, however the F74 and F76 samples show the opposite behavior. The studied monomers have different polymerization rates which causes variation in the degree of inhibition and amount of uncured material. This uncured material causes a decrease in bulk mechanical properties and a tacky layer on the mushroom tip surface. These properties have opposing effects on the shear performance of the fibers and without proper analysis of the degree of curing, these result are inconclusive. However, this data highlights the importance of achieving full cure in order to differentiate performance between sample formulations.

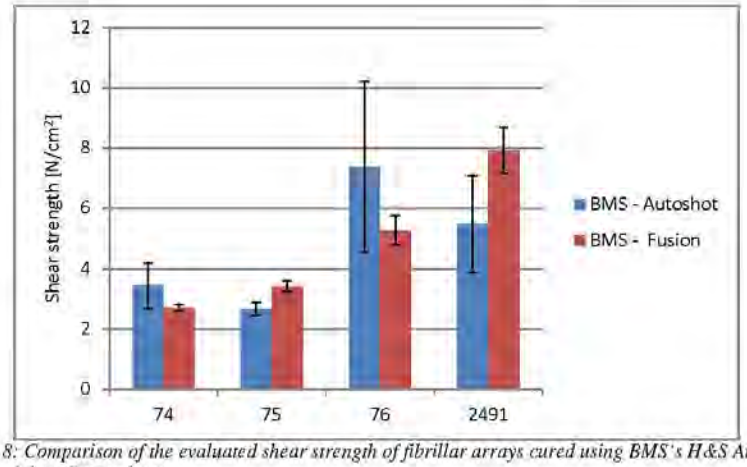

Figure 8: Comparison of the evaluated shear strength of fibrillar arrays cured using BMS's H&S Autoshot lamp and their Fusion lamp.

B.1.2.2 Studying the effect of material formulation on aging

Fibular arrays composed of Desmolux 2491 experience an aging effect that was noted by a substantial drop in adhesion performance when testing older manufactured materials. In order to quantify this behavior, new samples were tested before and after 21 days of aging on a windowsill. Samples were prepared using the Fusion system to ensure full curing of the material. Figure 9 displays the effective stiffness of the materials before and after aging using methods described in section 1.4.1.3. The stiffness of all materials decreases as the materials age. Desmolux 2491 exhibits a 50% loss of effective stiffness over the 21 day aging time. Formulation F76 displays the next largest loss at 43%. Since both monomers are essentially identical (one is *meth*acrylate versus acrylate), it leads us to believe that the isobornyl moiety plays a large role in the aging of 2491. Formulations F74 and F75 show a lower loss of material stiffness when aged. For example, the stiffness of F75 was only shown to decease by 6%. This finding is quite unexpected, especially since the F74 material contains an aromatic ring which is known to be more susceptible to aging and degradation than aliphatic structures such as the isobornyl moiety of 2491.

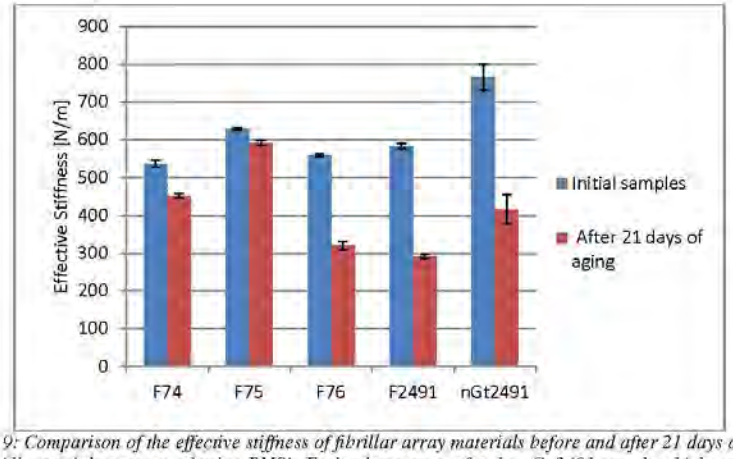

Figure 9: Comparison of the effective stiffness of fibrillar array materials before and after 21 days of aging. All materials were cured using BMS's Fusion lamp except for the nGt 2491 sample which was cured using nanoGriptech's inhouse H&S Autoshot lamp.

The samples were also tested to evaluate the effect of aging on the adhesion and shear performance of the fibrillar adhesives using shear characterization methods described in 1.4.1.1 and 1.4.1.3. This data is displayed in Figure 10 and 11. As the material ages, the pull-off force of the 2491 sample decreases by 47% which corresponds very well with the loss of stiffness of the material. This occurs with 2491 with both the nGt and Fusion curing processes. The methacrylate isobornyl monomer, F76, displays an increase in adhesion force with aging. This is due to the formation of a degraded tacky layer which acts similar to a pressure sensitive adhesive. We do not understand why this behavior occurs with F76 and not 2491 when both materials have the same isobornyl structure and loss of stiffness during aging. However, both materials failed shear testing and data was not collected because of a large amount of fiber damage during the first test. The adhesion and shear performance of the F74 and F75 materials showed very little change upon aging, attributed to the resiliance of material mechanical properties.

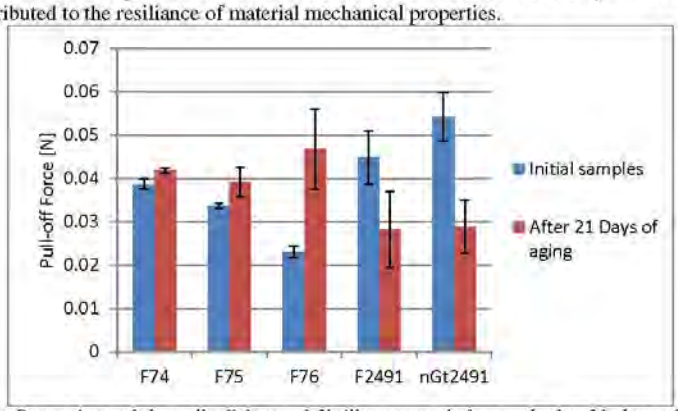

Figure 10: Comparison of the pull-off force of fibrillar arrays before and after 21 days of aging. All materials were cured using BMS's Fusion lamp except for the nGt2491 sample which was cured using nanoGriptech's inhouse H&S Autoshot lamp.

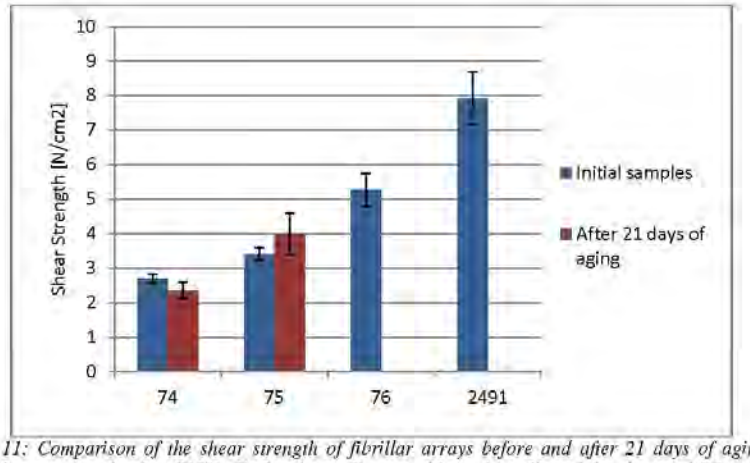

Figure 11: Comparison of the shear strength of fibrillar arrays before and after 21 days of aging. All materials were cured using BMS's Fusion lamp. Data could not be collected for the aged 76 and 2491 samples because they deteriorated after a single test cycle.

In contrast to the fully polyurethane BJB ST-1060 two-part curing system, the UV cured system has 20 wt-% of chemically different material in its formulation. Here, we have shown this addional material can have drastic effects on the overall properties.While 2491 initially performs the best of the UV materials in adhesion and shear tests, the aging effect severely limits the practical use of this material for our fibular adhesives. Therefore, our focus will be shifted to the F74 and F75 formulation because they have been shown to maintian stiffness and adhesive properties over time. However, fibrillar arrays made from F74 and F75 have a lower adhesion and shear performance than 2491. This can be attributed to a change in surface energy and mechanical properties of the material. Suprisingly, isobornyl acrylate (2491 comonomer) is relatively non polar compared to the F74 and F75 comonomers desipte having higher adhesion. Therefore, we believe that the difference in adhesion is due to the change of mechanical properties of the two systems. Future work will involve adjustment of the comonomer compostion of F74 and F75 to tune material properties in order to regain adhesion and shear properties comparable to the 2491 and BJB 1060 polyurethanes.

B.1.3. T3: Fabrication and use of mass production system

Fabricate the first generation mass-produced polymer micro/nano-fiber array samples with fabric backing using materials selected in Task 2 and design selected during Task 1. Achieve 10% of the length specified in S6.

B.1.3.1 Design and Fabrication of Mass Production System

Before this project begun, nanoGriptech had previously developed a proof-of-concept roller-to-roller mass production system for other project efforts. In this project term, work was conducted to redesign and manufacture a second generation mass production system more capable of reliably and repeatedly producing high quality samples to meet Under Armour's performance specifications.

A CAD rendering of the new design is illustrated in Figure 12. Some of the improvements, which are labeled in Figure 12, include:

- Replacing the DC gearmotor which drove the system with computer-controllable stepper motors (Figure 12A); This will allow the operator to more precisely control the belt speed for every fabrication run.

- Improving the overall alignment of system by:
  - Replacing the cantilevered single-bearing mounted shafts of the proof-of-concept system with shafts mounted by two bearings (one at either end) in the new system (Figure 12B);
  - Fabricating the system from outsourced CNC-machined aluminum plates (for example, Figure 12C) rather than in-house cut plywood and in-house machined aluminum;
  - Using an off-the-shelf tensioning system (Figure 12D) to apply uniform pressure at the molding interface pinch point;

  These changes will accelerate the setup time between tests by eliminating any alignment time. They will also ensure that the system does not fall out of alignment in the middle of a fabrication run.

- Inclusion of a separate release layer application/final product storage subsystem (Figure 12E); This will prevent any contamination of our produced samples by immediately applying a backing layer and storing them in a safe place for eventual characterization and/or transfer to Under Armour.

The overall system design is made up of several interconnected subsystems including the material dispensing subsystem (Figure 12F), the custom micropatterned belt mold (Figure 12G), the belt drive subsystem (Figure 12A), the UV-curing subsystem (Figure 12H), the backing layer storage subsystem (Figure 12I) and release layer application/final product storage subsystem (Figure 12E). Each of these subsystems is described in the sections below.

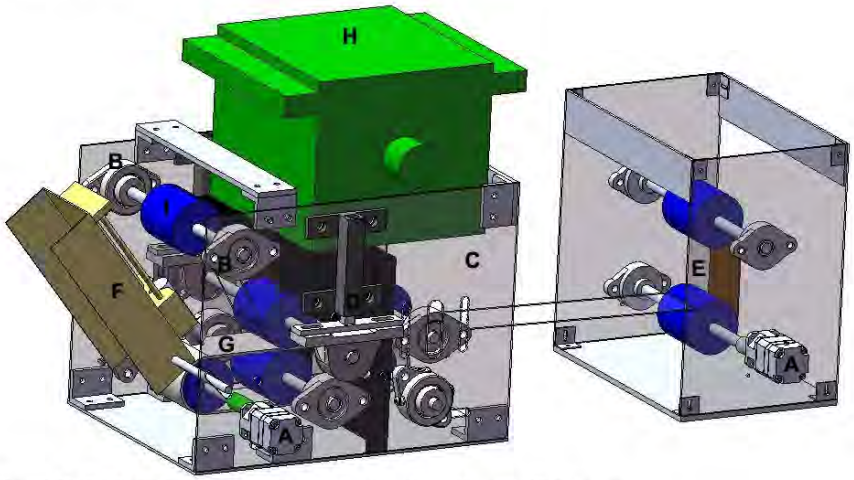

Figure 12: CAD rendering of the new mass production roller-to-roller system.

Material dispensing subsystem
nanoGriptech mixes and stores the UV cured material prior to use. The material is safe to use once mixed for some time, as long as it is not exposed to UV light. The material is manually loaded into a syringe and dispensed onto the custom micropatterned belt mold via a Multi-Phaser™ Model NE-500 syringe pump from New Era Pump Systems Inc. (illustrated in Figure 12F) to accurately dispense the BMS material onto the belt. The pump is mounted and the dispensing flow rate is controlled via custom built software for the pump hardware. The material is dispensed onto the front end of the belt mold that has the negative features of the fibrillar adhesive designed for this application.

Custom micropatterned belt mold
A custom belt mold that has the negative of the desired fiber geometry and spacing was manufactured for this prototyping effort and is illustrated in the CAD model in Figure 12G. The belt is made from silicone rubber (HS-II, Dow Corning) and is a conglomeration of multiple individual belt pieces that have been spliced together to create an approximately 24" long continuous loop. A similar belt was fabricated for previous efforts and the splicing methodology was described in previous reports issued to the PA NanoMaterials Commercialization Center.

For research conducted during this project term, a 40 µm diameter fiber geometry with mushroom tip shape was selected because it has shown good performance in previous lab scale testing. Once the UV-curable material is dispensed onto the belt, it passes through a roller set that creates a pinch point. The pinch point levels out the dispensed material, provides the pressure needed to fill the mold, and introduces the backing material onto the uncured product.

Belt drive subsystem
The BMS material is dispensed onto the micropatterned belt mold which is driven by a controllable stepper motor (Figure 12A, S9117C-S18GM018, SDP-SI). This motor controls the linear belt speed and can be adjusted using the motor software. Because of the scale of the mass production system, a belt speed ranging from 3-5 inches/minute is used. While relatively slow belt speed allows the BMS material to exposed to a sufficient amount UV light needed for curing.

UV curing subsystem
Following the roller pinch point, the micropatterned belt is exposed to UV light(Figure 12H, CureTek UVA 400, H&S Autoshot). This lamp provides the ultraviolet energy needed to initiate the photocuring reaction of the BMS material. An opaque barrier prevents the UV light from prematurely curing the BMS material before the backing layer is applied and mold properly filled.

Backing layer storage subsystem
The backing layer is stored on a separate subsystem (Figure 12I) and is continuously spooled to the molding pinch point where it is applied to the UV-curable BMS material. For this project term, a 0.002" thick Mylar(PET) film was used as the backing material, however, alternative backing materials such as UA textiles may be used in the same manner.

Release layer application/final product storage subsystem
A separate assembly illustrated in Figure 12E spools the finished micropatterned adhesive tape in contact with a protective release film. An identical controllable stepper motor (Figure 12A) drives this spooling process and will be synchronized with the belt drive speed. This module was not included during this project term due to the need for only small length samples in order to optimize other subsystems.

The overall system design was conducted using SolidWorks 2007. CNC machining of the aluminum frame was outsourced to emachineshop.com. The system was assembled in-house.

B.1.3.2 Production of samples using new system

A photographs of the system being operated during the mass-produced sample fabrication runs during this project term is shown in Figure 13 along with a picture of one of the first samples. As with any startup of a newly designed system, initial uses provide information on improvements for continued development. Such was the case in starting up the production process using the new equipment. The interactions between dispensing rate, belt speed, roller pressure, UV exposure time, backing material tension, material temperature, mold temperature, and post manufacturing UV exposure all generate differences in the quality of the fibular adhesive. Each of these variables has an upper and lower limit that creates a processing "space" where good product can be manufactured. The ideal setting for each of the input parameters is desired and should be based on some performance index. For instance, if shear force is the principal performance property for a specific application, it is desirable to know which manufacturing parameter has the largest effect on that property and to establish the ideal manufacturing setting (ie. pressure, speed, temperature, etc).

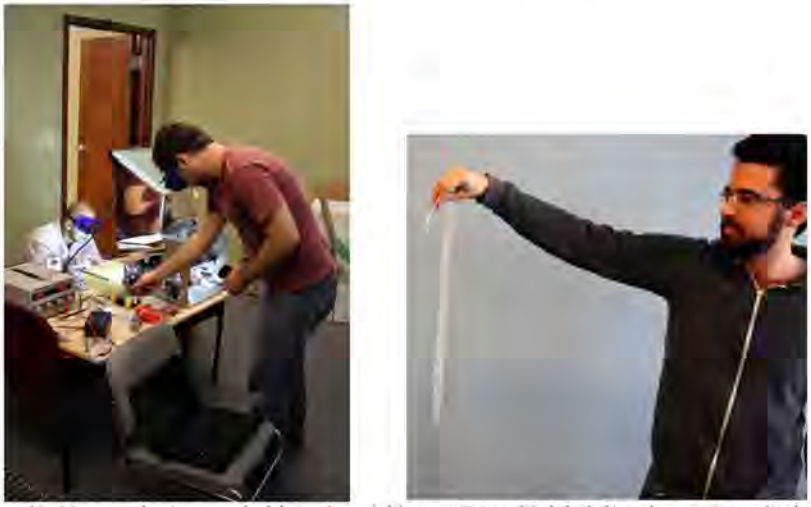

Figure 13: Mass-production sample fabrication trial in nanoGriptech's lab (left) and an engineer displays a length of one of the first samples produced using the new mass-production system (right).

B.1.4. T4: Sample Characterization

Characterize the first generation mass-produced polymer micro/nano-fiber array samples using setups described in 1.2.3. Achieve 40% of the full performance for S1, S2, S3, S4 and S5 in dry conditions and 25% of the full performance of S1, S2, S3, S4 and S5 in wet conditions.

B.1.4.1 Experimental methods

During this project term, we evaluated samples produced using small batch fabrication methods to assist in the material selection tasks outlined in T2 as well our mass-produced samples to

compare their performance with the specifications outlined in our statement of work. For our small batch samples, we evaluated shear force in contact with a glass substrate, adhesive force in contact with a glass hemisphere, and effective stiffness of a fiber array using a glass hemisphere. For our mass produced samples, we evaluated shear force in contact with closure and football substrates (S1 and S2), peel force in contact with closure substrates for single cycle testing (S3), durability testing (S4), and usability evaluation (S5).

Shear force measurement

All shear testing for this milestone was performed using nanoGriptech's manual shear force testing apparatus, shown in Figure 14. The 1 inch^2 substrate (either glass, closure, or leather removed from the exterior of a football (Figure 14A)) was mounted to a fixed surface. A similarly sized fabricated material sample (Figure 14B) was mounted to a small rigid plate, connected by a flexible thread to a load cell (Figure 14C, MLP-10, Transducer Techniques) which was fixed to a linear motorized stage (Figure 14D, MFA-CC, Newport Corporation). For every test, the material sample was carefully aligned and placed on top of the fixed substrate. A weight (Figure 14E) was placed on top of the fabricated sample, preloading the material into contact with the substrate. Custom software was then initiated to retract the stage away from substrate section while measuring the shear force in the y-direction at the interface of the two materials through changes in the load cell voltage.

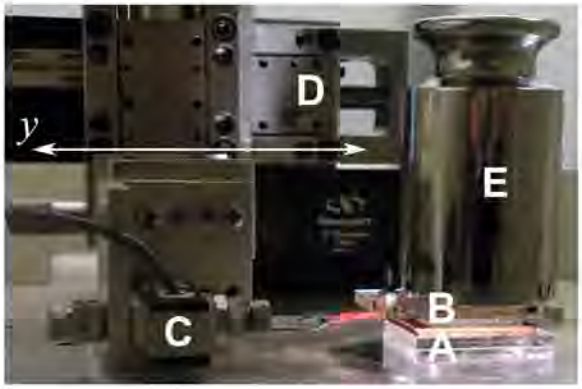

Figure 14: A photograph of the automated shear strength testing apparatus.

Experiments were performed at speeds 0.1 mm/s. The contact area (A) was approximately 1 inch^2 for all tests and to account for small deviations in the contact area of each sample, shear strength (σ_s) values were calculated from the shear force F_s according to $\sigma_s = F_s / A$. Reported results are the mean and the standard deviation of 5 tests per fabricated sample.

All tests were performed in "dry" conditions except for the specific evaluation of samples for S1 and S2 which were additionally tested in "wet" conditions. Dry conditions refer to conditions at room temperature. For experiments in "wet" conditions, the sample was soaked in water until saturated and then placed in position for testing.

Peel force, durability, and usability measurement

All of these specifications were evaluated using a custom automated peel strength characterization apparatus, which is illustrated in Figure 15. One feature of this setup is that it automatically presses the fiber sample back into contact with the test substrate after each test cycle, allowing for data collection for multiple cycles without a human operator. To collect data, the fiber array (Figure 15A) was first manually pressed into the substrate (Figure 15B). Then, using a computerized controller and data collection software, a linear stage (Figure 15C) is actuated to move a spring-loaded preloading roller mechanism (Figure 15D) toward the substrate. As the mechanism comes into contact with the substrate, the rubber roller rolls down along the length of the substrate, evenly pressing the fiber tips into contact until a predefined preload force, measured by a 10 lb load cell (Figure 15E), is reached. At this point, the stage is retracted away from the fiber/material interface, peeling the sample as it is withdrawn and uses the load cell to measure the peeling force required to separate the fibers from the substrate. At the end of the test cycle, the top of the fiber array remains in contact with the substrate, allowing the process to be repeated for any desired number of test cycles by iteratively preloading the rest of the fiber array back into the substrate and peeling it off.

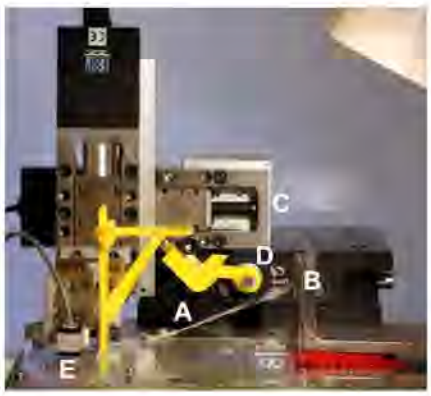

Figure 15: *A photograph of the automated peel strength repeatability testing apparatus.*

Adhesion force and effective stiffness measurement

A custom-built tensile adhesion testing apparatus (shown in Figure 16) was used to evaluate the adhesive force of some of the samples described for T2 in Section 1.2 in contact with a glass hemisphere. Developed material samples (Figure 16D) were fixed to an inverted optical microscope (TE200, Nikon) stage. A contacting surface, a 6 mm diameter glass hemisphere (Figure 16C) was fixed to the stem of a load cell (Figure 16B, GSO-50, Transducer Techniques), which was attached to a linear stage (Figure 16A, MFA-CC, Newport Corporation). Custom software was written to control the motion of the glass hemisphere while collecting data from the load cell. A hemisphere is used in these experiments because it represents a special type of non-at surface with a well-defined roughness, and is also immune to misalignment problems during testing. Furthermore, the transparent hemisphere and transparent cantilever to which it is attached allow for real-time magnified imaging of the fiber-hemisphere interface using the inverted microscope. This imaging can allow the user to visualize the material interaction during testing to help make sense of the complex fiber interactions occurring at the interface.

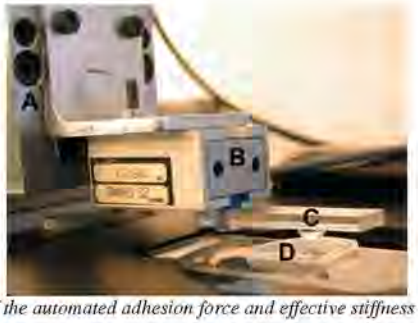

Figure 16: A photograph of the automated adhesion force and effective stiffness testing apparatus.

To measure the tensile adhesion of a sample in contact with the glass hemisphere, the sample was indented with the hemisphere at a rate of 0.01 mm/s until a pre-defined preload force of 20 mN was met. At this point, the hemisphere was retracted from the fiber array at the same rate until the tensile strength of the interface was exceeded and the hemisphere was no longer in contact with the sample. Fifteen data points were collected across three different areas (5 at each area) for each tested material.

To help determine whether the aging of the fibers had an effect on the material properties of the array, the effective stiffness (E_{eff}) of different fiber arrays were calculated from the measured preload force (F_p) and the preload indentation depth (d) according to the equation $E_{eff} = F_p / d$. Fifteen data points were collected across three different areas (5 at each area) for each tested material.

B.1.4.2 Results

Shear force results

The results of all shear force testing of developed mass-produced fibrillar samples are given in Table 2 along with the performance goals for this milestone. These results show that we met or exceeded our Milestone #2 goals for all shear strength measurements on football and closure substrates in both wet and dry conditions.

Test Substrate	Specification	Condition	Generation 1 Mass-Produced Sample Data	Milestone #2 Goal
Football (S1)	Shear Strength (N/cm^2)	Dry	1.2 ± 0.1	1.2
		Wet	0.9 ± 0.01	0.4
Closure (S2)	Shear Strength (N/cm^2)	Dry	5.6 ± 0.5	4.0
		Wet	3.2 ± 0.3	1.5

Table 2: Comparison of shear strength data of developed mass-produced fibrillar samples in contact with football and closure substrates and Milestone #2 goals for these applications.

Peel force, usability, and durability results

The results of peel force testing of developed mass-produced fibrillar samples on a closure substrate and our goals for this milestone are compared in Table 3. From these results, we can see that also we met or exceeded our Milestone #2 goals for both dry and wet peel strength measurements on closure substrates. Methods to additionally improve the shear and peel strengths of our tested interfaces will be attempted in future project terms. These methods will consist of including a softer backing layer for the football application, improving the mass-production manufacturing methods to produce fibers with larger tips, and improving the material properties of the bulk material used to form the fibrillar materials.

Test Substrate	Specification	Condition	Generation 1 Mass-Produced Sample Data	Milestone #2 Goal
Closure (S3)	Peel Strength (N/cm)	Dry	0.4 ± 0.06	0.2
		Wet	0.3 ± 0.02	0.08

Table 3: Comparison of peel strength data of developed mass-produced fibrillar samples in contact with a closure substrate and Milestone #2 goals.

Peel strength data was collected over 1,000 test cycles in dry conditions to determine to what extent the performance of the mass-produced samples decreases with repeated testing. Data for this testing is illustrated in Figure 17. From these results, we can see that the mass produced fibers retain approximately 65% of their initial peel force after 1000 cycles of peel testing over a 20 hour period, exceeding our goal for Milestone #2 of this project.

Under Armour defined a usability specification (S5) which states that our developed materials must not exceed a peel force of 0.5 kgf / inch (approximately 1.9 N/cm). We can see from the data in Table 3 that our peel strengths of 0.4 N/cm (dry) and 0.3 N/cm (wet) are not exceeding this value.

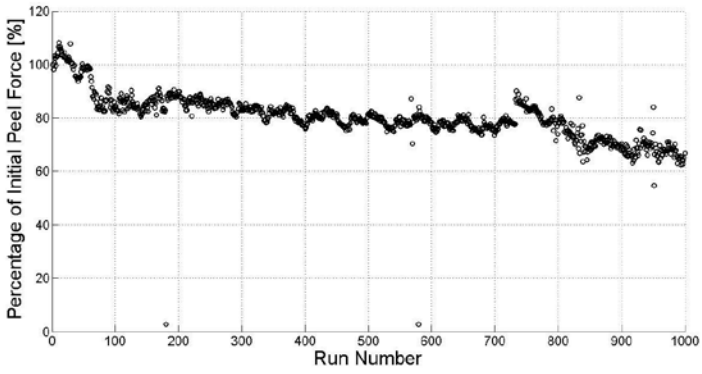

Figure 17: Peel data for a mass-produced microfiber array in contact with a closure substrate in dry conditions.

B.2. MILESTONE 3: TECHNICAL DEVELOPMENT

Develop the second-generation mass-manufactured fiber adhesives. The adhesives would have properties roughly 40% of the desired S1, S2, S3, S4 and S5 specifications given in Table 1 for wet conditions at room temperature.

B.2.1. T5 Fiber Adhesive Models

Compare the fiber characterization from Milestone 2 with the adhesive models and tune and improve the design models; develop a fiber adhesive design model for wet surfaces.

B.2.1.1 Using Milestone 2 model to guide fiber design

Developed Milestone 2 model examined the effect of fiber backing thickness and modulus on the shear performance of fibers in contact with the football surface. It was determined that softer, thicker backing would benefit shear performance the most by allowing more fibers to contact the football surface for an applied compressive load. Experimental effort was designed to estimate the effect of backing thickness and modulus, and determine how this idealized model applies to the experimental results. Two materials with different moduli were fabricated in various thicknesses as backing layer for the fiber adhesive and were tested for shear performance on a football surface. Fabrication techniques, experimental methods and results are discussed in Sections 2.3.3.

B.2.1.2 Wet surface adhesion based on previous modeling

As described in the Milestone #2 research, adhesive models developed at nanoGriptech are based on 1) The distribution of stress at the interface due to loading on the fiber, and 2) the adhesive properties of the interface between the fiber tip and the adhering surface. The design aims first to develop geometries which distribute the stress evenly at the fiber-adhering surface interface while secondly choosing material combinations with the highest possible intrinsic adhesive strengths and work of adhesions. Wet conditions mainly effect the interface, reducing both the intrinsic adhesive strength and work of adhesion. This reduction can be mitigated by the selection of the fiber material so that water is pushed away from the interface between the fiber tip and the adhering surface.

Another design option is suction. The 'mushroom tipped fibers' used for adhesive design are similar to suction cups. They do not utilize the suction cup effect in dry conditions because the intrinsic adhesive strength is usually much greater than atmospheric pressure. However, in wet conditions, the reduction in intrinsic adhesive strength leads to a more dominant suction effect. This effect is particularly visible when either one or both surfaces are hydrophobic.

Finally, both designs require selection of materials that are hydrophobic. Therefore, fiber design will continue to optimize the stress distribution at the tip while choosing hydrophobic materials for fiber fabrication to enhance wet performance.

B.2.2. T6: Material Compositions for Mass-Production
Select and develop the polymer fiber material compositions for second generation materials with Bayer MaterialScience (BMS) for wet surface closure applications.

In milestone 2, we showed that fibrillar adhesives comprised of UV-curable Desmolux XP 2491 (2491, Bayer MaterialScience) display a substantial decrease in shear strength and fiber stiffness over time. Formulation studies identified an alternative material which replaces the isobornyl methacrylate monomer of 2491 with a urethane bearing monomer, Genomer 1122. At the completion of Milestone 2, BMS supplied us with a gallon sample of this new material, which they called F-75. This section will detail our findings from our evaluation of F-75 and other results gathered while using batch processed UV cured polyurethanes.

B.2.2.1 Principles of UV curing on BMS polyurethane (PU) formulations

To understand the curing differences between F-75 and 2491, we must consider all variables of the system including the mold material, the UV curable resin, and the light source. Such a system, and the corresponding variables, is depicted in Figure 18. The UV light source may be of variable intensity, spectrum, and distance from the material to be cured. We can modify the UV-curable resin through changes in its formulation, for example by changing the photoinitiator concentration or monomer composition. The use of silicone rubber as the molding material is desired due to its ability to mold undercut, micron-sized features because of its demolding compliance. Therefore, the adjustable variables in the system are transparency and hardness of the silicone rubber mold. Silicone rubber is naturally soft due to the high flexibility of its polymer chains. In turn, this flexibility creates gaseous, free - volume in the material [1]. At room temperature and above, these molecules are dynamic, continuously permeating gas molecules.

Free radical polymerization, the mechanism of UV-curing of PU, is inhibited by oxygen. This means that polymer-forming free radicals can react with present oxygen molecules which "inhibit" further polymerization. Combined with the high oxygen permeability of silicone rubber, UV curing on silicone rubber surfaces can be quite complicated, and controlling this will be one challenge of scaling up nGt's roll-to-roll manufacturing process.

There are two regions in the fiber volume of polymerization to consider which will affect the adhesive performance of microfibers; the polymerization of the bulk material and the polymerization at the mold/material interface. The bulk material polymerization rate and properties are controlled by the number of polymerizing sites and the initiator efficiency and concentration. However, at the mold/UV material interface, during the curing process, the polymerization rate and final amount will be additionally affected by the quantity of oxygen at the interface and the rate of transfer of oxygen to the UV material surface from the mold rubber. Generally, the polymerization rate at the surface will be slower due to oxygen inhibition and polymerizing polymer chains will be terminated. This creates less crosslinking and fibers ultimately have softer or sticky tips.

The rate of monomer polymerization compared to the rate of oxygen permeation from the silicone mold will determine the surface material properties. For example, if the rate of polymerization is slower than the rate of oxygen permeation, less crosslinking will occur and this results in major inhibition at the fiber tips. This is the case for the curing of 2491 using our in-house Autoshot curing system, where full curing never occurs in the mold and residue is left on adhering surfaces. This can be compensated by increasing the polymerization rate via increased light intensity. This could be accomplished, for example, by using BMS's Fusion system. At nGt, the method to stop

major inhibition is to remove the partially crosslinked fiber array from the mold after one minute of UV exposure while in the mold and finishing the curing in an oxygen-free vacuum chamber.

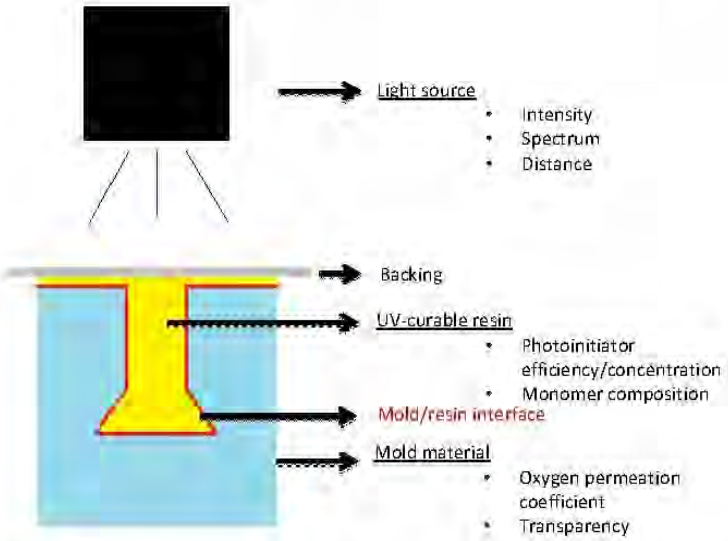

Figure 18: Schematic of UV-cured microfiber fabrication with listed variables that will effect curing.

Material formulation, such as monomer composition and photoinitiator concentration also play a role in the rate of polymerization. Increasing monomer polarity and adding hydrogen bonding sites have dramatic increase on the overall rate of the polymerization [2]. Genomer 1122, a butyl urethane acrylate monomer, is much more polar than the 2491 constituent, isobornyl methacrylate. A study of similar monomers found that the rate of polymerization of the urethane acrylate was approximately six times greater than monomers with isobornyl groups [3]. Because of this, we do not observe inhibition problems with F-75 materials as had with Desmolux 2491. In fact, the two stage vacuum curing process developed for 2491 is not necessary to get fully cured F-75 fibers. Furthermore, F-75 cures in the mold under our Autoshot curing system without the need to peel it from the mold to finish curing. In this case, the polymerization rate of the F-75 monomers is much faster than the permeation of oxygen through the silicone rubber mold using nGt's light source.

B.2.2.2 Experimental evaluation of different F-75 formulations

In the previous quarter, we also showed that the shear performance of F-75 was inferior to that of 2491. We believe that 2491 material had a combination of properties that lead to the better performance over F-75. Firstly, the bulk modulus of 2491 is greater than that of F-75 as shown by effective fiber stiffness in the Milestone 2 research above. Secondly, due the slower polymerization rate, the surfaces of the tips were less crosslinked and much softer.

The effect of the thin soft tip coating and fiber modulus can be explained by referring to the fiber shear model described in the previous milestone's research efforts. The stress at the fiber tip due to shear loading has two main components, stress due to the applied moment and stress due to uniaxial tension. The moment stress is the first and the uniaxial tension effect is the second term on the right of the equation below.

$$\sigma_{zz}(m) = B_1 \frac{M_a}{I} + B_2 \frac{P_z}{A},$$

It is assumed that when the total stress (the left side of the equation above) reaches the intrinsic adhesive strength, fiber detaches from the adhering surface. The soft layer at the fiber tip is very thin and therefore we can assume that it changes the interfacial properties rather than the bulk properties. This thin layer at the tip acts as a tacky adhesive layer which increases the effective adhesive strength, causing the fiber to withstand greater stress and shear load before detachment. The effect of modulus is less intuitive and needs some explanation. When shear load is applied to the fiber, it bends sideways. In addition, due to the fixed-fixed boundary conditions on the fiber, it has to stretch as it bends. It is the stretching that causes uniaxial tension. Therefore, if the fiber is stiffer, it will bend less, and the stress due to stretching (the second term in the equation) will be negligible. Therefore, stiffer fibers also enhance shear performance.

We wanted to produce a fibrillar structure using F-75 with similar properties as our 2491 fibers, with similarly high adhesive and shear strengths. Additionally, we want to identify the curing conditions and formulation that would result in the small degree of inhibition in the F-75 fibers to yield fibers with softer tips. During this project term, we mixed different F-75 formulations where the photoinitiator concentration varied between 0.5-3 wt-%. We evaluated the formulations for the degree of observable inhibition (evaluated by whether residue was left on a glass substrate after pushing a cured material in contact with it), and for the shear strength, effective stiffness and peel strengths of fibrillar samples measured on glass substrates. All materials were evaluated using the same experimental setups described in our Milestone #2 research above.

Inhibition and shear strength of F-75 formulations

At inhibition-favorable conditions, e.g. full curing in the silicone mold and no vacuum, we still could not force inhibition with 3 wt-% photoinitiator. Therefore, we decided to decrease the amount of photoinitiator in the F-75 formulation. Even with photoinitiator concentrations as low as 0.5 wt-%, we observed no inhibition when cured in-mold for eight minutes in atmosphere.

Figure 19 displays the shear strength of F-75 fibers on a glass surface cured with initiator concentrations ranging from 0.5-3 wt-%. The shear performance increases from 3.5 to 5.2 N/cm^2 when decreasing photoinitiator from 2 to 2.5 wt-%. Further decrease in the amount of photoinitiator produces a corresponding decrease in shear strength to 3.4 N/cm^2 at 0.5 wt-%. Interestingly, the 3 and 0.5 wt-% photoinitiator samples have identical shear performance. These shear tests were viewed under the microscope and images of these samples prior to failure are shown in Figure 20. We can see that the 0.5 wt-% initiator sample shows roughly 2.5-3 times more elongation at similar failure shear forces. This suggests that a drop in initiator concentration also lowers the bulk modulus of the material.

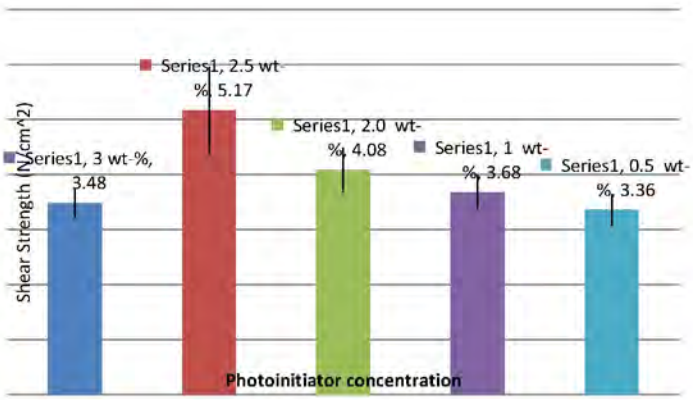

Figure 19: Shear strength of F-75 microfibers cured with photoinitiator concentrations ranging from 3-0.5 wt-% on a glass surface.

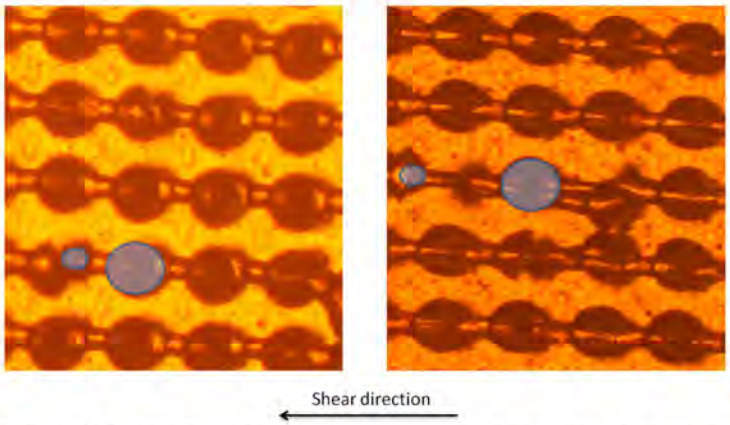

Figure 20: Image of 3 wt-% (left) and 0.5 wt-% photoinitiator (right) F-75 samples taken just before shear failure. Larger highlighted area represents fiber tip and the smaller area corresponds to the tip's fiber base.

In this quarter, we also produced several F-75 fibrillar samples using BMS's Fusion system. A sample was run with 3 wt-% photoinitiator using a clear mold made from silicon rubber (27T, Smooth-On). Only 1 N/cm^2 of shear strength was measured in shear testing this material. The gallium bulb in the Fusion system enables for a very fast polymerization. While this was essential for 2491, which polymerizes very slowly, in combination with the fuller exposure due to the clear mold, it proved to be too fast for F-75. While this is favorable to achieve the maximum bulk density, it also stiffens the tip surface, which we suspect is why it performed so poorly.

Effective stiffness of F-75 formulations

Figure 21 shows the effective fiber stiffness each of the formulations. The fibers stiffness test measures the bulk material properties. Indeed the bulk modulus of the material decreases in correlation with a reduction in photoinitiator from 3-0.5 wt-% by about 10% due to less crosslinking of the material. If we could measure the properties of the inhibited material on the tip surfaces, we would see the same modulus trend, e.g. a decrease in modulus of the tip surface with a decrease in photoinitiator. However, the overall values would be smaller than that of the bulk modulus at each photoinitiator concentration due to oxygen inhibition.

At failure, both the 3 and 0.5 wt-% samples are under a very similar loading. Under this loading, the 0.5% sample deflects much greater, and because of this, the peeling force on each tip is much greater when compared to the 3 wt-% sample. To resist peeling and failure of the 0.5 wt-% samples, the adhesion of the tip to that surface must be greater. The stiffness of the 3 wt-% photoinitiator causes less deflection at the same force, therefore relying less on the peel resistance of the tip surface. The softer tip of the 0.5 wt-% sample compensates for the loss of bulk modulus and performs similarly to the 3 wt-% sample where the higher bulk modulus compensates for the harder tip surface.

Furthermore, we feel that it is a combination of the stiffness of the bulk material and the softer tip surface of the 2.5 wt-% photoinitiator sample result in the best shear performance we have seen with the F-75 formulation. Recall that the previous quarter's research described above gave a shear value for F-75 to be 3.5 N/cm^2, so we have improved upon that value by approximately 40% through the modification to the photoinitiator concentration.

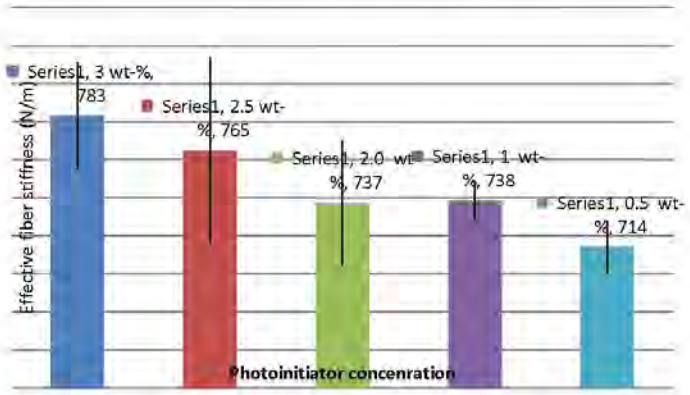

Figure 21: Effective stiffness of F-75 microfibers cured with photoinitiator concentrations ranging from 3-0.5 wt-%. This was tested using a glass hemisphere indentation test.

Peel strength of F-75 formulations

In Figure 22, the peel strength of F-75 cured with various amounts of photoinitiator is displayed. With decreasing photo initiator the peel strength of the materials increases from 0.52 N/cm to 0.72 N/cm on a glass substrate. We hypothesize that with less photoinitiator, the tip surface is softer, which allows for better adhesion to the substrate and greater peel strength.

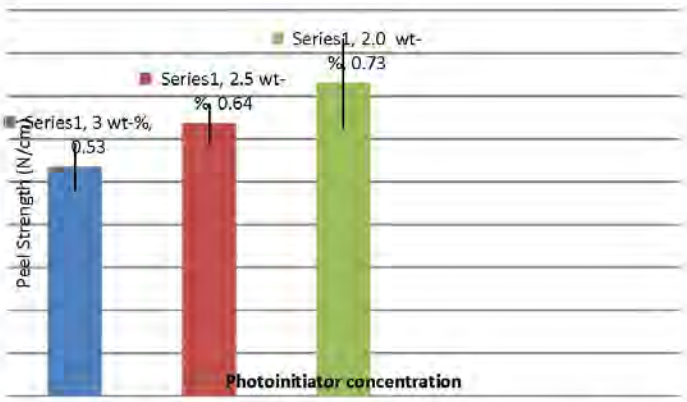

Figure 22: Peel strength of F-75 microfibers cured with photoinitiator concentrations ranging from 3-0.5 wt-% on a glass surface.

The absence of the 1 wt-% and 0.5 wt-% samples addresses a practical concern with the F-75 material. Compared to 2491, F-75 does not adhere to mylar very well and this effect seemed to get worse as the material got softer. Therefore, long enough samples of uniform thickness of the 1 and 0.5 wt-% samples could not be produced for peel testing.

B.2.2.3 Implications of formulation studies

This is an important set of findings because it shows that by only adjusting the curing conditions, with no change in the chemical composition of the monomers, adhesive properties of the fibers can be significantly changed. With every material composition, there will be a window of curing conditions that need to be met in order to fabricate a good fibrillar adhesive. Obtaining this knowledge of curing of UV curing on silicone surfaces is what nGt's can leverage against competitors. A hypothetical graph is given in Figure 23, where shear strength is plotted as a function of the tip surface stiffness. An actual graph is not given because we have not identified the right combination of formulation and curing conditions that can fit all areas of the curve.

As described above, the tip surface stiffness is a function of the ratio between the curing rate (or polymerization rate), and the rate of oxygen through the silicone mold to the tip surface. The larger the ratio (fast curing rates) the harder the tip will be. This is best represented by the F-75, clear mold, Fusion cured sample which only displayed a shear strength of 1 N/cm^2. This is displayed hypothetically as A on Figure 23. While keeping the modulus of the bulk material constant and forming a softer tip by altering the curing conditions, a better shear performance should be expected. For instance, F-75 curing in an opaque mold in our Autoshot system decreases the light intensity of the system, thus decreasing the curing rate. Doing this, the shear performance of the fibrillar adhesive increases to 3.5 N/cm^2. At some point the polymerization rate will be slowed significantly to the point where permeation of oxygen from the mold will inhibit the curing to the extent where residue is left on the adhering surface. This defines point C and D on the curve. In the past, we have noted that the degree of residue can vary considerably with different formulations and curing conditions. While F-75 shows no inhibition within the limits of our curing because of its fast rate, 2491, with a much slower curing rate, is in the B-D regime on the curve. We do not know on what side of the maximum shear strength value will lie,

or, stating it physically, will a sticky, residue leaving tip be stronger than a very soft, non-residue leaving tip.

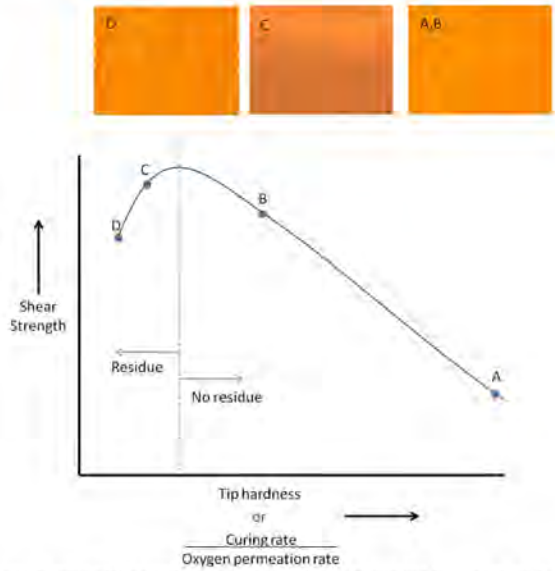

Figure 23: Hypothetical curve of displaying the effect of fiber tip surface hardness on the shear strength of UV-cured fibrillar adhesives.

Due to its softer tip (slower curing rate) and higher modulus, 2491 has shown superior shear strength. However, this analysis leads us to believe that there is a fine curing window that will get F-75 into the B-D regime and improve overall properties. Combined with a stiffening of the bulk modulus, we feel that F-75 can compete with 2491.

B.2.3. T7: Mass Produced Sample Fabrication

Fabricate the second-generation mass-produced polymer micro/nano-fiber array samples with fabric backing in foot-long areas using materials selected in Task 2 and design selected during Task 1. Achieve 20% of the length specified in S6.

B.2.3.1 Modifications to the mass production system to improve output

In order to produce an excellent product that meets our market and client needs, there were four distinct areas that could be varied in the roll to roll mass production system: (1) modifications to increase the speed of the system, thus improving output, (2) modifications to improve the yield of the system, thus decreasing the amount of waste per unit length (3) modifications to increase the amount of output per linear length of belt travel, thus increasing output and (4) modifications to improve the functional performance of the tape

Modifications to the roll to roll system to increase the speed of the system

The current iteration of the roll to roll mass production system is Version 2. The team is

continuously making small modifications to the system which are deviations to the original system design, in order to test the effect of system and parameter changes on the quality of the tape product being produced. The objective is to capture all of the learnings with this current system and use them to improve the design and function of future iterations of the system and to dictate an optimal design for an eventual pilot or commercial scale production facility.

The first change made to the roll to roll system to improve the speed was to modify the drive rollers. In the current configuration, a silicone belt mold is manufactured with a continuous pattern of the fibrillar microfeatures. The silicone material is backed with a fabric backing to provide strength in tension. Once made, the belt mold is mounted on hard plastic rollers. The rollers can be spaced at varying distances from each other, providing the ability to increase the tension on the belt mold. Belt tension is desirable, to an extent, because it assists in providing friction to the mold to keep it moving and also helps maintain the feature geometry in the mold. If the belt tension is increased too high, it causes distortions in the feature shape being molded (the microfibrillar features begin to exhibit an elliptical shape, rather than the target round shape. In some cases, the belt tension must be kept lower in order to maintain the molded fibrillar shape. When the belt tension is too small in magnitude, the belt drive roller began to slip on the mold due to a lack of friction between the roller and the belt. This challenge was easily solved by covering the drive roller with sandpaper. This created enough friction between the roller and the mold to allow the belt tension to be reduced.

This seemingly inconsequential detail provides an important insight for the design of the next system. Any drive system on a scaled up roll to roll continuous line must have a robust connection between the drive motor, drive shafts, rollers, and belt mold. The nanoGriptech team has noted the desire to have the mold mechanically lock into the rollers to eliminate the need to rely on friction to make the system turn. When there is slippage between the belt and the drive rollers, UV-curable material that is already in the mold and in contact with the mylar backing material also experiences a slippage at the interface, which ruins the connection between the fibrillar material and the backing material and results in an unusable product.

The second change to the roll to roll system was to replace the UV bulb for the material curing system. The UV exposure region on the manufacturing line plays a large part in determining the speed of the manufacturing line, and the age of the bulb has an impact on the intensity of the light provided by the lamp. We are learning that the exposure time and amount of UV energy received in the UV cured materials while in the roll to roll system plays a critical aspect in final performance of the sample materials. The exposure time in the roll to roll system is determined by a combination of the exposure length on the manufacturing line and the line speed. These collectively determine how much UV exposure the Bayer Desmolux XP 2491 material receives prior to being removed from the belt mold. In our previous quarter research we outlined comparisons of the evaluated shear strength of the Bayer Desmolux XP 2491 fibrillar arrays using several different UV curing sources. That section discussed the importance of proper curing and how different curing systems produce variations in product performance. The previous bulb had approximately 450 use hours. The light intensity/output, processing line speed, mold material, fibrillar raw material and initiator compositions and ratios are all intricately related.

Modifications to the roll to roll system to increase the yield of the product

For the roll to roll manufacturing process, yield is defined as the ratio of useful and good product produced verses the total length of tape coming from the manufacturing line. Events such as incomplete mold filling, incorrect or excessive curing, or smearing (where the mylar backing becomes detached from the UV cure materials on the mold) decrease the yield.

The first change made to the roll to roll system to increase the yield was to modify the locations of the pinch points and contact rollers. Figure 24 below illustrates a schematic of the sideview of the roll to roll system. The original design used a matching set of rollers, one on top and one on the bottom of the belt mold, that compress the mylar and the dispensed Bayer 2491 material to create a pinch point where the mold is filled. This configuration successfully fills the mold, but also creates a processing challenge down line after the rollers. A consistent challenge to manufacturing successful products is ensuring that the mylar film stay in contact with belt mold immediately after coming out of the pinch rollers. With the "over/under" configuration of pinch point rollers, the film would always curl up away from the belt mold surface after it passed through the pinch point and had become filled, thus breaking the required contact with the Bayer 2491 material. When the backing film is not in contact with the fiber materials during the curing process, the fiber material cures while in the belt mold and does not stick to the backing. This necessitates stopping the manufacturing line, cleaning the belt mold, and restarting the process. This occurrence also limited the length of a continuous piece of tape that could be manufactured. It is theorized that the reason for this phenomena is that the silicon mold is compressed in the rollers and re-expands after coming out of the rollers. This re-expansion occurs only with the softer mold material and not the rigid mylar backing. Once the belt mold is no longer under compression and expands back to original shape, the mylar backing becomes detached.

In order to remedy this situation, the nanoGriptech team investigated changing the location of the pinch point and forcing the mold to deform without undergoing a compression/elongation event, rather than having the mylar material deform after going through the rollers. Figure 25 shows the current configuration of the rollers. Using this setup, very consistent tape product has been manufactured. Following this modification, the team was able to manufacture a continuous piece of tape that was 11 feet long (44% of specification S6). And this length was only stopped due to a lack of prepared resin.

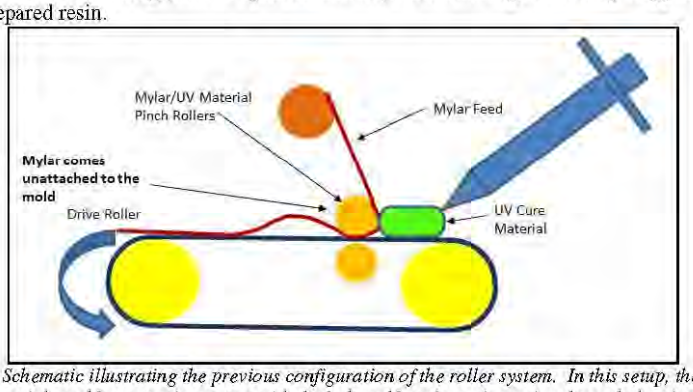

Figure 24: Schematic illustrating the previous configuration of the roller system. In this setup, the mylar backing material would not stay in contact with the belt mold surface after going through the pinch rollers.

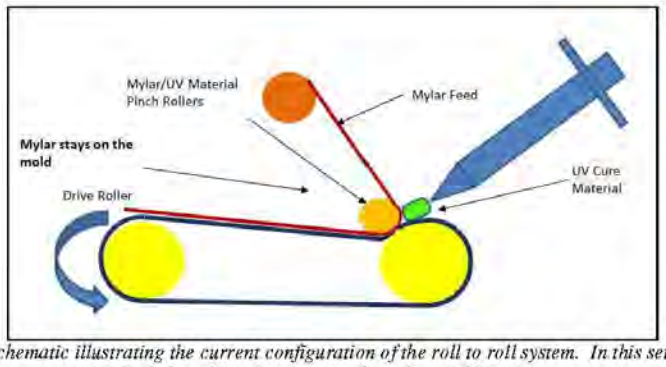

Figure 25: Schematic illustrating the current configuration of the roll to roll system. In this setup, the mylar stays in contact with the belt mold and an improved product yield is given.

The second change made to the roll to roll system to increase the yield was to study the use of a simulated dispensing blade for the system. These are commonly used in the printing industry to assist in spreading ink across a surface that is being coated. For our studies, a simulated dispersing blade was manually utilized. Figure 26 below show the variation in filling patterns when a blade is not used and not used. The bright white portion on the right side of the image has fibers that are completely filled, and the left side of the tape is missing fibers.

Figure 26: A piece of tape from roll to roll system showing fiber filling variations

The blade equally distributes the material across the surface area and essentially provides a pre-filling mechanism for the rollers. The mold filling is finished as the mylar film and fiber material are compressed into the mold at the compression rollers. The effectiveness of the blade is evident both at the micro and macro-level.

Modifications to the roll to roll system to increase the amount of output per linear length of belt travel

The manufacturing processing studies done this quarter have fairly consistently shown that for the high viscosity UV cured materials being used, slower manufacturing line speeds produce better results. In order to manufacture a cost effective product, as fast a line speed as possible is needed. One way to increase the output of tape product per given time is to extend the width of the mold. New silicone fiber masters with a larger starting area (2.5" x 2.5") have been manufactured in this quarter. These are described in Section 2.3.2, and will be critical in producing larger molds for improved product output.

Modifications to the roll to roll system to increase the performance of the final product

The most significant change has been in the redesign of the molds and the fiber masters used to create the molds. Previously, the fibrillar adhesive geometry of the molds was created utilizing the standard sequence of production.

For producing the new mold, a similar process to the original was used with one important variation. Master fibers were molded using a thermoplastic SEBS material. The tips on the thermoplastic fibers took the dimensions of the mold they were created in. Once the fibers were removed from the mold, they were placed on a heated plate and allowed to melt briefly.
In the original process, the final belt mold fibrillar tip size matches the tips that are created during the dipping process. From the previous quarter's research, it was shown that the master fibers used to create the belt mold had an average tip diameter of 95.5 ±1.9 µm. The mass-produced fiber arrays from this belt mold had an average tip diameter of 91.5 ±1.9 µm. Therefore, the previous set up for the manufacturing process was able to achieve 96% of the original tip size. In this quarter, molds were made that had tip sizes greater than 100 µm. This is an important development because as tip size increases, surface area coverage increases, and functional performance of the tapes can increase. In addition to increasing the tip size of the molds, two variations in mold design were investigated. These new molds can be seen in Figure 27. One of the early on problems the team had was getting mold to fill. In order to locally increase the pressure at the nip roller at the point of filling, a plateau type mold was developed. The thought behind this mold was to decrease the contact area of the mold with the rollers, thus increasing the compression pressure. The second mold developed was to make a mold with a clear silicone, and to use 2 strips of black support backing rather than one continuous piece. The thought behind the clear mold was to allow the UV material to be cured through the bottom to enable a fabric backing to be used for the tape material.

Figure 27: Two new belts fabricated during this project period. A multi-level silicone rubber mold (left) and a transparent silicone rubber mold (right)

B.2.3.2 New belt mold fabrication

To identify trends on the processing line, a small scale design of experiments was run to determine cause/effect relationships between manufacturing inputs and performance outputs. For the case of the initial study, the studied variable was final average tip diameter and percent of area

coverage with complete fibers. In future work, the studied variable will be expanded to include shear strength and peel strength. To run the study, the following inputs were varied for the Bayer 2491 material:

- Heated material vs. unheated material at the time of mold filling
- Four different line speeds (1 in/min, 2 in/min, 4 in/min, 8 in/min)

The trends showed that the tip diameter is larger for slower fill speeds, and that material that is heated (to lower the viscosity to assist in mold filling) also provides better filling patterns. These trends are shown in Figures 28 and 29.

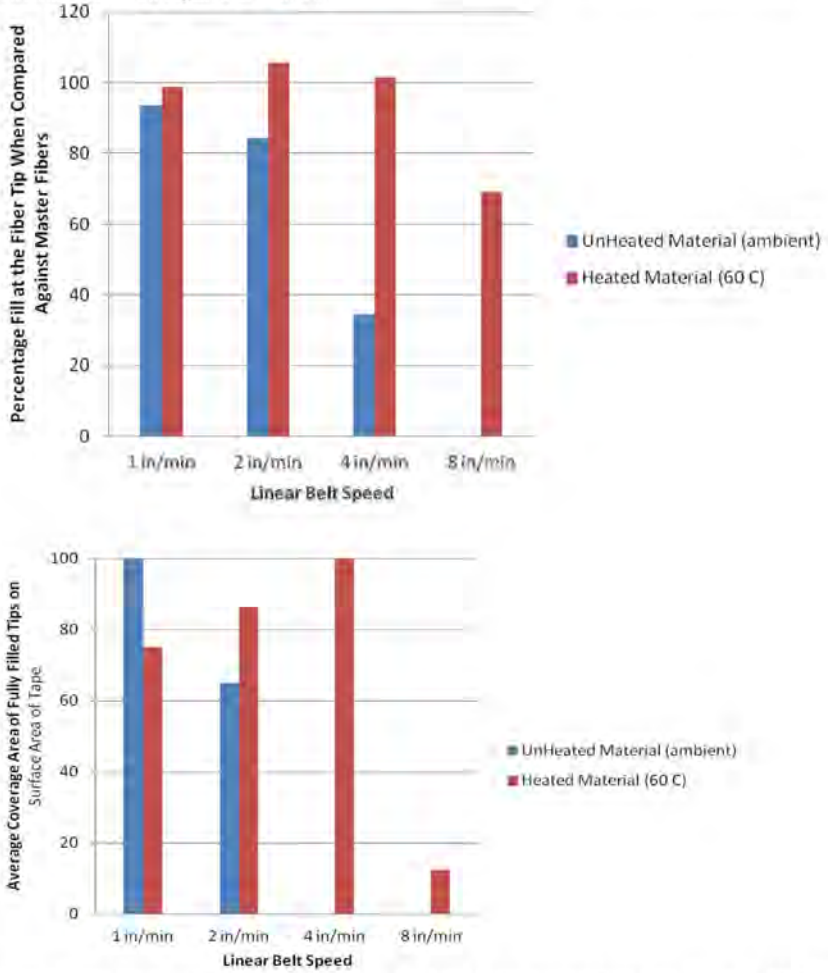

Figure 28: Resulting average percent fill of the tip (top) and average percentage area coverage of full tips (bottom) for different production speeds and heating conditions. The measurements were taken in four different spots from tape molded on the same square inch section of the mold each time and averaged.

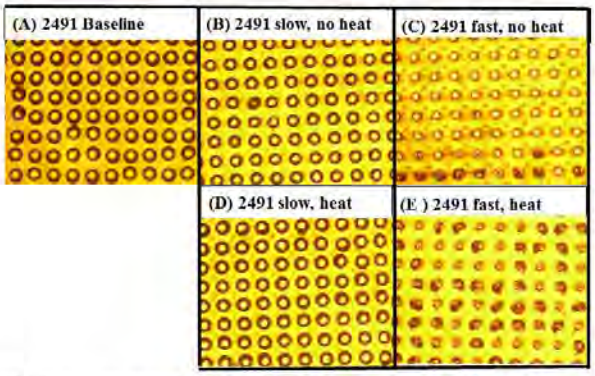

Figure 29: Optical microscopy images of the resulting tapes produced for different line speeds and heating conditions on the mass-production line (B-E) when compared to a baseline sample produced using manual small batch methods (A). The slow speed is made on the belt mold with a speed of 1 inch/minute, and the fast speed is 8 inches/minute.

B.2.4. T8: Sample Characterization

Characterize the second-generation mass-produced polymer micro/nano-fiber array samples using setups described in 1.2.3. Achieve 60% of the full performance for S1, S2, S3, S4 and S5 in dry conditions and 40% of the full performance of S1, S2, S3, S4 and S5 in wet conditions.

Shear force results

The results of all shear force testing of developed mass-produced fibrillar samples are given in Table 4 along with the performance goals for this milestone. These results show that we exceeded our Milestone #3 goals for all shear closure substrates in both wet and dry conditions as well as for wet shear strength in contact with a football with mass-produced materials. In fact, we have achieved our final target performance

Test Substrate	Specification	Condition	Generation 2 Mass-Produced Sample Data	Milestone #3 Goal
Football (S1)	Shear Strength (N/cm^2)	Dry	1.1 ± 0.05	1.8
		Wet	1.0 ± 0.03	0.6
Closure (S2)	Shear Strength (N/cm^2)	Dry	12.7 ± 0.6	6.0
		Wet	6.6 ± 1.6	2.4

Table 4: Comparison of shear strength data of developed mass-produced fibrillar samples in contact with football and closure substrates and Milestone #2 goals for these applications.

Peel force, usability, and durability results

The results of peel force testing of developed mass-produced fibrillar samples on a closure substrate and our goals for this milestone are compared in Table 5. From these results, we can see that also we met or exceeded our Milestone #3 goals for both dry and wet peel strength measurements on closure substrates. Note that for both dry and wet samples, the 2491 fibers delaminated from the mylar backing, and that the reported value of 0.7 N/cm is the minimum peel value for these materials.

Test Substrate	Specification	Condition	Generation 2 Mass-Produced Sample Data	Milestone #3 Goal
Closure (S3)	Peel Strength (N/cm)	Dry	0.7 ± 0.1	0.3
		Wet	0.7	0.12

Table 5: Comparison of peel strength data of developed mass-produced fibrillar samples in contact with a closure substrate and Milestone #2 goals.

Under Armour defined a usability specification (S5) which states that our developed materials must not exceed a peel force of 0.5 kgf / inch (approximately 1.9 N/cm). We can see from the data in Table 3 that our peel strengths of 0.7 N/cm (dry and wet) are not exceeding this value.

B.3. MILESTONE 4: TECHNICAL DEVELOPMENT
Produce the third-generation mass-produced fiber adhesives, using the improved UV curable polyurethane products, for dry and wet conditions at room temperature. The adhesives would achieve roughly 80% of the desired S1, S2, S3, and S4 specifications given in Table 1 in dry conditions and roughly 70% of the desired specifications in wet conditions.

B.3.1. T9 Fiber Adhesive Models
Tune, improve and complete the wet fiber array design models using the performance characterization results from Milestone #3.

Fiber adhesive and friction models were completed in the first two quarters of this project. No additional modeling was needed based on the characterization results from Milestone #3.

B.3.2. T10: Material Processing and Compositions for Mass-Production
Develop the third generation, polymeric fiber material compositions with BMS to achieve 80% of the full performance for S1, S2, S3, S4 and S5 in dry conditions and 70% of the full performance of S1, S2, S3, S4 and S5 in wet conditions as listed in Table 1.

B.3.2.1 Material processing optimization for mass production

In Quarter 2, the theoretical groundwork of the relationship between curing conditions and fibrillar adhesive properties was laid. This focused on the idea that at the mold/material interface, oxygen from the silicone would diffuse into the UV curing material causing less reaction or "inhibition" on the surface of the formed microfibers. By changing the curing conditions of the same material formulation, e.g. light spectrum, intensity, or exposure time, this surface can be altered from a hardness ranging from that of the bulk material to a pressure sensitive, residue

leaving adhesive. Here, we will provide data that tests this hypothesis and optimizes the curing conditions that are applied to our high throughput R2R system.

Clear Molds

The use of clear molds is a pivotal finding for our R2R manufacturing. By using a clear or translucent mold, the whole fiber area receives direct light from the UV source. In contrast, the tip area of opaque molds receives no direct light (Figure 30). Complete curing is limited by these areas of low light intensity using opaque molds. This is why using our old standard curing distances and times, full cure of the material could not be achieved without vacuum conditions. In other words, the rate of oxygen permeation from the silicone to the mold surface was comparable to the rate of curing at these tips edges resulting in extensive, residue-leaving inhibition.

Using clear molds, this effect is mitigated. By using proper curing times and intensities we can create fibrillar adhesives without the use of inert atmosphere or vacuum conditions, which will make scale-up of our continuous R2R manufacturing processes more affordable.

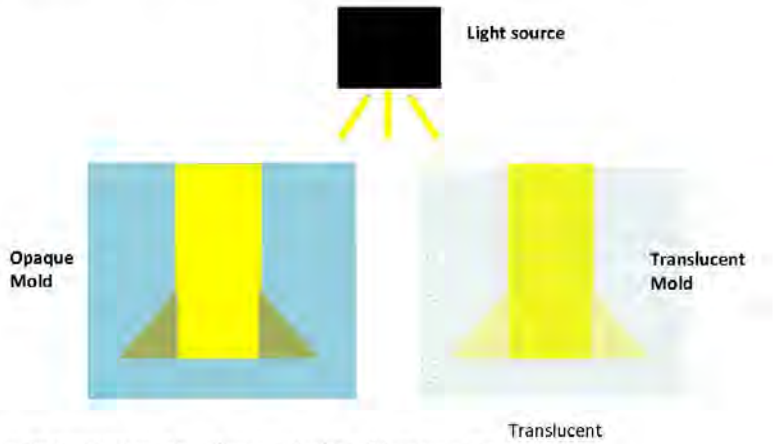

Figure 30: Comparison of translucent and solid mold exposure areas.

Lamp distance study

The first study performed this quarter was to determine the effect of the lamp distance from the curing surface on the resulting cured Desmolux 2491 (Bayer MaterialScience) properties. Since the nGt UV Light Source (UVA400, H&S Autoshot) voltage cannot be changed, the distance from the lamp to the sample was used as an artificial means to adjust the light intensity. All other variables were left constant, such as a photoinitiator concentration of 3.5 wt-% and translucent, new molds were used to produce each sample. The distance of the sample from the light was varied from 5 to 45 inches. Curing times were estimated from prior protocols and were 4 minutes from <15 inches from the light, 8 minutes at 15-30 inches, and 20 minutes when >30 inches from the light. The shear performance data from these samples is shown in Figure 31.

Notably, all samples, cured at their respective distances and times, displayed no residue leaving inhibition. However, their shear performances have a large variation. By moving from 10 inches to 25 inches from the lamp, the shear strength of the fibrillar adhesive was shown to increase from approximately 2 to 12 N/cm^2. Shear performance of UV-cured microfiber adhesives is dependent on the bulk modulus of the material as well as the hardness of the surfaces. Assuming that the bulk modulus of each sample was the same, it is the extent of inhibition of the tip surface that leads to this remarkable change in shear strength.

Samples closest to the light receive a higher light intensity and therefore have higher rates of cure. This is favorable for less inhibition and enables the UV curable material at the mold interface to more fully cure. More curing results in a stiffer tip surface which limits the ability to conform to micro/nanoscale surface roughnesses. Furthermore, it will reduce the peel resistance of the tip surface when the microfiber stalk deforms in shear. Therefore, the sample cured 10 inches from the lamp had a very low shear value of 2 N/cm^2. This will be referred to "over-curing" of the fibrillar adhesive.

Moving further from the light decreases the light intensity and the curing rate. The reduction of the curing rate allows further oxygen inhibition at the mold/material interface resulting in softer, more compliant tip surfaces. This increases the peel resistance of the tips under shear loading and greatly enhances the shear performance. For example, increasing the curing height from 10 inches to 18.5 inches increases shear performance by 350% to 7 N/cm^2. Shear performance peaks at 11 N/cm^2 curing for 8 minutes at a distance 25 inches from the light and seems to reach an asymptote with a further increase in distance.

The closest sample to the light (5 inches) does not fit the expected trend. We feel this is due to the large increase in temperature as the sample gets closer to the light. The effect of temperature will be discussed later.

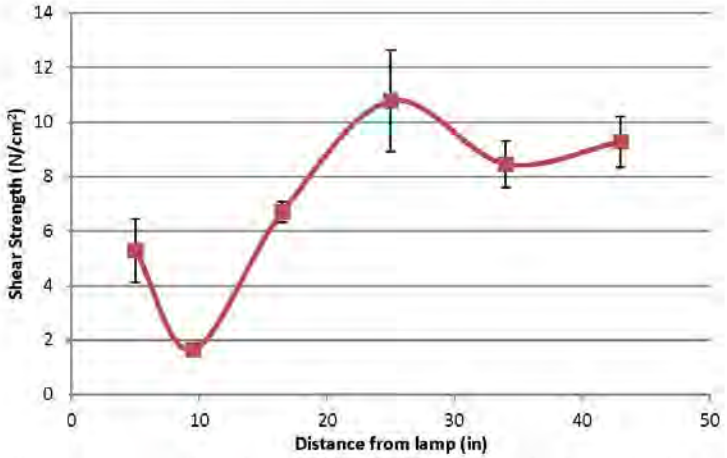

Figure 31: Shear performance of Desmolux 2491 microfibrillar arrays cured at different heights.

Time study at several lamp heights

To further track this inhibition effect on the shear performance of the UV-cured microfibers, a curing time study was performed. Here, several samples were placed at the same height from the UV lamp and were cured for times ranging from 30 seconds to 70 minutes to examine how the final properties develop during curing. This data is complied in Figure 32 for 12, 24, and 54 inch exposure heights.

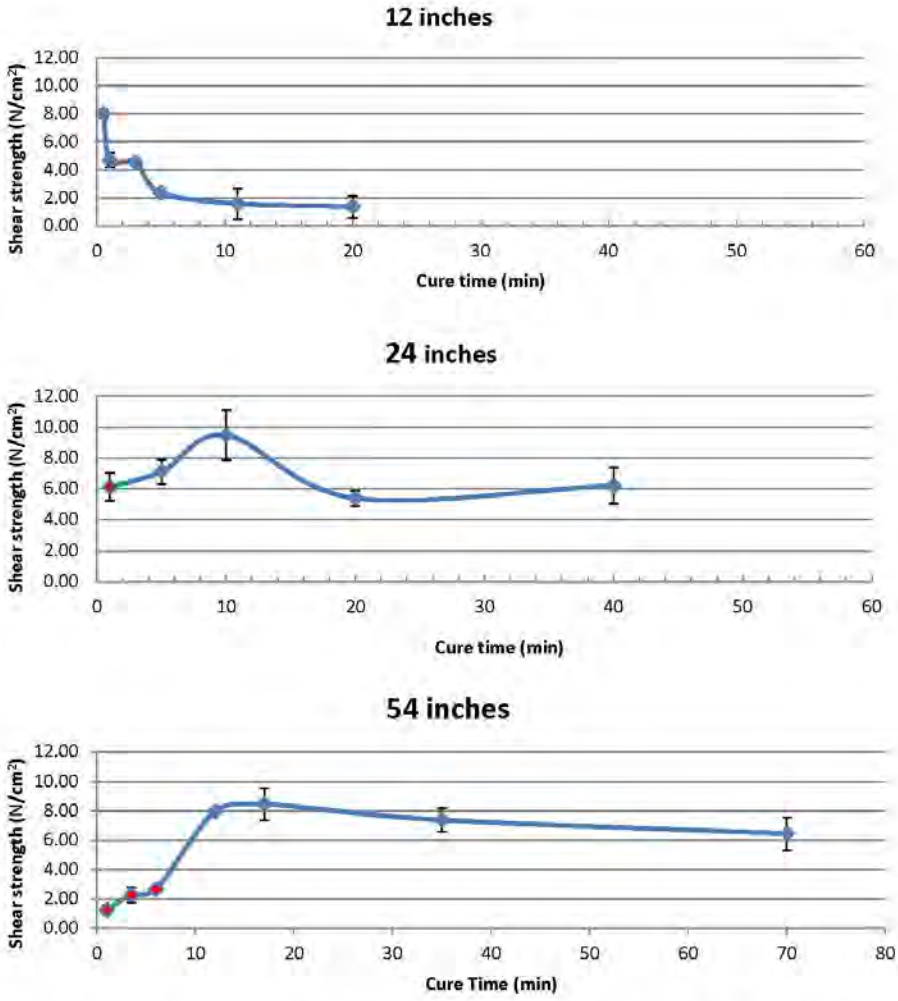

Figure 32: Shear strength of fibrillar adhesives as a function of time for sample heights of 12, 24, and 54 inches from the UV lamp. Note that red data points represent samples with residue leaving inhibition.

When the sample is 12 inches from the lamp, 30 seconds of curing gives the optimum shear strength of 8 N/cm^2. This value correspondingly decreases with cure time, reaching an asymptotic 1 N/cm^2 at approximately 11 minutes of curing. Curing less than 30 seconds, results in residue leaving inhibition, and is shown in Figure 33. This will now be referred to as "under-cured".

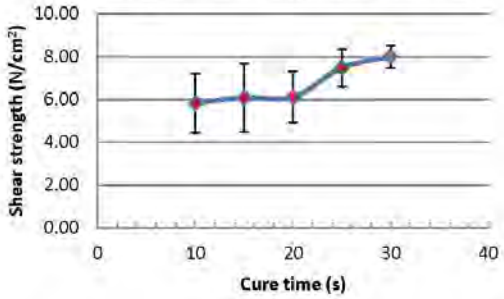

Figure 33: Shear strength as a function of curing time from 10 to 30 seconds at a curing distance of 12".

At 24 inches the optimum curing time was found to be 10 minutes, achieving a shear strength of 9.5 N/cm^2. Interestingly, it was observed that at 5 minutes of curing, the sample was undercured based on shear performance, but showed no residue leaving inhibition. Whether this implies that there is optimum tip softness or if this is a result of change in the bulk modulus throughout the curing process is not known. At this 24" distance, overcuring occurs past 10 minutes of UV exposure. This overcuring was also apparent at the 12" height. However, the drop in performance between optimum exposure and maximum overcured exposure is much less for the 24" exposure distance. Since the rate was slower at this height, the amount of inhibition during the curing process was greater, therefore limiting the hardness that the tip surfaces can achieve.

Curing at 54 inches, these characteristics shift even further. It takes 17 minutes of exposure to reach the optimally cured materials which generate 8.4 N/cm^2 of shear strength. Overcure is even less pronounced because oxygen is given more time to impart its inhibiting effect.

Finally, it is important to put this UV time and distance data in perspective with regards to the R2R fabrication system. It appears that there is a certain processing window that is needed to create good fibrillar adhesives and it is simply not a matter of being cured or uncured. The size of this window will be determined by the belt speed of the system. If the system belt speed is fast, then the light intensity must be high and the exposure time brief. For instance, in the samples 12 inches from the lamp, 5-10 seconds from either side of the optimum value results in either an uncured, residue-leaving or overcured adhesive, as shown in Figure 33. Note that even at these conditions on the nGt's H and S Autoshot system, this is an order of magnitude less intense then Fusion systems. In turn, this makes the processing window very small. However, slower belt speeds and lower light intensities make this optimum processing window on the scale of several minutes as shown with the 54 inch sample heights.

Temperature Study

The temperature of the system will also have an effect on the curing conditions and final performance properties. This is quite an important consideration for the R2R system because heat will be generated from the UV lamp. Additionally, heating the UV material may be necessary to lower its viscosity to aid in filling of the mold.

An increase in temperature will increase the rate of the curing reaction; however, it is not known how temperature will change the inhibition effect. To test this, a series of experiments were run at different temperatures while keeping the curing distance and time constant. It is important to note that for these experiments, both the mold and the curing material were heated or cooled and the results may vary significantly if material was just heated to aid in the R2R process filling.

Figure 34 shows samples cured at 0-65 °C at a distance 12 inches from the UV lamp for one minute. Samples were kept at the respective temperatures for 15 minutes prior to curing. The cooled sample at 0 °C was under cured given the 1 minute exposure time, while all others showed no residue leaving inhibition. Raising the temperature to 45 °C from room temperature, a drop in shear performance occurred while a further increase to 65 °C yielded better performance at identical cure conditions. This highlights that while in production, where cure conditions will be fixed, a change in temperature will have an effect on the overall performance and that curing conditions will need to reflect the production steady-state temperature. What this data does not suggest is that curing at 65 °C provides the best adhesive. Because we kept the curing time fixed in these experiments, we have deviated from optimum curing conditions for each temperature. This is exemplified by the severe undercure of the 0°C sample.

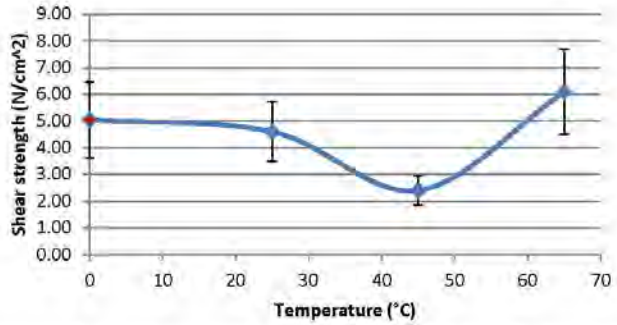

Figure 34: Shear strength as a function of curing temperature at a 12 inch sample distance and a one minute curing time.

B.3.2.2 Material compositions for mass production

In our previous quarter studies, the effect of photoinitiator concentration on the shear performance of the aging resistant F-75 formulation supplied by Bayer Materials Science (BMS) was investigated. We showed that by decreasing the photoinitiator concentration from 3.0 to 2.5 wt-% using identical curing conditions, we could improve the F-75 shear performance from 3.5 N/cm^2 to 5 N/cm^2. This was concluded to be due to formation of a softer tip surface because of the slowed rate of curing due to the decrease in photoinitiator concentration. Through both visual imaging of the fibers under shear as well as fiber stiffness testing (Quarter 1), it was apparent that the F-75 formulation was less stiff than Desmolux 2491. Therefore, F-75 elongates much more with shear and the tips peel more ready than 2491 fibers for a given force. At the end of the quarter, it was the goal to combine our newly proven curing theory with techniques to harden the formulation to advance the properties of the aging resistant F-75.

Improving F-75 formulation

To harden the F-75 formulation, we used Sartomer 351 which was used previously to harden Desmolux 2491. Sartomer 351 is chemically known as trimethoylpropane triacrylate (TMPTA) and has three UV curable sites. This is in contrast to other species in the F-75 material that have either one or two reactive sites. Because of this higher reactivity, more crosslinking sites are formed when cured which results in a harder material with a higher bulk modulus.

For these experiments, we cured F-75 and F-75 with 10 wt-% Sartomer 351 using the same curing conditions. A time study was performed in order to be sure that near optimum curing conditions were reached. The distance of 54 inches was chosen because F-75 is known to cure relatively fast compared to 2491 and fast overcuring was not desirable. A photoinitiator concentration of 2.5 wt-% was used because this proved to be optimum in previous studies.

Figure 35 displays the shear performance of the two materials versus curing time. Note that the red markers denote residue-leaving inhibition. Addition of the 351 causes the F-75 material to cure faster. At 3 minutes, the 10% Sartomer 351 sample is fully cured, while F-75 still shows signs of residue-during shear. At optimum curing, the addition of 10 wt-% 351 causes the shear strength of the F-75 formulation to increase from 7 to 10.5 N/cm^2. This demonstrates the F-75 can compete with, if not exceed the properties of 2491, with optimization of both the hardness and curing conditions. For next Quarter, the 351 concentration will be varied from 1-10% in order to identify an optimum bulk modulus and an aging resistant formulation that has good performance properties.

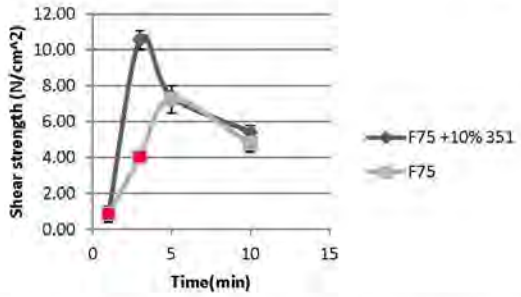

Figure 35: Shear strength of F-75 and F-75 +10 wt-% Sartomer 351 formulations as a function of curing time 54 inches.

B.3.3. T11: Mass Produced Sample Fabrication

Fabricate the third generation fiber adhesives from the polymer fiber materials determined in the Task 2; Integrate the hierarchical, soft backing layer, and/or angled fiber properties into mass-production system to enhance fiber properties as dictated by the results of the models developed during Task 1. Achieve 50% of the length specified in S6.

Modifications to mass production system to enable direct curing of fibers on UA textiles

All previous UV material sample manufacturing performed and reported at nanoGriptech, both bench scale and using the roll-to-roll system, required a two-step curing process. Typically, the UV material would be partially cured in the mold with UV energy on a mylar film backing.

peeled from the mold, then placed under vacuum and cured for an additional time under UV light. This process enabled the manufacture of tape samples with excellent shear and peel properties. However, it was not a process that could easily be translated into large scale production. The challenge to eliminating the two-step curing process was in being able to manipulate and control UV exposure time and exposure energy to create fibrillar adhesives with adequate shear and peel performance but no inhibition. To reiterate details from previous sections, inhibition is the material condition that occurs when UV material at the silicone mold interface is left uncured due to the oxygen content of the mold. Inhibited material on the fibrillar surface leaves a residue on the substrates it comes in contact with, and material performance ends up being inconsistent with repeated use.

The studies described above showed that the need for a post-mold vacuum step can be eliminated if the UV light distance from the mold is increased, along with increasing the UV exposure time. Based on the distance and time benchtop studies discussed above, the UV light distance on the roll to roll system from the belt mold was increased from the previous 12" to 30". At this distance, sample quality similar to the previous reported results can be manufactured exclusively on the roll to roll system. Figure 36 below shows the new roll-to-roll set up that allows for repeatable, variable UV light exposure distances.

Figure 36: Photograph of the new prototype mass-production system used to produce our Q3 matertals

Modifications to mass production system to enable incorporation of release paper to finished roll

The nanoGriptech team has continually been working to improve the roll-to-roll system to make it similar to a hands off manufacturing line. Part of this effort in the third quarter was to create a post molding take up system to gather the manufactured tape and include a release paper in contact with our microfiber tips. This will ultimately protect the finished product. As the research team has been in discussions with manufacturers of pilot and full scale roll-to-roll manufacturing equipment, it has become apparent of the difficulties and technical challenges in making a roll-to-

roll system for manufacturing product. Part of the understanding gained on the bench top scale manufacturing system and also via supplier conference calls is that any roll-to-roll manufacturing process can be broken down into various process components, and that each component is related to and affects the others. In the case of the post molding take up system, a critical parameter to be studied is the effect of the backing material tension on the curing and final product formed in the process. The manufacturing line speed and the take up roller speed can be decoupled, and this effect needs to be further studied as the team moves towards scale up.

Development of Improved Belt Molds

The previous belt molds consisted of a 1" wide fibrillar strip to create the fiber geometry. New silicon master templates were made and are discussed in Section C.2.3. In this quarter, dipping of the fibers produced from this mold to form the mushroom tip shape and replicating this geometry through previously-developed molding processes was performed. This new mold and fiber array geometry was used to create a new belt mold for the roll-to-roll system. The new mold has hexagonally spaced fibers on a 2.25" wide belt, which provides an improved surface area coverage. This pattern also creates fibers that have identical spacing from every other fiber, which makes fiber collapse isotropic regardless of shear direction. This allows tighter control for tip size during fabrication and improves the consistency of the fiber performance during use. This step from a 1" wide mold to a 2.25" wide mold is part of the natural progression towards scale up. Eventually, the team will utilize belts that are 3 feet or wider for production, and will likely use the same belt mold making techniques as are used now, just at a larger scale.

Curing through the bottom of the mold

In the Milestone 2 research for this PA Nanomaterials effort, the belt mold that was used on the roll-to-roll system was an opaque white silicone material. This had been the standard roll-to-roll belt material for manufacturing in the company. Experiments were performed using a translucent silicone mold material in place of the white silicone mold material, as discussed above, and several improvements were realized using it. The translucent mold allows UV energy to be exposed to all of the UV cured material while in the mold. It also provides an opportunity to cure through the bottom of the mold, thus enabling the use of opaque backing materials such as fabric. In order to test this theory, the team used small mirrors to reflect the UV light from the lamp above the mold back up to the bottom side of the translucent mold material. This configuration was used to create micropatterned adhesives cured directly on textiles provided by UA using our roller system.

New material substrates

In this quarter of work, the nanoGriptech team increased the number of material backing substrates that were used on the roll to roll system. The standard backing material for all previous research was a 0.004" mylar sheet. This material is strong in both the X and Y directions, has a surface energy sufficient to enable adequate adhesion of the UV cured material, and is clear to allow UV energy to pass through to cure the UV material. For many product applications, however, it is not an ideal material for use. Also, as reported above, our fiber geometry and final cured conditions are such that their adhesion to a closure substrate exceeded that of the fibrillar adhesion to the mylar itself. This limited the performance of the fibrillar adhesion, and is not ideal for product applications. Based on these findings, and the collaboration with Under Armour, several other backing material candidates were desired for use. The first was a thin flexible TPU material that is commonly used in the apparel industry. These TPUs are desirable for apparel because they are flexible and can easily be heat welded to fabric substrates in the garment

manufacturing process. Also, putting fibers directly on fabric is desirable for apparel closure and glove applications. Putting UV material fibrillar features directly on fabric requires the use of a thin tie layer of the UV material that is placed on the fabric. For our studies, the tie layer was a 200 µm layer of UV cured material. The nanoGriptech team tried various UV formulations as backing material. The viscosity of the tie layer material is important because it determines how well the material wicks into the fabric material. The amount of wicking is ultimately important because it determines how rigid the backing material becomes.

The use of TPU materials as a backing material creates UV adhesion issues similar to the mylar material. When the UV material was cured on TPU backing, low adhesion to the material occurred. In some cases the UV material would stick to the mold surface instead of the TPU backing material. The nanoGriptech team consulted with TPU and PU experts from our collaborative partner Bayer Material Science for insights on how to improve adhesion of the materials. Our collaborative partner from Under Armour also had some insights on how to improve the adhesion. The several options for increasing the adhesion of the UV cured material to a TPU substrate include: (1) Applying the UV material to TPU backing material while the TPU is heated, (2) surface treating the TPU via heat or plasmaher, or (3) specialized coatings that tie together the TPU and UV material.

The nanoGriptech team successfully investigated heating the TPU material, and was able to increase the adhesion of the TPU backing material to a useful level. Another backing material that was discovered, somewhat accidentally during prototyping for Under Armour, was 0.01" and 0.02" thickness sheets of polycarbonate (PC). This PC material is somewhat rigid and could be useful for other market areas, including wall hanging.

B.3.4. T8: Sample Characterization

Test the performance of the third generation fibers in dry and wet conditions. Achieve 80% of the full performance for S1, S2, S3, S4 and S5 in dry conditions and 70% of the full performance of S1, S2, S3, S4 and S5 in wet conditions.

One significant difference between the samples tested in this quarter and the samples evaluated previously in this project is that with the new curing configuration and parameters described in Sections 1.2 and 1.3, no vacuum post-cure was required to produce samples with no residue-leaving inhibition. As such, the samples tested in this milestone were all cured in one step in atmospheric conditions. This represents a major step towards affordable scaled-up manufacturing.

Shear force results

The results of all shear force testing of developed mass-produced fibrillar samples are given in Table 6 along with the performance goals for this milestone. These results show that we exceeded our Milestone #4 goals for all shear closure substrates in both wet and dry conditions as well as for wet shear strength in contact with a football. In fact, we have achieved our final target performance for these measures for the entire project. For glove friction in dry conditions, we did not achieve our ambitious goal for this quarter. However, the sample tested this quarter has our highest measured coefficient of friction (C.O.F.) ever in contact with a football substrate. It is higher than our previously measured shear strength for the UA Blur glove in both dry conditions (UA Blur shear strength = 1.7 N/cm^2) and wet conditions (1.2 N/cm^2).

Test Substrate	Specification	Condition	Generation 3 Mass-Produced Sample Data	Milestone #4 Goal
Football (S1)	Shear Strength (N/cm^2)	Dry	2.1 ± .02 (C.O.F. = 2.1)	2.4
		Wet	1.8 ± 0.1 (C.O.F. = 1.6)	1.1
Closure (S2)	Shear Strength (N/cm^2)	Dry	14.0 ± 2.5	8.0
		Wet	5.9 ± 2.3	4.2

Table 6: Comparison of shear strength data of developed mass-produced fibrillar samples in contact with football and closure substrates and Milestone #4 goals for these applications.

Peel force, usability, and durability results

The results of peel force testing of developed mass-produced fibrillar samples on a closure substrate and our goals for this milestone are compared in Table 7. From these results, we can see that also we met or exceeded our Milestone #4 goals for both dry and wet peel strength measurements on closure substrates.

Test Substrate	Specification	Condition	Generation 3 Mass-Produced Sample Data	Milestone #4 Goal
Closure (S3)	Peel Strength (N/cm)	Dry	1.2 ± 0.1	0.4
		Wet	0.6 ± 0.1	0.21

Table 7: Comparison of peel strength data of developed mass-produced fibrillar samples in contact with a closure substrate and Milestone #4 goals.

Under Armour defined a usability specification (S5) which states that our developed materials must not exceed a peel force of 0.5 kgf / inch (approximately 1.9 N/cm). We can see from the data in Table 7 that our peel strengths of 1.2 N/cm and 0.6 N/cm (dry and wet) are not exceeding this value.

Peel repeatability of a textile-backed microfiber array in dry conditions in contact with a Desmolux 2491 substrate was measured using the same system described previously over 1000 test cycles. The results of this testing are illustrated in Figure 37, and show that the sample maintained approximately 82% of its peel strength after 1000 cycles, exceeding the 72% target for this project Milestone.

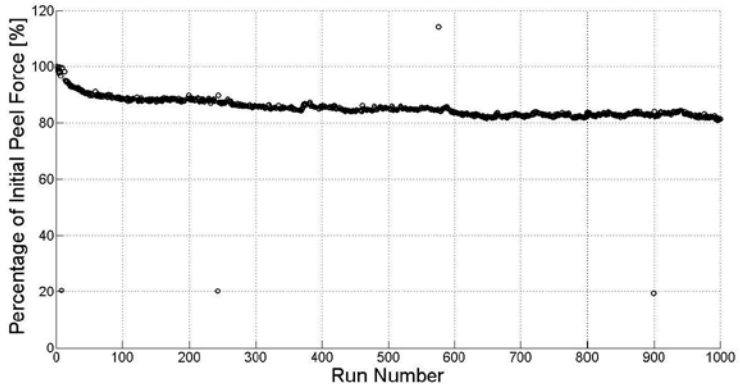

Figure 37: Data demonstrating the repeatability of these materials over 1000 testing cycles

B.4 MILESTONE 5: TECHNICAL DEVELOPMENT

Produce the optimized mass-manufactured fiber adhesive using the tailored polyurethane materials and fiber geometry to perform at a variety of temperatures in dry and wet conditions. At room temperature conditions, the performance would have properties greater than 100% of the desired S1, S2, and S3 specifications given in table 1 in dry conditions

B.4.1. T13 Material Compositions

Optimize the polymeric fiber material compositions with BMS to achieve 100% of specifications S1, S2, S3, S4 and S5 in Table 1.

In Milestone 4, the effect of curing conditions on the shear properties of fibrillar adhesives was investigated. It was found that there are optimum curing conditions that lead to the best adhesive performance. This is in contrast with most UV-cured resins, where they are either fully cured or under-cured. In addition to the possibility of being under-cured, it was determined that our fibrillar adhesives can also be over-cured. Deviation from optimum curing yields poorer performance. Under-cured microfibers typically display residue leaving inhibition when peeled from the adhering surface, while over-cured samples have harder, less compliant tip surfaces. Optimum curing results in a fully cured fiber that has a soft, non-residue leaving surface which leads to the best performance properties.

These phenomena were proven in Milestone 4 on nanoGriptech's in-house curing lamp. Because of its low intensity and longer curing times, it was essential to put this idea into perspective of our future pilot production system which will include higher light intensities and faster curimg times. To do this, several formulations were cured using BMS's Fusion curing system. In their system, the sample travels on a belt which passes under a fixed light. Unlike nGt's in-house process where light height can be adjusted to change the light intensity, the height of the Fusion system is fixed at the distance in which the light is focused (2.5").

A gallium-doped (Type V) bulb was used and its intensity was fixed at 100% output. Exposure time, the variable of the experiments, was changed by adjusting the conveyor belt speed. Figure 38 shows the relationship between the total energy of exposure and the belt speed of the system. At faster belt speeds the exposure time of the sample is decreased which corresponds to a

decrease in UV exposure. By changing the belt speed from 30 to 150 feet per minute (fpm) the exposure energy is decreased from 2.8 J/cm2 to 0.35 J/cm2 in a non-linear fashion. This data was obtained placing a UV detecting puck on the conveyor belt.

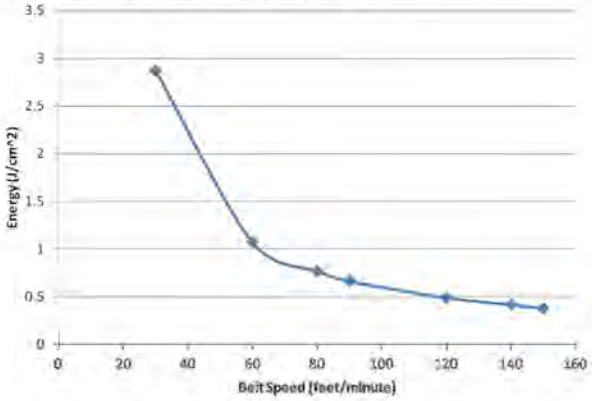

Figure 38: Total UV energy of BMS's Fusion curing system as a function of the system belt speed.

Qualitative results

Experiments focused on two formulations of BMS's UV-curable materials. The first was a mixture of Desmolux 2491 with 15% Desmolux 2513. The second formulation was the age-resistant, F-74 formulation with 5% added hardener (Sartomer CN351 – trimethylolpropane triacrylate). Both formulation consisted of 3 wt-% photoinititator (Irgacure 2022) based on weight of the total monomers. To evaluate the effect of the photoinitiator of the F-75 formulation, samples were also prepared with 3, 2, and 1% photoinitiator. For making fibers on fabric, the F-75 formulation with 3% photoinitiator was cured through the bottom of the mold.

Samples were prepared using the batch process. First the molds were cleaned and the premixed formulation was spread across the mold followed by application to the backing material. For filling, vacuum (25-30 mm Hg) was then applied for 2 minutes. The vacuum was then released and excess material was removed via added pressure atop the backing material. The samples were then taped to a metal panel to ensure stability through the turbulent forced-air cooling of the Fusion lamps. With the belt adjusted to desired speed, the panel was then set on the middle of the belt where it was carried under the fixed light. The cured samples were then collected on the other side of the conveyer. Following curing, the samples were peeled and labeled for testing.

Qualitative trial runs were first performed to roughly determine that upper and lower bounds of belt speed. Over-cure was determined by weak adhesion to a test glass slide while under-cure was determined by the presence of residue when the material was removed from glass. Table 8 summarizes these results. From these tests it was clear that F-75 required faster belt speeds for good adhesion and the Desmolux 2491 formulation required slower speeds. For instance, no presence of inhibition was observed at all, except the fastest belt speed, while for the 2491 formulation the onset of inhibition was noticed from 60-80 feet/minute. This relationship was expected from past curing studies described in Milestone 4, where it was found that the F-75 material cures much faster than Desmolux 2491.

Decreasing the amount of photoinitiator in the F-75 formulation decreases the belt speed needed for full curing. Less photoinitiator decreases the rate of the curing reaction, therefore more light is needed. When decreasing the photoinitiator concentration from 3 to 2 wt-%, the onset of inhibition is changed from 140 to 20 ft/minute. Furthermore, the 1 wt-% photoinitiator formulation could not be cured at the lowest belt speed of 10 ft/min and with this intensity bulb.

In addition, curing through the bottom of the mold proved to have a dramatic effect on the proper curing speed. For instance, it was seen that the onset of inhibition occurred between 20-30 feet/min. This is significantly lower than the 140 feet/min onset of when curing through the top of the mold. It appears that the silicone either absorbs or deflects most the UV light. However this effect could be mitigated by using a thinner mold. Here, the mold thickness was approximately 2.5 mm.

Table 8: Qualitative curing results with several formulations on BMS's Fusion curing system. (green – no inhibition, red – inhibition, PI = photoinitiator concentration)

Belt Speed ft/min	2491 +15% 2513 + 3% PI Top cure	F-75 +5% hardener +3% PI Top cure	F-75 +5% hardener +2% PI Top cure	F-75 +5% hardener +1% PI Top cure	F-75 +5% 351 +3% PI Bottom cure
10					
20					
30					
60					
80					
90					
100					
120					
140					
150					

Effect of base resin on cure properties

From the qualitative study, several speeds in the area of interest were run with larger samples for data collection. A shear strength comparison of the F-75 and 2491, both with 3% photoinitiator, is shown in Figure 39 as a function of the system belt speed. Samples of each formulation were run at 10 feet/minute to quantify the over-cured properties of each formulation. Both have poor shear properties when over-cured, approximately 3.5 N/cm^2. By increasing the belt speed and reducing the exposure time, shear strength is raised significantly due to the effects reported in the Milestone 4 section. The optimum belt speed for the 2491 formulation is 50 feet/min corresponding to a shear strength of 10 N/cm^2. Faster speeds resulted in samples with residue-leaving inhibition as viewed during testing (indicated in red in Figure 39). The F-75 sample showed optimum shear performance at 100 feet/minute with 12.2 N/cm^2 strength. Faster speeds seemed to have little effect on the performance and no inhibition was observed for any sample. Note that the optimum values may lie 5 feet/min faster or slower than these values. Additionally, any change in the formulation or environment will shift this optimum value.

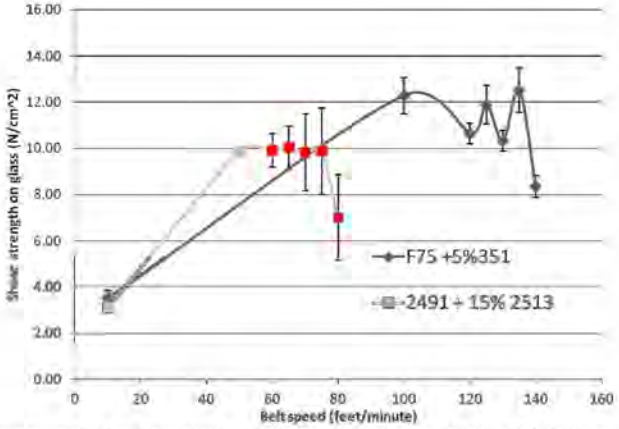

Figure 39: Shear strength of two formulations (F-75 +5% SR351 and 2491 + 15% 2413) cured at various belt speeds on BMS's Fusion UV-curing system. Red data points indicate residue-leaving inhibition.

Effect of photoinitiator concentration on cure properties

The data above defines the maximum belt speed that can be obtained for each formulation using Fusion microwave type lamp. Since other processes could limit the line speed of the system, such filling the microstructure cavities, it was important to determine formulation variables that could be used to tune the curing parameters. To do this, we examined the effect of the photoinitiator on the optimum belt speed and shear performance of the microfibers. Figure 40 shows the shear strength of the F-75 formulation cured as\t various belt speeds having a 2 and 3 wt-% photoinitiator concentration. Note from the results described in Table 8 that 1% photoinitiator concentrations were not tested due to incomplete cure at even the slowest belt speed.

F-75 formulations with 2% photoinitiator have an optimum belt speed of 20 feet/min, corresponding to a shear strength of 12.5 N/cm^2. This is substantially decreased from the 3% photoinitiator sample where the optimum speed was 100 feet/min. Therefore, with the using the same light, the formulation can be tuned to afford optimum curing by changing the photoinitiator concentration. For instance, if a line speed of 60 feet/min is desired, the photoinitiator concentration should be adjusted to 2.5 wt-%.

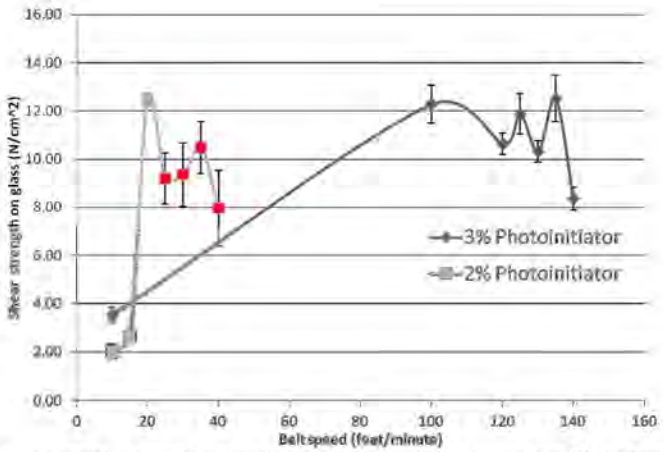

Figure 40: Shear strength of new F-75 formulation cured at various belt speeds on BMS's Fusion UV-curing system and different photoinitiator concentrations. Red data points indicate residue leaving inhibition.

Effect of light position on cure properties

Forming microfibers on backing material in which UV cannot penetrate requires the curing to occur through the bottom of the mold as shown in Figure 41. Using identical formulations (F-75, 5% hardener, 3% photoinitiator), samples were cured from the top and bottom at different belt speeds. The shear properties of these samples are shown in bottom of Figure 41. As discussed above, the optimum top curing speed is 100 ft/min. Curing through the bottom of the mold drastically decreases this value to 40 ft/min. This is likely due to the absorption of deflection of some of the UV energy by the thickness of the mold, thereby decreasing the rate of polymerization. More exposure time is needed for optimum cure, thus resulting in lower belt speeds. If faster speeds would need to be acquired when curing through the back of the mold, the mold would need to be thinned. Note that these experiments were performed with molds that were 2.5 mm thick.

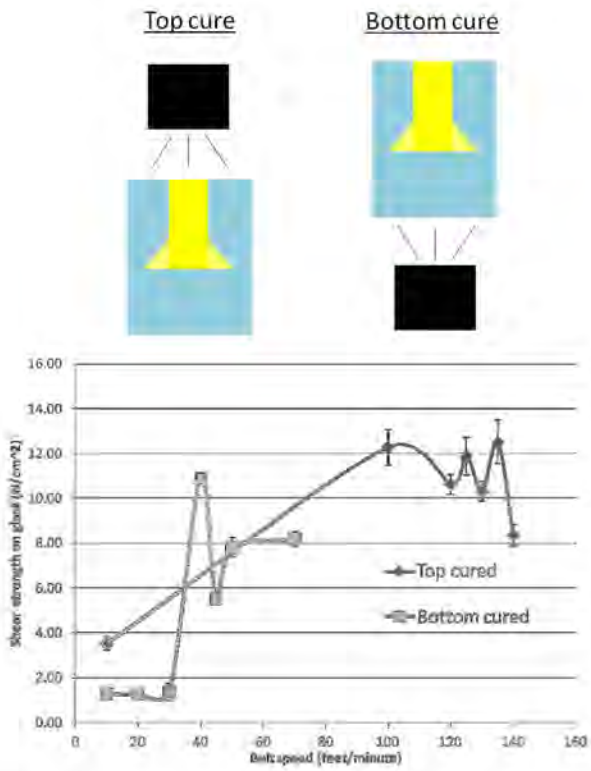

Figure 41: Schematic of top and bottom curing (Top) and shear strength of fibrillar adhesives cured from top and bottom positions at different belt speeds (Bottom).

B.4.2. T14: Fabricate 4th Generation Fiber Adhesives

Fabricate the fourth generation fiber adhesives from the polymer fiber materials determined in Task 2. Target benchmark is 100% of the length specified in S6.

A 25 foot long continuous microfiber tape sample satisfying specification S6 was presented to the audience at the Milestone #5 meeting on June 20th, 2012.

B.4.2.1 New Configuration for Roll-to-Roll System

Part of the work of this project effort has been to determine the best configuration for a scaled up roll-to-roll system to be manufactured for pilot scale production volumes. Previously, all of the work has been done on a lab scale production system that utilized a belt mold in a conventional conveyor-like configuration. In an effort to explore new ways to create a production scale system, the engineering team has been in the process of researching the printing industry for inspiration. During that research, and also during a meeting with an engineer from the local start-up company

Plextronics (http://www.plextronics.com), the concept of a single roller system was developed. The schematic in Figure 42 below show the high level operations of the modified system.

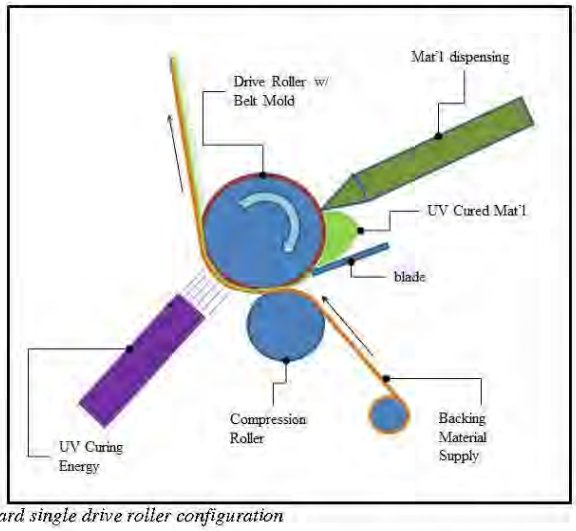

Figure 42: Standard single drive roller configuration

Based on the previous project work from this PA Nano effort, the manufacturing process of closures using fibrillar adhesive geometry can be broken down into the following steps:

Mold Filling

- Start with the correct UV curable material. This includes the base resin, photo-initiator, and any modifying agents (hardeners, etc)
- Material is dispersed onto a moving silicone belt mold that has a negative shape of the fibrillar features to be created
- The material is spread out on the belt mold using a wiper or a blade
- A backing material is introduced on top of the uncured UV material

Material Curing

- The uncured UV material and backing material are compressed together as they travel through a set of compression rollers in the system
- UV energy is directed on the backing and UV material to fully cure the system
- The combination of (backing + UV fiber material) is removed from the belt mold, and release paper is added to prevent product sticking until final use

This basic process can be performed on a 2-roll system, or on a system such as the one described in Figure 42. Figures 43 and 44 show a front view and top view of the desktop system reconfigured the existing roll-to-roll system to mimic a single roller system. The team was successful in getting the system up and working, and believes this configuration has merit for continued investigation.

Figure 43: Front View: nanoGriptech single roller configuration

Figure 44: Top View: nanoGriptech single roller configuration

During this project quarter, this new nanoGriptech single roller configuration used two different UV LED systems loaned from Phoseon Technology (http://www.phoseon.com/).

There are several potential benefits anticipated in using a single roller system, including:

- Lower system cost
- More robust molds and longer mold life
- Improved filling of the mold

Lower System Cost

A single roller system creates the potential for a much smaller footprint machine, and eliminates many of the components in a larger roller/conveyor type of set up. Additionally, depending on the product being manufactured and the size of the market being served, a single machine could be dedicated for each product, or a new master roller and mold could be exchanged. Finally, these single machines create the potential to use UV LED systems, which have a lower cost and longer use life than some of the larger UV systems investigated previously.

More Robust Molds and Longer Mold Life

At this point in the research, the life and durability of the silicone molds used in large scale production is unknown. For a conveyor type of system, long silicone belt molds are cast onto a structural member to carry the load of the tension the belt is placed under. If the conveyor style of pilot system is selected to move forward with, large scale belt mold manufacturing methods must be developed and optimized and improved, and their durability must be assessed. Additionally, the research must be performed to determine the best way to assess mold health while the belt is in use. In a single drive roll system, the belt could be cast directly onto the roller which would create a more robust structure for increased durability.

Improved Filling of the Mold

In addition to the need to study mold durability, more research is needed with the mold filling process. Specifically, understanding the effect of mold durometer and mold thickness on the filling process and needed pressure still needs to be understood. Regardless of the mold material specifics, by casting directly onto a roller, the filling process should be improved.

B.4.2.2 UV LED Systems

During this research quarter, nanoGriptech became familiar with the UV LED Curing Association (http://www.uvledcuring.org/) and began to investigate the potential for using this new type of curing energy. As noted earlier, Phoseon Technology loaned us two different UV LED systems, a 4 W system and an 8W system, for assessment.

In an effort to correlate the curing performance of the UV LED systems with the full scale curing systems tested at Bayer and outlined in the preceding section, curing studies were performed at nanoGriptech with these LED systems. The objective of these studies was to determine the line speeds that can be accommodated with UV LED systems. Table 9 outlines the line speeds that cure and do not cure. The exposure times that do not cure are denoted by red, those that do cure are denoted by green.

Table 9: Qualitative curing results with several formulations on the loaned UV LED systems (green – no inhibition, red – inhibition, PI = photoinitiator concentration)

Line Speed		F-75 +5% 351 +3% 2022		2491 +15% 2513 + 3% 2022	
in/sec	ft/min	4W light	8W light	4W light	8W light
.5	2.5				
1	5				
2	10				
3	15				
4	20				
8	40				
12	60				
16	80				
20	100				
24	120				
28	140				
32	160				
36	180				

The data correlates with the data that was obtained in the BMS Fusion Studies. The F-75 material allows for a much faster line speed to be used than the modified 2491 material. Depending on the

market needs and annual production requirements, a production line running at 40 ft/min may be fast enough to produce some materials at a profitable level. These results and the results of the BMS Fusion lamp studies indicate that any of these lamps can be used to produce working material prototypes, and that the ultimate lamp selection should be dictated by line speed requirements and capital equipment budgets.

B.4.3. T15: Sample Characterization

Test the performance of fourth generation fibers in dry and wet conditions. Achieve 100% of the full performance for S1, S2, S3, S4 and S5 in dry conditions and 100% of the full performance for S1, S2, S3, S4 and S5 in wet conditions.

As we reported above in our Milestone #4 results, all of these project specifications except for the shear force on a dry football glove were achieved. While we attempted several new formulations for football glove shear, we have not yet been able to improve upon the Milestone #4 reported results.

Per the statement of work collectively developed by the Pennsylvania Nanomaterials Commercialization Center and nanoGriptech, the specifications which apply to this project are included in Table 10. For each specification, the best measured results from our project are described.

Table 10: Project specifications compared with measured results

Specification Number	Specification Name	Desired Specification (mass-produced fibers)	Project Results
S1	Shear force (football glove)	• 3 N/cm^2 at 0.8 N/cm^2 load in contact with dry football • 1.5 N/ cm^2 at 0.8 N/cm^2 load in contact with wet football	• **2.1 N/cm^2** at 0.8 N/cm^2 load in contact with dry football • **1.8 N/cm^2** at 0.8 N/cm^2 load in contact with wet football
S2	Shear force (closure)	• 10 N/cm^2 in dry conditions • 6 N/cm^2 in wet conditions	• **14 N/cm^2** in dry conditions • **6 N/cm^2** in wet conditions
S3	Peel force (closure)	• 0.5 N/cm in dry conditions • 0.3 N/cm in wet conditions	• **1.2 N/cm** in dry conditions • **0.6 N/cm** in wet conditions
S4	Durability	Number of cycles over the product life: • 1,000 cycles – 0.45 N/cm in dry conditions (90% of original strength; closure) • 2,000 cycles – 70% of original strength • 5,000 cycles – 65% of original strength	• 1000 cycles - **0.98 N/cm** in dry conditions (82% of original strength) (closure)
S5	Usability	Open and close forces of <0.5 kgf per inch	Maximum measured open and close forces of **0.31 kgf / inch** (<0.5 kgf per inch)

While the maximum measured closure durability was 82% of its original strength (and not the 90% project specification), because our initial closure strength vastly outperformed the desired S3 peel force specification, the performance after 1000 cycles was still more than double the value that UA requested.

Based on the results of the football glove field trials (described below in Section C.4.1) we have several ideas for continued development of microstructures for football receiver glove applications which should result in improved shear strength and user satisfaction.

C. COMMERCIAL DEVELOPMENT

C.1 MILESTONE 2: COMMERCIAL DEVELOPMENT

C.1.1. C1: Renew the JDA between nanoGriptech and Under Armour

A renewed Joint Development Agreement between nanoGriptech and Under Armour was signed in September 2011.

C.1.2. C2: Prototype delivery

Provide 4x10-inch long first generation mass-produced adhesive samples to Under Armour, UA, for testing S1, S2, S3, S4 and S5 in dry and wet conditions at room temperature.

Prepared samples were brought to the Milestone #2 meeting and transferred to Under Armour at that time.

C.1.2.1 Additional Prototyping: Prototyping of Under Armour products using nanoGriptech microfibrillar arrays

As a part of the collaboration between Under Armour and nanoGriptech, the teams collaborated on a joint prototyping effort during this project period. We were invited by Jason Berns and Under Armour to visit their new R&D facilities at their company headquarters in Baltimore, MD. Even though we are still operating at small batch fabrication scales, we took the necessary steps to prepare a working football receiver glove prototype during this visit to test whether our developed materials would be compatible with Under Armour's prototyping facilities and fabrication processes.

Preparation for Under Armour Visit

Several research tasks were performed to prepare for our visit. These tasks included:

1. **Procuring the pattern template for the football contacting surfaces on an Under Armour glove**

   An Adobe Illustrator .ai template for the UA Blur II, a football receiver glove currently sold by Under Armour was provided to us by Joseph Trachta in Under Armour's Innovation Department.

2. **Fabrication of a micropatterned mold large enough to produce the glove pattern in a single fiber array**

   Using techniques developed in our first year of PA NanoMaterials Commercialization Center funding, a negative micropatterned mold large enough to produce a single micropatterned array which could be shaped into the football-contacting areas of the UA Blur II glove pattern was produced using silicone rubber (HS-II, Dow Corning). A picture of the produced mold is shown in Figure 45.

Figure 45: Negative micro-patterned mold for glove prototyping

3. **Production of micropatterned fibrillar arrays from the large mold**
   To fabricate a micropatterned fibrillar array suitable for incorporation into UA textiles, a 2-part polyurethane (ST-1060, BJB Enterprises) was mixed, degassed, and applied to the negative mold. A thermoplastic urethane (TPU) film was pressed into the back of the liquid polymer and the whole system was allowed to cure in the mold.

Under Armour Visit

We visited Under Armour on August 19, 2011 with the goal of conducting this glove prototyping. The following three benchmarks were met during our site visit.

1. **Integration of nGt microfibrillar array with UA textiles**
   A pneumatic hot press (CS-500B, H&H) was used to join the TPU-backed array with UA HeatGear® textiles both with and without a foam core. While still in the mold, the mold-fiber-TPU assembly was placed on the hot press with an optional foam core followed by UA HeatGear in contact with the TPU surface. 30 psi of pressure was applied to these materials at 173°C for 20 seconds to melt the TPU and bind the HeatGear to the microfiber array. Once the system had fully cooled, the microfiber array was peeled from the mold.

2. **Laser cutting integrated fabric/fiber sample into glove pattern**
   An automated laser cutter (Legend 36EXT, Epilog Laser) was used to cut the integrated array into the necessary glove pattern. The 120W laser was set to 50% power, 15% speed, and a frequency of 531 Hz. The resulting pattern was cut with no damage to the microfiber structure. A photograph of the laser-cut pattern is illustrated in Figure 46.

Figure 46: nGt microfiber array integrated with UA HeatGear and laser cut into football contacting surface pattern for the UA Blur II glove

3. **Prototyping of first glove**
With the assistance of a skilled seamstress at Under Armour, this array was integrated into a UA Blur II glove. A photograph of the finished glove is shown in Figure 47.

Figure 47: Produced UA Blur II glove with nGt micropatterned football-contacting surfaces

Prototyping directions for future work

Several improvements to the glove prototyping are suggested:

1. **Improving glove tactility, flexibility, and dexterity**. While we had speculated that incorporating a foam layer into the glove would improve our fiber performance, this added thickness increased the stiffness of the glove in a detrimental way that prevents the wearer from properly gripping a football. Furthermore, the use of the HeatGear as the hand contacting surface caused a high degree of slipping between the hand and glove

which additionally affected the gripping ability. The next prototypes should be fabricated without the foam layer and attached to a more established hand-contacting glove material, such as suede.

2. **Accelerating prototyping speed**. We may need to determine ways to accelerate the glove prototyping process as it took a highly skilled seamstress several hours to sew a single glove prototype. One possibility is to focus on a different pattern that may be simpler for the UA team to put together, or even to switch focus to a soccer goalie glove which is larger and less intricate.

C.2. MILESTONE 3: COMMERCIAL DEVELOPMENT

C.2.1. C3: Provide Under Armour with the second-generation mass-produced fiber adhesive samples

Prepared samples were brought to the Milestone #3 meeting and transferred to Under Armour at that time.

C.2.2. C4: Contact with different roll-to-roll manufacturing machine equipment manufacturers to get pricing for the required custom machines for mass-production of the fiber adhesives.

We have been in contact with PolyWorks Inc (North Smithfield, RI) as a potential roll-to-roll equipment manufacturer and have solicited a preliminary quote for a pilot-scale production system for our customized process. After several conference calls with PolyWorks engineers, they generated a quote of $174,900 for a production line which includes a customized UV curing system, off the shelf dispensing and control mounted to a steel frame. A combination of pneumatic actuators and motors will apply the appropriate tension to the belts and backing layers and torques to the production line. This system will include an enclosed curing chamber that can be nitrogenated if we ultimately determine that curing in an oxygen-free environment is necessary to control inhibition. This $174,900 price tag includes: $89,200 in Direct Labor, $34,980 in Mechanical and Electrical Design & Engineering, $29,733 for Machining & Assembly, $24,486 for Electrical Assembly & Wiring, and $85,701 for Purchase of Capital Equipment.

C.2.3 Additional task: Update on prototyping efforts

As a part of the ongoing product development effort between Under Armour and nanoGriptech, the teams continued making progress on glove prototyping during this project period. This progress, including material selection, clean room work, material dimension optimization, and the development of new prototyping methods is described in the remainder of this section.

New textile and pattern procurement in collaboration with UA

As a result of our prototyping efforts in the first quarter of this project which were described in our previous Milestone #2 research, we learned the value of using appropriate textiles which will be suitable for the intended football receiver glove application. Under Armour provided us with samples of the same faux suede material that they use in many of their commercially-available gloves. This material has been identified by Under Armour as one that is comfortable when used in tightly-fitted gloves while allowing for good dexterity and tactility of the user while manipulating a football. Additionally, it is familiar to those who sew and assemble gloves both at UA's existing Chinese production facilities and at their Baltimore prototyping laboratory.

Additionally, UA digitized and provided us with a new glove pattern which we will be working with over the duration of the prototyping effort. This pattern was identified by the UA team as one that would be easier to prototype than the UA Blur II pattern that we used in our first round of prototyping which we reported on in our Milestone #2 research.

New master template clean room fabrication

In preparation of future glove molding effort, preliminary deep reactive ion etching (DRIE) microfabrication work at Carnegie Mellon University's NanoFabrication clean room facility was conducted to produce a new silicon wafer template of hexagonally-packed 40 µm diameter pillars. This template is 2.5" x 2.5", unlike our previous template which was 1" x 1". This is the largest size rectangular template that we can produce on a 4" silicon wafer, which is the largest size wafer that can be processed using CMU's DRIE equipment. The larger size of the wafer will result in few seams when stitching multiple clones of this wafer together for belt and glove palm mold making. Additionally, the wider wafer size will make it easier to produce belts of increased width when compared to our previous 1" belt width. A photograph of the produced wafer is illustrated in Figure 48.

Figure 48. A 2.5" x 2.5" array of 40 µm diameter fibers etched into a silicon wafer.

In the next project term, we will replicate this silicon wafer through several molding steps, dip the replicated elastomeric template using our custom process to add mushroom tips to the wafer, and clone this tipped template for such mold making purposes.

Backing layer thickness characterization study

In the Milestone #2 research, we examined the ability of a compliant backing on a fibrillar surface to increase the contact area of fibers on football type features by finite element analysis using COMSOL software. The results showed that a thicker and softer backing would indeed result in better contact with rough football surfaces. To prove this we carried out a series of experiments to test this generated by these computer modeling efforts.

Sample fabrication and characterization

Samples for these tests were produced by our manual batch process using 2-part polyurethanes. First, sheets of soft polyurethanes (F-15 and F-25, BJB Enterprises) were made at different thicknesses. These are both 2-part, fast curing polyurethanes that have shore A hardness values of

15 and 25, respectively. They were mixed, degassed and then either poured into a mold with a certain thickness or between two plates with appropriate sized metal shims. The sheets were allowed to cure overnight at RT. These served as the backing material for the fibers. Next, the fiber material, ST-1060 or ST-1085 (BJB Enterprises), was mixed, degassed, and poured onto a cleaned fiber mold. Mylar backing was applied and then the system was then held under vacuum for 5 minutes to ensure proper filling of the mold. Excess material was then forced out to get a minimal ST-1060 (or ST-1085) layer and then the mylar was peel from the mold. The F-25 or F-15 sheet was then applied to the mold and pressed lightly to release any air pockets. The composite was then left to cure overnight followed by a 24 hour curing at 70 °C. The samples were then peeled from the mold and mounted on sample testing plaques. Mylar backed samples without a soft backing were also made as controls during testing. Samples were shear tested using our automated shear system on a football substrate using a 500 g force as shown in Figure 49.

Figure 49: Schematic of a fiber array with flexible backing under shear loading on a football substrate

Results

Figure 50 and 51 shows the coefficient of friction data for 1085 and 1060 fibers on the F-15 and F-25 backing at thicknesses at 0.5, 1, and 2 mm thick. All the samples that had F-15 and F-25 backing gave higher coefficient of friction than the mylar backed samples. The friction factor of BJB 1060 fibers increases from 1.3 to 1.7 as the F-15 backing thickness increases from 0.5 to 2 mm. The harder F-25 backing shows the opposite effect, where the friction factor decreases from 1.95 to 1.7 with increasing thickness from 0.7 to 2 mm. Despite compliant backing thickness and hardness, all BJB 1085 fibers showed friction factors ranging from 1.1 to 1.3 showing slight improvement over the mylar backed control of 0.93.

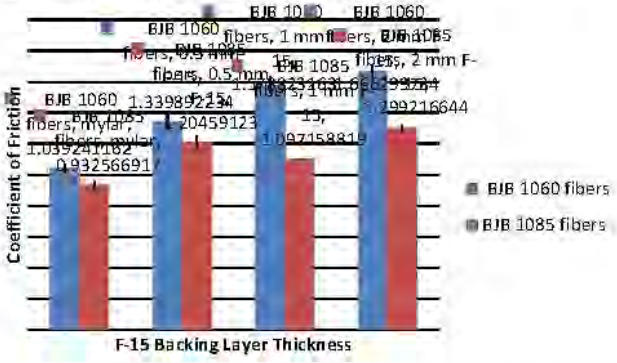

Figure 50: Coefficient of friction of BJB 1085 and 1060 fibular arrays with various thicknesses of BJB F-15 (shore A hardness = 15) with a 500 g preload force

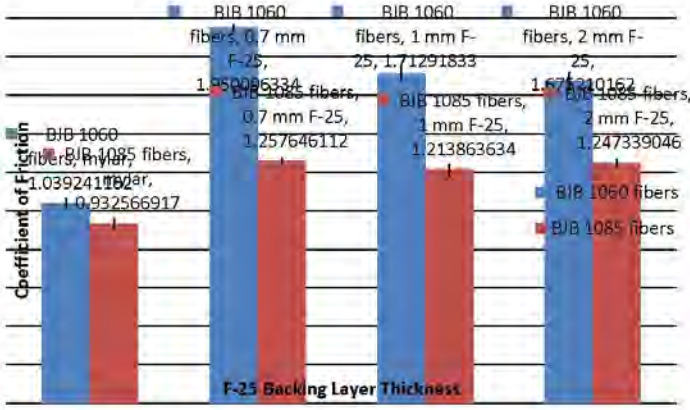

Figure 51: Coefficient of friction of BJB 1085 and 1060 fibular arrays with various thicknesses of BJB F-25 (shore A hardness = 25) with a 500 g preload force.

All compliant-backed fibers demonstrated better coefficients of friction compared to the rigid mylar backing because it allows better individual fiber conformability to create better contact with the rough football surface. In this general regard, our data fits this conclusion from the computer simulation and all compliant backed fibers give improved friction factors on the football surface. However, while the simulation concluded that a softer and thicker compliant backing is best for more fiber contact, this does not necessarily translate to higher shear forces and coefficients of friction in our system. For instance, the thicker the compliant backing, the larger the distance between the plane where the shear force is applied and the plane of the fiber tips, which results in a larger moment acting on each fiber tip to force the fibers out of contact with the football. Another factor is the deflection of the backing layer. These two effects create a peeling-like force on the trailing edge of the fibers and would decrease fiber contact. It is the combination of the competing effects on the system induced by the compliant backing (which increases the number of fibers which can contact the football) and the increased backing thickness (which results in increased moments and peeling force at the fiber tips which reduces the number of fibers in contact with the football) which will determine the performance of the material

In the case of F-15-backed 1060 fibers, the added compliance of thickening the backing has a greater effect on the shear performance than the imposed moment induced by this added thickness. Therefore, we see an increased friction factor when the backing layer is increased. However, the opposite is the case for the harder F-25 backed fibers. Here, we see that the thinner layer gives the best friction factor as the added compliance from the harder F-25 does not create enough conformability to offset the induced moment on the fiber tips.

Furthermore, the data suggests that BJB 1060 fibers perform significantly better than the 1085 fiber. BJB 1060 is softer, having a modulus at 100% elongation of 2 MPa compared to 5.2 MPa of 1085. The softer 1060 fiber also add to the compliance in the over system. 1060 fibers have the ability to be compressed, allowing more fibers to come into contact.

Glove prototype improvements

Over this project term, we have taken several steps to improve upon the first glove prototypes that we reported on in our Milestone #2 research. There, we described a method of integrating our fibers with UA textiles using thermoplastic urethane films and a hot press. To accelerate our prototyping efforts and simplify the process, in this quarter, we developed a new microfiber/textile integration method compatible with the faux suede textile which does not require a thermoplastic binding layer. Additionally, eliminating the hot press of a fibrillar structure will prevent the fibers from getting damaged during the application of heat and compression, which was a problem with our first round of glove prototyping. This new process also allows for the integration of a backing material of the appropriate thickness and hardness, as determined from our modeling in our Milestone #2 research and experiments presented above.

First liquid polyurethane (F-25, BJB Enterprises) which will form the soft backing layer was mixed, degassed, and spread over a faux suede textile swatch. Time was allowed to elapse for the viscosity of the polyurethane to increase as it begins to cure. Doing so prevented the polyurethane from penetrating so far into the faux suede textile weave that it would affect both the surface finish of the glove lining and the stiffness of the resulting composite material. After this time had elapsed, 0.5 mm shims, found to be an optimal backing layer thickness in the above study were placed on the suede and a smooth, rigid, release layer compressed the curing liquid polyurethane down to the desired thickness. The polyurethane was allowed to finish curing.

The photographs in Figure 52 illustrate the polyurethane side (top) and faux suede side (bottom) of fabricated swatches produced using this method. The samples on the left were allowed to sit for 27 minutes before pressure was applied to flatten the polyurethane to its desired thickness, while the sample on the right was put under pressure after 4 minutes. While both polyurethane surfaces are equally smooth and thick with excellent bonding between the textile and the elastomer, it is apparent that the polyurethane has seeped through the faux suede on the 4 minute sample from the darkened material region. This results in a stiffer composite which is undesirable for a form-fitting athletic glove where a high degree of manual dexterity and tactility are essential.

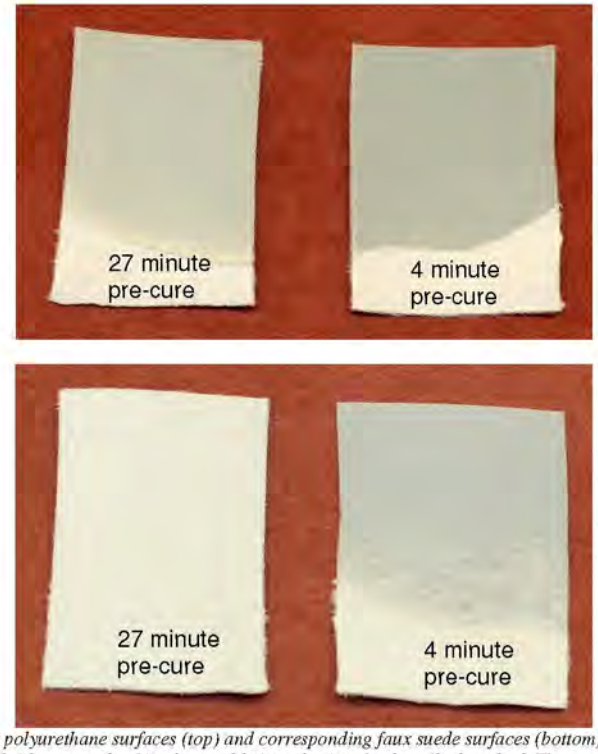

Figure 52. The polyurethane surfaces (top) and corresponding faux suede surfaces (bottom) of the composite textile/elastomer backing layers fabricated using the described method. The samples on the left were allowed to cure for 27 minutes before pressure was applied to bond the materials while the samples on the right were only allowed to cure for 4 minutes before pressure was applied.

To apply fibers to this polyurethane/faux suede composite, a second liquid polyurethane was mixed, degassed, and spread evenly and thinly into a previously fabricated mushroom-tipped microfibrillar silicone rubber mold. During this project term, ST-1060 (BJB Enterprises) was used to form the fibers. The polyurethane side of the faux suede/F-25 swatch was brought into contact with the filled mold and pressure was evenly applied to remove any excess ST-1060 from the interface. The ST-1060 was allowed to cure, and then the entire material was peeled from the silicon rubber mold. An approximately 1-inch square sample of a resulting faux suede/F-25/ST-1060 micropatterned material with an approximate thickness of 1 mm is illustrated in Figure 53. ST-1060 and F-25 are both aromatic 2-part polyurethanes with similar catalysts which allows them to both fully cure and bond with one another.

Figure 53: Photograph of a produced mushroom-tipped microfiber array with a soft elastomer backing robustly embedded with UA faux suede. The total sample thickness is ~1 mm, comparable to UA's existing glove product lines.

We expect this process should be compatible with our roller system as we scale up production. The two processes, first applying the soft backing, then applying the fibrillar structures, may be performed either in series on the same line or on two parallel production lines. In the latter case, the output of the first line (faux suede with a soft elastomer backing) would be used as the backing layer for the second, fibrillar patterning, line.

C.3. MILESTONE 4: COMMERCIAL DEVELOPMENT

As our adhesive development started to meet the project specifications identified in Table 1, we arranged a meeting with Jason Berns of Under Armour to coordinate our prototyping efforts to ensure that we were delivering samples that were useful to the UA team. Jason visited our site for a meeting on January 20th, 2012 for a brainstorming meeting where we outlined a subsequent prototyping timeline and generated several different prototype ideas for our respective teams to pursue.

Based on the ideas discussed in this meeting, preliminary micropatterned glove palm samples were sent to UA on February 9th for assembly by their prototyping team. Feedback on these gloves was provided by Jason Berns via a Skype meeting on February 19th, wherein a modified glove pattern was generated by UA for second generation glove prototyping. These second glove prototypes were sent to UA on March 2nd. Prototype closures were sent to UA on March 6th for preliminary evaluation. A theme of this quarter was constant communication and mutual feedback between the nanoGriptech engineering team and Under Armour as we focus more heavily on developing prototypes to meet the technical specifications of their product line.

C.3.1. C5: Determine the method of attachment of the fiber array samples to the sports fabric surface for field-testing at Under Armour. Under Armour will provide the textiles, adhesives, films and other materials to be used as substrates.

C.3.1.1 Closure prototyping

In support of the Under Armour collaboration, the nanoGriptech team developed prototypes for both gloves and garment closures. For the garment closures, the preferred configuration was to have a thin UV-cured polyurethane coated textile as the mating material, and a fibrillar mating surface that opposes and engages it. As the fibers cannot be easily created directly on fabric, a thin coating of flat UV-cured material must first be applied to the fabric that acts as a backing layer for the fibrillar layer. Under the guidance of Jason Berns of Under Armour, different prototype closure concepts were produced this quarter including 1" x 6" long continuous strips, 1" x 6" long discrete strips, closures with some rigid polycarbonate component, and elliptical closures. These closures were fabricated on different woven textiles as well as TPU films provided by Under Armour which were identified by their textile engineers as promising for our application.

In an e-mail dated March 14, 2012, these closure prototypes were described by Jason Berns as "AMAZING" and "a huge step forward" adding that "[The UA] team is blown away."

C.3.1.2 Football glove prototyping

In the last quarter, we showed that by applying a flexible backing to our fibers, the shear performance on the football surfaces was markedly increased. It was the goal of this quarter to apply this backing to our football glove prototypes.

At our January 20th meeting with Jason Berns, it was decided that leaving a polyurethane-free stitch area of uncoated fabric would improve the ease of glove manufacturing as well as the tactility and fit of the glove. Therefore, one challenge to overcome this quarter was how to add a layer of flexible backing onto the fabric in a specific pattern, allowing for such a fringe. To do this, we used a masking technique. Furthermore, UA provided us with several yards of the same faux suede textile that they use on the palms of their football glove line for improved prototyping. They also provided us with the exact glove palm pattern used in their glove production facilities. The newly developed batch process will now be described and is depicted in Figure 54.

Figure 54: A schematic depicting the fabrication process for micro-fiber coated glove prototypes directly fabricated on UA textiles.

First, a mask was made by laser cutting the glove pattern from a transparency sheet. A light adhesive (Repositionable 75, 3M) was sprayed onto the mask and was applied to the faux suede material. Next, a thin layer of compliant polyurethane backing (F-25, BJB Industries) material was applied to a separate transparency sheet and was allowed to partially cure for 30 minutes. After this time the F-25 coated transparency was pressed onto the masked fabric with metal shims that dictated the backing thickness. The system was then placed in between two metal plates and compressed with a bench top hydraulic press for several seconds. The F-25 coated fabric was

allowed to cure overnight. After cured, the top transparency sheet was peeled, exposing the layer of F-25. Polyurethane microfibers were then put onto the coated fabric using techniques detailed in the Milestone #3 research. After this, the microfiber and F-25 layer was cut following the mask. Then the mask was peeled leaving the flexible backed microfiber array in the original glove pattern.

Three different transparency masks and design concepts were produced during this project quarter, and are illustrated in Figure 55. These range from a simple entirely micropatterned glove palm to increasingly complex pattern shapes. In addition to an aesthetic or marketing interest in different glove patterns, making the fingers patterned area discrete rather than continuous may help improve finger flexibility and dexterity, improving the grip of the glove on a football. Field trials and user studies should be conducted with these or similar glove concepts to evaluate customer interest in such designs. Additional designs could allow for incorporation of the Under Armour "UA" trademark as well as different team logos for different customers.

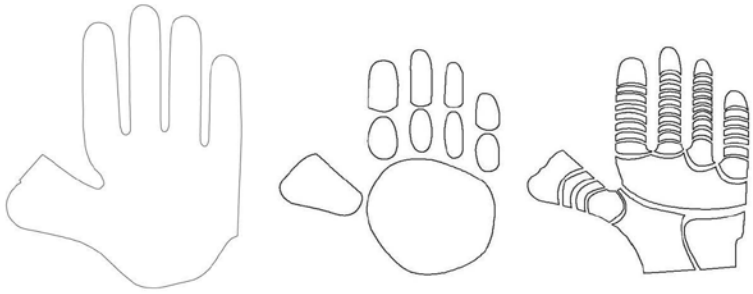

Figure 55: *Three* different glove palm design concepts developed and prototyped during this quarter

Preliminary gloves prototyped this quarter by UA using the technique described above were sent back to nGt to evaluate whether the glove assembly process caused any friction performance degradation. Glove assembly involves manual manipulation of the textile by a seamstress, and the microfibrillar surface may come into contact with the airborne textile particles generated by the stiching process.

Glove performance was measured of a virgin glove palm prototype before shipment to UA. After assembly into a glove prototype, the glove was shipped back to nGt. A small square region of this glove palm was then tested in our shear testing apparatus to measure the performance deterioration, if any, induced by the assembly process. The sample was then cleaned through blotting with a commercially available pressure-sensitive adhesive (Scotch Tape, 3M) and the friction coefficient was measured again. Finally, the sample was lightly cleaned with hand soap and tap water, rinsed with DI water, and dried before a final measurement was taken. The results of these measurements are illustrated in Figure 56. We can see that about 20% of the performance was lost due to the assembly process, but this loss was recovered during the post assembly cleaning steps. As such, during eventual glove manufacturing, either glove palms should be assembled with a protective film to eliminate the risk of particle contamination or a post-assembly cleaning process should be incorporated into the manufacturing process.

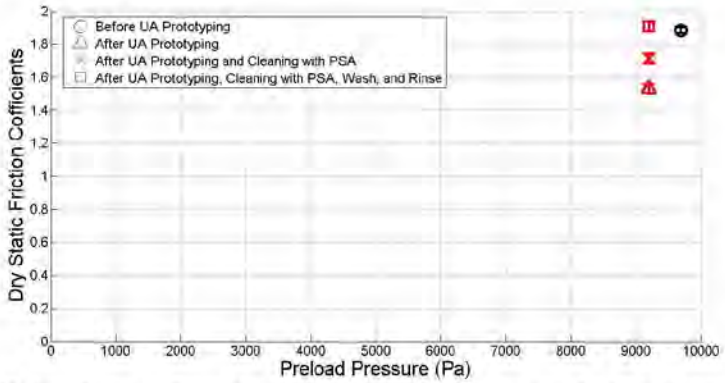

Figure 56: Static friction coefficient of glove prototypes before UA prototyping, after UA prototyping, and after UA prototyping and different cleaning processes.

C.3.2. C6: Provide Under Armour with the third-generation mass-produced fiber adhesive samples to for field-testing of the product specifications S1, S2, S3, S4, S5, S7, S8, and S9 as listed in Table 1.

Glove palm prototypes were provided to Under Armour on February 9th and March 2nd of this quarter. New closure prototypes were provided on March 6th.

C.3.3. Additional task – C4: Pilot system pricing (revisited)

During this last quarter, conversations were initiated with two different potential pilot system build-up partners: Foresight Technologies (Tempe, AZ) and Web Industries (Marlborough, MA). These two companies offer a different production approach. Foresight would be involved with the design and construction of a pilot production system from the ground up, and deliver a turnkey ready system for us to produce materials.

Web Industries' model of business would have them likewise design and build a pilot manufacturing system. However, their business model would have them produce this system at a lower cost in exchange for an arrangement whereby they operated as a contract manufacturing partner on our behalf for a negotiated fee.

Details of the preliminary quotes provided by these companies are included in Table 11 below. A second wave of conversations with these companies, as well as with PolyWorks Inc., who provided the quote that we discussed in our Milestone #3 research, were conducted in our final project quarter as we move toward an ultimate decision on who will build our pilot system for us.

Company Name	Foresight Technologies	Web Industries
Quote Highlights	Turn key horizontal & vertical configuration Fully Integrated Northfield Automation winders PC/PLC control Fully enclosed & exhausted environment Equipment and Process Startup 1 Year parts and labor warranty	Become familiar with process by observing proof-of-concept machine. Determine pilot-line deliverables, financial agreements and design/build resources. Design/build less than 12" wide continuous pilot-line process and locate at Web Industries Fort Wayne plant. DOE to optimize process parameters and reliability. Develop products with different materials or substrates. Determine commercial project details and secondary converting, die-cutting, slitting or sheeting. Design/build commercial process and optimize.
Estimated System Cost	$589,000 (up to 20" wide web) $776,000 (up to 1m wide web)	$275,000
Contract Manufacturing Fee	Contract manufacturing not available	~ $200/hr of operation + raw material costs + system depreciation costs

Table 11: Comparison of quotes for two different pilot manufacturing business models

Contact different UV lamp manufacturers to obtain lighting quotes for pilot manufacturing system

As shown above, microfiber performance properties are very sensitive to the curing conditions. Overcuring increases tip hardness and decreases adhesion while undercuring will cause inhibition and residue. Therefore, a uniform exposure area is critical. This includes uniformity within the one lamp and between two lamps in parallel. Additionally, the ability to adjust the intensity of the system is also needed to be able to account for formulation and temperature variation.

The ultimate line speed of the system will determine the intensity of the light needed and the distance the of belt exposure. Since most commercial UV lamps have a relatively fixed exposure distance ranging from 0.5 – 1 inch, light intensity will be our major source of curing control. For these quotes it was assumed that we will need the most intense light offered for each product. In this quarter, nGt contacted UV lamp manufacturers Fusion and Xenon in order to obtain lighting quotes for a 3-foot belt pilot R2R system that address the concerns above. Table 12 includes a summary of the lamp properties and costs.

As discussed at the Quarter 2 meeting, there are two types of UV lights, arc and microwave. Fusion supplies microwave UV lights which have some very attractive properties. For instance, the bulbs on fusion lamps last 8000 hours and the light intensity and spectrum do no fade over this duration. In comparison, the Xenon pulsed arc system does fade over time and only has a 1,000 hour lifetime at average intensities. Despite this, there are some advantages to the Xenon system. By pulsing the light, the temperature of the system can be better controlled and with the ability to change the pulse width and intensity, sample exposure can be precisely controlled. Xenon lamps are 20 inches wide and Fusion lamps are 10 inches wide and we would need 3 and 4 of them respectively for a 3-foot belt. This gives an extra knit line with the Fusion system. Depending on the sensitivity of the UV conditions this may or may not be a problem.

Due to the high uniform intensity of the Fusion microwave system, it is double the cost of the pulsed arc lamps of Xenon. It is the line speed will determine what type of system we choose. If the line speed is fast, higher light intensities will be needed. The shortcomings of the arc-type lamps (Xenon) such as drop in intensity over time and short bulb lifetime, will be magnified when maxing out the lamp power, and therefore a Fusion system would be the better option. However, at slower to moderate belt speeds, a less intense light is needed and a cost savings using the arc lamps.

Table 12: Property and cost comparison of Fusion (microwave) and Xenon (arc) lighting systems for a pilot systems featuring a 3 feet wide belt.

Company	Fusion	Xenon
Type	Microwave	Pulsed arc
Bulb lifetime	8000 hrs	1000 hrs
Bulb durability	No fading with time	Fades with time
Maximum bulb output	300 or 600 W/in	10-13 W/cm^2 pulse
Variable control	35-100% in 5% increments	2-2000 watts/pulse
Maximum light length	10 inches	20 or 30 inches
Amount needed pilot system	4	2
Cost/light	$15,000	$19,000
Total light cost (including controller)	$60,000	$29,600
Housing cost	$9,000	$4,500
Total system cost	**$69,000**	**$34,100**

C.4 MILESTONE 5: COMMERCIAL DEVELOPMENT

C.4.1 Prototype field testing

During this project quarter, we interfaced closely with Jason Berns and the Under Armour innovation and product development teams to provide them with multiple sets of fiber adhesive samples, both closures and football glove palms, for prototyping and field testing.

Closure field-testing

Several rounds of closure samples were sent to Under Armour for inclusion in new high performance outerwear and also for some user studies that were performed. The samples continue to initially perform well, however Under Armour has noted that some of the samples are not performing as consistently as desired or maintaining their performance after several months of aging. Also, the big challenge at this point for the closures is how they react to contaminants, specifically machine and skin oil, throughout the manufacturing and use life cycle.

From the user studies, Kerrie Timmons, Sr. Development Manager, Innovation at Under Armour, sent the nanoGriptech team the following update:

"We received positive feedback from the user studies. Most people think it's a nice idea and like the idea of having a velcro alternative. They are concerned about strength and durability, "will it really be strong enough to replace my velcro?" was a common question. The users were very engaged with the samples and were interested in seeing it in product."

Football glove field testing

Now that we had developed a good glove manufacturing technique and assembly process in earlier quarters in collaboration with UA, we sent three sets of glove palms to Under Armour for prototyping and field trials with elite student-athletes at the football programs at the Universities of Maryland and South Carolina, with whom UA works very closely.

At the University of South Carolina, four players gave qualitative evaluations of the glove when throwing and catching a football in dry and wet conditions. The wet conditions were obtained by submersing the wearer's hands in a bucket of water until the gloves were saturated. According to Jarred Law, Product Line Manager/Developer for Under Armour:

"[the gloves] didn't get a good reception when dry and was even worse when wet. Need to do more testing on this but I think initial tack or a tacky feel when wet is essential for consumer buy in."

The second day of testing at the University of Maryland produced better results. The results of this testing were transmitted to us by telephone by Alex Stone, Football Glove Product Manager for Under Armour.

The positives to take away from this testing include:

- The gloves performed better on this second test day than on the first test day
- The glove clearly was rated better than UA's commercially-available glove in wet conditions
- The glove got great feedback for very hard passes

The negatives which we will need to improve include:

- Because the glove is not tacky like their other products, there is a perception of slickness when players hold the ball
- The gloves were not rated as high for very soft passes

From these results, it appears as though our "dry adhesive" non-tacky materials may deviate too far from what habitual users of these gloves are used to. Even if our gloves perform better in wet conditions or for hard passes, this lack of tack may give users the perception of poor performance and prevent sales. As such, as a follow-up to these tests, we are in the process of preparing a slightly tackier formulation and modified fiber geometry that is compatible with this formulation for an additional round of testing and prototyping.

C.4.2. Intellectual property filing opportunities

C7: Assess the patent filing opportunities with the partners on the mass-produced fiber material design and manufacturing, fiber material composition, or fiber material integration to sporting fabrics.

During this project term, innovative work was done on both the material formulations and the processes necessary to optimize the development and integration of bio-inspired micro-fibrillar adhesives for sports apparel applications. There are several innovations that could eventually be filed for patents that were developed during this project term. The first is the concept of using transparent micro-patterned molds to cure through the mold to allow for direct integration of our adhesives into a customer's optically opaque product backing. This technique allowed us to mass-produce our materials directly integrated to textiles provided by Under Armour, which they could then easily assemble into their products. This direct integration during manufacturing eliminates the need for additional processing steps by our client, which could make it more desirable. We anticipate that this process will be useful for future clients who have product requirements which involve non-transparent fiber backing materials as this would mean that curing through the mold would be essential to our process. Additionally, using transparent molds reduces the exposure time to UV light necessary to properly cure the fibers, and it also results in a more uniform microfiber curing surface due to the increased exposure to light.

A second innovation which could eventually be filed as a patent is the ultimate material formulation used these for sports apparel applications. Research is ongoing to finalize this formulation and the processing parameters to produce optimized results, but once we have finalized these parameters, we may consider protecting them with a patent application. However, internal discussions will be held to evaluate whether this should instead be kept as a trade secret to eliminate the risk of overseas patent infringement.

C.4.3 nanoGriptech/Under Armour commercialization strategy

As the next step with UA, we are preparing a term sheet towards a commercialization agreement between our two companies. As the first component of this agreement, we will jointly continue to improve the sports closure and glove product prototypes until field study users and UA are fully satisfied with their performance, robustness, and durability. Moreover, during this development phase, more details related to the delivery of exact closure and glove prototypes with integrated gecko adhesives will be jointly determined. Next, the timeline, volume, and purchase price of our adhesive materials will be finalized. While this development phase is continuing, a pilot production system will be purchased and installed at nanoGriptech for production of these

adhesive materials for UA to allow us to meet the technical and production specs (microstructure geometry, material formulation, backing, volume, sales price) decided upon in this joint agreement. UA is interested in partially funding the pilot production facility production costs depending on the terms of this agreement.

Our joint development agreement with BMS runs through the end of this summer. At that time, nanoGriptech and BMS will jointly evaluate whether a continued joint development relationship makes sense for both parties as we move toward commercialization.

D. FUTURE DIRECTIONS

Under Armour and nanoGriptech are in the process of preparing and negotiating a term sheet for a joint development project which would involve UA partially funding a pilot production line in exchange for continued development of closure and football glove prototypes with milestones to meet for development, and delivery sales price and volume. Additional technical hurdles include producing samples that satisfy the real-world environmental handling of UA's product line. This will be accomplished through repeated protyping and field trials in collaboration with the UA team. Once these technical and financing hurdles have been overcome, the nanoGriptech engineering team will focus on the procurement, installation, and optimization of the pilot-scale production system to delivery product to Under Armour for incorporation in their product line.

E. REFERENCES

[1] Zhang, H. and Cloud, A. 2006 SAMPE Fall Technical Conference, "*Global Advances in Materials and Process Engineering", proceedings, Coatings and Sealants Section*, Nov. 2006, Dallas, TX.

[2] Berchthold, K. A. Nie, J. Elliot, J. E. Hacioglu, B. Luo, N. Trotter, A. J. N. Stansburry, J. W. Bowman, C. N. *Proc. Radtech Europe* 2001, 265.

[3] Jansen, J. Dias, A. A. Dorschu, M. and Coussens, B. *Macromolecules* 2002, *35,* 7529-753.

Appendix Q – 11-057 (EC Power)

Novel Nanocomposite Electrode Materials for High Performance Cylindrical 18650 Li-ion Batteries

A Final Report Submitted to
Pennsylvania NanoMaterials Commercialization Center

PI: Dr. Christian E. Shaffer
Project Manager: Dr. Rong Kou
Prepared by EC Power PA-Nano Project Team
In Collaboration with Penn State University Subcontract Team

EC Power
200 Innovation Blvd.
State College, PA 16803
Ph: 814-861-6233
Fax: 814-861-6234
http://www.ecpowergroup.com

January 15, 2013

Introduction

With the generous support from Pennsylvania NanoMaterials Commercialization Center, EC Power excitedly carried out the development of novel nanocomposite electrode materials for and the fabrication of high capacity cylindrical 18650 Li-ion batteries over the past year. There is great need for high capacity, high energy storage systems than can meet military requirements in addition to plug-in hybrid vehicles (PHEV), electrical vehicles (EV) requirements. In collaboration with our partner in Penn State, EC Power targeted to fabricate 3Ah high capacity 18650 cells with high capacity Si-carbon as anode materials and lithium-rich as cathode materials. Although there were quite a few technical challenges encountered during the material synthesis and battery fabrication process, the researchers and engineers at EC Power and Penn State have worked hard to solve the problems, meet the milestones on time, and strive for high capacity 18650 cells.

Milestone 1: Contract Signing and Project Kickoff

The project started in January, 2012.

Milestone 2

C1: Reach agreement with initial customer(s).

C1.1. Provide a list of customer(s) that will evaluate the prototype cells and provide feedback. These customers will likely have products with military applications, or be the military itself. This fits into our near-term market strategy for the final product, which targets primarily military applications that require power sources with an extremely high energy density, above all other attributes.

EC Power teamed with C&D Technologies, of Blue Bell, PA for evaluation of the developed prototype high energy density 18650 cells. C&D Technologies has designed and developed batteries for more than 100 years. C&D is a market leader in the North American Telecommunications, Uninterrupted Power Supply (UPS), and Utility markets for energy storage solutions and has a proven track record of supplying government, military, and commercial customers with high quality products. C&D has developed lithium ion energy storage solutions for both commercial and military products. Currently, C&D is in the midst of a four-year ($18M) U.S. Army program to develop a domestic source of affordable, large format lithium-ion cells, Battery Management Systems, and battery packs for both military and commercial applications.

We are proud to have C&D Technologies as our business partner and we believe that there is a great opportunity to continue work with C&D Technologies to further commercialize the high energy density 18650 lithium-ion batteries once our prototype battery meets the design criteria. With their long history of battery engineering, already-existing customer base, and strong reputation in serving commercial and military customers, we believe C&D is one of the most competitive companies in the market to further manufacture EC Power's products and provide the U.S. military with high energy density lithium-ion batteries.

C1.2. The agreement(s) will outline the terms of the prototype evaluation, including product specifications and the protocol/guidelines for the characterization tests to be performed. Figure

1 shows a copy of the signed letter of agreement for C&D's prototype evaluation of EC Power's 18650 high energy density cell. As noted in the letter, C&D is most interested in testing the cell capacity (through charge/discharge cycles) under various C-rates. The two deliveries of the prototype cells will occur in concert with the time frame scheduled in the EC Power/PA-Nano agreement.

Figure 1 shows a copy of the signed letter of agreement for C&D's prototype evaluation of EC Power's 18650 high energy density cell. As noted in the letter, C&D is most interested in testing the cell capacity (through charge/discharge cycles).

C&D TECHNOLOGIES
Power Solutions

Dr. Christian Shaffer
EC Power
200 Innovation Blvd.
Suite 250
State College, PA 16803

Mr. Daniel Boyer
C&D Technologies, Inc.
1400 Union Meeting Road
P.O. Box 3053
Blue Bell, PA 19422

March 25, 2012

Dear Dr. Shaffer:

Re: Evaluation of EC Power's prototype 18650 Li-ion batteries

C&D Technologies is excited to evaluate EC Power's prototype 18650 Li-ion cell, based on Li-rich metal oxide cathode and Si-C anode technologies. Given our current Li-ion battery products and our ongoing $18M Army project to deliver Li-ion battery systems for military applications, C&D Technologies is interested in the energy dense nature of this cell chemistry under development by EC Power.

As a part of the evaluation, the following tests will be performed:

- Charge, discharge, and capacity tests at 0.1 A current.
- Charge, discharge, and capacity tests at 1.0 A current.
- Charge, discharge, and capacity tests at 3.0 A current.

The first cell(s) to be evaluated will be given to C&D in July, 2012, and the second cell(s) to be evaluated will be given to C&D in October, 2012.

We look forward to working with EC Power in the evaluation of these cells.

Sincerely,

Daniel Boyer
Technical Manager
New Technology Development

Figure 1. Prototype evaluation agreement letter with C&D Technologies.

T1: Identify the Si-based nanocomposite anode with optimal composition, crystalline phase, interface properties, and nanostructures.

T1.1. Synthesize carbon-based nanocomposites with different functional groups, such as hydroxide, nitrogen groups.

Penn State synthesized Si-carbon nanocomposites with using two approaches. The first approach is to ball mill Si and carbon materials in formation of nanocomposites. In details, Si nanomaterials and Super P carbon are ball milled to form nanocomposite. The second approach is to use polymer precursor to grow and coat on Si nanoparticles followed by carbonization process. Penn State has specifically using nitrogen-containing polymer precursor to form nitrogen containing group in the carbon materials.

T1.2. Synthesize carbon-based nanocomposites with different surfactants, such as P123, F127.

We optimized the synthesis procedure with/without surfactant.

T1.3. Synthesize Si-Carbon nanocomposites following the optimized synthesis condition obtained from T1.1 and T1.2.

After optimization, Penn State successfully synthesized Si-carbon nanocomposites with Si coated with carbon layer. Penn State also synthesized Si-carbon nanocomposites with different weight ratio of Si to carbon.

T1.4. Characterize as-synthesized nanomaterials with TEM and XRD and select 4-5 nano-composites best suited for the anode materials.

The nanocomposite material prepared by ball mill process was characterized by TEM (Fig. 2) and the carbon additive can be seen coated on the Si nanoparticles. The Si-carbon nanocomposite material prepared by coating methods was also characterized by TEM (Fig. 3). The spherical Si nanoparticles were all coated with a layer of carbon materials. Penn State has also characterized the material using XRD. XRD pattern show typical reflection peaks for both Si-carbon nanocomposite materials (Fig. 4)

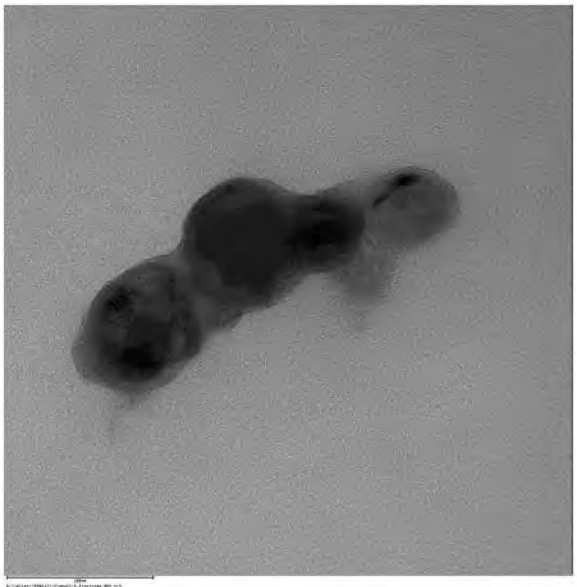

Figure 2. TEM of Si-C nanocomposite prepared by ball mill process (scale bar is 100 nm). The carbon additive seems to act as a coating to the Si nanoparticles.

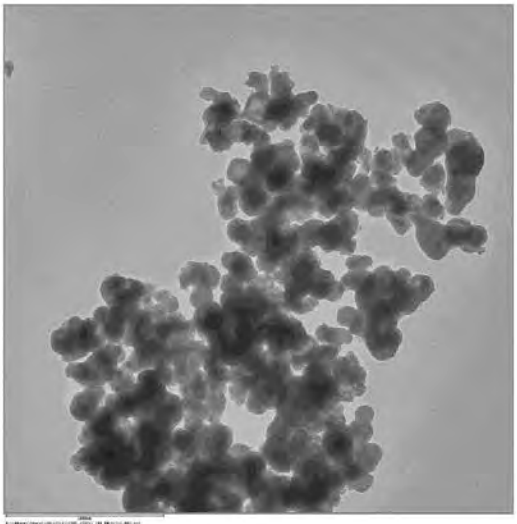

Figure 3. TEM of Si-C nanocomposite prepared by polymer coating process followed by carbonization (scale bar is 1000 nm).

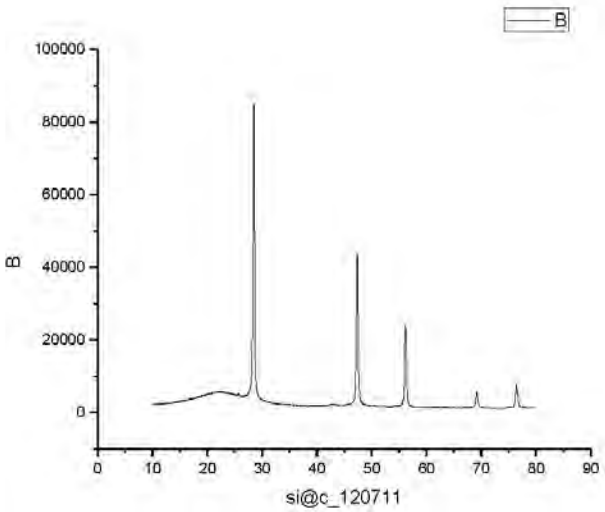

Figure 4. XRD profile of as-prepared Si-C nanocomposite.

Penn State also did a preliminary battery test on Si-C nanocomposites prepared by ball-mill process. The Si-C nanocomposite show discharge capacity above 1800 mAh/g nanocomposite at the first few cycles (Fig. 5). Penn State will continue to optimize and characterize the Si-C nanocomposite and test its battery performance.

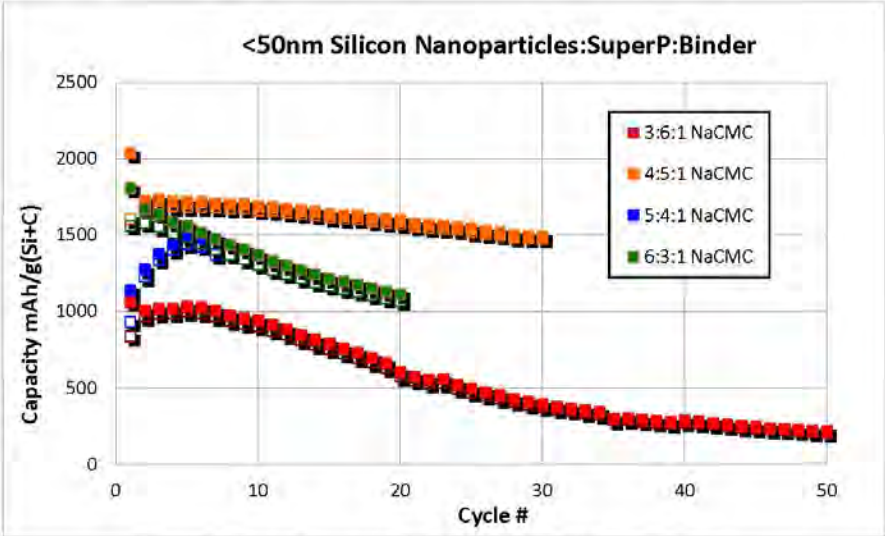

Figure 5. The performance of Si-C anode with different Si:C ratios.

C2. Market Synopsis

Along with the increasing demands for energy in modern society, the military faces its own energy challenge. As reported, the military consumed 93 percent (120 million barrels costing $16 billion) of all oil used by the U. S. Government in 2008. Moreover, the warfighting is about 16 times more energy-intensive than the peace time. The oil consumption per warfighter rose 2.6 percent annually during the past 40 years and is projected to rise another 1.5 percent annually through 2017 due to greater mechanization, remote expeditionary conflict, rugged terrain, and irregular operations.[1] The Department of Defense (DOD) is probably the world's largest institutional oil buyer. The DOD is looking for alternative energy source for military use for three reasons: security, climate and the cost. The 2010 National Defense Authorization Act requires the DOD to use renewable energy sources for 25 percent of its facilities by 2025. The DOD itself highlighted that "reducing the demand for energy must be the most immediate operational energy priority for the Department" in its Operational Energy Strategy released May 2011.

High energy density energy storage devices are critical in providing alternative energy. Lithium-ion battery technology attracts a lot of attention due to its low weight, high energy density and long cycle life. The US military drastically needs high energy density lithium-ion batteries for use in various applications. The Figure 6[1] from the reference shows the approximate amount of liquid petroleum used by the DOD in FY2005. As it shows, the Air force consumed 53%, the Navy consumed 33%, the Army consumed 12%, and the Marines and others consumed 2% of the 136 million total barrels used by DOD. High energy density lithium-ion batteries could contribute to multiple military applications and significantly decrease the usage of liquid petroleum. Several examples of near-term targeted applications which require a high energy density are shown below.

Target Li-Ion Army Applications include:

- Long endurance aerial vehicles (UAV's)
- Long endurance autonomous systems
- Unattended sensors

Target Li-Ion Air Force Applications include:

- Long endurance aerial vehicles (UAV's)
- Space applications such as Directed Energy and Satellite Power

The future market of lithium-ion batteries is huge. According to the forecast from cleantech market intelligence firm Pike Research, the installed cost of lithium-ion batteries will drop more than one-third and the market of lithium-ion batteries will grow to more than $14 billion by 2017 driven by the plug-in hybrid electric vehicles (PHEVs) and battery electric vehicles (BEVs).[2] Although the military market is more dynamic depending on if the new battery chemistry and technology can meet the standards and specifications of the sophisticated modern military

equipments, it is estimated that the current military market is already over $0.1 billion and the demand is projected to steadily increase over the next five years.

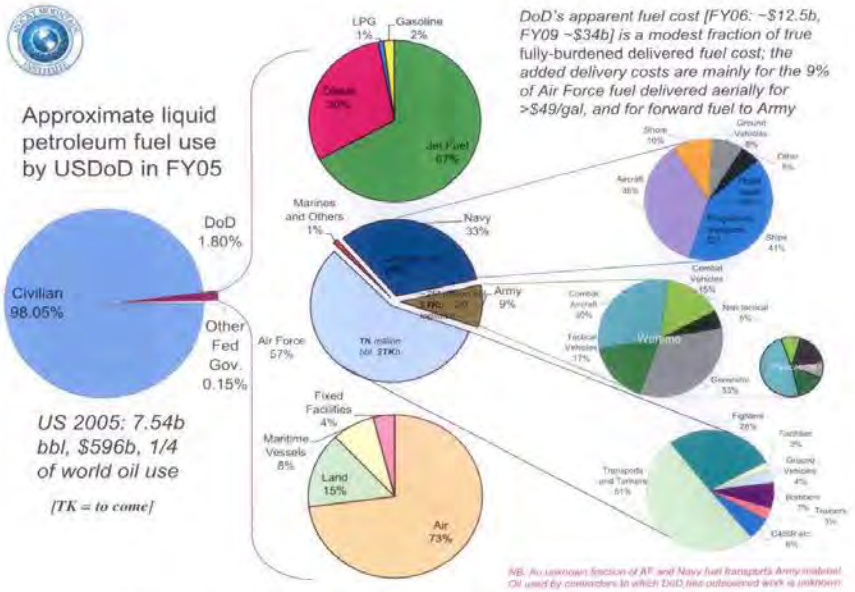

Figure 6. Approximate liquid petroleum fuel use by DOD in 2005.[1]

Milestone 3

T2: Identify the Si-based nanocomposite anode with optimal composition, crystalline phase, interface properties, and nanostructures.

T2.1. Continue to optimize Si-based nano-composite by adjusting the surfactants and experimental conditions, such as the incubation time, temperature, etc.

Penn State has continued to test new compositions by varying the Si:C ratio, the binder type and content, the electrode preparation method, and the Si particle size. We tested the performance of NaCMC, PVA, LiPAA, PAA, xanthan gum, and chitosan based materials as binders, coming to the conclusion that PAA or LiPAA provided the most stable data. Additionally, Penn State was able to test the effect of silicon particle size by using several different sizes of silicon nanoparticles; obtaining very good performance with particles with average diameter less than 100 nm. In testing binders we found the most reliable performance and coating with ball milled slurries using PAA and LiPAA in aqueous solution.

T2.2. Characterize as-synthesized nanomaterials with XRD, TEM

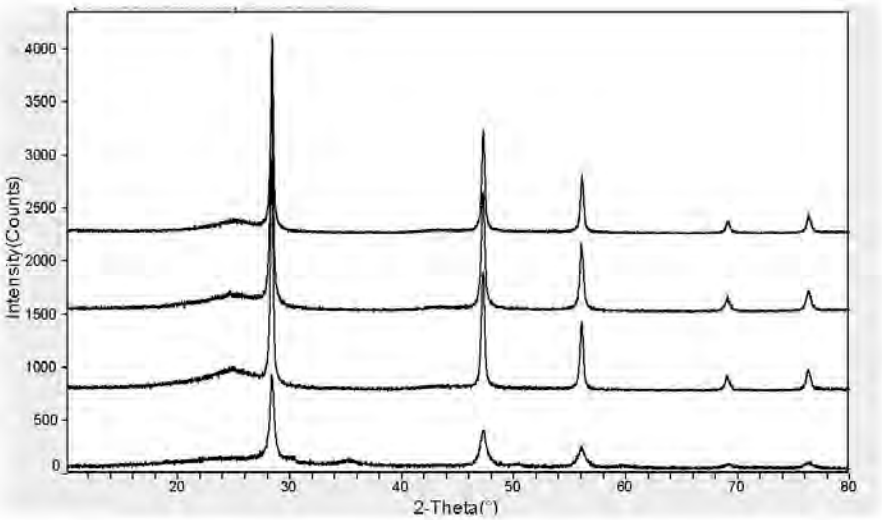

Figure 7. Powder XRD profiles of as synthesized ball milled Si-C nano-composite materials. Materials produced with 4:5 silicon to carbon ratio by planetary milling using different Si-nanoparticles. From top: <50nm particles milled for 1hr; <50nm particles milled for 5hrs; <100nm particles milled for 5hrs; and <30nm particles milled for 5hrs.

Figure 8. TEM of Si-C milled composite prepared from < 50nm Si-nanoparticles. Scale bar is 100nm.

T2.3. Select the nanocomposites (as many as possible) which have highly crystalline Si nanoparticles uniformly dispersed on carbon substrates with controlled porosity, Si/carbon ratio for next step.

Penn State has chosen several compositions of Si-C composites to primarily test centering around a 4:5 ratio of < 50nm silicon nanoparticles to conductive carbon prepared by mechanical milling.

T3: Identify appropriate composition, crystalline phase, interface properties, and nanostructures of high $xLi_2MnO_3{\cdot}(1\text{-}x)LiMO_2$ composite cathodes

T3.1. Synthesize $xLi_2MnO_3{\cdot}(1\text{-}x)LiMO_2$ composites by adjusting the surfactants and the experimental conditions, such as temperature, calcinations time, etc.

We have synthesized $xLi_2MnO_3{\cdot}(1\text{-}x)LiMO_2$ with different compositions. A number of experiments were carried out to study the effect of the following factors:

1) Acid and basic conditions. The synthesis was carried out under both acid and basic conditions, respectively. The reaction under basic condition was more controllable and

repeatable. We also optimized the amount of the acid and basic. The experiments showed that unbalanced acid/base ratio causes the unwanted precipitation of the raw materials.

2) The calcinations temperatures and calcination times. The calcinations were used to burn out the organic residues and make the solid reaction sufficient. However, lithium starts to lose from the compound and the crystalline structure may change when the temperature is too high or the calcinations time is too long. We calcinated the samples under different temperatures for various times in order to optimize the calcination condition for the solid reaction but without the loss of Lithium.
3) The different compositions and different compounds. We investigated the various compounds with different compositions and different metal oxides. The changes of the composition didn't make obvious changes on XRD patterns. However, the big difference was reflected on the coin cell test results. Table 1 shows the composition of the compounds we have studied. Although they all showed the similar XRD patterns, $Li(Li_{0.17}Ni_{0.25}Mn_{0.58})O_2$ and $Li(Li_{0.2}Ni_{0.13}Mn_{0.54}Co_{0.13})O_2$ showed better capacity in coin cell tests.

Table 1. Different compounds were studied

x	Composition
0.14	$Li(Li_{0.14}Ni_{0.24}Mn_{0.55})O_2$
0.17	$Li(Li_{0.17}Ni_{0.25}Mn_{0.58})O_2$
0.20	$Li(Li_{0.2}Ni_{0.2}Mn_{0.6})O_2$
0.22	$Li(Li_{0.22}Ni_{0.17}Mn_{0.61})O_2$
0.2	$Li(Li_{0.2}Ni_{0.13}Mn_{0.54}Co_{0.13})O_2$

T3.2 Characterize as-synthesized nanomaterials with XRD, TEM.

Figure 9 shows the XRD pattern of $Li(Li_{0.2}Ni_{0.13}Mn_{0.54}Co_{0.13})O_2$, the XRD pattern shows the highly crystalline structure of the nanocomposite. The pattern is similar as reported in the literature. Because the product is solid nanoparticles and the particle size is about 200-300nm, we use SEM instead of TEM for the characterization. SEM is a more convenient measurement for the size and surface morphology of the large size nanoparticles. Figure 10 shows a few SEM images under different magnifications. Figures 10a and 10b show the final product of $Li(Li_{0.2}Ni_{0.13}Mn_{0.54}Co_{0.13})O_2$are packed nanoparticles and Figure 10c clearly shows the size of nanoparticles are around 200-300 nanometers, with irregular shape.

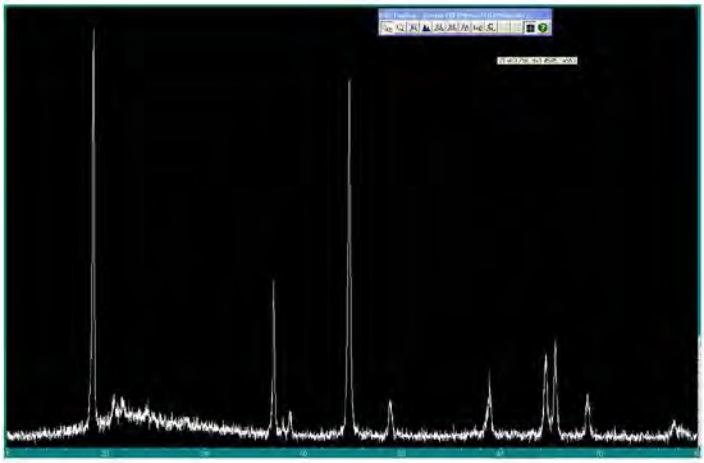

Figure 9. XRD pattern of high crystalline structure $Li(Li_{0.2}Ni_{0.13}Mn_{0.54}Co_{0.13})O_2$.

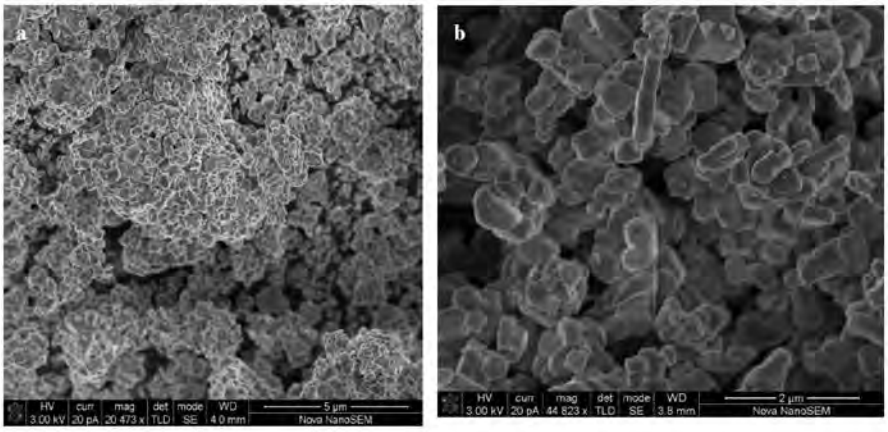

Figure 10. SEM images of $Li(Li_{0.2}Ni_{0.13}Mn_{0.54}Co_{0.13})O_2$nanoparticles under different magnifications.

T3.3. Select the nanocomposites which have highly crystalline structure, uniform particle size for the next step.

A few of nanocomposites with highly crystalline structure and uniform particle size are selected for the following coin cell tests.

T4: Improve the specific capacity of the Si anode to more than 1,000 mAh/g (double that of commercial graphite) with minimal capacity fade in 100 cycles. Improve the high capacity cathode with discharge capacity larger than 250 mAh/g. Reaching these anode and cathode material specific capacities, will facilitate the fabrication of a 3Ah capacity 18650 cell, according to preliminary design work and experience. The 3Ah capacity goal for the 18650 cell would be a world-class performance for a multitude of "energy applications", where energy density is of paramount concern (i.e. where the cell is chosen largely due to its available capacity or energy density).

T4.1. Fabricate half coin cell with carbon-Si nanocomposites from T2, and test the electrochemical performance to obtain charge-discharge profile, capacity, voltage and rate performance.

The carbon-Si nanocomposites from T2 were fabricated and tested in coin cells. The results are shown under T4.3.

T4.2. Fabricate half coin cell with xLi_2MnO_3•$(1-x)LiMO_2$ nanocomposites from T3, and test the electrochemical performance to obtain charge-discharge profile, capacity, voltage and rate performance.

The Li-rich cathode materials from T3 were fabricated and tested in coin cells. The results are shown under T4.3.

T4.3. Optimize the synthesis for both anode and cathode materials and improve the capacity of Si anode to 1,000 mAh/g (double that of commercial graphite) with minimal capacity fade in 100 cycles, and Improve the high capacity cathode with discharge capacity larger than 250 mAh/g. (Note: Currently we have reached the capacity of Si anode to 1000 mAh/g for 30 cycles and cathode capacity larger than 200 mAh/g).

Anode:

As shown in Figure 11, the optimum composition obtained (4:5 ratio of <50nm Si-nanopaticles and conductive carbon) has produced a high and relatively stable gravimetric specific capacity. The capacity was over 1500mAh/g after the first 20cycles and was still over 1000mAh/g after 100 cycles. Penn State has also continued to optimize the preparation of the material and the electrodes particularly to improve the higher rate performance of the material. Figures 12 and 13 show the cyclic performance of electrodes produced with NaCMC, LiPAA, and PAA binders cycled at a higher rate (800 mA/g) and a sample of the charge discharge curves of the LiPAA sample.

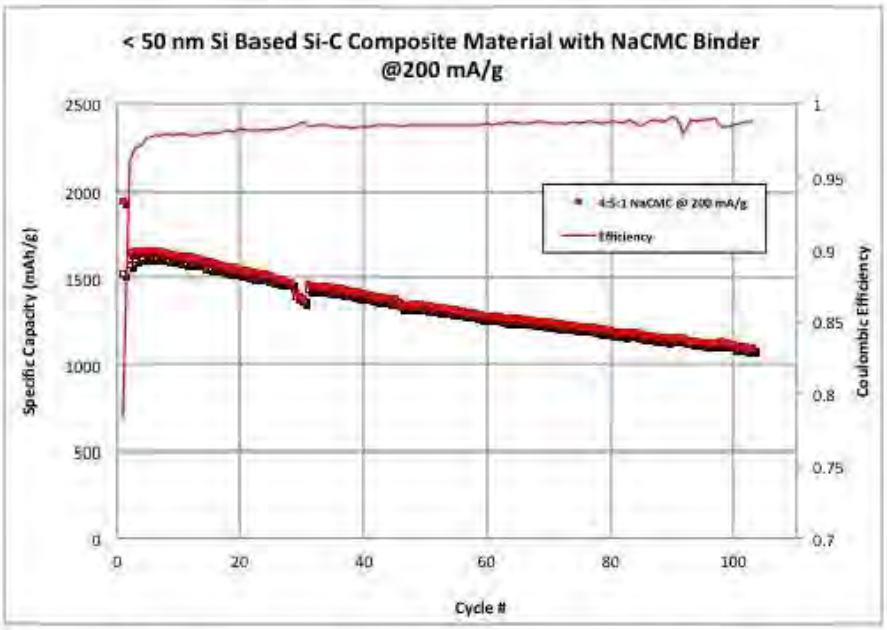

Figure. 11. Cyclic performance data for 4:5 Si-C composite material with <50 nm diameter silicon nanoparticles. The electrode was prepared using 10% NaCMC as the binder material in a 2032 coin cell with Li as the counter electrode. Cycled at a rate of 200 mA/g from 0.01 to 1.00V, this material shows a specific capacity of ~1100mAh/g at 100 cycles.

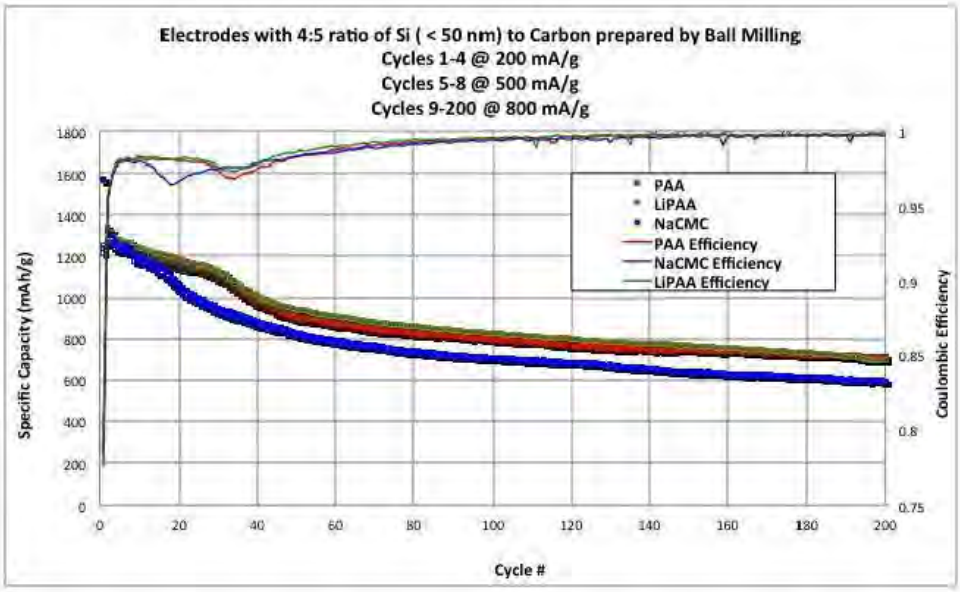

Figure 12. Cycling performance of Si-C composite anodes in half-cells with Li as the counter electrode. Cells were cycled from 0.01-1.00V in Newware Battery test unit. The electrodes were prepared by milling the composite material with LiPAA, PAA, and NaCMC binders in 1wt% solution. After initial cycling at 200 mA/g and 500 mA/g the cells were cycled at 800 mA/g. Initial coulombic efficiencies are all greater than 78%.

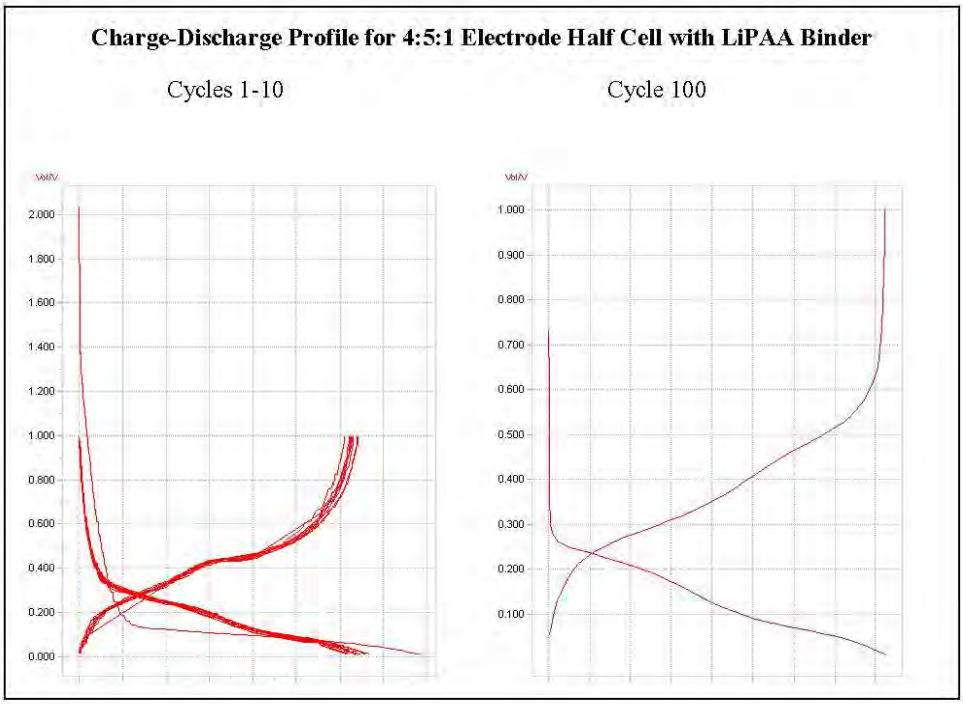

Figure 13. Charge-discharge profiles of 4:5 Si-C composite electrode with 10% LiPAA binder in half-cells with Li as the counter electrode. Cells were cycled from 0.01-1.00V in Newware Battery test unit at 200 mA/g for 4 cylcles then 500 mA/g for 4 cycles followed by continued cycling at 800 mA/g. The electrodes were prepared by milling the composite material with LiPAA binderin 1wt% solution.

Cathode:

We use the nanocomposites passed T3 selection to fabricate 2016 coin cells. The coin cells were tested under different currents and voltages. Many cells died quickly or showed poor capacity during the test. With the further optimization of the synthesis, we successfully produced the lithium rich cathode with desired capacity. Figure 14 shows the charge-discharge profile of as-synthesized cathode material. The charge curve shows a plateau around 4.5V before it is fully charged to 4.8V, which is a signature of Li-rich cathode charge profile; this data is charged and discharged at a current of 15 mA/g. The first cycle charge capacity is around 287mAh/g and the discharge capacity is around 224mAh/g, however, the discharge capacity increased in the second and the third cycles and reached to 240mAh/g. Figure 15 gives the same test data as for the tests given in Figure 14, but gives the capacity up to 14 cycles. Figure 15 clearly shows the cathode keeps high capacity of roughly 240 mAh/g over multiple cycles. We also tested the cathode

material under different currents. Figure16 shows the charge-discharge profile of the cathode tested under much higher current (50mA). Naturally, the capacity drops when the charge current increases. The cathode material only shows the first cycle discharge capacity of 143mAh/g but the capacity continually increases to over 180mAh/g after 20 cycles.

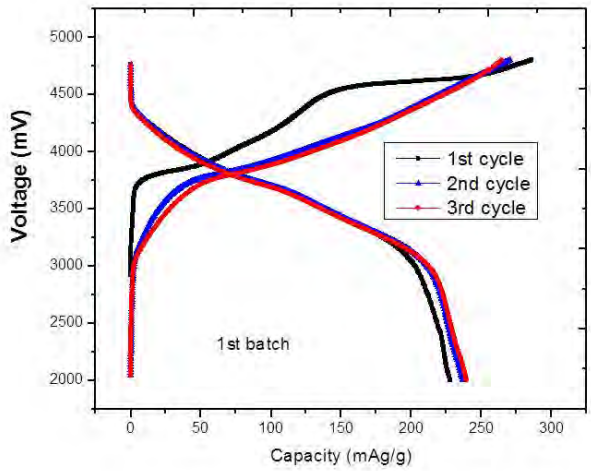

Figure 14. Charge-discharge voltage- capacity profile of Li-rich cathode under the current of 15mA/g.

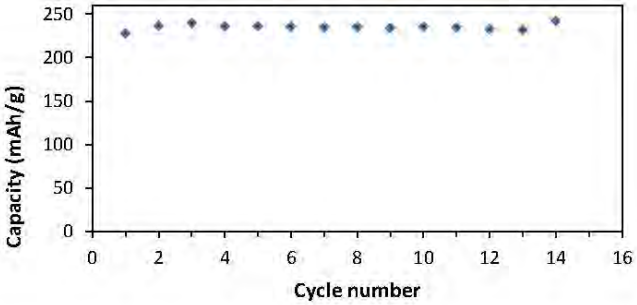

Figure 15. The capacity of $Li(Li_{0.2}Ni_{0.13}Mn_{0.54}Co_{0.13})O_2$ is around 240mAh/g in multiple cycles; current of 15mA/g.

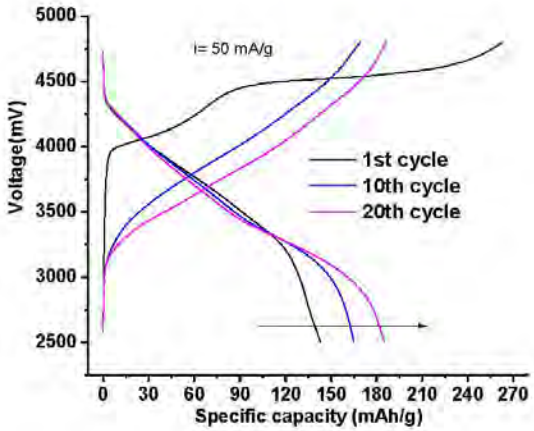

Figure16. Charge-discharge voltage-capacity profile of Li-rich cathode under the current of 50mA/g.

T4.4. Select one cathode and one anode material which has best performance for the next step to fabricate optimized 18650 cells.

Anode:

PSU has selected Si-carbon as the anode for the fabrication of 18650 cells. The selected materials show high capacity of over 1000mAh/g after 100 cycles. The use of low cost carbon material in substitution of graphene also saves the cost in battery fabrication

Cathode

With a number of times of optimization, we select $Li(Li_{0.2}Ni_{0.13}Mn_{0.54}Co_{0.13})O_2$ as the cathode material for the fabrication of 18650 cells. The choice is not only because the compound shows high capacity (240mAh/g) in the coin cell test but also the synthesis approach is more convenient to scale up. Currently, EC Power has successfully reached 30g/batch with the capability to further scale up. This will benefit our 18650 cell fabrication and the large scale production in the future.

C3: Deliver one initial 18650 cell to customer(s) for testing and evaluation, as per terms of agreement reached in C1. The cell to be delivered for testing will use most promising Si-based nanocomposite anode and xLi2MnO3(1-x)LiMO2 materials.

The initial cell design was completed. We observed gassing problems during the testing of thick electrode coin cells. It became evident that gassing was an issue with the cathode active material, as most of the fabricated coin cells popped open during testing. This was obviously a safety issue, particularly for the larger to-be-fabricated 18650 cell. As the gassing primarily occurs during the first few cycles due to high voltage charge, we developed a method that would allow us to cycle the 18650 cell for a few cycles before fully sealing. After a short delay, we successfully and safely fabricated the first batch of prototype 18650 cells, and milestone C3 was reached.

C4: Provide a report on that outlines the cost structure as anticipated for the production of the cell, viz. anode and cathode. Included in the report will be (a) an update of the graphene production technology and issues related to volume (manufacturing and scalability) and related cost, and (b) an estimated cost breakdown for production of the battery and how it compares to current market pricing.

The following cost estimate is based on the current market price of the all cell components, for our anticipated near-term military market production quantities. To better understand the cost, we break down the cost structure to the cost of active material (Table 2), and the cost of other cell components, labor, etc. of 18650 cells (Table 3).

In the first and second project periods, the researchers at PSU have synthesized Si anode with different kinds of carbon materials. They have successfully synthesized the Si-carbon anodes in which highly conductive, commercially available, low-cost carbon materials are used in substitution of expensive graphene materials. The Si-carbon anode not only shows the better capacity than Si-graphene anode but also decreases the cost of the anode material. Although it has been predicted that graphene nanoplatelets can be produced at $5 per pound, the mass commercialization of graphene may still be years away due to a number of product and process obstacles, including the cost of the development, the technological complication that pertains to the high electrical conductivity and the difficulties relating to health and safety in nanotechnology. On the contrary, the carbon employed here only costs less than 1cent per gram benefited by the established long-term massive production. The use of the low cost carbon also protects the cost of our cells from the current fluctuations of the graphene market price.

As shown in Table 2, while the replacing graphene with lower-cost carbon materials is cost-effective, the cost of high-quality Si nano-particles still leads to a rather expensive anode. To reach the 3Ah goal, 12.1g of Li-rich cathode materials and 6.2 g of Si/carbon anode materials are needed (0.62g of Si and 5.58g of carbon). We further assume an 85% fabrication materials efficiency (15% of active materials essentially wasted, i.e. does not make it into the cell, during the cell production process). Since both cathode and anode are the top leading materials for their ultra high capacities and made with advanced nanotechnology, the cost of the cathode and anode materials is higher than that in traditional Li-ion battery.

Table2. The estimated cost of cathode and anode materials at near-term market production quantities.

	Cost $/g	Mass in Cell(g)	Fab. Materials Efficiency	Materials Mass per Cell (g)	Total ($)
Cathode	0.035	12.1	0.85	14.24	0.50
Anode	Silicon: 2	0.62	0.85	0.729	1.49
	Carbon: 0.005	5.58	0.85	6.56	
Total					1.99

Table 3. The estimated cost of 18650 fabrication at near-term market production quantities.

Anode & Cathode Materials	Separator and electrolyte	Can, cap, etc.	Labor	Mark up	Total
$1.99	$0.55	$0.20	$1.00	$1.60	$5.34 or ~ $500/kWh

As a summary from Table2 and Table 3, the estimated cost of our 18650, Li-rich metal oxide cathode, Si-carbon anode Li-ion battery will be $5.34, or ~ $500/kWh. It should be noted that the greatest cost of the cell is from the anode materials. Over the long term, we expect the cost of high-quality silicon nanoparticle to continue to drop; naturally, the price of our cells will likewise drop significantly if/when this happens.

The military's immediate and great need for high specific energy batteries is highlighted, for example by the Air Force's recent Title III call, where the main technical target was listed as 250 Wh/kg[3]. Given the current state-of-the-art specific energy in the automotive field (EVs) of ~ 170 Wh/kg, this represents a nearly 50% increase over these widely available and cheaper cells. Further, best estimates for these automotive cells put them at ~ $350 - $450/kWh. The roughly 50% increase in capacity will come at a premium, and given the already-attractive estimated cell price of ~ $500/kWh, we strongly believe that our technology will be quite attractive to the military as a low-cost, near-term solution to approaching their high specific energy needs.

MILESTONE 4

T5: Identify appropriate design parameters for fabrication of 3Ah 18650 Li-ion battery cells.

T5.1. Formulas for the anode and cathode slurries and their electrode dimensions will be selected and optimized using EC Power proprietary design software.

The end result from our software design is given in figure 18. This figure is the culmination of many iterations of parameters such as packing density, electrode slurry compositions, etc., in designing a cell reaching 3 Ah.

In addition to simply using EC Power software to identify appropriate design parameters, a series of studies was also performed using thick coin cells, in effort to ensure the fabricated thick electrodes and resultant cell would scale up properly. The formulas of anode and cathode slurries were identified in order to obtain robust thick film while maintain the high capacity. Compared to anode, cathode is more difficult to prepare because of the requirement of the thicker film.

In order to achieve 3Ah capacity, thick electrode has to be used in 18650 cells. Based on the calculation and design from EC Power's cell design engineer, the thickness of Li-rich cathode should be around 150 micro meters with 75 micro meters in each side. However the thick electrode is more likely to peel off and shows poor performance during the battery tests (as shown in Figure 17a).

We have carried out many experiments to optimize the ratio of active material, carbon and PVDF in order to obtain robust thick electrode with high capacity. We finally reached a combination and successfully fabricated the electrode with density over 8mg/cm^2 (as shown in figure 17b). In the meantime, we observed the effect of particle size in preparation of the electrode and decided to use Grill mill to decrease the particle size before it was used to prepare the slurry for the electrodes.

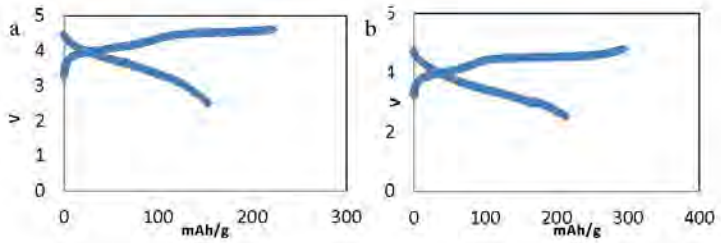

Figure 17. The thick electrode shown decreased capacity a), and the capacity was improved with optimized slurry formula b).

T5.2. Factors such as electrode packing densities and porosities will be optimized for the target specification of 3Ah.

A series of studies was performed to test the packing densities of both cathode and anode. EC Power's engineer has improved the parameters of packing densities and porosities based on thick coin cell tests, software, and the experience of making the first batch 18650 cells. The decided upon design is given in figure 18.

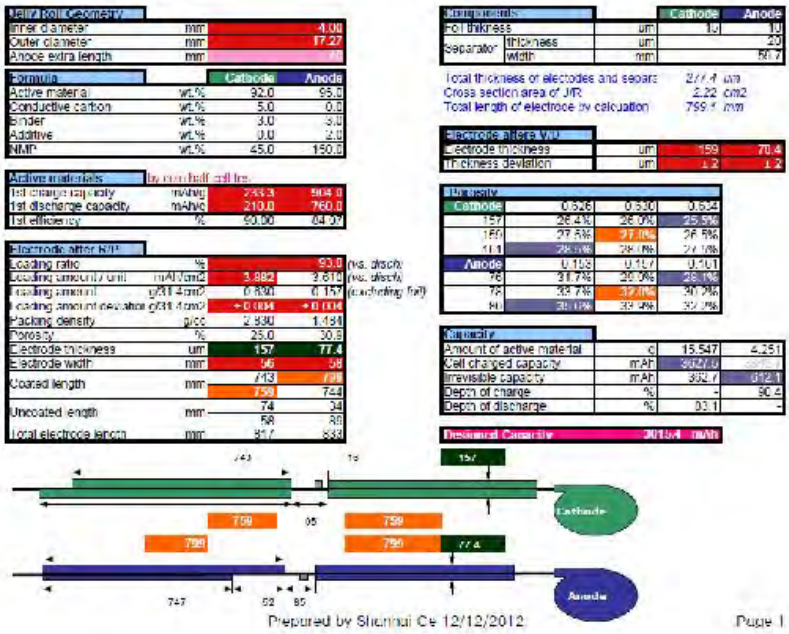

Figure 18. Design sheet for 3Ah 18650 cell.

T6: Show data for the improved performance testing for the optimized design of the novel nanocomposite electrodes by fabricating >3Ah 18650 Li-ion battery cell.

The performance target is an 18650 cell with > 3Ah capacity. This will require anode material of ~ 1000 mAh/g and cathode material of ~ 250 mAh/g (i.e. 3 Ah cell will deliver much greater than 200 Wh/kg @ the cell level).

EC Power and Penn State partner have successfully synthesized Li-rich cathode materials and Si-carbon anode materials during the last two quarters. The researchers in Penn State have identified that Si-carbon nanoparticle with 4:5 ratio and NaCMC as binder which shows high capacity of over 1500mAh/g and capacity of 1100mAh/g after 100 cycles with the minimal capacity fade. EC Power has successfully synthesized $Li(Li_{0.2}Ni_{0.13}Mn_{0.54}Co_{0.13})O_2$ as the cathode for the 18650 cell fabrication which shows a capacity of 240mAh/g in coin cell test.

In this quarter, EC Power focused on fabrication of 18650 battery cells with as-synthesized materials. However, there are a few technical challenges surfaced during the design and fabrication process. Many efforts were put into material and process optimization in order to overcome these challenges. Since it will greatly increase the time and efforts if we carry out the optimization experiments in 18650 cells, we performed all the tests in coin cell level and all the knowledge and data from the coin cell tests were applied to 18650 cell fabrication.

One challenge in the process was gassing problem of cathode materials during the charge-discharge of the battery.

The Li-rich materials release the gas during the charge-discharge cycles because of the unstable nature of the material. The coin cells were likely to pop open during the tests when thick electrodes were used. The gassing problem not only affects the performance of the battery but also increases the safety concerns in 18650 cells.

In order to solve the gassing problem, we tried two approaches. Firstly we used acid treatment to activate the Li-rich material before it was fabricated into the electrode. The gassing problem was greatly reduced with the as-treated materials and we did not observe any coin cells popped open during the tests.

Secondly, EC Power designed and made an open system to form18650 cells (formation during first few cycles). With our open system set-up, the gas produced in 18650 cell was released before the final seal of 18650 cell. This fabrication feature greatly decreases the possibility of the accidents such as explosions during the battery tests. After filling the electrolyte, the cell was put in a cell holder as shown in figure 19. A pressure controller (on the top) was used to release gas produced during charging. The pressure is keep at lower than 0.7 atm to prevent building up of the high pressure and the possible explosion.

Figure 19. The testing holder designed by EC Power.

During the design of 18650 cells, we also find the 1st cycle efficiency is a key parameter in order to achieve designed capacity.

To increase the 1st cycle efficiency of Li-rich material, we applied acid treatment and thermal treatment to the materials after they were synthesized. With many efforts on experiments, we have successfully produced Li-rich material with over 90% 1st cycle efficiency while keeping the high capacity. Figure 20 shows the improvements on performance of the Li-rich material using acid treatment under different conditions. It clearly shows the first cycle efficiency was improved with the acid treatment. Under the optimized conditions, the 1st cycle efficiency is increased from 63.3% to 97.7%.

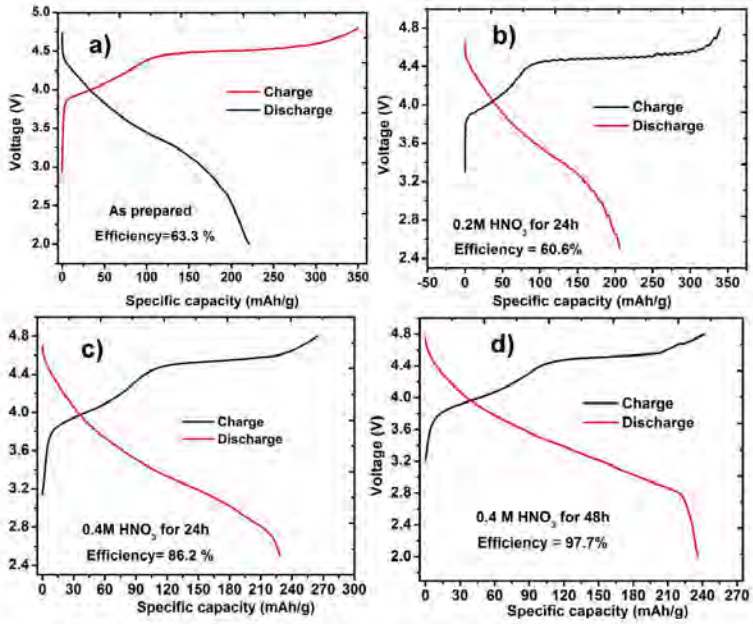

Figure 20. The 1st cycle efficiency of Li-rich cathode is greatly increased with the acid treatment.

We have investigated and solved the technical problems under coin cell level and applied our knowledge to the design and fabrication of 18650 cells. We have also evaluated the performance of the cells. **The capacity for the 0.1A discharge of our second batch of 18650 cells is around 2.584Ah as shown in figure 21, which is greater than the first prototype cell by ~ 13%.** While the capacity at low discharge rate is encouraging, the capacity at discharge rate of 1A and 3A tests were low, coming in at 0.453A and 0.252 A, respectively. It indicates a high electronic resistance within the electrode which prevents the transportation of electrons at high charging rate. The engineer also identified the similar problem during the fabrication of Li-rich cathode. As figure 22 shows, the Li-rich cathode has many cracks on the surface during the coating process. The surface becomes shinning and the cracks are more serious after the pressing. It indicates a bad adhesion between the materials and the substrates. In spite of our best efforts experimenting with thick coin cells, the slurry formula optimized for thick electrode coin cells did not work as well when scale up to large electrode films. More defects were observed on the surface of the large electrodes. Si-carbon anode shows a smooth and uniform surface before the pressing and no obvious cracks were observed after pressing as shown in figure 23a and 23b. Comparing the anode and cathode electrodes after pressing, the Si-carbon anode is more soft and uniform, while Li-rich cathode has more cracks and is more rigid (figure23c). The rigid nature of the cathode also brings more difficulties in rolling process, including observed flaking of the material during the rolling process.

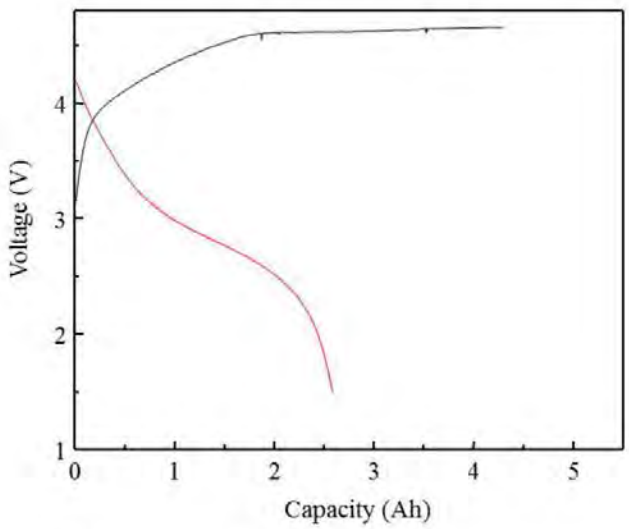

Figure 21. The charge-discharge curve of Li-ion battery with Li-rich material as cathode and Si-carbon as anode at discharge rate of 0.1A. The discharge capacity is 2.584Ah.

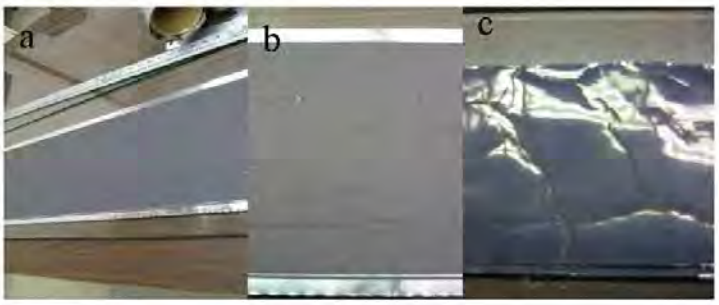

Figure 22. Li-rich cathode before pressing a) and b), after pressing c).

Figure 23. Si-carbon anode before pressing a), after pressing b) Li-rich cathode and Si-carbon anode after pressing c).

T7: Deliver the optimized cell to customer for testing and evaluation.

The optimized cells have been tested in EC Power. The capacity at 0.1A discharge rate is 2.584Ah. Although the 13% improvement from the last prototype cells is very encouraging, there is still room to improve to reach our 3Ah target. We have communicated with our customer, C&D Technologies, and we both agreed there is no need to test the cells at the current point in order to save the time and efforts of our customer. As highlighted in the letter of support in section C7, C&D Technologies remains highly interested in our technology, and would like to continue support EC Power on the development of high capacity Li-ion cell technology.

C5: Provide a report outlining the feedback received from the customer evaluation and testing of 18650 Li-ion cells. The feedback report will describe the results of the tests performed by the customer, in accordance with the agreement in C1.

Two feedback letters are given below. The first one, given in figure 24, is the evaluation of the first prototype, and the second letter, given in figure 25, is the evaluation of the second prototype. In addition to these two evaluation letters, we have remained in steady contact with C&D over the course of the project, including a meeting at EC Power on September 21, 2012.

Dr. Christian Shaffer
EC Power
200 Innovation Blvd.
State College, PA, 16803

Mr. Daniel Boyer
C&D Technologies, Inc.
1400 Union Meeting Road
P.O.Box 3053
Blue Bell, PA, 19422
September, 24, 2012

Dear Dr. Shaffer,

The evaluation of EC Power's first prototype 18650 cells, based on Li rich metal oxide as cathode and silicon carbon nanoparticles as anode, is complete. The cells were tested under the protocol originally agreed to in the support letter dated March 25, 2012. The 18650 cells show the performance as follows:

Discharge Current (A)	Capacity (Ah)
0.1	2.287
1	2.169
3	2.086

L&D Technologies will keep in touch with EC Power and pay close attention to the development of the high capacity 18650 battery while EC Power continues optimizing both material synthesis and battery fabrication to strive for 3Ah goal.

We look forward to continuing our work with EC Power and the future development of their high energy density technology.

Sincerely,

Daniel Boyer
Technical Manager
New Technology Development

Figure 24. Evaluation of EC Power's first prototype 18650 cell.

C&D TECHNOLOGIES, INC.
Power Solutions

Dr. Christian Shaffer
EC Power
200 Innovation Blvd,
State College, PA, 16803

Mr. Daniel Boyer
C&D Technologies, Inc.
1400 Union Meeting Road
P.O.Box 3053
Blue Bell, PA, 19422

December 12, 2012

Re: Evaluation of second batch of EC Power 18650 cells

Dear Dr. Shaffer,

The evaluation of EC Power's second prototype 18650 cell, based on Li-rich metal oxide as cathode and silicon-carbon nanoparticles as anode, is complete, based on the data provided by EC Power, which shows the performance as follows:

[illegible]	[illegible]
0.1	2.584
1	0.453
3	0.252

The capacity for the 0.1 A discharge, being greater than the first prototype cell by ~ 13%, is encouraging. While the 1A and 3A tests were shown to have low capacity, EC Power has discussed with us the issues related to large-scale electrode fabrication, including those related to electrode slurry solvent and binder.

Furthermore, given the demonstrated electrode active material capacities of over 1500mAh/g for anode and nearly 250mAh/g for cathode materials, there is good reason to believe that a greater capacity will be reached in the future, after final scale-up issues have been resolved.

We look forward to continuing our work with EC Power and the future development of their high energy density technology.

Sincerely,

Daniel Boyer
Technical Manager
New Technology Development

Figure 25. Evaluation of EC Power's second prototype 18650 cell.

C6: Submit report outlining improvements to original cell delivered to customer. This report will include both improvements in active material specific capacity, as outlined in T4, and cell design improvements, as outlined in T5.

We have optimized the cathode materials with acid treatment and thermal treatment to further increase the 1st cycle efficiency and decrease the gassing problem. The as-treated materials show high 1st cycle efficiency over 90% and the coin cells made with thick electrodes didn't pop open during the test any more. We also improved the design by optimizing ratio of components in the electrode slurries, test of packing densities and optimizing porosities. Moreover, the engineer designed and made an open system for battery testing to decrease the possibility of explosion.

C7: Based on the performance of the prototype, provide a Letter of Support, outlining a plan to continue with from the customer evaluating the cell, describing potential commercialization path/s going forward, based on the results of the first evaluation.

EC Power had a meeting with C&D Technologies on Sep. 21, 2012 to discuss the ongoing work in this project in addition to several other EC Power technologies and software. C&D remains quite interested in the high capacity technology being developed under this project. As outlined in the letter of support given in figure 26, even in light of the less than desirable results from the second prototype, C&D remains interested in the EC Power technology, and will continue to support future activities.

C&D TECHNOLOGIES, INC.
Power Solutions

Dr. Christian Shaffer
EC Power
200 Innovation Blvd.
State College, PA 16803

Mr. Daniel Boyer
C&D Technologies, Inc.
1400 Union Meeting Road
P.O. Box 3053
Blue Bell, PA, 19422

December 12, 2012

Re: Letter of Support for EC Power high capacity Li Ion cell technology

Dear Dr. Shaffer,

We continue to support the development of the EC Power high capacity Li ion cell technology, based on high capacity layered metal oxide cathode and Si/carbon anode materials. While the 3Ah goal has not been reached to date, due to some unforeseen challenges related to scale-up, the anode and cathode active material specific capacities of over 2500 mAh/g and nearing 250 mAh/g, reached over the past year, are quite attractive, particularly to high energy military applications.

We have been in touch with EC Power several times over the course of the past year, including a meeting on September 21, 2012, where we discussed at great length EC Power's high-capacity Li ion technology and recent technology developments in this regard. We remain optimistic that EC Power will overcome the remaining hurdles, resulting in a high-capacity commercial cell technology.

Sincerely,

Daniel Boyer
Technical Manager
New Technology Development

Figure 26. C&D letter of support.

C8: Provide a report that outlines the commercialization pathway opportunities for the technology development and the identified application/s. update the center on the IP arrangements with PSU as it relates to licensing.

We anticipate our high energy density technologies being adopted in Navy critical information backup systems on sea-going vessels. C&D is already has quite active in this market, and desires a more energy dense solution technology.

EC Power has developed considerable IP from the activities of this work, both in cathode active material synthesis and cell fabrication/engineering. We anticipate filing patents in the near future (1yr) from these activities. In addition to patents, we have developed multiple trade secrets, particularly in the cell fabrication/engineering. Penn State is likewise moving towards patenting their anode technology.

The most likely commercialization pathway forward is for C&D to license the cathode and cell fabrication technology from EC Power, and the anode technology from PSU. C&D has expertise in large-scale battery manufacturing and will incorporate our technologies in various form factors.

Summary:

In the first quarter, Penn State successfully met the milestones in the technical part by synthesizing, optimizing, and characterizing Si-carbon nanocomposites . EC Power also met the milestones in the commercialization part: the prototyping agreement was reached , and our market synopsis was delivered.

During the second quarter, PSU successfully synthesized Si-carbon nanoparticles as the anode for 18650 cells. The researchers identified that Si-carbon nanoparticle with 4:5 ratio and NaCMC as binder shows high capacity of over 1500mAh/g. With the minimal capacity fade in 100 cycles, the Si-carbon anode still keeps the capacity as high as 1100mAh/g. In the meantime, PSU researchers successfully used the low cost carbon in substitution of graphene. The anode material does not only have high capacity but also save the cost on the raw materials.

EC Power carried out a number of experiments to assess the effects of different experiment conditions and optimize the synthesis of Li-rich cathode materials. The researchers successfully selected Li(Li0.2Ni0.13Mn0.54Co0.13)O2 as the cathode for the 18650 cell fabrication. The choice is based on two facts. Li(Li0.2Ni0.13Mn0.54Co0.13)O2 cathode shows a high capacity of 240mAh/g, which nearly reaches our target of 250mAh/g; and the synthesis approach is easy to scale up, which is very important for 18650 fabrication and the large scale production in future. We also plan on the investigation of new electrolyte and carbon doping in the synthesis in order to further increase the capacity in future.

EC Power also carried out a cost estimate based on near-term market size and production quantity. The demonstrated ability of the PSU anode to use low-cost carbon in lieu of expensive graphene removes the highest-cost item from the cell production. Thus our latest cost production for the 18650 cells is ~ $500/kWh, which should be quite attractive for a cell technology nearing 250 Wh/kg.

Our initial batch of 18650 cells was evaluated by our customer, C&D technologies. As the evaluation letter the y provided later shows, the capacity of the prototype cell is 2.287Ah. It is also worth to mention that we observed serious gassing problems during the testing. We

documented that gassing of the cathode during the first few cycles is a potential safety issue, as several coin cells popped open during testing. The cumulated gas not only decreased the capacity of the cell but also may cause explosion. Before finalizing the prototype cells, the researchers and engineers in EC Power took the problems seriously and successfully developed a solution to the gassing problem while maintain a high capacity.

In the last quarter, EC Power focused on fabrication of 18650 battery cells with optimized materials. There are a few technical challenges surfaced during the design and fabrication process. Many efforts were put into material and process optimization in order to overcome these challenges. We also developed additional methods in attempt to further minimize the gassing problems. This was accomplished from both material synthesis and engineering approaches. Firstly we used acid treatment to activate the Li-rich material before it was fabricated into the electrode in order to relieve the gassing problem. Secondly, EC Power has designed an open system to form18650 cells (formation during first few cycles). With our open system set-up, the gas produced in 18650 cell was released before the final seal of 18650 cell. The combination of the materials acid treatment approach and fabrication feature greatly decreases the possibility of the accidents such as explosions during the battery tests. Acid and thermal treatments were also investigated to increase the 1st cycle efficiency in order to further increase the capacity of the cell. We also studied and optimized the coating of thick electrodes. Because of the limit of the time, to date we only can optimize the coating with coin cell tests. Unfortunately, the thick film was not as good as we expected when we used the same formula to large-scale thick film coating using large batches. There are more challenges in preparing large thick film and the cracking problem is more severe after pressing and rolling process. Although we have studied and solved the problems in coin cell level, there were still some engineering challenges in the fabrication of 18650 cells which impedes the capacity at high discharging rate. EC Power has fabricated the second batch of prototype 18650 cells and the capacity is 2.584Ah. Although there is 13% improvement from the last batch, the cell falls short of our 3Ah target and the capacity at high discharge rate requires further improvement as well. The short of the capacity may be caused by the low electrical conductivity of the cathode film which is attributed to the poor electrode film structure as we discussed before. We believe with the optimization of the large format electrode films, the capacity of the cell would be further increased.

We have kept open and frequent communication with our customer C&D technologies. On September 21, 2012, C&D technologies visited EC Power in State College to discuss this project and possible collaboration in future. C&D remains quite interested in the high capacity technology being developed under this project. They acknowledged the efforts of EC Power and agreed on our approaches to solve the technical problems. As outlined in the letter of support, even in light of the less than desirable results from the second prototype, C&D remains interested in the EC Power technology, and will continue to support future activities.

References

1. http://www.ndu.edu/press/lib/images/jfq-57/lovins.pdf
2. http://seekingalpha.com/instablog/21153-sufiy/410591-revenue-for-lithium-ion-battery-market-set-to-grow-by-700-by-2017
3. Broad Agency Announcement "BAA-11-17-PKM", CFDA 12.800_AF.

Appendix R – 11-058 (SenSevere)

Pennsylvania NanoMaterials Commercialization Center

Final Report

Project Title: Commercialization of Novel Sensors for Chemically and Thermally Challenging Environments: Detection of Hydrogen within Chlor-alkali Product Streams

Project Leader: Dr. Jason Gu

Name of Project Leader's Organization: SenSevere, LLC

Date: 11/26/2012

Table 1: Schedule summary for Milestones and Payments

Milestone	Date	Description (T,C)	Payment
Milestone 1	4, January, 2012	Project Kickoff	$30,000
Milestone 2	31 March 2012	T1, T2, T3, T4, T5, C1	$50,000
Milestone 3	30 June, 2012	T6, T7, T8, T9, C2, C3	$55,000
Milestone 4	31 October, 2012	T10, T11, C4, C5, C6	$35,000
Final Paperwork	November 15, 2012	Closeout documents	$15,000

T = Technical Milestone
C = Commercial Milestone

1

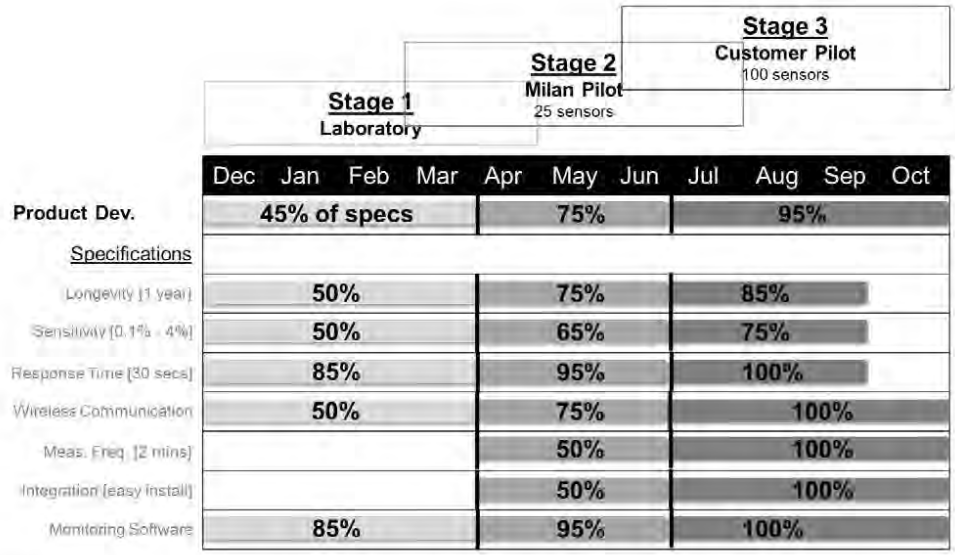

Table 2: It is important to note that the Stages at the top of the image represent different states in testing, which does not correspond to the different phases of the project. This offset allows for time to respond to suggested changes that result from the testing, and iteratively evolve towards the milestones within each phase. *Accelerated lifetime testing will allow completion of the longevity requirement. Both increases in temperature and removal of protective over-layers have been considered. Initial tests on protective over-layer removal indicate significantly (8 times) faster degradation; this is however dependent upon the operative failure mode.

Miletone 1 : Project Kickoff January 1, 2012

Milestone 2 : Prototype Development

The overall aim of this milestone was to complete the first scale-up of SenSevere technology and build a prototype business case for deploying sensors in chlor-alkali plants. At the date of completion, SenSevere has delivered a prototype product, which includes at least 50% of the previously agreed upon specifications to a scale-up facility owned by De Nora in Milano Italy. The risk of running a cell without hydrogen sensors has been calculated. Based upon responses from PPG Industries and Sabic, a prototype of the utility model for these sensors has been built. The calculated risk and the empirically determined value add per cell was $2000 and $1500, respectively. Additional surveys to the remaining plants in North America will be administered closer to the pilot deployment of SenSevere sensors into a live chlor-alkali plant. A visit to PPG Industries Natrium plant drew significant interest in being our beta site. De Nora aims to approach PPG Industries during the Chlorine Institute meetings in the summer about a potential beta installation. Due to the positive technical developments and customer feedback, the management at De Nora has made reaching a long-term business agreement a priority. SenSevere expects a term sheet for a long-term arrangement in either April or May. Next milestone focuses upon channel development, identification of a test site, completion of a product to-be-deployed into a customer site. Positive progress has been made on all fronts.

Milestone 3: Prototype Refinement

SenSevere has complied with the deliverable, save acquiring specific market information regarding the pricing of the sensor. SenSevere has chosen a modular approach for product development. The base sensor product will contain the sensor device, fixture, and electronics. SenSevere will offer modular battery backup, wireless, and analog out modules. Additional modules can/will be offered given feedback from the customer. De Nora was unable to complete the surveys due to certain unforeseen circumstances, but is dedicated to completing such a survey in Q3, 2012. SenSevere will drive the completion of such a survey, or identify additional routes to achieving such information.

Milestone 4: Prototype Deployment

SenSevere has complied with the deliverable, save the executed distribution agreement with De Nora. This was held up by the lack of a customer pilot trial. To remedy this, the previous LOI was extended for 6 months to the end of 2012, and a customer pilot trial is currently ongoing. SenSevere has identified and engaged contract manufacturers and is currently capable of delivering on orders of up to 1000 sensors. Through interactions with the plant, a two-product marketing strategy was identified. Initially, a high precision chlorine header hydrogen monitoring system will be marketed first, to be followed by a less precise per-cell hydrogen and other process variables monitoring system. The cost of marketing should be low due to the

existing sales network owned by De Nora, and the eminent need for these products, as confirmed by SenSevere's interaction with 3 of the 4 largest chlorine operators in the world.

Closeout: Strategic Path Forward

Throughout the course of this project, SenSevere was able to move from laboratory demonstrations of our technology to a completed product currently in a pilot deployment. Moving forward, SenSevere aims to complete the pilot test in March, en route to commercial sales of the product via our distributor, De Nora. SenSevere projects to complete negotiations of the distribution agreement with De Nora by January 2013. The initial target customer is PPG Natrium.

On other fronts, SenSevere aims at exploring other commercial opportunities for our technology. We have identified the need for hydrogen sensors within the nuclear, automotive, energy, and other electrochemical industries as good points of entry. De Nora will serve a strong partner for exploration and penetration into other electrochemical industries. SenSevere is currently engaged in discussion with EPRI for exploration into the nuclear field. We are currently looking for partners for all of these potential sensor markets.

LIST OF ACRONYMS, ABBREVIATIONS, AND SYMBOLS

Acronym	Description
CPO	Collaborative Project Order
AFRL/RX	Air Force Research Laboratory, Materials and Manufacturing Directorate
WBI	Wright Brothers Institute
PA NanoCenter	Pennsylvania NanoMateials Commercialization Center
TAC	Technical Advisory Committee
SOW	Statement of Work
OPV	Optionally Piloted Vehicle
PL	Photoluminescence
FTIR	Fourier Transform Infrared
NREL	National Renewable Energy Laboratory
CNT	Carbon Nanotube
CF	Carbon Fiber
CB	Carbon Black
t-CNT	Treated Carbon Nanotube
TGA	Thermal Gravimetric Analysis
NanoRDC	NanoResearch, Development and Consulting LLC
MPIs	Materials Performance Indices
MIL	Military
ANSI	American National Standard
NHA	Nickel Coated Copper Alloy
NCU	Ultra-high Strength Copper Alloy
MTS	Modular Wire Takeup System
OPV	Organic Photovoltaic
PET	Polyethylene Terephthalate
HTL	Hole Transport Layer
ITO	Indium Tin Oxide
PEN	Polyethylene Naphthalate
PI	Polyimide
PC	Polycarbonate
IPA	Isopropyl Alcohol
ROIC	Return on Invested Capitol
SPS	Strategic Polymer Sciences, Inc.
SJM	St. Jude Medical
PSU	Pennsylvania State University
ICD	Implantable Cardioverter Defibrilator
VDF	Vinylidene Fluoride

LIST OF ACRONYMS, ABBREVIATIONS, AND SYMBOLS (cont'd)

Acronym	Description
TrFE	Trifluoroethylene
CFE	Chlorofluoroethylene
CTFE	Chlorotrifluoroethylene
PP	Polypropylene
CARTS	Capacitors and Resistors Technology Symposium
ERC	Engineering Research Center
HIS	Human Interface Software
TPU	Thermoplastic Urethane
DOPA	Dihydroxyphenylalanine
VER	Vinyl Ester Resin
UPR	Unsaturated Polyester Resin
PCB	Printed Circuit Board
JDA	Joint Development Agreement
SFIL	Step and Flash Imprint Lithography
CIS	CMOS Image Sensor
CMOS	Complementary Metal Oxide Semiconductor
SAAD	Sective Aluminum Area Deposition
AES	Auger Electron Spectrometry
TE	Transmitted Electron
HAADF	High-Angle Annular Dark Field
SE	Secondary Electron
SEM	Scanning Electron Microscope
STEM	Scanning Transmission Electron Microscope
iLS	Industrial Learning Systems
HRG	Horizontal Ribbon Growth
XRD	X-ray Diffraction
LXPM	Liquid X Printed Metals
σ	Conductivity
OFET	Organic-based Field Effect Transistor
PET	Polyethylene Terephthalate
PV	Photovoltaic
ARC	Anti-reflective Coating
PECVD	Plasma-Enhanced Chemical Vapor Deposition
DSSCs	Dye Sensitized Solar Cells
IV	Current Voltage
TCO	Transparent Conductive Oxide

LIST OF ACRONYMS, ABBREVIATIONS, AND SYMBOLS (cont'd)

Acronym	Description
GaAS	Gallium Arsenide
NWA	Nanowire Array
FE	Finite Elements
BMS	Bayer MaterialScience
PU	Polyurethane
TPU	Thermoplastic Urethane
PHEV	Plug-in Hybrid Vehicle
EV	Electrical Vehicle
UPS	Uninterrupted Power Supply
DoD	Department of Defense
UAV	Unmanned Aerial Vehicle